New Concept of Multidisciplinary Optimization for Weight Saving and Stiffness Improvement of a Morphing Variable Span of Tapered Wing MVSTW - Application to the UAS-S4

by

Mohamed ELELWI

MANUSCRIPT-BASED THESIS PRESENTED TO ÉCOLE DE TECHNOLOGIE SUPÉRIEURE IN PARTIAL FULFILLMENT OF THE REQUIREMENTS FOR THE DEGREE OF DOCTOR OF PHILOSOPHY PH. D.

MONTREAL, AUGUST 29, 2022

ÉCOLE DE TECHNOLOGIE SUPÉRIEURE
UNIVERSITÉ DU QUÉBEC

BOARD OF EXAMINERS

THIS THESIS HAS BEEN EVALUATED

BY THE FOLLOWING BOARD OF EXAMINERS

Mrs. Ruxandra Mihael Botez, Thesis Supervisor
Department of System Engineering at École de technologie supérieure

Mr. Thien-My Dao, Thesis Co-supervisor
Department of Mechanical Engineering at École de technologie supérieure

Mr. Philippe Bocher, President of the Board of Examiners
Department of Mechanical Engineering at École de technologie supérieure

Mr. Yvan Beauregard, Member of the jury
Department of Mechanical Engineering at École de technologie supérieure

Mr. Rosario Pecora, External Evaluator
University of Naples "Federico II"- Aerospace Engineering Faculty

THIS THESIS WAS PRENSENTED AND DEFENDED

IN THE PRESENCE OF A BOARD OF EXAMINERS AND PUBLIC

ON AUGUST 18, 2022

AT ÉCOLE DE TECHNOLOGIE SUPÉRIEURE

ACKNOWLEDGMENT

Firstly, and foremost, I would like to express my sincere gratitude to Prof. Ruxandra Mihaela Botez, my thesis supervisor, for providing me with the opportunity to join her team and to convince me to pursue and to complete my Ph.D. thesis at the Laboratory of Applied Research in Active Control, Avionics AeroServoElasticity (LARCASE), and for her valuable advice, constant motivation, and high support during this entire period. In addition, I wish to acknowledge her multiple efforts to make my research and educational goals achievable.

Special thanks are extended to Prof. Thien-My Dao for his advice, guidance, and company; and valuable directives to pursue independent work. I offer my appreciation for his support, feedback, and time, as well as to PhD committee member.

I am extremely grateful to my extended family, near and far for all affection and encouragement.

Of course, my special thanks extend to my lovely wife for her patience and her efforts to create a supportive environment so that I could complete my research.

Lastly, I am grateful to all LARCASE members and researchers, and especially to all of the students with whom I had the pleasure of working together and sharing ideas. Moreover, I would wish to extend my sincere thanks to the employees of the ÉTS for their support.
My sincere gratitude to all these people without your encouragement and support, I could never have reached finished my PhD.

Nouveau concept d'optimisation multidisciplinaire pour l'économie de poids et l'augmentation de la rigidité d'une aile à envergure variable - Application à UAS-S4

Mohamed Elelwi

RÉSUMÉ

Cette thèse présente une nouvelle approche sophistiquée d'utilisation de l'optimisation numérique multidisciplinaire pour développer une aile légère déformable basée sur les données d'un système aérien sans pilote (UAS-S4). La conception optimale de l'aile de l'UAS-S4 pour atteindre un haut niveau de performance. Le calcul et la sélection des matériaux de fabrication appropriés ont été également prises en compte. La méthodologie, les outils de conception et les résultats ont été obtenus via la conception assistée par ordinateur (CAO), l'ingénierie assistée par ordinateur (IAO) et le logiciel MATLAB. Dans la première, phase comprenait une étude comparative de conception et de développement d'une aile déformable à envergure variable de morphing de l'aile conique (MVSTW) pour un système aérien sans pilote (UAS-S4) a été présenter. L'objectif principal était d'analyser et de comparer les propriétés aérodynamiques des ailes de différentes longueurs d'envergure et angles de balayage et de déterminer leurs plus conceptions géométriques efficaces. Cette conception peut être utilisée pour le contrôle du mouvement de roulis d'un avion au lieu de mécanismes de contrôle conventionnels et elle est plus sensible aux changements d'angle de la section intérieure, qui influencent les caractéristiques aérodynamiques. La deuxième phase a présentée l'optimisation de la topologie et évaluée la faisabilité des composants internes de l'aile. L'optimisation de la topologie a été effectuée pour placer les composants de l'aile dans ses segments fixes et mobiles en utilisant l'alliage d'aluminium 2024-T3. Selon les résultats de la recherche, les segments d'aile fixes et mobiles devraient être conçus pour des configurations à deux longerons et sept nervures en utilisant des composants de support dans la région à forte contrainte. La troisième phase traite de l'intégration du dimensionnement structurel, de la topologie et de l'optimisation aérodynamique pour une MVSTW dans le but de réduire son poids. Les techniques d'optimisation ont pris en compte la répartition de la charge aérodynamique le long de l'envergure dans sa pleine extension et à vitesse maximale. Les composants de l'aile ont été optimisés en termes de taille et de topologie et ont été conçus à partir de l'alliage d'aluminium 2024-T3. Des économies de poids allant jusqu'à 51,2 % et 55,7 % ont été obtenues pour les sections d'aile fixe et mobile, respectivement, selon les résultats de l'optimisation. La quatrième phase est une continuation des phases précédentes effectuées sur l'optimisation numérique multidisciplinaire pour la conception d'une MVSTW pour minimiser son poids en utilisant des matériaux composites. En intégrant l'optimisation simultanée de la sélection des matériaux, l'optimisation de la taille structurelle et l'optimisation topologique selon les analyses aérodynamiques, un environnement informatique pour l'optimisation multidisciplinaire a été considéré pour déterminer si l'optimisation des ailes de déformables était faisable. Le poids du MVSTW pourrait être considérablement réduit en utilisant les résultats de l'optimisation.

Mots-clés : analyses aérodynamiques ; performances aérodynamiques; corde à la racine de l'aile; accord de pointe ; aile déformable à envergure fuselée variable (MVSTW); UAV ;

Mécanisme télescopique ; Optimisation de la taille et de la topologie par l'analyse d'éléments finis ; Solveur OptiStruct ; SoildThinking; MATLAB

New Concept of Multidisciplinary Optimization for Weight Saving and Stiffness Improvement of a Variable Tapered Span-Morphing Wing - Application to the UAS-S4

Mohamed ELELWI

ABSTRACT

This thesis presents a new approach of multidisciplinary numerical optimization used to develop a lightweight morphing wing based on data from an Unmanned Aerial System (UAS-S4). The optimal design for the UAS-S4 wing was determined, in order to achieve a high level of performance. The computation and selection of appropriate manufacturing materials were also considered. The methodology, design tools, and results were obtained via Computer-Aided Design (CAD), Computer-Aided Engineering (CAE), and MATLAB software. The first phase included a design and development comparative study of a Morphing Variable Span of the Tapered Wing (MVSTW) for an Unmanned Aerial System UAS-S4. The main objective was to analyze, and to compare the wing aerodynamic properties for various span lengths and sweep angles, and to determine its most efficient geometric design. This design can be employed for aircraft roll motion control instead of its conventional control mechanism, and is more sensitive to changes in the angle of its inner section influencing the aerodynamic characteristics. The second phase presented the topology optimization and evaluated the feasibility of internal wing components. Topology optimization was performed to place the wing components within its fixed and moving segments done in aluminum alloy 2024-T3. According to research findings, the fixed and moving segments should be designed with two spar and seven ribs configurations with their support components in the high-strain region. The third phase discusses the integration of structural sizing, topology, and aerodynamic optimization for MVSTW with the objective of reducing its weight. The optimization techniques considered the aerodynamic load distribution along the wingspan at its full wingspan extension and maximum speed. The wing components were optimized for size and topology optimization, and were designed using aluminum alloy 2024-T3. Weight savings of up to 51.2% and 55.7% were obtained for the fixed and moving wing sections, respectively, according to the optimization results. The fourth phase is a continuation of earlier phases performed for the multidisciplinary numerical optimization for the of MVSTW design to minimize its weight using composite materials. By integrating simultaneous material, structural size, and topological optimizations according to aerodynamic analyses, a computational environment for multidisciplinary optimization was considered to determine if morphing wings optimization was feasible. The MVSTW weight could be significantly decreased by using of the multidisciplinary numerical optimization methods.

Keywords: aerodynamic analyses; aerodynamic performance; root chord; tip chord; morphing variable span of the tapered wing (MVSTW); UAV; Telescopic mechanism; Finite element analysis size and topology optimization; OptiStruct solver; SolidThinking; MATLAB

TABLE OF CONTENTS

Page

LIST OF TABLES

Page

LIST OF FIGURES

LIST OF ABREVIATIONS

ABS	Acrylonitrile Butadiene Styrene
CAE	Computer-Aided Engineering
CFD	Computational Fluid Dynamics
FAA	Federal Aviation Regulations
FEM	Finite Element Method
FRPs	Fiber-reinforced plastics
HDPE	High-Density Polyethylene
MDO	Multidisciplinary optimization
MVSTW	Morphing Variable Span of Tapered Wing
SIMP	Solid Isotropic Material with the Penalization
SO	Sizing optimization
STO	Sizing and topology optimization
TO	Topology Optimization
UAVs	Unmanned Aerial Vehicles

LIST OF SYMBOLS

A	Laminate extension stiffness matrix
AR	Wing aspect ratio
b	Wingspan (m)
B	Laminate coupling stiffness matrix
c_g	Geometric chord (m)
C_L	Lift coefficient
C_D	Drag coefficient
C_L/C_D	Lift to drag ratio
c_t	Fuel consumption rate
D	Laminate bending stiffness matrix
D	Drag (N)
E	Flight endurance (h)
E_1	Lamina longitudinal Young's Modulus
E_2	Transverse Young's Modulus
E_{f1}	The longitudinal Young's Modulus of the fiber
E_m	The longitudinal Young's Modulus of the matrix
$E_{(xi)}$	Young's modulus of each element
E_{solid}	Young's modulus of solid regions
E_{void}	Very low Young's modulus
E_x	longitudinal Young's Modulus

XXX

E_y	Transversal Young's Modulus
f	Distributed body force
F	Force vector
Fi	Point load on the i^{th} node
G_{xy}	Shear modulus
I_{xx}	Mass moment of inertia (kgm^2)
K	Global stiffness matrix
k_0	Elemental stiffness matrix
L	Lift (N)
L_{roll}	Rolling moment (Nm)
m_w	Wing mass (kg)
p	Roll rate
q	Dynamic pressure (Pa)
R	Flight range (km)
S	Wing reference area (m^2)
S	Surface area of the continuum
t	Traction force
u	Displacement area
U	Global displacement
Ui	i^{th} displacement degree of freedom
V	Speed (m/s)
V	Total volume

v_f	The volume fractions of the fiber
v_m	The volume fractions of the fiber and the matrix
V_0	Initial volume
V_i	Volume of the i^{th} element
V_{xy}	Poisson's ratio
W_0	Takeoff weight (N)
W_1	landing weight (N)
Xi	Pseudo density
ρ	Air density (kg/m^3)
$\Gamma_{(y)}$	Circulation distribution
ρ_0	Density of the base material
ρ_i	Density of the i^{th} element
τs	Time constant

INTRODUCTION

More than a century has passed since the Wright brothers invented the first controlled aircraft. One of the most astonishing technologies at the time was the pilot's ability to control the aircraft in three dimensions in rotation mode (pitch, yaw, and roll) (Allen, 2003).

This thesis offers research findings to establish a novel concept for utilizing Multidisciplinary Design Optimization (MDO) to develop a sophisticated, robust and lightweight morphing system for an UAV wing. All the data and information used in this thesis were gathered in accordance with the manufacturing data and specifications of the Unmanned Aerial System (UAS-S4) Ehécatl, from Hydra Technologies. Our LARCASE laboratory at the ÉTS has conducted a wide range of research activities in the multidisciplinary domain of aeroservoelasticity (R. Botez, 2018). This research evaluated the structural analysis and optimization of the UAS-S4 based on CFD optimization results. Figure 0.1 depicts the UAS-S4 version, used as a reference (baseline) model for conducting structural and aerodynamic optimization at the LARCASE laboratory.

Figure 0.1 Unmanned Aerial System UAS-S4 Ehécatl from Hydra Technologies

The primary characteristics of the UAS-S4 Ehécatl are given below in Table 0.1:

Table 0.1 Primary characteristics of the UAS-S4 Ehécatl

Specification	Symbols	Value
		UAS-S4
Wing span (in meters)	b	4.191
Wing area (in square meters)	S_w	2.307
Wing root chord at the fuselage centerline (in meters)	C_r	0.705
Wing tip chord (in meters)	C_t	0.396
Maximum take-off weight in kilograms	W_{TO}	80
Operational ceiling (in feet and meter)		20000 *ft*, 6096 *m*
Maximum speed (in knots and kilometers per hour)	V_H	135 *knots*, 250 *km/h*
Loitering speed (in knots and kilometers per hour)	V_c	50 *knots*, 92.59 *km/h*
Operational range (in kilometers)	R	120 km
Sweep distance (in meters)	d	0.309
Aspect ratio	AR	11.6
Taper ratio	λ	0.56
Mean aerodynamic chord (in meters)	$\bar{C}$	0.56
Sweep angle of the wing	Λ_w	8.93°
Sweep distance at the mean aerodynamic (chord in meters)	d_{MAC}	0.103
Mean aerodynamic chord from the root chord (in meters)	y_{MAC}	0.95
Mean aerodynamic chord in the x-axis (in meters)	x_{MAC}	0.14
%MAC Distance from the Root (%MAC)	$\%MAC$	20%
The distance of the center of gravity in meter	CG	0.253

The objective of this thesis is to create a new geometric wing shape based on the UAS-S4 Ehécatl reference wing, that can accomplish several multi-missions within the whole UAS's flight envelope. The research strategy encompasses the steps below:

- Investigation of the possibility of developing a more effective wing shape than its baseline shape with the ability to adjust its aspect ratio, so that it will act under the condition of a morphing wing to identify ways to increase the span-chord, and thus, the lift/drag ratio. In addition, one of the fundamental considerations of optimal design in aerospace is to maximize performance while minimizing structural weight within an adequate range. The most significant aspect of wing design is the consideration of both aerodynamics and structures studies in order to improve wing flexibility and performance. A variable morphing wingspan uses efficiency enhancement technique instead of conventional control

surfaces. Aviation performance enhancements result in an increase in flight range and endurance.

- A novel vision-based structural analysis and topology optimization (TO) has been presented for a morphing variable span of the tapered wing (MVSTW) design based on the NACA 4412 airfoil. Based on the TO approach, that optimization was performed to properly locate the wing components inside its segments. Candidate elements were then chosen within the design area of the wing segments. Constraints imposed by materials, such as the volume of a structural design, substantially affect the mechanical properties, including their total stiffness and robustness (Plocher & Panesar, 2019). The TO technique enhances the structural design of the wing by determining the most feasible structural layouts for its various structural components (L. Zhao, Li, Chang, & Li, 2019). Additionally, the positions of a wing's parts should provide maximum stiffness to the overall structural design of the wing. An optimization setting was therefore developed for solid wing segments in order to predict the positions of variable span morphing wing components inside the design area.
- An aerodynamic-structural analysis and optimization were carried out using data from the unmanned aerial systems UAS-S4, and then they coupled this data to the results of the CFD optimization (Y. Tondji & Botez, 2017). The aerodynamic lift distribution over the whole surface of a wing was determined using a numerical investigation based on the XFLR5 code results. The TO was used to develop the optimal structural configuration that resulted in a tremendous reduction in structural weight. For the high efficiency of the optimized wing components, they should correspond to the structural wing configuration's maximum stiffness requirements (Y.-b. Zhao, Guo, Duan, & Xing, 2017). Finite Element Analyses (FEA) were then performed, and their findings revealed that the optimized MVSTW possessed the required mechanical properties, including linear elasticity and structural wing integrity. The design of the morphing variable span of tapered wing (MVSTW) design was developed using the recent progress in integration of aerodynamic and optimization methodologies. The results of the aerodynamic study were incorporated into sizing optimization (SO) and TO, and then they were used to solve pertinent optimization problems. The main purpose was to specify and examine the feasibility of this optimization

approach for skin and interior wing components such as ribs, spars, and others. The optimization approach was applied using a conventional material (Al-2024-T3) and extended the challenge by requiring close attention to various components materials during the optimization process. As a result of the weight savings achieved by sizing and topology optimization (STO) techniques on the wing components, the optimized wing shape met the structural integrity design parameters and could withstand structural failure in extreme flight conditions.

- To minimize weight by utilizing composite materials, multidisciplinary numerical optimization was developed for a morphing variable span tapered wing (MVSTW). To determine if optimizing morphing wings is feasible, a numerical domain of (MDO) was created by simultaneously merging material selection, structural sizing, and topology optimization according to aerodynamic performance improvement computations. The optimization process was performed using multiple solvers to evaluate their results in a variety of disciplines, including aerodynamics, material selection, structural optimization, and in their interactions. Our MATLAB new algorithm selected the best composite materials based on a variety of criteria such as physio-mechanical properties, availabilities in the markets, and cost. The size and topology optimizations were then achieved using Altair's OptiStruct and SolidThinking Inspire solvers. Both solvers have been linked to the aerodynamic analysis results produced by ANSYS Fluent and the XFLR5 code. The MDO technique has required the management of enormous quantities of data and information collected from various optimizations attaching them to each numerical solver and by paying close attention to wing components during the optimization process. The weights of the optimized wing components were greatly decreased significantly by using composite materials. Based on the optimization results for both MVSTW components, the wing components, including the spars, ribs, and support elements, were remodeled and further developed using the new MATLAB code to find the optimal material for specific wing components.

CHAPTER 1

LITERATURE REVIEW AND TECHNICAL BACKGROUND

The morphing wing design is expressed as a multidisciplinary problem, as it requires proper materials and structural configurations, accurate aerodynamic calculations, and optimization. This chapter provides an overview of the literature review, including the morphing wing methodology, material selection, and optimization methodologies indicated in the introduction. For consistency, the literature review is organized to provide the previous work on morphing wing done by the LARCASE team, followed by a general view of recent multidisciplinary design optimization methods, that address aircraft performance and optimization approaches using various materials. The subsequent chapters will provide more detailed literature reviews, as each chapter includes its technical literature review.

1.1 Morphing wing concepts and their applications

1.1.1 Variation of Wing Airfoil Shape

The LARCASE team has developed large research on morphing wings, including studying and developing novel approaches for morphing wing technology. Cooperation between teams at LARCASE at the École de Technologie Supérieure (ÉTS), Thales Canada and the Institute for Aerospace Research – National Research Canada (IAR - NRC), Bombardier Aerospace, and École Polytechnique de Montréal took place from 2006 to 2009 as part of the project CRIAQ 7.1. The primary goal was to enhance and control the laminar flow past a morphing wing with the aim to obtain significant drag decreases. The prototype of the morphing wing contained three noteworthy components: (i) an adaptable surface, fabricated of a composite material and stretching across between 3% and 70% of the airfoil chord, (ii) a rigid inward surface, and (iii) an actuation system placed within the wing box. The actuators were situated at 25.3% and 47.6% of the chord and could morph the adaptive skin in two points (Popov, Grigorie, Botez,

Mébarki, & Mamou, 2010). Shape memory alloys (SMAs) were utilized as morphing actuators to integrate a morphing wing with a flexible upper skin, as shown in Figure 1-1.

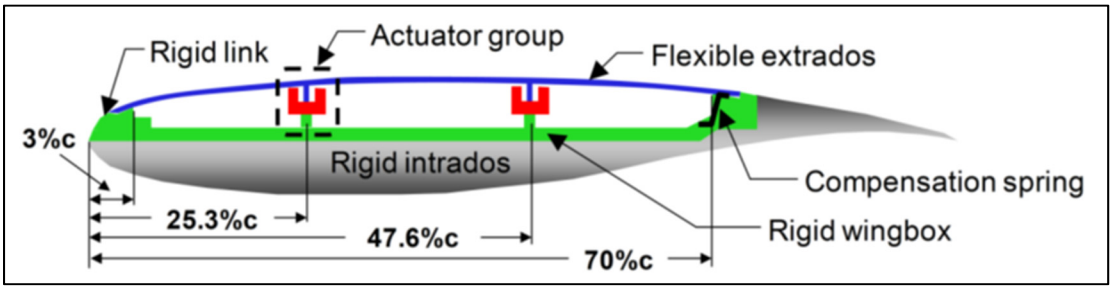

Figure 1.1 Wing section WTEA CRIAQ 7 project

The wing skin was produced using an epoxy resin, crossover Carbon-Kevlar filaments and low-modulus unidirectional carbon. The actuation system was manufactured of a smart memory alloy (SMA) and a dynamic element cam transmission. The reference profile WTEA was selected for its large laminar flow surface. CFD and wind tunnel tests evaluations were conducted for the flight conditions of Mach 0.2 to 0.3 and incidence angles of -1 to 2 degrees. The simulation results demonstrated a shift of the transition to the trailing edge of up to 30% of the chord and a drag reduction up to 22%. Wind tunnel tests were performed in the subsonic wind tunnel at the IAR-NRC. The rigid part of the model was outfitted with static pressure taps and the adaptive upper surface was supplied with sixteen pressure sensors for detecting the edge position. Infrared images were taken to validate the transition region. These experimental results have shown that the acquired deformation allowed the flow transition delay on the wing. Since this research utilized an ideal rectangular wing, no structural constraints for an actual wing were addressed.

Another large international project, CRIAQ MDO 505, was established later, sponsored by the same Canadian and new Italian partners (Ruxandra M Botez et al., 2017). In this project, a morphing wing equipped with a morphing aileron were developed for a Bombardier regional aircraft. The project's goal was to design and test an aileron-equipped wing that could delay the transition from laminar to turbulent flow along the wing chord. The CRIAQ MDO 505 project's major focus was the development of a bench test, followed by wind tunnel tests of a

prototype system of a morphing wing-tip. Both teams worked on the development, manufacturing, and testing of the morphing wing was integrated with and rigid aileron (Canada) and the morphing aileron (Italy) to enhance the aerodynamic performance of the morphing system. Then, the morphing wing was integrated with the morphing aileron.

1.1.2 Variation of the Wing in the Camber and Spanwise Directions

Morphing technology allows aeronautical engineers and aircraft designers to develop a wing that can modify its geometrical shape. The capacity of a wing to morph according to its planform and cross-sectional dimensions allow it to better perform its tasks under various flight conditions. In 2015, a research team led by Christopher Beaverstock of the University of Swansea investigated the effect of span and camber morphing on the mission performance of a 25-kg UAV (Christopher Simon Beaverstock, Woods, Fincham, & Friswell, 2015). They have used models representing the fishbone dynamic camber (FishBAC) and an adaptive aspect ratio (AdAR).

The wing span morphing approach with optimized fixed camber at its root increased its aerodynamic efficiency by 25%. That same team proved that improvements in the effectiveness are dependent by the speed range in the mission (Christopher Simon Beaverstock et al., 2015) (JHS Fincham & Friswell, 2015).

1.1.3 Chord-wise Variation of the Wing

Chord-wise wing camber modifications, guided by the morphing wing design, can provide the optimum feasible wing shape for various flight missions. Within the SARISTU (Smart Intelligent Aircraft Structures) European program, 13 companies, research organizations, and universities collaborated on the "Adaptive Trailing Edge Device" project (ATED), that was completed in December 2014. The researches deepened their understanding of the performance of a morphing wing.

Conformal morphing along the trailing edge (TE) can reduce both the drag and the root bending moment, so that chord-wise actuation can improve the L/D ratio by up to 10%. The redistribution of span-wise lift results in a 10% reduction in the root bending moment. Furthermore, these results reveal a reduction in overall weight and fuel consumption (Dimino, Flauto, Diodati, & Pecora, 2014).

1.1.4 Variation of a Morphing Wing with Radical Geometry

Lockheed Martin's Skunk Work collaborated with the Air Force Research Laboratory (AFRL) from January 2003 to January 2006 to design and develop Z-wing morphing for unmanned aerial vehicles (UAV). The main concept of the Z-wing is to fold the wing by simulating a bird's folded wing (Joshi, Tidwell, Crossley, & Ramakrishnan, 2004).

Wing shifting geometry enables aircraft to perform many missions simultaneously, such as long-range cruise and loitering, transitioning into a high-speed dash. Lockheed Martin and the Air Force Research Laboratory have researched advanced materials' technology morphing techniques, including those of piezoelectric actuators (Compact Hybrid Actuators Program) to transform it to an appropriate position. These piezoelectric actuators were found to be efficient at both high and low frequencies.

Another type of morphing wing is the one with a changing sweep angle. The concept for this morphing UAV is called the Bat Wing. NextGen Aeronautics renamed it the MFX1, and presented a new generation of unmanned aerial vehicles (UAVs) with a wing geometry that was able to adjust its shape according to flight conditions. Controlled by electro-mechanical actuators, it could switch from a high span geometrical shape for slow-speed flights to a low span configuration for high-speed flights (Zingg, Diosady, & Billing, 2006).

In August 2006, the main effective flight test of the MFX1 model was performed. The UAV reached up to 40% in span length, 30% and sweep angles variable from 15° to 35°, with speeds of close to 100 knots (Zingg et al., 2006).

1.1.5 Material Selection

Many companies and academic institutions are keen to develop new materials capable of changing their structural and mechanical properties to adapt themselves to changing flight conditions. Dynamic and shape-changing wing geometry has become a popular area for aeronautical researchers and developers. Aeronautical engineers seek to develop an active structure capable of static and dynamic shape management. The fundamental objective of shape morphing is to maintain its variation following multiple flight missions by targeting very good functionality and performance. Flexible materials are being employed in aircraft design to achieve the following goals (Baier & Datashvili, 2011):

- Weight reduction
- Aerodynamic wing parameters improvement
- Multiple-requirements of different flight regimes adaptation; and
- Self-healing wing shapes design

Some examples of the advanced materials that can be used in wing morphing are given next.

1.1.6 Shape Memory Polymers

Shape Memory Polymers (SMPs) respond perfectly to external influences (e.g., heat, electricity, light, magnetism, moisture, and others). Since the 1980s, a substantial amount of research has been conducted on this topic to develop a new range of promising smart materials (Leng, Lan, Liu, & Du, 2011). SMPs can drastically transform from a stiff to an extremely elastic polymer under certain conditions, and then revert to their original shapes. A SMP is a polymer that can be stretched, folded, and shaped to any geometry form. It has an elongation potential of up to 200% without compromising the material's characteristics (Sun, Guan, Liu, & Leng, 2016). Morphing skins made from SMP composites have been designed and tested in telescope wings.

1.1.7 Shape Memory Alloys (SMAs)

Because of their super-elastic characteristics, SMAs can respond to a wide range of conditions (e.g., high applied loads, large inelastic deformations, high strains). Due to their unique properties, SMAs are particularly appealing for actuators, and they are already widely utilized in the aviation field for morphing structures (Sun et al., 2016). The European Research Establishments Association launched a project to develop an adaptive airfoil in 1998 in collaboration with other European research centers, such as the French Aeronautics and Space Research Center (ONERA), the German Aerospace Center (DLR), the Italian Aerospace Research Centre (CIRA) and the Swedish Deference Research Agency (FOI). They introduced shape-adaptive wing, including the camber curvature, capable of absorbing and blowing the flow passing over the wing's surface using flow control, and put optical fibers on the wing to identify its structural deformations.

The concept of SMAs is to apply the tensile force in a vertical direction; the morphing flap is designed to be pivoted with the SMAs. Supporting the SMA springs, high-heat-resistant carbon fiber was installed, as of the high temperature of more than 100 °C (Sun et al., 2016).

1.1.8 Piezoelectric Materials

Piezoelectric materials are used for aerodynamic vibration control due to their relatively high forces yield over a wide frequency range (Bilgen, Friswell, Kochersberger, & Inman, 2011). The NASA Langley Research Center developed a type of piezoelectric fiber composite actuator called Macro Fiber Composite actuator (Williams, Park, Inman, & Wilkie, 2002), which outperformed the monolithic piezoceramic (PZT) actuators. Different morphing wing sections have been actuated by Lightweight Piezoceramic Composite Actuators (LIPCA). Piezoelectric composites can be used to change the wings camber. The main aim of the use piezoelectric composites is morphing wing design, then, lift increase and drag decrease. A piezoelectric composite-controlled micro air vehicle (MAV) was built and tested in a wind tunnel (Sun et al., 2016).

1.1.9 Composite Materials

Composite materials have become increasingly important in the aerospace industry. Composite materials offer several important characteristics, including low weight mass, high strength, and resistance to external factors (corrosion, rust), and they are part of a combination of materials that can achieve specific structural properties. Composite materials offer new properties that can give specific physical and mechanical characteristics. The technique of producing an advanced composite material is to combine fibrous materials installed in a resin network. These fibrous materials are equipped with fibers oriented in alternative directions, with the aim to achieve the desired material strength and stiffness (Lubin, 2013).

NASA's green aviation project aims to develop new technology in order to deliver future aircraft, that will be both more quitter and fuel-efficient. In 2015, researchers used a new flap made from an advanced composite material instead of conventional aluminum flaps. The major goal of this project was to determine if adjustable trailing-edge wing flaps could be a feasible way to reduce the noise during takeoffs and landings as well as to improve aerodynamic efficiency. In the Adaptive Compliant Trailing Edge (ACTE) project, the use of advanced lightweight materials gives engineers more capabilities than those using conventional materials. They have better aerodynamical shapes needed to reduce fuel and green-gas consumption (Beutel, 2014).

Another good example of using advanced composite materials is the UAS-S4 Ehécatl, that is mainly used in our research. The UAS-S4 wing is made from several composite materials to reduce its weight and improve its flight efficiency and fuel economy. Hydra Technologies use light composite materials, such as balsa wood, carbon fiber, aluminum 6065, high-density foam, E-glass, S-glass, and plywood to manufacture the UAS-S4 wing. Figure 1.2 shows the UAS-S4 Ehécatl.

Figure 1.2 The UAS-S4, produced by Ehécatl Hydra technology

The properties of various types of materials used to manufacture aircraft parts are provided in Table 1.1.

Table 1.1 Properties of various types of material (typical values)

Material	Density ρ-kg/m^3	Elasticity, Young's Modulus E-10^6 kg/m^2	Ultimate tensile E/ρ	Specific strength	Relative cost
2014-T6 Alclad sheet	0.101	10.7	68	106	base price
2024-T4 extrusion	0.100	10.7	57	107	slightly less
7076-T6	0.101	10.3	78	102	slightly more
7076-T6 extrusion	0.101	10.4	78	103	slightly more
Stainless steel	0.276	29	177	103	
Maraging steel	0.283	29	252	94	more
H-11	0.281	30	280	107	more
Nickel alloy	0.300	31	155	103	much more expensive
Magnesium alloy	0.064	6.5	40	102	
Beryllium alloy–rolled	0.067	42.5	65	63.4	expensive
Composite nonmetals					
Fiberglass/epoxy	0.065	5	80	77	relatively inexpensive
Kevlar/epoxy	0.050	12	160	240	more expensive
Carbon/epoxy	0.056	22	170	393	more expensive

CHAPTER 2

RESEARCH PROPOSAL, OBJECTIVES, AND THESIS ORGANIZATION

With the growing interest in Unmanned Aerial Vehicles (UAV) design and development in both civilian and military sectors, an improvement in their agility and versatility is becoming critical for their continuous exploitation. Numerous efforts have been made to develop UAVs capable of performing multiple missions in a single flight, without needing them to return to base for any geometrical or equipment modifications (Popov et al., 2010). Morphing wing technology offers a compromise between requirements while meeting the optimum performance mandate. There are multiple reasons for developing morphing wings, which can be summarized according to the following objectives (Oliviu, Koreanschi, & Botez, 2015):

- Adaptability by making aircraft more flexible, so that it can fly in a wider range of flight conditions;
- Ideal efficiency by improving multi-efficiency in terms of weight, volume, and fuel economy; and
- Multi-purpose capability by allowing a single aircraft to accomplish various missions as efficiently as possible (Barbarino, Bilgen, Ajaj, Friswell, & Inman, 2011).

The Unmanned Aerial System Éhecatl UAS-S4, produced in Mexico by Hydra Technologies, was obtained by Prof. Ruxandra Botez with the support of the Canadian Foundation for Innovation (CFI), and the Ministère du Développement Économique, Innovation et Exportation (MDEIE). The S4 Éhecatl was designed to meet the security and reconnaissance needs of the Mexican military and police forces, as well as non-military service situations (Oliviu et al., 2015).

This thesis is focused on substituting the conventional wing of the UAS-S4 with a morphing wing capable of dynamically modifying the wing's shape during various flight phases. The primary objective of the morphing wing design is to adjust the wing geometry (by modifying its span) to increase the UAS-S4 aerodynamic efficiency by adding larger regions of laminar flow over the wing span and thereby reducing the drag coefficient.

2.1 Objectives

This thesis aims to provide the understanding of the aerodynamic performance of morphing wing structural-dynamics design, and to understand how morphing wings can be used to achieve the main goals of the technological modeling of the UAS-S4 wing. The primary purpose is to design and develop a wing for the UAS-S4 that can perform a variety of missions in its flight range, with the overall goal to increase the UAS-S4 performance at a given flight speed (Mestrinho, Gamboa, & Santos, 2011). The key points covered in this thesis are listed below:

- The improvement of the aerodynamic characteristics of a UAS's wing takes utmost importance in this project, given that the research objectives are dependent on the aerodynamic loads. Since the main objective of manufacturing UAS-S4s is to use them for aerial surveillance systems over long time intervals, the aerodynamic optimization has mainly been concentrated on enhancing the wing's aerodynamic performance (Ivanco, Scott, Love, Zink, & Weisshaar, 2007) (Cauzard, Antoine, & Botez, 2013). The dynamic behavior of the forces and moments on the wing during its morphing phases is evaluated and tested using a broad range of simulations of various fidelity (high and low) (Xfoil, XFLR5, CFD by ANSYS, and others) (Christopher Simon Beaverstock et al., 2015).
- The optimal geometrical shape of the airfoil must be determined to cover all potential flight regimes, and then the wing planform shape can be developed. The best structural solution must be found through numerical optimization techniques to determine the morphing wing's optimal design shape and to evaluate the aerodynamic results while ensuring its structural integrity and safety. According to the optimization outcomes, the axial forces on wing morphing affect the sizing and power requirements of the actuation system; hence the number and positions of actuators must be identified for each morphing wing (Usher, Ulibarri, & Camargo, 2013) (Abdelkefi & Ghommem, 2013).
- The aim of the work on the UAS's variable span-chord wing work (as part of the morphing wing project) is to investigate ways to increase the wingspan during various flight speeds, and thereby improve its performance. Due to wing flexibility and the trade-offs between wing performance and structural weight, two essential considerations must accounted for

its design: aerodynamics and structures (G. Kennedy & Martins, 2012). These considerations are in turn incorporated into the numerical algorithm techniques to optimize the materials used in UAS-S4 manufacturing, as well as the process of selecting the most appropriate for the design needs (low weight and optimal performance) (O. S. Gabor, Simon, Koreanschi, & Botez, 2014).

- An extensive analysis of the various impacts of the morphing wing structure on the flight envelope must be performed as the aerodynamic coefficients and optimized shapes must be studied in the beginning of a project. Comprehensive testing and data collection were conducted on the baseline UAS-S4 wing. Comparing the flight test data and novel estimation approaches are used to determine the wing geometrical model based on the obtained data from the optimization processes.
- Once the structural model is developed based on the aerodynamic loads, a simulation of the variable span wing utilizing composite materials can be performed under real flight conditions as a conclusive phase of the configuration cycle. Modeling specifications should be compatible with the Finite Element Method (FEM) results. Validation of these numerical results were realized via testing in the Price-Païdoussis wind tunnel.

2.2 Constraints

The strategy presented here is to redesign and develop a revolutionary morphing strategy for the UAS-S4 wing to achieve the optimal aerodynamic performance. This strategy is based on costs minimization, and incorporates both the performance standards and wing characteristics. The variables are optimized to incorporate all-wing design parameters (e.g., design range, wing zone, wing components, and skin thickness). The UAS-S4 wing configuration variables are determined by numerical optimization applications, utilizing penalty functions to determine the optimization constraints. The most valuable technique consists in the investigation different morphing wing components in a synchronous way and in enhancing performance. Before the beginning of the design phase, the major design problems should be first identified, then the desired objectives, and finally the design constraints. These design constraints are the following:

- The morphing wing must meet dimensions constraints, as dictated by various design requirements.
- The variable span morphing wing must be designed to contain all its components, such as spars, ribs and others, in a limited space while maintaining the wing's high physical and mechanical characteristics.
- The novel wing weight must be kept as low as possible to achieve maximum performance.
- New wing components' size and static edges that produce the desired aerodynamic characteristics must be determined and verified.
- A variable span morphing wing with higher processing qualities complies with those achieved in a sequential optimization design procedure.

2.3 Methodology

The engineering system approach MDO methodology can yield optimal design and modeling for variable span morphing wings that should meet their design requirements. The entire process of the MDO methodologies should be integrated to achieve the desired objectives. The main methodology for designing a variable span morphing wing for the UAS-S4 is performed in the following three fundamental steps:

- Solving problems associated with new design shapes research via mathematical computations using previous studies conducted at the LARCASE laboratory under Prof. Ruxandra Botez supervision and validating new results using original data from Hydra Technologies.
- Conducting trade-off studies of new MDO results to select the preferred methodology and to identify the most appropriate characteristics of the wing and its components deign.
- Compromising and correlating the various results of the MDO design to accomplish the desired objective of remodeling the UAS-S4 wing using variable span morphing wing.

Several fundamental hypotheses have been assumed in this thesis using aerodynamic, mechanical, and composite material optimizations. Aerodynamics and structural optimizations have been performed using appropriate materials.

2.3.1 Analysis and optimization approach

The thesis focuses on Unmanned Aerial Vehicles (UAVs) morphing wing MDO design; all aspects of the design problem, such as its objectives and constraints, are evaluated in converged aero-structural methodologies and their solutions. The structural optimization of the variable span morphing wing allows the design to be enhanced by means of advanced materials. The aero-structural effects on the wing components within the design space are evaluated to obtain the wing's optimal performance. High-fidelity methods programmed in high-fidelity Finite-Element and optimization and CFD solvers, have been used to identify the optimal values of wing design parameters (G. J. Kennedy, Kenway, & Martins, 2014) .

2.3.1.1 Aerodynamic analysis and optimization

Aerodynamic optimization analyses were performed utilizing Xfoil, XFLR5, and Computer-Aided Engineering (CAE) software packages, in which the aerodynamic forces, moments, and pressures were computed using two- and three-dimensional models. For the high-fidelity aerodynamics cases, a special CFD package, an efficient Computer-Aided Engineering software, was utilized for the aerodynamic forces analysis that impacts the wing design. Computational Fluid Dynamics (CFD) is one of the types of aerodynamic analysis methods needed to accomplish an excellent wing design shape. Expectations in the areas of stability and control, performance, handling qualities, and different other areas including single and multiple-component airfoil investigation and design, static and dynamic aeroelastic loads, distribution, and aerodynamic loads optimization along wingspan can be achieved with CFD codes (Kenway, Kennedy, & Martins, 2014).

2.3.1.2 Structural analysis and optimization

Structural analysis and optimization of the variable span morphing wing determine the impacts of dynamic and mechanical strains on physical wing structures and their components (spar,

ribs, stringers, and others). The entire optimized wing components' structure, subjected to internal forces, stresses, support reactions, and external forces (lift, drag, and the wind), must meet all the analytical requirements. To conduct an objective investigation, data such as the structural loads, support conditions, and material parameters must be determined. Typically, the results of such investigations conduct to the enhancement of aerodynamic capabilities. The obtained investigation morphing wing results are then compared with the original wing shape. Advanced structural investigation of wing manufacturing materials includes their dynamic response, stiffness, and nonlinear behavior. There are several ways to deal with this type of investigation:

- The mechanics of materials approach;
- The elasticity theory approach;
- Finite element methods; and
- Structural optimization based on finite element methods (FEMs).

The optimization-based finite element approach is a numerical method for solving numerous simulation problems. These problems employ a variety of modern computer applications to solve such an optimization-based FE approach. On the other hand, the optimization-based finite-element method depends highly on computer processing power and to structures of arbitrary size and complexity.

2.3.2 Tools and Software Definition

This sub-section describes the computation tools utilized for different aspects of aero-structural analysis and optimization. They include all the elements within the framework for the MDO of the airfoil and variable span morphing wing configurations with high fidelity, X-Foil, XFLR5, ANSYS, and the Altair product software. These tools have been used to optimize the aerodynamic and aero-structural design of the variable span morphing wing shape (Burdette, Kenway, Lyu, & Martins, 2015) (G. Kennedy & Martins, 2012).

2.3.2.1 2D Optimization with Xfoil and XFLR5 Codes

The two-dimensional (2D) aerodynamic coefficients as functions of the angle of attack (AOA) and the Reynolds number (Re) in assigned locations along the wingspan are obtained with Xfoil and XFLR5 codes. These codes were selected because they have demonstrated their effectivenesses over time and because they have reached a converged solution very rapidly. Xfoil and XFLR5 codes use a high-order panel technique to solve the flow field around a 2D airfoil (Gamboa, Aleixo, Vale, Lau, & Suleman, 2007). In this thesis, these codes are employed to compute the viscous drag in each wing spanwise strip utilizing the Reynolds number and sectional airfoil shape. Every parameter of the present analysis (Mach number, Reynolds number, the angle of attack) is written in an input Xfoil and XFLR5 file. Estimations are made for each individual of every generation of the algorithm in a genetic algorithm. The aerodynamic outcomes are then imported back into the genetic algorithm code within Xfoil and XFLR5 file.

2.3.2.2 Aero-structural optimization solvers

This thesis employed ANSYS software as the CFD and as a topology optimization solver. ANSYS is used for solving of turbulence models. The main flow is solved with a multi-stage Runge-Kutta explicit, geometric multigrid algorithm. A discrete adjoint method of Euler and RANS equations has been developed and further implemented to compute the gradients required for optimization for a successful (J Fincham et al., 2014) (Lyu, Xu, & Martins, 2014).

ANSYS Workbench was implemented for structural analysis and optimization. The TO algorithm used herein relies on combining the FEM with an optimization code. ANSYS Workbench links the TO results obtained from the numerical solver with Finite Element Analysis (FEA) to determine a layout design for the variable-span morphing wing. ANSYS Workbench can accurately estimate a product's performance under a real-world environment by integrating all its physical phenomena (Ghosh, Ghosh, Ghimire, & Barman, 2016).

Another commercial application used in this thesis is Altairs' product software such as HyperMesh OptiStruct and SolidThinking’s Inspire, which manage the given design constraints by establishing the objective functions for individual load cases. These applications were created to manage constraints to ensure that design standards were met; they therefore define a design's critical materials and the procedure for eliminating redundant elements. OptiStruct and SolidThinking’s Inspire both use algorithms to optimize material distribution within the design area to create the optimal geometrical shape of the wing. They compute the design structure that provides the best solution under specified boundary conditions by minimizing the compliance of the wing components while adhering to the design limitations and thereby minimize their weights. The optimal solution is obtained by an iterative approach to reach its convergence. The methodology and validation of design and optimization for MVSTW used in this thesis are shown in Figure 2.1.

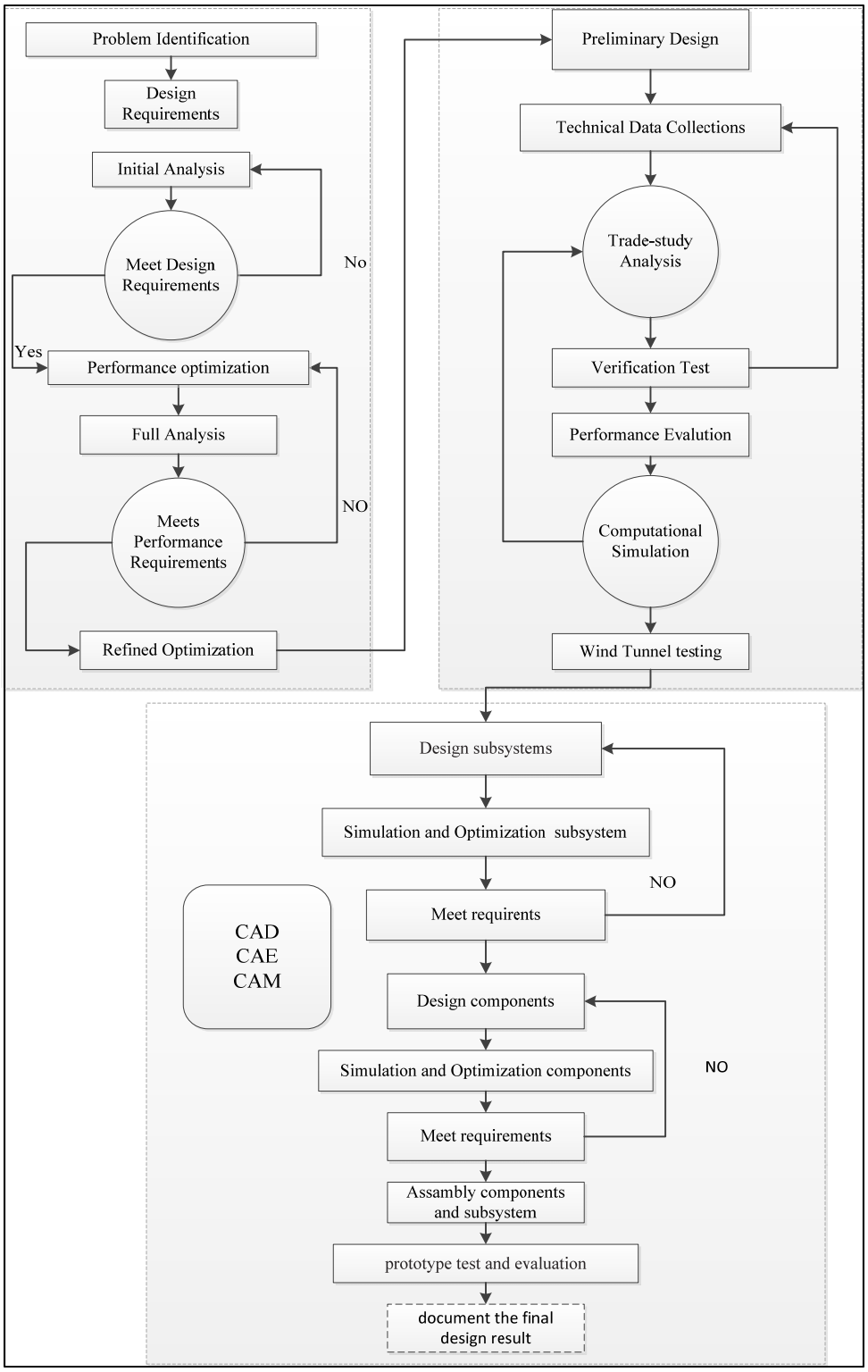

Figure 2.1 Methodology and validation for the research study

2.4 Thesis organization

This thesis describes MDO process needed to develop a variable span morphing wing project to develop for the UAS-S4. The research was conducted in the following phases:

1. A literature review analyzed current aero-structural optimization methods with the objective of determining a novel variable span morphing wing. This review discussed the objectives, constraints, and tools and identified approaches that could be used to improve the proposed optimized morphing wing.
2. A statement of the research proposal, objectives and constraints to be addressed in the research.
3. The research work was then divided into four phases, and each phase was presented in a scientific journal article. These technical articles were distributed to the scientific community in the relevant field, and were written under the supervision of Professors Dr. Ruxandra Botez and Professors Dr. Thien-My Dao. Professor Ruxandra Botez is the thesis supervisor, and Professor Thien-My Deo is co-director. They were responsible for supervising all of the work described in this thesis.

In the first paper, PhD student Maxime Kuitche has worked as co-author following contribution to the research methodology development.

During his internships, Mr. Thomas Calvet, a bachelor's in engineering degree student, was also included as a co-author in the second journal article as he contributed to the development and testing of the proposed methodology, and he has performed results comparisons using commercial software (Hypermesh).

In the fourth article, Mr. Felipe Schiavoni Pinto, Master student contributed as co-author to implementing the MATLAB code for composite materials selection and by comparing the results obtained with this MATLAB code to select the proper composite materials and the best state-of-the-art optimizers.

2.4.1 First journal paper

Chapter 3 contains the first technical research paper, “Comparison and analyses of a variable span-morphing of the tapered wing with a varying sweep angle” that was published by Cambridge University Press on behalf of the Royal Aeronautical Society in 2020. It involves the development of a 2D airfoil, an analysis of its aerodynamic performance, and the design of a variable span of tapered morphing wing. Three parameters were used to analyze innovative geometric shapes, and the optimal variable span was chosen to design and develop a 3D morphing wing using conventional and composite materials. Preliminary optimization findings for the morphing wing were presented using UAS-S4 data.

This paper provided a comparative design and development study of variable span morphing of the tapered wing (VSMTW) for the Unmanned Aerial System (the UAS-S4). The proposed approach involved sliding the inner section into the fixed part along the wing while altering the angle of its inner section within the fixed part (parallel to the leading edge while the moving-wing axis was coincident with the fixed-wing axis) in two configurations. Morphing wing analysis was done in four predetermined locations. The main objective was to examine the aerodynamic characteristics of various span lengths and sweep degrees and to determine the most efficient geometrical combinations. The wing was optimized for various speeds and altitudes during flight phases. The XFLR5 code was used for 2D aerodynamic analysis, while the ANSYS Fluent solver was used for studying the flow field on the 3D wing structure. The morphing of the span of a tapered wing technology with a variable-sweep angle was found to greatly improve its aerodynamic efficiency. The wing design was more sensitive to the changing angle of the inner section and therefore it was more aerodynamically efficient.

2.4.2 Second journal paper

Chapter 4 contains the second technical research paper called, “Wing component allocation for a morphing variable span of tapered wing using finite element method and topology optimization – application to the UAS-S4” published by Cambridge University Press on behalf

of the Royal Aeronautical Society in 2021. It offers a revolutionary approach to efficiently position the inner components within the wing design. The topology optimization strategy was determined to be the most effective method for achieving this objective. Specific factors were utilized to assign the wing components to their proper position, and the optimized wing segments were tested in terms of their parameters such as deformations, stresses, and strains. The optimized morphing wing's results demonstrated that the optimized wing was robust enough to overcome mechanical failures, even in extreme flight conditions.

The purpose of this paper was to perform the Topology Optimization of the Morphing Variable Span of a Tapered Wing (MVSTW) using a finite element method. This topology optimization was designed to determine the feasibility of inner wing components, such as ribs, spars, and other structural components. The optimization was performed utilizing ANSYS Workbench, which can solve topology optimization (TO) problems. The main objective was to minimize its structural compliance and maximize structural stiffness to improve structural performance and meet the MVSTW's structural integrity standards. Topology optimization was therefore used to identify the locations of the wing components within the fixed and moving segments of a solid wing developed with aluminum alloy 2024-T3. According to the results, both the fixed and moving wing segments must be designed using two spar configurations and seven ribs, as well as they would be able to support components in the high-strain area. Additionally, the results demonstrate the optimal mechanical behavior and structural wing integrity required for multi-flight missions.

2.4.3 Third journal paper

Chapter 5 contains the third technical research paper, "Structural sizing and topology optimization based on weight minimization of a variable tapered span-morphing wing for aerodynamic performance improvements", published by Biomimetics on behalf of the Molecular Diversity Preservation International (MDPI) in 2021 following the invitation of Guest Editors of the Special Issue: It presents a weight-saving optimization strategy for the wing components of a variable span morphing wing. The topology and sizing optimization

methodologies were the most effective techniques for achieving weight savings while maximizing stiffness. The optimized morphing wing demonstrated that its components' weights could be reduced considerably without affecting its structural integrity.

This paper's main objective was the discussion of the integration of structural sizing, topology, and aerodynamic optimization for a morphing variable span of a tapered wing (MVSTW) with the objective of minimizing its weight, and to offer an innovative optimization technique for an MVSTW. In the optimization processes, the aerodynamic loads distribution along the wingspan at its full extension and maximum speed was adopted. The wing components size and topology were optimized, and they were entirely designed with aluminum alloy 2024-T3. Using its weight-saving possibility, the optimized variable-span morphing wing may enable an aircraft to conduct specified flight missions perfectly and without mechanical failures.

2.4.4 Fourth journal paper

Chapter 6 contains the fourth technical research paper, "Multidisciplinary Optimization for Weight Saving of a Variable Tapered Span-Morphing Wing Using Composite Material - Application to UAS-S4", published in Actuators, invited by special session on behalf of the Molecular Diversity Preservation International (MDPI) in 2022. It presents work in the continuation of the earlier-published optimization paper (section 2,3 ,4) for weight reduction of the wing components for variable span morphing. However, this optimization was performed to minimize the weights of wing components by using appropriate composite materials. For more practical weight savings while maximizing stiffness, similar approaches have been applied for topology and sizing optimization as those used for conventional materials (Al 2024-T3). The optimized morphing wing developed with composite material components proved that the weight of selected composite materials can be significantly reduced while maintaining its structural integrity.

The main objective of this paper was to discuss the application of MDO methodologies to the development of a MVSTW to minimize its weight using composite materials. A MDO

numerical environment was constructed and demonstrated that weight can be reduced by simultaneously integrating material selection optimization, structural sizing, and topological optimization according to aerodynamic performance requirements. Aerodynamic optimization was performed using CFD and XFLR5 codes, while material selection was performed using MATLAB code, and STO was performed using Altair's OptiStruct and SolidThinking Inspire solvers. The MVSTW's weight was significantly lowered to 5.5 kg, which was of course smaller than the original UAS-S4 wing's weight (6.5 kg).

2.5 Contributions

The originality of this thesis is based on the following major contributions, which include those presented in these four journal papers. The main contribution of this research was to design novel methods for the development of an adaptive UAV wing by using advanced materials and testing them for their mechanical and physical properties. The shape of the wing was considered the essential varying parameter to design the most efficient wing configurations that meet the required physical and mechanical properties, such as mechanical tension and aerodynamic strain.

- The design of an UAS-S4 morphing wing that can achieve high-performance (lift/drag ratio) with low fuel consumption, helping to reduce greenhouse gas emissions and lower operating cost.
- The design of a morphing wing that using sophisticated techniques and proper composite materials while maintaining low manufacturing costs and operating costs.
- Aero-structural analysis and optimization of an adaptive wing based on the UAS-S4 data.
- The development of the application of (MDO) methods for the improvement of an adaptive wing (variable span) design.
- The performance of topology and sizing optimizations of an adaptive wing span using advanced composite materials.

2.6 Conclusion

The initial evaluation of an optimum redesign of the UAS-S4 wing required preliminary data and the baseline wing obtained by Hydra Technologies to validate the original wing geometry with its new optimized shape. The optimized wing design was simulated and optimized via specialized computer software (Xfoil, XFLR5, MATLAB, ANSYS, Altair Engineering). The results obtained by simulation, analysis, and optimization software were compared with the computational process and the available resources from baseline UAS-S4 wing and materials database such as mechanical, physical, and chemical properties. An optimum optimization method for the design of an adaptive wing span showed that integrating the mechanism design with aero-structural, sizing, and topological optimization techniques leads to an optimal design. Obtaining the ideal shape of a wing involves the distribution of materials. Based on the studies performed herein, in future work, the location of the actuation system will vary according to the whole mechanism utilized to support the structure. This work seeks to exploit the benefits of simultaneously optimizing the mechanism design, the location of pivot points, and the configurations of the actuation system. Based on the available computational resources, the proposed approach can be used in reaching the main objective.

In general, the morphing wing technique can increase the aerodynamic performance of a UAV, making it the ideal aircraft for performing multiple-missions within its in-flight envelope, such as in long-time endurance flights. Morphing wings overcome the many obstacles that conventional wings may encounter, providing significant advantages over them. Their excellent structural capabilities made possible the use of adaptive wings during various phases of a typical flight mission with different flight speeds could offer improved aerodynamic capabilities that could reduce the detrimental environmental effects of aircraft offering more efficient fuel consumption.

The main reasons by scientific research on Unmanned Aerial Vehicles are that their findings could be used for designing and experimenting with different morphing methodologies and their solutions, solutions that can be extended to commercial or military aircraft.

CHAPTER 3

COMPARISON AND ANALYSES OF A VARIABLE SPAN-MORPHING OF THE TAPERED WING WITH A VARYING SWEEP ANGLE

Mohamed Elelwi [a], Maxime Kuitchea [a], Ruxandra Mihaela Botez [a]* and Thien-My Dao [b]

[a] Department of Laboratory of Active Controls Avionics and AeroServo Elasticity
LARCASE
ÉTS - École de technologie supérieure
1100 Notre-Dame West, Montréal QC H3C 1K3 Canada

[b] Department of Research Team in Machines Dynamics Structures and Processes
ÉTS - École de technologie supérieure
1100 Notre-Dame West, Montréal QC H3C 1K3 Canada

Paper published in *The Aeronautical Journal*, Volume 124, Issue 1278, August 2020, pp. 1146 - 1169
DOI: https://doi.org/10.1017/aer.2020.19

Résumé

Ce travail présente une étude comparative de la conception et du développement, en plus des analyses de l'aile déformable à envergure variable (VSMTW) pour le véhicule aérien sans pilote (UAV). Le concept proposé consiste à faire glisser la section intérieure dans la partie fixe le long de l'aile en faisant varier l'angle de la section intérieure à l'intérieur de la partie fixe (parallèle au bord d'attaque où l'axe de l'aile mobile est confondu avec l'axe de l'aile fixe) dans deux configurations. La conception de l'aile est basée sur un profil aérodynamique NACA 4412 avec une corde à sa racine de 0,675 m et une corde à son bout de 0,367 m pour le segment fixe et de 0,320 m pour le segment mobile. L'analyse de l'aile déformable se produit à trois emplacements sélectionnés qui ont été spécifiés pour étendre et évident la longueur de l'envergure de (25 %, 50 % et 75 %) de sa longueur d'origine afin de répondre aux diverses exigences de la mission de vol. L'objectif principal de cet article est de comparer les caractéristiques aérodynamiques pour plusieurs longueurs de l'envergure et angles de balayage et de trouver leurs plus efficaces combinaisons. L'aile est optimisée pour différentes vitesses

pendant toutes les phases de vol (vitesse min, loiter, croisière et vitesse max), qui sont de 17, 34, 51 et 68 m/s, respectivement. Les analyses sont effectuées en calculant les forces (traînée et portance) et les moments à différentes altitudes, par exemple, niveau de la mer, à 5,000 et 10,000 pieds. Des analyses aérodynamiques bidimensionnelles sont effectuées à l'aide du code XFLR5, de ainsi que ANSYS Fluent pour étudier le champ d'écoulement sur la structure tridimensionnelle de l'aile. Il a été observé qu'une aile déformable avec un angle de balayage et une envergure variable peut offrir jusqu'à 32,93% d'amélioration de l'efficacité aérodynamique. Cette conception conceptuelle peut également être utilisée pour la technique de mouvement de roulis de l'avion au lieu d'utiliser des dispositifs de commande conventionnels. De plus, la mission de vol en distance augmente jusqu'à 46,89% lorsque l'aile se trouve sur toute sa longueur par rapport à une position d'origine. Enfin, il a été conclu de cette étude que la conception de l'aile est plus sensible au changement d'angle de la section intérieure et plus efficace en termes de caractéristiques aérodynamiques.

Abstract

This work presents a comparative study of design and development, in addition, to analyses of variable span morphing of the tapered wing (VSMTW) for the unmanned aerial vehicle (UAV). The proposed concept consists of sliding the inner section into the fixed part along the wing with varying the angle of the inner section inside the fixed part (parallel with the leading edge and the moving wing axis is coincident to the fixed wing axis) within two configurations. The wing design is based on a NACA 4412 airfoil with a root chord of 0.675m and the tip chord of 0.367m for the fixed segment and 0.320m for the moving segment. Morphing wing analysis occurs at three selected locations that have been specified for extending and modifying span length by (25%, 50%, and 75%) of its original length to fulfill various flight mission requirements. The main objective of this paper is to compare the aerodynamic characteristics for several span lengths and sweep angles and find their most efficient combinations. The wing is optimized for different velocities during all phases of flight (min speed, loiter, cruise, and max speed), which are 17, 34, 51, and 68m/s, respectively. The analyses are performed by computing forces (drag and lift) and moments at various altitudes, such as at the sea level,

5,000 and 10,000ft. Two-dimensional aerodynamic analyses are carried out using XFLR5 code, and the ANSYS Fluent solver is used for investigating the flow field on the three-dimensional wing structure. It has been observed that a variable span morphing of tapered wing technology with a variable-sweep angle can deliver up to 32.93% improved aerodynamic efficiency. This concept design can also be used for the aircraft roll motion technique instead of conventional control devices. Furthermore, the range flight mission increases up to 46.89% when the wing is placed at its full length compared to an original position. Finally, it has been concluded from this study that the wing design is more sensitive to the changing angle of the inner section and more efficient in terms of aerodynamic characteristics.

3.1 Introduction

The goal of designing a morphing wing is to allow the UAV to achieve its mission requirements in various flight conditions. Enhancing the performance and improving the controllability and maneuverability of aerial vehicles have attracted considerable attention in aerospace research (RM Ajaj, Bourchak, & Friswell, 2014) (Murugan, Woods, & Friswell, 2015) (Pecora, Barbarino, Concilio, Lecce, & Russo, 2011). The capability of changing the wing aspect ratio allows the UAV to achieve its mission smoothly during various flight stages (RM Ajaj et al., 2013). Moreover, it enables the UAV to increase its aerodynamic performance and efficiency. For instance, prolonged spans led to significant improvements in aerodynamic performance and fuel efficiency. However, they also decrease the maneuverability and limit the cruise velocities. On the opposite side, the low aspect ratio wings give more maneuverability and increase aircraft speed with an in-flight reduction performance and an increase in fuel consumption (R. Ajaj et al., 2014) (RM Ajaj et al., 2013) (Della Vecchia et al., 2017).

The main concepts of the morphing wing can be classified into three major types as follows (Tarabi, Ghasemloo, & Mani, 2016):

- Planform alternation: In this type, the wing can manipulate its shape dimensions, such as its span, chord length, and sweep angle.

- Out-of-plane transformation: Wing out-of-plane transformation is mainly based on three parameters, which include the span-wise bending, the chord-wise bending, and the wing twisting.
- Airfoil adjustment: Airfoil adjustment is mainly affected by two parameters: camber variation and thickness, which can reshape the airfoil (Sofla, Meguid, Tan, & Yeo, 2010) (Barbarino et al., 2011).

With the growing use of the UAV in various domains, civil and military applications, the morphing aircraft technology area is reinforced in the current and upcoming periods of time (Arena, Concilio, & Pecora, 2019). The morphing concept provides massive benefits such as:

- Increasing the flight range by improving aerodynamic efficiency.
- Achieving multiple tasks to carry out radically new maneuvers without using conventional control surfaces.
- Reducing drag force to enhance fuel-efficiency, which leads to the flight envelope extension.
- Reducing vibration and flutter by enhancing structural capability.

The variable span morphing wing provides an excellent capacity for achieving multiple tasks (Concilio et al., 2018). By changing the span length and wetted area, the wing addresses numerous mission segments such as cruising, loitering, long flight range, maneuverability, and controllability more efficiently than a conventional wing (Barbarino et al., 2011) (Burdette et al., 2015) (Cascio, Milazzo, Amendola, Arena, & Dimino, 2018). Another advantage of adaptive span wing is the roll control through asymmetric wing changes rather than through conventional control surface. An asymmetric loading in the wing contributes to coupling the yawing and rolling motions (Dimino, Lecce, & Pecora, 2017) (Pecora, Amoroso, & Lecce, 2012).

Numerous studies of morphing concepts have been accomplished in the last few decades (O. Ş. Gabor, Koreanschi, & Botez, 2016) (O. Ş. Gabor, Koreanschi, Botez, Mamou, & Mebarki, 2016) (O. Ş. Gabor, Koreanschi, Botez, et al., 2016) (Koreanschi, Sugar-Gabor, & Botez,

2016a) (Koreanschi, Sugar-Gabor, & Botez, 2016b). They have been done on the advantages of the variable span morphing wing technology based on the effect of increasing aspect ratio on the performance and maneuverability (Mestrinho et al., 2011) (Rafic Ajaj, Friswell, Saavedra Flores, Little, & Isikveren, 2012) (Christopher S Beaverstock et al., 2014) (Christopher Simon Beaverstock et al., 2015) (Vale, Leite, Lau, & Suleman, 2011). The majority of these studies has been focused on the design and investigation of the telescopic mechanisms with rectangular wing shape at the zero-sweep angle.

Ivan Makhonine has presented a variable-span wing in 1931. He designed the first telescoping wing on the MAK-10 aircraft. The mechanism allowed the span to extend up to 62% and wing space to increase up to 57% (RM Ajaj et al., 2013) (Weisshaar, 2006). The Defense Advanced Research Projects Agency (DARPA) led successful efforts to develop Morphing Aircraft Structures (MAS) from 2002 to 2007 (Ivanco et al., 2007). This program was defined as a multirole platform, which can change its geometrical shape according to the alteration of mission requirements, reconfigure the excellent system capability, and enable the use of innovative combinations of advanced materials, actuators, and mechanisms (Seigler, 2005).

Joao R. C. Mestrinho et al. designed and validated variable-span wing (Mestrinho et al., 2011). They have estimated the wing weight based on empirical data gained from a wing prototype. The speeds varied from 12 to 35m/s, which was the maximum speed, while the drag reduction was 20%. An analysis with asymmetric span was also carried out to estimate the rate roll. Vale et al. conducted an aerodynamic analysis of telescoping wing and a conformal camber morphing for high- and low-speed airfoils (Vale et al., 2011). The structural optimization was performed using the Finite Element Model to find optimal airfoil shape and minimum weight. The comparison study was carried out between two concepts.

Beaverstock et al. have done a comparative study of the influence of camber and span morphing on the mission performance of a 25 kg unmanned aerial vehicle (Christopher Simon Beaverstock et al., 2015). The study showed the effect of the low and high velocities on the calculation of the mission parameter to increase aerodynamic efficiency and flight range. An

adaptive aspect ratio span (AdAR) and a fish-bone active camber were used in this study. The results indicated that the span concept could improve the aerodynamic performance up to 25% for speeds ranging between 13.9 and 30.6 m/s. Tarabi et al. carried out an experimental analysis on a variable span morphing wing (Tarabi et al., 2016). The model was tested in the wind tunnel at low steady wind velocities (35, 60, and 80 m/s). The aerodynamic performance increased to 5% and 17% in flight range and endurance, respectively.

R. M. Ajaj et al. (R. Ajaj et al., 2014) have designed a new span morphing concept called Gear Driven Autonomous Twin Spar (GNATSpar). The wing could extend with an extra 20% to reduce drag and increase flight range. Wencheng Li and Dongping have done a study regarding the dynamical behavior and stability of a variable-span wing (W. Li & Jin, 2018). The Kane method and piston theory were used to govern the equations of motion.

The results showed that the morphing wing could achieve flutter suppression, and the upper bound of the morphing wing decreases swiftly at its critical span extent. Gao et al. (B. Gao, Kang, & Chen, 2016) tested and applied the Single-Degree-of-Freedom (SDOF) on the span morphing wing to improve its performance. The analysis showed that span modifications have slight effects on the lift coefficient and drag coefficient when the span changes, whereas the improvement of lift force and drag force was by 50%. The results of Finite Element Methods pointed out that the base link of the mechanism was affected by the maximum stress (45.5MPa). Parkash and Pant have studied the benefits of telescoping span wing in order to increase the flight endurance for HALE UAV (Prakash & Pant, 2017). Three morphing configurations were determined for the Global Hawk. Two penalties were taken into account the weight of the mechanism and the bending and shear calculations were made to gain the base weight by considering the stability characteristics.

3.2 Development of Tapered Span Morphing Model

3.2.1 Description of the model

McCormick investigated the influence of a span on aircraft dynamics (McCormick, 1995). It showed that aircraft with a large span has good aerodynamic efficiency, which leads to a good range and fuel efficiency. On another side, aircraft with reduced span are faster and highly maneuverable. A variable span concept is thus a good way to obtain the advantages of both designs. Our study is focused on the relationship between span increase, range, and fuel efficiency.

Furthermore, the influences of asymmetric wingspan strategy on the roll control are considered in this work, too. This study also investigates the impact of a sweep angle variation of the morphed span of the aircraft performance. The wing is divided into a fixed segment and the morphing segment. The fixed part is the basic wing without morphing. It is a straight tapered wing designed based on a NACA 4412 airfoil. The morphing part consists of an inner section that can slide while varying its sweep angle.

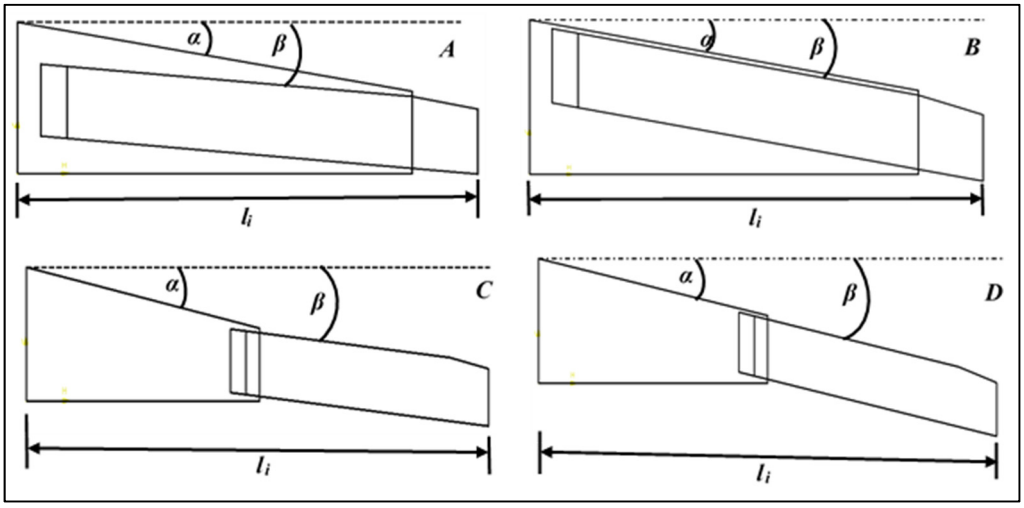

Figure 3.1 Morphing wing geometry of two models (A), (C): first sweep angle model (B), (D): second sweep

In Figure 3.1, l_i is the length of the wing at the original position and full extended wingspan, α is the sweep angle of the fixed section, and β is the sweep angle of the inner section slide out of the fixed wing. The focus of this work is to investigate the influence of both l_i and β parameters.

The inner wing is designed to have a swept angle geometrical shape according to its position in the fixed wing. However, the end of the inner wing (about 15% of its length) is shaped as a tapered wing with the aim to fit with the fixed wing at the original position. The geometrical parameters of the morphing part as well as of the fixed part used in this project are shown in Table 3.1.

Table 3.1 Airfoil Parameters

Parameters for fixed wing		Parameters for morphing part	
The wing root chord (in meters)	0.675	The wing root chord (in meters)	0.320
Thickness at root chord (in meter)	0.081	Thickness at root chord (in meter)	0.0128
Max camber at root chord (in meter)	0.027	Max camber at root chord (in meter)	0.0384
Location of max camber at the root chord	0.27	Location of max camber at the root chord	0.128
The wing tip chord (in meters)	0.315	The wing tip chord (in meters)	0.290
Thickness at tip chord (in meter)	0.0375	Thickness at tip chord (in meter)	0.0116
Max camber aft at tip chord (in meter)	0.0126	Max camber aft at tip chord (in meter)	0.0348
Location of max camber at tip chord	0.126	Location of max camber at tip chord	0.116

Figure 3.2 shows the two configurations of the wing for two different sweep angles of their inner sections $\beta = 4.5^\circ$ and $\beta = 8.9^\circ$, as considered in this study.

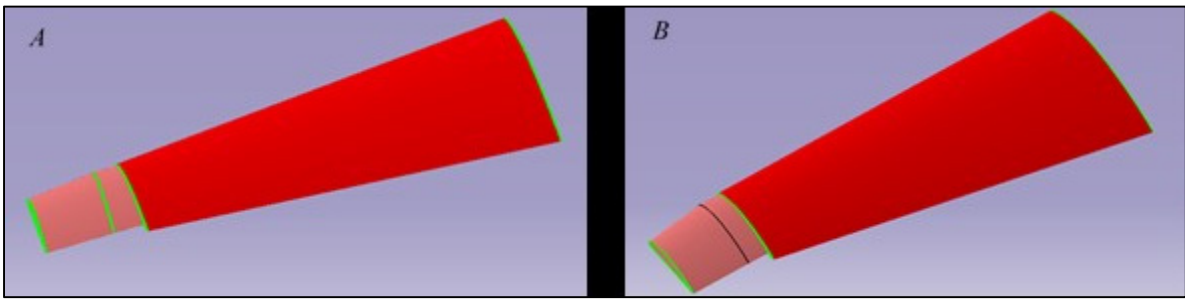

Figure 3.2 Variable span of the tapered morphing wings for (A): the first sweep angle model and (B): second

The first design configuration shows that the central axis line of the moving segment is coincident with the central axis line of the fixed wing. The second design configuration represents the leading edge of the moving segment located parallel to the leading edge of the fixed segment.

Both configurations of the wing are designed using Computer-Aided Design (CAD) with CATIA software and allow three various span extensions. Table 3.2 shows the wing geometries of their two configurations at the original position and for the specific span extensions.

Table 3.2 Wing Parameters

Parameter	Original wing	25% extension	50% extension	75% extension
The wing half-span (in meters), $b/2$	2.100	2.625	3.150	3.675
The wing area (in square meters), S	1.921	2.258	2.595	2.933
The wing root chord (in meters), c_r	0.675	0.675	0.675	0.675
The wing tip chord (in meters), c_t	0.290	0.290	0.290	0.290
Aspect ratio, AR	9.18	12.2	15.29	18.42
The taper ratio, λ	0.43	0.43	0.43	0.43
The mean aerodynamic chord in meter	0.51	0.51	0.51	0.51
MAC distance from root chord	0.91	1.14	1.37	1.59

3.3 Aerodynamic analysis

3.3.1 Aerodynamic wing studies using Xfoil and ANSYS Fluent

The aerodynamic investigation is performed in two steps. First, the 2-dimensional (*2D*) aerodynamic analysis used the Xfoil code to obtain aerodynamic forces and moments coefficients as functions of Reynolds number (*Re*) and the angle-of-attack (*AOA*). The Vortex Lattice Method is used for numerical analysis based on the XFLR5 code solver. The aerodynamic coefficients were conducted at various Reynolds numbers and angles of attack. The airfoil was operated at Reynolds numbers of (610263, 1220525, 1830788, and 2441050 relatively to the chord), which correspond to speeds of 0.05, 0.10, 0.15, and 0.20 Mach. The selected angles of attack were ranged between -3˚ and 15˚.

Moreover, the number of panels was 160, with the aim of obtaining more realistic results. The NACA 4412 includes four-digit code used to define the airfoil by:

- The first digit gives the maximum camber in terms of a percentage of the chord, more Specifically 4% of the chord length.
- The second digit gives the location of maximum camber from the airfoil leading edge in 10’s of the chord percentage, such as 40% from the airfoil leading-edge.
- The third and fourth digits give the maximum thickness of the airfoil in terms of percentage of the chord, such as 12% of the chord length (Kevadiya & Vaidya, 2013).

The NACA 4412 airfoil geometrical shape is shown in Figure 3.3.

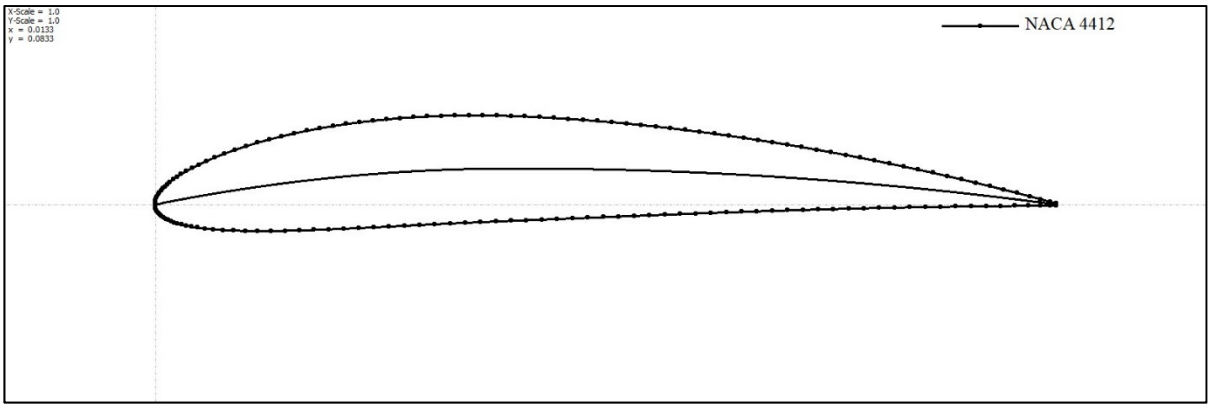

Figure 3.3 Geometry of the NACA 4412 Airfoil

The variation of lift and drag coefficients with the angle-of-attack are shown in Figure 3.4; these variations were obtained by the use of the XFLR5 software, which uses both Xfoil algorithms and the Vortex Lattice Method (Deperrois, 2009).

Once the aerodynamic characteristics for the NACA 4412 airfoil have been analyzed numerically in the XFLR5 solver, the novel design concept for creating the span morphing wing was developed. The variable span morphing wing, proposed in this study, aims to benefit from the aerodynamic and structural advantages of tapered wing shape. The main benefits of tapered span design with respect to its baseline design wing might be, for example, better aerodynamic efficiency (lower drag and better lift distribution along its span), better structural efficiency (stronger and lighter) as the chord's lengths is varying between the root and tip, and maneuverability would be better. The lift to drag ratio efficiency is influenced by the taper ratio at the low flight speed (Traub, Botero, Waghela, Callahan, & Watson, 2015).

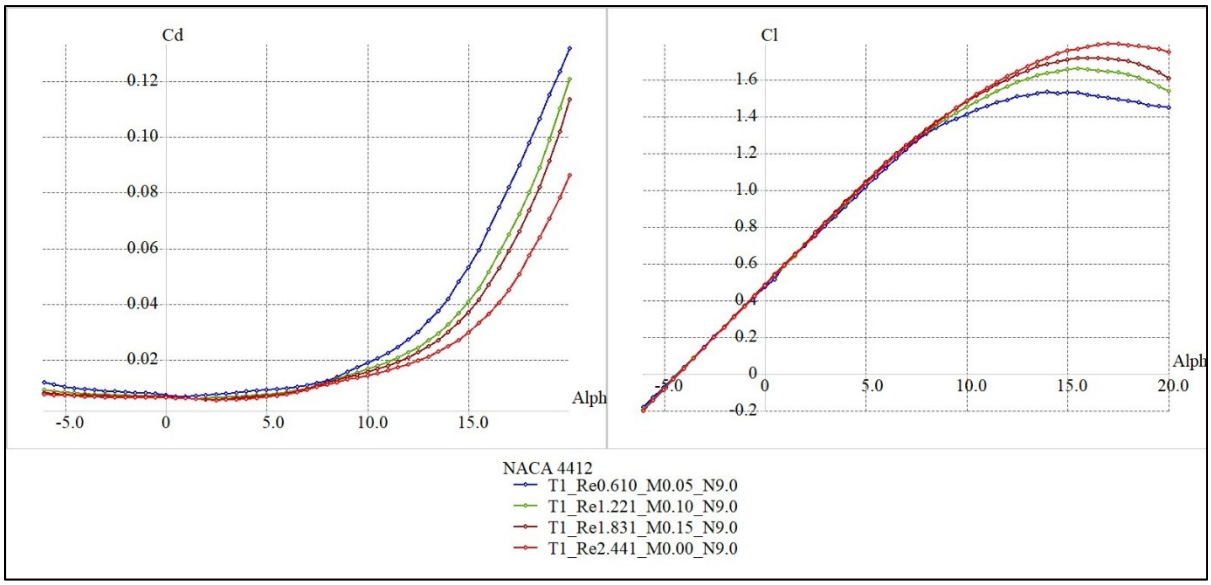

Figure 3.4 Lift and drag coefficients variation versus the angle of attack

Second, by the numerical investigations, four versions (based on the wingspan extension stages) of Variable Span Morphing of Tapered Wings (VSMTW) are implemented by using a Computational Fluid Dynamics (CFD) ANSYS Fluent solver that is used as it can offer beneficial tools for geometry editing, meshing, simulation setup, and results of the analysis (C. d. Liauzun, 2010). The use of ANSYS Fluent solver provides accurate solutions and speeds up the simulations of complex scenarios such as transonic or turbulent flows. The results obtained from this numerical study will be analyzed for the variable morphing wingspan experimental performance validation using a wind tunnel. In this comparative design study, the following procedure is performed for both sweep angle models (C. Liauzun, Le Bihan, David, Joly, & Paluch, 2018) (C. d. Liauzun, 2006).

- The geometrical shape and physical outlines of the design are determined using Computer Aided Design (CAD), as represented in Figure 3.2.
- The data is then processed, and the fluid chamber volume (or fluid domain) is defined.
- The fluid volume and the wing shape are divided into discrete cells (meshes). The number of elements and nodes is varied as the wing length changed and in correlation with the wing geometrical shape. The physical modelling is selected based on the equations of fluid motions.

- For the simulation, boundary conditions, such as fluid behavior and properties (density, speeds, viscosity, pressure, etc.), must be defined.
- To obtain the final solution and to visualize the results, a postprocessor is used after solving the equations iteratively, which allows creating contour plots, vector plots, 2D and 3D surface plots, etc. Moreover, it can offer animation for dynamic results display.

Figure 3.5 shows the numerical analysis methods carried out in this study using ANSYS Fluent solver.

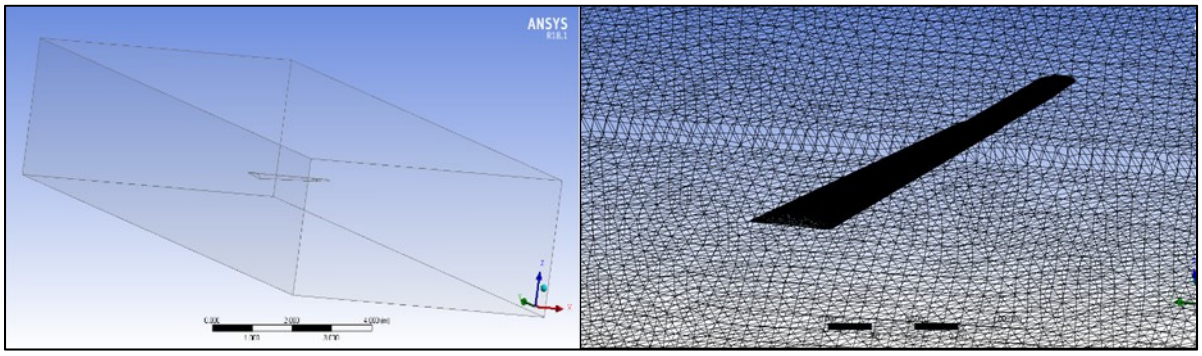

Figure 3.5 Numerical analysis phases using ANSYS Fluent

The 3D unstructured tetrahedral mesh for both design shapes was employed to flow around the model. For more accuracy, the “inflation layers” were applied to smooth the mesh of edges around the wing surface. Thus, the inflation layers provide a highly precise resolution of the boundary layer. The number of ten inflation layers was situated within the boundary layers to obtain the accurate solving of the boundary layer. The meshing method is described in Fig. 3.5(b). The two modeling methods based on the Reynolds-Averaged Navier-Stokes (RANS) were applied for computing the flow past the wing. First, the k-ε turbulence model was used to simulate mean flow characteristics around the wing to investigate the turbulent flow conditions because of the fact that the free-shear layer flows with relatively small pressure gradients. The k-epsilon model was based on two equations, and it provided the flow simulation, including its rotation, recirculation, and separation (Grisval & Liauzun, 1999). According to the results obtained with means of the k-ε model, two wing design shapes (with

two sweep angles) were selected among their preliminary design shapes; thereafter, the Transition Shear-Stress Transport (Transition SST) turbulence model was implemented as it could predict the flow separation correctly, provide robust, accurate results including steady-state solutions (Langtry & Menter, 2009) (Coughtrie, Borman, & Sleigh, 2013). The Transition SST turbulence model was based on four equations and solves flow turbulence for smooth transition based on the k–Ω model near the wall. The transition SST turbulence model is rated for aerodynamic applications as one of the most precise models used for aerodynamic performance evaluation. Boundary condition, solution control parameters, and material properties were defined.

3.3.2 Aerodynamic performance and mission range

To evaluate the performance improvements, the rolling moment, the roll rate, the range, and the endurance were calculated from the aerodynamic coefficients obtained using the morphing technique.

3.3.2.1 Rolling moment calculation

The adjustment of the variable-span wing asymmetrically is predicted to obtain a rolling moment as given otherwise by conventional ailerons. However, the challenge of this technique is from the structural viewpoint; the root wing will be influenced by considerable sizeable bending moment ((R. M. Ajaj et al., 2014). The bending moment of a variable wingspan increases as the product of lift distribution, wing area, wing panel span, and free-stream dynamic pressure increases due to the span extension. Weight is also a critical factor for increasing the bending moment, especially when an added actuation system would be located at the wing root. According to some studies (Rafic Ajaj et al., 2012), the root bending moment of a variable wingspan can be 60% higher than the root bending moment of conventional ailerons.

The semi-span of one side extends to the desired distance y_1 while maintaining the other side fixed, as shown in Figure 3.6.

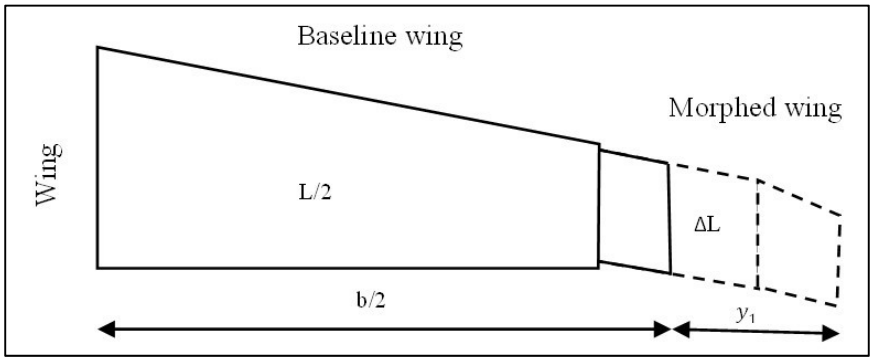

Figure 3.6 Increase of Wing Span y/b (%)

The total lift at the beginning of the roll motion can be determined as Ref. (R. M. Ajaj et al., 2014):

$$L + \Delta L = qC_L(S + \Delta S) \tag{3.1}$$

where L is the lift produced by the original wing, ΔL is the acquired lift due to span extension, q is the dynamic pressure, C_L is the lift coefficient, S is the original wing area, and ΔS is the additional wing area after span extension. The lift is equal on both sides of the wing due to its symmetric span. However, as the wing area changes on one side due to the asymmetric span extension or retraction, the lift will increase more on one side of the wing.

The area S of a tapered wing and the changing area ΔS of the swept angle geometrical shape of the wing become:

$$S = b * \frac{[c_r + c_t]}{2} \tag{3.2}$$

where b is the wingspan at the original wing, c_r is the root chord, and c_t is the tip chord. The changing area is:

$$\Delta S = \frac{[c_r + c_t]}{2} * y_1 \tag{3.3}$$

where y_1 is the additional wingspan after span extension, c_r is the root chord, and c_t is the tip chord.

The total lift coefficient can be found with the following equation.

$$C_L = \frac{L + \Delta L}{q * \frac{[c_r + c_t]}{2}(b + y_1)} \tag{3.4}$$

The rolling moment L_{roll} can be approximated with the following equation (R. M. Ajaj et al., 2014):

$$L_{roll} \approx \Delta L \left(\frac{b}{2} + \frac{y_1}{2}\right) \approx q * \frac{[c_r + c_t]}{2} y_1 C_L \left(\frac{b}{2} + \frac{y_1}{2}\right) \tag{3.5}$$

As the assumption of the Equation, the lift influences in the midpoint of the wing extension; because of that, it has a total moment arm of (($b/2$) + ($y1/2$)). By substituting Equation (3.4) in the rolling moment Equation (3.5), Equation (3.6) becomes:

$$L_{roll} = \frac{L + \Delta L}{2} y_1 \tag{3.6}$$

where L_{roll} is the rolling moment, L is the lift at the original position, and ΔL is the gained lift through span extension.

Equation (3.6) shows that by extending the wing on one side, the rolling moment produced relies on the difference between a generated lift in both semi-spans.

3.3.2.2 Roll rate

The asymmetric span configurations can vary the lift distribution in morphing wing. For example, when one side of the wing (starboard or port) extends its span longer than the other side of the wing, the lift distribution symmetry point will transfer to the long wingspan (Nelson, 1998). The generated roll moment is expected to be the one given by the deflection of conventional ailerons for roll maneuvers control (R. M. Ajaj et al., 2014). For the pure roll rate due to varying mass moment inertia, the first-order equation can be defined as Refs. (Christopher S Beaverstock et al., 2014) and (R. M. Ajaj et al., 2014):

$$L_{roll} = I_{xx}\dot{p} + p\dot{I}_{xx} \tag{3.7}$$

where I_{xx} is the mass moment of inertia around the x-axis and p is the roll rate. With the assumption of wing mass distribution and neglection of the contribution of other components such as fuselage and empennage, the equation of mass moment of inertia becomes:

$$I_{xx} \approx \frac{m_w b^2}{12} \tag{3.8}$$

where m_w the mass of wing. The mass moment of inertia with variable-span wing can be expressed by:

$$I_{xx_s} = I_{xx} + \frac{m_w}{6}(y_1^2 + y_2^2 + by_1 + by_2) \tag{3.9}$$

I_{xxs} is a mass moment of inertia with a variable-span wing around the *x*-axis, and y_1 y_2 are the extensions of starboard and port, respectively. In the previous equations, the mass moment of inertia of fuselage and empennage are neglected. Hence, the rate of alteration of the wing inertia is time-dependent and is defined as:

$$\dot{I}_{xx_s} = \frac{m_w}{6}(2y_1\dot{y}_1 + 2y_1\dot{y}_2 + b\dot{y}_1 + b\dot{y}_2) \tag{3.10}$$

Based on Equation (3.7), the rolling moment equation for span morphing can be defined as Refs. and (Körpe et al., 2016):

$$L_{roll} = I_{xx_s}\dot{p} + p\dot{I}_{xx_s} = \frac{\partial L}{\partial y_1}y_1 + \frac{\partial L}{\partial y_2}y_2 + \frac{\partial L}{\partial p}p \tag{3.11}$$

where $(\partial L/\partial y_1)\ y_1 + (\partial L/\partial y_2)\ y_2$ is the roll moment due to the extension of starboard and port, respectively, and $(\partial L/\partial p)\ p$ is the roll damping moment. To alleviate the bending moment at the wing root, the appropriate extensions of both wing sides should be determined at a given flight condition (Körpe et al., 2016). Therefore, the governing equation of rolling motion becomes.

$$I_{xx_s}\dot{p} - \left(\frac{\partial L}{\partial p} - \dot{I}_{xx_s}\right)p = \frac{\partial L}{\partial y_1}y_1 + \frac{\partial L}{\partial y_2}y_2 \tag{3.12}$$

where

$$\frac{\partial L}{\partial p} = \frac{\rho V \bar{c}(b + y_1 + y_2)}{4}C_{l_{ps}} \tag{3.13}$$

and

$$C_{l_{ps}} = \frac{\pi(b + y_1 + y_2)}{3(b + y_1 + y_2 + 2\bar{c})} \tag{3.14}$$

where the C_{lps} is the rolling moment damping coefficient.
The steady roll rate is determined by:

$$L_{p_s} = \frac{\left(\frac{\partial L}{\partial p} - \dot{I}_{xx_s}\right)}{I_{xx}} \tag{3.15}$$

and

$$L_{\partial y} = \frac{\left(\frac{\partial L}{\partial y_1} + \frac{\partial L}{\partial y_2}\right)}{I_{xx}} \tag{3.16}$$

The time constant τ_s is time for roll mode response.
where the time constant can be defined as:

$$\tau_s = -\frac{4I_{xx_s}}{\rho V c (b + y_1 + y_2)^3 C_{l_{ps}}} \tag{3.17}$$

The steady-state roll rate of the variable-span wing is Ref. (Körpe et al., 2016):

$$p_{ss}^* = -\frac{\left(\frac{\partial L}{\partial y_1} + \frac{\partial L}{\partial y_2}\right)}{L_p^*}(\partial y_1 - \partial y_2) \tag{3.18}$$

3.3.2.3 Improved range and endurance estimation

The efficiency of the morphing wing was also estimated in terms of range and endurance increases. As the wingspan extends, the aerodynamic performance (lift-to-drag) increases, thus increasing the range and endurance contribute to an improvement of aircraft efficiency. For the purpose of investigating the increase of performance, the geometrical characteristic of a real aircraft was considered.

The estimations were made using the characteristic of the UAS-S4 (Kuitche & Botez, 2019) (Yvan Tondji & Botez, 2016) (Segui, Kuitche, & Botez, 2017). The UAS-S4 is an unmanned

aerial system designed and manufactured by Hydra technologies for military and civilian purposes (Figure 3.7). Its general characteristics are presented in Table 3.3.

Figure 3.7 Hydra Technologies UAS-S4 Ehecalt

Table 3.3 The characteristics of the UAS-S4

Geometrical data	**Values**
Wing Span	4.2 m
Wing Area	2.3 m²
Total length	2.5 m
Mean Aerodynamic Chord (MAC)	0.57 m
Empty weight	50 kg
Maximum Take-off Weight (MTOW)	80 kg
Loitering Airspeed	35 knots
Maximum Speed	135 knots
Service Ceiling	15, 000 ft
Operational Range	120 km

The range and endurance of the UAS-S4, assuming steady level flight based on the Breguet formulas are (Anderson & Bowden, 2005):

$$R = \frac{\eta}{c}\frac{C_L}{C_D}\ln\frac{W_0}{W_1} \tag{3.19}$$

$$E = \frac{\eta}{c}\frac{{C_L}^{3/2}}{C_D}\frac{\sqrt{2\rho_\infty S}}{\sqrt{W_1}-\sqrt{W_0}} \tag{3.20}$$

Where R and E are the range and endurance, η, c, W_0, and W_1, are the propulsive efficiency, the fuel consumption rate, takeoff weight, and landing weight, respectively. For a given morphing aircraft, in Equations (3.19) and (3.20), the values of airspeed and weight are constant.

Note that for a given altitude and weight, the range and endurance are maximized when the $\frac{C_L}{C_D}$ and $\frac{{C_L}^{3/2}}{C_D}$ are maximum (Blondeau & Pines, 2004). Their maximum values are given by the following equations:

$$\left(\frac{C_L}{C_D}\right)_{max} = \left(\frac{C_{D_0} * \pi * e * AR}{2 * C_{D_0}}\right)^{1/2} \tag{3.21}$$

$$\left(\frac{{C_L}^{3/2}}{C_D}\right)_{max} = \left(\frac{3 * C_{D_0} * \pi * e * AR}{4 * C_{D_0}}\right)^{3/4} \tag{3.22}$$

where e is the span efficiency factor, and C_{D0} is the zero-lift drag coefficient. The aerodynamic efficiency is dependent on the wing aspect ratio. As a result, an increase in wing aspect ratio would lead to the boost up of both flight range and endurance. Moreover, the flight endurance is further increased for a variable wing because the wing area also increases based on a change of aspect ratio.

3.4 Performance Evaluation of Designed Models

This comparative study gives an evaluation of the performance characteristics for selecting the best geometrical shape. The results obtained in this work include varying parameters obtained using Computational Fluid Dynamics (CFD) solver. The wings have been designed by considering the advantages of the structural and aerodynamic design points of view. For accomplishing the simulation processes, the morphing wingspan has been extended in this investigation by 25%, 50%, and 75% of the original wing. The analyses were carried out at four airspeed values, 17, 34, 51, and 68m/s, corresponding to Mach number values of 0.05, 0.10, 0.15, and 0.20, respectively. Furthermore, the air density and dynamic pressure were determined at various altitudes, such as at the sea level, 5,000 and 10,000 ft.

3.4.1 Comparison results obtained for aerodynamic efficiency

The results present the comparison of the aerodynamic efficiency variation for the various airspeeds, for which the length and the sweep angle of the inner section were varied. Figure 3.8 shows the variation of the lift coefficient with the drag coefficient (CL vs. CD) changes substantially for the first and second sweep angle models ($\beta = 4.5^{\circ}$ and $\beta = 8.9^{\circ}$), respectively, when both wingspan and speed vary (lift increase and drag decrease). However, as seen in Figure 3.8, the aerodynamic performance generated by varying the wingspan length was more efficient than that generated by varying the speed at all selected altitudes in this investigation. For instance, the lift and drag coefficients obtained at sea level for the entire wing were equal to 0.350 and 0.0123 for the first sweep angle model and were equal to 0.340 and 0.0122 for the second sweep angle model at low speed (Mach number of 0.05), and for full wingspan extension.

On the other hand, the lift and drag coefficients at maximum speed (Mach number of 0.2) but the original position was 0.362 and 0.0109, and of 0.352 and 0.0109 for the first and second sweep angle models, respectively.

Furthermore, the main parameters in this investigation are the sweep angle of the moving segment inside the fixed wing, the wingspan, and the flight speed variation. However, the effects of these two parameters (wingspan lengths and flight speeds variations) on the UAV wing are different for the two sweep angles models. For instance, it is evident that the increase of the wingspan length (at the same flight speed) can conduct, for example, to the increase of the lift coefficient at the cruise speed. Therefore, when the wing extended to 75% from its original length, for the first and the second sweep angle models, the lift coefficient increased up to 11% and up to 9.4%, respectively. It was noticed that the lift coefficient increases with the sweep angle decrease. Moreover, the drag coefficient decreased for the first and the second sweep angle models, up to 16.2% and up to 12.3%, respectively (it decreased with the decrease of the sweep angle).

On the other side, by taking into account the varying speed, for example, when the wingspan was at 75% of its length, and the speed varied from its minimum to its maximum value, the lift coefficient increased up to 3.6% and 3.3% for the first and the second sweep angle model, respectively. The drag coefficient was reduced to 12.7% and 11.1%, respectively, for the first and the second sweep angle models.

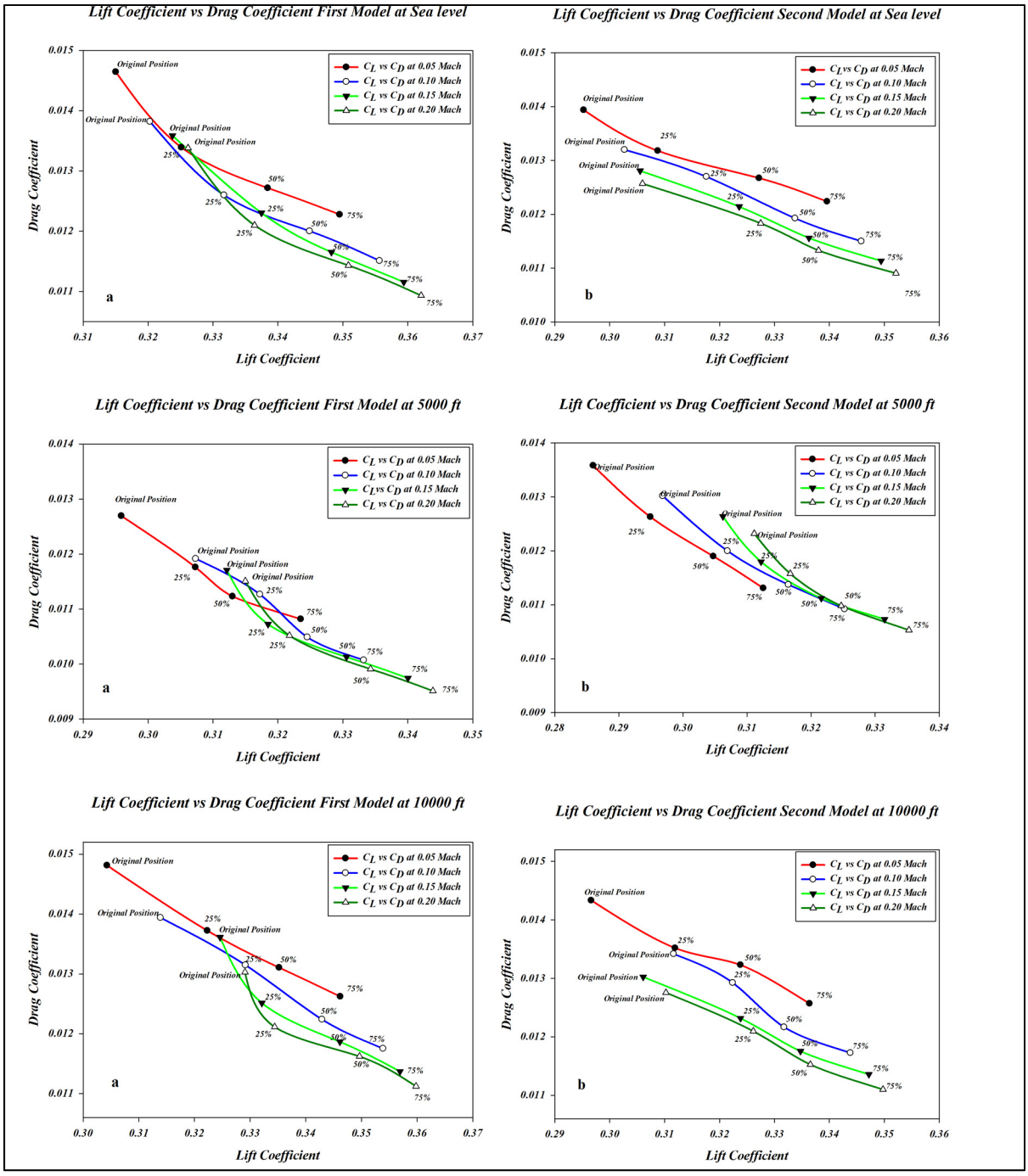

Figure 3.8 Drag coefficient versus lift coefficient of span extension at various velocities for a) first sweep angle model and b) second sweep angle model at Sea level, 5000 ft., and10000 ft.

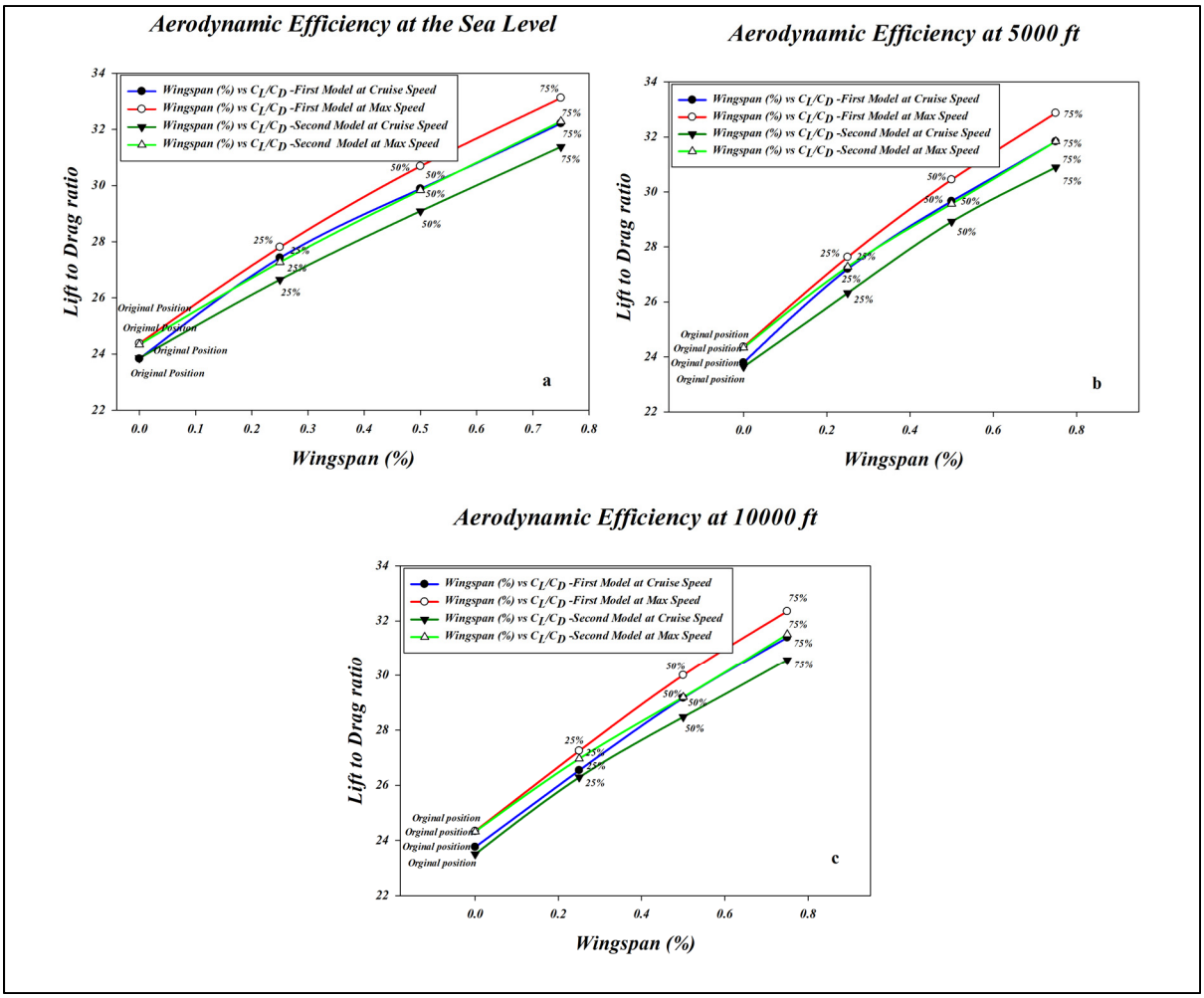

Figure 3.9 Aerodynamic efficiency comparison at cruise and maximum speed at a) the sea level, b) at 5000 ft. and c) 10000 ft.

Figure 3.9 illustrates that the performances of the wing with the first sweep angle model (β = 4.5◦) are more effective than the performances of the wing with the second sweep angle model (β = 8.9◦).

The aerodynamic efficiency, for instance, increases with the full-extended span at the cruise speed and altitude 1,000 ft for the first sweep angle configuration to 31.39, and the second sweep angle configuration to 30.57. Therefore, the improving ratio of aerodynamic efficiency for both configurations at this speed when the span extends from its original position to its full

extension was 32.39% and 29.5%, respectively. For more details, Table 3.4 contains the values of aerodynamic efficiency for span configuration extension at selected speeds.

Table 3.4 The increase of the aerodynamic efficiency for selected speeds from wing original position to its full span extension

	First shape, $\beta = 4.5^{\circ}$			Second shape, $\beta = 8.9^{\circ}$		
Wingspan (%)	Original Position	75%	Increase Ratio	Original Position	75%	Increase Ratio
C_L/C_D at Loiter Speed	23.358	30.112	28.92%	23.224	29.320	26.25%
C_L/C_D at Cruise Speed	23.760	31.392	32.11%	23.501	30.567	30.07%
C_L/C_D at Max Speed	24.337	32.350	32.93%	24.320	31.510	29.56%

The results indicate that as the span increases, the aerodynamic efficiency increases. Figure 3.10 shows the drag coefficient versus the lift coefficient variations for the four morphing wing configurations at the sea level, at 5,000 and 10,000 ft altitudes. As expected, changing from the original position to maximum span extension increases the lift coefficient and decreases drag coefficient; therefore, the maximum lift coefficient increases, and the induced drag decreases. Since the angle-of-attack is constant at 0˚ in this investigation, therefore, the effect of angle-of-attack on the wing is out of scope for this study. Thus, the aerodynamic efficiency increases based on the influence of wingspan extension (0%, 25%, 50%, and 75%) and the variation of the speed (Mach numbers of 0.05, 0.10, 0.15, and 0.20) for two sweep angle models. The aerodynamic performance rate for each extended span decreases slightly for both configurations. For example, the aerodynamic performance rate differs in the first sweep angle configuration, at 10,000 ft altitude, and the cruise speed when the span is extended from its original position to 25%, from 25% to 50%, and from 50% to 75% of its length to 11.70%, 9.92%, 7.61%, respectively.

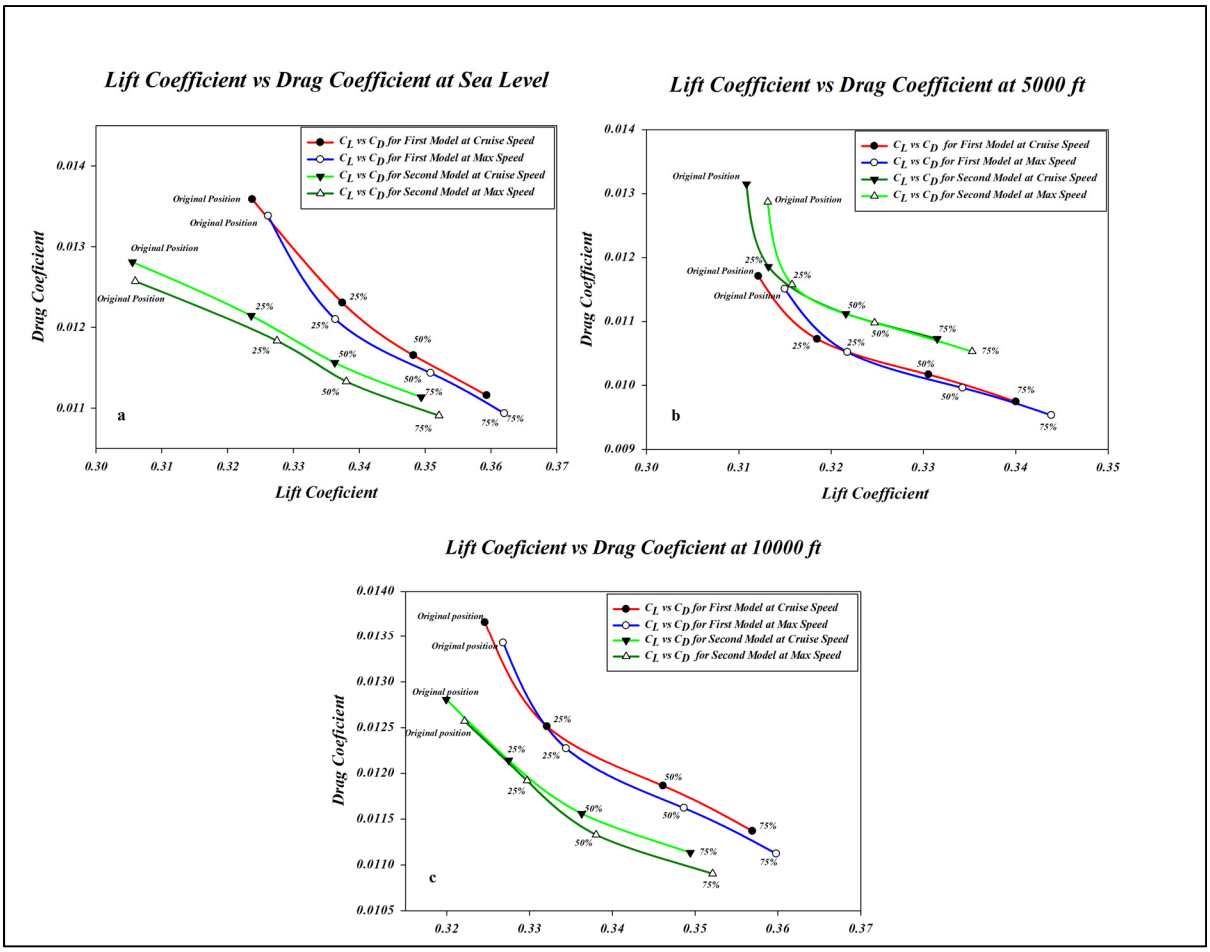

Figure 3.10 Drag coefficient versus lift coefficient variation at a) the sea level, b) at 5000ft, and c) at 10000 ft

In the same way, as in the first sweep angle configuration, the aerodynamic performance rates for the second sweep angle configuration are 11.65%, 8.48%, and 7.33%, respectively. Table 3.5 contains all aerodynamic performance values for the first sweep angle model and second sweep angle model at cruise and maximum speed. The induced drag average based on the full-extended span (from the original position to 75% of its length) decreased to approximately 7% for both shapes at all selected speeds.

Table 3.5 The increasing rate of aerodynamic performance for the first and second sweep angle models when span length changes at cruise and maximum speeds

	51 m/s (cruise)		68 m/s (maximum speed)	
	First Model	Second Model	First Model	Second Model
Original Position – 25%	11.7%	11.35%	11.96%	10.86%
25% - 50%	9.92%	8.48%	10.1%	9.16%
50% - 75%	7.61%	7.33%	7.83%	7.65%

It is clear that the change of the position of the moving wing axis inside the fixed-wing noticeably influences the performance of the morphing wing. For instance, the difference in aerodynamic performance between the first and the second sweep angle configuration suggests that the difference in the improvement of performance between the first sweep angle and the second one reached up to 27.43%, 28.44%, and 28.81% for loiter, cruise, and max speed respectively, when wingspan is modified to full extended span.

3.4.2 Asymmetric span morphing at cruise and maximum velocity

As one of the benefits of a variable morphing wing, the roll control is accomplished by using different spanwise lift distribution between the port wing (PW) and the starboard wing (SBW). However, it is obvious that this technique is not the best method to achieve roll control due to the structural perspective because of the increasing of the bending moment at the wing root noticeably. Thus, the reinforcement of the wing structure must be taken into account in the mechanical design and optimization to overcome the bending moment increase. The roll control must be calculated for the differential of span extension. Span retraction of varying extension rates (from 75% to original wing) is applied, where the rate of change is held constant from maximum to minimum. The results in Figure 3.11 indicate that increasing span leads to delay in the roll rate while decreasing span tends to speed up the roll rate Equation (3.18) as shown in Figure 3.11 for both altitudes of 5,000 and 10,000ft. On the contrary, Figure 3.12 illustrates that the roll damping moment increases as the wingspan increases.

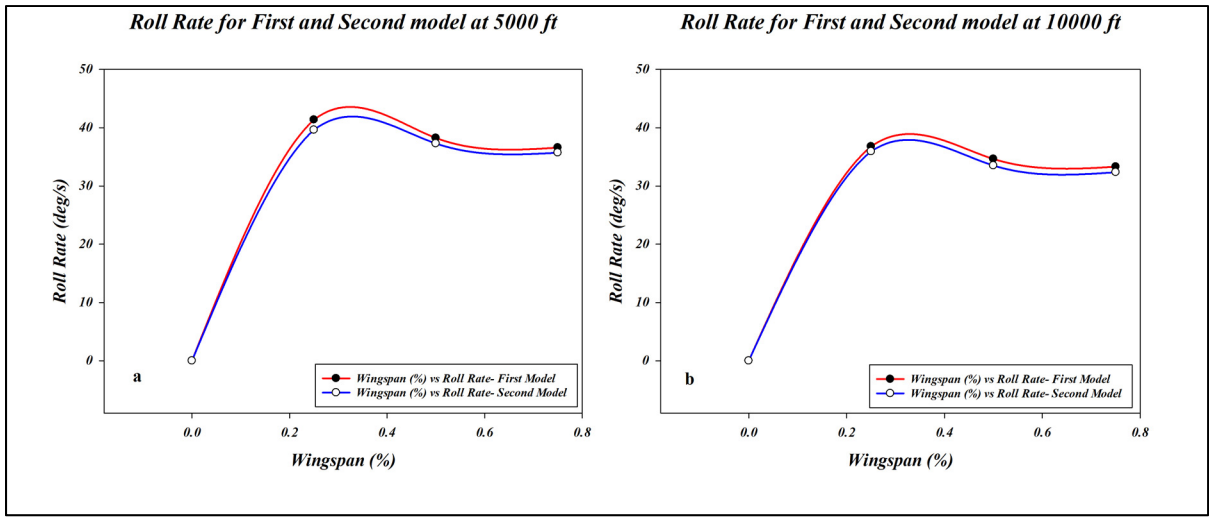

Figure 3.11 Roll rate versus the wingspan locations for the first and second sweep angles model a) at 5000 ft and b) 10000 ft

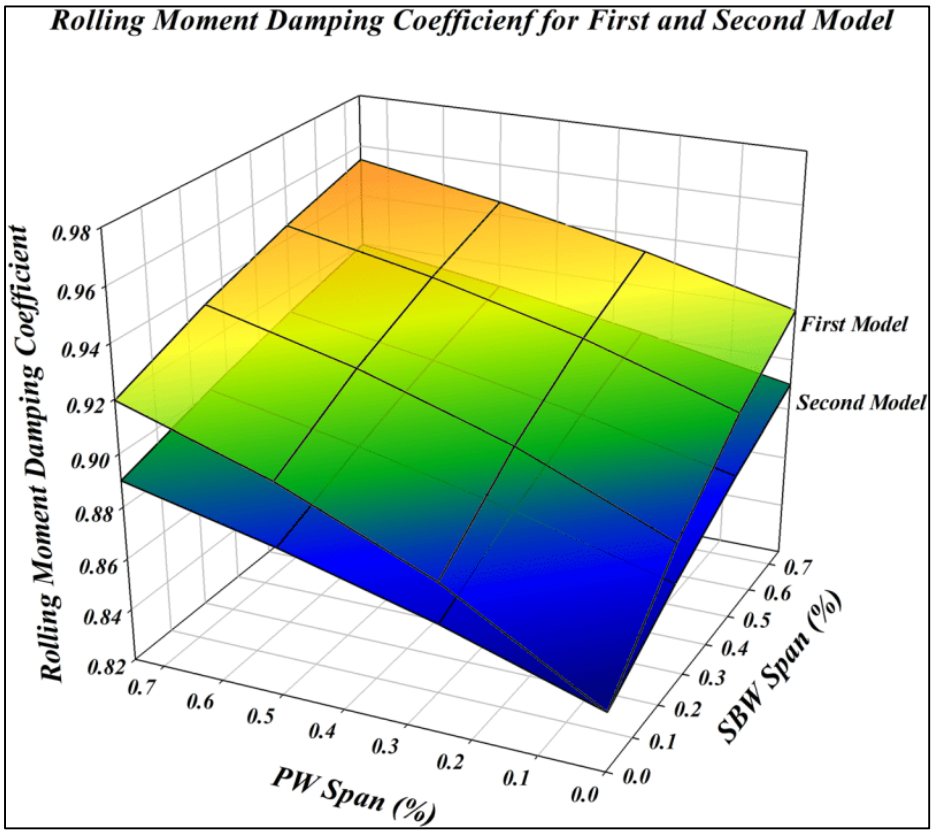

Figure 3.12 Rolling Moment Damping Coefficient for the first and second Model PW: Port Wing, SBW: Starboard Wing

The roll rate increases significantly as the speed increases. As the flight speed increases, the tendency of the aircraft reduces to roll as the damping increases, which is very consistent with the rolling moment damping coefficient. The purpose of this study is to compare two design options for selecting the best shape in terms of the performance of three characteristics (aerodynamic, roll control, and range and endurance). The results of the rolling moment damping coefficient Equations (3.13) and (3.14), are shown in Figure 3.12, indicate that the first sweep angle generates a more rolling moment as the span increases. Nevertheless, the changing of the rolling moment is about 2.8 % at full span extension.

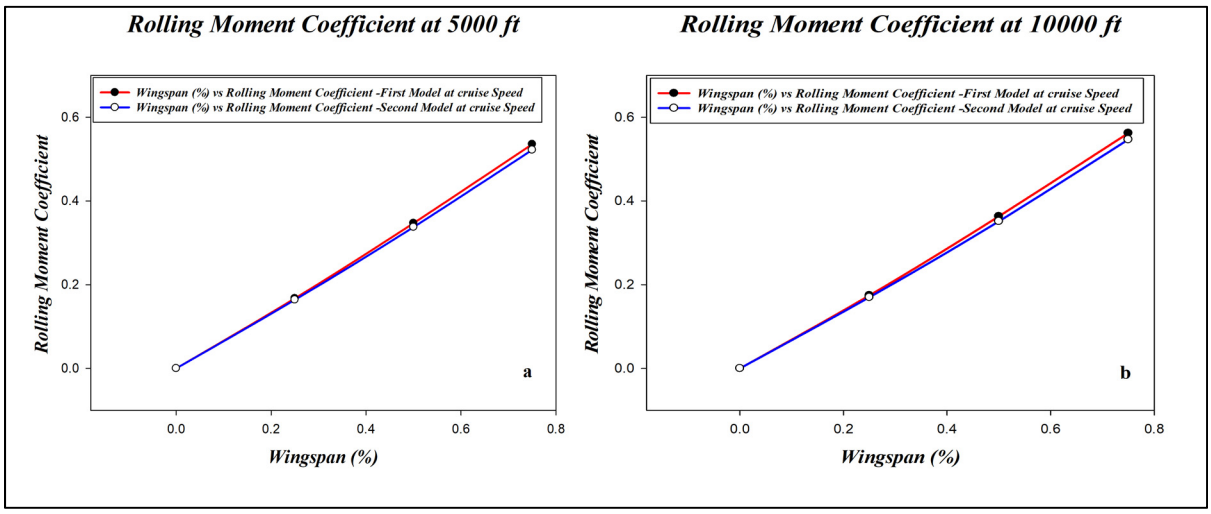

Figure 3.13 Rolling moment coefficient versus wingspan locations for the first and second sweep angle models a) at 5000 ft. and b) 10000 ft

It can be summarized that the asymmetrical variable span can be used for rolling control, and it can achieve steady turns. Since generating the lift distribution is different for the first and the second sweep angle model in the present case, the rolling moment coefficient is slightly larger for the first sweep angle model, as shown in Figure 3.13. The time constant of roll mode response is identical for both sweep angles models as the parameters in Equation (3.17) are constant. Figure 3.14 refers to the time response of both variable morphing span wing models for roll control at the altitudes of 5,000 and 10,000ft. The rolling time constant increases with the wings span location, as seen in Figure 3.14.

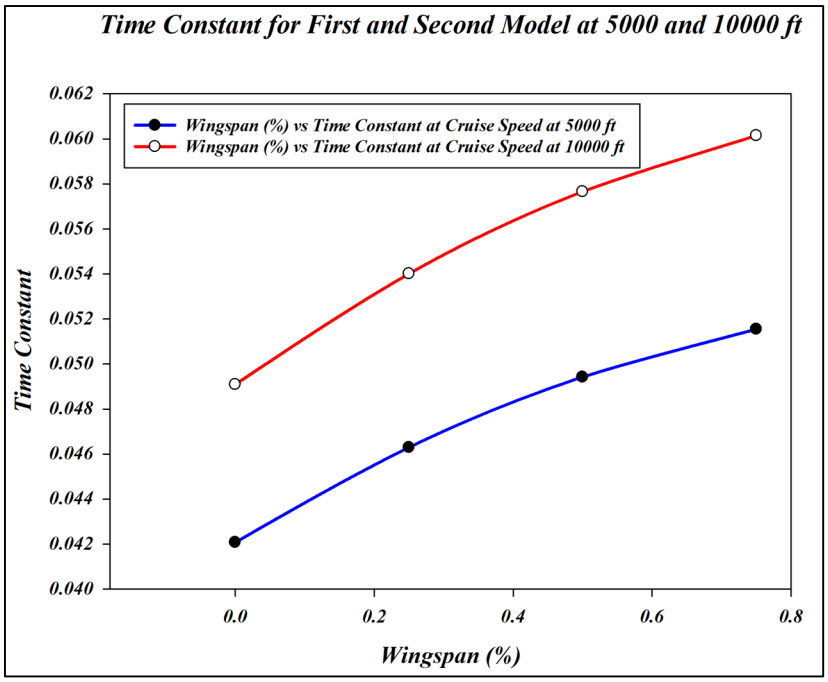

Figure 3.14 Time constant vs. wingspan locations calculated for the first and second sweep angle model

3.4.3 Comparison results for the range and the endurance

The results provide a clear image of the benefits of a variable morphing wing for range and flight endurance. This investigation indicates that the increase of the flight range and endurance due to wingspan extension influences all selected speeds considerably. For instance, Figure 3.15 represents the significant improvement of the range and endurance metrics for loitering velocities at 5,000 and 10,000 ft.

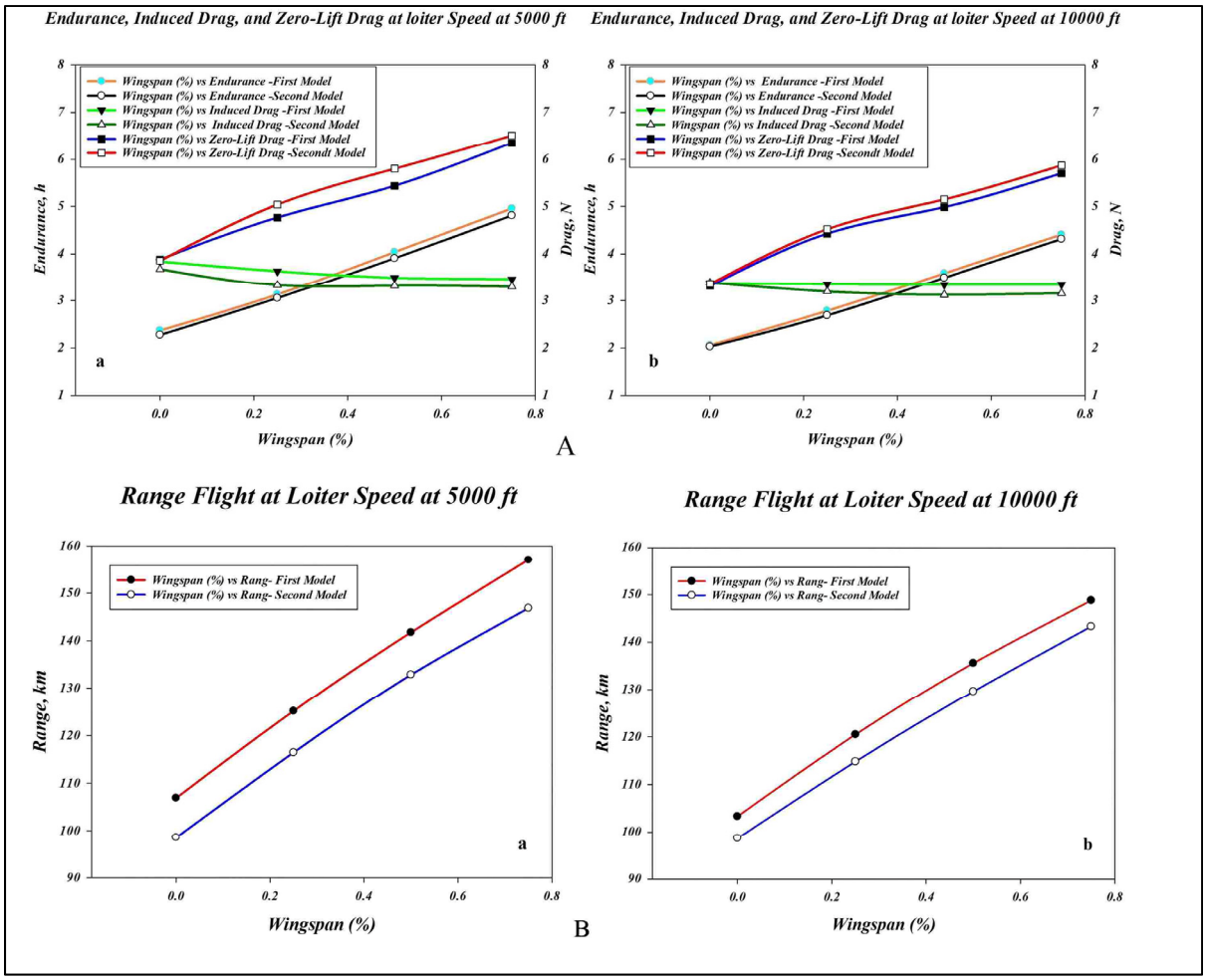

Figure 3.15 A) Endurance and B) Range vs. wingspan variation for first sweep angle model and second sweep angle model at loiter velocity

The assessment of the increased endurance and range is based on the change of the $\frac{C_L}{C_D}$ and $\frac{C_L^{3/2}}{C_D}$ ratios. The total drag computed for morphing wingspan is a combination of the induced drag and zero-lift drag. As shown in Figure 3.15, the wingspan area of the wing has an important influence on endurance and drag. Furthermore, Figure 3.15 shows that the induced drag decreases when the wingspan extends, while the opposite occurs when the wingspan extends the zero-lift drag increases. The maximum extension of the flight range to 5,000 ft is up to 46.89% for the first sweep angle model and 43.16% for the second sweep angle model when the span extends from its original length to its full extension. The same pattern is found at the altitude of 10,000 ft, where the flight range is up to 43.94% for the first sweep angle model

and is up to 41.31% for the second sweep angle model. Therefore, the first sweep angle model improves the flight range at the altitude of 5,000 ft by 8.64% and by 6.37% at the altitude of 10,000 ft with respect to the second sweep angle model.

3.5 Conclusions and future work

A variable morphing wingspan is an effective technology for enhancing aerodynamic efficiency and replacing conventional control surfaces. The improvement of flight performance leads to an increase in the flight range and endurance for a given flight. The purpose of this comparative study was to implement the analysis and the examination of three key characteristics using aerodynamics solver.

The major findings of this investigation resided in the fact that the variable span-morphing of the tapered wing can deliver the required improvements of performance because of the variation of wingspan extension, and sweep angle variation. However, estimated weight increases due to an equivalent stiffness of the structure and actuation system in comparison with the conventional wing. “In addition, flutter parameters (speed, damping) might change as they are sensitive to wingspan elasticity increase during the flight envelope. The aeroelastic parameters would also change depending on the motion of the moving segment (extension or retraction), and these changes should be taken into account in the wing design and optimization process.” The obtained results show the significant improvement in aerodynamic performance (for instance, at the cruise phase) by 32.39% for the first sweep angle model, and by 29.5% for the second sweep angle model. The rolling moment is sensitive to the lift distribution generated by span extension. The roll rate of variable wingspan decreases when the flight speed increases. The varying moment generated by variation of wingspan extension between the port and starboard wings suggests that the wing structures must be designed by taking into account the bending moment impacts at the wing root. The main advantages of variable morphing wingspan are the drag reduction; therefore, increase of range flight and endurance. The findings show that around 43.94% and 41.31% increase in flight range for the first and second sweep angle model can be achieved when the full wing extension is used.

Finally, it has been inferred that for future work, the best design shape of the variable morphing wing is the first sweep angle model. It is clear that for aerodynamic efficiency, the first sweep angle model is more efficient than the second sweep angle model for all speeds. For instance, at the cruise speed, the incremented ratio from the original position to 75% extension of its original length for the first and the second sweep angle models were of 32.39% and 29.5%, respectively, which corresponded to the difference in the aerodynamic performance improvement between the two models of 9.34%. However, the efficiency of the rolling moment reduces to 2.5%. Regarding the range and endurance of flight, the first sweep angle model is 8.6% better than the second sweep angle model.

To accomplish the primary objective, several steps will be taken in future work. Additional analysis phases will be carried out for the stability and control derivatives. The variable tapered span-morphing wing structure and mechanism integration will be tested together. Numerical topology optimization techniques will be generated to examine compliant adaptive wing structures for reducing the wing weight.

CHAPTER 4

WING COMPONEMT ALLOCATION FOR A MORPHING VARIABLE SPAN OF TAPERED WING USING FINITE ELEMENT METHOD AND TOPOLOGY OPTIMIZATION – APPLICATION TO THE UAS-S4

Mohamed Elelwi [a], Thomas Calvet [a], Ruxandra Mihaela Botez [a]* and Thien-My Dao [b]

[a] Department of Laboratory of Active Controls Avionics and AeroServo Elasticity
LARCASE
ÉTS - École de technologie supérieure
1100 Notre-Dame West, Montréal QC H3C 1K3 Canada

[b] Department of Research Team in Machines Dynamics Structures and Processes
ÉTS - École de technologie supérieure
1100 Notre-Dame West, Montréal QC H3C 1K3 Canada

Paper published in *The Aeronautical Journal*, Volume 125, Issue 1290, August 2021, pp. 1313 - 1336
DOI: https://doi.org/10.1017/aer.2021.29

Résumé

Ce travail présente l'optimisation de la topologie de l'aile déformable à envergure variable (MVSTW) à l'aide d'une méthode d'éléments finis. Cette optimisation topologique vise à évaluer la faisabilité des composants internes de l'aile tels que les nervures, les longerons et les autres composants structurels. Cette approche innovante est proposée pour le mécanisme télescopique du MVSTW, qui comprend le coulissement de l'aile allongée télescopiquement dans le segment de l'aile fixe. L'optimisation est effectuée à l'aide des outils d'ANSYS Mechanical, qui permettent de résoudre les problèmes d'optimisation topologique. Cette étude vise à minimiser la conformité structurelle globale et à maximiser la rigidité pour améliorer les performances structurelles, et ainsi répondre aux exigences d'intégrité structurelle du MVSTW. Cette étude évalue les déplacements maximaux, les paramètres de contraintes et de déformations de l'aile à déformable à envergure variable optimisée en comparaison à ceux de l'aile d'origine. Les analyses d'optimisation des ailes sont menées pour quatre extensions d'envergure, soit 0%, 25%, 50% et 75% de l'envergure d'origine, et pour différentes vitesses

de vol afin d'inclure toutes les phases de vol (17, 34, 51 et 68m/ s, respectivement). L'optimisation de la topologie est effectuée sur l'aile pleine conçue en l'alliage d'aluminium 2024-T3 pour répartir ses composants dans ses segments fixes et mobiles. Les résultats montrent que les segments d'aile fixes et mobiles doivent être conçus en utilisant deux configurations de longerons et sept nervures avec leurs éléments de support dans la zone de forte contrainte. Les valeurs de poids structurel des segments d'aile fixe et mobile ont été réduites à 16,3 et 10,3 kg de 112 à 45 kg, respectivement. Le MVSTW optimisé a été testé en utilisant différents paramètres mécaniques tels que les déformations, les déplacements et les contraintes de von Misses. Les résultats obtenus pour le MVSTW optimisé montrent le comportement mécanique optimal et l'intégrité structurelle de l'aile nécessaires pour réaliser les missions multi-vols.

Abstract

This work presents the Topology Optimization of the Morphing Variable Span of Tapered Wing (MVSTW) using a finite element method. This topology optimization aims to assess the feasibility of internal wing components such as ribs, spars and other structural components. This innovative approach is proposed for the telescopic mechanism of the MVSTW, which includes the sliding of the telescopically extended wing into the fixed wing segment. The optimization is performed using the tools within ANSYS Mechanical, which allows the solving of topology optimization problems. This study aims to minimize overall structural compliance and maximize stiffness to enhance structural performance, and thus to meet the structural integrity requirements of the MVSTW. The study evaluates the maximum displacements, stress and strain parameters of the optimized variable span morphing wing in comparison with those of the original wing. The optimized wing analyses are conducted on four wingspan extensions, that is, 0%, 25%, 50% and 75%, of the original wingspan, and for different flight speeds to include all flight phases (17, 34, 51 and 68m/s, respectively). Topology optimization is carried out on the solid wing built with aluminum alloy 2024-T3 to distribute the wing components within the fixed and moving segments. The results show that the fixed and moving wing segments must be designed with two spar configurations, and

seven ribs with their support elements in the high-strain area. The fixed and moving wing segments' structural weight values were reduced to 16.3 and 10.3kg from 112 to 45kg, respectively. The optimized MVSTW was tested using different mechanical parameters such as strains, displacements and von Misses stresses. The results obtained from the optimized variable span morphing wing show the optimal mechanical behavior and the structural wing integrity needed to achieve the multi-flight missions.

4.1 Introduction

The aviation industry and its related markets are expanding widely due to increased air travel customers. Engineers and researchers in the aerospace field have been investing substantial effort in producing advanced aircraft with high-performance capabilities to accomplish its mission requirements efficiently under various flight conditions (Torenbeek, 2013). Presently, the main concern of engineers around the world is to produce new-generation aircraft through research and innovative technologies with the aim of increasing performance and decreasing ecological impacts. Morphing structures are considered to be successful techniques for achieving these objectives.

An effective example is the Adaptive Trailing Edge Device (ATED), which was designed in the Smart Intelligent Aircraft Structures (SARISTU) project coordinated by Airbus, aimed to improve aircraft performance by reducing fuel consumption by up to 5% (Diodati et al., 2013) (Concilio, Dimino, Pecora, & Ciminello, 2016) (Arena et al., 2019). In the aviation industry, efforts are currently being exerted to produce a new generation of aircraft that can achieve a 50% reduction in aircraft fuel consumption and CO2 emissions by 2020 while ensuring safety. Such objectives have driven engineers to reduce aircraft weight by using new design technologies involving optimized composite materials, morphing wings, and others (Zhu, Zhang, & Xia, 2016) (Michel Joel Tchatchueng Kammegne, Grigorie, & Botez, 2016).

Topology Optimization (TO) is one of the most important structural optimization methods and is applied to determine an optimized material distribution over a given design space and

thereby reduce the weight of an aircraft (Rao, Kiran, Kamesh, Padmanabhan, & Chandra, 2009). Thus, the best structural load distribution is found using this method (Zhu et al., 2016) (Mitropoulou, Fourkiotis, Lagaros, & Karlaftis, 2013).

Various optimization techniques have been applied in engineering design over the years, and their use has been increasing in the aerospace domain (Krog, Tucker, Kemp, & Boyd, 2004). Engineers have used TO to design individual aircraft components, such as wing and fuselage elements (Eves et al., 2009). Airbus used TO methods to find the shapes of new components needed to reduce the weight of the A-380 aircraft. The most well-known example of successful application of such optimization is the Airbus A-380's leading-edge ribs alongside the fuselage door intercostals, achieving a weight reduction of approximately 1,000 kg (Grihon, Krog, & Hertel, 2004). Another interesting project was carried out at Boeing to design the wing's leading-edge ribs for its B-787 Dreamliner aircraft. It integrated TO with sizing and shape optimization, which led to a reduction of the weight of the B-787 leading-edge ribs by 24–45% in comparison with those of the B-777 aircraft (Q. Wang, Lu, & Zhou, 2011) (James, Kennedy, & Martins, 2014). At Bombardier, engineers investigated the aerodynamic design loads for wing-box rib by using two-dimensional TO (Buchanan, 2007).

Oktay et al. (E. Oktay, Akay, & Merttopcuoglu, 2011) (Erdal Oktay, Akay, & Sehitoglu, 2014) carried out estimation studies on the material distribution optimization of an aircraft wing using TO tools. Coupled Computational Fluid Dynamics (CFD) and a structural optimization solver were used to reduce the overall aircraft weight.

The Finite Element Method (FEM) and TO have been considered to represent significant tools in the aircraft design area (Ramesh, Handal, Jensen, & Rusovici, 2020). Integrated application of FEM and TO for an aircraft can result in a significant weight reduction, thereby saving material costs without impacting the final model's robustness or strength properties (Tang, Xi, Zhang, & Hu, 2013) (Gawel, Nowak, Hausa, & Roszak, 2017). The optimization processes achieved by combining CFD with Computational Structural Mechanics (CSM) result in the

determination of a wing shape with optimal aerodynamic performance in all operational flight conditions while keeping its minimum design weight (Morlier & Charlotte, 2012).

The present study provides a novel vision-based structural analysis and TO for a MVSTW design based on the NACA 4412 airfoil. The optimization was implemented to effectively locate the wing components (spars, ribs, stringers, and others) within the wing sections, based on the TO method. Candidate materials were then selected inside the design domain of the wing. The material constraints, such as the volume of a structural design, significantly affect the mechanical properties, such as the total stiffness and robustness (Plocher & Panesar, 2019). The TO method improves the wing structural design by finding the most feasible structural layouts for its different structural components (L. Zhao et al., 2019). The positions of the wing elements must also provide the maximum rigidity to the overall structural configuration of the wing (Y.-b. Zhao et al., 2017).

The previous part of this study investigated the aerodynamic performance of the MVSTW by studying the effects of changing the sweep angle on the morphing wing by varying its span extension (to 0%, 25%, 50%, and 75% of its length) (M. Elelwi, Kuitche, Botez, & Dao, 2020). That analysis was carried out at different speeds, representing all flight phases. The wing shape with the best aerodynamic efficiency was selected for this TO study. The wing shape chosen consisted of two parts, a fixed part, and a moving part, while both axes coincident. This TO of the MVSTW aims to improve the structural performance of the wing in all flight conditions and span extensions while reducing its weight.

4.2 Design and Modelling of the MVSTW Model

Many studies have shown that an aircraft with a morphing wingspan can perform different missions (M. Elelwi et al., 2020). For example, an aircraft with a large wingspan exhibit enhanced aerodynamic efficiency, characterized by a flight range increase, as well as decreased fuel consumption. In contrast, an aircraft with a small wingspan can offer higher flight speeds and better maneuverability (McCormick, 1995). The asymmetric telescopic wingspan

technique can be employed for roll control instead of using conventional control surfaces (L. Gao, Jin, Zhao, Cai, & Zhu, 2018) (Chen, Guo, & Wang, 2016). However, the constant challenge facing designers regarding variable span morphing wing design is to overcome the weight penalty as well as its design complexity (Barbarino et al., 2011). The TO method is one of the approaches for reducing the structural weight without affecting the strength properties of the wing.

The wing shape model selected at this stage from the MVSTW project was finalized at our LARCASE laboratory and includes two models based on the results obtained by aerodynamic analysis (M. Elelwi et al., 2020). These results showed that the first model is more efficient than the second. The solid wing models for both segments were designed using Computer-Aided Design (CAD) with CATIA software. The TO method was then carried out based on the aerodynamic analysis results for the selected wing shape using a CFD solver. After obtaining the wing TO results, its components were designed and distributed inside both sections. The final wing shape was validated by using the FEM code.

A variable-span morphing wing was designed using the telescopic mechanism concept. Both segments of the morphing variable span of the tapered wing were designed based on a NACA 4412 airfoil shape (Communier, Botez, & Wong, 2020). The wing was divided into two sections, as shown in Figure 4.1.

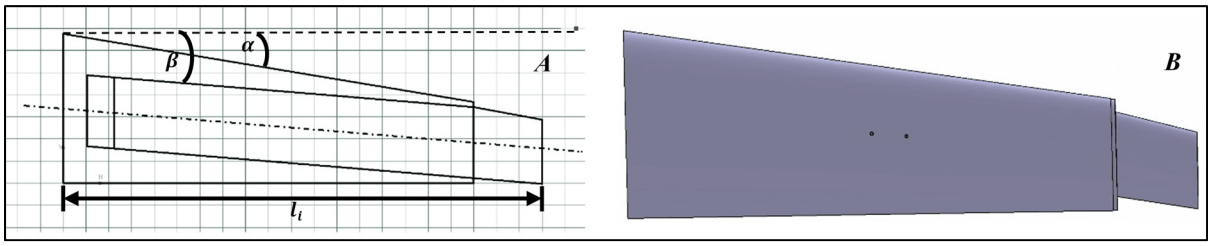

Figure 4.1 Geometrical Shape of a Variable Span of a Tapered Morphing Wing

The selected model was designed such that the central axis line of the moving segment coincided with that of the fixed wing segment. In addition, the inner wing was positioned within the fixed wing at a swept angle of 4.5˚. The geometrical parameters of the wing sections

are presented in Table 4.1 (for MVSTW) and Table 4.2. Table 4.1 shows the main parameters of the variable morphing wing for four different span lengths, while Table 4.2 lists the main parameters for the fixed segment and the moving segment.

Table 4.1 Wing Parameters a three Modified Wing Spans and at the Original Length

Parameter	Original wing	25% *b/2*	50% *b/2*	75% *b/2*
Wing-span (half) (in meters), ***b/2***	2.10	2.63	3.15	3.68
Wing area (in square meters), S	1.92	2.26	2.60	2.93
Wing root chord (in meters), C_r	0.68	0.68	0.68	0.68
Wingtip chord (in meters), C_t	0.29	0.29	0.29	0.29
Aspect ratio, ***AR***	9.18	12.20	15.29	18.4
Taper ratio, λ	0.43	0.43	0.43	0.43
Mean aerodynamic chord in meter $\bar{C}$	0.51	0.51	0.51	0.51
MAC distance from root chord	0.91	1.14	1.37	1.59

Table 4.2 Wing Parameters for Fixed and Moving Wing Segments

Parameters	Fixed Segment	Moving Segment
Wing span (half)	1.8 m	1.98 m
Wing area	1.87 m^2	0.63 m^2
Aspect ratio	6.92	6.22
Root chord	0.68 m	0.32 m
Thickness at root chord	0.08	0.04
Max camber at root chord	0.03	0.01
Location of max camber at the root chord	0.28	0.13
Middle chord	-	0.32 *m*
Tip chord	0.37 m	0.29 *m*
Thickness at tip chord	0.04	0.04
Max camber at tip chord	0.02	0.012
Location of max camber at the tip chord	0.15	0.12
Sweep angle of leading-edge	9.05˚	4.53˚
Section profile	NACA 4412	NACA 4412

In the previous study, the aerodynamic investigation was performed (M. Elelwi et al., 2020) for wings with different span-wise extensions, viz. 25%, 50%, and 75% of the original position, as shown in Figure 4.2. Different span extensions were studied for the Hydra Technologies' UAS-S4 wings with the aim of achieving multiple missions within a single flight (M. Elelwi

et al., 2020). The selected speeds were 17, 34, 51 and 68 m/s, representing the minimum, loiter, cruise, and maximum speed, respectively. Furthermore, aerodynamic simulations were conducted at three altitudes: sea level, 5,000 ft, and 10,000 ft, to evaluate aerodynamic forces and moments.

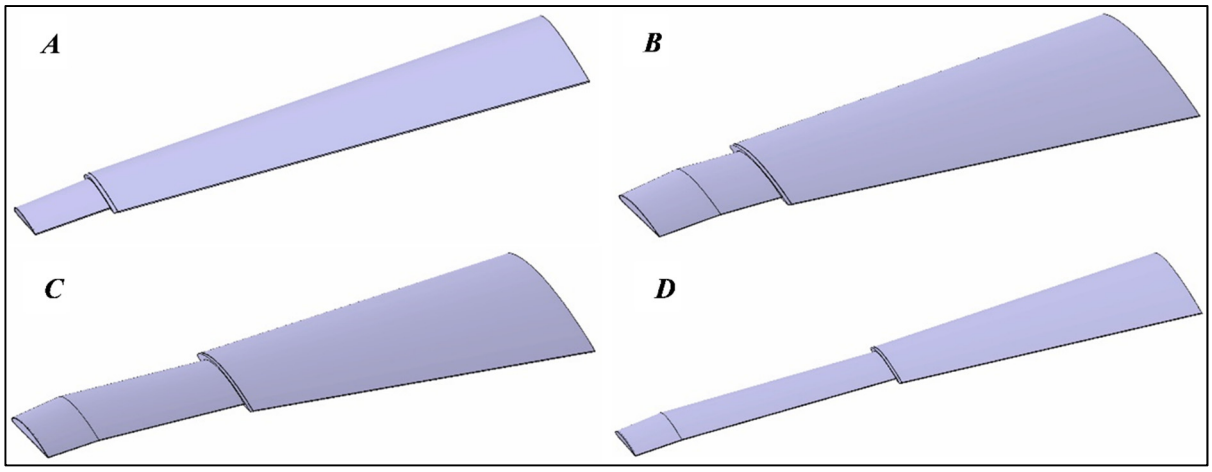

Figure 4.2 A Variable Morphing Span at Various Lengths: A) Original Position; B) 25%; C) 50%; D) 75%

4.3 Topology Optimization Method

The TO method is considered to be one of the most efficient techniques to reduce the weight of a wing structure while maximizing its global stiffness (Rao et al., 2009). The TO algorithm applied herein is based on a combination of the FEM with an optimization code.

The primary objective of this investigation is the distribution of the wing components inside the MVSTW design while supporting its baseline structural integrity. The CFD code collected the applied pressure values for extreme flight conditions to achieve this objective (Michel Joël Tchatchueng Kammegne et al., 2018). The initial wing components were located using the TO by matching the aerodynamic loads on the fixed and moving wing segments to achieve a required level of structural, mechanical behavior, such as deformation, stress, and strain, for a robust structure (Carossa et al., 2016).

The TO results obtained from the numerical solver were further analyzed by Finite Element Analysis (FEA) to determine a proper layout design for the variable-span morphing wing. This process was executed iteratively to define the best possible locations of the elements within the wing. More specifically, two FEMs were carried out: the first on both sections of the original morphing wing to optimize them with the TO code, and the second to ensure that the TO output results satisfied the design requirements.

4.3.1 Theoretical Background of TO

The TO method can be used to find an optimized material distribution over a given design wing space. Material that is significant for the structure is retained while eliminating the undesired weight, thus resulting in the best structural load distribution. The TO approach in the numerical codes is used to respect the given constraints by defining objectives. To ensure that the design requirements are met, minimum material thicknesses are set and exclusion areas defined. The objective of TO is to minimize the compliance, i.e., maximize the stiffness, while satisfying the design constraints.

The material density is considered as a variable of the objective function. For every finite element, the pseudo-density x_i may vary between 0 and 1, $0 \leq xi \leq 1$, where 0 represents void material and 1 represents solid material. The pseudo-density variable can be expressed a shown in Equation (4.1) (Tamta & Saxena, 2016):

$$x_i = \frac{\rho_i}{\rho_0} \tag{4.1}$$

where x_i is the pseudo-density of the i^{th} element, ρ_i is the density of the i^{th} element, and ρ_0 represents the density of the base material. The effect of the pseudo-density on the stiffness properties can be described as

$$E_{(x_i)} = E_{soild}(x_i)^p \tag{4.2}$$

$$E_{(x_i)} = E_{void} + x_i{}^p(E_{solid} + E_{void}) \qquad p \geq 1 \tag{4.3}$$

where E_{void} is a very low Young's modulus allocated to void regions, E_{solid} is Young's modulus of solid regions, and $E_{(xi)}$ is Young's modulus of each element.

The penalty parameter, expressed by the exponent p, has a value greater than 1 (in this paper, p = 3), therefore in combination with the pseudo-densities, it will have a great effect on the optimization results. The stiffness often approaches 0 as the density ρ_i gets close to 0 as well. In the Solid Isotropic Material with Penalization (SIMP) approach, if the intermediate densities approach 0, then the rate of reduction of the modulus of elasticity $E_{(xi)}$ is low. Otherwise, if the intermediate densities p reach 1, the rate of growth in the modulus of elasticity $E_{(xi)}$ increases considerably (M. P. Bendsøe & Sigmund, 1999) (Gunwant & Misra, 2012). The total volume can be represented as the volume of all units with their relevant pseudo-densities, as shown in Equation (4.4):

$$V = \sum_{i=1}^{n} x_i V_i \tag{4.4}$$

where V is the total volume, x_i is the pseudo-density of the i^{th} element, and V_i is the volume of the i^{th} element.

The TO objective function is to minimize compliance and maximize the stiffness of the structure while meeting the design constraints. The objective function can be described mathematically as

$$\begin{aligned} \min_x : \quad & c(x) = U^T K U = \sum_{e=1}^{N} (x_i)^P u_e^T k_0 u_e \\ & subject\ to: \ \frac{V(x)}{V_0} = f \\ & : KU = F \\ & : 0 < x_{min} \leq x_i \leq 1 \end{aligned} \tag{4.5}$$

The function of the design variable vector x is called $c(x)$. The volume fraction is expressed as $\frac{V(X)}{V_0} = f$, where f is the load vector, V is the final volume, and V_0 is the initial volume. F is the force vector, U is the global displacement, and K is the global stiffness matrix in the displacement $KU = F$. Meanwhile, u_e represents the displacement vector and k_0 the elemental stiffness matrix.

The shape of the density filter is chosen in our mathematical optimization, as explained by Sigmund (Sigmund & Petersson, 1998). The physical relative density filtering is donated by $\widetilde{x_i}$ and can be expressed as

$$\widetilde{x_i} = \frac{\sum_{j \in \mathbb{N}_e} w(r_i) v_j \tilde{x}_j}{\sum_{j \in \mathbb{N}_e} w(r_i) v_j} \tag{4.6}$$

where $N_e = \{i | \|r_i - r_e\| \leq R\}$ is a neighborhood set with filter radius R. Here, r_i and r_e are the filter radii about the center of elements i and e, respectively. Also, $w(r_i, r_e) = R - \|r_i - r_e\|$ is the weighting function, and v_i is the volume of element i (Aage, Andreassen, Lazarov, & Sigmund, 2017).

The global stiffness of the structure is maximized by applying a given load. Thus, the optimization problem is solved by minimizing the compliance of the Three-Dimensional (3D) morphing wing while constraining its volume.

The compliance optimization problem can be formulated as

$$C = \int_V fudV + \int_S tudS + \sum_i^n F_i u_i \tag{4.7}$$

where f is the distributed body force, u is the displacement area, t is the traction force, F_i is the point load on the i^{th} node, u_i is the i^{th} displacement degree of freedom, V is the volume of the continuum, and S is the surface area of the continuum.

4.3.2 Parameterization Formulation of the TO Problem

The aim of the discrete TO of the structural design problem is to maximize the stiffness while minimizing the weight. Density-based approaches are applied here, and the optimization problem is solved using the static linear method. The topology design problem can be described using the following mathematical formulation:

$$\begin{gathered} \min f(x) = f(x_1, x_2, \dots\dots, x_n) \\ g_j(x) \le 0, \quad j = 1, \dots\dots, m \\ x_{i_{min}} \le x_i \le x_{i_{max}} \quad i = 1, \dots\dots, n \end{gathered} \tag{4.8}$$

where the design variables x are the independent variables of the $f(x)$ objective function, $g(x)$ are the constraints, and x_{max} and x_{min} are the upper and lower bound constraints, respectively.

In this investigation, solid elements are used, and the optimization process is performed using linear analysis (Lee & Park, 2015). The calculation of the given constraints whose gradients are required can be facilitated by utilizing the constraints screening process to differentiate between active and idle constraints, thereby limiting the number of responses within the optimization problem that form a representative set. The optimization algorithm, which is written and run-in numerical codes, is applied in combination with the approximate method.

The Optimality Criteria (OC) approach is applied to a robust algorithm that can reliably solve the problem using a large set of design variables. Therefore, iterative optimization methods are commonly employed to solve this problem.

The analysis process minimizes the compliance of the variable-span morphing wing while meeting the given constraints using the minimal volume of material. Clearly, this iterative process continues until reaching convergence (Tamta & Saxena, 2016) (Jankovics, Gohari, Tayefeh, & Barari, 2018).

4.4 Optimization Methodology

The research methodology for optimizing the MVSTW designed based on the NACA 4412 airfoil is described in this paper. The model wing was designed based on Hydra Technologies' UAS-S4 and UAS-S45 Baalam data (Kuitche & Botez, 2019). The design workflow was subdivided into three phases: conceptual, preliminary, and optimization design phases. The TO was then implemented using ANSYS Workbench for structural analysis and optimization. Modifications were then applied to the wing structure on the basis of the TO results.

The wing is constrained at the root rib in all degrees of freedom for both segments (Eves et al., 2009). The maximum value of the lift force was obtained for the sea-level fight at a speed of 68m/s and 75% wingspan extension of the MVSTW. Previous aerodynamic studies were conducted, and the aerodynamic loadings were computed at the following flight speeds, altitudes, and wingspan extensions, that were also considered in Ref. (M. Elelwi et al., 2020):

- Flight speeds: 17, 34, 51 and 68m/s
- Flight altitudes: sea level, 5,000ft, 10,000ft
- Wingspan extensions from the original length: original position, 25%, 50%, and 75%.

Table 4.3 presents the aerodynamic forces computed via the ANSYS solver:

In addition, a safety factor of 1.5 was chosen following Federal Aviation Administration (FAA) regulations (FAR 25.303), which state that aircraft structures should withstand the static loads calculated from their corresponding aerodynamic pressures without experiencing structural failure (Acar, Haftka, & Kim, 2010).

Table 4.3 Lift Forces at Sea Level for Various Speeds and Wingspan Extensions

	17 m/s	34 m/s	51 m/s	68 m/s
Original	53.6	217.8	495.4	887.2
25%	65.1	256.1	608.3	1078
50%	78	317.8	722	1293.3
75%	91.1	370.8	843.1	1509.9

The fixed wing was clamped at its root, which represents its connection with the fuselage. The applied forces and stresses will be the same for both the fixed and moving segments of the wing. The moving wing is considered to be an independent solid part in the simulations; thus, the two wing assemblies were not considered for the morphing wing.

4.4.1 Material Selection

The wing design concept of the MVSTW was discussed in Section 2.1. For the first optimization process, aluminum alloy 2024-T3 was selected. Aluminum 2024-T3 is an isotropic material with good versatility; it is easy to work with this due to its high mechanical strength. Commonly used for structural applications, this material is quite prevalent in the aerospace industry. Its material properties are described in Table 4.4.

Table 4.4 Material Data for Aluminum Alloy 2024-T3

Physical and Mechanical Properties	
Density	2780 kg/m^3
Ultimate Tensile Strength	483 MPa
Tensile Yield Strength	345 MPa
Modulus of Elasticity	73100 MPa
Poisson's Ratio	0.33
Fatigue Strength	138 MPa
Shear Modulus	28000 MPa
Shear Strength	283 MPa

4.4.2 Load estimation and pre-processing approach

The load was calculated at the maximum speed and sea level for a full-extension wingspan. A load factor of 3*g* (three times the acceleration due to gravity) and a safety factor of 1.5 were applied. The solid wing was modeled in 3D using aluminum alloy 2024-T3. The numerical analysis was performed separately on the two wing segments of the basic structure. The basic wing structure of the MVSTW represents the initial solid wing of the moving and fixed segments before the optimization process. Figure 4.3 shows the geometry wing planform for both segments.

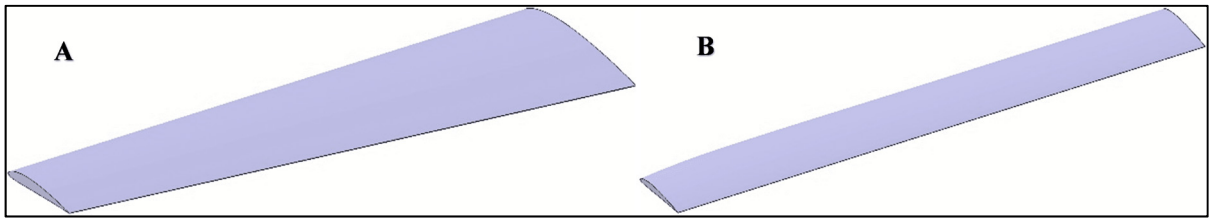

Figure 4.3 Wing Planform: - A) Fixed Part, B) Moving Part

The procedure was implemented for both the fixed and moving wing segments and is presented in the next paragraphs. The basic structure and physical configuration for both wing shapes of the design were defined as shown in Figure 4.3.

The data were processed at zero angle-of-attack. The study parameters of the semi wingspan were selected at the extreme flight conditions to ensure compliance through all flight phases, as presented in Table 4.5.

Table 4.5 The Parameters used in the TO

General Study Parameters	
Lift load	1508 N
Load factor	3 g
Safety factor	1.5
Ultimate pressure	3537 Pa

4.4.3 Finite Element Model of the MVSTW

The numerical analyses of the MVSTW were implemented using a static structure within ANSYS Workbench, which can predict the performance of a product under a real-world environment by incorporating all the occurring physical phenomena with very good accuracy (Ghosh et al., 2016). Structural analysis is one of the most common applications of FEA. The process for static analysis involves meshing, boundary conditions, and loading. In this simulation study, the following procedures were adopted for the static analysis and TO:

- The geometrical shape and physical outlines of the design for the fixed and moving segments were defined, as illustrated in Figure 4.3.
- Mesh generation by the ANSYS solver offers efficient and high-quality grid partitions for both wing shapes. Two meshing elements types were used in the FEM and TO methodologies. The meshing elements are high-quality hexahedral and tetrahedral. The total number of nodes and elements for the fixed segment were 54,185 and 10,152, respectively, while for the moving segment, their total numbers were 25,077 and 4,704, respectively. Figure 4.4 shows the meshed models of the fixed and moving span morphing wing segments.
- The boundary conditions expressed by the desired mechanical behavior and properties (material properties definition, analysis settings, and loading conditions) were defined. The variable span morphing wing was mounted on the aircraft fuselage, with the moving segment sliding inside the fixed segment. The boundary conditions, fixed supports, and load applications for both wing segments are shown in Figure 5.5. Static structural analysis was performed for the fixed and moving segments by enforcing identical boundary conditions. Therefore, in the static structural domain, fixed support was inserted at the root chord for both segments. The load is distributed uniformly on all nodes situated on the bottom surfaces of the moving and fixed wing segments. This load is applied with the same values along the *Y* direction for both segments. To apply the load on the wing segments. The pressure calculated following the aerodynamic results was considered to apply the load on the wing segments, and the magnitude of the load was 3,537 Pa (M. Elelwi et al., 2020) (Chethan, Zuber, Shenoy, & Kini, 2019).

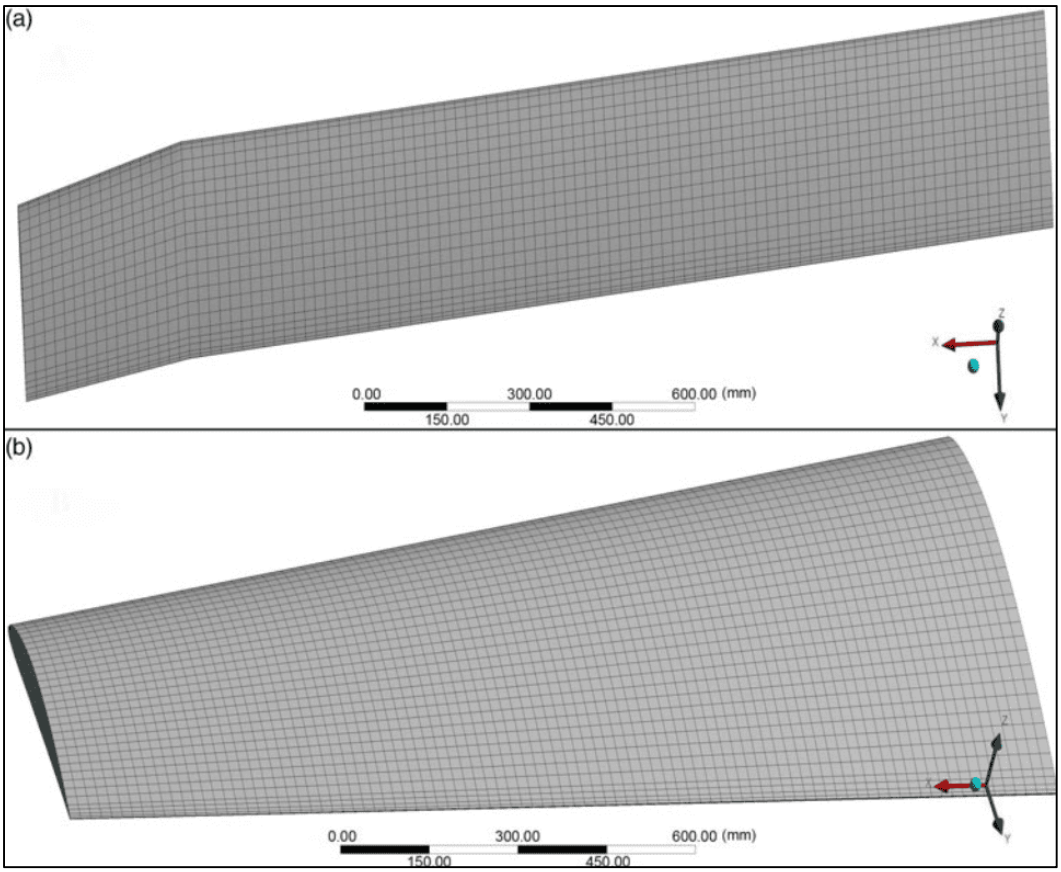

Figure 4.4 Meshing Model of a) Moving, and b) Fixed Wing Segments

- Post-processing was applied after solving the equations of the structural calculations such as stress, deformation, and strain to obtain the converged solution. The static analysis solver allows contour plots, vector plots, 2D and 3D surface schemes to be designed to visualize the finite element analysis results. It can also offer animation to display the results dynamically.
- The results are obtained by static structural analysis. Following the optimization process, von Miss stresses, strains, and deformation values are obtained from the static structural analysis. The FEM results, expressed in terms of deformation, stress, and strain, for the morphing wing segments, respect the safety limits of the selected material's mechanical properties. The FEA results obtained on the considered wing segments are described in Table 4.6 and further shown in Figures. 4.6(a), (b) and (c).

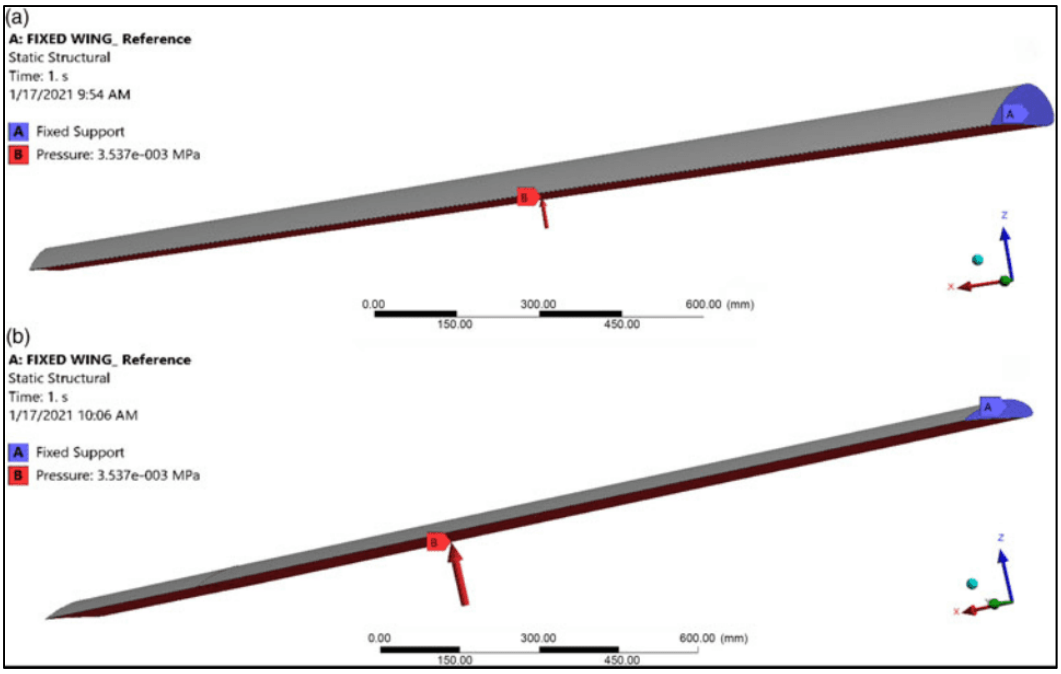

Figure 4.5 Boundary Condition, Fixed Support and Loading Application for a) Fixed and b) Moving segments

Table 4.6 The Results of the Three Parameters (Deformation, Stress, and Strain) for Fixed and Moving Segments at Ultimate Pressure

Finite Element Analysis Results	Deformation	Von-Mises Stress	Strain
Fixed wing segment	3.04 mm	8.35 MPa	0.00011 mm/mm
Moving wing segment	30.71 mm	54.22 MPa	0.00075 mm/mm

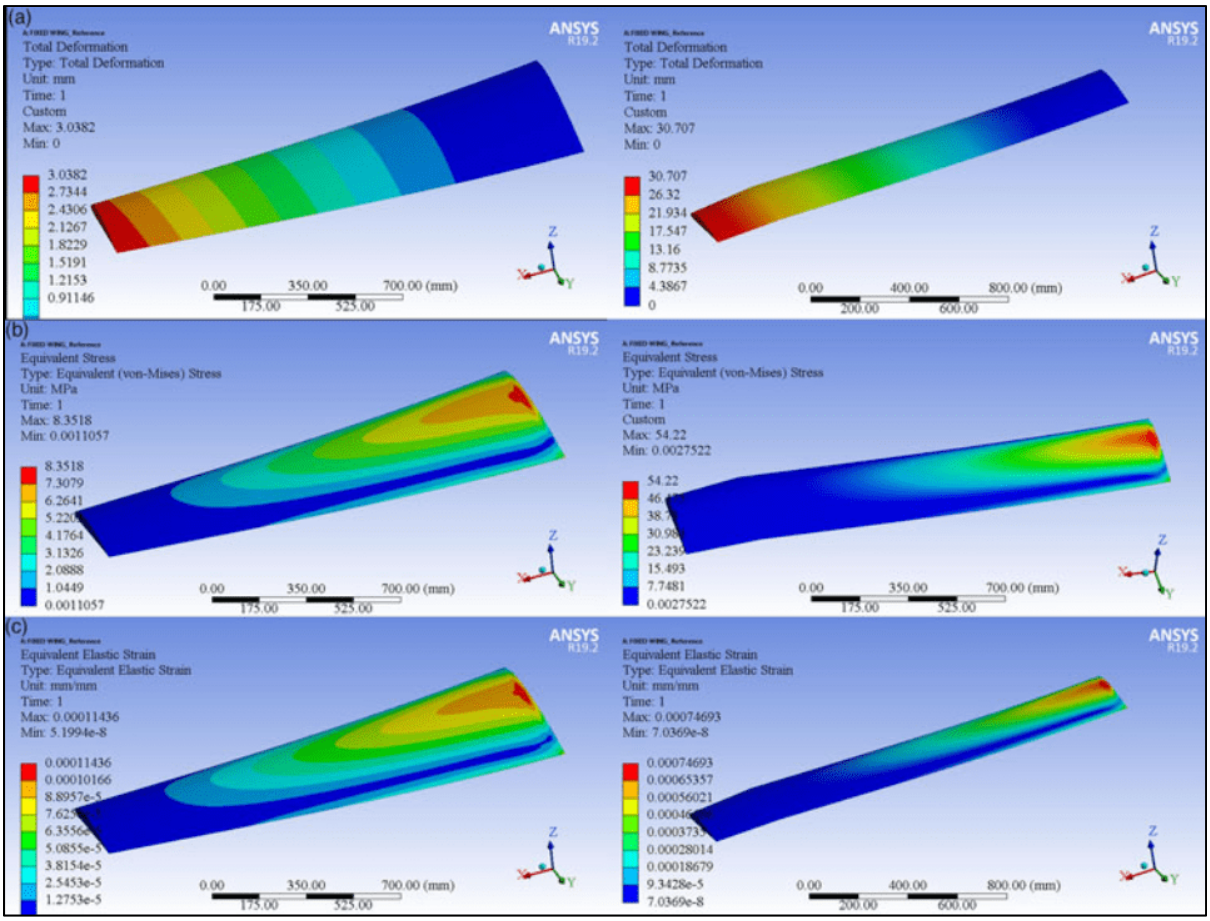

Figure 4.6 (A) Total Deformation, (B) von Mises Stress, and (C) Elastic strain for a) Fixed, and b) Moving, Segments of the Variable Span Morphing of a Tapered Wing Airfoil

4.5 Topology Optimization Results for Wing Components Locations

After finalizing the FEA model analysis, linear static analysis was conducted. The obtained results were checked before setting up the optimization process, as shown in Figure 4.7. The material density was determined as a design variable to optimize the material density distribution from its continuous range (X.-p. Li, Zhao, & Liu, 2017). Two responses were considered for our design case: minimizing the structural compliance and the volume fraction. The volume fraction is considered a constraint. The optimization results show that all elements are located in high-stress/deformation zones, and ensure that the elements inside these zones are essential for structural design. It can be observed that the elements outside such high-pressure areas can be removed (Q. Wang et al., 2011) (X.-p. Li et al., 2017).

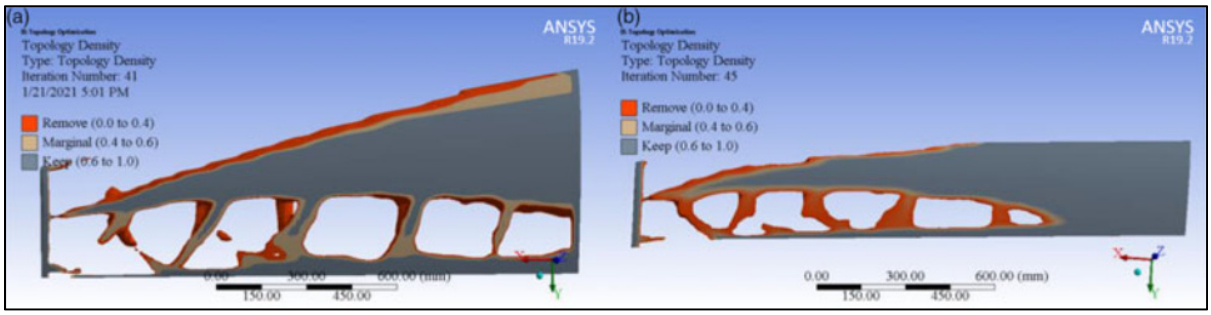

Figure 4.7 TO results for (a) fixed and (b) moving segments of the variable-span morphing of a tapered wing

The TO process shows how the objective function changes with the number of iterations. In this investigation, 41 and 49 iterations were required for the fixed and moving segments, respectively, until convergence was achieved, as shown in Figure 4.8.

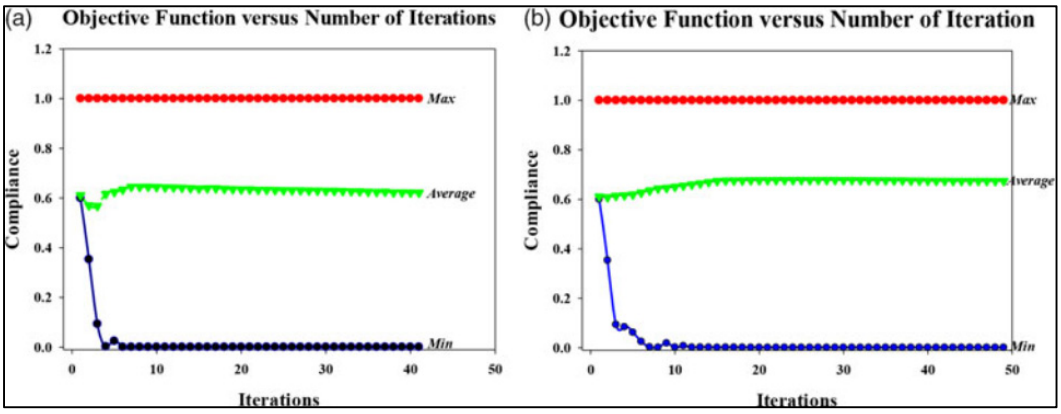

Figure 4.8 Convergence graph of TO for (a) fixed wing and (b) moving wing.

The iterative process modifies the strain energy, so as the strain energy decreases, the structural rigidity gradually increases.

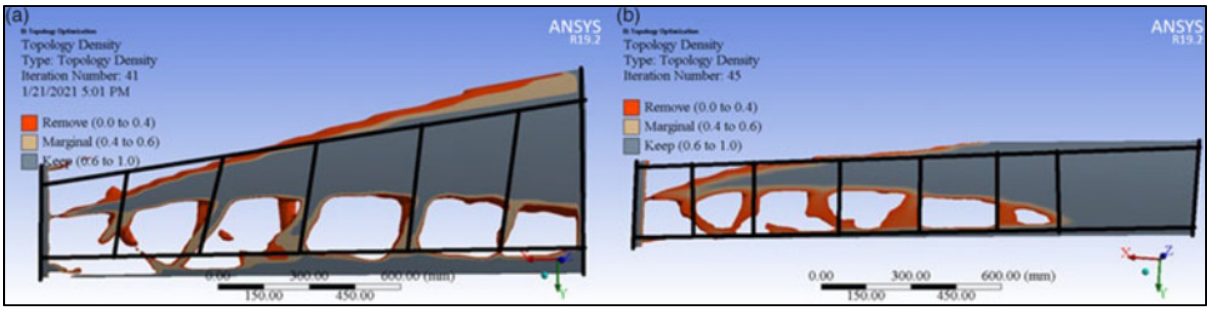

Figure 4.9 Wing components locations based on the topology optimization results for a) Fixed b) Moving Segments

The main objective of the analysis for TO for the variable span morphing wing is to define the wing components that must be redesigned efficiently. The most suitable locations of the components inside the wing with maximum efficiency will be found in the new optimized structure. The TO of the variable span morphing wing for the maximum speed case at the selected wing component locations is shown in Figure 4.9. It can be seen from Figure 4.9 that the analysis provides the approximate locations of the wing components, such as ribs and spars, required to support their loads correctly.

4.6 Remodeling Wing Design Based on Topology Optimization

Based on the TO results shown in Figure 4.9, the wing components are redesigned and analyzed for both wing segments using the same selected material. The first investigation evaluated a potential lightweight structure for the first wing model, as described in Section 2.1. The basic wing model was composed of 100% solid aluminum 2024-T3, with masses of 112 and 45kg for the fixed and moving segment, respectively.

The ribs were first placed at the distances proposed by the TO method at the locations indicated in Table 4.7.

Table 4.7 The Proposed Locations for Wing Ribs for Fixed and Moving Segments

Rib No.	Fixed Wing	Moving wing
1	0 mm Reference	0 mm Reference
2.	269 mm	245 mm
3.	534 mm	626 mm
4.	932 mm	919 mm
5.	1198 mm	1234 mm
6.	1503 mm	1502 mm
7.	1800 mm	1875 mm

For this case study, the TO method suggested that the fixed segment must be designed with two-spar configurations, as its ribs are housing the moving segment. Accordingly, the moving segment must be designed with two-spar configurations to support the wing components, especially at full wing extension, as shown in Figures 4.9 and 4.10.

The baseline TO results show that the high-strain area is located in the middle of the wing area. It can thus be concluded that it is necessary to support the high-strain area in both wing segments by strengthening the shear stress generated by the reactions to the aerodynamic loads under various flight conditions.

After remodeling the TO results for both wing segments, a parametric CAD model of the wing components (Figure 4.10) was developed based on their density distribution (Figure 4.9) (Komarov, Kishov, Kurkin, & Charkviani, 2015).

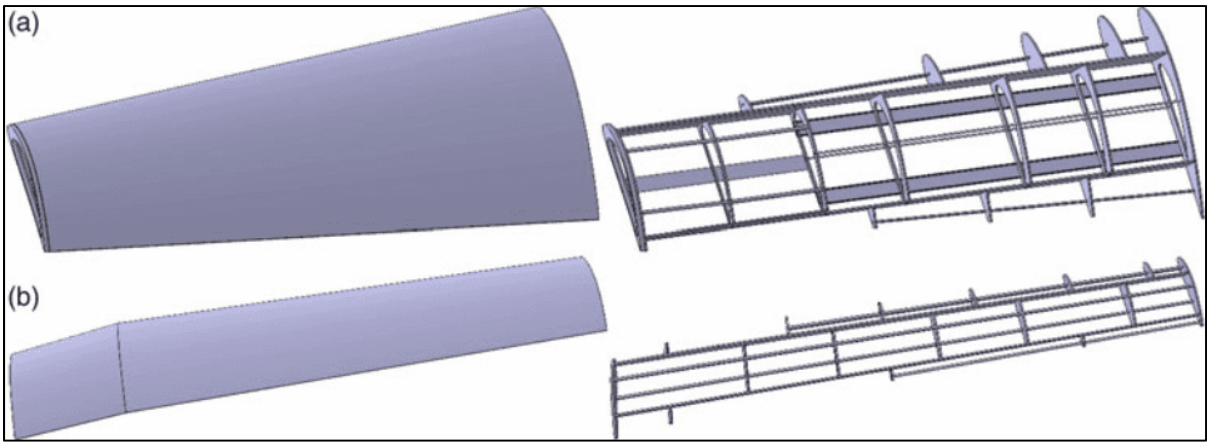

Figure 4.10 Parametric CAD model of (a) fixed and (b) moving segments with their components

Comparison of the weight of the initial structure of the solid wing segments with the weight of the optimized wing segments reveals those reductions of the total wing weight by 16.3kg for the fixed wing segment and 10.3kg for the moving wing segment were achieved.

4.6.1 FEM based on TO

The described approach based on the simulation-based TO method can provide a detailed structural design of the variable-span morphing wing. This offers a new way to reduce the aircraft's structural weight. The redesign based on the TO method suggested a variable-span morphing wing model consisting of thin skin, twin spars, seven ribs, and multiple support elements, as shown in Figures 4.9 and 4.10. The baseline design consists of the external surface skin to sustain the aerodynamic loads and distribute the aerodynamic loads to the internal components, such as spars, ribs, and stringers. The main function of the two spars is to support the multiple loads acting on the wing, including the bending moment and shear force, as well as to support the wing structure against any torsion created by load lifting. The ribs are used to retain the geometrical shape of the wing section with the aim of distributing the external loads evenly on the wing skin and thereby prevent undesired wing deformation. The stringers are applied in the design to enhance the wing's rigidity (X. Zhang, Zhao, & Si, 2018).

To achieve a stiffened and reliable variable-span morphing wing, the main parameters of its fixed and moving wing segments components are defined as follows:

- A wing skin thickness of 2 mm for both segments
- A spar thickness of 6 mm for both segments
- A rib thickness of 6 mm for both segments
- Flat stringers with a thickness of 4 mm for the fixed segments, and round stringers with a diameter of 3 mm and thickness of 1 mm.
- A stringer thickness of 8 mm for the moving segment.

Furthermore, as they are parallel, the distance between the two spars is defined as 351.56 mm for the fixed segment and 163.38 mm for the moving segment of the wing.

The objective for designing such a wing is to enhance the capabilities of the Unmanned Aerial Vehicle (UAV) to accomplish multiple missions during the same flight. This UAV is mainly used for surveillance and security purposes, as it can cover all its targets in one flight by reaching its intended destination rapidly while expanding the flight range without refueling.

The variable-span morphing wing shapes for various wingspan extensions and different flight speeds were re-analyzed using the CFD calculations. The static analysis parameters for the optimized wing were selected for four flight speeds at all three wingspan extensions to ensure compliance throughout each flight phase, as described in Table 4.8.

The same material properties were selected as explained in the previous analysis for the solid wing segments, as described in Table 4.4. Hexahedral meshing was performed using the MultiZone mesh method with the aim of obtaining highly accurate results. The mesh size was selected to be the same for both wing segments: 15 mm for the wing skin, 6 mm for wing spars, and 3 mm for the ribs and stringers. The total number of nodes was equal to 836,885, and the total number of elements was equal to 243,976 for the entire wing. Figure 4.11 shows the meshing of the wing structure and its components.

Table 4.8 Finite Element Analysis Specifications for a MVSTW all Span extensions for different flight speeds

Finite Element Analysis Specifications	17 m/s	34 m/s	51 m/s	68 m/s
Lift Load at Original Position	53.56 N	217.75 N	495.4 N	887.23 N
Lift Load at 25%	65.12 N	259.12 N	608.28 N	1078 N
Lift Load at 50%	77.97 N	317.82 N	722.04 N	1293.29 N
Lift Load at 75%	91.1 N	370.8 N	843.2 N	1509.89 N
Load Factor	3 g	3 g	3 g	3 g
Safety Factor	1.5	1.5	1.5	1.5
The semi-wingspan area at Original Position	1.921 m^2	1.921 m^2	1.921 m^2	1.921 m^2
The semi-wingspan area at 25%	2.26 m^2	2.26 m^2	2.26 m^2	2.26 m^2
The semi-wingspan area at 50%	2.60 m^2	2.60 m^2	2.60 m^2	2.60 m^2
The semi-wingspan area at 75%	2.95 m^2	2.95 m^2	2.95 m^2	2.95 m^2
Ultimate Pressure Original Position	125.47 Pa	510.09 Pa	1160.49 Pa	2078.36 Pa
Ultimate Pressure 25%	129.49 Pa	515.3 Pa	1209.57 Pa	2143.61 Pa
Ultimate Pressure 50%	182.67	549.43 Pa	1248.24 Pa	2235.81 Pa
Ultimate Pressure 75%	213.4 Pa	566.59 Pa	1288.2 Pa	2307.13 Pa
Air Density	1.225 kg/m^3	1.225 kg/m^3	1.225 kg/m^3	1.225 kg/m^3

The same methodology as mentioned in Section 6 was used in this case study. The boundary conditions applied on the variable-span morphing wing were defined. The root chord of the variable-span morphing wing was fixed, and the load was applied for wingspan extensions of 50% and 75%, at a speed of 17m/s, and for the wingspan extension of 0% (original) and 25% at a speed of 51m/s, as shown in Figure 4.12.

The given loads for the multiple wingspan extensions and speeds were applied along the Y direction for the variable-span morphing wing, with the pressures calculated according to the aerodynamic results described in Table 4.8.

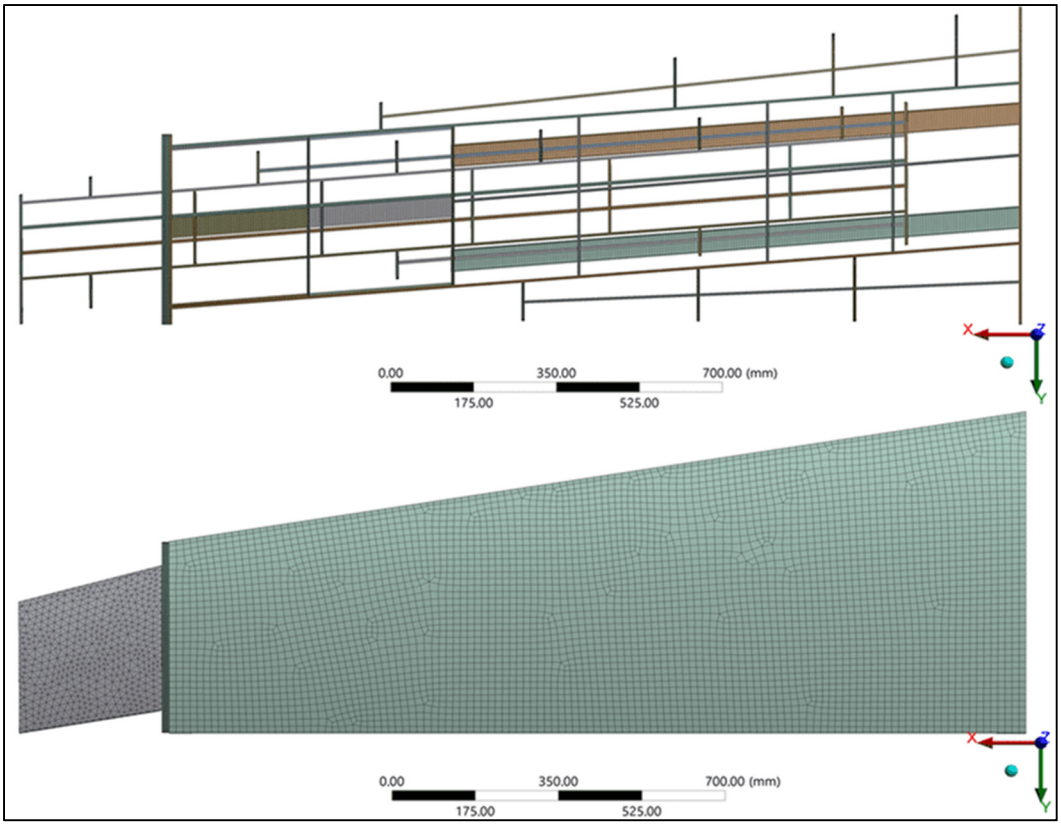

Figure 4.11 Grid meshing of the variable-span morphing tapered wing and its components

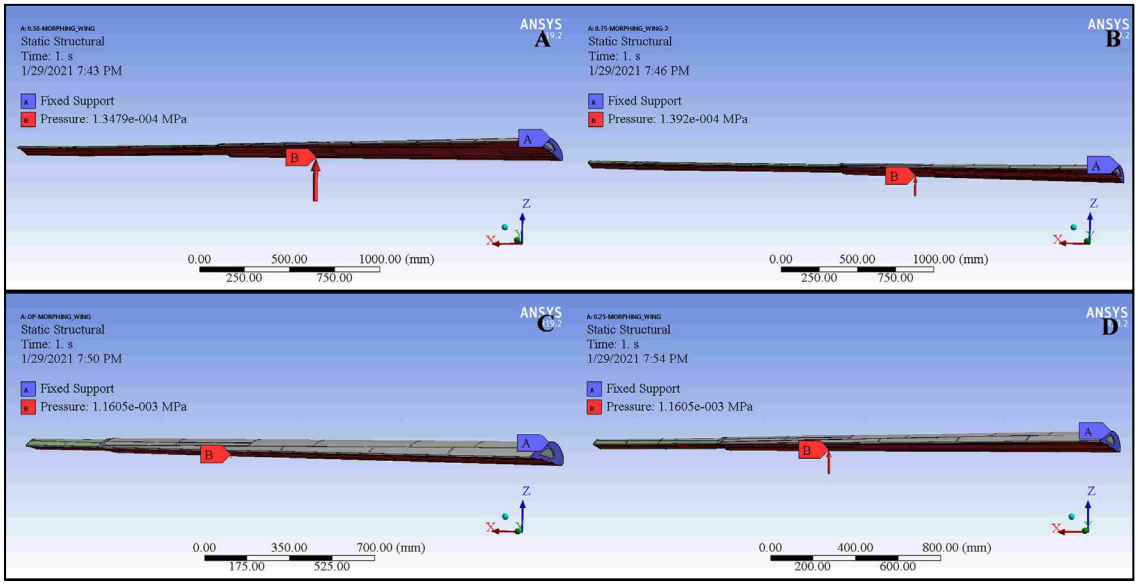

Figure 4.12 Boundary conditions for variable morphing for wingspan extensions of (a) 50%, (b) 75% at 17m/s and (c) 0%, (d) 25% at 51m/s.

4.6.2 Evaluations of the static structural analysis of the optimized MVSTW

Static analysis was performed to evaluate the optimized MVSTW. The loads were defined as per the lift forces that were obtained for the various wingspan extensions and flight speeds. The same boundary conditions were also considered in this investigation and the safety factor, as given in Table 4.8. The results of the static structural analysis are expressed in terms of deformations, von Mises stresses, and strains for eight selected cases (Table 4.9); the results are illustrated in Figures 4.13, 4.14, and 4.15.

Table 4.9 Results for the three characteristics (deformation, stress and strain) at selected wingspan extensions and flight speeds

Finite Element Analysis Results	Deformation	Von-Mises Stress	Strain
Extension 50% at 17 m/s	2.08 mm	24.06 MPa	0.00051 mm/mm
Extension 75% at 17 m/s	4.48 mm	52.35 MPa	0.00093 mm/mm
Extension 50% at 34 m/s	8.49 mm	98.07 MPa	0.0021 mm/mm
Extension 75% at 34 m/s	18.27 mm	213.06 MPa	0.0038 mm/mm
Extension 0% at 51 m/s	4.57 mm	110.43 MPa	0.0015 mm/mm
Extension 25% at 51 m/s	7.57 mm	143.93 MPa	0.0021 mm/mm
Extension 0% at 68 m/s	8.18 mm	197.78 MPa	0.0027 mm/mm
Extension 25% at 68 m/s	13.988 mm	265.84 MPa	0.0038 mm/mm

The results obtained from the MVSTW simulations are depicted in Figures 4.13, 4.14, 4.15, and in Table 4.9. Note that the values of the mechanical properties, that is, the deformation, stress, and strain, increased with increasing aerodynamic loads. Meanwhile, the aerodynamic loads increase with the wingspan extension (increasing the wing surface area) and also changes the flight speed (R. M. Ajaj et al., 2014). The mechanical properties increase dramatically at the large wingspan extensions of 50% and 75% and increased cruise and maximum flight speeds. Therefore, the wingspan extensions of 50% and 75% are suggested only for the minimum speed and loiter phases. The main benefit of symmetric wingspan extension is to increase aerodynamic efficiency for maximized range flight and reduce take-off and landing distances. The wingspan at the original position without extension (0%) and 25% extension

can be used to ensure high maneuverability and reduce the flight time, as the mechanical properties remain within the safe domain of the wing's resistance to failure.

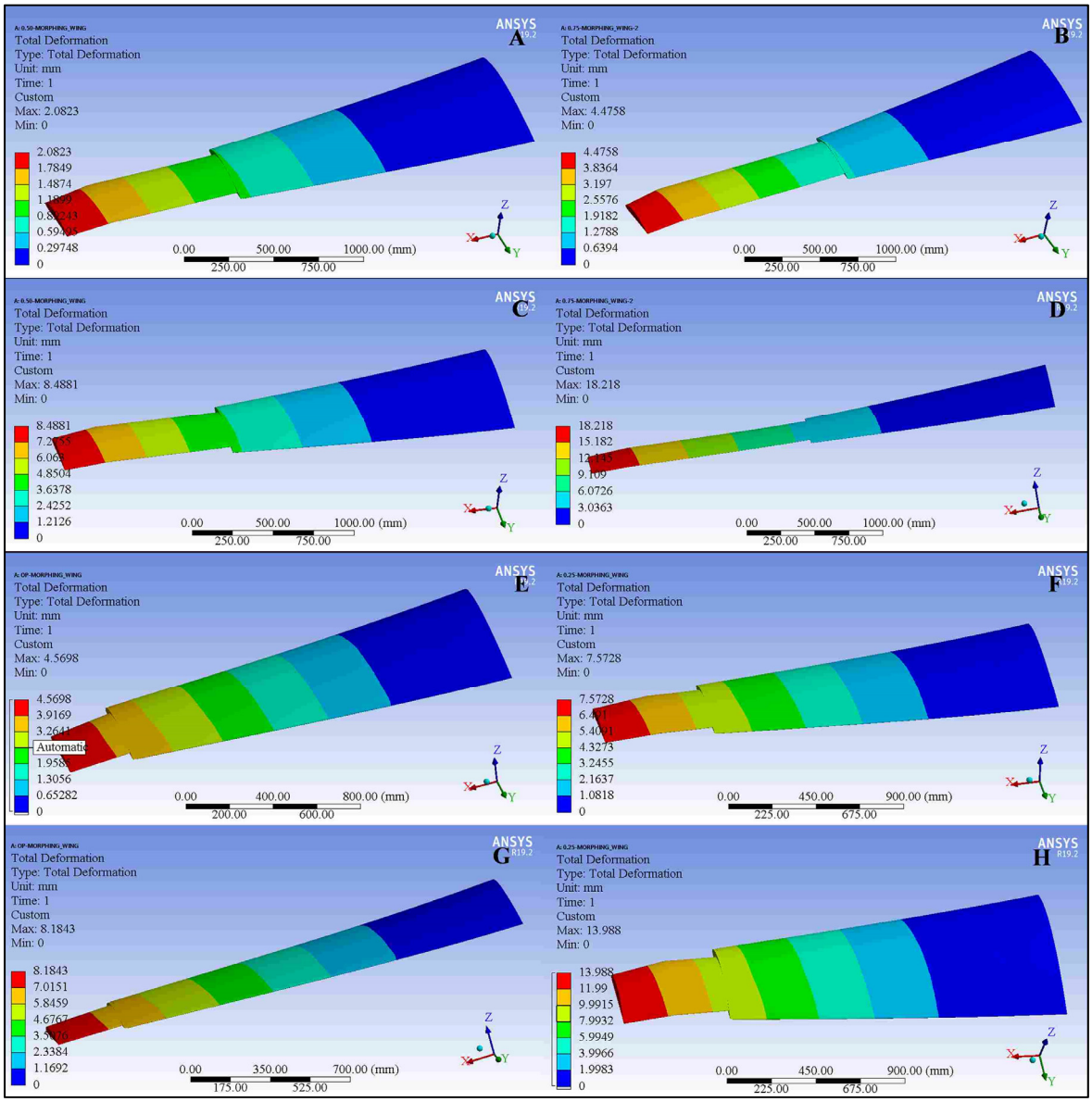

Figure 4.13 Total deformation of the MVSTW for (a) Wing extension of 50% and speed of 17m/s, (b) wing extension of 75% and speed of 17m/s, (c) wing extension of 50% and speed of 34m/s, (d) wing extension of 75% and speed of 34m/s, (e) wing extension of 0% and speed 51m/s, (f) wing extension of 25% and speed of 51m/s, (g) wing extension of 0% and speed of 68m/s and (h) wing extension of 25% and speed of 68m/s.

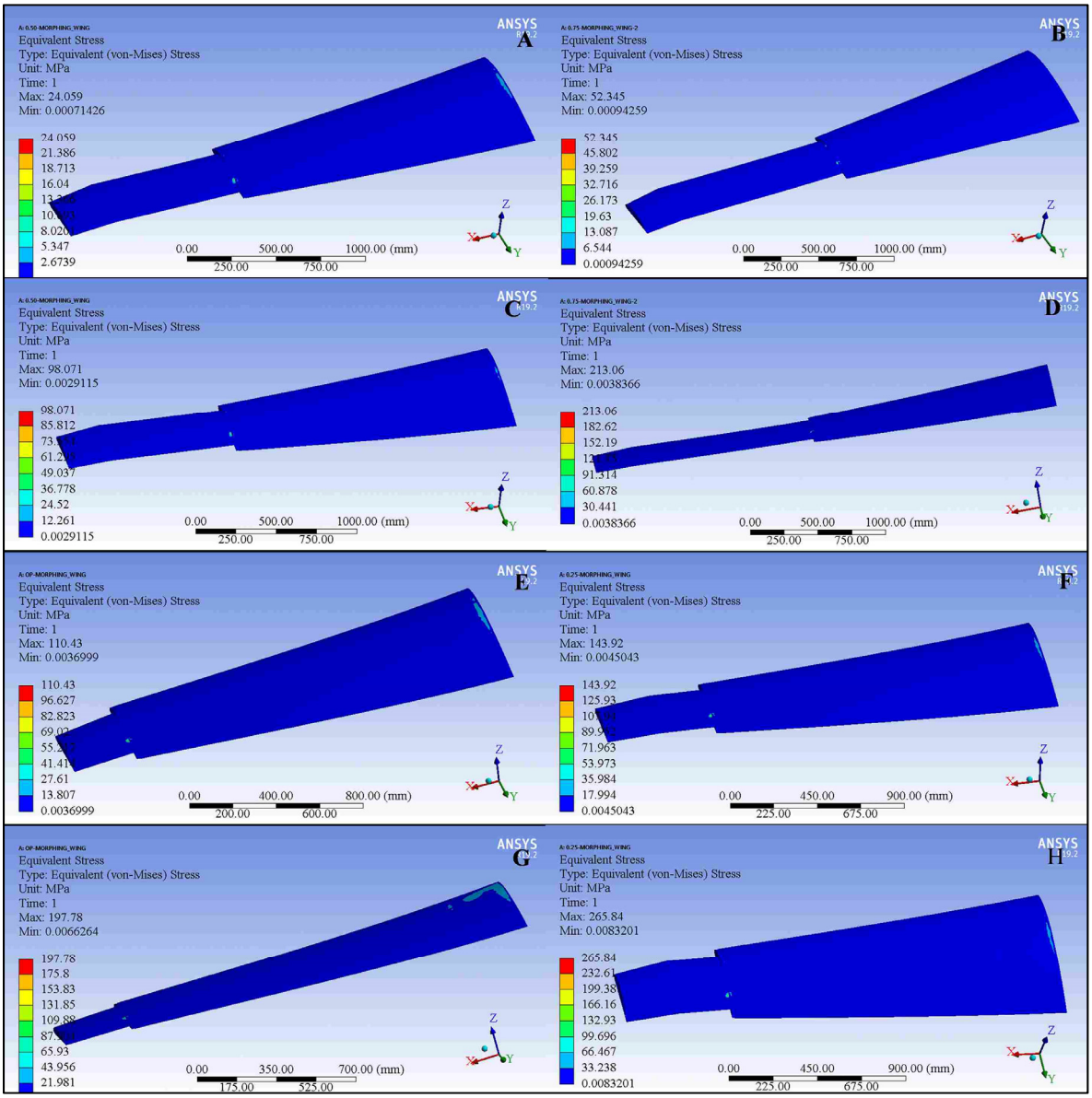

Figure 4.14 Von-Mises Stress of the MVSTW for (a) Wing extension of 50% and speed of 17m/s, (b) wing extension of 75% and speed of 17m/s, (c) wing extension of 50% and speed of 34m/s, (d) wing extension of 75% and speed of 34m/s, (e) wing extension of 0% and speed 51m/s, (f) wing extension of 25% and speed of 51m/s, (g) wing extension of 0% and speed of 68m/s and (h) wing extension of 25% and speed of 68m/s.

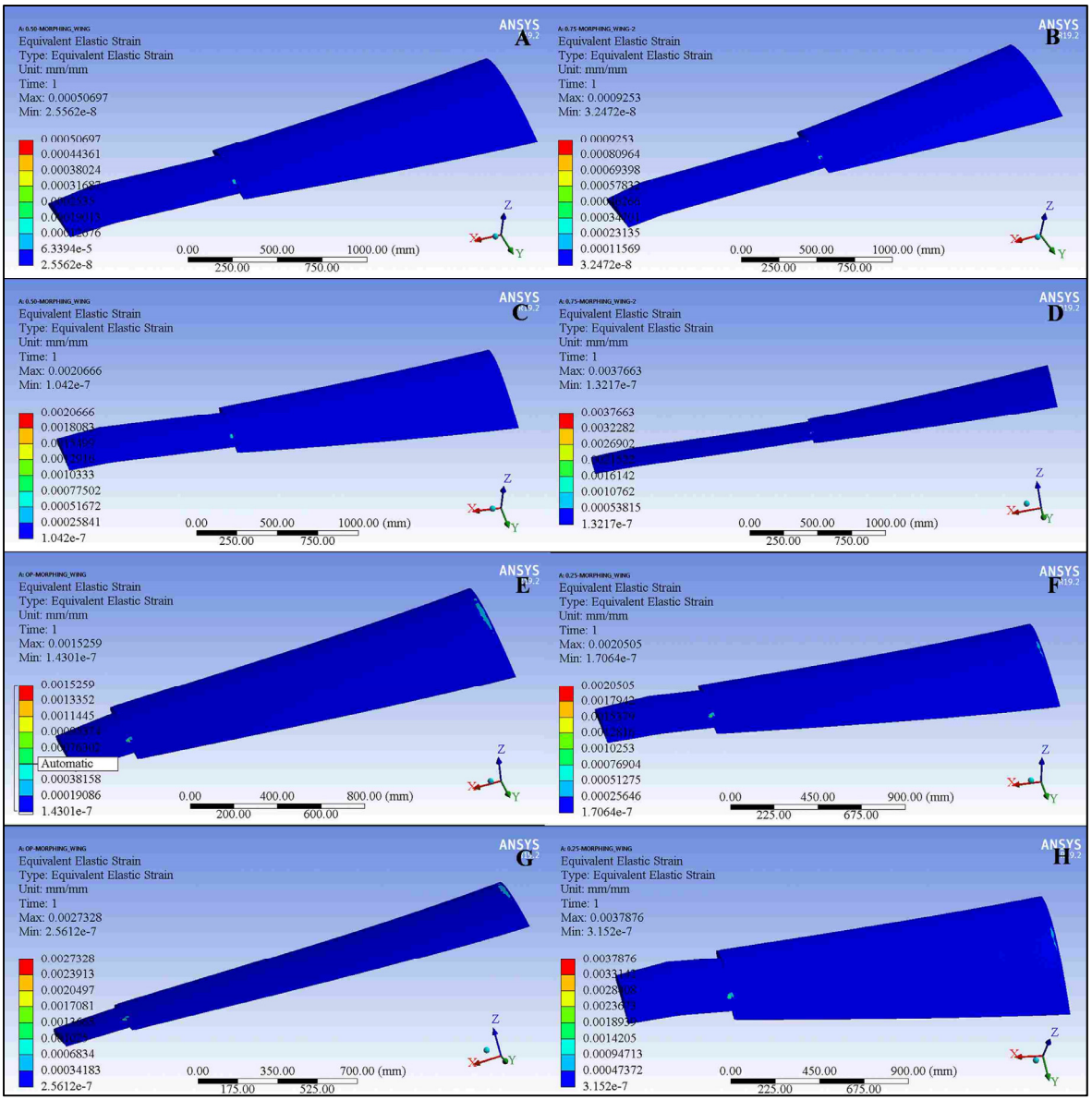

Figure 4.15 Equivalent Strain of the MVSTW for (a) Wing extension of 50% and speed of 17m/s, (b) wing extension of 75% and speed of 17m/s, (c) wing extension of 50% and speed of 34m/s, (d) wing extension of 75% and speed of 34m/s, (e) wing extension of 0% and speed 51m/s, (f) wing extension of 25% and speed of 51m/s, (g) wing extension of 0% and speed of 68m/s and (h) wing extension of 25% and speed of 68m/s.

According to the FEA results, it is clear that the morphing of the structure of the designed wing is suitable for the rolling control strategy using the asymmetric span morphing technique. However, the optimum rolling mechanism should consider that both sides of the wing's span

must expand gradually and symmetrically. In addition, the wingspan should extend smoothly and effectively to avoid structural fatigue since the results obtained for the changes of the deformation, stress, and strain show dramatic increases, being severely affected by the aerodynamic loads. An example of these increases is presented in Table 4.9 for a wingspan extended from its original position to 75% of its length.

The structural optimization of the MVSTW under stiffness requirements is used to predict the perfect layouts of the wing components within the design space. The TO results suggest that the best possible weight values of the MVSTW for both segments are the following: the optimized weight of the fixed segment is 16.3 kg, and the optimized weight of the moving segment is 10.3 kg, compared with the calculated values of 112 and 45 kg for both solid wing segments, respectively. The structural layouts based on the mechanical characteristics, such as stiffness and strength, involve two-spar and seven-rib configurations. Moreover, to achieve the multi-mission requirements, additional support parts, such as stringers and stiffeners, are added to overcome mechanical fatigue (Figure 4.10) by enhancing structural integrity and avoiding structural failure. The proposed arrangement and allocation of wing components were proved to attain the robustness and integrality required for the MVSTW and achieve important weight reductions through topological optimization (Amendola, Dimino, Amoroso, & Pecora, 2016).

4.7 Conclusions and Future Work

This paper addresses the current progress in the field of TO techniques applied in UAV design and new component allocation for the MVSTW. The optimization was carried out using the ANSYS Mechanical tools, enabling the formulation and then a solution of appropriate TO problems. The optimization framework was developed for solid wing segments with the aim of predicting the locations of the variable span morphing wing components within the design space.

The main objective of this optimization was to define and understand the feasibility of internal wing components, such as ribs, spars, and other structural components. This innovative

approach was proposed for the telescopic mechanism of the MVSTW, which includes the sliding of the telescopically extended wing into the fixed wing segment. The study aimed to minimize the overall structural compliance and maximize its stiffness to enhance the structural performance and meet the structural integrity requirements of the MVSTW. The TO results suggested that the fixed and moving wing segments must be designed with two-spar configurations and seven ribs with their support parts. The solid wing weight for both segments was reduced significantly from 112 to 16.3 kg for the fixed wing segment and from 45 to 10.3 kg for the moving segment for the optimized MVSTW. The wing structural components, such as ribs, spars, and support elements, were designed and further developed based on the TO results for both MVSTW segments. Sequential FEAs were performed on the assembled variable-span morphing wing at various wingspan extensions and four different flight speeds. This study is a follow-up to the previous aerodynamic optimization study, in which the aerodynamic loads associated with wingspan lengths and speeds were obtained for multiple flight conditions.

The FEA results for the topology-optimized MVSTW at different wingspan extensions and flight speeds highlight the important benefits of using TO. The results also show that the optimized MVSTW configuration can achieve multiple-mission flight. The optimized wing shape satisfies the structural integrity's design criteria because the wing components' allocation was based on the TO approach.

Future research will include the optimization of the novel MVSTW obtained in this investigation. Numerical TO techniques will be applied to the wing components to enhance the wing stiffness while providing weight savings for better performance. The TO approach will be performed for each wing component individually. This optimized wing will be used as a baseline reference for the subsequent optimization process to produce a lightweight wing while maintaining its structural stiffness and robustness. The weight of the optimized wing could thereby be reduced by 30–50% from the initial value. Additional investigation phases will be carried out to obtain a robust and reliable adaptive morphing wing. The TO will be performed using composite material to obtain a greater weight reduction for the MVSTW. The

MVSTW structure and actuation mechanism integration will be investigated after carrying out the TO of the wing using composite materials.

CHAPTER 5

STRUCTURAL SIZING AND TOPOLOGY OPTIMIZATION BASED ON WEIGHT MINIMIZATION OF A VARIABLE TAPERED SPAN-MORPHING WING FOR AERODYNAMIC PERFORMANCE IMPROVEMENTS

Mohamed Elelwi [a], Ruxandra Mihaela Botez [a]* and Thien-My Dao [b]

[a] Department of Laboratory of Active Controls Avionics and AeroServo Elasticity
LARCASE
ÉTS - École de technologie supérieure
1100 Notre-Dame West, Montréal QC H3C 1K3 Canada

[b] Department of Research Team in Machines Dynamics Structures and Processes
ÉTS - École de technologie supérieure
1100 Notre-Dame West, Montréal QC H3C 1K3 Canada

Paper published in *Biomimetics* 2021, 6(4), 55; https://doi.org/10.3390/biomimetics 6040055

Résumé

Cet article propose l'intégration du dimensionnement structurel, de la topologie et de l'optimisation aérodynamique pour une aile déformable l'envergure variable (MVSTW) dans le but de minimiser son poids. Afin d'évaluer la faisabilité de l'optimisation du MVSTW, ce travail crée un environnement numérique en incorporant simultanément le dimensionnement structurel et l'optimisation topologique basées sur son analyse aérodynamique. Cette nouvelle approche est proposée pour un MVSTW. Une approche d'optimisation spécifique au problème pour déterminer la structure de poids minimum des composants de l'aile pour ses segments fixes et mobiles est d'abord présentée. Cette optimisation a été effectuée à l'aide du solveur OptiStruct dans HyperMesh. Cette investigation vise à minimiser la conformité totale de la structure tout en maximisant la rigidité afin de satisfaire aux exigences d'intégrité structurelle du MVSTW. La répartition de la charge aérodynamique le long de l'envergure en pleine extension et à la vitesse maximale a été prise en compte dans les processus d'optimisation. Les composants de l'aile ont été optimisés en termes de taille et de la topologie, et tous ont été conçus en alliage d'aluminium 2024-T3. Les résultats d'optimisation montrent que des

économies de poids allant jusqu'à 51,2 % et 55,7 % ont été obtenues pour les segments d'aile fixe et mobile, respectivement. En se basant sur ces résultats, l'aile morphing à envergure variable optimisée MVSTW peut parfaitement effectuer certaines missions de vol sans subir des défaillances mécaniques.

Abstract

This article proposes the integration of structural sizing, topology, and aerodynamic optimization for a morphing variable span of the tapered wing (MVSTW) with the aim to minimize its weight. In order to evaluate the feasibility of the morphing wing optimization, this work creates a numerical environment by incorporating simultaneous structural sizing and topology optimization based on its aerodynamic analysis. This novel approach is proposed for an MVSTW. A problem-specific optimization approach to determine the minimum weight structure of the wing components for its fixed and moving segments is firstly presented. The optimization was performed using the OptiStruct solver inside HyperMesh. This investigation seeks to minimize total structure compliance while maximizing stiffness in order to satisfy the structural integrity requirements of the MVSTW. The aerodynamic load distribution along the wingspan at full wingspan extension and maximum speed were considered in the optimization processes. The wing components were optimized for size and topology, and all of them were built from aluminum alloy 2024-T3. The optimization results show that weight savings of up to 51.2% and 55.7% were obtained for fixed and moving wing segments, respectively. Based on these results, the optimized variable-span morphing wing can perform certain flight missions perfectly without experiencing any mechanical failures.

5.1 Introduction

Aeronautical engineering research has made substantial progress in the past few decades due to the aviation industry requirements (Ameduri & Concilio, 2020). In global aerospace engineering centers, engineers and researchers have made extraordinary efforts to develop aircraft capable of adapting very well to various flight conditions (Concilio, Dimino, & Pecora,

2021) (Concilio et al., 2017). The optimal aircraft performance capabilities refer to multiple missions' realization under various flight conditions. The significant weight reduction obtained for robust and reliable structural aircraft configurations requires the integration of multidisciplinary design optimization approaches by use of a combination of advanced computer-aided design (CAD) with advanced computer-aided engineering (CAE) tools (Armendáriz, Millán, Encinas, & Olarrea, 2016) (Muneiah, Bhaskar, & Rajesh, 2014).

The aviation industry has invested in developing novel types of aircraft with very good performance, capable of meeting diverse flight requirements. These objectives have prompted engineers to develop new design techniques for reducing aircraft weight. Our structural optimization method to reduce aircraft weight needs to utilize topology, size, and shape optimization approaches. Hence, aircraft configurations are subjected to different constraints that must be addressed during the optimization (Rao et al., 2009) (Liu, Mulani, & Kapania, 2014). Topology optimization (TO) seeks to find the optimal distribution of materials across a certain design area under given constraints. Thus, it can determine an optimal structure by finding its optimal load, and therefore, its optimized material distribution. In the TO, when the material density of the design variables is equal to 1, these variables can be considered solid, which is critical for structural design. On the other hand, when the material density is equal to 0, they can be considered void, thereby determining the best material distribution (Zhu et al., 2016) (Mitropoulou et al., 2013).

Multiple optimization techniques have been used in a variety of engineering design domains, and their application has spread throughout the field of aerospace engineering (Michaud, Joncas, & Botez, 2013) (Krog et al., 2004). For example, several successful optimization techniques for finding the optimal structure of aircraft components are utilized in aircraft design, as seen in (Eves et al., 2009) (Rinku & Ananthasuresh, 2015).

Airbus has applied Topology optimization in the A380 aircraft design program to generate its new lighter aircraft components. The most well-known optimized components for the Airbus A380 are the leading-edge ribs and the fuselage door intercostals, which led to weight savings

of approximately 1000 kg for each aircraft (Grihon et al., 2004). The Boeing Company took a similar approach when designing the wings' leading-edge ribs for the B-787 Dreamliner. Topology optimization was incorporated with sizing and shape optimization to find the optimal wing leading-edge shape in the design process. As a result, the leading-edge ribs' weight of the B-787 was reduced by 24 45% compared to the B-777 aircraft (Q. Wang et al., 2011) (James et al., 2014).

Oktay et al. (E. Oktay et al., 2011) (Erdal Oktay et al., 2014) conducted research by combining the results from Computational Fluid Dynamics (CFD) analysis with the Computational Solid Mechanics (CSM) results obtained from Topology optimization. They investigated the aerodynamic load on wing lifting surfaces and used a Solid Isotropic Material with the Penalization (SIMP) topology optimization method to determine a wing's optimal material distribution.

The Finite Element Method (FEM) and topology optimization (TO) have been linked with computer-aided engineering (CAE), and they are now considered the most advanced tools and methodologies in the aircraft design field. The combination of the FEM with TO makes it possible to obtain major weight reductions, thus resulting in material and fuel savings while maintaining the final product's robustness properties (Tang et al., 2013) (Gawel et al., 2017). Furthermore, optimization methods based on merging CFD with CSM allow the determination of the optimal wing shape, which could decrease the aircraft's weight by obtaining its optimal aerodynamic performance (Morlier & Charlotte, 2012).

The LARCASE laboratory at ÉTS presented a wide range of research activities in the multidisciplinary fields of aeroservoelasticity. Some of these studies were applied to unmanned aerial systems (UAS). The LARCASE team developed sophisticated methodologies for predicting the aerodynamic behavior and performance of the unmanned aerial systems UAS-S4 and UAS-S45 of Hydra Technologies (R. M. Botez, 2018) (Kuitche, Botez, Viso, Maunand, & Moyao, 2020) (Kuitche, Botez, Guillemin, & Communier, 2020). This work concentrated on the structural analysis and optimization of unmanned aerial systems UAS-S4 and UAS-S45

based on CFD optimization results (aerodynamic performance, viscous damping, and oscillations) (Y. Tondji & Botez, 2017) (C. Liauzun, Daniel Mortchéléwicz, & Lepage, 2019). The aerodynamic lift distribution over a wing's entire surface was calculated using a numerical analysis based on the XFLR5 code results (Communier, Salinas, Carranza Moyao, & Botez, 2015). This wing was designed based on the variable-span morphing of the tapered wing (VSMTW) concept (M. Elelwi et al., 2020). The optimization was implemented for the morphing wing, and it was developed based on the results of the preceding optimization process (Michaud et al., 2013). The topology optimization technique was used to determine the optimal positions of the wing components (M. Elelwi, Calvet, Botez, & Dao, 2021). The optimization approach evaluated the efficiency of selecting candidate materials inside wing components, such as spars, ribs, and stringers, for high weight savings. Mechanical constraints impacted material characteristics, such as their overall strength, hardness, and robustness. TO established the optimal structural configuration with the highest reduction in its structural weight (L. Zhao et al., 2019). The optimized components of the wing must comply with the maximum rigidity of the structural wing configuration (Y.-b. Zhao et al., 2017).

The first part of this investigation deals with allocating the best locations of wing components inside the VSMTW, based on the results of our TO methodology (M. Elelwi et al., 2021). TO was applied based on the aerodynamic performance results obtained at the full wingspan extension and the maximum speed (68 m/s); a safety factor and a 3 g load factor were considered. TO also suggested incorporating two spars, seven ribs, and several other support elements on the fixed and the moving segments with the aim to decrease the solid wing weights of fixed and moving segments for the optimized morphing wing from 112 kg to 16.3 kg and from 45 kg to 10.3 kg, respectively. The Finite Element Analyses (FEA) were then executed, and their results indicated that the optimized VSMTW fulfilled the required mechanical properties such as linear elasticity and structural wing integrity. Thus, the optimized wing will withstand structural failure under extreme flight conditions.

5.2 Parametric Layout of the Optimized VSMTW

Global aerospace and aviation centers have conducted a high number of studies, which demonstrated the wing shape modification benefits. Our initial investigation dealt with calculating wing aerodynamic performance by utilizing Computational Fluid Dynamics (CFD). That work proved that the wing area's increase using its span morphing technique led to increased aerodynamic performance, with its associated fuel consumption savings and expanded flight envelope range (Kammegne, Botez, Grigorie, Manou, & Mebarki, 2016). Furthermore, instead of using conventional control surfaces, the asymmetric wingspan mechanism was used as a roll control system (M. Elelwi et al., 2020). However, the main obstacle that design engineers must overcome is the structural wing weight penalty. Structural optimization is the most efficient method for reducing structural weight without compromising the wing's structural integrity and its strength properties.

An optimized baseline wing was designed based on the TO results and subsequently examined using Finite Element Analysis. Based on several test cases, this optimized wing demonstrated excellent mechanical behavior and reliable structural integrity for given boundary conditions (M. Elelwi et al., 2021).

5.2.1 Wing Design Configurations

A baseline wing was designed using the telescopic mechanism and the variable-span morphing wing theory based on the aerodynamic optimization results (M. Elelwi et al., 2020). The wing was divided into two sections, including moving and fixed segments, as shown in Figure 5.1. The CATIA V5 software was utilized to design the variable-span morphing wing.

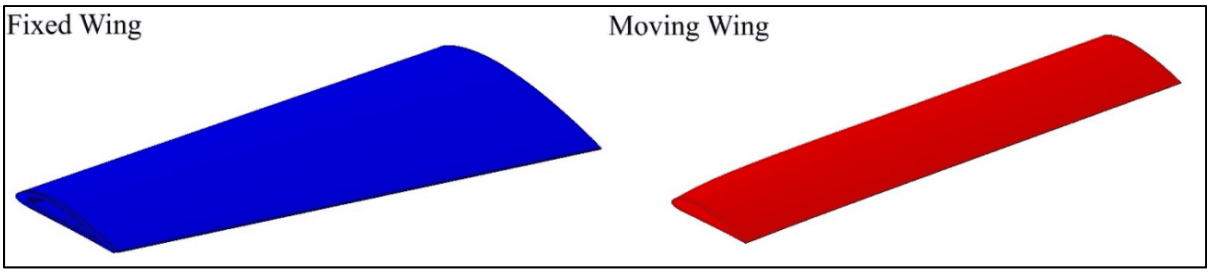

Figure 5.1 The initial geometrical shape of a variable-span morphing wing; fixed segment and moving segment

The topology optimization method was performed in order to effectively allocate the internal structural elements inside both segments. The data and boundary conditions were computed at sea level altitude and maximum speed. Moreover, a safety factor of 1.5 and a 3 g load factor was added to the designed wing to overcome the various flight conditions. TO found that both segments must have two spars, with an optimal distance between them of 351.559 mm for the fixed segment and 163.379 mm for the moving segment. TO also suggested seven ribs; the new configurations of spars and ribs are therefore illustrated in Figure 5.2.

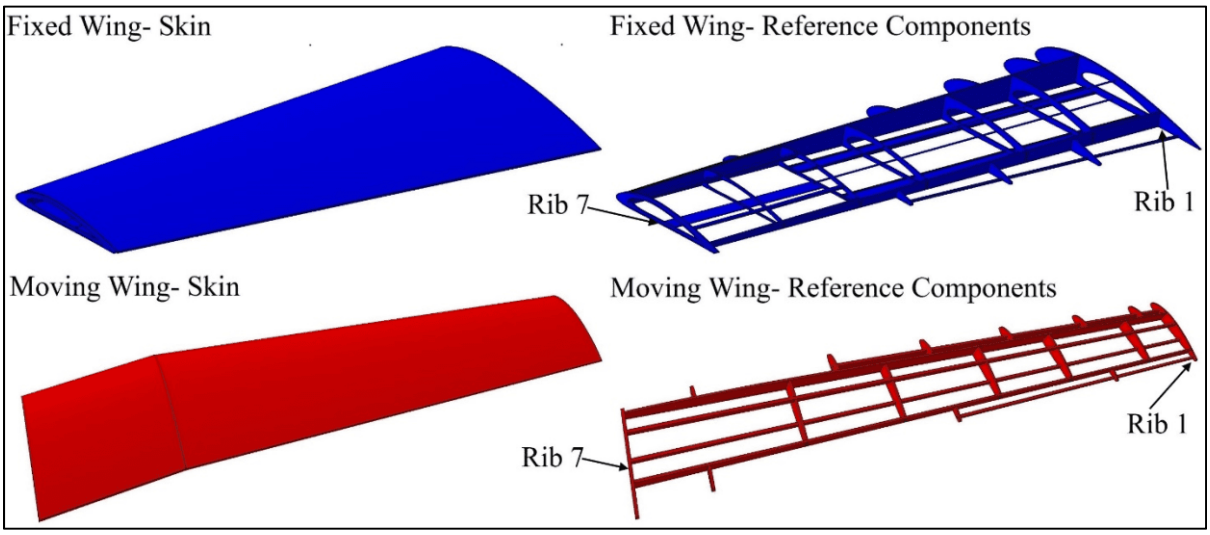

Figure 5.2 Geometrical model configuration of fixed and moving segments with their components, according to topology optimization

The ribs are situated in both segments in accordance with the topology optimization results from analyzing solid wing segments at the proposed locations, as listed in Table 5.1:

Table 5.1 Proposed locations of wing ribs for fixed and moving segments; these locations are measured with respect to the reference rib

Rib No.	Fixed Wing	Moving Wing
1.	0 mm Reference	0 mm Reference
2.	269 mm	245 mm
3.	534 mm	626 mm
4.	932 mm	919 mm
5.	1198 mm	1234 mm
6.	1503 mm	1502 mm
7.	1800 mm	1875mm

5.2.2 Material Choice

The aluminum alloy 2024-T3 was selected for the first topology optimization process. This investigation chose the same material to continue the optimization process with the aim to reduce wing component weight. The aluminum alloy 2024-T3 is an isotropic material with good durability and mechanical properties combined with high strength and resistance to fatigue. This material is commonly employed in the design of aircraft components. The aluminum alloy 2024-T3 material properties are represented in Table 5.2.

Table 5.2 Wing aluminum alloy 2024-T3 material properties

Physical and Mechanical Properties	
Density	2780 kg/m^3
Ultimate Tensile Strength	483 MPa
Tensile Yield Strength	345 MPa
Modulus of Elasticity	73,100 MPa
Poisson's Ratio	0.33
Fatigue Strength	138 MPa
Shear Modulus	28,000 MPa
Shear Strength	283 MPa

5.3 Load Cases

This section assesses the lift distribution along the wingspan. First, the VSMTW was divided into sections with the aim to estimate the flow circulation distribution G(y). For this reason, CFD Fluent code was combined with XFLR5 software results to evaluate the lift distribution

along the VSMTW. Finally, the aerodynamic loads along the wing were measured using the lifting line theory, as illustrated in Figure 5.3.

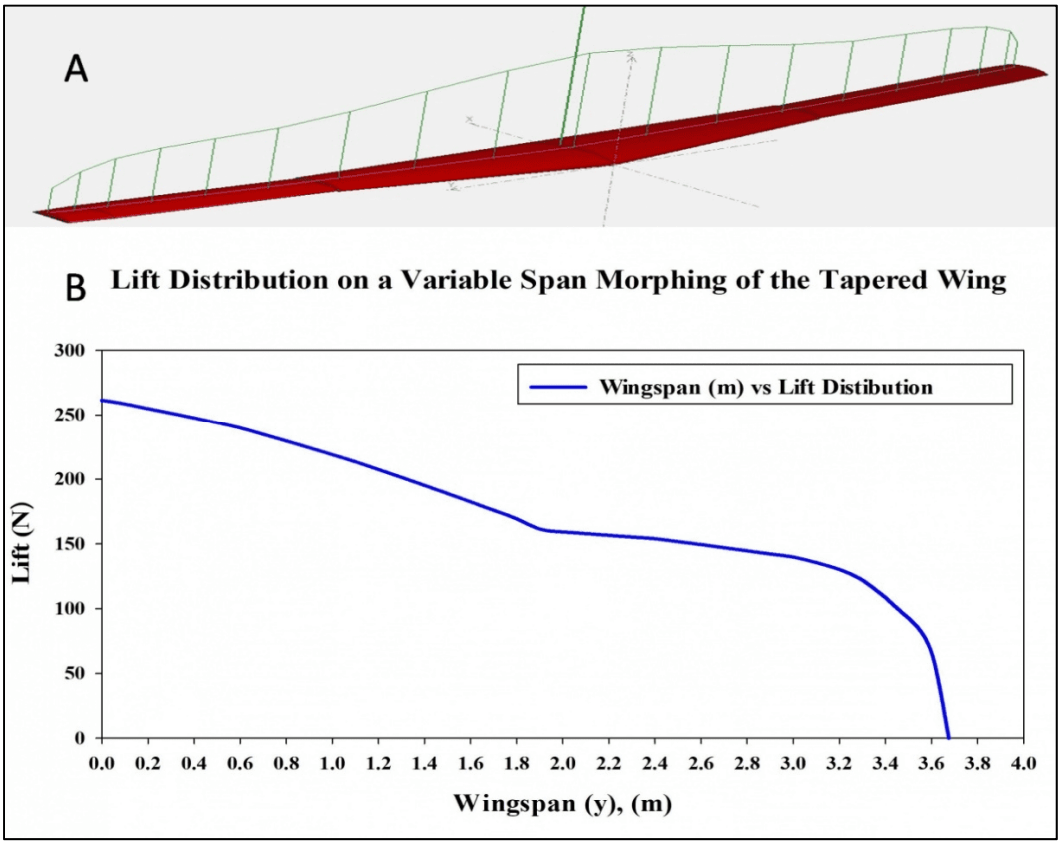

Figure 5.3 Lift distributions for the VSMTW along the wingspan by using (A) Fluent XFLR5 code, and (B) the chart of lift forces distribution along wingspan length

The Kutta–Joukowski theorem was applied to estimate the flow circulation distribution along the span of the VSMTW by use of the following equation (Q. Zhang & Liu, 2017) (Gross, Fasel, & Gaster, 2015):

$$\Gamma_{(y)} = \Gamma_0 \left(1 - \left(\frac{2y}{b}\right)^2\right)^{1/2} \tag{5.1}$$

where $\Gamma_{(y)}$ is the flow circulation distribution calculated at any arbitrary location along the wingspan. $\Gamma_{(y)}$ is maximum when y = 0 and tends towards zero when y = ±b/2. Hence, the circulation at the wing mid-span Γ_0 can be obtained according to:

$$\Gamma_0 = \frac{4L}{\rho V b \pi} \tag{5.2}$$

and thus, the lift distribution which acts on each wing segment was obtained using the following equation:

$$L_{(y)} = \rho V \Gamma_{(y)} \tag{5.3}$$

After establishing the number and position of wing components for the VSMTW, the number of spars and ribs was determined based on the first topology optimization process. The Prandtl lifting-line theory was found to be the most efficient approach, as it allowed the lift to be distributed appropriately over the whole wingspan. The main parameters of the wingspan and its ribs were then determined. The first topology optimization suggested the use of seven ribs inside the moving wing segment and fixed wing segment at the proposed locations, as shown in Figure 2. The VSMTW was divided into 11 sections based on the rib locations at the full wing extension (75%) of its original length, as illustrated in Figure 5.4.

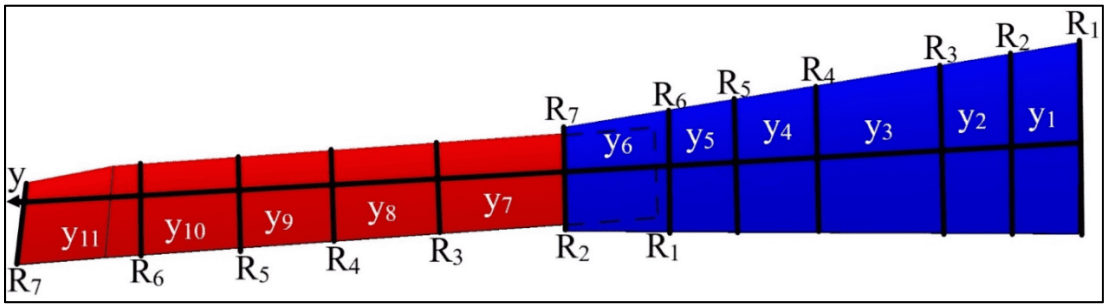

Figure 5.4 Generic planform wing with its span sections (y_n)and chord numbers for the VSMTW

A safety factor of 1.5 and a 3 g load factor were also included in the modeling of the wing structural components. A safety factor of 1.5 was selected in accordance with the FAA regulations (FAR 25.303). According to these regulations, aircraft structures must withstand static loads, which were determined in this paper by their corresponding aerodynamic pressures without causing any structural damage or failure. The fixed wing ribs were evaluated using the average values of lift loads calculated for the fixed segment. The same approach was chosen for the moving segment, with its load's values listed in Table 5.3.

Table 5.3 Loads calculated for each section of a VSMTW

Section Number	Lift Load (N)	Ultimate Load
y_1	257.36	1158.1
y_2	243.77	1096.97
y_3	232.15	1044.65
y_4	213.325	959.96
y_5	198.29	892.28
y_6	175.96	791.8
y_7	158.62	713.77
y_8	152.7	687.15
y_9	147.12	662.04
y_{10}	134.61	605.75
y_{11}	79.11	355.995

5.4 Optimization Mathematical Model

The combination of sizing and topology optimization (STO) is a powerful approach for reducing structural configuration weight while maintaining its overall stiffness and structural integrity (Jensen, 2018) (Raheel & Toropov, 2018). Furthermore, the sizing and topology optimization tools can be integrated into multiple-computer-aided engineering software. In this investigation, STO was performed based on the integration of the Finite Element Method (FEM) into an optimization solver.

This study's main objective is the determination of the most efficient solution for producing lightweight components of a variable morphing wing while maintaining their optimal mechanical properties. Therefore, the STO results were obtained for ribs, spars, and support

elements for each segment and then were tested for the validation of their mechanical properties (displacements and stresses).

5.4.1 Topology Optimization Methodology

Topology optimization is a mathematical method used to formulate and then to determine an optimum distribution of a material within a pre-defined design space. An optimized structural material configuration within a design domain can be obtained by considering its specific boundary conditions and constraints. The structural design fundamental materials are treated as solid, whereas null materials are regarded as void. Hence, the unnecessary structural weight can be eliminated. A commercial topology optimization application, Atair's OptiStruct, is used in this investigation to manage the given design constraints by defining the objective functions for individual load cases. This application was designed to manage the constraints with the aim to ensure that design specifications were satisfied; therefore, in this paper, essential materials of the design are established, and the process to eliminate redundant elements is defined. Minimizing the compliance while maximizing the structural stiffness under specific design constraints can indeed meet the design requirements.

As mentioned above, the TO used in this study is combined with Finite Element Analysis (FEA), while the density-based approach is conducted. The design loads and parameters are applied to the wing components in order to deal with the material density distribution and its other mechanical properties (displacement, stresses, etc.).

TO is based on the Solid Isotropic Material with Penalization (SIMP) method. The design domain is optimized by minimizing the objective function, which refers to structural compliance. The objective function variable is the material density that defines whether a finite element is solid or void. The pseudo-density, x_i, of the i^{th} element may take values between 0 and 1, or x_i $(0 \leq \mathrm{xi} \leq 1)$, wherein the 0 value represents a material as void, and the 1 value represents the material as solid. The pseudo-density variable can be defined with the following equation:

$$x_i = \frac{\rho_i}{\rho_0} \tag{5.4}$$

where ρ_i is the density of the i^{th} element, ρ_0 is the density of the base element, and x_i is the pseudo-density of the i^{th} element.

The formulation of the SIMP method defines the relationship between the material pseudo-density variable and its stiffness properties, as follows (Gunwant & Misra, 2012):

$$E_{(x_i)} = E_{solid}(x_i)^p \tag{5.5}$$

where E_{solid} denotes the base material's isotropic property and p is the exponent of the penalty parameter. Equation (5.5) can then be expanded using the young modulus for solid and void regions:

$$E_{(x_i)} = E_{void} + {x_i}^p(E_{solid} + E_{void}) \qquad p \geq 1 \tag{5.6}$$

where E_{void} is the low Young's modulus assigned to void regions, E_{solid} is Young's modulus assigned to solid regions, and $E_{(x_i)}$ is Young's modulus assigned to each element.

The penalty factor value, p, should be selected to be large enough ($p \geq 3$ is generally considered) so that the volume constraint is active when the intermediate densities are penalized. Since the intermediate densities are close to 0, the material is unnecessary and may be therefore considered void. Contrarily, if the intermediate densities are close to 1, the material is critical to the structure's integrity and can be considered solid (Aage et al., 2017).

The volume fraction is a constraint to the total volume of the design domain related to the pseudo-density, as represented in the following equation:

$$V = \sum_{i=1}^{n} x_i V_i \tag{5.7}$$

where V denotes the total volume and V_i expresses the volume of the i^{th} element.

The objective function of the TO is to minimize the structural compliance that is subjected to the design constraints and can be defined with the following mathematical statement:

$$\begin{aligned} \min_x : \quad & c(x) = U^T K U = \sum_{e=1}^{N} (x_i)^P u_e^T k_0 u_e \\ \text{subject to: } & \frac{V(x)}{V_0} = f \\ & : KU = F \\ & : 0 < x_{min} \leq x_i \leq 1 \end{aligned} \tag{5.8}$$

in which the design variable vector, x, in the formulation $c(x)$ presents the volume fraction $\frac{V(x)}{V_0} = f$, where f is the load vector, V_0 is the initial volume, and V is the final volume. K is the global stiffness matrix, and U is the global displacement, such that KU equals F, the force vector. In addition, u_e represents the displacement vector, and k_0 is the elemental stiffness matrix.

The shape of the density filter is selected as defined by Sigmund (M. P. Bendsøe & Sigmund, 1999) (Höke & Bozca, 2020). The filtration is defined for the physical relative density by $\widetilde{x_i}$ and can be demonstrated using the following equation:

$$\widetilde{x_i} = \frac{\sum_{j \in \mathbb{N}_e} w(r_i) v_j \tilde{x}_j}{\sum_{j \in \mathbb{N}_e} w(r_i) v_j} \tag{5.9}$$

where $N_e = \{i \,|\, \|r_i - r_e\| \leq R\}$ denotes a neighborhood set defined by the filter radius, R. The filter radii around the centers of elements i and e are denoted by r_i and r_e, respectively. The

weighting function is $w(r_i, r_e) = R - \|r_i - r_e\|$ and the volume of the i^{th} element is v_i (M. P. Bendsøe & Sigmund, 1999).

In this study, the major objective is to minimize each component's weight within the optimized span morphing wing. TO ensures the lightest possible wing weight by maximizing its static stiffness. Therefore, minimizing compliance is a means to increase the structural stiffness subjected to the set load. The compliance optimization can be expressed as follows (Aage et al., 2017):

$$C = \int_V fudV + \int_S tudS + \sum_i^n F_i u_i \tag{5.10}$$

where V denotes the volume of the continuum, f is the distributed body force, u is the displacement area, t is the traction force, Fi represents the point load on the i^{th} node, u_i is the i^{th} displacement degree of freedom, and S is the surface area of the continuum.

5.4.2 Formulation of the Stiffness and Topology Optimization Problem

The static stiffness can be obtained by applying static loading to wing components (for both segments). The deformation value under a static load refers to the mechanical displacement resistance (Bakhtiarinejad, 2015). The stiffness can be calculated based on the displacement, as follows:

$$\mathrm{K}(x)u = F \tag{5.11}$$

where F is the nodal forces vector, and u is the nodal displacement. The nodal displacement can then be found with the following equation:

$$u(x) = K(x)^{-1}F \tag{5.12}$$

As already mentioned, the main objective of the structural TO of the morphing wing design problem is to maximize the wing's stiffness while minimizing its weight. The density-based approach is coupled with the static linear method (Daynes, Feih, Lu, & Wei, 2017) so that the TO problem can be formulated mathematically as follows:

$$\begin{gathered} \min f(x) = f(x_1, x_2, \dots\dots, x_n) \\ g_j(x) \leq 0, \quad j = 1, \dots\dots, m \\ x_{i_{min}} \leq x_i \leq x_{i_{max}} \quad i = 1, \dots\dots, n \end{gathered} \tag{5.13}$$

where $f(x)$ represents the objective function, $g(x)$ denotes the constraints, x are the design variables, which are considered as independent variables of the $f(x)$, and x_{min} and x_{max} are the upper and lower bound constraints, respectively.

The TO algorithm coordinates the distribution of the material throughout the design domain by optimizing the user-defined objective function under certain constraints. In this study, each wing component's design space for both segments was defined as a separate element in the optimization process.

The gradient-based optimization method is widely utilized, as it is recognized as a very efficient method. The constraints' screening process was applied to compute the set constraints, thereby minimizing the required gradients.

The compliance of the static structural stiffness is completely transformed into potential deformation energy (Mou, He, Zhao, & Chau, 2017). The static structural stiffness can be calculated using Finite Element Analysis (FEA). The TO solver OptiStruct uses algorithms to set up the optimal material distribution inside the design domain in order to achieve the optimal wing geometrical shape. Then, it computes the design structure that offers the optimum solution under given boundary conditions by minimizing the wing components' compliance while respecting the design constraints to decrease their weights. The optimum solution is reached when the solution convergence is obtained in an iterative approach.

5.5 Wing Component Structure Design Optimization Process

This investigation's primary goal is to design a robust structure by reducing the weight of a variable-span morphing tapered wing (VSMTW). The main challenge is to combine the strength with the lightweight properties of the wing. The objective is to maximize the stiffness by optimizing the material distribution within the wing components' volume space. Many factors must be considered in the optimization process, including the computational area, mesh generation, and boundary condition settings. For more accurate and reliable results, the pressure was calculated separately for each wing component. The optimization settings of the wing components were found as described in the following sub-sections (Vasista et al., 2016).

5.5.1 Wing Skin Thickness Size Optimization

A baseline wing for both segments had a skin thickness of 2 mm for its optimization process. Size optimization (SO) was conducted in a 2D environment, and then the results were extended to a 3D environment, and they were further chosen to design the best possible wing skin (Coroian & Lupea, 2013). In fact, it is known that SO is an iterative process. Wing skin optimization was performed using the aerodynamic loads calculated with the CFD solver and the XFLR5 code at the maximum speed and full wingspan extension. A 20 mm tetra quadrilateral element size meshing was applied on both segments, as shown in Figure 5.5.

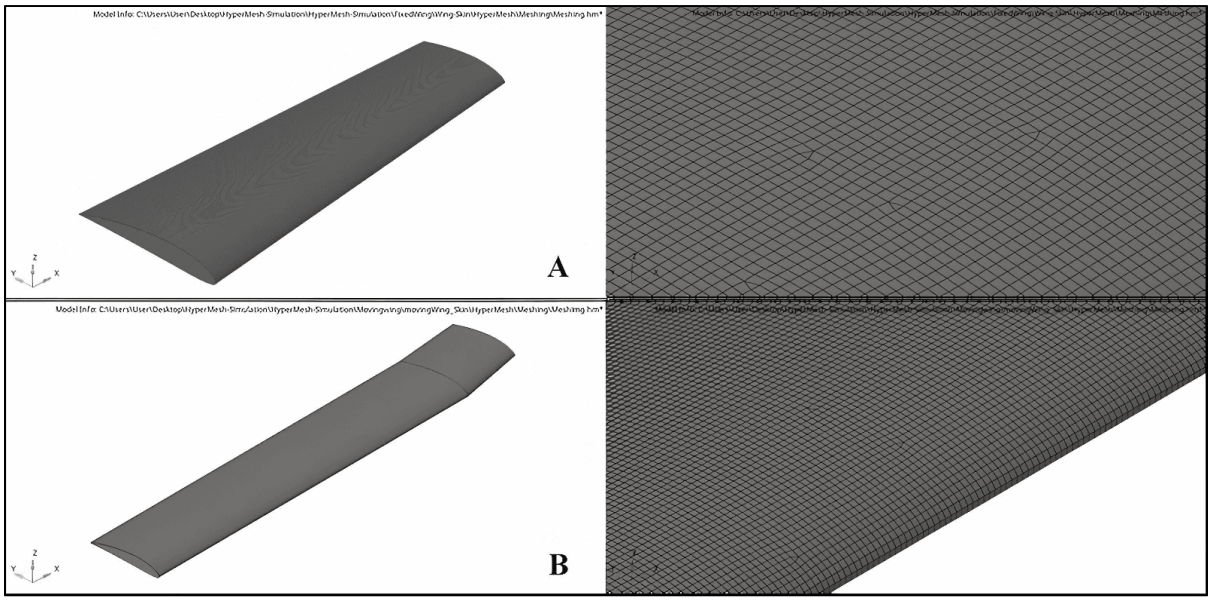

Figure 5.5 Finite Element for (A) fixed wing and (B) moving wing

The aerodynamic loads were applied, and the design variables were considered scalar parameters. These parameters were defined for the optimization problem in this investigation because of the fact that the wing skin thickness influences the system responses. The optimization responses were defined for two variables, which were the design volume and the selected stress. The objective function concerned the minimization of the structural mass of the wing skin. The design constraints were determined in this investigation as the lower and upper bounds of the maximum stress values, which was less than 200 MPa due to the stress response based on the design variable. The design variable was defined with an initial value of 2 mm, with a lower bound of 0.5 mm and an upper bound of 2 mm (Rinku & Ananthasuresh, 2015) (Girennavar, Soumya, Subodh, Heraje, & PY, 2017). The optimization problem was formulated as follows:

$$\begin{gathered} \min M \\ \sigma_{max} = 200 \text{ MPa} \\ 0.5 \leq T \leq 2 \end{gathered} \tag{5.14}$$

5.5.2 Spar Structure Topology Optimization

The spar is one of the most important wing components, as it can support the heaviest aerodynamic loads affecting the aircraft wing. A spar is designed as an extended beam along the wingspan, which supports the wing submitted to the bending load. Thus, it should withstand the impacts of shear, tensile, and compressive loads. In our project, the previous TO of baseline solid wings design suggested the use of two spars for each wing segment at defined locations, as shown in Figure 5.6 (M. Elelwi et al., 2021). The aerodynamic loads were calculated with the ANSYS and XFLR5 software, where the spars were modeled as beams with discrete loads at different locations (their values are presented in Table 5.3).

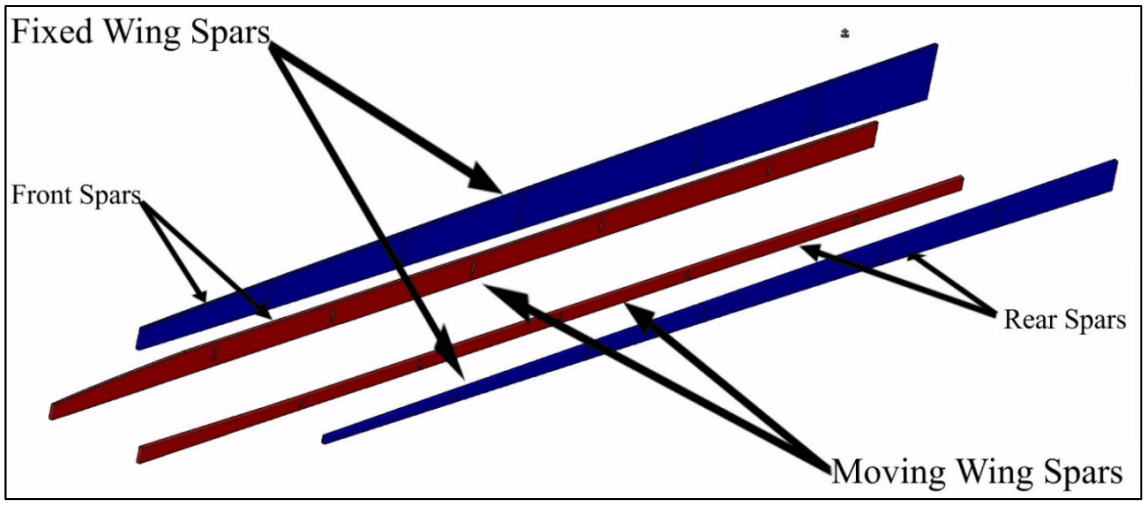

Figure 5.6 Baseline geometry shape for morphing wing spars for fixed and moving segments at their original position on the wing

The structural weight was considered in the problem formulation for the wing spars, as the main aim of our design was to find the optimal wing structural parameters. This objective was used to determine the minimum wing weight while satisfying its strength, durability, and versatility constraints (Zhu et al., 2016).

The I-beam section was selected for modeling the wing spars (except at their connecting points with the ribs) because it provided high mechanical advantages compared to other beam section

shapes. The I-beam shapes bear higher loads than the other beam section shapes, supported very well the other wing components, withstood mechanical fatigue (such as torsions and deformations), reduced the load intensity on the other wing components, and led to low costs and weight (Grbović, Kastratović, Sedmak, Balać, & Popović, 2019) (Grisval & Liauzun, 1999).

TO is an iterative process needed to reach the optimized system's best-converged solution based on the objective function and certain design constraints. In a 3D environment, all wing spars are subjected to the same analyses procedures (C. Li, Kim, & Jeswiet, 2015). As the selected loads are proportional to the wing spar length, the objective function includes both the designable region, as well as the flange and the attachment areas used to link the ribs inside the spars, which is considered a non-designable region. The non-designable regions were fixed during the optimization process as they were excluded from the design domain. Figure 5.7 illustrates the determined designable and non-designable regions of the front wing spar by creating various areas and thus leading to more feasible optimizations (Bashir, Longtin-Martel, Botez, & Wong, 2021). The spars meshed into uniform tetrahedrons with elements of 3 mm thickness; the uniform grids were needed to reduce the computation errors.

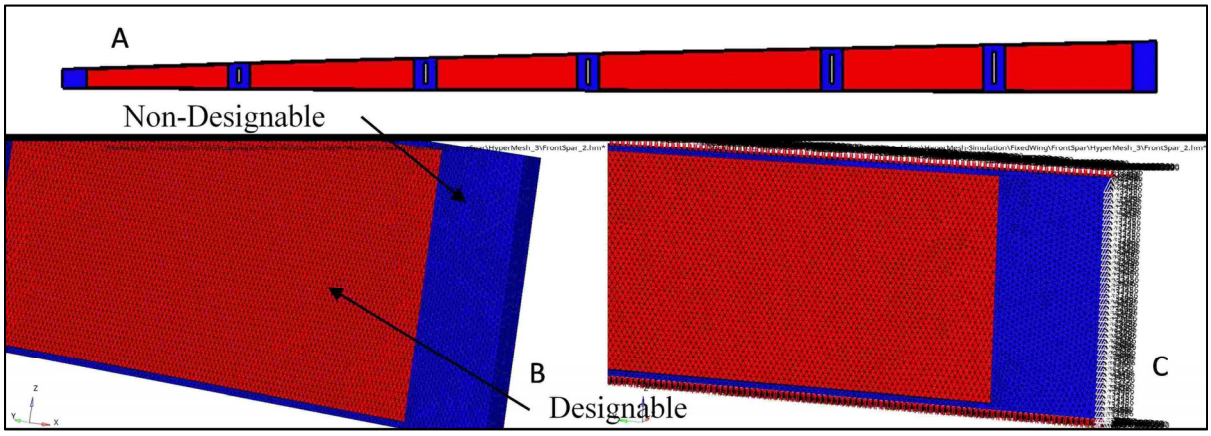

Figure 5.7 An example of the meshing and boundary conditions for the front spar - fixed wing. (A) Front spar for a fixed wing, (B) The meshing and the designable and non-designable areas of the front spar and (C) The boundary conditions of the front spar

5.5.3 Rib Structure Topology Optimization

The baseline TO proposes seven ribs for both wing segments, as shown in Figure 5.8, with approximate distances between ribs inside the wings (M. Elelwi et al., 2021). These ribs are used to minimize the wing deformation by maintaining its segment's geometrical structure. Thus, the external loads are evenly distributed on the wing skin. Fixed wing ribs should be designed with a cavity, as they house their moving segment, as illustrated in Figure 5.8. Therefore, the TO was implemented on the inner six ribs for both segments. The external ribs were not considered for the fixed and moving wing segments within the design optimization region, as the fixed wing's last rib should only contain the cavity for the moving wing segment. Additionally, the ribs of the moving wing segment should have a closed geometrical shape.

The optimum material distribution inside the ribs was determined by the original design space configuration and the boundary conditions. A uniform tetrahedron mesh with elements of 3 mm in size was generated for the wing ribs for the two segments in order to implement TO. Both wing ribs were discretized into various elements, and their node numbers were based on their rib's sizes.

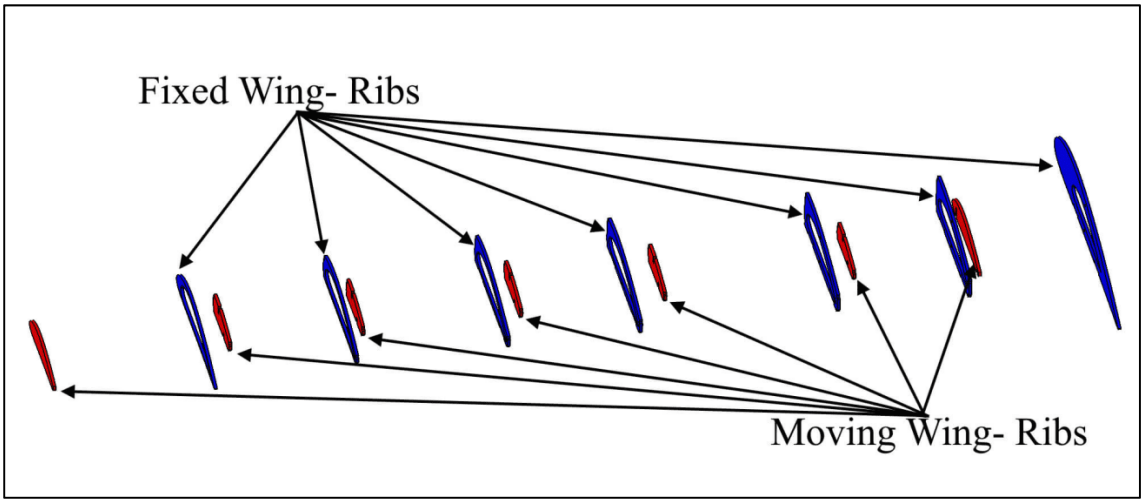

Figure 5.8 Baseline geometrical shape for morphing wing spars for fixed and moving segments at the original position

Figure 5.9 shows the meshing and its boundary conditions of the ribs for the fixed wing. A volume constraint was applied to all wing ribs in the optimization problem by its consideration as an opposite constraint. The aerodynamic analysis (see Table 5.3) can define the loads for each rib. The objective function was extended to the designable region and the rib edge. The link spots connecting the ribs inside the spars were considered as a non-designable region. The non-designable regions at the link spots with spars were stabilized during the optimization process, as they were excluded from the design domain.

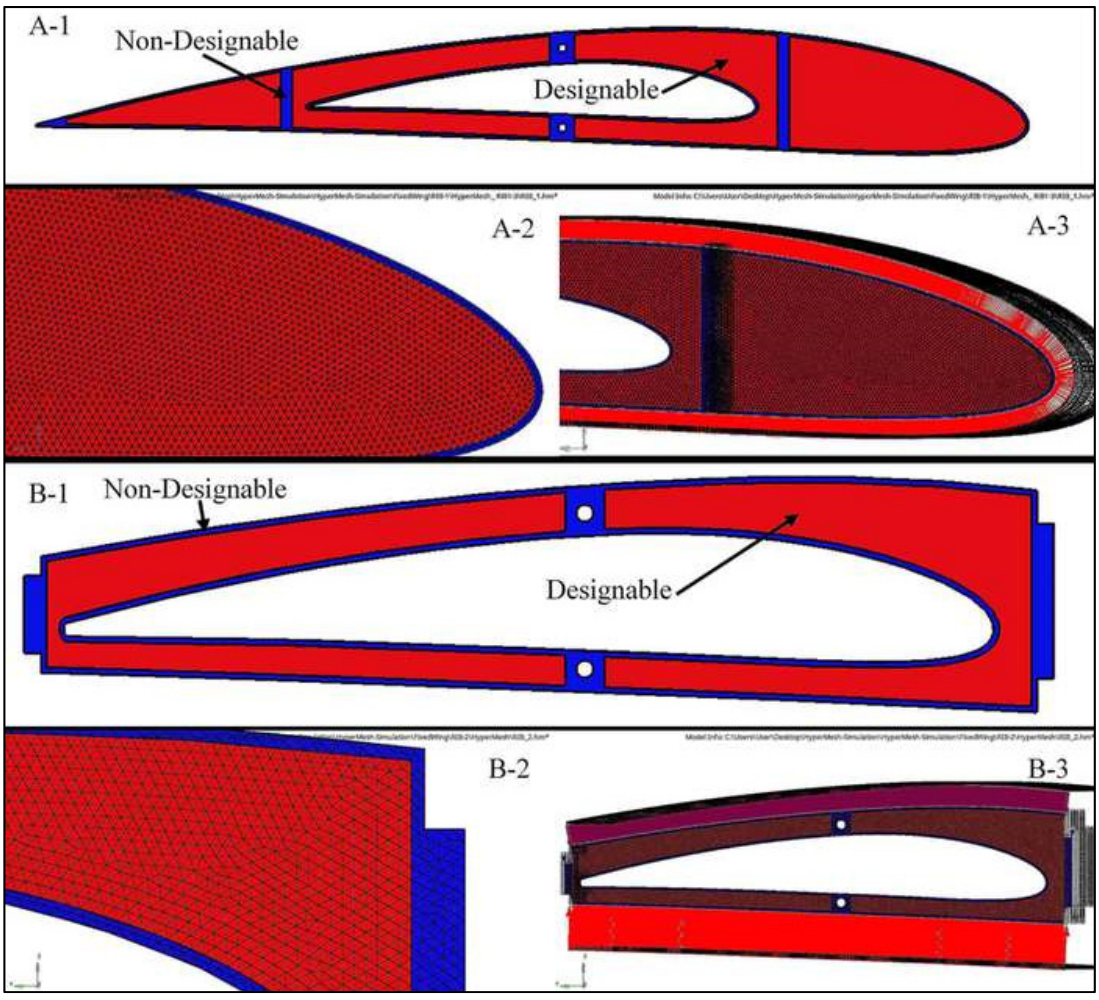

Figure 5.9 Geometry, meshing and boundary conditions for the ribs 1 and 2—fixed wing as an example. (A-, B-1) Geometry for ribs 1 and 2 and the designable and non-designable areas for a fixed wing; (A-, B-2) ribs 1-2 meshing; and (A-, B-3) Boundary conditions of the ribs (1-2.)

5.5.4 Topology Optimization (TO) of the Support Element's Structure

The initial design of the wing support elements, including its leading-edge ribs, trailing edge ribs, stringers, and stiffeners for the optimized wing based on the TO method were designed. The support elements of both wing segments were designed as shear webs to be stabilized against buckling loading, bending loading, torsion loading, and vertical shear loading. Other loads besides the aerodynamic loads and inertial loads applied to the wings can be considered in the design process according to their shapes and structural masses. In addition, the payload, expressed by electronic devices or surveillance cameras, can be carried on the wings and/or on the fuselage. This extra equipment adds more weight, thus contributing to the existing bending, shear, and torsion loads of the wing.

The shear web structure of wing components provides a reliable design by enabling them to carry loads on the wing in different directions. The support elements' structure for both segments of a VSMTW is shown in Figure 5.10.

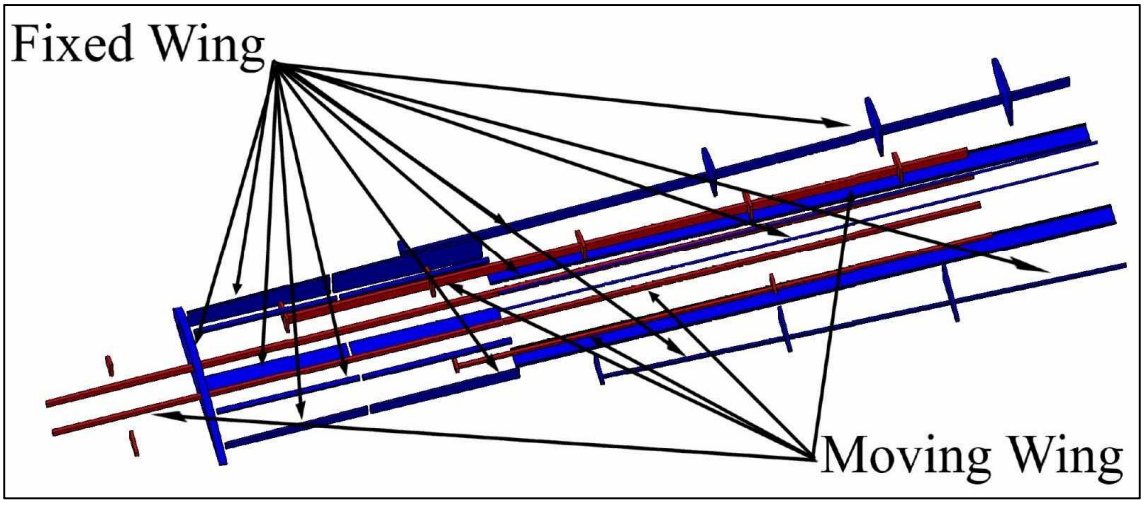

Figure 5.10 Support elements for fixed and moving wings at their original positions

The current meshing and boundary conditions of support wing elements were similar to those of the spars and ribs. The layout of the support elements' structure of the wing, the geometry

of the mesh model, and its boundary conditions were established based on parametric data obtained from the aerodynamic investigation, as listed in Table 5.3. Since the support elements' weight contributes significantly to the total weight of the wing, it is important to reduce it while maintaining the wing stiffness. The rigid meshes of the support elements for both segments were designed by applying the TO using uniform tetrahedrons with their element's sizes of 3 mm.

The number of meshing elements and nodes differs for each component, depending on its dimensions. Figures 5.11 and 5.12 illustrate some support components' meshing and boundary conditions for a fixed wing and a moving wing, respectively. A volume constraint was applied to the entire support element and served as an opposing constraint in the optimization problem.

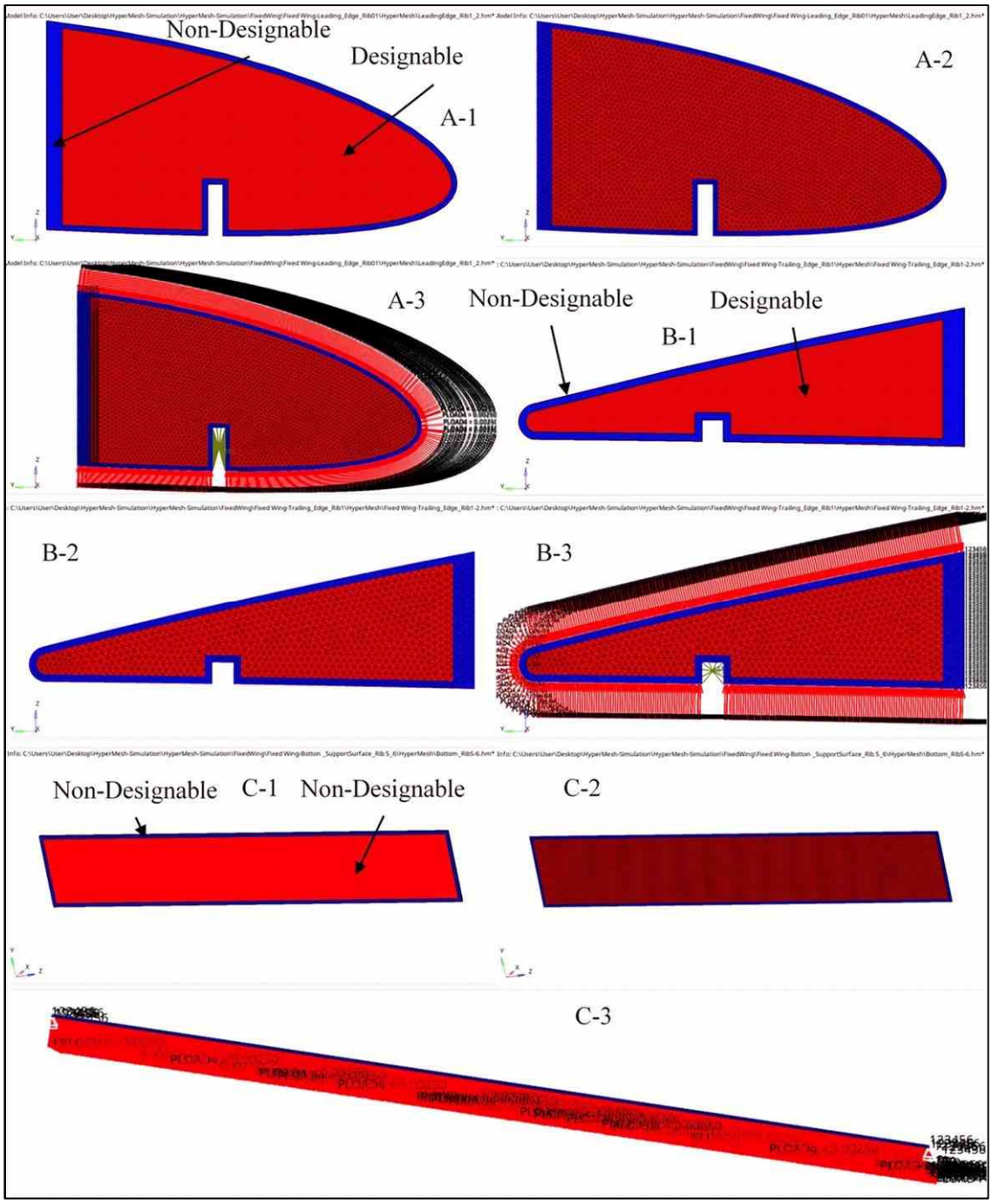

Figure 5.11 Examples of A - geometry, B - meshing and C - boundary condition for support elements (leading-edge rib 1, rib 2, and bottom support lamina between ribs 5 and 6). (A-, B-, C-1) Geometry for support elements and the designable and non-designable areas for a fixed wing; (A-, B-, C-2) -Support elements meshing; and (A-, B-, C-3) Boundary conditions of the Support elements.)

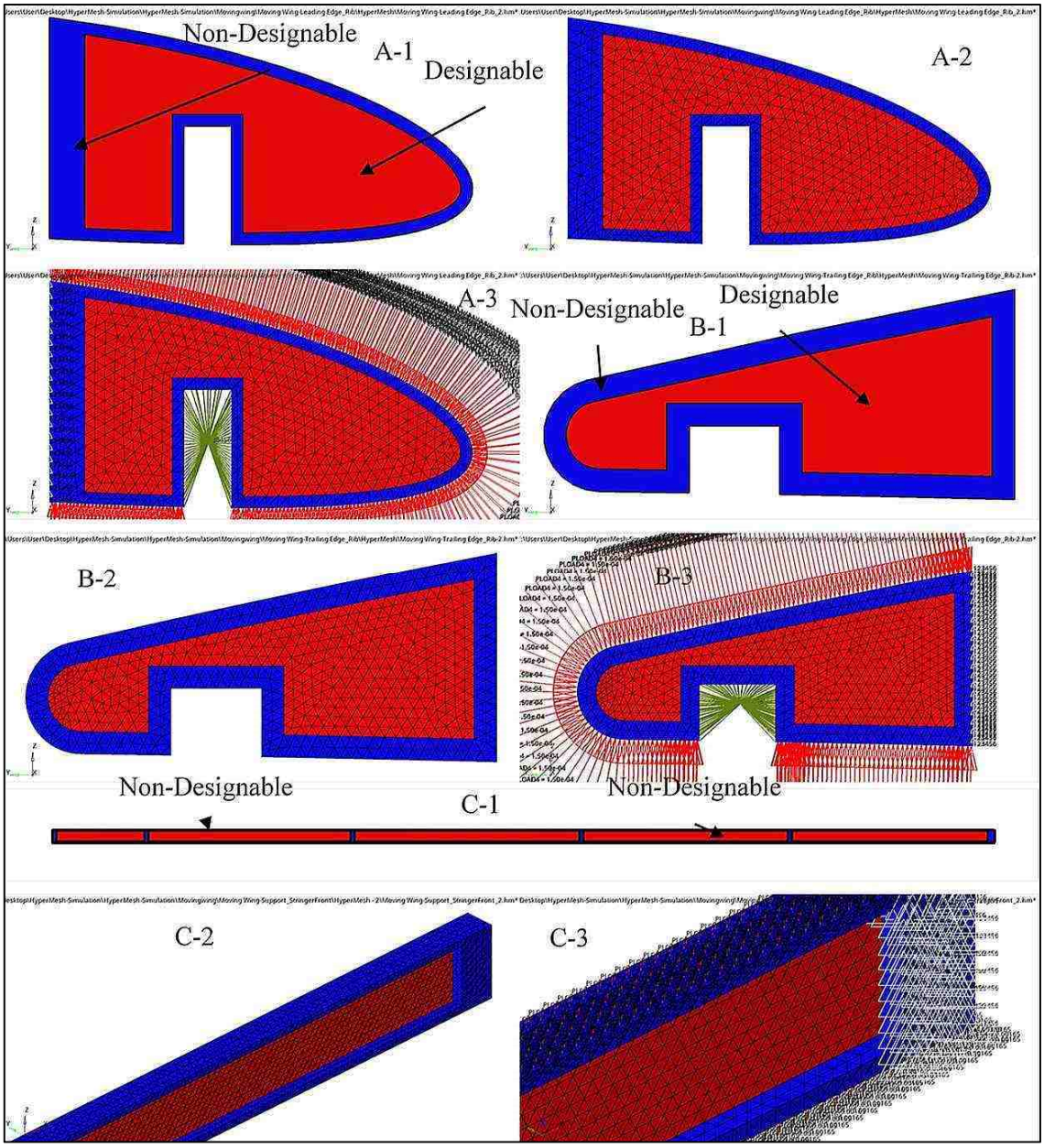

Figure 5.12 Examples of A - geometry, B - meshing and C - boundary conditions for support elements (leading-edge rib 1, trailing edge rib 2, and support stringer front). (A-, B-, C-1) Geometry for some support elements and the designable and non-designable areas for a moving wing; (A-, B-, C- 2) support elements meshing; and (A-, B-, C-3) Boundary conditions of the support elements.)

The attached area between wing components cannot change from its initial design. Therefore, the edges of the support element components and the loci binding to other wing components were considered as non-designable areas. Since there are various places where links must be

made to connect the wing components, such as spars and ribs, these components were defined with fixed areas during the TO. They represent the bonding with other wing components, and thus they can be altered throughout the optimization.

5.6 Results and Discussion

As described in the previous sections, aerodynamic analysis and optimization were conducted on the VSMTW for the UAS-S4 under different flight conditions (Bashir et al., 2021). Thus, their results were then integrated into the optimization problem. This optimization problem considered the parameters that characterized a structure's overall performance.

All these parameters were considered as either optimization objectives or constraints. Skin thickness and other wing components are known as sizing and topology variables, respectively. Sizing optimization (SO) of the wing skin for both segments was performed by adding the design constraints to the structural stiffness. A very small number of optimization iterations were used to converge rapidly towards the optimal solution by obtaining a highly efficient skin thickness, as shown in Figure 13.

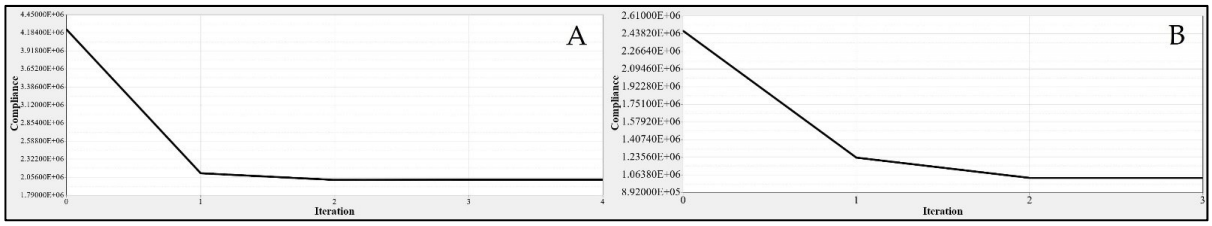

Figure 5.13 Convergence graph of the objective function for (A) fixed wing skin and (B) moving wing skin

SO was performed on both wing segments. The interpretations of its results for both wing segments are shown in Figure 5.14.

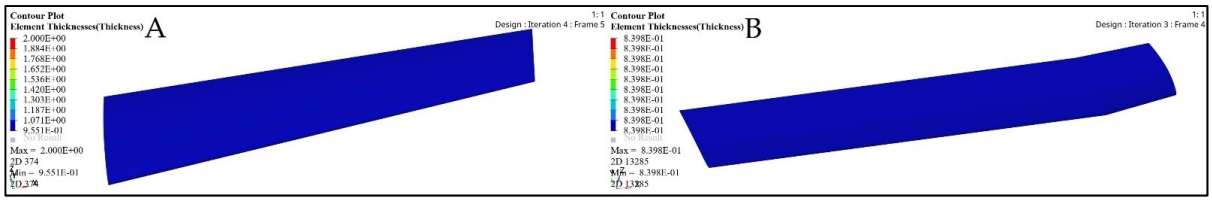

Figure 5.14 Sizing optimization (SO) results for (A) fixed wing and (B) moving wing

An initial wing skin thickness was chosen to be 2 mm for both wing segments. The FEM evaluations of a fixed and a moving wing skin are shown in Figure 5.15. This optimization relies on an FEM static analysis under extreme flight conditions, and it creates stress and deformation.

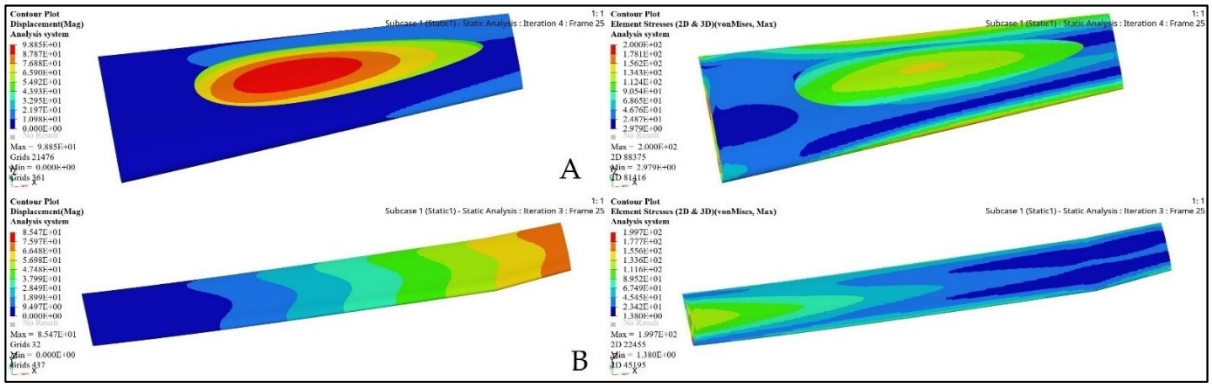

Figure 5.15 FEM results for fixed and moving wing segments: (A) fixed wing, and (B) moving wing, obtained using the sizing optimization problem

The maximum stress value of the wing two segments skin was restricted to 200 MPa for the highest efficiency in order to withstand the aerodynamic loading acting on its surface. The same boundary condition was applied to both wing segments. Hence, SO and FEAs were based on the wing design volume and shape. The maximum deformations and stresses obtained under extreme flight conditions, as well as other important parameter values obtained from the optimization results, are shown in Table 5.4.

Table 5.4 Values obtained from the sizing optimization and Finite Element Analysis for wing skins (a fixed and a moving wing)

	Iterations	Deformation	Stress	Original Skin Thickness	Optimized Skin Thickness	Weight Reduction Ratio
Fixed Wing	4	98.85 mm	200 MPa	2 mm	0.995 mm	52.4%
Moving Wing	3	85.47 mm	199.7MPa	2 mm	0.84mm	58.3%

TO was implemented to determine the spars that would achieve wing maximum stiffness and reduce the weight. A Computational Fluid Dynamics (CFD) study of the wing structure was conducted to obtain high levels of fidelity. This analysis provided the pressure loading cases for extreme flight conditions. The aerodynamic analysis of the wing structure was performed at the sea level altitude and maximum speed (68 m/s) to ensure the optimal distribution of aerodynamic loading over the wingspan, as shown in Table 5.3. The minimum structural compliance was obtained for the initial wing spars' design for both segments by a various number of iterations based on the size and shape of each spar, as illustrated in Figure 5.16.

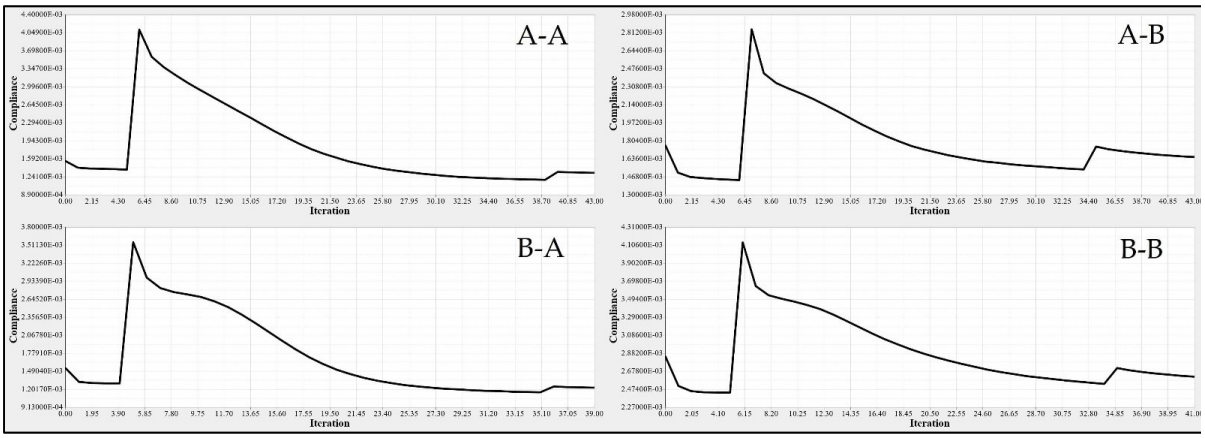

Figure 5.16 Convergence graph of the objective function: (A–A) front spars of a fixed wing, (A–B) rear spars of fixed wing, (B–A) front spars of a moving wing, and (B–B) rear spars of a moving wing

The minimization of structural compliance using constraints is defined as a volume fraction by 30%. The design variable is the structural weight for an allocated global compliance-based stress. The TO results are summarized in Table 5.5.

Table 5.5 Parameters of the wing segments for spars obtained by TO based on Finite Element Analysis

	Fixed Wing		Moving Wing	
	Front Spar	Rear Spar	Front Spar	Rear Spar
Iterations	43	43	39	41
Initial Weight	1.79 kg	0.82 kg	1.1 kg	0.59 kg
Optimized Weight	0.58 kg	0.37 kg	0.43 kg	0.29 kg
Weight reduction Ratio	67.6%	54.9%	60.9%	50.9%
Deformation	0.00064 mm	0.00117 mm	0.00073 mm	0.00227 mm
Stress	0.13MPa	0.185 MPa	0.134 MPa	0.225 MPa

TO based on the FE modeling of the wing spar is an iterative process, as shown in Table 5.5, and in Figures 5.16 and 5.17. Table 5.5 shows the parameters of the most important wing spars by calculating them as a function of the design parameters.

The merit of TO within OptiStruct is that the FE properties were updated depending on the optimization results. Figures 5.18 and 5.19 illustrate the FE characteristics obtained with TO, and Table 5.5 shows the weights of the initial spars and those of the optimized spars, which reveals the significant reduction in the average weight of the wing spars.

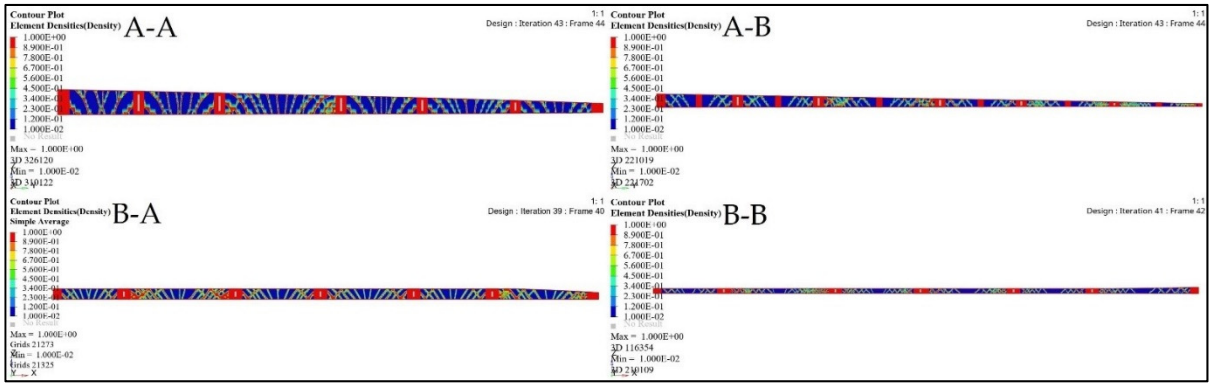

Figure 5.17 Element density variation with the numbers of iteration for (A–A) fixed wing front spars, (A–B) fixed wing rear spars, (B–A) moving wing front spars, and (B–B) moving wing rear spars

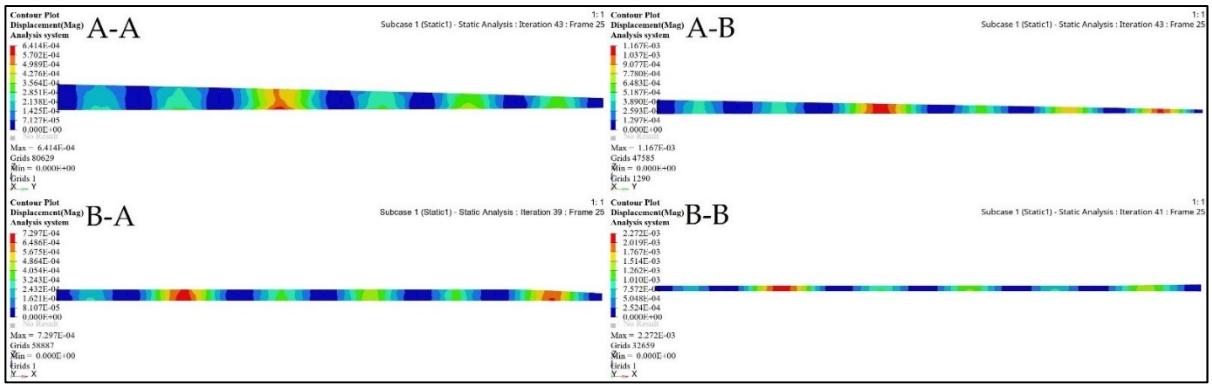

Figure 5.18 Deformation results based on topology optimization for (A–A) fixed wing front spars, (A–B) fixed wing rear spars, (B–A) moving wing front spars, and (B–B) moving wing rear spars

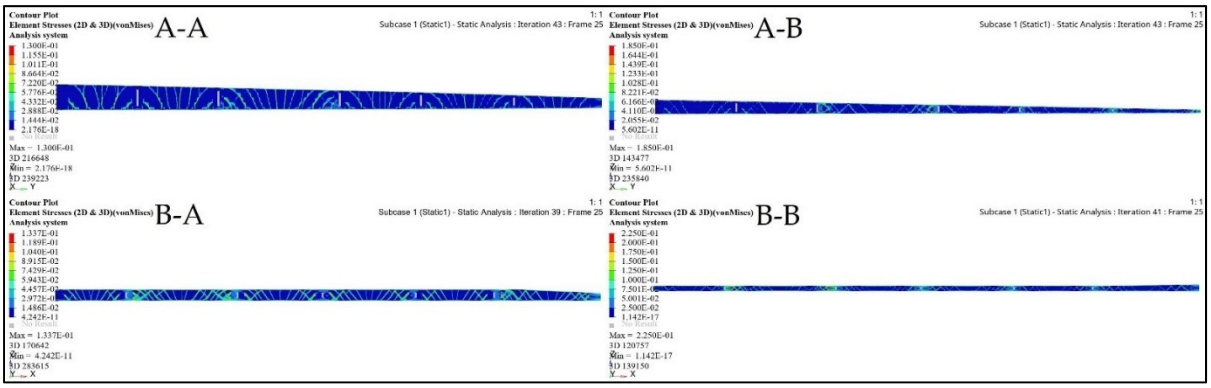

Figure 5.19 Stress results based on topology optimization for: (A–A) fixed wing front spars, (A–B) fixed wing rear spars, (B–A) moving wing front spars, and (B–B) moving wing rear spars

This component simulation-based TO approach guides detailed structural design and provides an alternative way to reduce wing spars' structural weight. Furthermore, Table 5.5 shows that the proposed component simulation-based TO approach can be an efficient, as well as logical design technique for the continuum design of wing components with high efficacy and reliability.

The same procedures applied to the wing spars were chosen for the wing ribs as well. An optimization approach based on the Finite Element Model (FEM) was implemented for each rib, depending on its calculated loading. The material density of each element was defined as

a design variable. Two analysis responses expressed in terms of structural compliance and volume fraction were identified, in which the volume fraction was classified as a constraint, and the compliance was defined as an objective function. The typical setup of the TO led to compliance minimization by using the volume fraction parameter as a constraint; the converged solution was obtained using an iterative process, as illustrated in Figure 5.20.

Figure 5.21 depicts the material density obtained by TO for the wing ribs (for simplicity, Figure 5.21 shows ribs 1 and 2 for the fixed wing, and ribs 1 and 6 for the moving wing).

The FE models based on the TO process for the selected ribs shown in Figures 5.22 and 5.23 demonstrate that an important weight reduction was obtained without affecting the components stiffnesses.

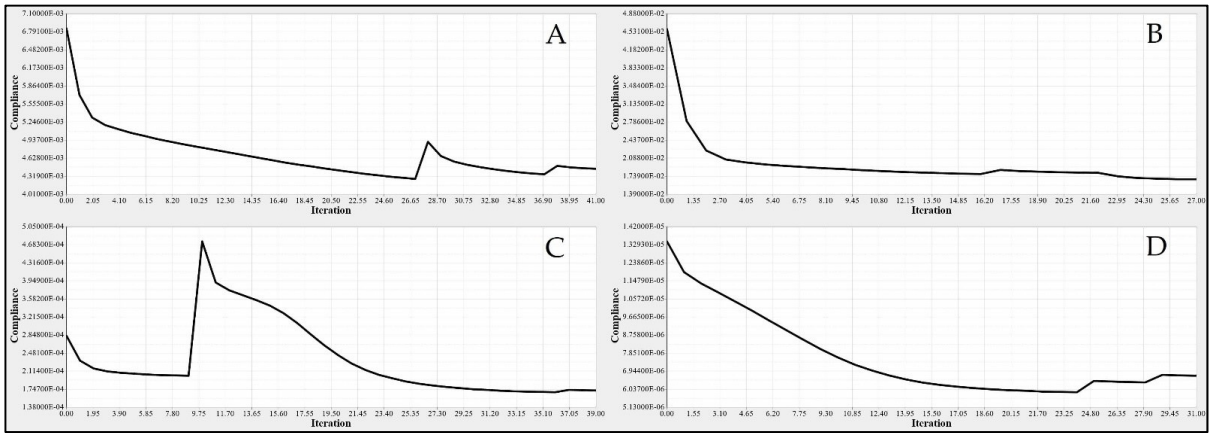

Figure 5.20 Convergence graphs of the objective functions for: (A) rib 1 of a fixed wing, (B) rib 2 of a fixed wing, (C) rib 1 of a moving wing, and (D) rib 6 of a moving wing

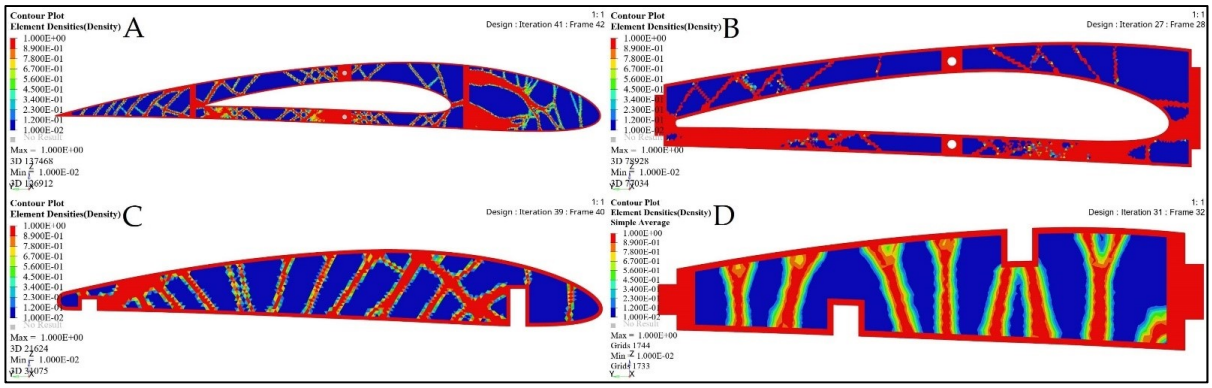

Figure 5.21 Element density variations with the iteration numbers for: (A) rib 1 of a fixed wing, (B) rib 2 of a fixed wing, (C) rib 1 of a moving wing, and (D) rib 6 of a moving wing

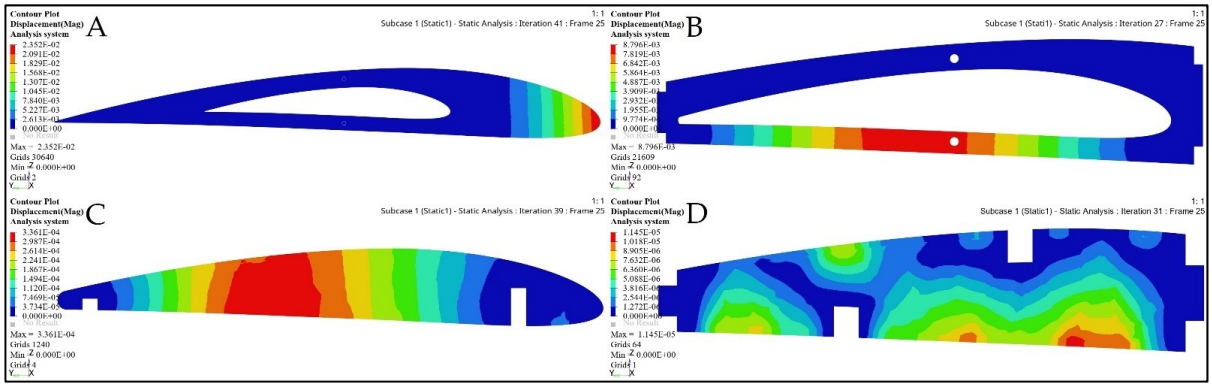

Figure 5.22 Deformation results based on TO for: (A) rib 1 of a fixed wing, (B) rib 2 of a fixed wing, (C) rib 1 of a moving wing, and (D) rib 6 of a moving wing

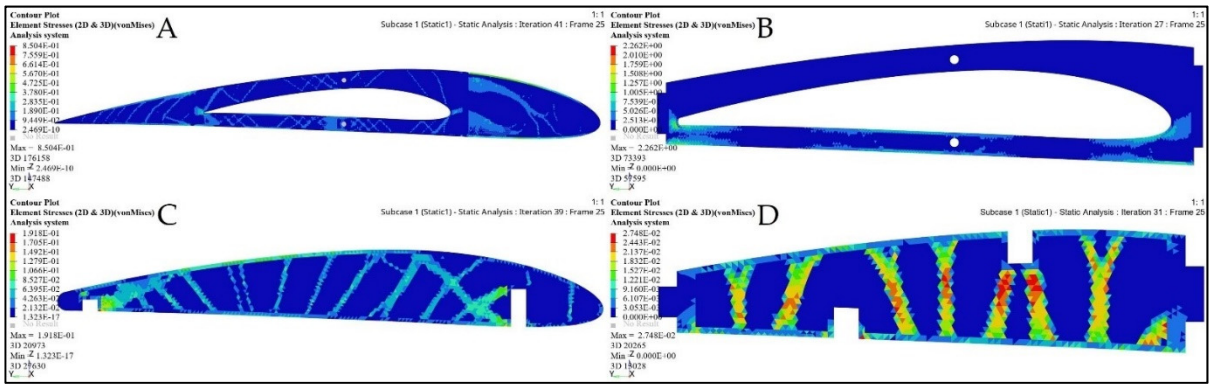

Figure 5.23 Stress results based on TO for: (A) rib 1 of a fixed wing, (B) rib 2 of a fixed wing, (C) rib 1 of a moving wing, and (D) rib 6 of a moving wing

Table 5.6 displays the VSMTW rib TO results obtained using their various starting values based on the aerodynamic loading distribution. The comparison of the weight values of ribs before and after optimization reveals that their weights were substantially reduced following the calculated loads acting on the rib. The maximum stresses and displacements of all ribs were very small; thus, the optimized ribs satisfied the strength and stiffness requirements. The seventh rib of both the fixed and moving wings models were excluded from the optimization process, as these wings must be solid without hollows.

Table 5.6 Parameters of the wing segments for the ribs obtained from topology optimization based on Finite Element Analysis

		Iteration	Initial Weight	Optimized Weight	Weight reduction Ratio	Deformation	Stress
Fixed Wing	Rib 1	41	0.539 kg	0.279 kg	48.2%	0.024 mm	0.85 MPa
	Rib 2	27	0.237 kg	0.1 kg	57.8%	0.0088 mm	2.26 MPa
	Rib 3	26	0.209 kg	0.095 kg	54.5%	0.003 mm	1.11 MPa
	Rib 4	24	0.167 kg	0.09 kg	46.1%	0.023 mm	3.813 MPa
	Rib 5	20	0.137 kg	0.086 kg	37.2%	0.04mm	5.462 MPa
	Rib 6	9	0.107 kg	0.086 kg	19.6%	0.082 mm	5.737 MPa
	Rib 7	0	0.086 kg	0.086 kg	0	0	0
Moving Wing	Rib 1	40	0.134 kg	0.04 kg	70.1%	0.00034 mm	0.19 MPa
	Rib 2	30	0.086 kg	0.028 kg	67.4%	0.00002 mm	0.047 MPa
	Rib 3	30	0.086 kg	0.028 kg	67.4%	0.00002 mm	0.047 MPa
	Rib 4	29	0.086 kg	0.028 kg	67.4%	0.00002 mm	0.045 MPa
	Rib 5	32	0.086 kg	0.028 kg	67.4%	0.00001 mm	0.032 MPa
	Rib 6	31	0.086 kg	0.028 kg	67.4%	0.00001 mm	0.027 MPa
	Rib 7	0	0.113 kg	0.113 kg	0	0	0

The optimized wing segments modeled as solid suggest that a wing should have strut elements obtained from TO in order to meet their strengths requirements. Various aerodynamic load scenarios obtained for extreme flight conditions were evaluated to design the support parts, as indicated in Table 5.3, and in Figures 5.3 and 5.4. The baseline TO was conducted on the support elements' structure for both wing segments using the required load conditions. Certain support elements were excluded from the TO due to their geometrical designs. The results obtained from various TOs were represented as density cloud maps for the support elements,

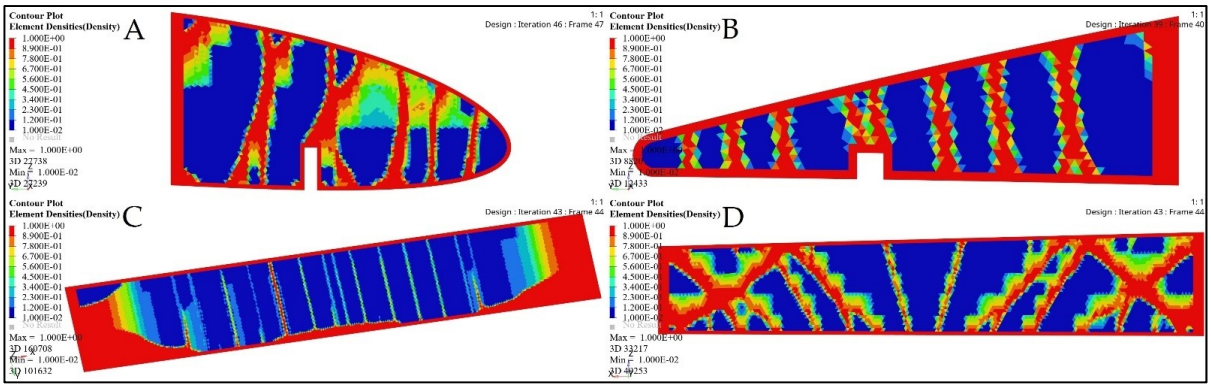

Figure 5.24 Element density plots with the iteration numbers for fixed wing: (A) leading edge of rib 1, (B) trailing edge of rib 1, (C) bottom support surface between rib 6 and rib 7, and (D) front spar support

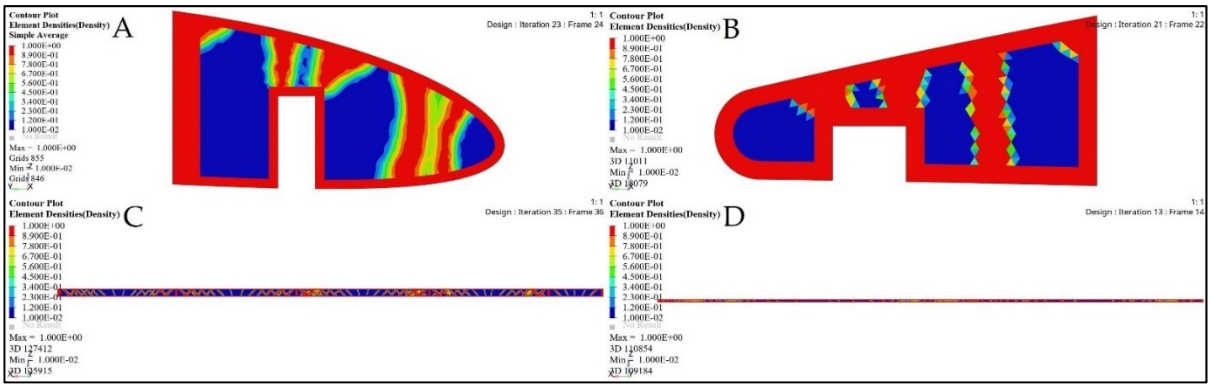

Figure 5.25 Element density plots with the iteration number for moving wing: (A) leading edge of rib 1, (B) trailing edge of rib 1, (C) support stringer of a front spar, and (D) support stringer of a rear spar

as shown in Figures 5.24 and 5.25 for fixed wing and moving wing segments, respectively. The red sections represent the solid region, while the blue sections represent the void region.

The basic structure of support elements was highly minimized based on the TO results, thereby reducing the support elements weights. Moreover, it is clear that the structural compliance decreased as the number of iterations increased, as shown in Figures 5.26 and 5.27.

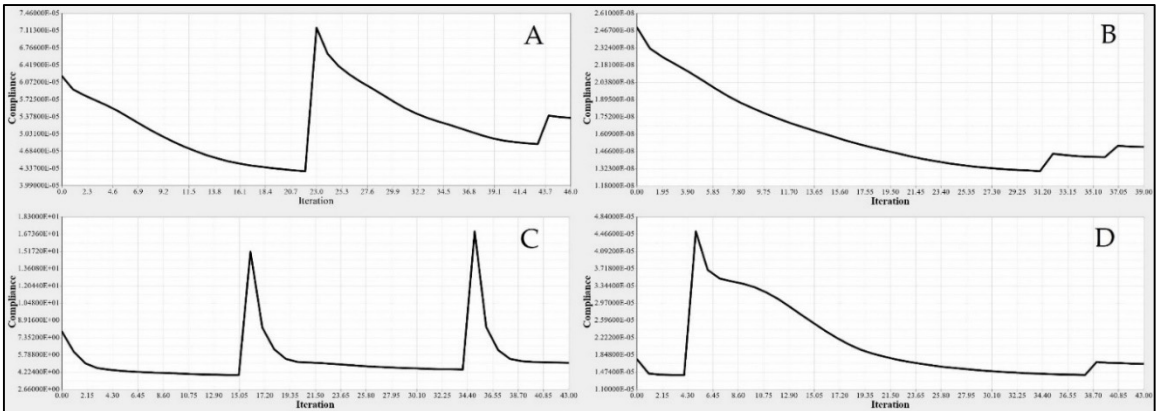

Figure 5.26 Convergence graphs of the objective function for a fixed wing: (A) leading edge of rib 1, (B) trailing edge of rib 1, (C) bottom support surface between ribs 6 and 7, and (D) support of a front spar

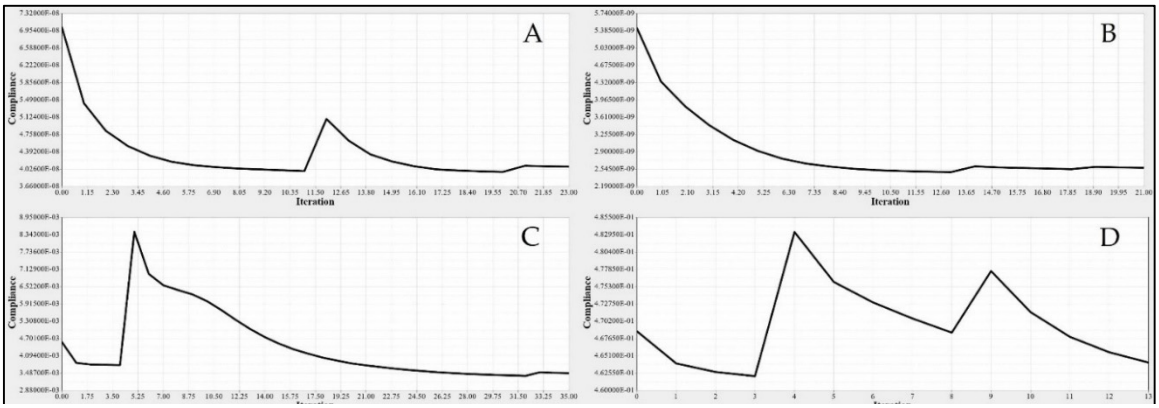

Figure 5.27 Convergence graphs of the objective function for a moving wing: (A) leading edge of rib 1, (B) trailing edge of rib 1, (C) support stringer of a front spar, and (D) support stringer of a rear spar

Figures 5.28 – 5.31 show the effects of a TO process on the structural changes in mechanical properties, such as deformations and stresses. These figures indicate that the strain can be reduced, while the structural stiffness progressively increases.

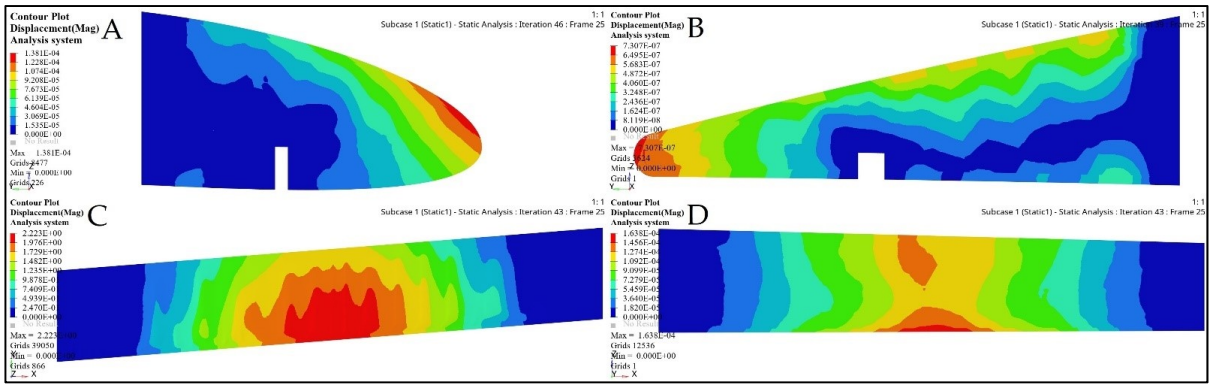

Figure 5.28 Deformation results based on topology optimization of a fixed wing: (A) leading edge of rib 1, (B) trailing edge of rib 1, (C) bottom support surface between ribs 6 and 7, and (D) support of a front spar

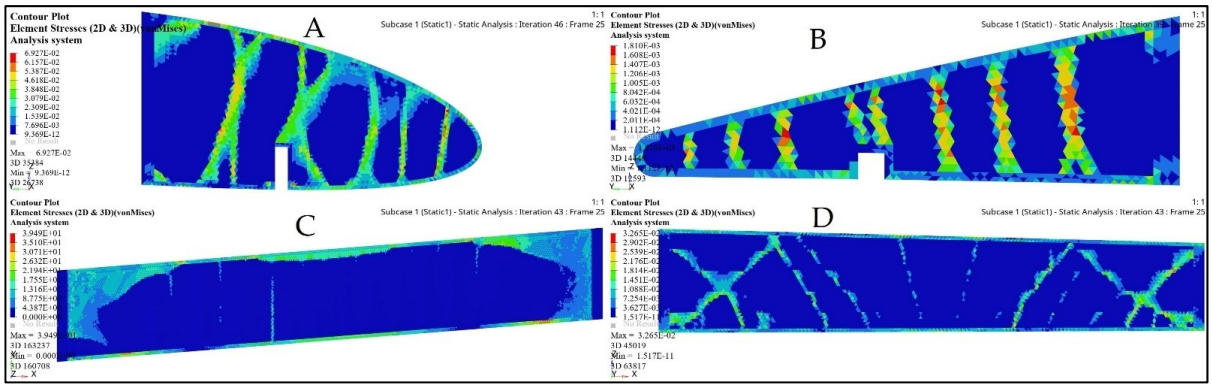

Figure 5.29 Stress results based on topology optimization of a fixed wing: (A) leading edge of rib 1, (B) trailing edge of rib 1, (C) bot-tom support surface between ribs 6 and 7, and (D) support of a front spar

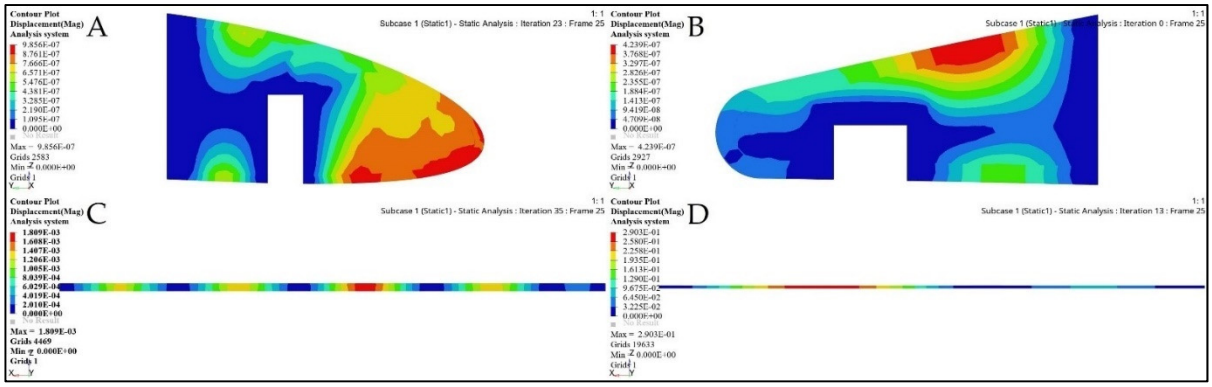

Figure 5.30 Deformation results based on topology optimization of a moving wing: (A) leading edge of rib 1, (B) trailing edge of rib 1, (C) support stringer of a front spar, and (D) support stringer of a rear spar

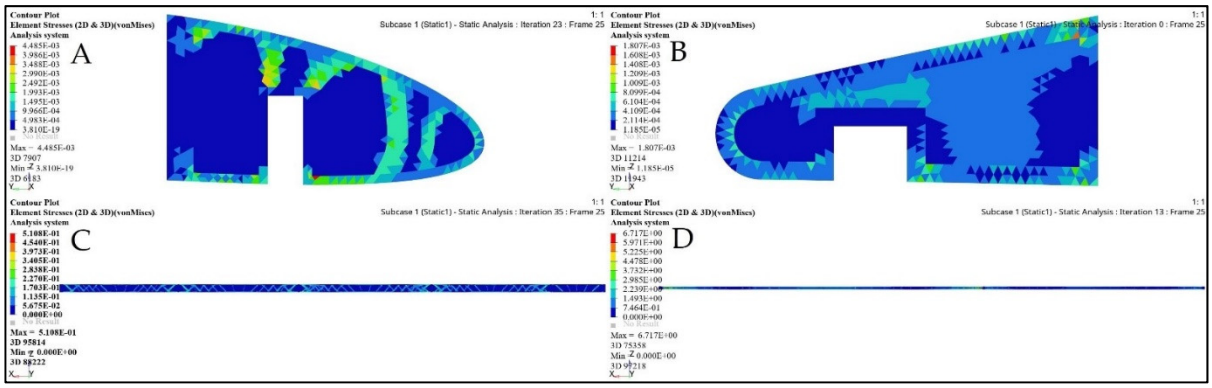

Figure 5.31 Stress results based on topology optimization of a moving wing: (A) leading edge of rib 1, (B) trailing edge of rib 1, (C) support stringer of a front spar, and (D) support stringer of a rear spar

The main parameters' values were calculated in the optimization analysis. The values of the results depended on the number of iterations and the mechanical analysis and they differed between each individual component of the support elements, as the forces and the geometric shapes differed from one support element to another. Several support elements were eliminated from the optimization process due to the difficulties in their implementation in terms of their geometrical and physical obstacles such as cylindrical shape.

5.7 Remodeling of the Optimized Wing Components and Their Final Design

Generally, the morphing wing configuration is used for the accomplishment of multiple missions in an individual flight. The work presented here was applied on both Hydra Technologies' UAS-S4 and UAS-S45 Baalam (Kuitche & Botez, 2019). First, SO was implemented on the wing skin to determine its optimum thickness. Next, TO was utilized to determine the optimum internal wing components that would reduce the components' weights while maintaining their strengths. Finally, remodeling based on optimization results was considered for the design of wing components' configurations. This optimization was performed for fixed and moving wing segments, so that the wing component's structure could be remodeled to further analyze their weight optimization.

The optimized wing model was built from aluminum 2024-T3, with its fixed and moving segments weighing 16.3 kg and 10.3 kg, respectively. The wing components' structure manufacturing includes the arrangement of the spars, ribs, and support elements based on the TO results, and then, the design of a skeleton model of the wing structure. In the present optimization investigation, the TO method was performed on the wing components, including its spars and ribs. Minor support elements were eliminated from the TO method, as they were ineffective from a structural perspective.

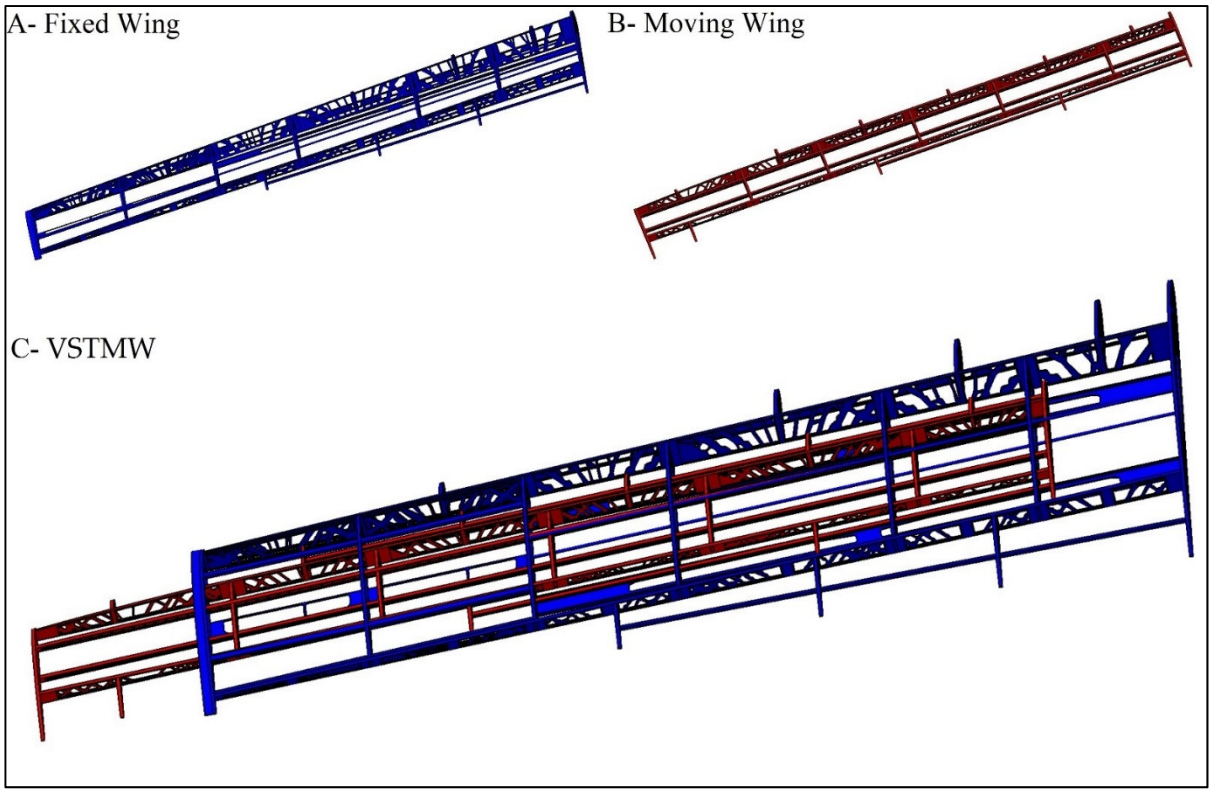

Figure 5.32 Detailed remodeling of the VSTMW (A) fixed wing segment, (B) moving wing segment, and (C) assembled VSTMW at the original position

The highest challenge in this phase of optimization was the implementation of the TO on the fixed segment ribs. Given the space required to house the moving segment, we assumed that there should be a cavity in the middle of each rib, as seen in Figure 5.8. Subsequently, it was decided that reinforcement of the fixed wing's middle area was needed to support the ribs in the impairment regions where the loads were large, as they resulted from the moving wing segment motion. Both wing segments had to be reinforced due to the shear stress produced by the aerodynamic loads' reactions under a variety of flight conditions. After remodeling the wing segment shapes based on the TO findings, the CAD model of the design of the MVSTW components was developed according to their density distribution. Figure 5.32 illustrates the optimized shapes for both wing segments.

5.8 Conclusions

This article addresses recent advancements in integrating aerodynamic approaches and optimization methods in order to develop the concept of the morphing variable span of tapered wing (MVSTW) design. This phase of wing component optimization is subordinated to the previous topology optimization phase, which was used to allocate the wing components inside the MVSTW. The optimization was performed using Altair's OptiStruct solver, connected with the aerodynamic research results obtained using the XFLR5 code. Then, these results were incorporated into SO and TO, and then utilized to solve relevant optimization problems.

The optimization framework for wing components was developed in order to minimize the weights of the MVSTW components while optimizing their structure stiffnesses. The study's main objective was to identify and thus assess the feasibility of implementing this optimization process for skin and internal wing elements, such as ribs, spars, and others. This novel technique was suggested for the MVSTW based on a telescopic mechanism, which involved sliding a telescopically stretched wing into a fixed wing segment. This approach increased the difficulty of our work by requiring us to pay high attention to wing several components during the optimization process. For example, the fixed wing ribs should have a cavity for sliding the moving segment into the wing to fit a complex geometric shape when applying SO and TO (or STO).

This analysis aims to minimize the weight of the MVSTW by maximizing its stiffness and minimizing its total structural compliance parameters in order to reinforce structural durability, and to satisfy the MVSTW's structural integrity criteria. The STO findings revealed an advantage in structural weight savings for fixed and moving wing parts components. When the weights of the baseline wing segments were compared to the weights of the optimized wing segments, the optimized wing components' weights for both segments decreased from 16.3 kg to 7.96 kg for the fixed wing segment, and from 10.3 kg to 4.57 kg for the moving wing segment. Based on the TO results of both MVSTW segments, the wing components' configurations, including the spars, ribs, and support elements, were redesigned and further

developed. In addition, the wing skin was chosen depending on the SO results. The aerodynamic loads were distributed along wingspan length and further obtained under extreme flight conditions. Following the weight savings obtained by the STO techniques on the wing components, the optimized wing shape fulfilled the structural integrity design criteria.

Future research will include additional investigations to develop a reliable adaptive morphing wing. Optimizations will be conducted on composite materials with the aim to achieve greater weight reduction in the MVSTW. Following the optimization of the wing segments using composite materials, the MVSTW configuration and its actuation mechanism integration will be evaluated. The gains obtained by these optimizations will further reduce the fuel consumption.

CHAPTER 6

MULTIDISCIPLINARY OPTIMIZATION FOR WEIGHT SAVING IN A VARIABLE TAPARED SPAN-MORPHING WING USING COMPOSITE MATERIALS - APPLICATION TO THE UAS-S4

Mohamed Elelwi [a], Felipe Schiavoni Pinto[a], Ruxandra Mihaela Botez [a]* and Thien-My Dao [b]

[a] Department of Laboratory of Active Controls Avionics and AeroServo Elasticity
LARCASE
ÉTS - École de technologie supérieure
1100 Notre-Dame West, Montréal QC H3C 1K3 Canada

[b] Department of Research Team in Machines Dynamics Structures and Processes
ÉTS - École de technologie supérieure
1100 Notre-Dame West, Montréal QC H3C 1K3 Canada

Paper published in *Actuators* 2022, 11(5), 121; https://doi.org/10.3390/act11050121

Résumé

Cet article fait suite à des travaux antérieurs en optimisation numérique multidisciplinaire pour développer une aile déformable (MVSTW) afin de réduire son poids en utilisant des matériaux composites. Cette étude crée un environnement numérique d'optimisation multidisciplinaire en intégrant la sélection des matériaux, le dimensionnement structurel et l'optimisation topologique suite aux résultats d'optimisation aérodynamique dans le but d'évaluer si l'optimisation déformable des ailes est faisable. Cette technologie sophistiquée est suggérée pour le développement de MVSTW. Dans un premier temps, une approche d'optimisation spécifique au problème est décrite pour spécifier la structure allégée des composants d'aile en utilisant des matériaux composites plutôt que des matériaux standard (tels que l'aluminium Al 2024-T3). L'optimisation a été réalisée à l'aide de plusieurs approches ; par exemple, l'optimisation aérodynamique a été effectuée avec les codes CFD et XFLR5, la sélection des matériaux a été effectuée à l'aide du code MATLAB, pendant que l'optimisation du dimensionnement et de la topologie a été effectuée à l'aide des solveurs OptiStruct et SolidThinking Inspire d'Altair. L'objectif de cette recherche a été d'atteindre les normes de

rigidité structurelle du MVSTW en minimisant la conformité tout en maximisant la rigidité. Le dimensionnement et l'optimisation de la topologie des composants de l'aile ont été conçus à l'aide de matériaux composites. Selon les résultats de cette optimisation, le poids du MVSTW a été considérablement réduit à 5,5 kg, par rapport au poids d'origine de l'aile de l'UAS-S4 de 6,5 kg. Les résultats de l'optimisation et de la méthode des éléments finis indiquent également que le MVSTW développée peut parfaitement accomplir des missions de vol spécifiées et sans aucune panne mécanique.

Abstract

This paper is a follow-up to earlier work on applying multidisciplinary numerical optimization to develop a morphing variable span of a tapered wing (MVSTW) to reduce its weight by using composite materials. This study creates a numerical environment of multidisciplinary optimization by integrating material selection, structural sizing, and topological optimization following aerodynamic optimization results with the aim to assess whether morphing wing optimization is feasible. This sophisticated technology is suggested for developing MVSTWs. As a first step, a problem-specific optimization approach is described for specifying the weight-saving structure of wing components using composite materials. The optimization was performed using several approaches; for example, aerodynamic optimization was performed with CFD and XFLR5 codes, the material selection was conducted using MATLAB code, and sizing and topology optimization was carried out using Altair's OptiStruct and SolidThinking Inspire solvers. The goal of this research is to achieve the MVSTW's structural rigidity standards by minimizing wing components' weight while maximizing stiffness. According to the results of this optimization, the weight of the MVSTW was reduced significantly to 5.5 kg in comparison to the original UAS-S4 wing weight of 6.5kg. The optimization and Finite Element Method results also indicate that the developed morphing variable span of a tapered wing can complete specified flight missions perfectly and without any mechanical breakdown.

6.1 Introduction

Aluminum alloy is a very well-known material in the aerospace sector due to its ideal strength–weight ratio. The space race in the 1960s introduced new materials and technology, including composite materials. At that time, those materials offered the chance to make airplanes stronger, lighter, and have great potential to reduce fuel consumption and thus be more cost-profitable (Judge, 1969) (Concilio et al., 2021) (Pecora et al., 2011) (Dimino et al., 2017).

A composite material is created by combining two or more different materials (reinforcement, fillers, and binder) with varying compositions and substantially different physical and chemical properties. When composite materials are considered, they provide a product with an appearance (and performance) that differs from the individual material components. Composites comprise a solid load-bearing material called reinforcement and softer materials arranged in a matrix. Reinforcement adds stiffness and strength to the structure by augmenting the load support. Composite materials are widely employed in the industry due to their exceptional resistance to chemicals and to most types of corrosion, as well as to their other interesting properties (Rajak, Pagar, Kumar, & Pruncu, 2019) (Rajak, Pagar, Menezes, & Linul, 2019).

Their numerous and valuable properties include low density, low weight, un-matched manufacturing and processing capabilities, complicated material bodies that are easily fabricated, their suitability for their use on tiny, as well as very large products, low tooling costs, and their ability to incorporate a suitable surface finish. Composite materials have been used extensively and recently to develop over 50% of aerospace components. The key advantages of composite materials consist of reducing the weight of the components and simplifying their assembly. Composites are used to fabricate a variety of aircraft surfaces, including rudders, spoilers, air-brakes, wing ribs, main wings, and turbine engines (Jerome, 2001) (Aamir, Tolouei-Rad, Giasin, & Nosrati, 2019).

The initial wide-ranging applications of fiber-reinforced plastics (FRPs) in aircraft wing development date back to the 1960s, when sailplane designers recognized the advantages of

their orthotropic properties and low masses. FRPs enable the optimization of laminate rigidity to meet loading requirements in combination with high stiff-ness-to-mass and strength-to-mass ratios. Using composites in commercial aircraft wings has since grown steadily, encouraged by advancements in manufacturing technology, such as automatic fiber positioning. The optimization of composites has been a field of study for many years, especially in aeroelasticity areas (Dillinger, Klimmek, Abdalla, & Gürdal, 2013). Fiber-reinforced composite materials can often provide designers with outstanding potential to achieve a wing structure's desired directional stiffness and aeroelastic behavior by optimizing its fiber directions while minimizing weight penalty and its corresponding high specific strength and stiffness (Guo, 2007).

Unmanned Aerial Vehicles (UAVs) have been in use since the 1950s, but with limitations regarding their operation, autonomy, and feasibility (Sullivan, 2006) (Arena et al., 2019). The new wingtip model was developed as part of an international CRIAQ project with the aim of exhibiting the wing upper surface and aileron-morphing capabilities in im-proving wing tip aerodynamic efficiencies (Ruxandra M Botez, Grigorie, Khan, Mamou, & Mebarki, 2021) (R. Botez et al., 2018). As the technology has improved, composite materials are increasingly being used in advanced design for modern aircraft such as the Bombardier-Series, the Airbus A-380, and the Boeing B-787, as well as for designing UAVs. However, UAVs can afford to have a smaller safety margin on the structural side, as a human pilot is on the ground (Pecora et al., 2011) (Concilio et al., 2016) (Dimino, Andreutti, Moens, Fonte, & Pecora, 2021). In this context, materials not typically used in the aviation industry, such as polymers and 3D-printed materials, have been incorporated for UAV structural design (Mieloszyk, Tarnowski, Kowalik, Perz, & Rzadkowski, 2019) (Easter, Turman, Sheffler, Balazs, & Rotner, 2013) (Dimino et al., 2014) (Rathod, Kumar, & Jain, 2017). Composites used in the aviation industry should exhibit high-reliability characteristics, namely a high degree of mechanical, impact, and thermal resistance (Rathod et al., 2017) (Setlak & Kowalik, 2019) (Setlak, Kowalik, & Lusiak, 2021).

No matter which design method is used, the sizing design must include optimal thickness allocation of different body components: spars, ribs, stringers, and skin (Locatelli, Mulani, &

Kapania, 2014). There exist significant interconnections between these two types of design factors (topology and sizing/layout) that are substantial, especially when skin-buckling metrics are considered. Concurrent optimization of sizing and topology is required to achieve the optimal weight-saving tradeoff; however, significant numerical challenges are presented. Layouts may be optimized using non-gradient optimization methodologies (W. Wang, Guo, & Yang, 2011) (Stanford, Jutte, & Coker, 2019).

Topology optimization was applied by Airbus in the A380 airplane design project to develop new lightweight surfaces. In particular, the leading-edge ribs and fuselage door intercostals of the Airbus A380 achieved a weight reduction of over 1000 kg per aircraft (Grihon et al., 2004). Similarly, when developing the wings' leading-edge ribs for the B-787 Dreamliner, Boeing incorporated topology, size, and shape optimization to find their optimum shapes. Due to the combination of various optimization techniques, the weight of the B-787's leading-edge ribs was decreased by 24–45% compared to the B-777 aircraft weight (Q. Wang et al., 2011) (James et al., 2014).

The fundamental objective of this research is to develop and accomplish the most effective solution for developing lightweight components of the variable morphing wing while maintaining optimal mechanical properties compared to the UAS-S4 baseline wing. Estimates were calculated using the UAS-S4 characteristic. Hydra technologies developed and manufactured the UAS-S4 Unmanned Aerial System for military and commercial applications (Figure 6.1). Table 6.1 summarizes its general characteristics.

Figure 6.1 Hydra Technologies UAS-S4 Ehecalt

Table 6.1 The characteristics of the UAS-S4

Geometrical Data	Values
Wing Span	4.2 m
Wing Area	2.3 m2
Total length	2.5 m
Mean Aerodynamic Chord (MAC)	0.57 m
Empty weight	50 kg
Maximum Take-off Weight (MTOW)	80 kg
Loitering Airspeed	35 knots
Maximum Speed	135 knots
Service Ceiling	15,000 ft
Operational Range	120 km

A telescoping mechanism was proposed as a novel approach for the MVSTW. This strategy adds more difficulties to our work by asking us to pay closer attention to various components' design throughout the optimization process. As a continuation of our previous research, this study is dedicated to the selection and use of composite materials rather than a single material (aluminum Alloy-2024-T3) using STO methods to reduce the wing components' weight. A multidisciplinary optimization approach has been used for adaptive wingspan using advanced composite materials for its performance enhancement.

6.2 The Optimized MVSTW and Load Distribution – Design Outline

A number of studies conducted in Aerospace Research Centers have proven the advantages of wing shape morphing. The LARCASE has accomplished many investigations of the Unmanned Aerial Systems UAS-S4 and UAS-S45 and other projects. The main objective of these investigations is to improve the aerodynamic performance and enhance green aircraft technology (Ruxandra M Botez, 2022) (R. M. Botez, 2018). These earlier works investigated the multidisciplinary numerical optimization of MVSTW, which integrated automated numerical analyses of aerodynamics, Finite Element Method, and structure optimizations (Mohamed Elelwi, Botez, & Dao, 2021). Aerodynamic analyses have established that

increasing the wing area via the span-morphing technique improved its aerodynamic performance, reduced fuel consumption, and increased flight envelope range (Kammegne et al., 2016) (Ruxandra Mihaela Botez, Molaret, & Laurendeau, 2007) (Noviello, Dimino, Amoroso, & Pecora, 2019). Another advantage was the ability to dominate roll control using the asymmetric wingspan mechanism rather than conventional control surfaces (M. Elelwi et al., 2020). Design engineers face the most significant challenge, which is the structural wing weight penalty. To overcome this challenge, structural optimization is considered the most successful technique for weight minimizing by enhancing the structural design and development of the wing. An optimized reference wing was developed based on multidisciplinary numerical optimization consisting of aerodynamic optimization, the Finite Element Method, and structural optimization (topology and sizing) (Mohamed Elelwi et al., 2021) (Zhu et al., 2016). The aerodynamic optimization was combined with topology optimization results to allocate the wing components within MVSTW segments (M. Elelwi et al., 2020). The topology and sizing optimization were then repeated for the entire component set using a single material (aluminum alloy-2024-T) to minimize the wing component weight (Mohamed Elelwi et al., 2021).

6.2.1 MVSTW Layout and Configurations

A reference wing relies on the concept of telescopic wing techniques. This concept was developed as a result of aerodynamic optimization findings, and it consists of parallel wing segments (swept angle geometrical shape) of the inboard and tapered outboard wings, as shown in Figure 6.2. To allow the inboard segment to move through the outboard segment, the outboard segment must be designed with an appropriate cavity (M. Elelwi et al., 2020).

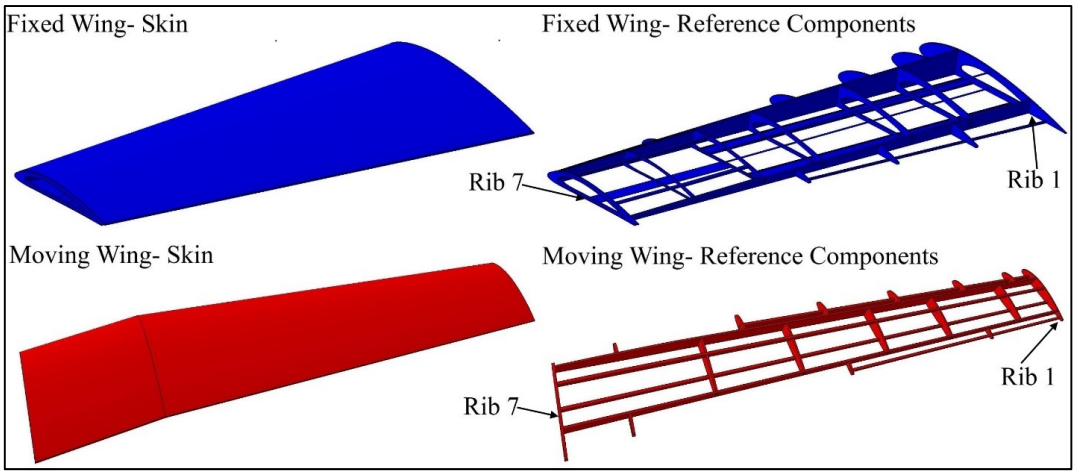

Figure 6.2 Configuration outline of fixed and moving segments with allocated wing components based on topology optimization

The previous work (M. Elelwi et al., 2021) concentrated on finding the appropriate location of internal structural components within wing segments. The topology optimization technique was chosen to achieve this objective. This technique has been linked to aerodynamic optimization outcomes and to the data and boundary conditions calculated under extreme situations (sea level altitude and maximum speed, as the maximum pressure was obtained at sea level, and maximum speed when the wingspan was fully extended) (M. Elelwi et al., 2020).

Table 6.2 Proposed wing rib locations for fixed and moving segments, as measured for reference rib no. 1

Rib No.	Fixed Wing	Moving Wing
1.	0 mm Reference	0 mm Reference
2.	269 mm	245 mm
3.	534 mm	626 mm
4.	932 mm	919 mm
5.	1198 mm	1234 mm
6.	1503 mm	1502 mm
7.	1800 mm	1875mm

In earlier optimization efforts, a 3 g load factor and a safety factor of 1.5 were used to design a high-strength morphing wing capable of withstanding realistic flight situations such as severe

weather (wind shear, thunderstorms, wake turbulence, and others) effects at various altitudes (from sea level to 10,000 ft) (M. Elelwi et al., 2021) (Mohamed Elelwi et al., 2021).

According to those topology optimization results; two spars and seven ribs were established within wing segments. The ribs were placed in both segments according to the acquired findings of topology optimization analysis of solid wing segments at the suggested positions, as shown in Figure 6.2 and Table 6.2 (M. Elelwi et al., 2021):

6.2.2 Evaluated Loads along an MVSTW

In the preliminary phase of MVSTW optimization, the lift distribution was calculated along the wingspan, as it is a significant factor in subsequent optimization phases (the first phase was performed on MVSTW optimization with aluminum 2024-T3). The adopted strategy consists of dividing the MVSTW calculation into parts according to the rib positions. The CFD Fluent code was integrated with the XFLR5 code to estimate the flow circulation distribution Γ(y). The aerodynamic load was then determined for each MVSTW section using the lifting line theory, as demonstrated in Figure 6.3 (Pecora, 2021).

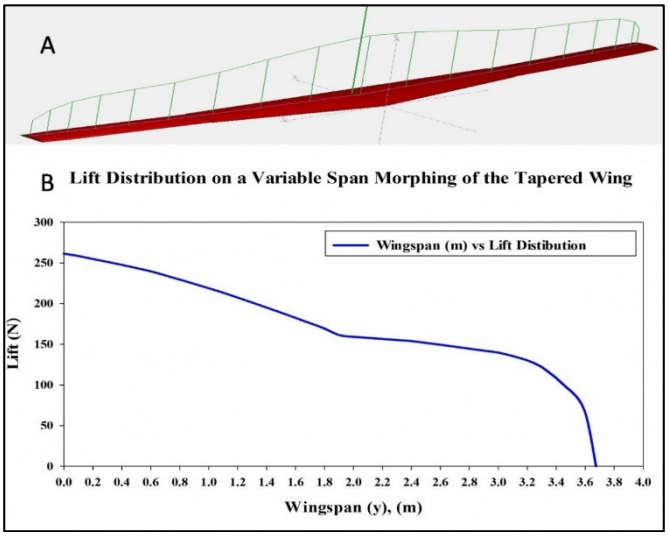

Figure 6.3 (A) Lift distributions for the MVSTW calculated using Fluent XFLR5 code; (B) lift force distribution chart

The Kutta–Joukowski theorem was developed as a way to calculate the distribution of the flow circulation with the following Equations (6.1)–(6.3), explained in (Sugar-Gabor, 2019) (Q. Zhang & Liu, 2017) (Gross et al., 2015).

$$\Gamma_{(y)} = \Gamma_0 \left(1 - \left(\frac{2y}{b}\right)^2\right)^{1/2} \tag{6.1}$$

In this case, $\Gamma_{(y)}$ denotes the distribution of flow circulation estimated at any random position along the wingspan. $\Gamma_{(y)}$ has its maximum value when y = 0 and it tends to zero when y = ±b/2. Thus, the flow circulation in the mid-span of the wing Γ_0 can be calculated as follows:

$$\Gamma_0 = \frac{4L}{\rho V b \pi} \tag{6.2}$$

where L is the lift force, ρ is the air density and V represents the air velocity. The following equation can be used to determine the lift loads acting on each wing segment:

$$L_{(y)} = \rho V \Gamma_{(y)} \tag{6.3}$$

As following the initial topology optimization, the number and type of wing components and their positions were determined. Each wing section had two spars and seven ribs. Al 2024-T3 was selected for all components during the following topology optimization process to reduce the wing structures' weight. The lifting load along the wingspan can be effectively estimated for each segment and it was calculated using the Prandtl Lifting-Line theory. The main parameters of the wing's span and ribs could then be determined. As shown in Figure 6.1, the initial topology optimization recommended the positioning of the seven ribs within the moving wing and fixed wing segments in the suggested locations.(M. Elelwi et al., 2021). The MVSTW was divided into separate 11 parts according to the locations of the ribs when the wingspan was extended to 75% of the original length of the wing, as depicted in Figure 6.4.

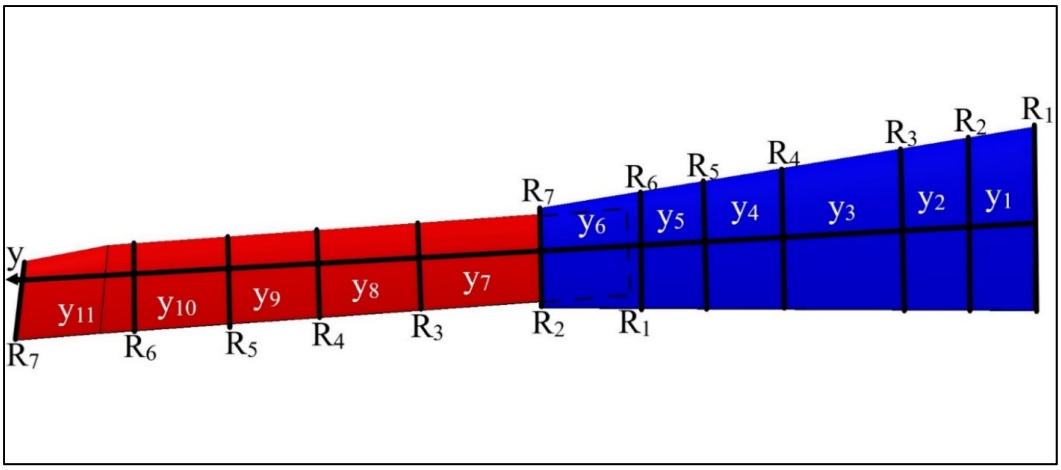

Figure 6.4 General scheme of an MVSTW with span sections (yn) and chord numbers (R)

As stated above, for a reliable and strong wing, the modeling of its structural components included a load factor of 3 g and a safety factor of 1.5. The safety factor of 1.5 was based on the FAA regulations (FAR 25.303). These regulations require aircraft structures to endure appropriate static loads determined by their related aerodynamic pressures without structural damage or failure. (Acar et al., 2010). The average lift loads measured for the fixed parts were used to evaluate the fixed wing ribs. The moving segment was treated similarly, with its lift load values shown in Table 6.3 for that segment (Mohamed Elelwi et al., 2021) (Dimino et al., 2021).

Table 6.3 Lifting loads computed for each section of an MVSTW

Section Number	Lift Load (N)	Ultimate Load
y1	257.36	1158.1
y2	243.77	1096.97
y3	232.15	1044.65
y4	213.325	959.96
y5	198.29	892.28
y6	175.96	791.8
y7	158.62	713.77
y8	152.7	687.15
y9	147.12	662.04
y10	134.61	605.75
y11	79.11	355.995

6.3 The Mathematical Approach to the Selection of Composite Materials

A MATLAB algorithm was developed to analyze the final analytical properties of composite materials based on fiber and matrix mechanical characteristics. The lamina longitudinal Young's Modulus, (E_1) for example, can be determined by the rule of mixtures, where E_{f1} and E_m represent the longitudinal Young's Modulus of the fiber and the matrix, respectively, v_f and v_m are the volume fractions of the fiber and the matrix, respectively.

$$E_1 = E_{f1} * v_f + E_m * v_m \tag{6.4}$$

where E_{f2} represents the transversal Young's Modulus of the fiber.

The transverse Young's Modulus (E_2) of a material can be calculated using a variety of methods. The Halpin-Tsai approach is applied in this research, a well-known method with reliable results (Shokrieh & Moshrefzadeh-Sani, 2016).

$$E_2 = E_m \left(\frac{1 + 2 * \left(\frac{\frac{E_{f2}}{E_m} - 1}{\frac{E_{f2}}{E_m} + 2} \right) * v_f}{1 - \left(\frac{\frac{E_{f2}}{E_m} - 1}{\frac{E_{f2}}{E_m} + 2} \right) * v_f} \right) \tag{6.5}$$

To obtain the equivalent laminate properties, an analysis of a simplified load case was analyzed in MATLAB. This case only considers a single axial load, for which E_x and E_y are determined. A more accurate result can be obtained by developing the full equation by considering the loads per unit length in all directions, a process that can be done iteratively. The laminate-equivalent properties were determined using for the load case by inverting the laminate stiffness matrix E, which is composed of three other matrices: A, B, and D, representing the

laminate extension stiffness, laminate coupling stiffness, and laminate bending stiffness matrices, respectively (Gibson, 2016).

$$[E] = \begin{bmatrix} [A] & [B] \\ [B] & [D] \end{bmatrix} \tag{6.6}$$

$$A_{ij} = \int_{-\frac{t}{2}}^{\frac{t}{2}} \left(\bar{Q}_{ij}\right)_k dz = \sum_{k=1}^{N} \left(\bar{Q}_{ij}\right)_k (z_k - z_{k-1}) \tag{6.7}$$

$$B_{ij} = \int_{-\frac{t}{2}}^{\frac{t}{2}} \left(\bar{Q}_{ij}\right)_k z\, dz = \sum_{k=1}^{N} \left(\bar{Q}_{ij}\right)_k (z_k^2 - z_{k-1}^2) \tag{6.8}$$

$$D_{ij} = \int_{-t/2}^{t/2} \left(\bar{Q}_{ij}\right)_k z^2\, dz = \sum_{k=1}^{N} \left(\bar{Q}_{ij}\right)_k (z_k^3 - z_{k-1}^3) \tag{6.9}$$

Equations (6.6) – (6.9) are functions of the transformed lamina stiffness matrix $\bar{Q}$, and of the distance of each layer (k) from the middle surface (z_k).

The inverted laminate stiffness matrix E is written under the following form:

$$[E]^{-1} = \begin{bmatrix} A' & B' \\ C' & D' \end{bmatrix} \tag{6.10}$$

The laminate equivalent longitudinal Young's Modulus (E_x), transversal Young's Modulus (E_y), shear modulus (G_{xy}) and Poisson's ratio (v_{xy}) are written as follows:

$$E_x = \frac{1}{t\, A'_{11}} \tag{6.11}$$

$$E_y = \frac{1}{t\,A'_{22}} \tag{6.12}$$

$$G_{xy} = \frac{1}{tA'_{66}} \tag{6.13}$$

$$\nu_{xy} = -\frac{A'_{12}}{A'_{11}} \tag{6.14}$$

where *t* is the laminate thickness.

The MATLAB code has been used to calculate the appropriate composite materials for output equal each wing component type, including its wing skin, spars, ribs, and support components.

6.4 Optimization Techniques of the MVSTW

Optimization techniques are receiving increased attention in the aviation field because they are considered the most effective approaches for decreasing a structure's weight while increasing its global stiffness (Degertekin, Lamberti, & Ugur, 2019). The topology optimization was performed using the SolidThinking Inspire software, while the sizing optimization was performed using the HyperMesh (OptiStruct) soft-ware. The Inspire and OptiStruct codes were designed using the (Solid Isotropic Material with Penalization) SIMP method (Martin P Bendsøe, 1989).

The wing elements' structural configuration weight can be minimized by enhancing the wing structure's overall strength and integrity via the application of sizing and topology optimization (STO) (Assimi, Jamali, & Nariman-zadeh, 2017).

This paper offers a new multidisciplinary optimization (MDO) framework based on design parameters for modeling and analyzing wing elements. It integrates several optimization methods into multiple-computer-aided engineering software. The Sizing and Topology

Optimization STO techniques were coupled with the aerodynamic optimization utilizing Computational Fluid Dynamics (CFD) via ANSYS FLUENT and XFLR5 codes.
The fundamental concept behind this investigation is to perform MDO on a composite morphing wing using different composite materials rather than a single metal material (such as aluminum alloy 2024-T3 in (M. Elelwi et al., 2021) (Mohamed Elelwi et al., 2021). The Finite Element Method (FEM) integrates with the STO into an optimization solver.

The multidisciplinary design optimization MDO was used to determine the appropriate composite materials (and their composition) for a morphing wing based on MATLAB calculations. Then, the STO was applied to the selected materials for the design of lightweight wing elements of a morphing wing while improving its mechanical characteristics. The structural and aerodynamic performance of the wing were evaluated using wing parameters that serve as optimization objectives and constraints. STO results based on the selected composite materials were obtained for all wing components; these components were then tested to validate their mechanical properties (displacement, factor safety, and stresses).

6.4.1 Theoretical Background of the Optimization Technique

Topology Optimization (TO) is a mathematical approach for identifying the optimal material distribution while minimizing its compliance within a predetermined design field. This optimized material configuration can be obtained because the critical material for the structural design is preserved while the undesirable material is re-moved. Thus, the outcome leads to the best structural load distribution under given boundary conditions and constraints. The TO approach via numerical solvers respects the predetermined constraints while meeting certain objectives. Hence, substantial materials are considered solid, whereas null materials are considered void. A commercial optimization numerical solver is utilized to cope with a set of constraints while relying on the objective functions for determining individual load situations. Sizing and topological optimizations have been implemented using Altair's OptiStruct and SolidThinking's Inspire. The design constraints were addressed within the solvers to ensure

that the design requirements were met. As a result, the primary objective of minimizing compliance while maximizing structural stiffness was satisfied.

Wing components are subjected to the design's pre-set loads and parameters to accommodate the density distribution of the material and its other mechanical characteristics (displacements, stresses, and others). Thus, the material density is considered to be the objective function variable, which determines whether a finite element is solid or void. The equations are elaborated on below.

The i^{th} element's pseudo-density, *xi*, may range between 0 and 1, i.e. ($0 \leq \text{xi} \leq 1$), where the 0 value indicates void material and the 1 value represents solid material. The variable denoted by the pseudo-density can be defined in equation (6.15):

$$x_i = \frac{\rho_i}{\rho_0} \tag{6.15}$$

where x_i denotes the pseudo-density of the i^{th} element, ρ_i represents the density of the i^{th} element, and ρ_0 indicates the density of the base material. According to the SIMP approach, equation (6.16) illustrates the effect of the pseudo-density variable on the material stiffness (Gunwant & Misra, 2012):

$$E_{(x_i)} = E_{solid}(x_i)^p \tag{6.16}$$

where E_{solid} stands for the isotropic property of the base material, while superscript p stands for the penalty parameter's exponent. Equation (6.17) can then be applied to link the Young's Modulus for (solid and void domains) with the pseudo-density.

$$E_{(x_i)} = E_{void} + {x_i}^p(E_{solid} + E_{void}) \qquad p \geq 1 \tag{6.17}$$

where Young's Modulus E_{void} is assigned to the void area, E_{solid} is assigned to the solid area, and each element's Young's Modulus is assigned by $E_{(xi)}$.

The penalty parameter p should be greater than 1 ($p \geq 3$ commonly defined) so that when it is included in the pseudo-density, which impacts the volume constraint while penalizing intermediate densities, there is a significant effect on the TO, as when the density ρi approaches 0, the stiffness also approaches 0. As a result, the material is considered as unnecessary and can be regarded as void. By contrast, when the inter-mediate density approaches 1, the material becomes crucial to the structural integrity and can be regarded to be solid (Aage et al., 2017).

The TO method's constraint is the volume fraction of the total volume of the designable region as function of to the pseudo-density, as stated in the following equation:

$$V = \sum_{i=1}^{n} x_i V_i \tag{6.18}$$

where V is the total volume of the designable region and V_i indicates the volume of the i^{th} element.

The objective function is defined to minimize the design structure's compliance while maximizing its stiffness that meets the requirements under the given constraints. The objective function can be mathematically represented as follows:

$$\begin{aligned} \min_x : \quad & c(x) = U^T K U = \sum_{e=1}^{N} (x_i)^P u_e^T k_0 u_e \\ \text{subject to: } & \frac{V(x)}{V_0} = f \\ & : KU = F \\ & : 0 < x_{min} \leq x_i \leq 1 \end{aligned} \tag{6.19}$$

where x represents the variable vector function in the formulation of $c(x)$, the volume fraction is expressed as $\frac{V(x)}{V_0} = f$, where V is the total volume and V_0 is the initial volume, K represents the global stiffness matrix, and U denotes the global displacement; thus, KU equals the force vector F. The displacement vector is u_e, while k_0 denotes the elemental stiffness matrix.

The following constraints must be satisfied during each optimization iteration: the target mass constraint, the global force-stiffness equilibrium, and the requisite functional constraints. Equation (6.20) expresses how the optimization respects the target mass constraint:

$$\sum_{e=1}^{N} (v_x)^T x_i \leq M_{target} \tag{6.20}$$

where M_{target} denotes the optimization's target mass.

In a mathematical TO, the density filter shape described by Sigmund is chosen (M. P. Bendsøe & Sigmund, 1999) (Höke & Bozca, 2020). The physical relative density filtration can be determined by $\tilde{x}_i$, as follows.

$$\tilde{x}_i = \frac{\sum_{j \in \mathbb{N}_e} w(r_i) v_j \tilde{x}_j}{\sum_{j \in \mathbb{N}_e} w(r_i) v_j} \tag{6.21}$$

The following formula expresses a neighborhood setting $N_e = \{i | \|r_i - r_e\| \leq R\}$, where R is the filter radius. The filter radii r_i and r_e are defined as those surrounding the centers of elements i and e, respectively. Additionally, the weighting function is denoted by the formula $w(r_i, r_e) = R - \|r_i - r_e\|$, where v_i denotes the volume of the i^{th} element.

Following our previous investigation (Mohamed Elelwi et al., 2021), the main objective in this stage is to apply the optimization to optimized composite materials chosen according to established criteria. Given that the STO has been used to minimize the structural compliance

while maximizing the global stiffness under given loads, the wing components' weight has been reduced to produce a lighter morphing weight.

The compliance optimization problem that we considered is formulated in the following equation:

$$C = \int_V fudV + \int_S tudS + \sum_i^n F_i u_i \tag{6.22}$$

where V represents the continuum's volume, f the distributed body force, t the traction force, F_i is the point load on the i^{th} node, u is the displacement area, u_i the i^{th} displacement degree of freedom, and S represents the surface area of the continuum.

6.4.2 Formulation of the Topology Optimization Objective Function

The structural design's discrete TO aims to minimize weight while maximizing stiffness and decreasing structural compliance. Thus, applying static loading on each wing component yields static stiffness (for both segments). The mechanical resistance to displacement represents the value of the produced deformation under static load (Bakhtiarinejad, 2015). Based on the displacement, the stiffness can be calculated mathematically as:

$$\mathrm{K}(x)u = F \tag{6.23}$$

where F denotes the vector of nodal forces, and u denotes the nodal displacement. The following equation can then be used to determine the nodal displacement:

$$u(x) = K(x)^{-1}F \tag{6.24}$$

Constraints on the design response, including limits on stresses and displacements, and other parameters, are indicated in the following equation.

$$\theta\{(x),(u)\}_1 \leq \theta_1^*, \theta\{(x),(u)\}_2 \leq \theta_2^*, \ldots \tag{6.25}$$

To estimate the influence of material density variation on the objective function of maximizing stiffness, the optimization code conducts a sensitivity analysis using the next equation.

$$\frac{dC}{dx_i} = -p(x_i)^{p-1}(x_i)^T(K_i)(u_i) \tag{6.26}$$

where K_i represents the displacement matrix element and u_i is the displacement vector for i^{th} element

When performing a sensitivity analysis, elements with a minimum material density are weighted, their characteristics become less significant for the structural design and; therefore, are eliminated in succeeding iterations. When the sensitivity of each element is calculated independently without considering the interconnection between these elements, the discontinuity of materials and volumes may appear, thus resulting in their discontinuity from the main geometry. The optimization iterations continue until the convergence of the objective function and therefore until the iterations meet their converge criteria.

As stated earlier, the main objective of the structural TO of the morphing wing design is to maximize the wing's stiffness while minimizing its weight. The density-based method is used in conjunction with the static linear method, (Daynes et al., 2017), thus resulting in the following mathematical formulation of the TO problem:

$$\begin{gathered} \min f(x) = f(x_1, x_2, \ldots\ldots, x_n) \\ g_j(x) \leq 0, \quad j = 1, \ldots\ldots, m \\ x_{i_{min}} \leq x_i \leq x_{i_{max}} \quad i = 1, \ldots\ldots, n \end{gathered} \tag{6.27}$$

where the independent variables of the objective function *f(x)* are the design variables *x*, the constraints denoted by *g*(*x*), and the upper and lower bound constraints x_{min} and x_{max}, respectively.

In the optimization procedure, the design space for each wing component was identified as a separate element. Gradient-based optimization is commonly employed due to its efficiency. The set of constraints were computed using their screening process, which minimized the required gradients. Calculating the gradients of given constraints can be facilitated by distinguishing between active and idle constraints, thus by employing the constraints' screening approach, minimizing the number of responses that include a representative set in an optimization problem. The approximate approach is used in conjunction with the optimization algorithm written and executed in numerical codes.

As a result of the TO, the compliance of static structural stiffness is entirely converted to potential deformation energy (Mou et al., 2017). The static stiffness of a structure can be determined using Finite Element Analysis (FEA). The design field's material distribution is optimized by the STO SolidThinking Inspire solver for TO, and by the OptiStruct solver for sizing optimization; the latter utilizes algorithms to obtain the shape of the best possible wing components. These two optimizations' strategies determine the best possible solutions for wing components' compliance under set boundary conditions, considering the design constraints to minimize their weights.

6.5 Materials Selection Strategy and Optimization Methodology

The design and development of a strong, lightweight variable span-morphing tapered wing (MVSTW) require the development of a Multidisciplinary Design Optimization (MDO) strategy so that the designed structure can meet all its constraints. Several optimization methodologies have been performed and combined to create a robust, lightweight wing (M. Elelwi et al., 2021) (Mohamed Elelwi et al., 2021).

This research presented here is using previous investigations and evaluates the wing design's performance and weight under design constraints. The key aspect is to balance the wing's strength and lightweight attributes by combining material selection with structural optimization. A literature search was carried out on the materials' parameters with the aim to define the optimal weight-to-strength ratios once their properties were obtained from published experimental results and analyses. The composite materials were selected based on the results of an in-house MATLAB code developed to evaluate their characteristics, such as physical–mechanical properties, availabilities, and costs. Optimization using multiple composite materials is more complicated than when a single material is used, as a high number of variables must be considered throughout the optimization process. The pressure was computed separately for each wing component to ensure more accurate results. The following sub-sections provide details on the settings identified for wing components optimization (Vasista et al., 2016).

6.5.1 Combination of Material Selection and Size Optimization for Wing Skin Thickness

After the material selection optimization, the wing skin will remain continuous, as sizing optimization will be performed rather than topological optimization. Consequently, long-fiber composites are a viable option for this application. The composite configurations vary in their fibers and matrix material types according to the stacking sequences and direction angles. Among the most crucial factors to consider are the costs of composite materials. For instance, glass fiber can be nearly ten times less expensive than carbon fiber.

The E-Glass composite has been considered in this work, as it is much less expensive than the other fibers and offers comparatively very good properties. The epoxy resin and E-glass properties were employed (Gibson & Plunkett, 1976).

Furthermore, the epoxy matrix is isotropic, while the fibers are anisotropic. The fiber/volume fraction was considered to be 60%, and the presence of voids was neglected. The longitudinal

properties and Poisson's ratio for the lamina were obtained from the equilibrium, compatibility, and stress–strain relationships, while the transversal Young's modulus was obtained using the Halpin–Tsai method (Shokrieh & Moshrefzadeh-Sani, 2016). The next phase is the calculation of the effective composite material mechanical characteristics.

This work will address a composite with eight layers (four symmetrical layers), in a configuration of $[0°/90°/0°/90°]_{syn}$, and the composite laminate can be considered isotropic. The initial thickness of each layer was set to 0.250 mm; therefore, the total thickness of the composite is 2 mm. However, the composite thickness can be adjusted depending on the sizing optimization results. It is feasible to obtain the laminate stiffness matrix and the ultimate properties of laminates by using the extensional stiffness, the coupling stiffness, and the bending stiffness matrices of the laminate (Gibson, 2016). Given that the acquired properties are determined analytically, the yield strength and ultimate strength will be considered as 2.5% of the Young's modulus and 1.5 times the yield strength, respectively. Table 6.4 below contains a summary of properties obtained using the method described above:

Table 6.4 Material properties of E-glass composite applied in the Sizing Optimization of the wing skin

Parameter	Value
Young's Modulus (quasi-isotropic)	30.578 GPa
Poisson's ratio	0.138
Yield strength	901.097 MPa
Ultimate strength	1351.645 MPa
Density	2.016 g/cm^3

This investigation used a technique identical to that used in prior optimizations (Mohamed Elelwi et al., 2021) with aluminum alloy 2024-T3. For all phases of this study, a baseline wing with an identical skin thickness of 2 mm was employed for both segments. The outcomes of size optimization (SO) in a 2D field were transferred to those in a 3D field to develop the best feasible wing skin (Coroian & Lupea, 2013). It is commonly understood that the Size Optimization (SO) is an iterative process. The CFD and the XFLR5 solvers were used to

calculate the aerodynamic loads on a full wingspan extension and at maximum speed to perform the Size Optimization on the wing skin. Meshing was applied to both segments, where the tetra-quadrilateral element size of 20 mm was used on both their lengths, as illustrated in Figure 6.5.

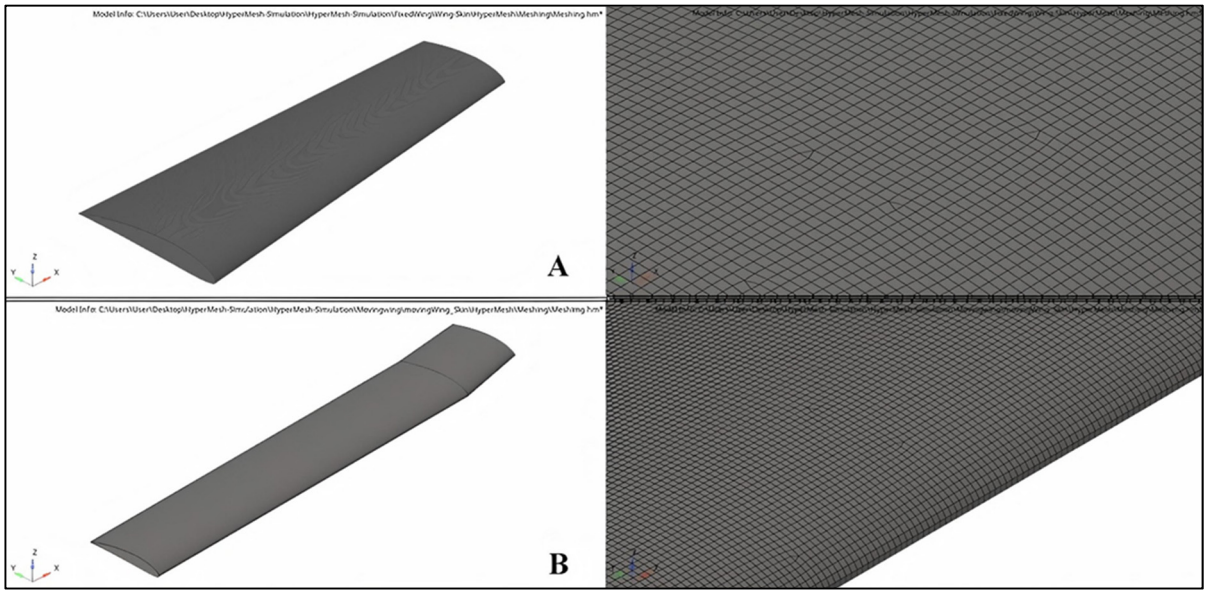

Figure 6.5 Meshing method for (A) fixed wing and (B) moving wing

Aerodynamic loads were used, and their design variables were considered as scalar parameters in the optimization computations. In this investigation, these parameters were determined to solve the optimization problem, as the thickness of the wing skin affects the system's responses. Design volume and set of the stresses were the variables applied to the optimization responses. The objective function was set to decrease the structural components' weights of the wing skin. The lower and upper bounds of the maximum stress values were given as the design constraints. Therefore, the design parameter of the maximum stress response was selected as 750 MPa. The design variable was given an initial value of 2 mm, as well as a lower and upper bound of 0.5 and 2 mm, respectively (Rinku & Ananthasuresh, 2015) (Girennavar et al., 2017). The following formulation was used to describe the optimization problem:

$$\begin{gathered} \min M \\ \sigma_{max} = 750 \text{ MPa} \\ 0.5 \leq T \leq 2 \end{gathered} \tag{6.28}$$

6.5.2 Combined Material Selection and Topology Optimization for Wing Spars

The spars design of the aluminum alloy 2024-T3 based on the Topology Optimization performs effectively, as demonstrated in (Mohamed Elelwi et al., 2021). The TO aims to maximize the structural stiffness, and then the maximum stress obtained for the optimized component should be less than the yield strength and is used as a reference for selecting alternative lighter materials. Aluminum 2024-T3 has a yield strength of around 345 MPa. The main limitations of this material in terms of its optimization are its geometric shape, i.e., areas that should be preserved intact due to the allocation of structures inherent to the mechanism or for the load distribution continuity.

Long-fiber composite materials, widely utilized in the aerospace industry, would be very good candidates for this application. However, the spars should be topologically optimized, and so there would be several regions with cut-outs, according to an earlier investigation in which aluminum alloy 2024-T3 was used for the wing spars' design (Mohamed Elelwi et al., 2021).

Avoiding the fibers' cut-out requires a more expensive manufacturing technique, and the material properties of such spars after machining will be less predictable. Therefore, composite materials with long fibers would be inappropriate for this application. Polymers, however, have a low manufacturing cost, moderate to high strength, and low-density properties (Batista et al., 2019). High-Density Polyethylene (HDPE) has been tested to evaluate its properties for use in structural applications (Batista et al., 2019) (Costa, Zanini, & Mulinari, 2021). HDPE could be derived from virgin manufacturing or from 100% recycled HDPE. While the environmental benefit of recycled HDPE is significant, the percentage of impurities in the material could be a limitation, as HDPE is commonly used in conjunction with other polymers, such as polypropylene (PP) (Vasconcelos, Basso, & Valera, 2019).

Numerous papers detail the mechanical characteristics of pure HDPE. The values acquired from various sources are averaged for this work (Batista et al., 2019) (Costa et al., 2021)

(Vasconcelos et al., 2019) (Awad, El Gamasy, Abd El Wahab, & Abdellatif, 2019). In terms of Poisson's coefficient, the value of 0.4 is considered as shown in Table 6.5, the same as the value used by Contino et al. in (Contino et al., 2020).

Table 6.5 Material properties of HDPE applied in the topology optimization of the wing spars

Parameter	Value
Young's Modulus	1250 MPa
Poisson's ratio	0.4
Yield strength	28 MPa
Ultimate strength	48 MPa
Density	0.95 g/cm^3

In aircraft wings, the spar is one of the most critical components, as it must be able to withstand the most severe aerodynamic loads and to provide support for other wing components. A spar is an extended beam that is installed on the length of the wingspan and provides support to the wing when subjected to bending loads. In other words, it should be strong enough to support the effects of tensile, compressive, and shear loads. The afore-mentioned TO for baseline solid wing design has been proposed, using two spars at predetermined locations for each wing segment, as seen in Figure 6.6 (M. Elelwi et al., 2021).

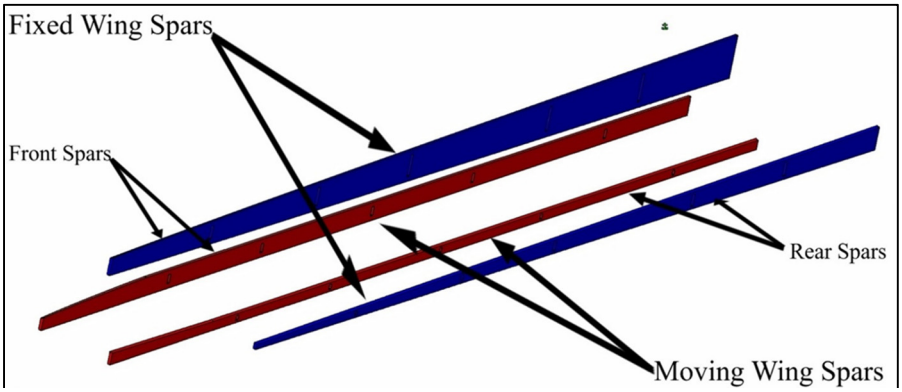

Figure 6.6 Baseline geometrical shape for morphing wing spars at their initial position for fixed and moving segments

The aerodynamic loads were calculated using the ANSYS Fluent and XFLR5 software tools, with the spars modeled as beams with discrete loads at various locations (Table 3 gives their values). The structural weights of wing spars were considered when formulating the problem for the wing spars, as the primary objective was to determine the ideal structural parameters of the wing. This objective made it possible to establish the wing's minimal weight while still meeting the constraints of strength, durability, and versatility (M. Elelwi et al., 2021).

The same approaches as those considered in the previous optimization were used to determine the I-beam sections. The fundamental motivation for using an I-beam section (except where it links to the ribs) is its significant mechanical advantages over other beam configurations. The I-beam shape supports the other wing components extremely well, resists mechanical strain (such as torsion and deformation), decreases the load intensity on the other components, and lowers weight and costs (Grbović et al., 2019) (Grisval & Liauzun, 1999).

All wing spars were undergone to identical analysis techniques in a 3D environment (C. Li et al., 2015).
Figures 6.7 and 6.8 show the specified designable and non-designable portions of the front and rear spars with their associated boundary conditions for fixed and moving wing segments, respectively.

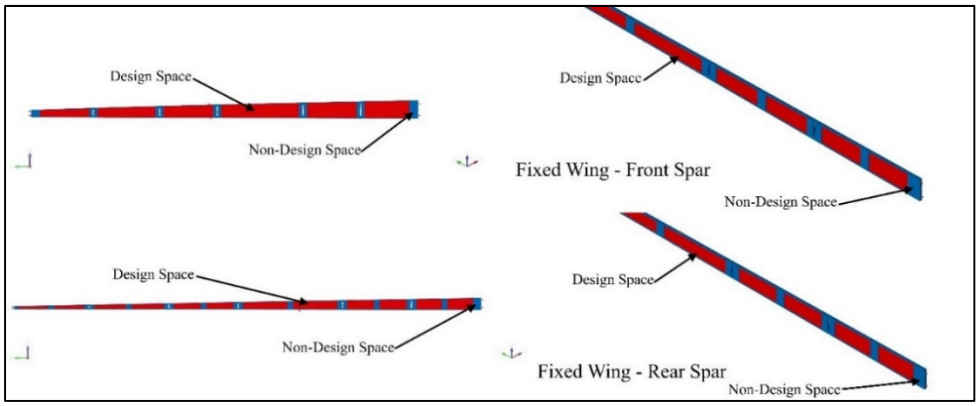

Figure 6.7 Boundary conditions with design and non-design spaces for the front and rear spars of a fixed wing

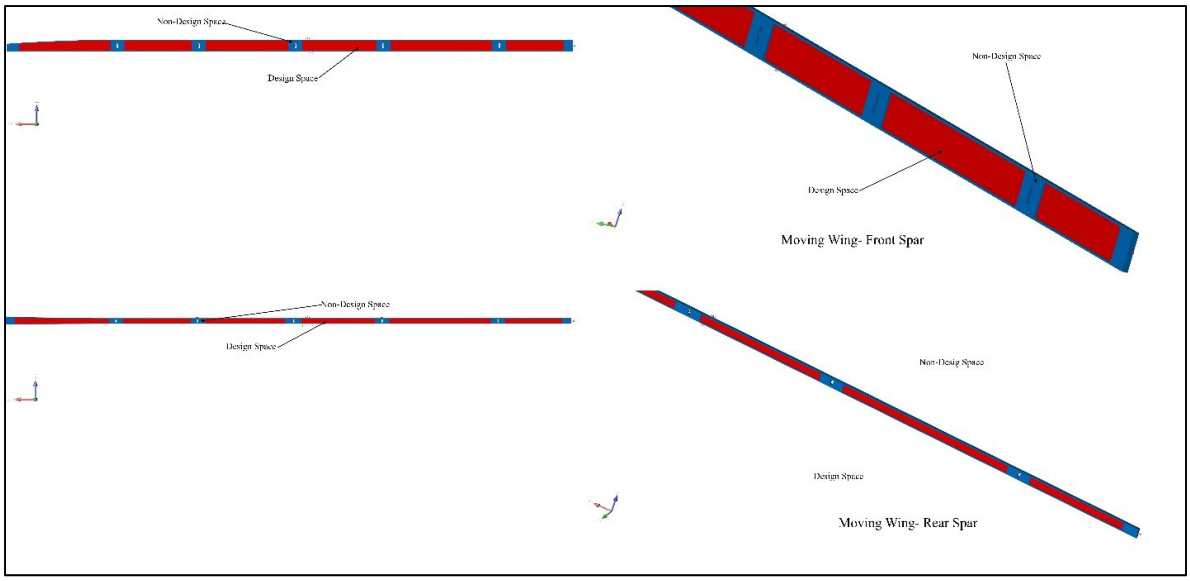

Figure 6.8 Boundary conditions with design and non-design spaces for the front and rear spars of a moving wing

6.5.3 Combined Material Selection and Topology Optimization for Wing Ribs

As in the case of spars, the priority for an initial analysis of unconventional materials for wing ribs was focused on polymers. Since the rib geometry is critical to the wing aerodynamics, its manufacturing should be precise and repeatable. Therefore, 3D printers were utilized to reduce costs, speed up production, and increase accessibility.

When considering three-dimensional printing, various factors in addition to the printing material affect the final product's mechanical qualities, such as the manufacturing method. Acrylonitrile Butadiene Styrene (ABS) is one of the first polymers that was widely used in 3D printers, and its properties are well known in the extensive documentation. Nomani et al. (Nomani, Wilson, Paulino, & Mohammed, 2020). Describe the thickness effects of each ABS layer on the final product's tensile and compression properties, revealing that, in general, increasing the thickness of each layer results in a decrease in the Young's modulus, ranging from 2.0 GPa for a thickness of 0.2 mm to 1.55 GPa for a thickness of 0.8 mm.

The ABS Poisson's ratio was investigated by Cantrell J. et al (Cantrell et al., 2017). According to their research findings, Poisson's coefficient exhibits little variation in relation to print/raster orientation. The values obtained ranged from 0.36 to 0.38.

Thus, Poisson's coefficient of 0.36 will be used for the ABS in this work. Table 6.6 below highlights the ABS properties that have been considered in the investigations mentioned above.

Table 6.6 Material properties of ABS applied in the topology optimization of the wing ribs

Parameter	Value
Young's Modulus	2000 MPa
Poisson's ratio	0.36
Yield strength	30 MPa
Ultimate strength	36 MPa
Density	1.05 g/cm^3

As illustrated in Figure 6.9, the wing baseline of the previous TO offers a total of seven ribs for each wing segment, with estimated lengths between the ribs on the wings (M. Elelwi et al., 2021). These ribs are intended to minimize wing deformation by keeping the geometrical structure of the wing's sections. Therefore, the wing's outward loads are distributed equally across the skin and wing components. As shown in Figure 6.9, a cavity should be included in the fixed wing ribs to accommodate the moving wing. The TO was therefore applied to the interior six ribs of each wing segment. The exterior ribs for each wing segment were excluded from design optimization as the last rib of the fixed wing should be solid and only hold the cavity of the moving wing. Furthermore, the ribs of the moving wing should have a solid shape for better aerodynamic efficiency.

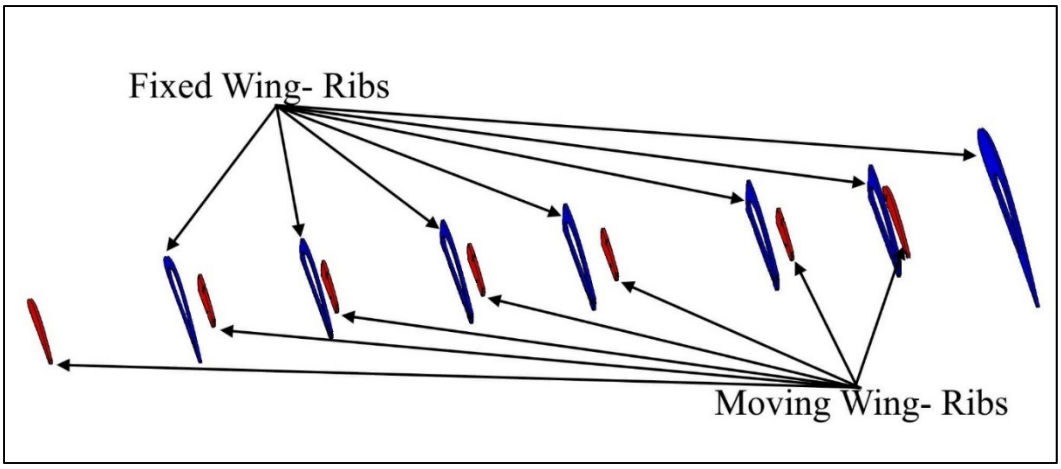

Figure 6.9 The geometric shape of morphing wing ribs for fixed and moving wings

The original design space layout and boundary conditions were applied to establish the optimal material distribution inside the ribs. Ribs for each wing were discretized into separate components, and node numbers were assigned to them according to their sizes on both wings. Figures 6.10 and 6.11 illustrate the boundary conditions of ribs of both wing segments.

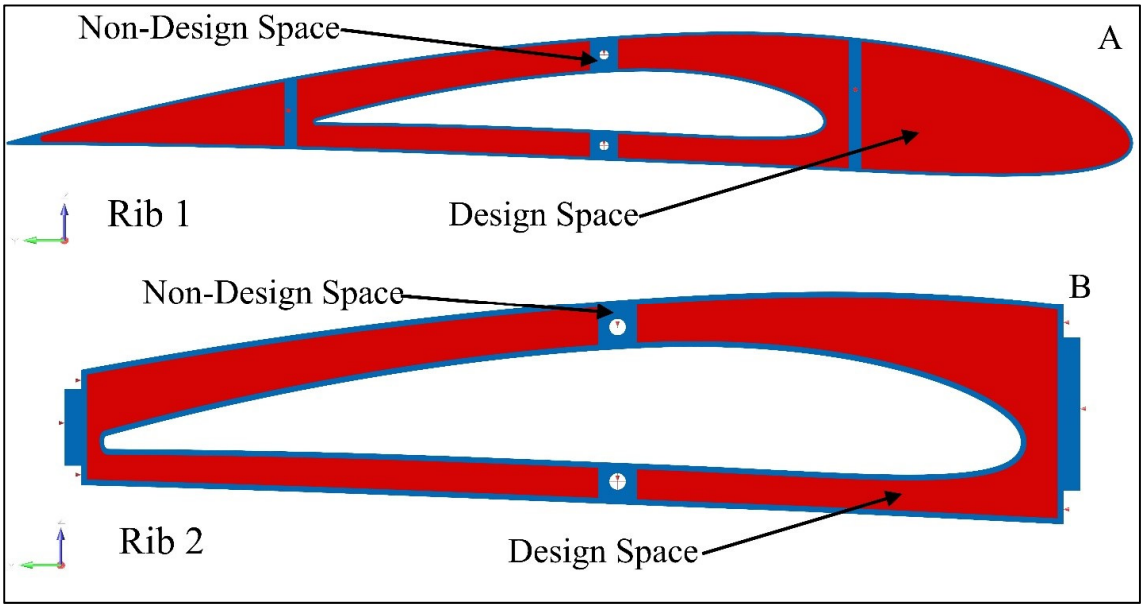

Figure 6.10 Examples of the boundary conditions, designable space, and non-designable space for ribs 1 and 2 of the fixed wing

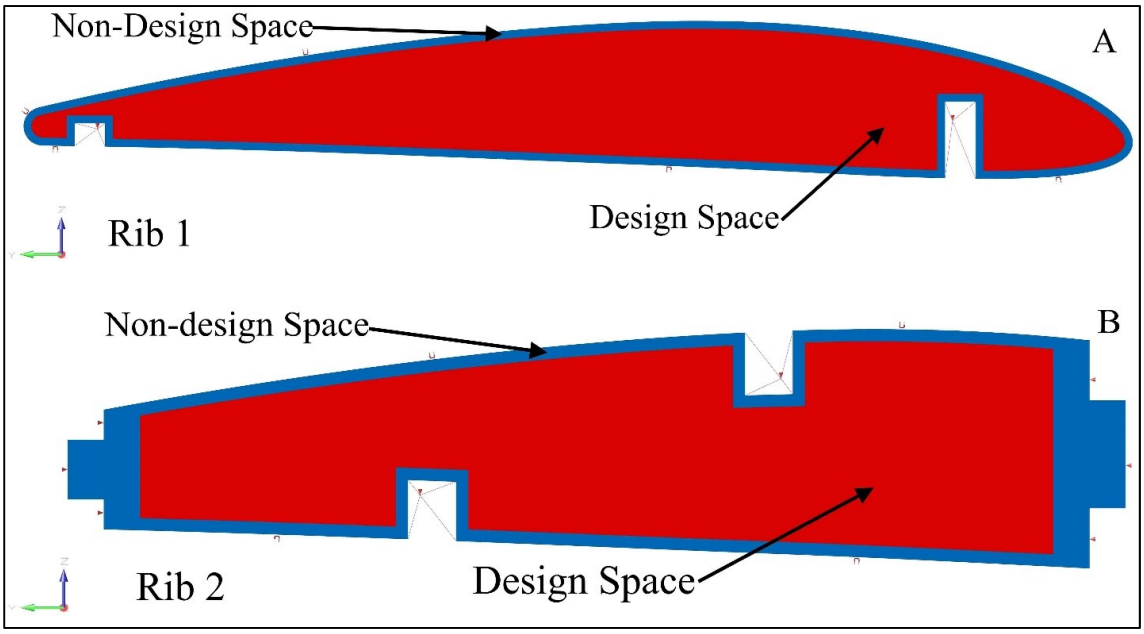

Figure 6.11 Examples of the boundary conditions, designable space, and non-designable space of ribs 1 and 2 of the moving wing as an example

By considering the wing ribs as an opposing constraint, a volume constraint was applied to all of them in the optimization problem. The loads acting on each rib can be computed efficiently by aerodynamic optimization, as indicated in Table 6.4. The designable areas and the rib edges were also included in the objective function. Connection locations linking the ribs within the spars were not included in the TO process; they were considered non-designable regions. Areas that were not designable at sparse connection locations were fixed during optimization because they were not included in the design field.

6.5.4 Combined Material Selection and Topology Optimization for Wing Support Element's Structure

The wing's support elements are crucial to a wing structure's integrity, and thus to the design of a robust wing. Several composite materials were investigated to determine the most appropriate materials for this project. The material selection criteria were subjected to various parameters, including cost, mechanical behavior, and availability on the market. Three

materials were adopted for support elements: balsa wood, white oak, and aluminum alloy 6063-T6.

The excellent lightweight and insulating characteristics of balsa wood have made it a commercially important material in many applications, where it was used as the core of sandwich-type constructions for critical weight applications in aircraft and ship structures. Its radial mechanical characteristics are affected by the bending of the fibers, as well as by the axial compression of the rays under radial stresses (Sadler, Sharpe, Panduranga, & Shivakumar, 2009) (Borrega & Gibson, 2015).

Table 6.7 shows the material properties of balsa wood.

Table 6.7 Material properties of balsa wood applied in the topology optimization of the wing support elements

Parameter	Value
Young's Modulus	3.4 GPa
Poisson's ratio	0.23
Yield strength	21.6 MPa
Ultimate strength	21.6 MPa
Density	0.16 g/cm^3

White oak is used in various industrial applications due to its desirable qualities. White oak (Quercus alba), a relatively high-density ring-porous hardwood, was used to build several support elements for our wing (Erchiqui, Annasabi, & Diagne, 2021);

Table 6.8 shows its material properties.

Table 6.8 Material properties of white oak applied in the topology optimization of the wing support elements

Parameter	Value
Young's Modulus	12.27 MPa
Poisson's ratio	0.369
Yield strength	104.8 MPa
Ultimate strength	104.8 MPa
Density	0.68 g/cm^3

The aluminum alloy 6063-T6 was used to design other support elements. Isotropic aluminum alloy 6063-T6 offers very good durability and high solidity and fatigue resistance. (Singh & Agrawal, 2015). Table 6.9 shows its material properties.

Table 6.9 Material properties of aluminum alloy 6063-T6 applied in the topology optimization of the wing support elements

Parameter	Value
Young's Modulus	68.9 GPa
Poisson's ratio	0.33
Yield strength	214 MPa
Ultimate strength	241 MPa
Density	2.7 g/cm^3

The leading-edge ribs, trailing-edge ribs, stringers, and stiffeners for the optimized wing based on the TO approach were developed using an initial design for the baseline wing. Each wing segment's support elements were built as shear webs to provide stability and to withstand buckling, bending, torsion, and vertical shear loading. Along with aerodynamic and inertial loads acting on the wings, various loads depending on their shapes and structural masses might be considered during the design process. Furthermore, the payload, which can be on electronic

equipment or a monitoring camera, may be carried on the wings or in the fuselage. This equipment adds weight as increases to the wing's bending, shear, and torsion loads.
Wing components with shear web structures offer a reliable design by distributing loads on the wing in multiple directions. The structure and materials of the support elements for both segments of a VSMTW are illustrated in Figure 6.12.

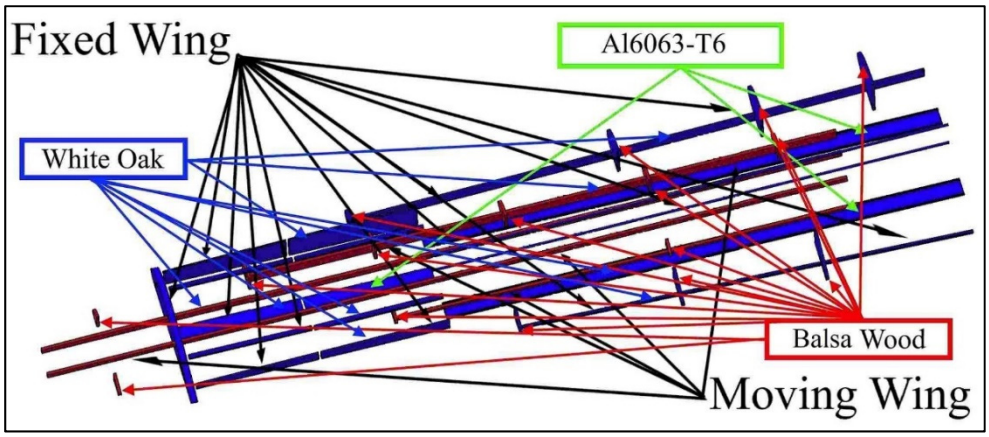

Figure 6.12 Support elements with their materials for each wing component for fixed and moving wings at their original positions

The boundary conditions applied to the support wing elements matched the boundary conditions for the spars and ribs. The structure of the wing's support elements and their boundary conditions were calculated using parametric data from the aerodynamic optimization, as shown in Table 6.3. Since the weight of the support elements greatly contributes to the overall weight of the wing, its minimization while preserving its stiffness is crucial.

The boundary conditions that apply to the support elements vary according to the component's dimensions. Figures 6.13 and 6.14 depict the boundary conditions of several support components for the fixed and moving wing, respectively. The volume constraint was applied to the support element structure, which functioned as an opposing constraint in the optimization process.

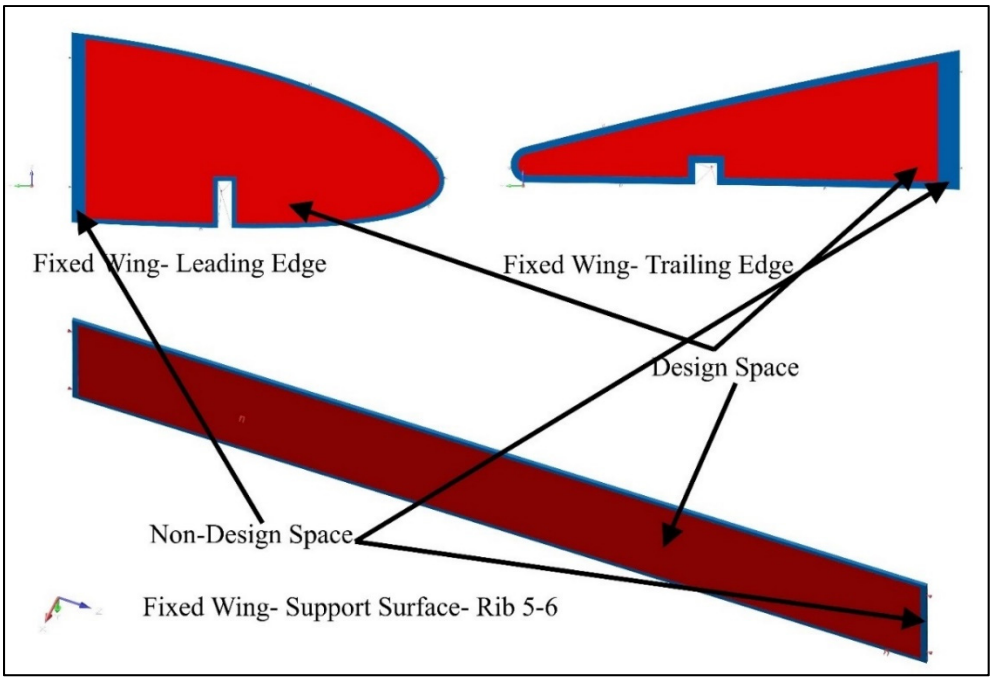

Figure 6.13 Boundary conditions, designable space, and non-designable space as examples for support elements (leading-edge rib 1, trailing-edge rib 1, and bottom support plate between ribs 5 and 6) for a fixed wing

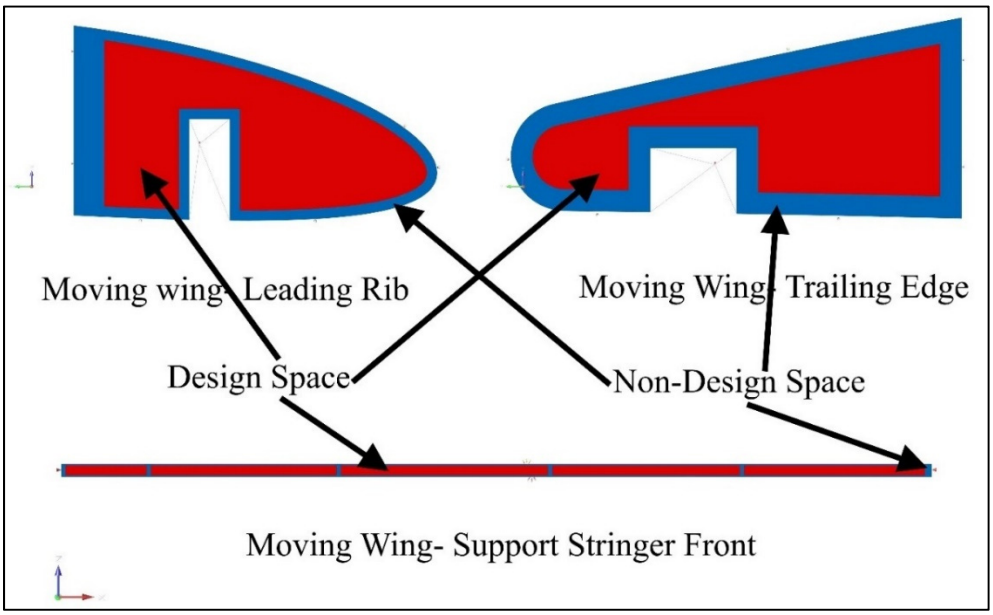

Figure 6.14 Boundary conditions, designable space, and non-designable space as examples for support elements (leading-edge rib, trailing-edge rib, and support stringer front) for a moving wing

The area between the wing components attached to others cannot be altered from its original design, as it links each component to the others. The edges of the support elements and the sites where the support element components are bound to other wing components were thus determined to be non-designable. Due to the multiple locations where connections between wing components must be established, these components were specified with their fixed regions throughout the TO. They indicate the connections with other wing components and can thus be modified throughout the optimization process.

6.6 Multidisciplinary Optimization Results and Evaluation

Aerodynamic analysis, material selection code, and structural optimization STO were performed on the VSMTW, as described in the preceding sections, to improve the UAS-S4′s capabilities under various flight scenarios. Altair's Inspire and OptiStruct tools provide design engineers with the most powerful and user-friendly generative design/optimization and quick simulation solutions. The optimization problem was then solved with multidisciplinary numerical optimizations. This optimization problem takes into account the parameters that define the overall performance.

These parameters were treated as either optimization objectives or constraints during the optimization process. Size and topology variables were used to determine the thickness of the skin and the optimized structure of the other wing components, respectively.

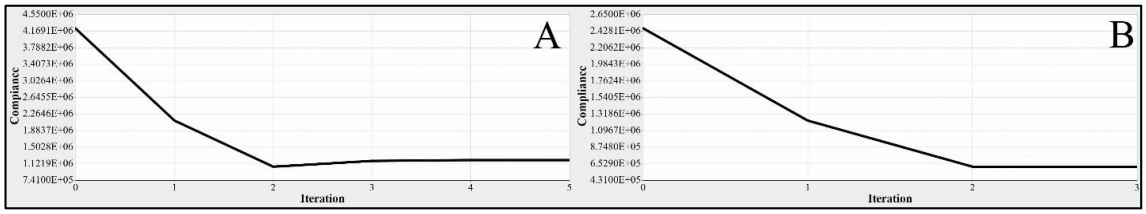

Figure 6.15 The objective function convergence graphs for (A) fixed wing skin and (B) moving wing skin

The same design constraints were imposed on the structural stiffness to conduct the wing skin's size optimization (SO) for both segments. Figure 6.15 shows how a few optimization iterations were applied to rapidly converge to the optimal solution with a highly efficient skin thickness.

The SO was carried out on each wing segment. Figure 6.16 illustrates the results of the study's interpretations for both types of wing segments.

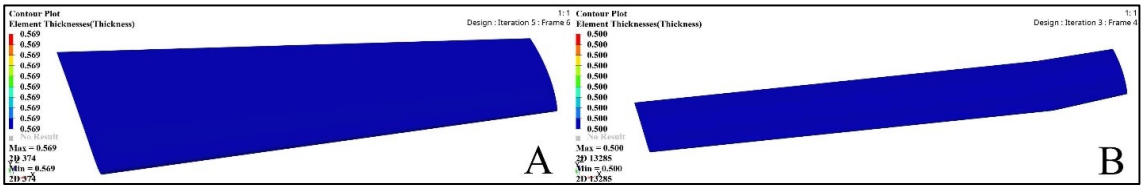

Figure 6.16 The thickness obtained based on sizing optimization (SO) results for (A) fixed wing and (B) moving wing

To serve as a reference for size optimization, the base wing for fixed and moving segments was designed with a thickness of 2 mm. Figure 6.17 illustrates the FEM results for estimating the optimized wing thickness for both wing skins. This optimization is based on a FEM static analysis performed under extreme flight conditions, during which stress and deformation were generated.

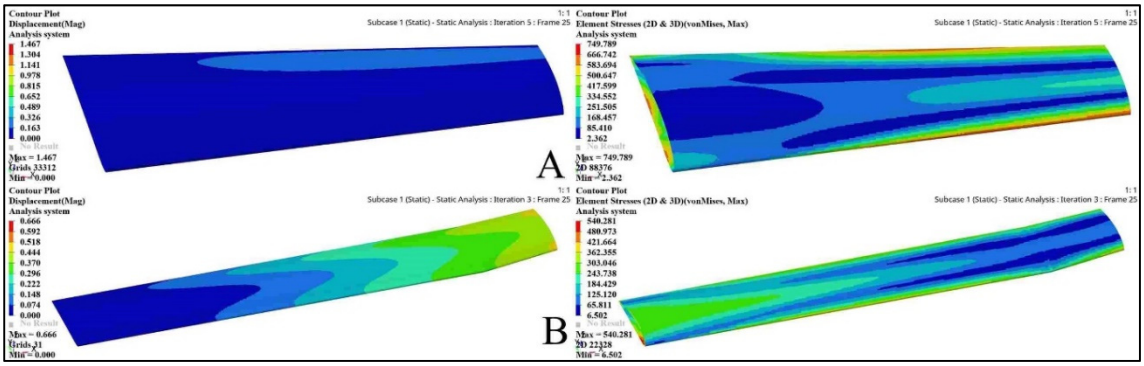

Figure 6.17 The sizing optimization problem FEM results for fixed (A) and moving (B) wing segments

The maximum stress value used in the Size Optimization (SO) of the wing applied to both segments' skins was limited to 750 MPa in order to obtain the optimal thickness capable of achieving the highest efficiency to withstand the aerodynamic loading. Both wing segments were subjected to identical boundary conditions, and SO and FEM analyses were conducted according to the wing volume and shape. The maximum deformations and stresses obtained under extreme flight scenarios, as well as other key parameter values resulting from the optimization results, are summarized in Table 6.10.

Table 6.10 Evaluations obtained via SO and FEM for the wing skins for both wing segments

	Iterations	Deformation	Stress	Original Skin	Optimized Skin	Weight Reduction
Fixed Wing	5	1.47 mm	749.79	2 mm	0.569 mm	81.45%
Moving	3	0.67 mm	540.29	2 mm	0.500 mm	81.80%

To apply the TO, multidisciplinary numerical optimization was used to define the optimized spars that would provide maximum wing stiffness while reducing the wing weight. The aerodynamic investigation determined the maximum aerodynamic pressures for extreme flight scenarios. The wing structure was investigated aerodynamically at sea level and at maximum speed (68 m/s) with the aim to achieve the appropriate distribution of aerodynamic loading across the wingspan, as depicted in Table 11. Altair's SolidThinking Inspire software was used to fulfill the TO objective. The initial wing spars' topology and shape were optimized to minimize the structural compliance and to maximize the structural stiffness to weight ratio while remaining within the target envelope's restrictions.

The volume fraction of 30% was used to obtain the maximum structural stiffness and then to use that value as an optimization constraint. The design variable is the structural weight associated with an assigned global compliance-based stress. The TO results are summarized in Table 6.11.

Table 6.11 The parameters of the wing segments for spars were determined by TO using Finite Element Analysis (FEA)

	Fixed Wing		Moving Wing	
	Front Spar	Rear Spar	Front Spar	Rear Spar
Initial Weight	0.29 kg	0.16 kg	0.19 kg	0.59 kg
Optimized Weight	0.17 kg	0.11 kg	0.12 kg	0.08 kg
Weight reduction Ratio	41.4%	31.3%	36.8%	86.4%
Displacement	0.00015 mm	0.00056 mm	0.00020 mm	0.00057 mm
Stress	0.2016 MPa	0.3191 MPa	0.1869 MPa	0.1973 MPa
Safety Factor	31830	66130	2864000	4264000

Figure 6.18 depicts an iterative process for determining the element density based on the TO results of the wing spar and as shown in Table 6.10. Table 6.11 shows the parameters of the most critical wing spars as a function of the design parameters. The advantage of using TO in SolidThinking Inspire is that the FE characteristics are changed according to the optimization results. The FE characteristics obtained using the TO are shown in Figures 6.19-6.21. Table 6.11 lists the weights of the original and optimized spars, thus revealing a considerable reduction in the average weight.

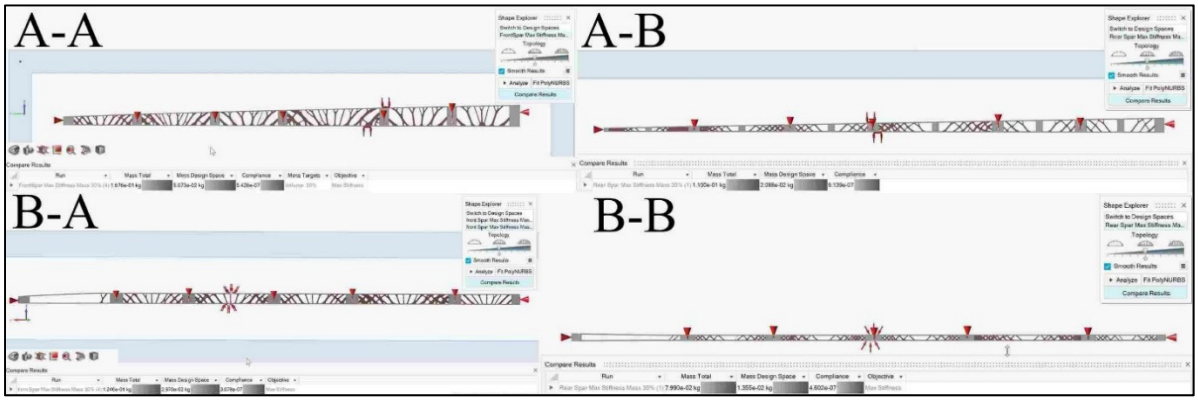

Figure 6.18 Variation in element density obtained using the TO for (A–A) fixed wing front spar, (A–B) fixed wing rear spar, (B–A) moving wing front spar, and (B–B) moving wing rear spar

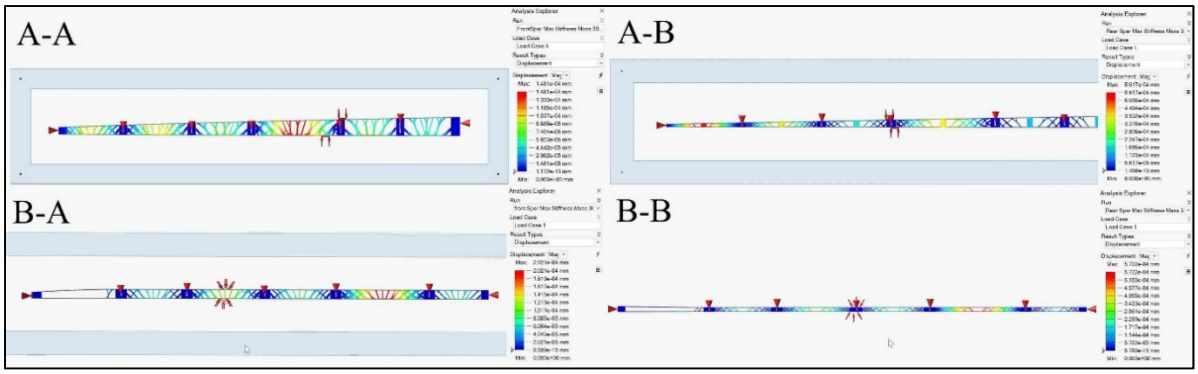

Figure 6.19 Displacement values obtained using the TO for (A–A) fixed wing front spar, (A–B) fixed wing rear spar, (B–A) moving wing front spar, and (B–B) moving wing rear spar

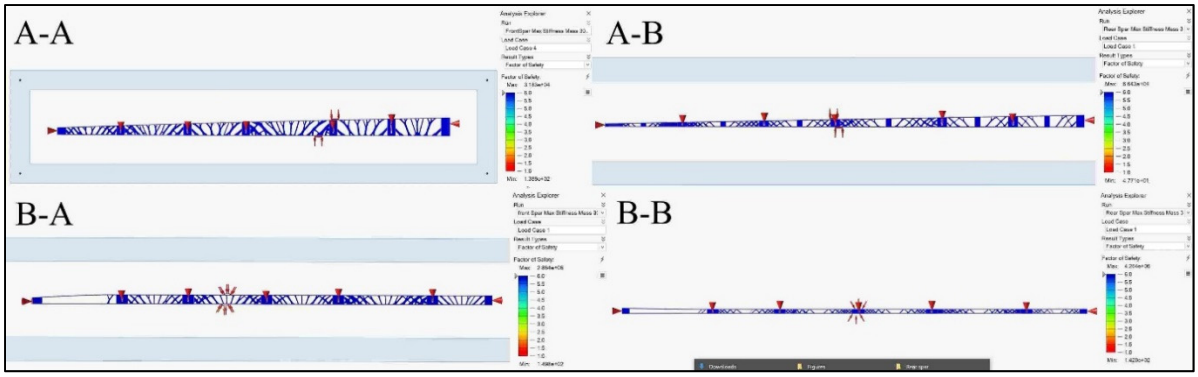

Figure 6.20 Safety factor evaluations obtained using the TO for (A–A) fixed wing front spar, (A–B) fixed wing rear spar, (B–A) moving wing front spar, and (B–B) moving wing rear spar

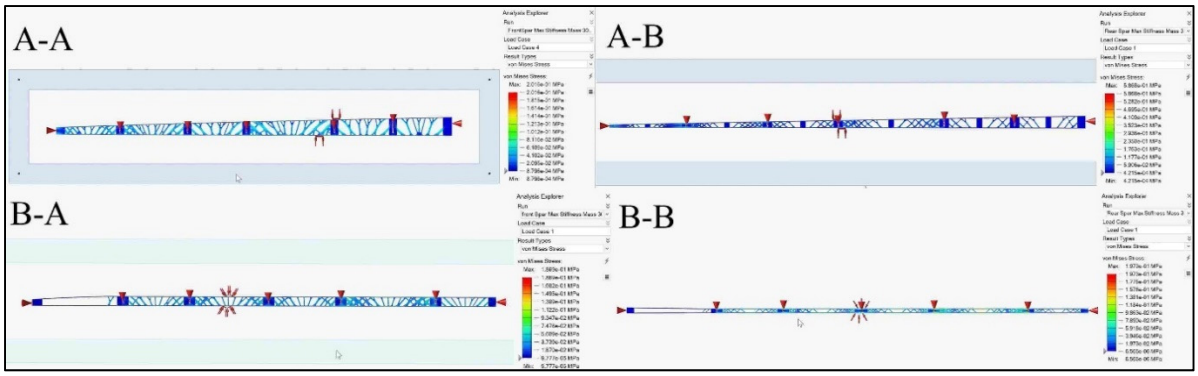

Figure 6.21 Von mises stress values obtained using the TO for (A–A) fixed wing front spar, (A–B) fixed wing rear spar, (B–A) moving wing front spar, and (B–B) moving wing rear spar

This component-analysis-based TO methodology leads to a comprehensive structural design and offers an alternate method for minimizing the structural weight of wing spars. The results shown in Table 6.10 also demonstrate that the component-analysis-based TO strategy for high effectiveness and reliability in the continuum design of wing components can be a practical and logical design technique.

The wing ribs were subjected to similar steps as those applied to the wing spars calculations. According to its computed aerodynamic loading, an optimization approach based on the Finite Element Model (FEM) was constructed for each rib. Design variables were determined, including the material density of each element. Two analysis responses were identified, which were described in terms of structural compliance and volume fraction, with the volume fraction classified as a constraint and the compliance characterized as an objective function. The volume fraction was used as a constraint in the standard TO configuration, which resulted in compliance minimization. Figure 6.22 illustrates the distribution of material density of the wing ribs as determined by TO. The FE models developed for the specified ribs based on the TO approach il-lustrated in Figures 6.23–6.25 reveal that significant weight savings were achieved without compromising component stiffness.

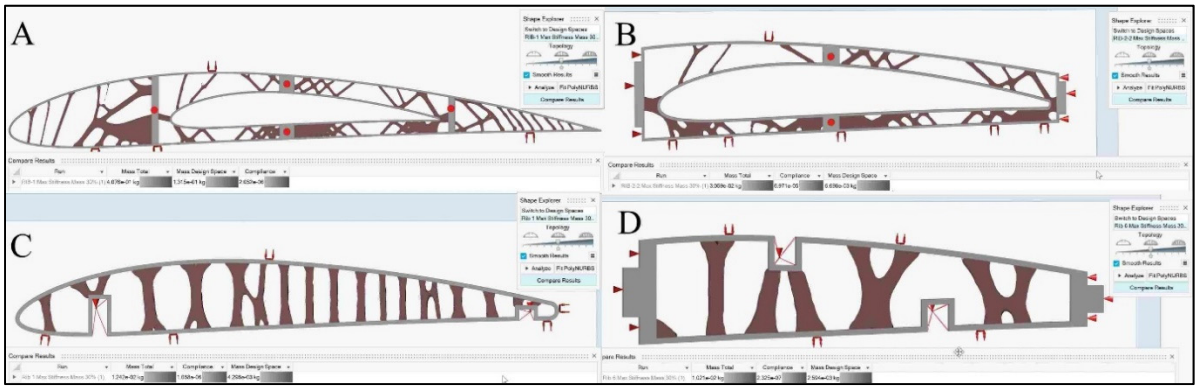

Figure 6.22 Variation in element density obtained using TO for (A) fixed wing rib 1, (B) fixed wing rib 2, (C) moving wing rib 1, and (D) moving wing rib 6

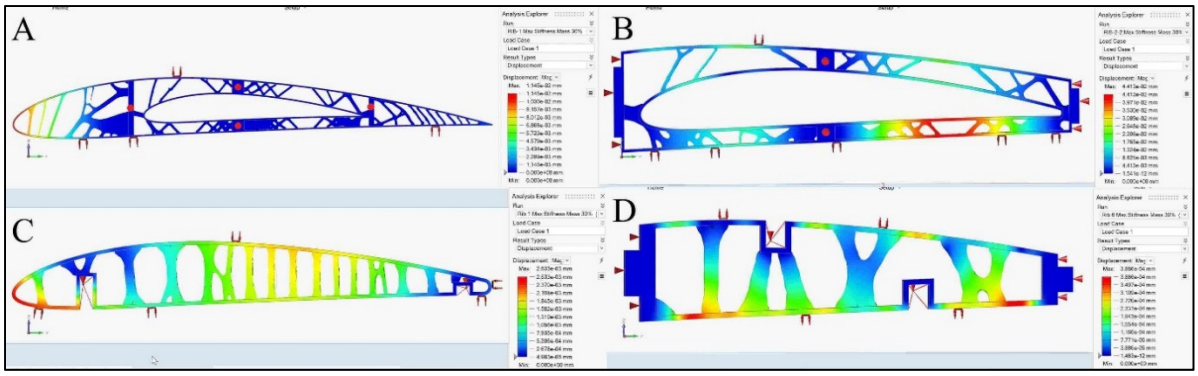

Figure 6.23 Displacement values obtained using TO for (A) fixed wing rib1, (B) fixed wing rib2, (C) moving wing rib1, and (D) moving wing rib6

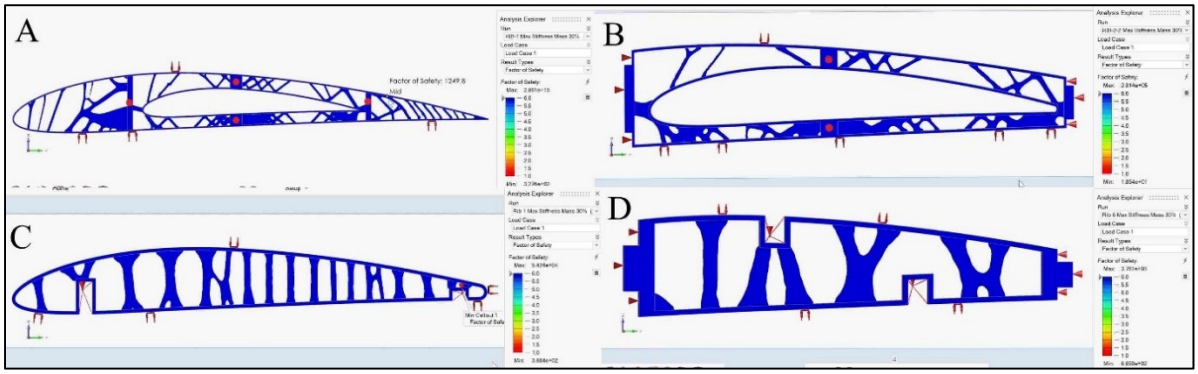

Figure 6.24 Safety factor evaluations obtained using TO for (A) fixed wing rib1, (B) fixed wing rib2, (C) moving wing rib1, and (D) moving wing rib6

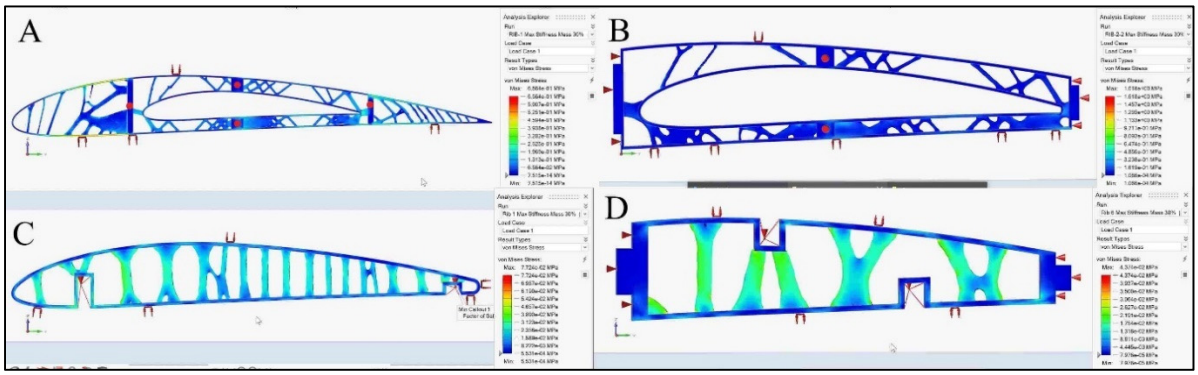

Figure 6.25 Von mises stress values obtained using TO for (A) fixed wing rib1, (B) fixed wing rib2, (C) moving wing rib1, and (D) moving wing rib6

The outcomes of the MVSTW rib obtained by TO are shown in Table 6.12 for their different initial values determined via the distribution of aerodynamic loads. When the ribs' weights before and after optimization were compared, their weights were minimized due to the calculated loads on them. All ribs had extremely low maximum loads and displacements; hence, the optimized ribs met the required strength and stiffness.

Table 6.12 Topology optimization according to Finite Element Analysis yielded these wing segment parameters for the ribs

		Initial Weight	Optimized Weight	Weight reduction Ratio	Deformation	Min Factor of safety	Stress
Fixed Wing	Rib 1	0.094 kg	0.054 kg	42.6%	1.02 mm	47.5	6.31 MPa
	Rib 2	0.0459 kg	0.0305 kg	32.6%	0.0044 mm	18.5	1.62 MPa
	Rib 3	0.042 kg	0.029 kg	31%	0.05 mm	38.9	0.77 MPa
	Rib 4	0.035 kg	0.026 kg	25.7%	0.094 mm	35.7	0.84 MPa
	Rib 5	0.031 kg	0.024 kg	22.6%	0.15 mm	30.7	0.98 MPa
	Rib 6	0.029 kg	0.026 kg	10.3%	2.07 mm	8.9	3.38 MPa
	Rib 7	0.033 kg	0.033 kg	0	0	0	0
Moving Wing	Rib 1	0.022 kg	0.012 kg	70.1%	0.0026 mm	38.8	0.078 MPa
	Rib 2	0.016 kg	0.01 kg	37.5%	0.00078 mm	310.9	0.097 MPa
	Rib 3	0.016 kg	0.01 kg	37.5%	0.00078 mm	310.9	0.097 MPa
	Rib 4	0.016 kg	0.01 kg	37.5%	0.00078 mm	310.9	0.079 MPa
	Rib 5	0.016 kg	0.01 kg	37.5%	0.00037 mm	68.6	0.032 MPa
	Rib 6	0.016 kg	0.01 kg	37.5%	0.00037 mm	68.6	0.027 MPa
	Rib 7	0.044 kg	0.044 kg	0	0	0	0

The wing components, including spars, ribs, and support elements, are shown entirely in blue color, and are not at risk of mechanical failure under corresponding load cases, as indicated in Figures 6.20, 6.24, 6.28, and 6.32. Thus, the optimized variable span-morphing wing can withstand the extreme aero-mechanical loads encountered throughout varied aircraft missions. Given that these wings should be solid, the seventh rib for both the fixed and moving wing segments was eliminated from the optimization procedure.

The optimized wing segments represented as solids imply that a wing should incorporate TO support elements to meet its design requirements. Table 6.3, as well as Figures 6.3 and 6.4, show the different aerodynamic load situations used to design the support elements for extreme

flight conditions. The TO was performed on the structure of the support elements for both wing segments under the specified load cases. The support elements' density cloud maps were represented using the results of several TOs, as illustrated in Figures 6.26 and 6.30 for fixed wing and moving wing, respectively. Figures 6.27–6.29 show how a TO method affects structural changes in mechanical parameters for fixed segments, such as deformations and stresses.

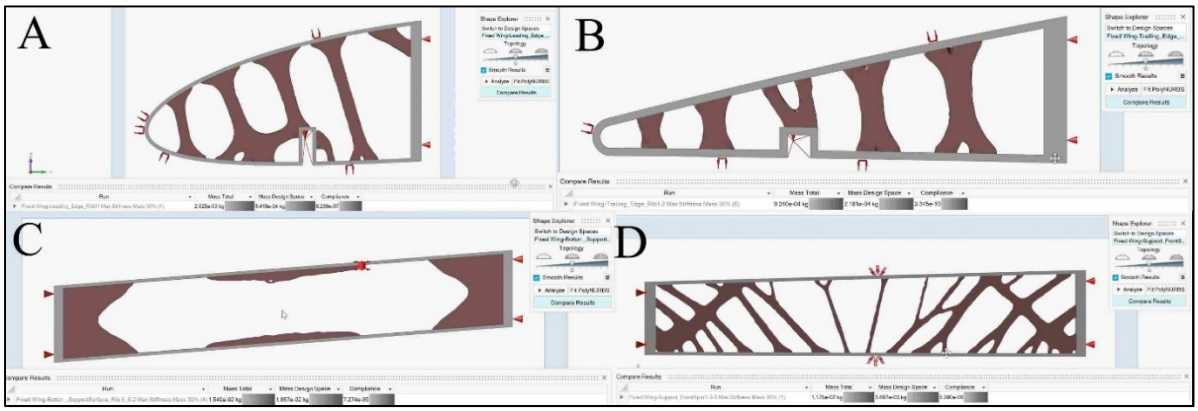

Figure 6.26 Variation in element density in relation to TO results of a fixed wing: (A) leading edge of rib 1, (B) trailing edge of rib 1, (C) bottom support surface between rib 6 and rib 7, and (D) front spar support

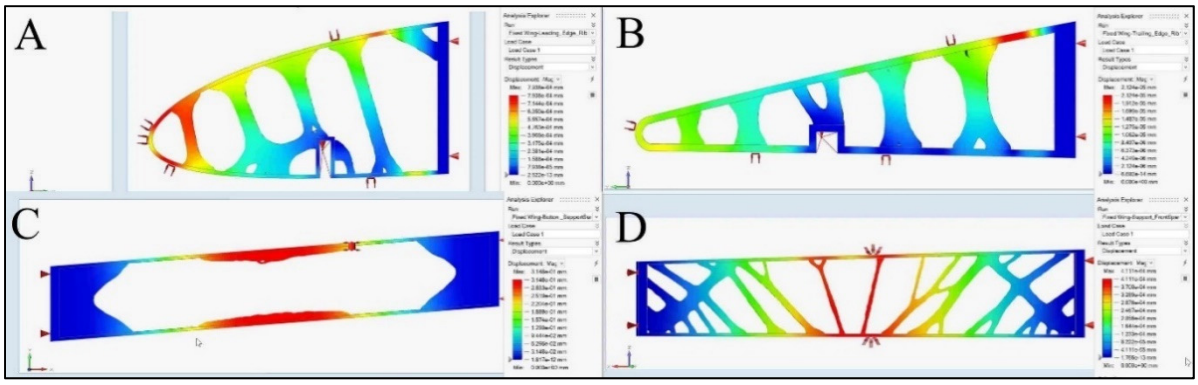

Figure 6.27 Displacement values in relation to topology optimization results of a fixed wing: (A) leading edge of rib 1, (B) trailing edge of rib 1, (C) bottom support surface between ribs 6 and 7, and (D) support of a front spar

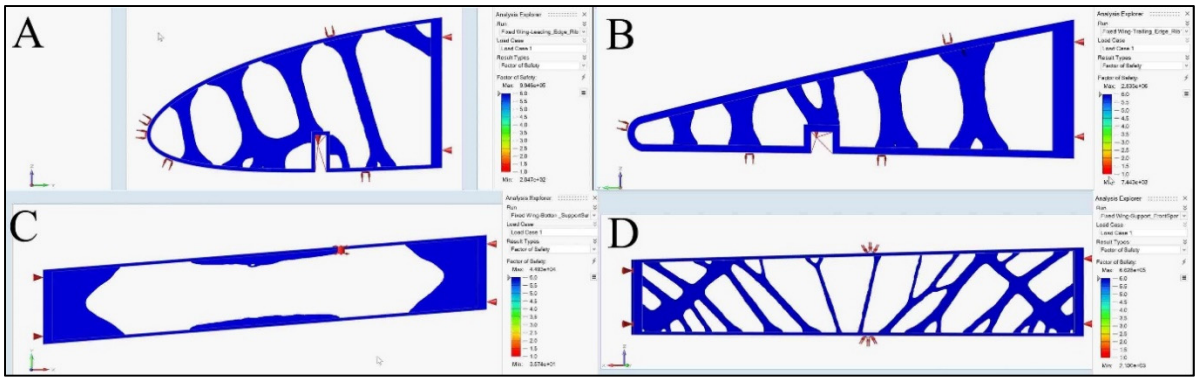

Figure 6.28 Safety factor evaluations obtained using TO for a fixed wing: (A) leading edge of rib 1, the (B) trailing edge of rib 1, (C) bottom support surface between ribs 6 and 7, and (D) support of a front spar

Based on the TO results, the fundamental structure of support components was substantially optimized by reducing the weights of the support elements. Furthermore, as seen in Figure 6.28, structural compliance decreases as the number of iterations increases and does not affect the stiffness of the components.

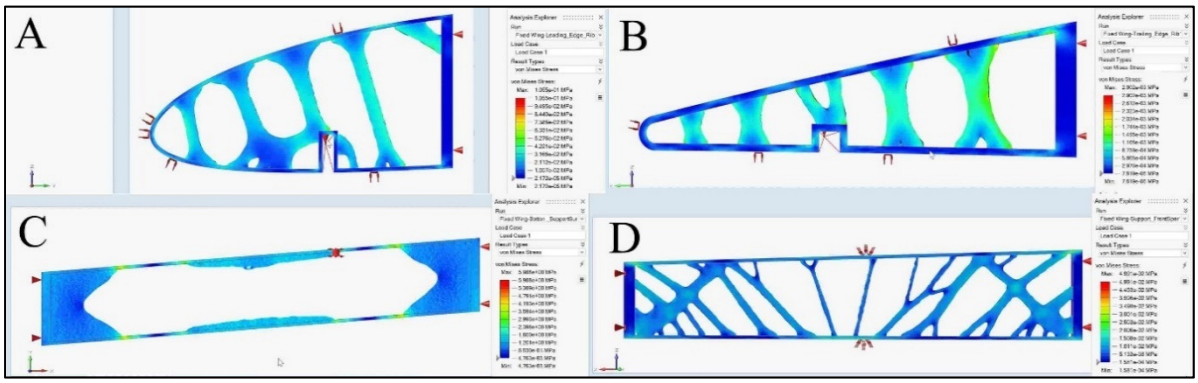

Figure 6.29 Von mises stress values obtained using TO for a fixed wing: (A) leading edge of rib 1, (B) trailing edge of rib 1, (C) bottom support surface between ribs 6 and 7, and (D) support of a front spar

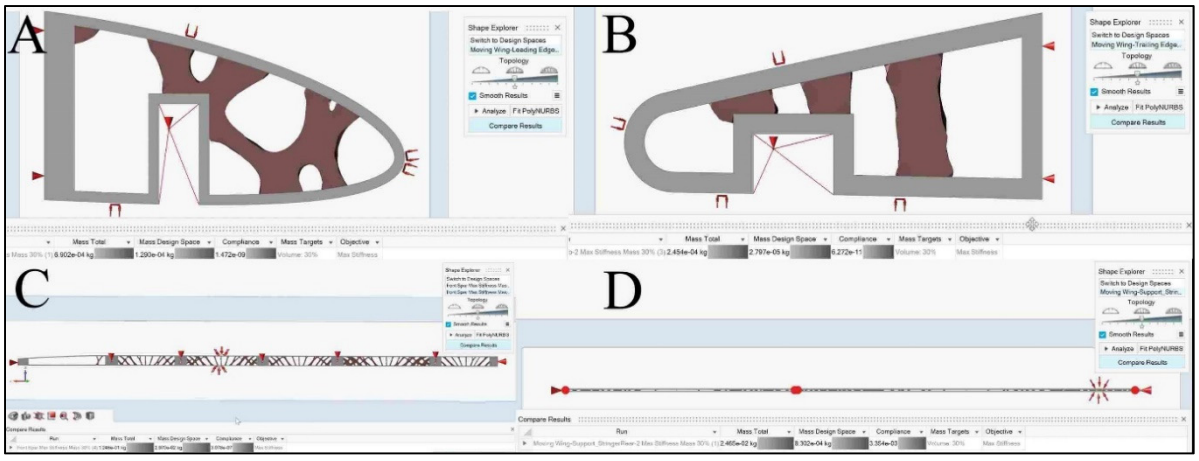

Figure 6.30 Variation in element density obtained using TO for a moving wing: (A) leading edge of rib 1, (B) trailing edge of rib 1, (C) support stringer of a front spar, and (D) support stringer of a rear spar

Figures 6.31–6.33 illustrate the impacts of a TO method on structural changes in mechanical parameters for moving segment, such as deformations and stresses. These figures show that the strain can be minimized while structural stiffness increases progressively.

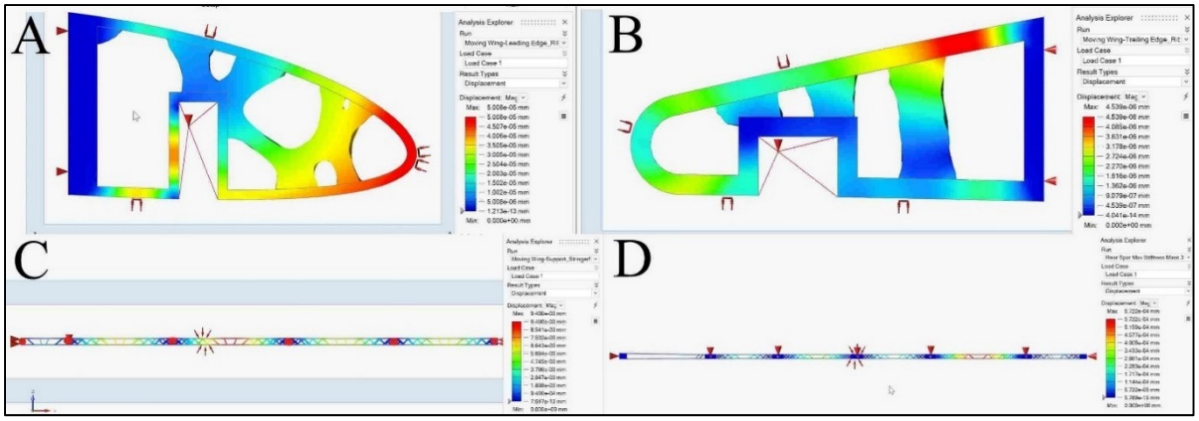

Figure 6.31 Displacement values obtained using TO for a moving wing: (A) leading edge of rib 1, (B) trailing edge of rib 1, (C) support stringer of a front spar, and (D) support stringer of a rear spar

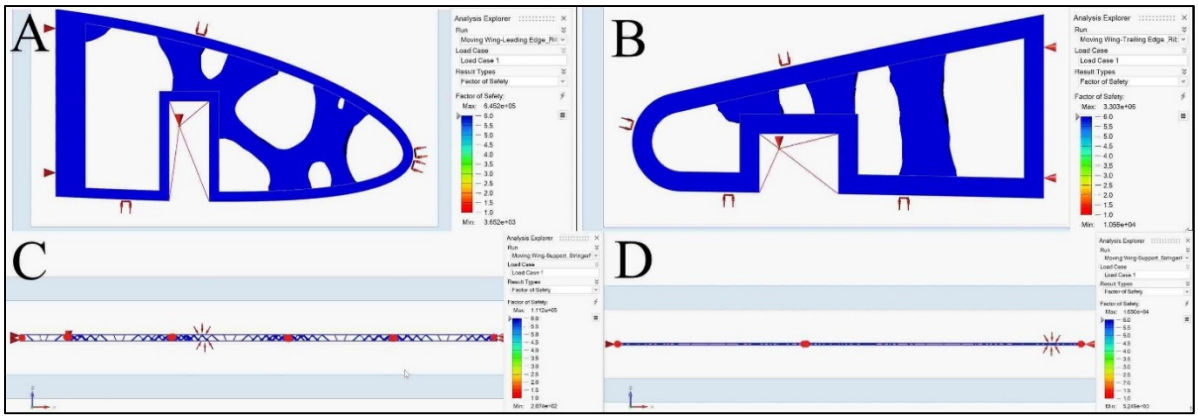

Figure 6.32 Safety factor evaluations obtained using TO for a moving wing: (A) leading edge of rib 1, (B) trailing edge of rib 1, (C) support stringer of a front spar, and (D) support stringer of a rear spar

The values of the primary parameters obtained from the FEA were obtained as part of the optimization analysis. The optimization outputs varied according to the number of iterations and the type of mechanical investigation, and due to various loads and geometrical shapes of the support elements, they differed between each component of the support elements. A few support elements were eliminated from the optimization process due to geometrical and physical limitations, such as their cylindrical shape and small geometrical dimensions.

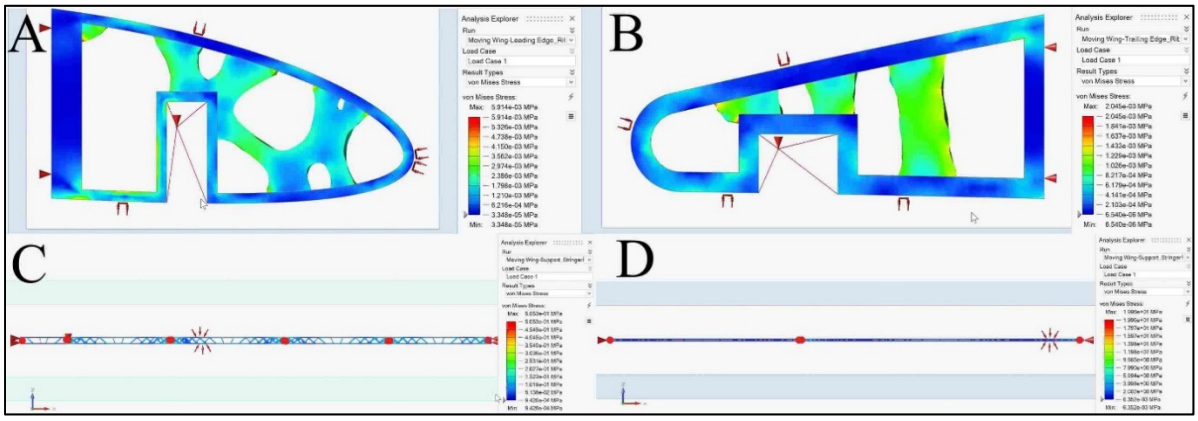

Figure 6.33 Von mises stress values obtained using TO for a moving wing: (A) leading edge of rib 1, (B) trailing edge of rib 1, (C) support stringer of a front spar, and (D) support stringer of a rear spar

6.7 Performance Comparison between the Optimized VSMTW, the UAS-S4, and the Wing Components' Final Design

The morphing wing configuration is generally employed to complete numerous missions during a single flight. The study described in this article was conducted on Hydra Technologies' UAS-S4 (Kuitche & Botez, 2019). First, the SO was used to determine the wing skin materials and then to calculate its optimal thickness. Then, the TO was used to establish the optimal internal wing components to minimize their weights while enhancing their structural stiffnesses. Finally, the wing component design configurations were evaluated based on the optimization results to determine which configuration should be the best to use. The optimization was conducted on both fixed and moving wings to allow the structure of the wing components to be redesigned and compared to a previous optimization of an aluminum alloy 2024-T3 wing (M. Elelwi et al., 2021). The optimized wing model was designed using composite materials and specified for individual components such as spars and ribs. Table 6.13 compares the performances and weights of optimized wings made of composite materials, aluminum alloy 2024-T3, and the original UAS-S4 wing. The aerodynamic performance data in Table 6.13 were collected at sea level altitude and maximum speed.

Table 6.13 Comparison of optimized VSMTW and UAS-S4 wing in terms of aerodynamic performance and weight

		Aerodynamic Performance			weight
		Lift	Drag	L/D	
UAS-S4 wing		347.02 N	16.34 N	21.2	6.5 kg
VSMTW at full wing extension	Alu 2024-T3	1509.89 N	45.59 N	33.1	12.4 kg
	Composite material	1509.89 N	45.59 N	33.1	5.5 kg

Table 6.13 clearly shows that the VWTSW technique's performance outperforms substantially compared to the UAS-wing. However, the greatest challenge is reducing weight while enhancing wing strength. The results in Table 6.13 demonstrate that the optimized wing made of composite material fulfilled its weight reduction and performance objectives. The optimized wing made with aluminum 2024-T3 is heavier than the UAS-S4 wing and so should be

modified to achieve the primary objective of designing a lightweight, strong wing. The majority of the weight is concentrated in the wing skin; the weight of the wing skin for both segments with aluminum is approximately 7.4 kg, while the wing skin for both segments with composite material weighs around 3.4 kg. Thus, based on the optimization method's data computation, the optimal wing with aluminum alloy 2024-T3 can be enhanced in terms of weight by replacing its skin with optimized skin of composite material. The wing segments with optimized internal components made with aluminum alloy 2024-T3 and optimized wing skin of composite materials weigh approximately 7.95 kg.

It is necessary to determine how the wing components are placed with respect to each other and then to build a frame model that accurately represents the final design. In this optimization part of the project, the TO approach was used for the wing com-ponents modeling, including the spars and ribs, similar to the previous TO work in this area (M. Elelwi et al., 2021). Since certain support components were structurally inefficient, the TO technique was not applied to these support elements. The most challenging aspect of the optimization approach was undertaking TO on the fixed wing ribs. Each rib in the fixed wing was assumed to have a cavity in the middle, as shown in Figure 6.8, to accommodate the moving wing. It was subsequently established that strengthening the fixed wing's center section would be necessary to boost the ribs in the impaired regions where the moving wing's motion generated substantially. Because of the shear stress generated by the aerodynamic loads' reactions in a range of flight conditions, both wing segments had to be strengthened. The CAD model for the MVSTW components was built using the density distribution of the wing segments after TO results. Figure 34 shows the optimal structures for both wing segments.

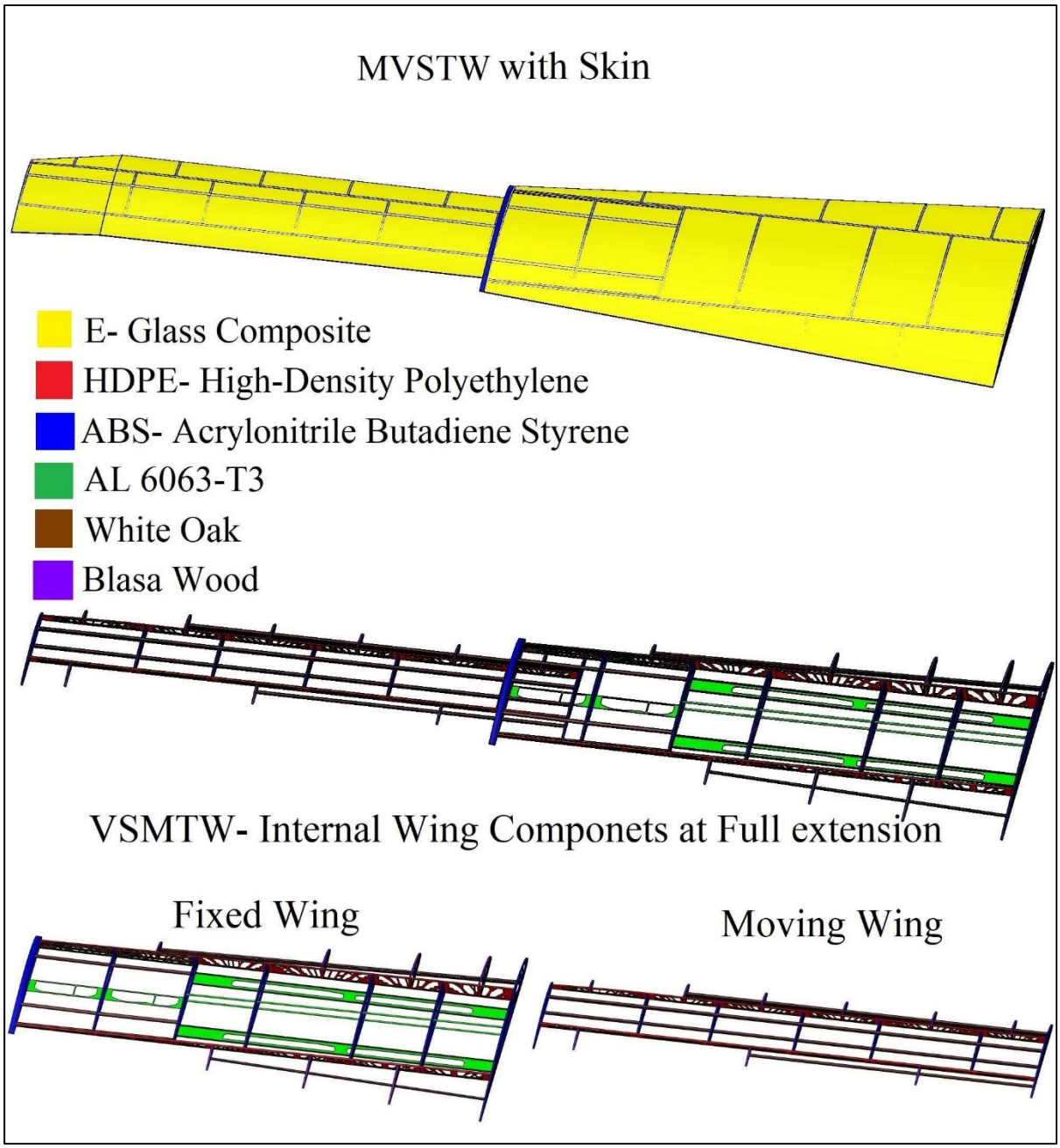

Figure 6.34 MVSTW remodeled in detail, using composite materials for its components

After incorporating the optimized components' structural configuration data into the overall design, the weights of the enhanced wing components were reduced to 2.13 kg for the fixed section and to 1.22 kg for the moving segment. As a result, the entire MVSTW was roughly 1 kg smaller than the original UAS-S4 wing weight.

6.8 Conclusions

This article discusses the progress in incorporating multidisciplinary optimization methodologies simultaneously to optimize and develop the concept of the morphing variable span of a tapered wing (MVSTW) using composite materials. The novel wing component optimization involved merging multi-codes of aerodynamic optimization, material selection, sizing, and topology optimization. The MATLAB algorithm was used to determine the most appropriate composite materials. Altair's OptiStruct and SolidThinking Inspire solvers were then utilized to perform both the size and topology optimizations. Both solvers' outputs were linked to the aerodynamic analysis results generated by ANSYS Fluent and XFLR5 code using CFD. The primary purpose of this investigation was to specify and evaluate the feasibility of executing these multi-optimization methods on the skin and interior wing components using certain composite materials.

The objective of this study was to reduce the weight of the MVSTW while increasing its global stiffness to improve structural durability accordingly to MVSTW's structural integrity standards. The STO results indicated that employing composite materials resulted in structural weight reduction when comparing an optimized wing with the UAS-S4 wing, and thus in a significant improvement in aerodynamic performance. The optimized wing components' weights for both segments were reduced to 2.13 kg for the fixed wing and to 1.22 kg for the moving wing. Based on the optimization outcomes for both MVSTW components, the redesigns of the wing components, comprising spars, ribs, and support elements, were modified using MATLAB code to determine the appropriate material for each type of component and were further developed. For example, E-glass was chosen for the skin, and its weight has been decreased by roughly 80%, while HDPE was chosen for the spars, and the findings reveal a weight reduction of up to 41%. Similar methodologies were considered for the ribs, and the ABS material was used; their weight reduction ranged between 10% and 70%. The support elements were designed from Al 6063-T3, white oak, and balsa wood, and the results displayed the same pattern as the other components.

Additional research will be undertaken in future work to advance the development of an adaptive morphing wing. The MVSTW arrangement will be integrated with an actuation mechanism and evaluated after the wing segments' optimization utilizing composite materials. The final design of the MVSTW, which was obtained through an optimization process and then integrated with an actuation system, will be manufactured as a prototype for experimental wind tunnel tests.

CHAPTER 7

GENERAL DISCUSSION OF THE RESULTS AND ORIGINALTY

The major focus of this thesis was to design and further develop a novel morphing wing technology using UAS-S4 data and information. The MDO methodology was used to design a morphing variable span tapered wing (MVSTW) while reducing its weight. A complete framework for the high-fidelity MDO analysis of morphing wings was developed. This MDO framework was analyzed by a set of well-known commercial software applications. The design process was divided into distinct phases to incorporate various disciplines. Aerodynamic analysis and optimization were conducted using CFD in ANSYS FLUENT software, Xfoil, and XFLR5 solvers. ANSYS workbench and Altair packages (OptiStruct by HyperMesh, and SolidThinking Inspire) were used for structural finite element modeling and optimization.
The primary focus of this research thesis has been the design and investigation of a morphing wing based on telescopic mechanisms with a tapered shape and various sweep angles of its moving section. The research results are described in Chapters 3 to 6, which together establish a general framework for the aerodynamic investigation and distribution of the wing components within a morphing wing design space based on FEM and Topology Optimization. These results show that significant weight savings are possible while maximizing stiffness using conventional material (Al 2024-T3), and by using the composite materials rather than a single type of material. The present section provides an overview and analysis of these results from an integrated perspective.

Aerodynamic investigation and optimization

Planform alternation, in which a wing may change its shape to increase its area by extending its span length and changing its sweep angle, was the key concept of the morphing wing used in this study. The first investigation presented a comparative study of its design and development, as well as an analysis of a VSMTW with varying sweep angles of its moving

section. The NACA 4412 airfoil was chosen for both wing segments based on the results obtained from Xfoil and XFLR5 codes; please note that its geometrical shape is very suitable as the ribs of the fixed wing must have cavities that act as housing for moving segment.

The analysis was conducted at four locations on the wing, established by extending its span by 25%, 50%, and 75% of its length, and starting at its original position, and for various flight speeds: minimum, loiter, cruise, and maximum speeds. Analyses were conducted at various altitudes: sea level, 5,000 ft, and 10,000 ft.

The flow field on the 3-D wing structure was investigated using the ANSYS Fluent solver. Two configurations of this wing were evaluated, according to the moving segment location within fixed segment. Three factors were chosen for the aerodynamic analysis to identify the optimal morphing wing shapes for their structural simulations and optimizations:

1. The relationships between performance, flight range, and fuel consumption reduction.
2. The amount of wing extension, the asymmetric wingspan strategy effects on roll control were also evaluated.

According to the results, the first design configuration (where the central axis line of the moving segment coincides with the central axis line of the fixed segment) was the optimum shape in terms of the three factors defined above. The investigation's findings showed that as the sweep angle decreases, the lift coefficient increases. For example, the improved aerodynamic efficiency ratios for configurations at a cruise speed and at an altitude of 10,000 ft, where the span extends from its original position to its full extension were 32.39% and 29.5%, respectively. These results reveal that when the span increases, the wing aerodynamic efficiency increases at all speeds and altitudes. Moreover, moving from the original position to the full span extension increases the lift coefficient while decreasing the drag coefficient. Another advantage of a variable morphing wing is that it can be used to manage roll control by adjusting the spanwise lift distribution between the port wing (PW) and its the starboard wing (SBW). However, to withstand the increased rolling moment, the wing structure must be reinforced and optimization in the mechanical design.

Another significant advantage of this strategy is the corresponding increase in flight range and endurance, that was made evidently by wingspan extension; this observation was the same at all altitudes and at all of selected speeds. When the span was extended from its original length to its full extension, the maximum flight range for 5,000 ft increased up to 46.89% for the first sweep angle model and to 43.16% for the second sweep angle model, for example.

To summarize the first investigation, a variable morphing wingspan can be considered an effective technology for improving aerodynamic efficiency and as to replace the conventional control surfaces. The enhancement of flight performance leads to an increase in flight range and endurance, by reducing fuel consumption. However, the main limitation of this technology is the predicted weight increase associated with the equivalent stiffness of the structure and actuation system weight compared to a conventional wing weight. Furthermore, flutter parameters (speed, damping) may change as wingspan flexibility increases during the flight envelope.

Wing component distribution inside a variable span of a tapered morphing wing

The work presented in the fourth chapter discussed the second research proposal and offers a novel strategy for allocating wing components within its structure. The Topology Optimization (TO) technique combined with Finite Element Analysis was applied to the Morphing Variable Span of a Tapered Wing (MVSTW) to evaluate the feasibility of modifying inner wing components, such as ribs, spars, and other structural components. This investigation was conducted as a continuation of the previous study presented above. This innovative approach evaluated the MVSTW's telescopic mechanism, including way in which the telescopically extended wing may slide into the fixed wing segment. The TO technique is one of the most promising approaches for reducing wing structural weight without impacting its strength properties. Computer-Aided Design (CAD) with CATIA software was used to design the solid wing model. The TO approach was then integrated with the results of the aerodynamic analysis for the chosen wing shape via a CFD solver. After obtaining the wing TO results, its components were designed and distributed inside both segments (fixed and moving). FEM code was used to validate the final morphing wing shape.

The main objective of this investigation was to determine the optimal distribution of wing components within the MVSTW design while maintaining the UAS-S4 baseline structural integrity. The CFD analysis collected pressure values under extreme flying conditions and the numerical solver's TO findings were analyzed using Finite Element Analysis (FEA) to establish the best layout design for the variable-span morphing wing. Material density was selected as a design variable in order to optimize its distribution throughout its continuous range. For our design case, we analyzed two responses regarding the minimization of the: 1) structural compliance and 2) volume fraction. The volume fraction was considered as a constraint. The optimization results have shown that all wing components were positioned within high-stress/deformation zones, and have ensured that the elements within these zones were those required for the structural design. The components outside these high-pressure locations were those that could be removed. The iterative process adjusts the strain energy, so that, the structural stiffness gradually increases as the strain energy decreases. The new optimized structure thus contains the most efficient positions for the components inside the wing.

The baseline wing model was developed entirely of solid aluminum 2024-T3, with fixed and moving section masses of 112 and 45 kg, respectively. The TO technique proposed that the fixed segment should have been designed with two-spar configurations in this case study, as its ribs were the housing the moving segment. The moving segment therefore must be designed with two-spar configurations to support the wing components, particularly during full wing extension. The TO results indicated that the high-strain area was near the center of the wing domain. Therefore, it was important to support the high-strain area in both wing segments by reinforcing the locations of the shear stress generated by the reactions to aerodynamic loads under different flight conditions. When the weight of the initial structure of the solid wing segments was compared to the weight of the optimized wing segments, the overall wing weight was reduced by 16.3 kg for the fixed wing segment and by 10.3 kg for the moving wing segment. The remodeled morphing wing was designed with the following parameters to obtain a stiffened and reliable variable-span morphing wing:

- A 2mm wing skin thickness for both segments;

- A 6mm spar thickness for both segments;
- A 6mm rib thickness for both segments;
- For the fixed segments, flat stringers with a thickness of 4mm, and round stringers with a diameter of 3mm and a thickness of 1mm; and
- For the moving segment, an 8 mm thick rectangle stringer.

Additionally, due to their parallel alignment, the distance between the two spars was determined to be 351.56mm for the fixed segment of the wing and 163.38mm for the moving segment. The optimized MVSTW was evaluated using static analysis. As can be seen from the FEA, the values of the mechanical characteristics, namely deformation, stress, and strain, increased as the aerodynamic loads increased. These mechanical properties significantly increased at large wingspan extensions of 50% and 75%, as well as at higher flight speeds. Therefore, 50% and 75% of wingspan extensions were recommended exclusively during the minimum speed and loiter phases. According to the FEA, the morphing of the designed wing's structure was suitable for the rolling control strategy, that employed the asymmetric morphing span technique. However, the optimal rolling mechanism should consider that both sides of the wing's span must gradually and symmetrically extend. The proposed arrangement and allocation of wing components achieved the required robustness and integrality for the MVSTW while obtaining significant weight reductions through topological optimization.

Structural sizing and topology optimization based on weight-saving using Al 2024-T3

The fifth chapter describes the advancement in the third research axis, which included sizing and topology optimization of a lightweight, and robust morphing wing. This work establishes a numerical environment by incorporating simultaneous structural sizing and topology optimization based on its aerodynamic analysis in order to evaluate the feasibility of the morphing wing optimization. The OptiStruct solver within HyperMesh was used to perform the morphing wing optimization. The purpose of this investigation was to minimize the total structure compliance while maximizing stiffness in order to meet the MVSTW's structural integrity standards. A baseline wing was designed using the telescopic mechanism and variable-span morphing wing theory based on the aerodynamic optimization results. Results

and boundary conditions were computed at sea level altitude at maximum speed. Additionally, a safety factor of 1.5 and a load factor of 3 g were added to the designed wing to ensure that it could withstand a combination of flight conditions. To continue the optimization process with the objective of reducing wing component weight, this investigation used the same material (aluminum alloy 2024-T3) as the previous one. The main objective was to maximize the wing stiffness by optimizing the material distribution inside the volume space of the wing components. The pressure was computed separately for each wing component to ensure more efficient and accurate results. This optimization problem considered the parameters that characterize a structure's overall performance. All these parameters were considered as optimization objectives or constraints. The wing skin sizing optimization (SO) was conducted for both segments by applying the design constraints to the structural stiffness. The original wing skin thickness for both segments was set at 2 mm. The maximum stress value of the skin of the wing's two segments was limited to 200 MPa in order to maximize efficiency and could withstand the aerodynamic loading acting on its surface. Topology optimization was used to design the spars that would maximize wing stiffness while minimizing its weight. Minimum structural compliance was achieved for both segments' initial wing spar design through a series of iterations dependent on the size and shape of each spar. The minimization of the structural compliance through the use of constraints was determined as a volume fraction of 30% of the entire volume.

The advantage of using the TO within OptiStruct is that the FE properties are updated accordingly to the optimization findings. The results show that the weights of the optimized spars are significantly smaller than those of the initial spars, indicating a high reduction in the average weight of the wing spars. An optimization approach based on the Finite Element Model (FEM) was developed for morphing wing ribs in according to the computed loading. Each element's material density was determined and used as a design variable. Two analyses responses were expressed in terms of structural compliance and volume fraction, where the volume fraction was classified as a constraint and the compliance defined as an objective function. When ribs' weights were compared before and after optimization, it was clear that their weights were significantly reduced due to the computed loads acting on the rib. The seventh rib of both the fixed and moving wings models was excluded from the optimization

process as these wing ribs must be solid with no cavities. The optimized wing segments designed as solid segments indicated that the strut elements obtained from TO should be used to fulfill the strength requirements of the wing. Based on the TO results, the fundamental structure of the support components was substantially minimized, resulting in a reduction in the weights of the support elements. Furthermore, it is obvious that structural compliance decreased as the number of iterations increased. As the forces and geometric shapes vary from one support element to another, the values of constraints varied for each individual component of the support elements. Several support components were eliminated from the optimization process due to implementation problems posed by their geometrical and physical constraints, such as their cylindrical and small dimensions shape. The optimized wing model was composed of 2024-T3 aluminum, with its fixed and moving segments weighing 16.3 kg and 10.3 kg, respectively. After incorporating the optimized wing components' structural layout data into the overall design, the weights of the optimized wing components were reduced by 7.96 kg and 4.57 kg, for the fixed and moving segments, respectively.

Structural sizing and topology optimization based on weight-saving using composite materials

The sixth chapter addressed the fourth research axis, that of incorporating multidisciplinary optimization using composite materials to reduce the wing's weight further while maximizing stiffness. This work develops a numerical environment for MDO studies by incorporating material selection, structural sizing, and topological optimization results after aerodynamic optimization, with the objective of determining if morphing wing optimization was feasible. Aerodynamic optimization was performed using CFD and XFLR5 algorithms, the material selection was performed using MATLAB code, and the size and topology optimization using Altair's OptiStruct and SolidThinking Inspire solvers. This research proposes a novel MDO framework for modeling and evaluating wing components based on their design parameters. The fundamental concept behind this study is to conduct MDO analysis on a composite morphing wing by employing a variety of composite materials rather than a single metal material. The design and development of a robust, and lightweight Morphing Variable-Span

Tapered Wing (MVSTW) requires a MDO approach to ensure that the developed structure can satisfy all of the constraints.

After the collection of all properties of the materials were collected from published studies, a literature search was conducted on their parameters to establish their appropriate weight-to-strength ratios. Composite materials were selected based on the output of an in-house MATLAB code, developed to analyze their physics-mechanical properties, availability, and cost. Optimization using multiple composite materials is more complex than the optimization of a single material as more variables must be addressed during the optimization process. E-Glass composite was considered to optimize the wing skin because it is significantly cheaper than the other fibers and has excellent properties. The properties of both epoxy resin and E-glass were exploited for the wing skin. The initial thickness of each layer was set at 0.250 mm, resulting in a total thickness of 2 mm for the composite, as 4 layers were employed.

A baseline wing with a skin thickness of 2 mm, identical to that of a previous study on both segments was used throughout this investigation. High-Density Polyethylene (HDPE) characteristics have been evaluated for use in structural applications of wing spar design. A spar is an elongated beam installed on the length of the wingspan and is designed to support the wing when subjected to bending loads. The main reason for employing an I-beam section (except where it connects to the ribs) is to take advantage of its substantial mechanical benefits in comparison to alternative beam arrangements. In a 3D environment, all wing spars were subjected to similar analysis methodologies.

ABS (Acrylonitrile Butadiene Styrene) is one of the first polymers to be widely utilized in 3D printers, and its properties have been documented extensively. ABS was therefore selected as the material for the wing ribs design. The original design space layout and boundary conditions were done to obtain the optimal material distribution inside the ribs. In the optimization problem, a volume constraint was applied to all wing ribs as an opposing constraint.

The support elements of a wing are crucial to its structural integrity and hence to its robust design. Several composite materials were analyzed to determine which would be the most suitable for this project. Three materials were evaluated for the support components design: balsa wood, white oak, and aluminum alloy 6063-T6. The leading-edge ribs, trailing-edge ribs,

stringers, and stiffeners for the optimized wing based on the TO method were designed using a baseline wing as a starting point. Aerodynamic and inertial loads acting on the wings were based on their shapes, while structural weights were considered throughout the design process. The support wing components' boundary conditions matched those of the spars and ribs. The boundary conditions that apply to the support elements vary according to the size of their components.

A volume constraint was applied to the support element design, which served as an opposite constraint throughout the optimization process. The baseline wing for fixed and moving segments was designed with a thickness of 2 mm to serve as a reference for the SO process. The maximum stress applied to the skins of both segments during the SO process was limited to 750 MPa to obtain the optimal thickness capable of sustaining aerodynamic loads. MDO was utilized to develop the optimal spars that would provide maximum wing stiffness with the lowest possible wing weight. A volume fraction of 30% was applied to determine the maximum structural stiffness, and then this value was used as an optimization constraint. This component analysis-based TO technique results in a comprehensive structural design and provides an alternative method for reducing wing spar structural weight.

The wing ribs design took place in the same phases as the wing spars calculations. When the weights of the ribs were compared before and after optimization, they were minimized as a function of their predicted stresses. Since all ribs had exceptionally low maximum loads and displacements, their optimized values satisfied the strength and stiffness requirements. Weight savings of 2.13 kg for the fixed segment and 1.22 kg for the moving segment were achieved by optimizing the wing components. The MVSTW's weight was decreased to 5.5 kg, in comparison to the 6.5 kg of the original UAS-S4 wing.

CONCLUSION

Several novel and sophisticated methods were developed in this thesis and used to study the multidisciplinary numerical design optimization obtained through the application of a morphing wing concept on an UAS-S4 wing. The morphing system consists of a telescopic mechanism with a tapered wing shape and a moving section capable of varying its span length via an actuation system. A wing geometry shape was designed in 2D using a NACA 4412 airfoil chosen based on aerodynamic optimization findings obtained with Xfoil and XFLR5 codes. ANSYS Fluent solver was utilized to investigate the flow field on the 3-D wing structure. This investigation was performed at four locations by extending the wingspan of a morphing wing and varying the flight speeds conditions (minimum, loiter, cruise, and maximum). These evaluations were performed at three different altitudes. The aerodynamic analysis used three criteria to assess the relationship between wingspan extension, performance, flight range, and fuel consumption reduction. The results established that when the sweep angle decreased, the lift coefficient increased, and the span increase improved the aerodynamic efficiency at all speeds and altitudes. Another substantial benefit of this technique was the increase in flight range and endurance, that were possible by wingspan extension, which had a large effect at all the selected speeds. A variable morphing wingspan can therefore be considered as an effective technology for improving aerodynamic performance and replacing conventional control surfaces.

The TO technique was integrated with the results of the aerodynamic analysis for the selected wing shape using Ansys CFD solver. Following the determination of the wing TO findings, its components were developed and then allocated inside both wing segments. The final wing shape was validated using the FEM code. The new optimized structure established the locations of the most efficient wing components. The basic wing model was designed completely of solid aluminum 2024-T3, weighed 112 kg for the fixed part and 45 kg for the moving section. The overall wing weight of the optimized wing segments was reduced by 16.3 kg for the fixed wing segment and by 10.3 kg for the moving wing segment.

The study the feasibility of the optimized morphing wing, a numerical environment was established by integrating size and topology optimizations to reduce the wing components based on their aerodynamic analysis results. The values and boundary conditions using in the MDO were calculated at sea level and at maximum speed. The designed wing was subjected to a safety factor of 1.5 and a load factor of 3 g to ensure that it could withstand a whole range of flight conditions. The wing skin SO for both segments was performed by applying the design constraints to the structural stiffness. The remainder of the wing components, including the spars, ribs, and support elements, were designed using TO to maximize wing stiffness while minimizing its weight. Minimum structural compliance was accomplished by a series of iterations dependent on the size and shape of each wing component. Aluminum 2024-T3 was used to design the optimized wing model. After incorporating the structural layout data for the optimized wing components into the overall design, the optimized wing components' weights were reduced from 16.3 kg for the fixed wing segment to 7.96 kg and from10.3 kg to 4.57 kg for the moving wing segments, respectively.

Following the aerodynamic optimization, a numerical MDO environment was developed by integrating the material selection, structure sizing, and TO findings. The main objective was to conduct MDO on morphing wing using a variety of composite materials rather than a single (metal) material. The composite materials were chosen based on the results of an in-house MATLAB code, developed to evaluate their physical-mechanical properties, availability, and cost. E-Glass composite was selected for wing skin optimization. High-Density Polyethylene (HDPE) was an appropriate material to use in structural applications of wing spar design, and ABS (Acrylonitrile Butadiene Styrene’s) characteristics were very documented; hence, they were used to design the wing ribs. Three materials were employed for the support components: balsa wood, white oak, and aluminum alloy 6063-T6. Most of the weight was contained in the wing skin; the weight of the optimized wing skin for both segments using aluminum was approximately 7.4 kg, while the weight of the optimized wing skin for both segments with composite material was around 3.4 kg. The weight was reduced by 2.13 kg for the fixed segment and 1.22 kg for the moving segment. The use of composite materials made it possible

to reduce the weight of the MVSTW from 6.5 kg to 5.5 kg in comparison to the baseline UAS-S4 wing.

RECOMMENDATIONS

The research presented in this thesis is focused on the use of MDO design to develop a novel morphing wing technology. This novel morphing wing modeling and influence on aircraft performance offer a promising avenue. Future investigation could lead to further improvements by considering the following perspectives and recommendations:

- Additional research could be performed on 2D airfoil shape optimizations such as modifications of the airfoil thickness, camber, and other parameters. The analyses of the aerodynamic performance provided in this thesis could be extended to flight flutter, deformation, and vibration testing, thereby verifying the analytical predictions over the flight envelope.
- A flight simulation environment could incorporate the techniques developed in this work to achieve realistic aerodynamic findings by employing specified airfoil performance databases.
- The research might be expanded by studying the impact of the morphing wing on flight performance during maneuvers (asymmetric wingspan extension) and take-off/landings (full wingspan extension). Further analysis may verify if the optimized skin can compensate for the loss of aerodynamic effectiveness under certain flight conditions.
- Future work and investigations should focus on integrating MDO design and with current knowledge to further develop reliable lightweight robust morphing wings, particularly for the study of aero-structural performance throughout all flight envelope.
- Further study of composite materials could be conducted to find the mechanical characteristics and behavior of composite materials most suitable for the design of morphing wings. New language programming and codes may be developed using different codes such as MATLAB, Python, and others to facilitate and improve the selection of composite materials.
- New techniques are needed to complete the methodology for an actuation system model that adjusts and optimizes the span length locations depending on the flight conditions. Due to design constraints (balance, location, weight, efficiency), this research effort would determine several parameters for the type of actuation system, (electromechanical,

hydraulic, or other systems). One approach would be to perform aero-structural optimizations using a FEM to redesign the wing components throughout the MDO design phase.

APPENDIX I

PARAMETERS OF OPTIMIZATION USED TO DESIGN MVSTW

Table-A.I-1 Parameters used in the design and optimization of the tapered wing's morphing variable span (MVSTW)

Parameter	Wingspan extension			
	Original position	25%	50%	75%
The wing half-span (in meters)	2.1	2.625	3.15	3.675
The wing area (in square meters)	1.921	2.263	2.603	2.945
The wing root chord (in meters)	0.675	0.675	0.675	0.675
The wing tip chord (in meters)	0.29	0.29	0.29	0.29
Aspect ratio	9.18	12.2	15.29	18.42
The taper ratio	0.43	0.43	0.43	0.43
The mean aerodynamic chord in meter	0.51	0.51	0.51	0.51
Min speed (m/s)	17	17	17	17
Loiter speed (m/s)	34	34	34	34
Cruise speed (m/s)	51	51	51	51
Maximum speed (m/s)	68	68	68	68
Air density - sea level kg/m^3	1.225	1.225	1.225	1.225
Air density - 5000 f kg/m^3	1.056	1.056	1.056	1.056
Air density - 10000 f kg/m^3	0.905	0.905	0.905	0.905
The moving wing chord (in meters)	320	320	320	320
Span extend (in meter)	0	0.525	1.05	1.575
Oswald's Efficiency factor	0.7782858	0.7011085	0.6282833	0.5591962
Span efficiency factor	-4.51031	-3.34569	-2.69022	-2.26858

APPENDIX II

MVSTW USING ALUMINUM ALLOY 2024-T

This appendix is for the detailed design of MVSTW and its components using conventional material (Al 2024-T3). It depicts the MVSTW with various wingspan extensions based on the location of the moving segment with the fixed wing. The detailed design also includes information such as the weight of each component and the design scale.

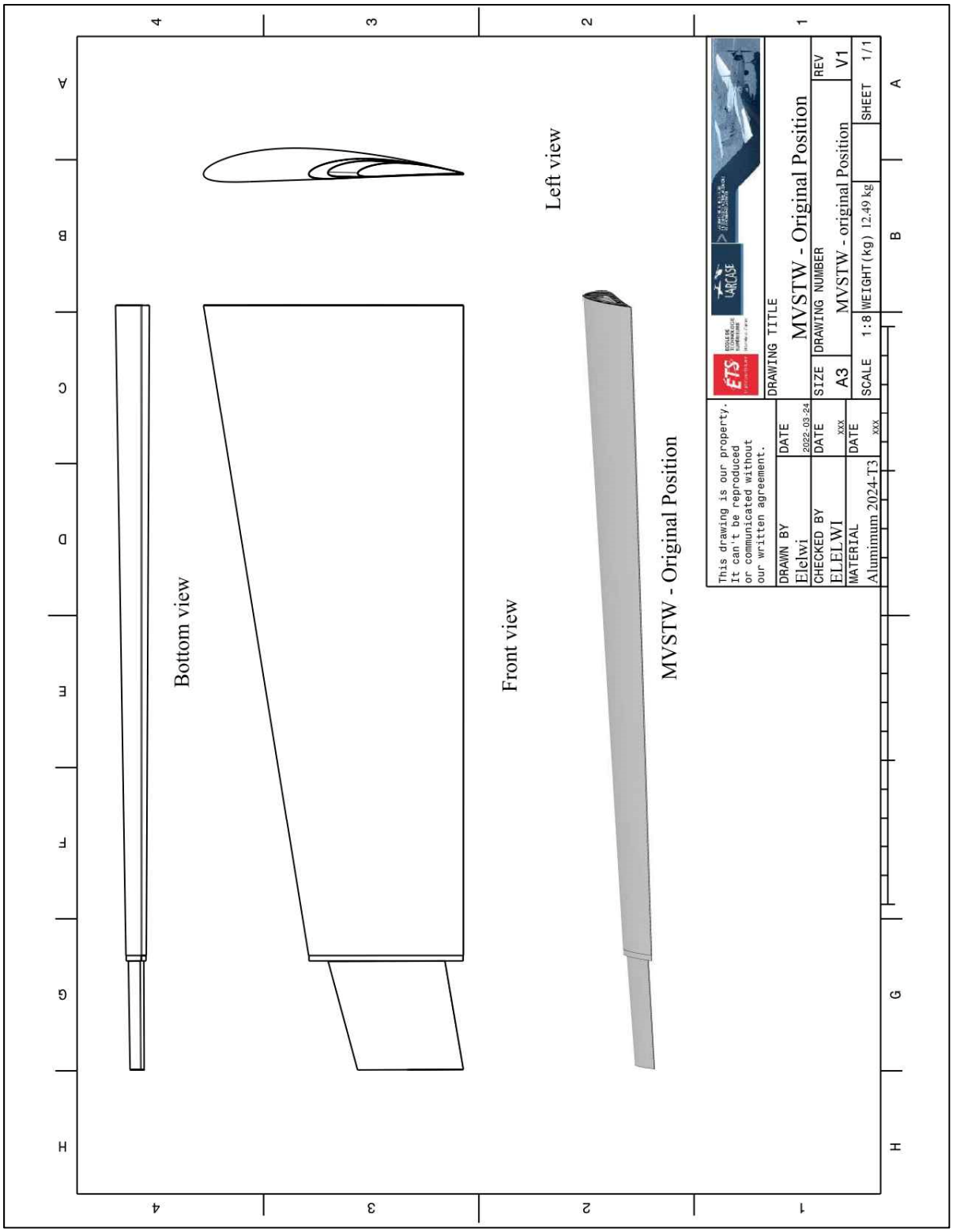

Figure-B II-1 MVSTW at Original Position Using Al 2024-T3

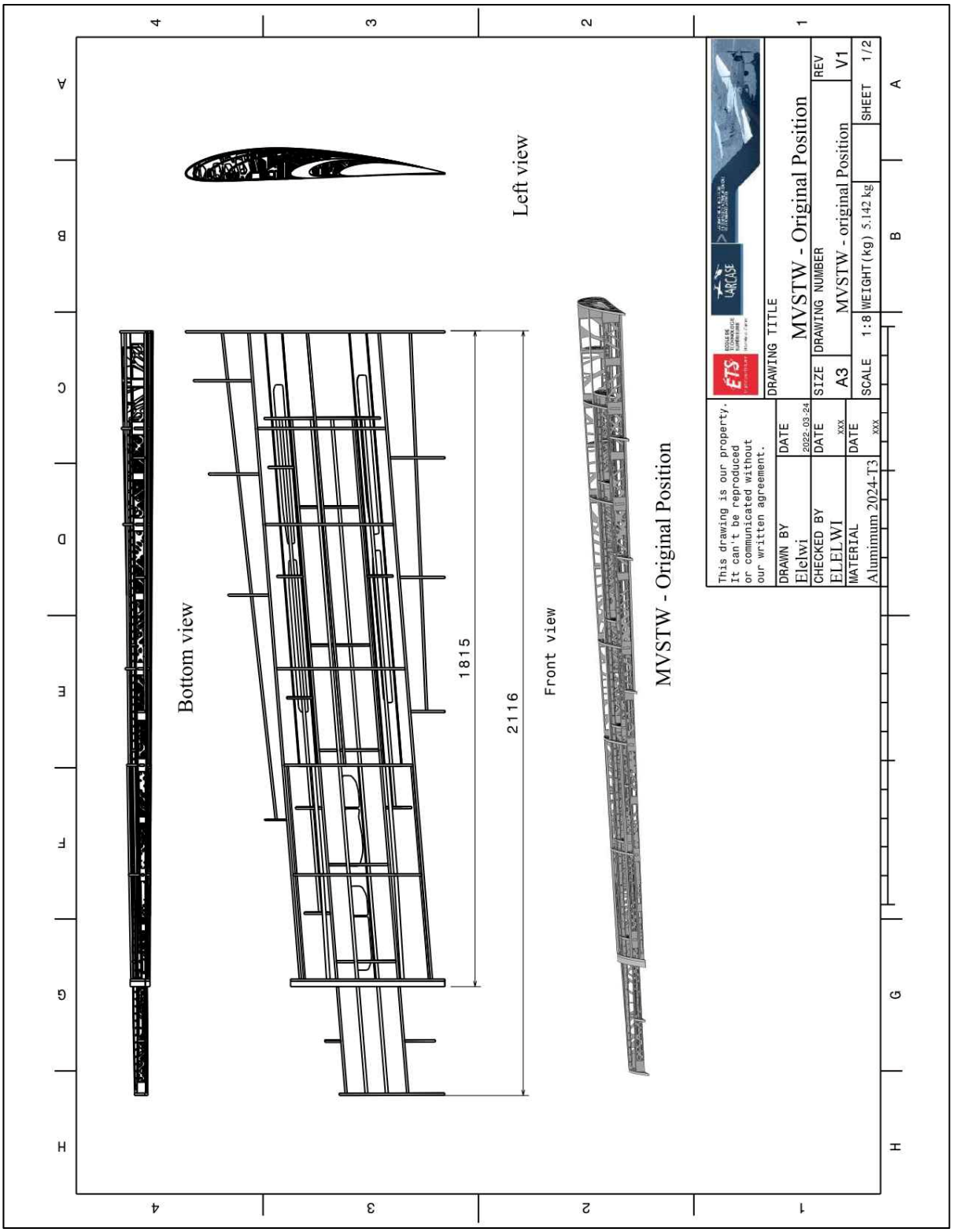

Figure-B II-2 MVSTW Skeleton at Original Position Using Al 2024-T3

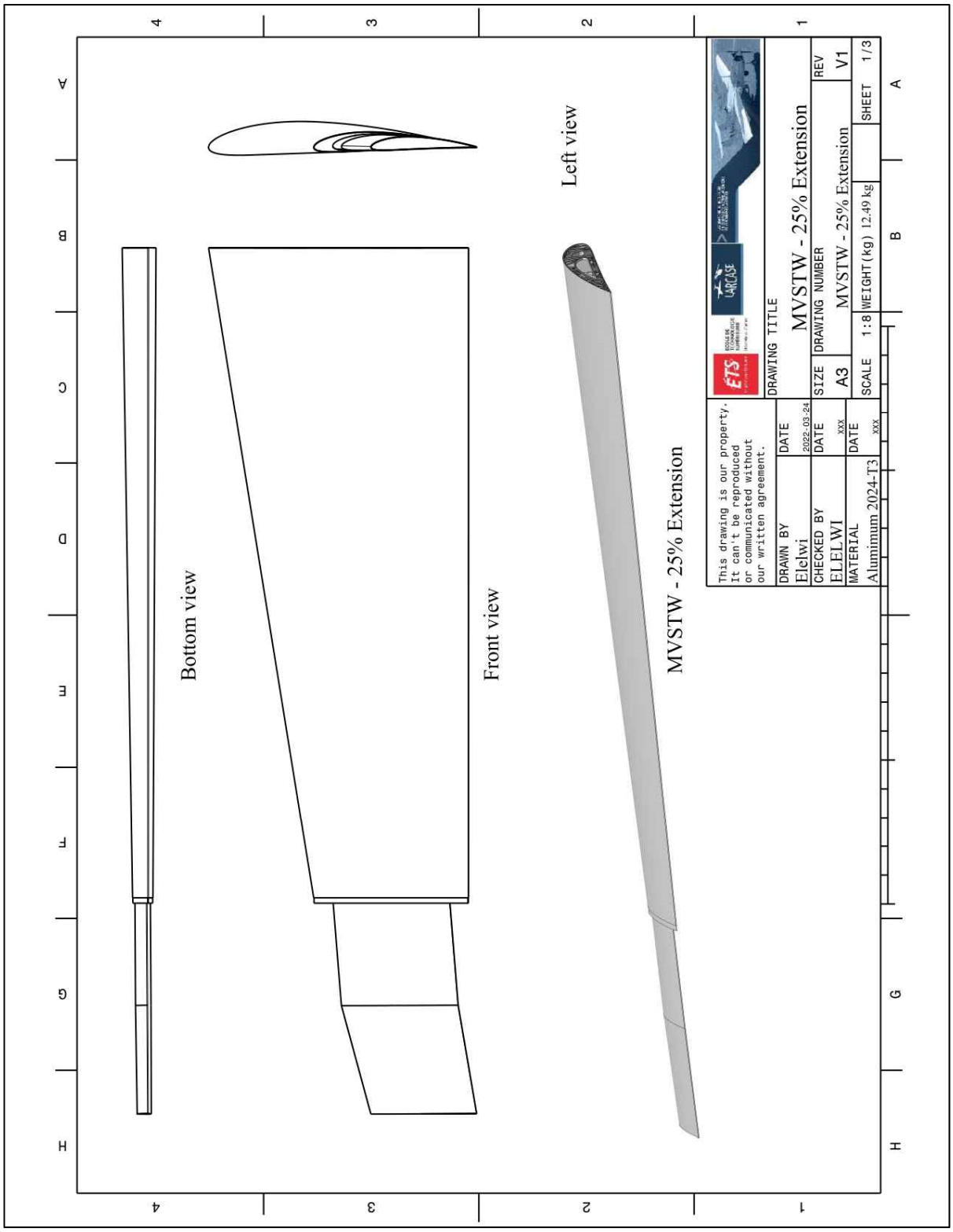

Figure-B II-3 MVSTW at 25% from its Original Position Using Al 2024-T3

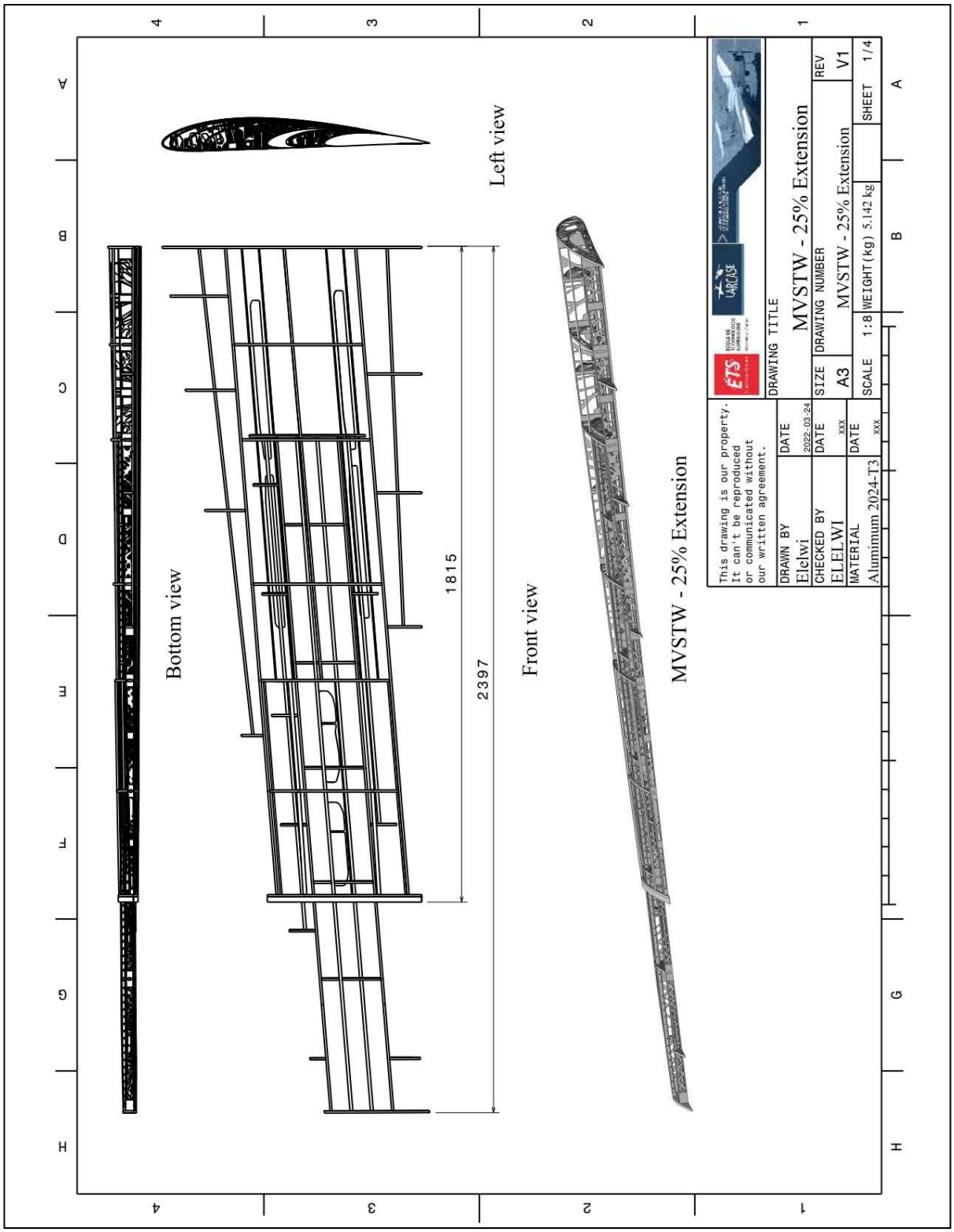

Figure-B II-4 MVSTW Skeleton at 25% from its Original Position Using Al 2024-T3

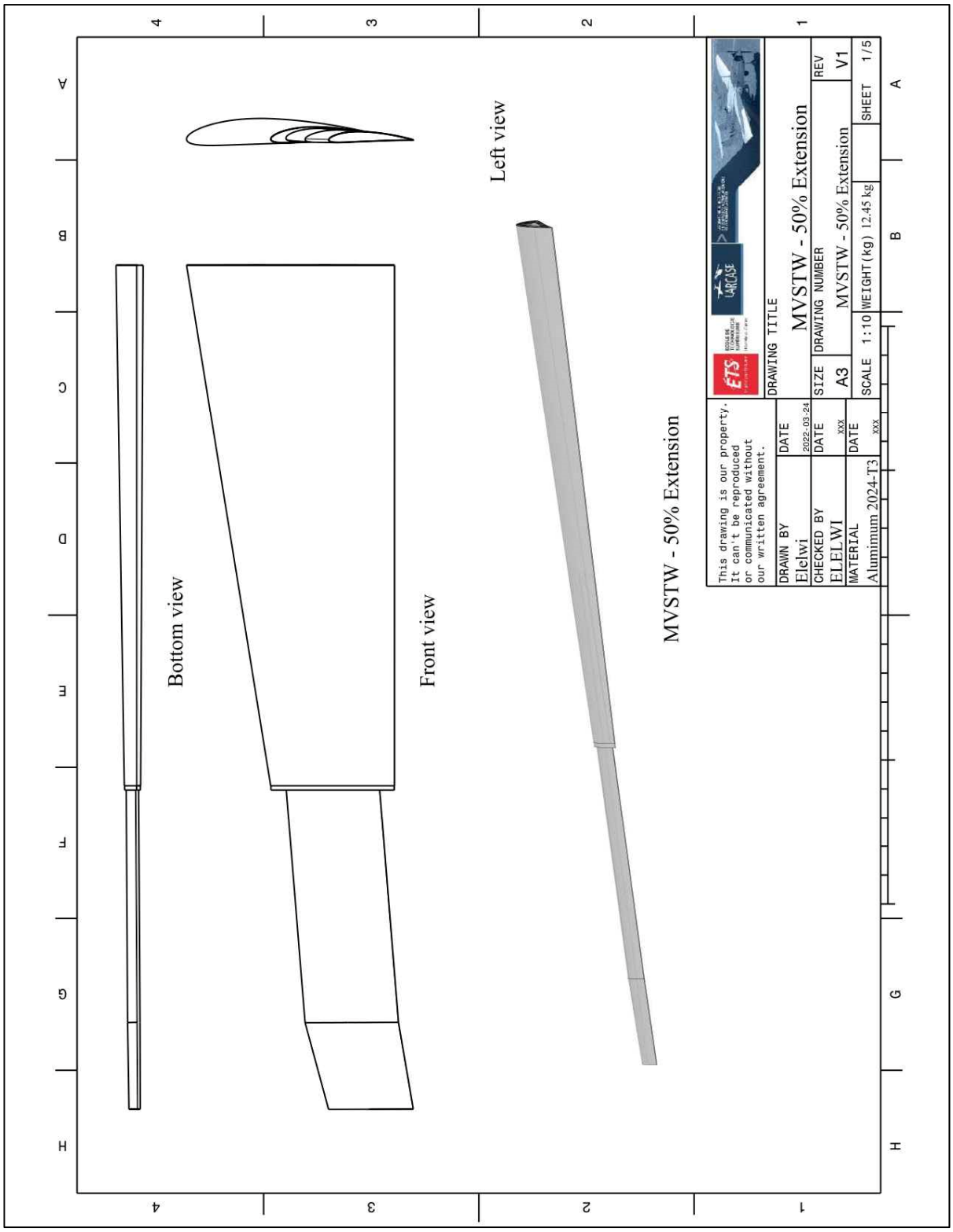

Figure-B II-5 MVSTW at 50% from its Original Position Using Al 2024-T3

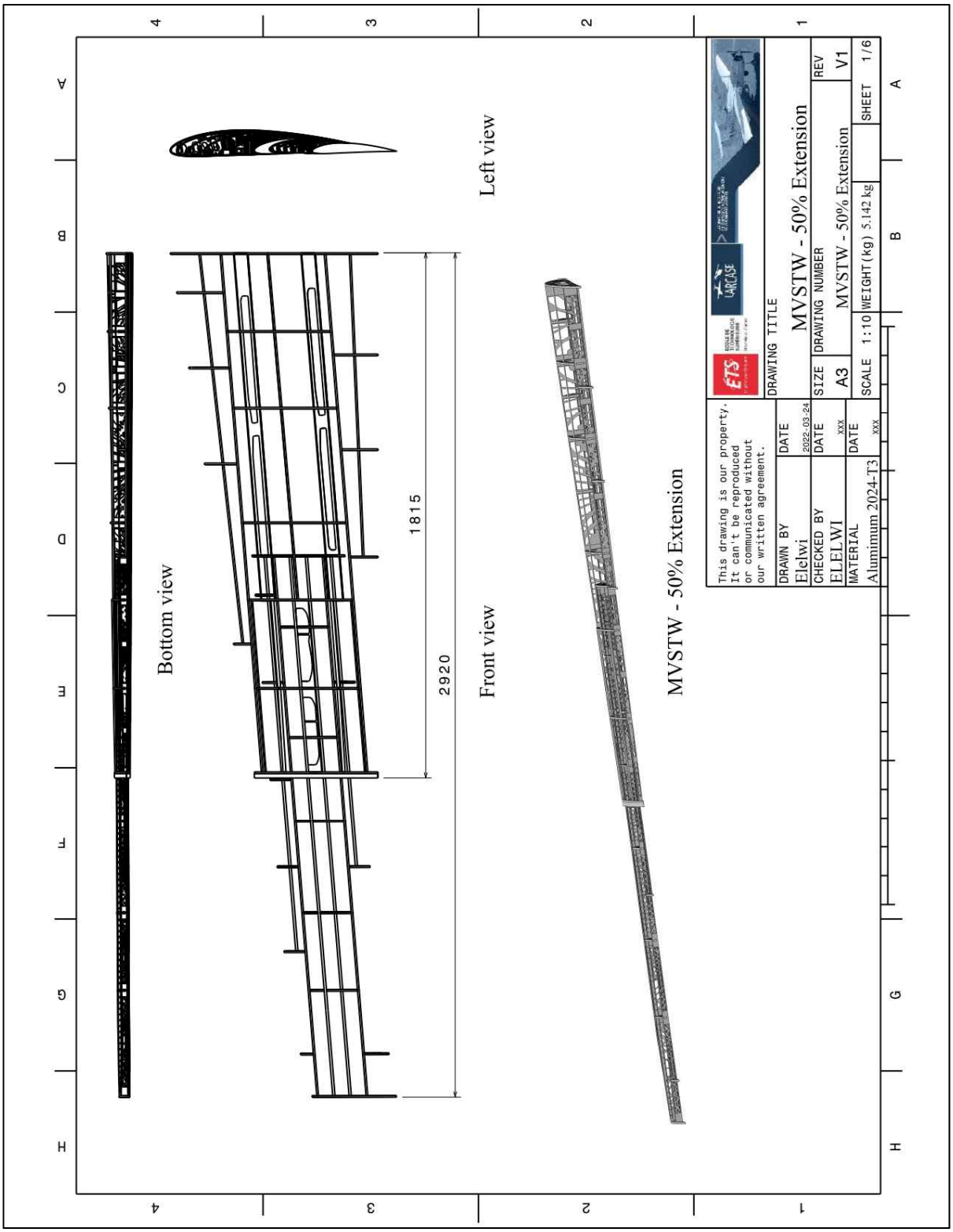

Figure-B II-6 MVSTW Skeleton at 50% from its Original Position Using Al 2024-T3

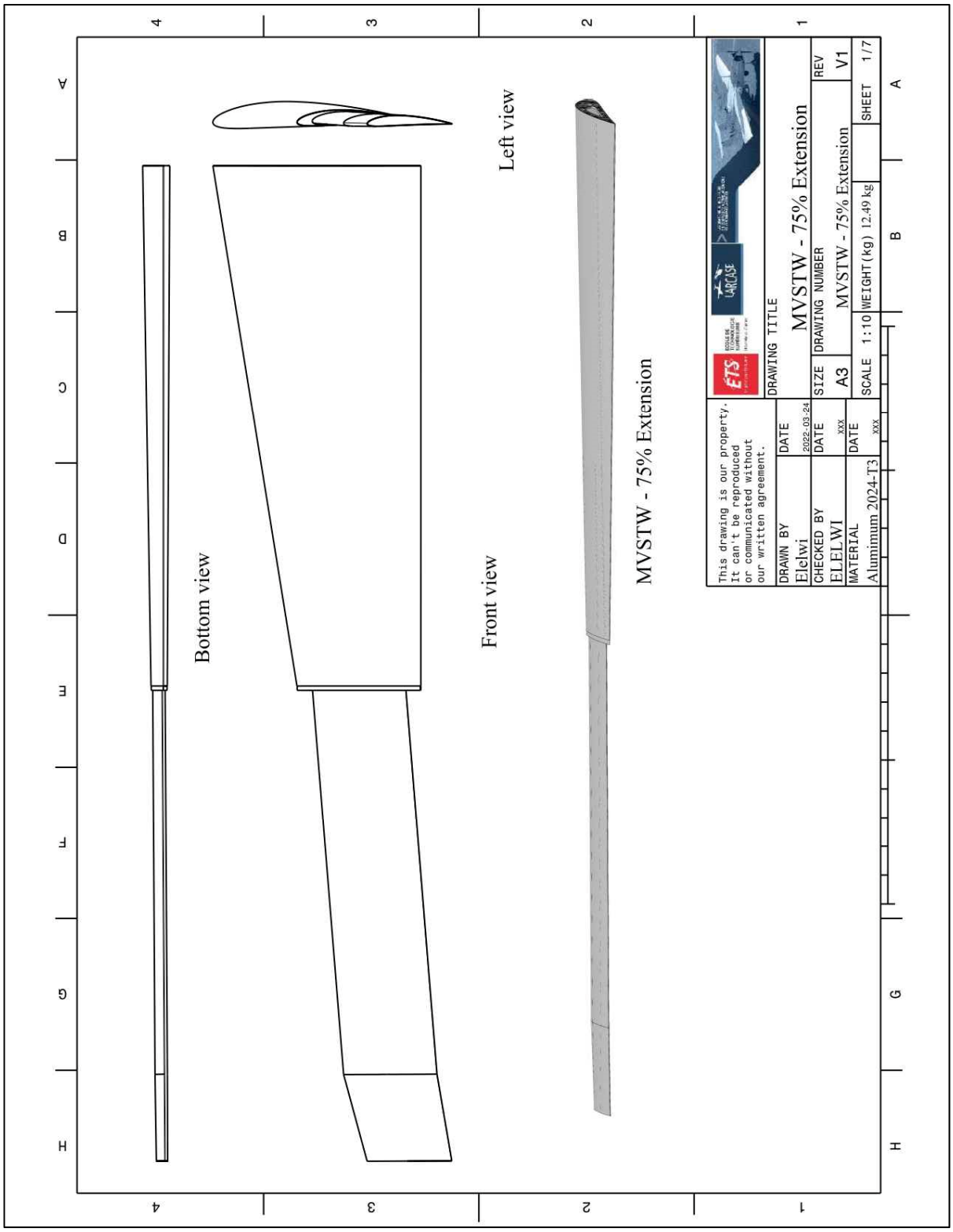

Figure-B II-7 MVSTW at 75% from its Original Position Using Al 2024-T3

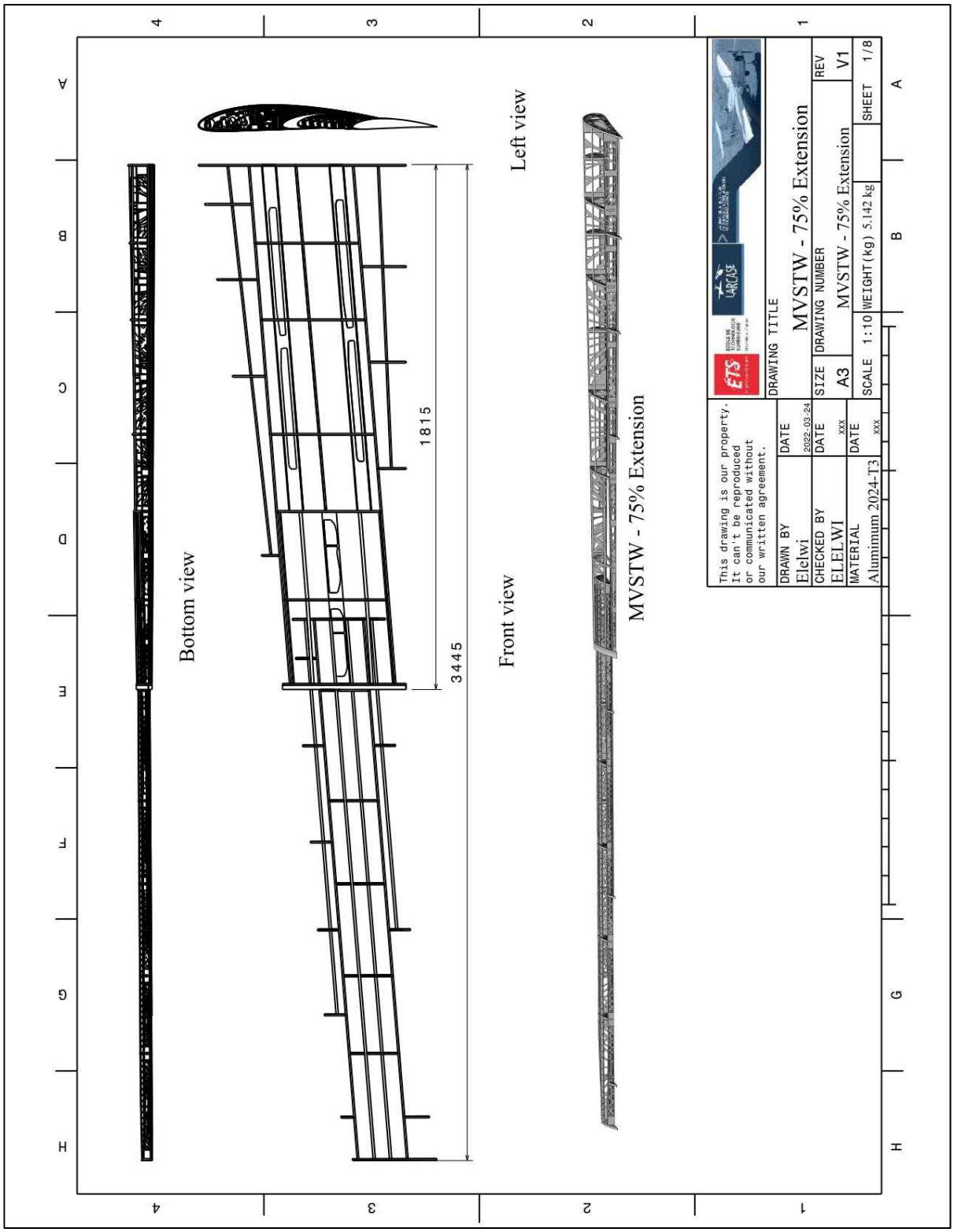

Figure-B II-8 MVSTW Skeleton at 75% from its Original Position Using Al 2024-T3

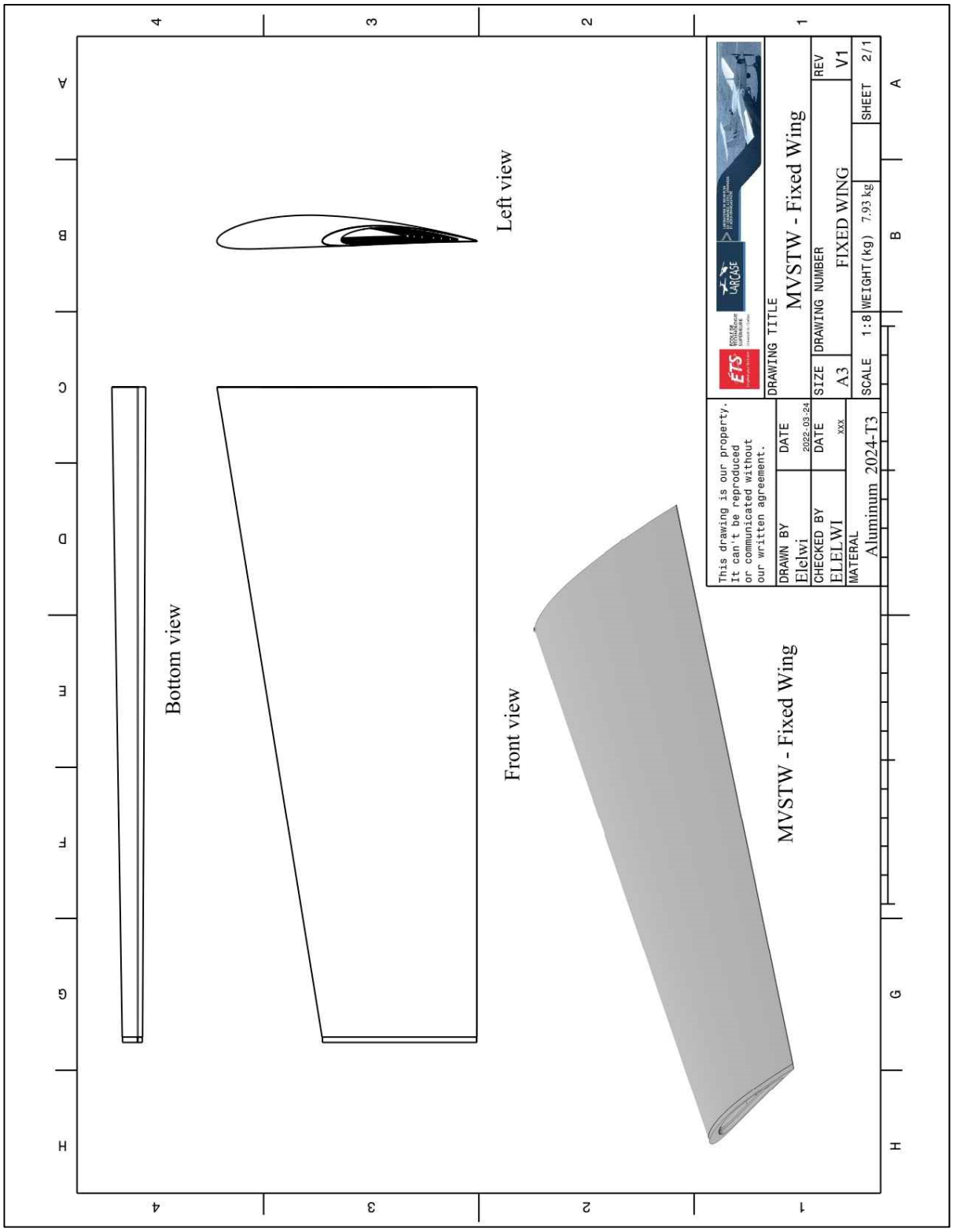

Figure-B II-9 MVSTW Fixed Wing Using Al 2024-T3

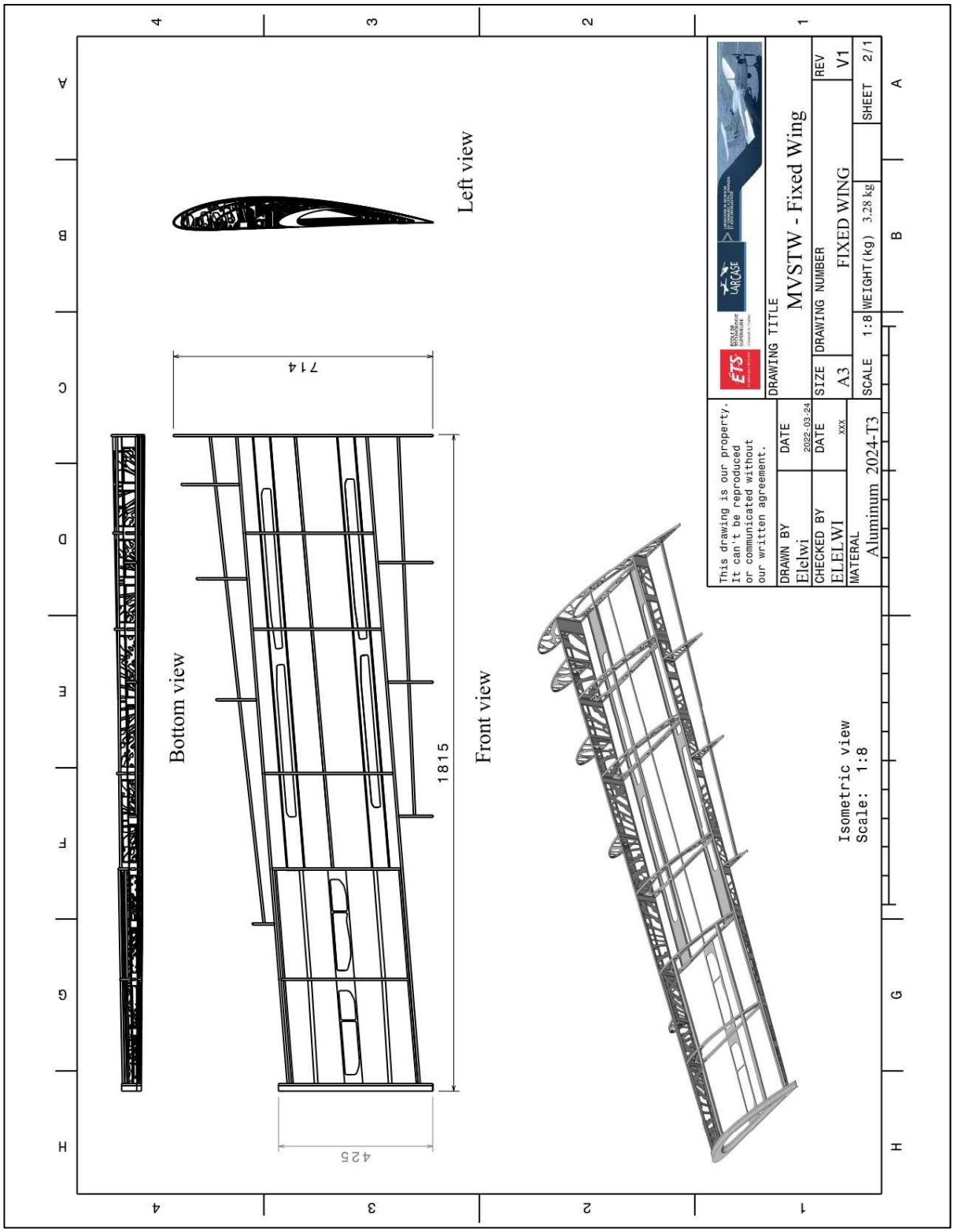

Figure-B II-10 MVSTW Fixed Wing Skeleton Using Al 2024-T3

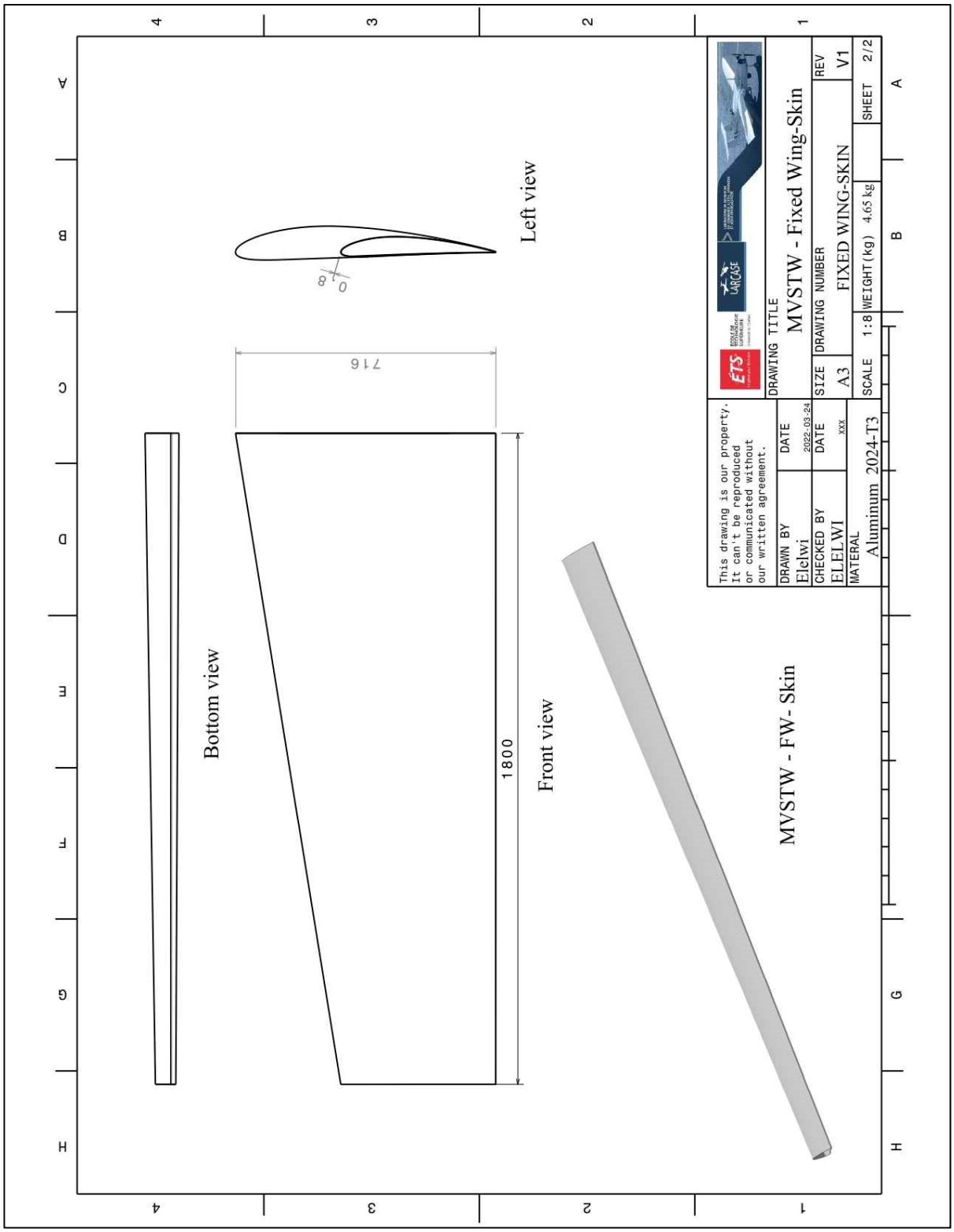

Figure-B II-11 MVSTW Fixed Wing Skin Using Al 2024-T3

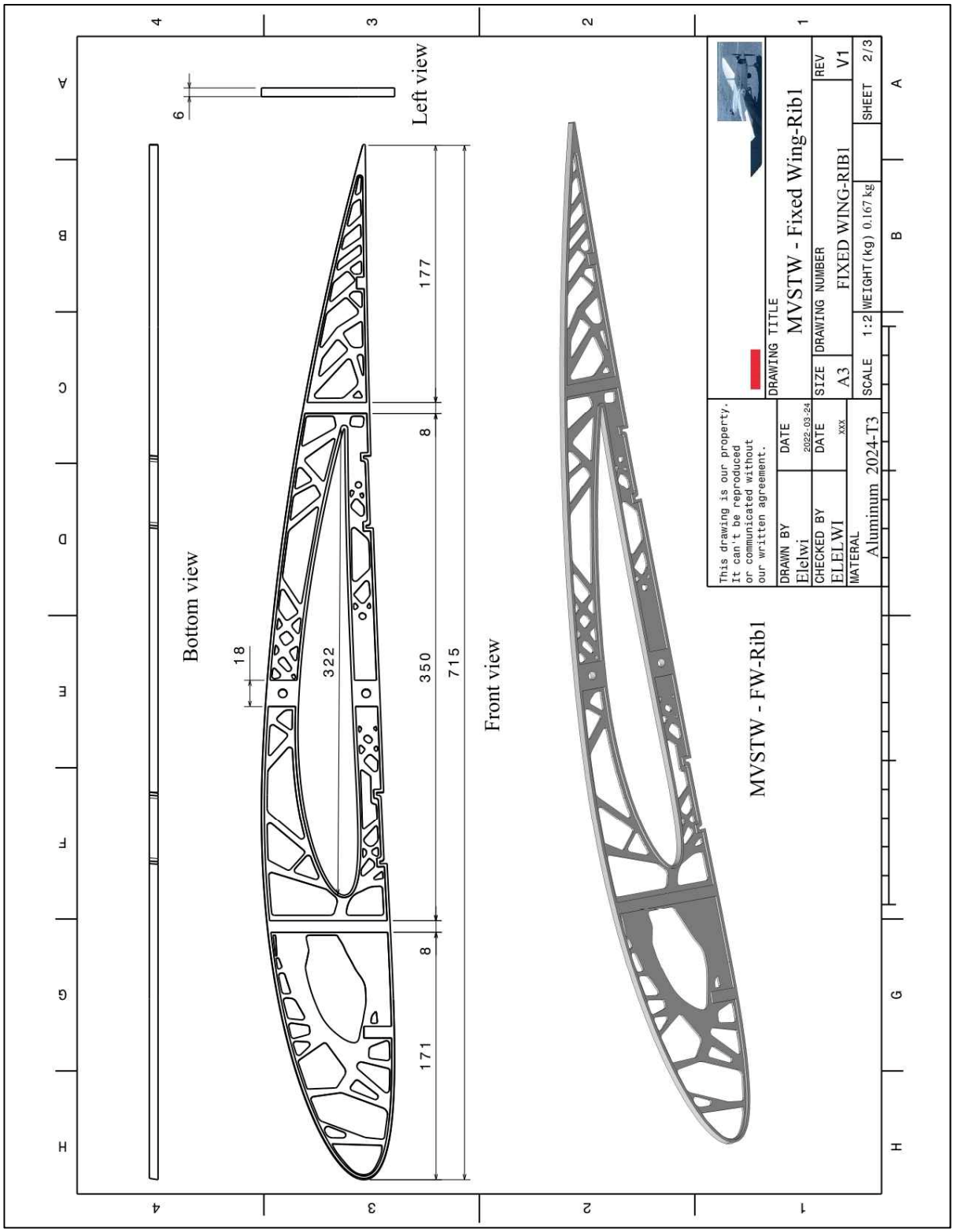

Figure-B II-12 MVSTW Fixed Wing Rib1 Using Al 2024-T3

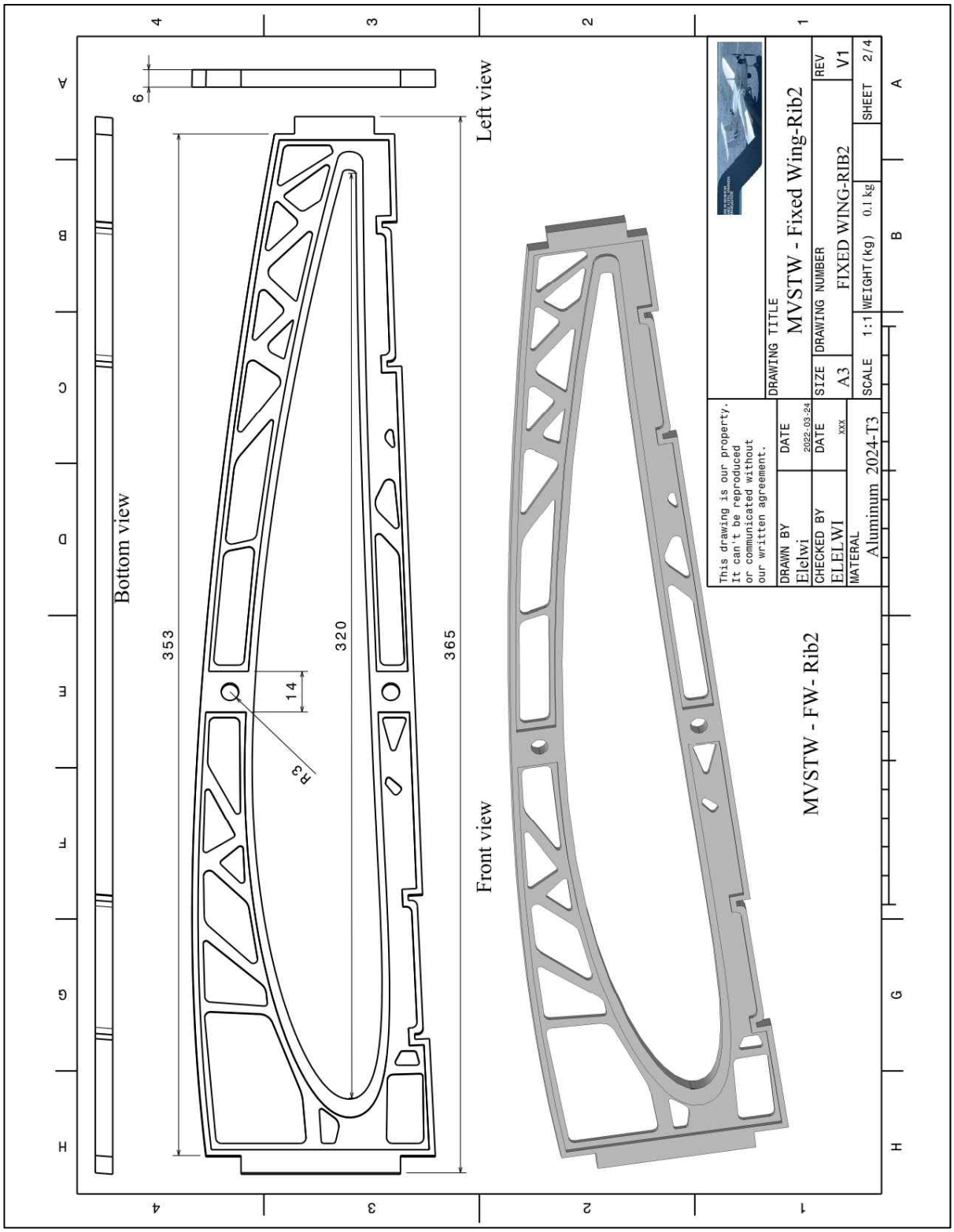

Figure-B II-13 MVSTW Fixed Wing Rib2 Using Al 2024-T3

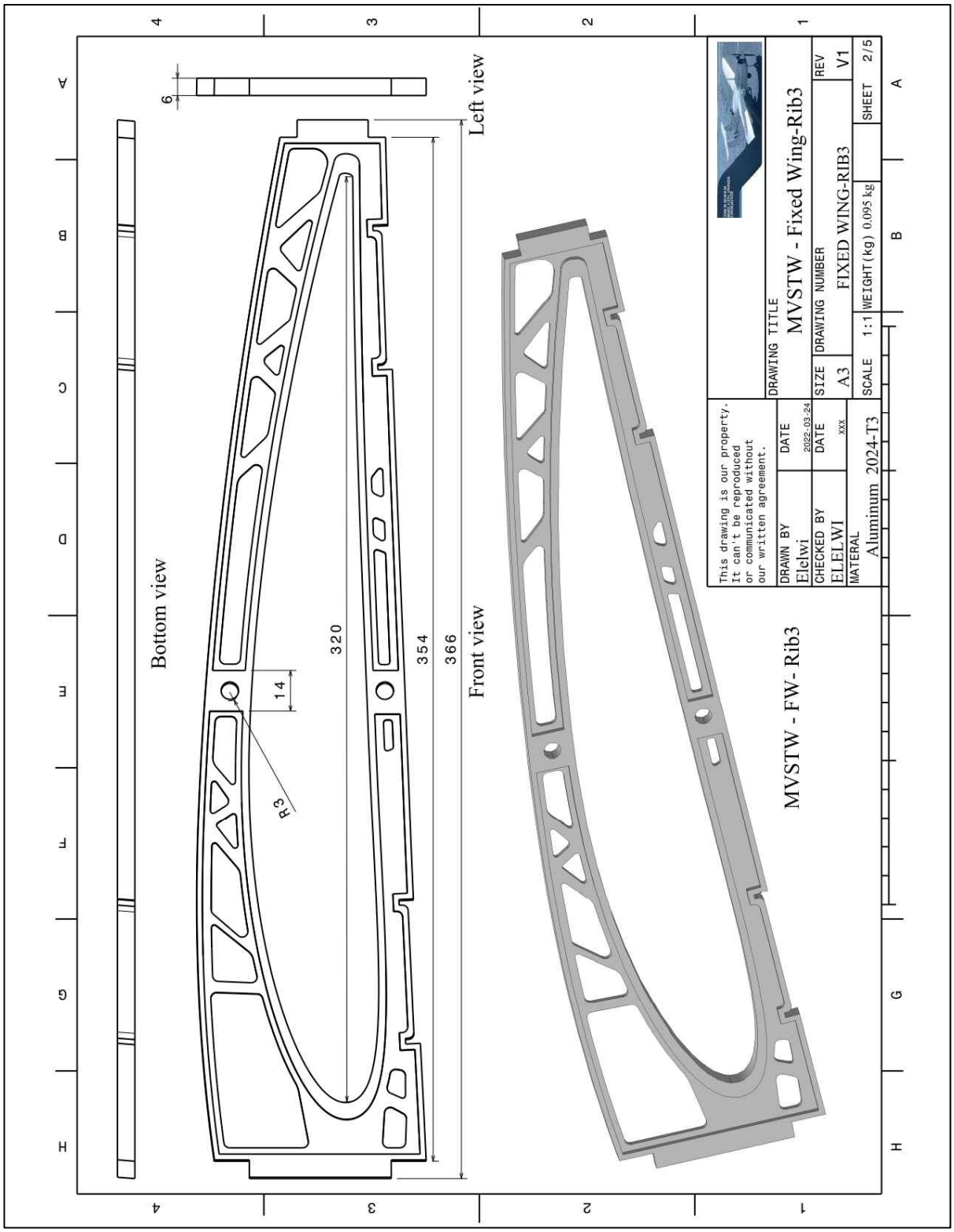

Figure-B II-14 MVSTW Fixed Wing Rib3 Using Al 2024-T3

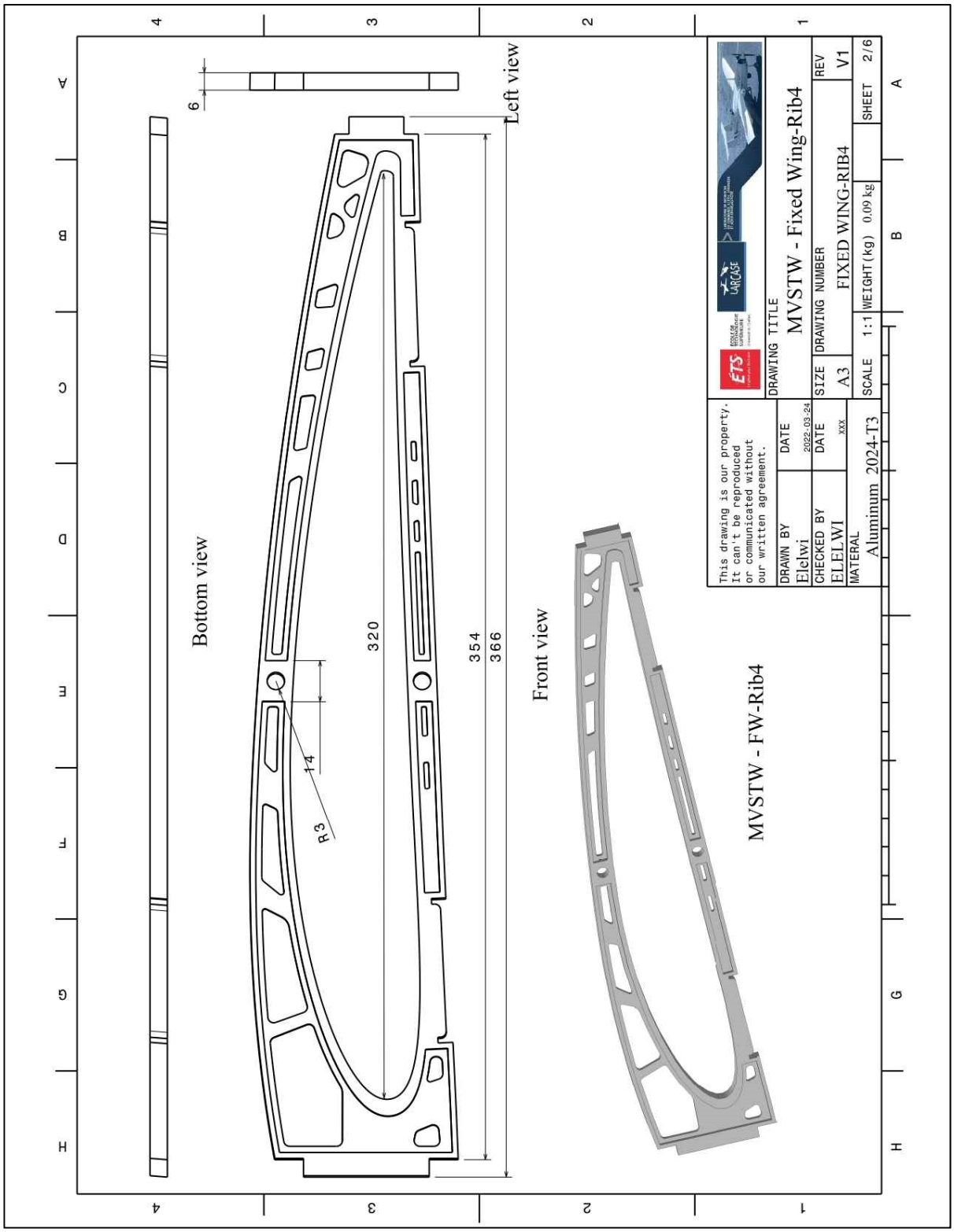

Figure-B II-15 MVSTW Fixed Wing Rib 4 Using Al 2024-T3

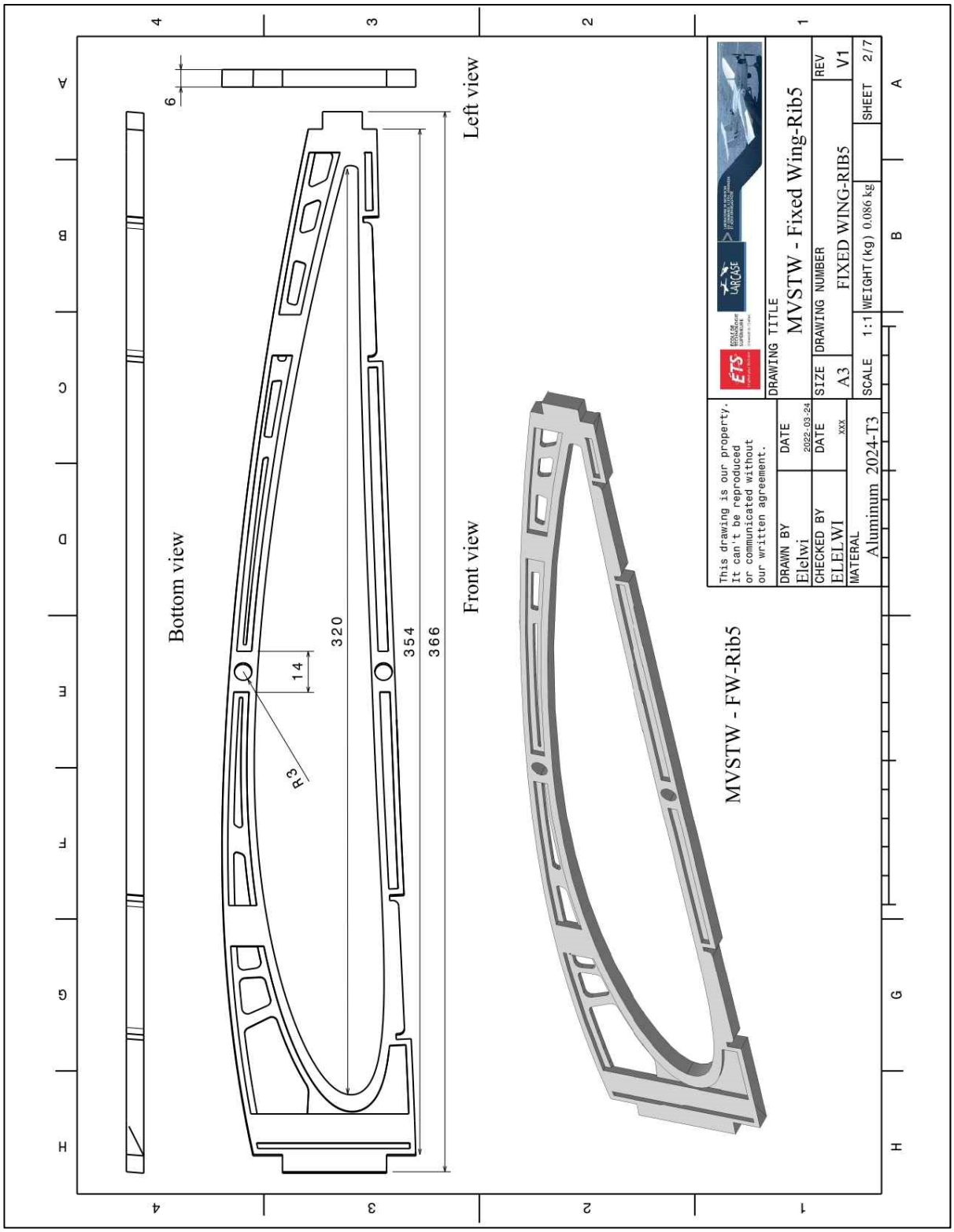

Figure-B II-16 MVSTW Fixed Wing Rib5 Using Al 2024-T3

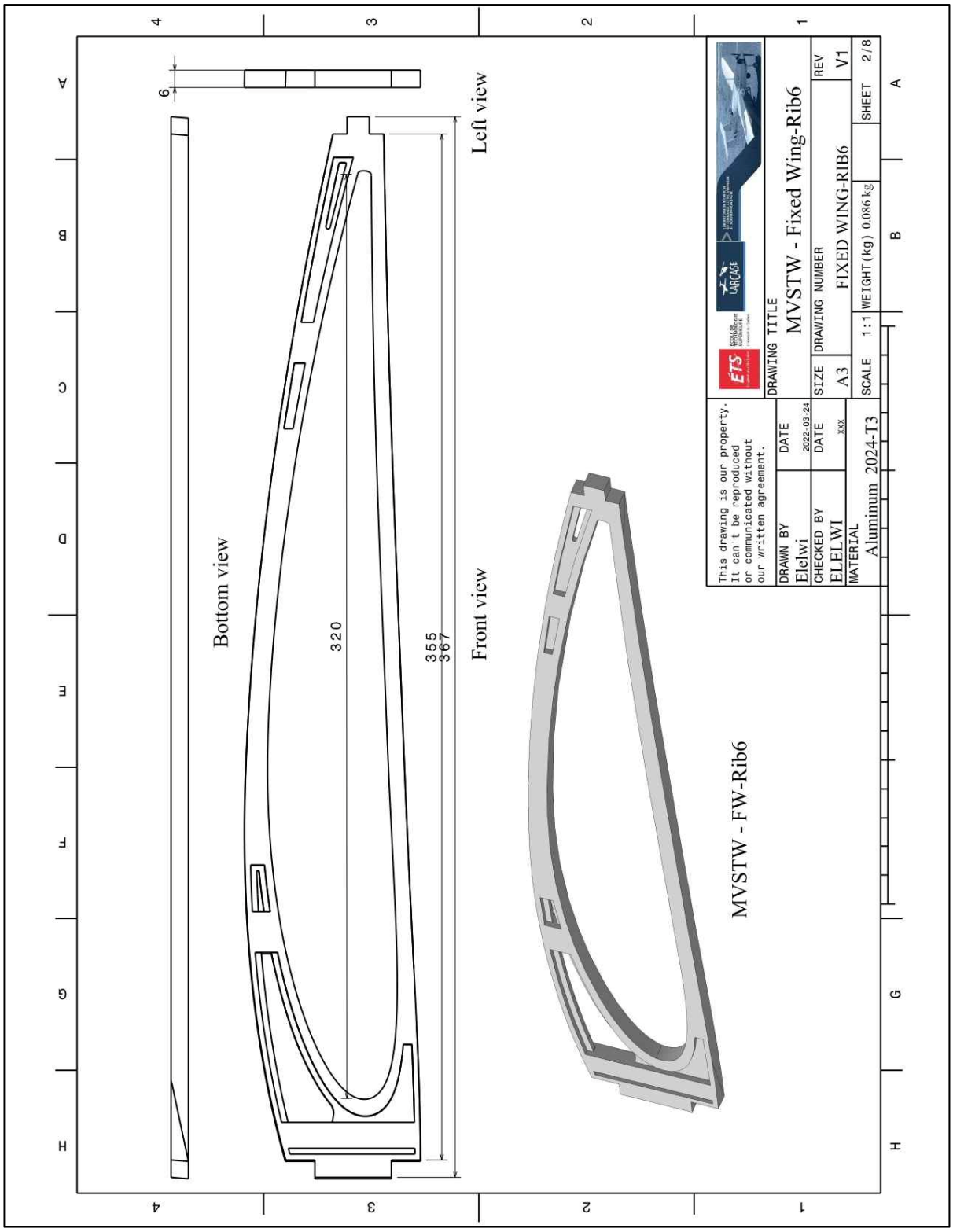

Figure-B II-17 MVSTW Fixed Wing Rib6 Using Al 2024-T3

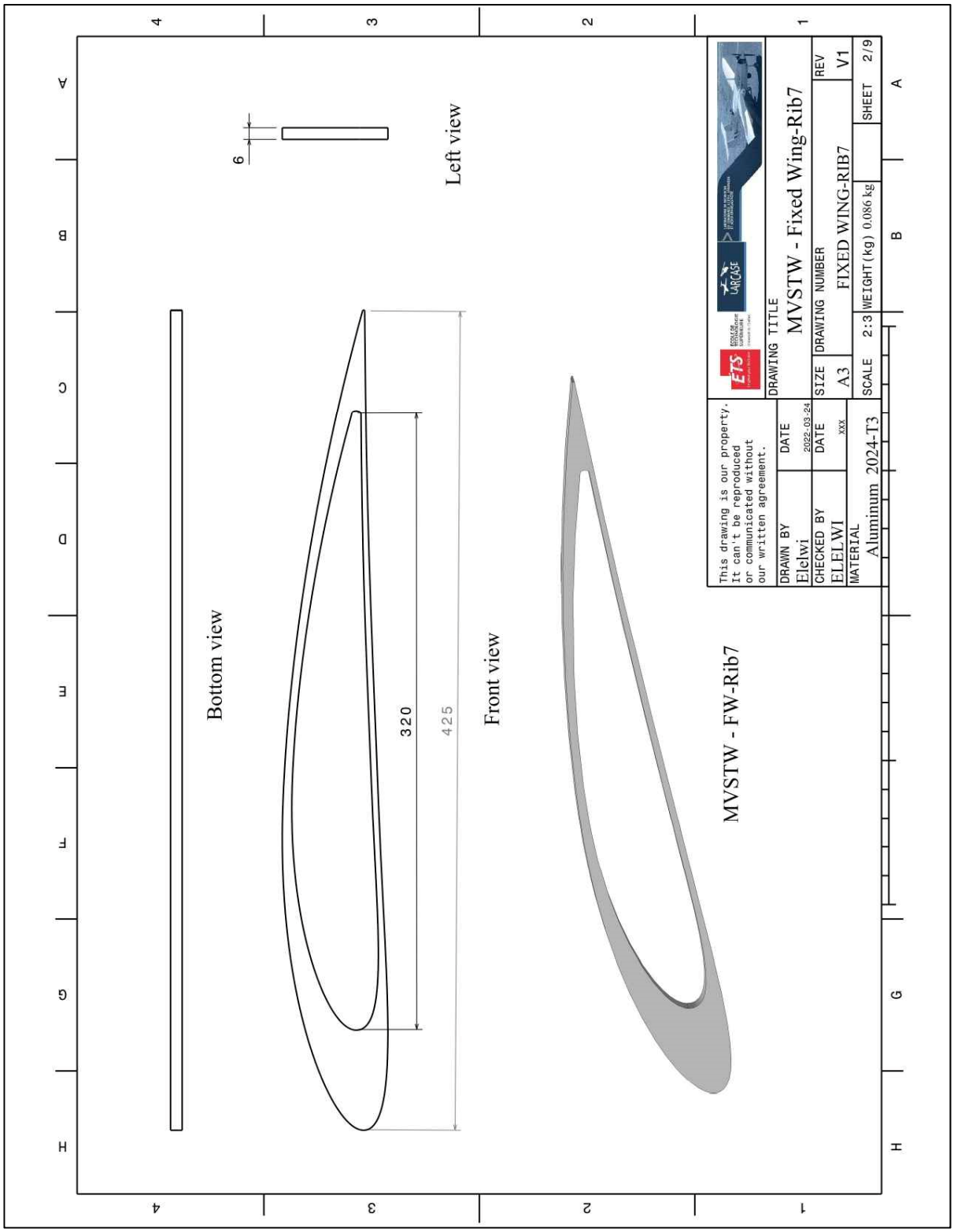

Figure-B II-18 MVSTW Fixed Wing Rib7 Using Al 2024-T3

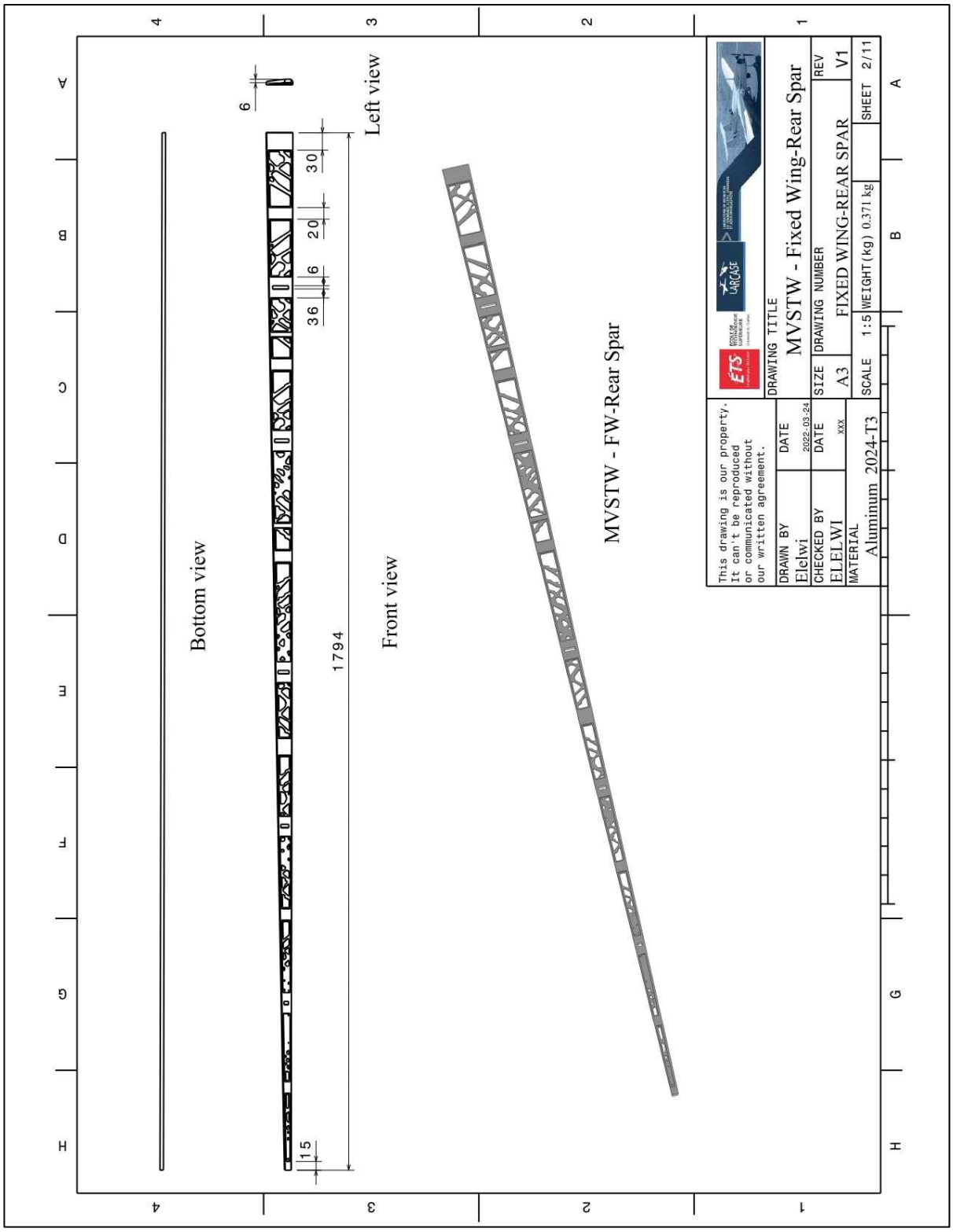

Figure-B II-19 MVSTW Fixed Wing Rear Spar Using Al 2024-T3

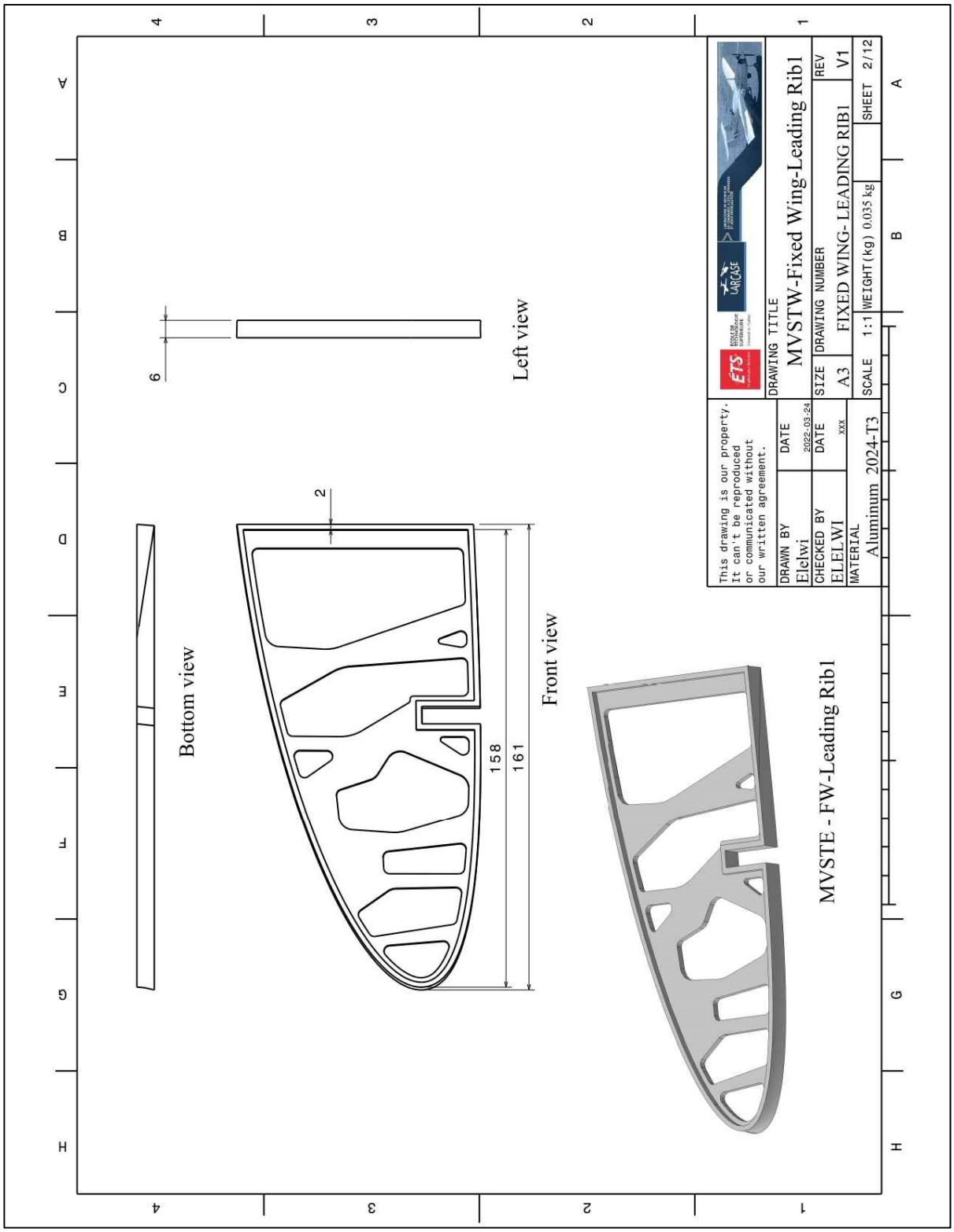

Figure-B II20 MVSTW Fixed Wing Leading Edge Rib1 Using Al 2024-T3

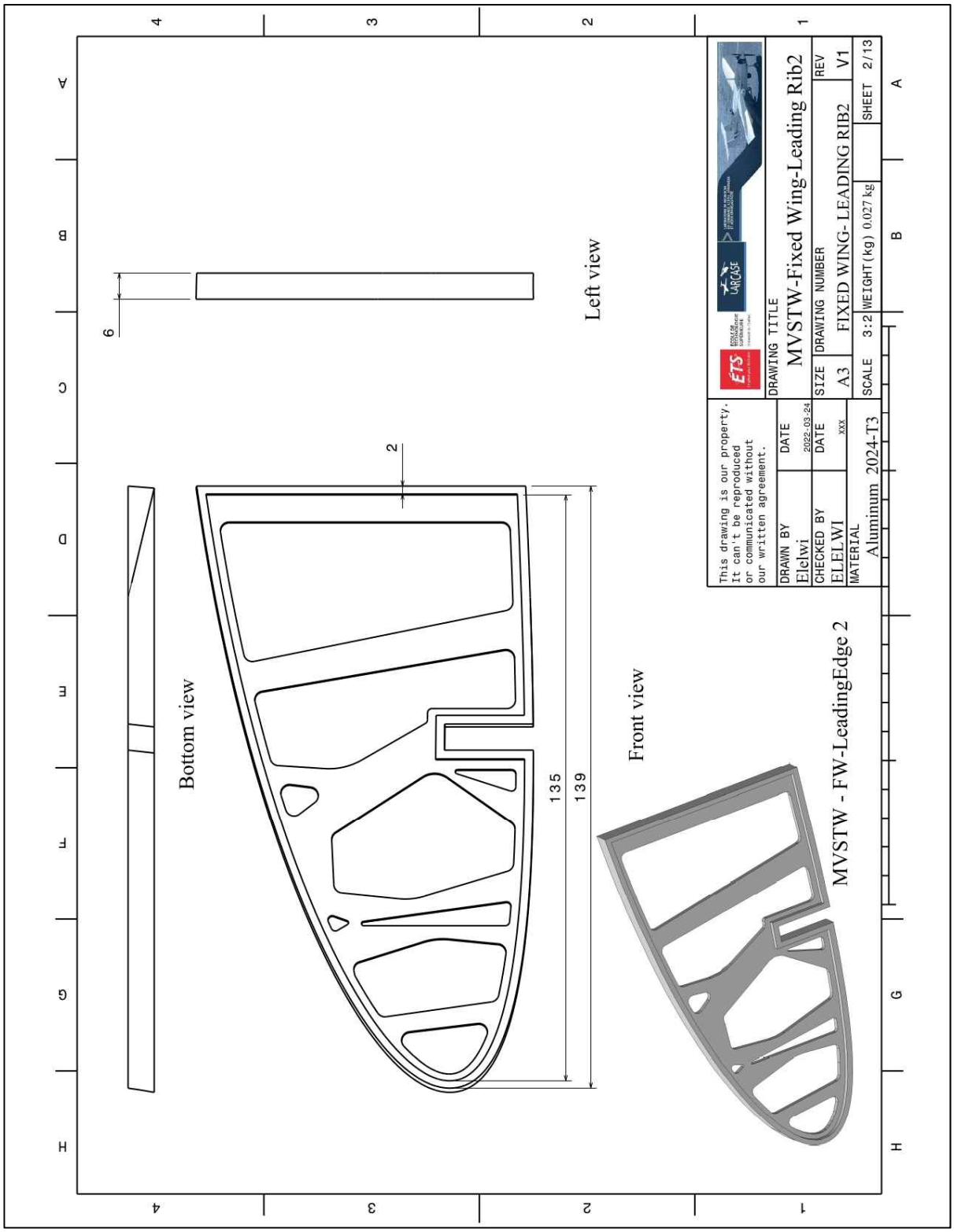

Figure-B II-21 MVSTW Fixed Wing Leading Edge Rib2 Using Al 2024-T3

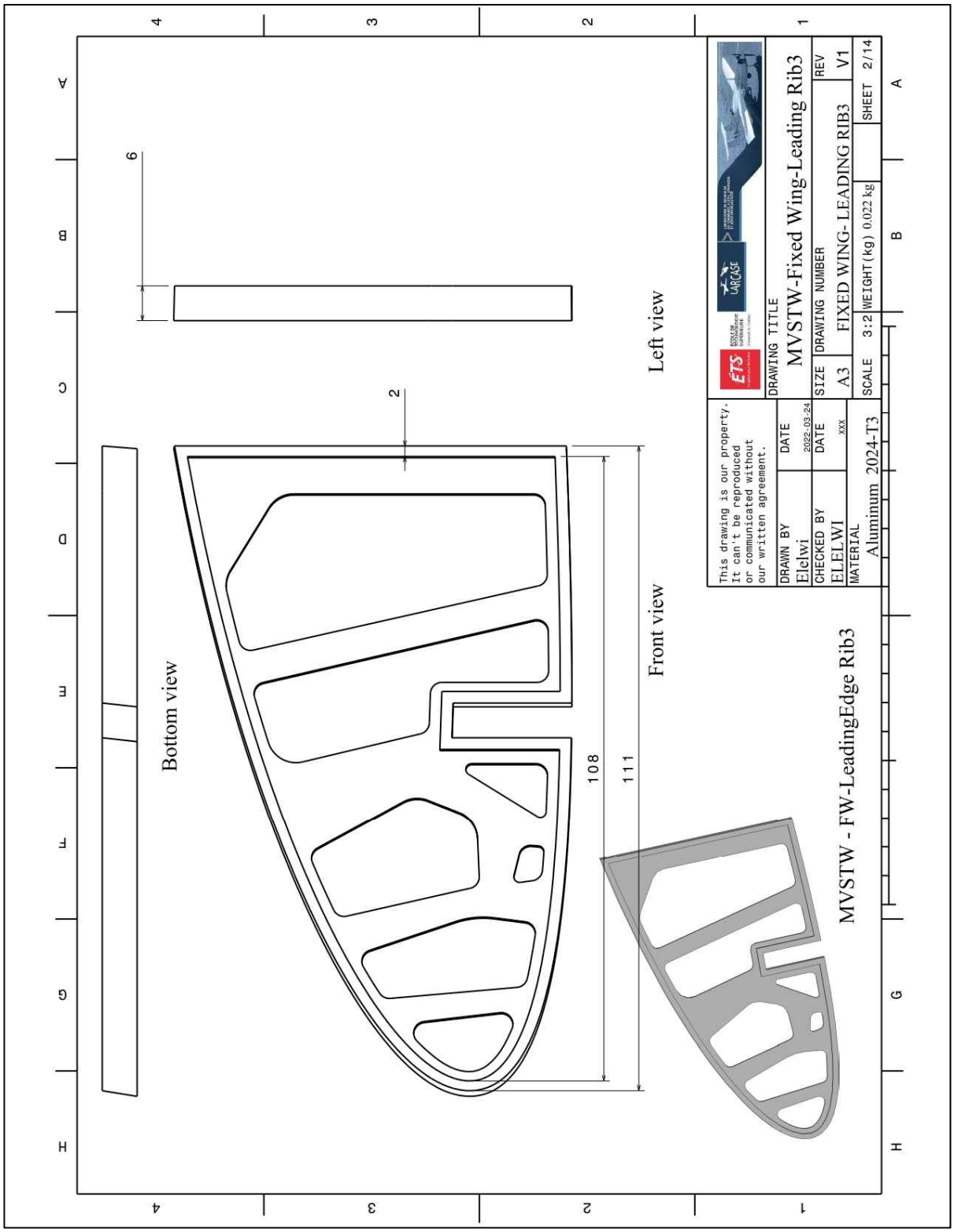

Figure-B II-22 MVSTW Fixed Wing Leading Edge Rib3 Using Al 2024-T3

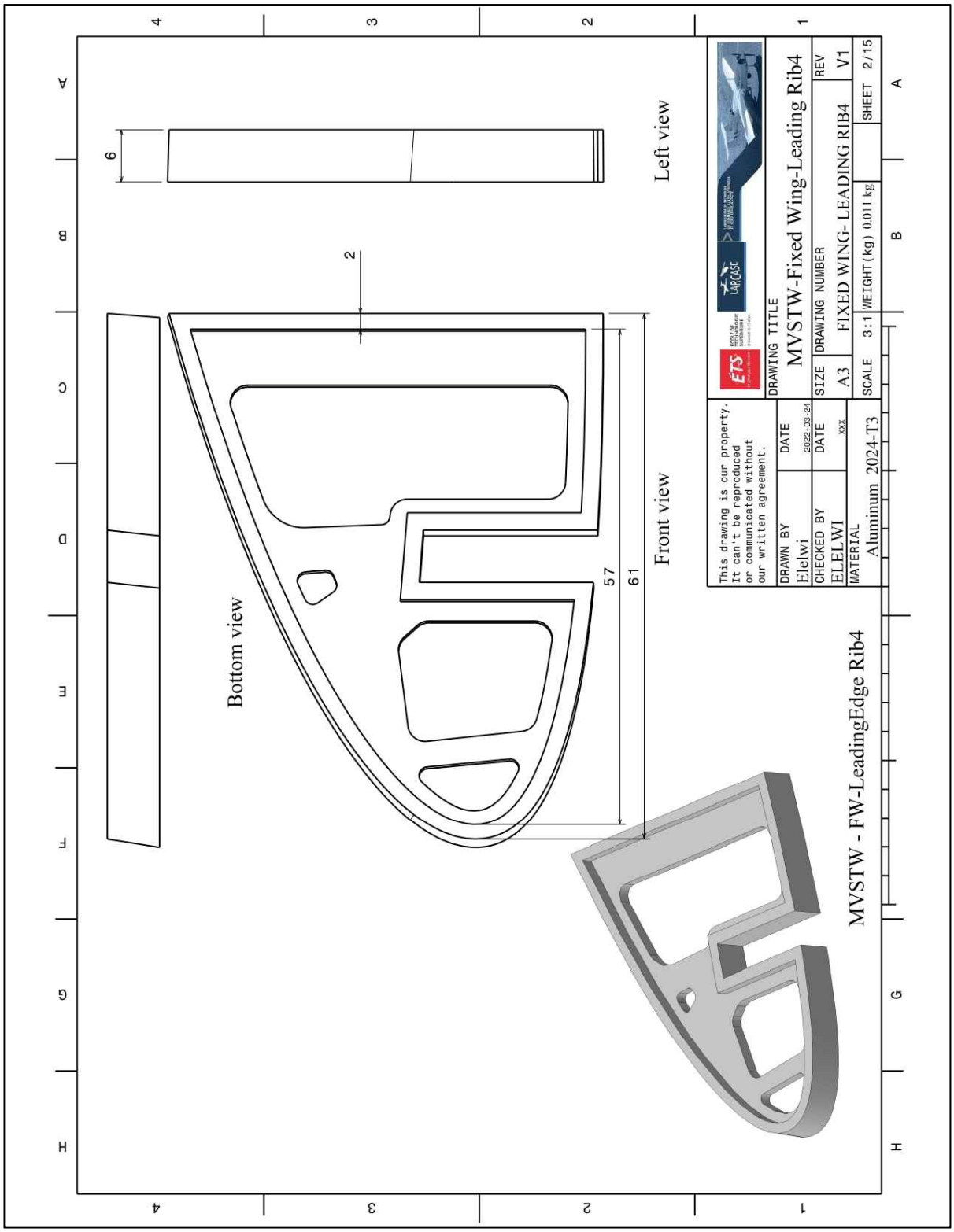

Figure-B II-23 MVSTW Fixed Wing Using Leading Edge Rib4 Al 2024-T3

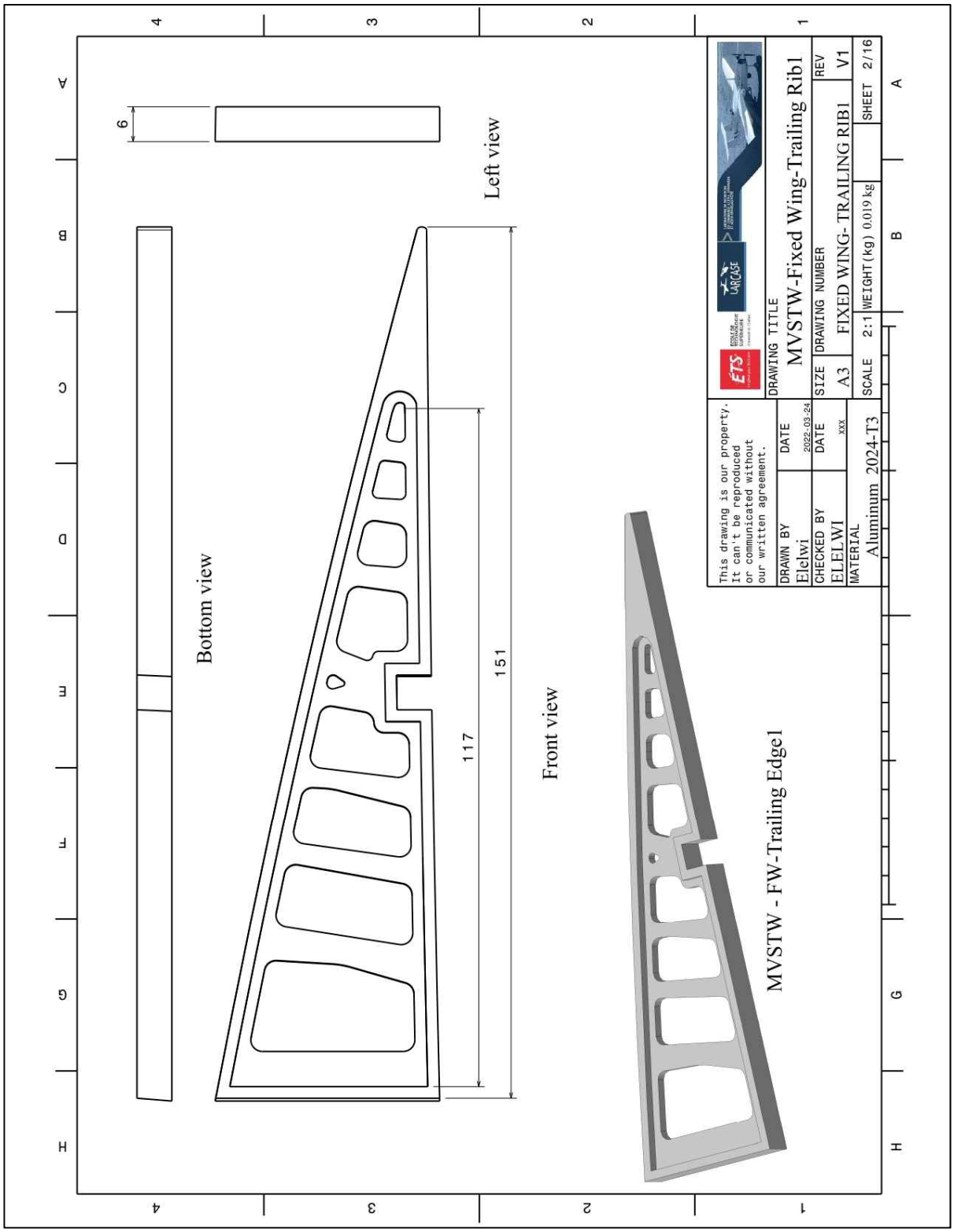

Figure-B II-24 MVSTW Fixed Wing Trailing Edge Rib1 Using Al 2024-T3

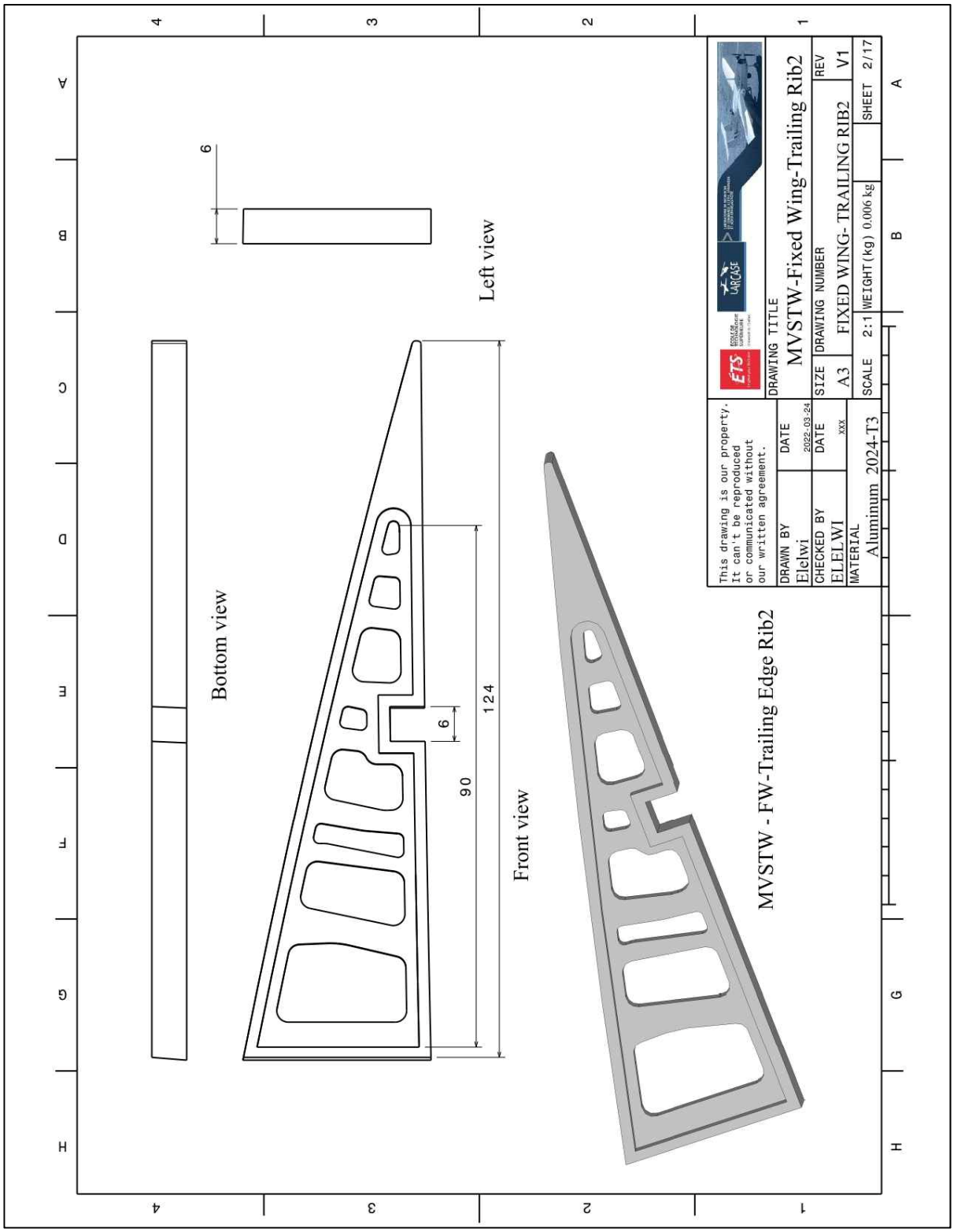

Figure-B II-25 MVSTW Fixed Wing Trailing Edge Rib2 Using Al 2024-T3

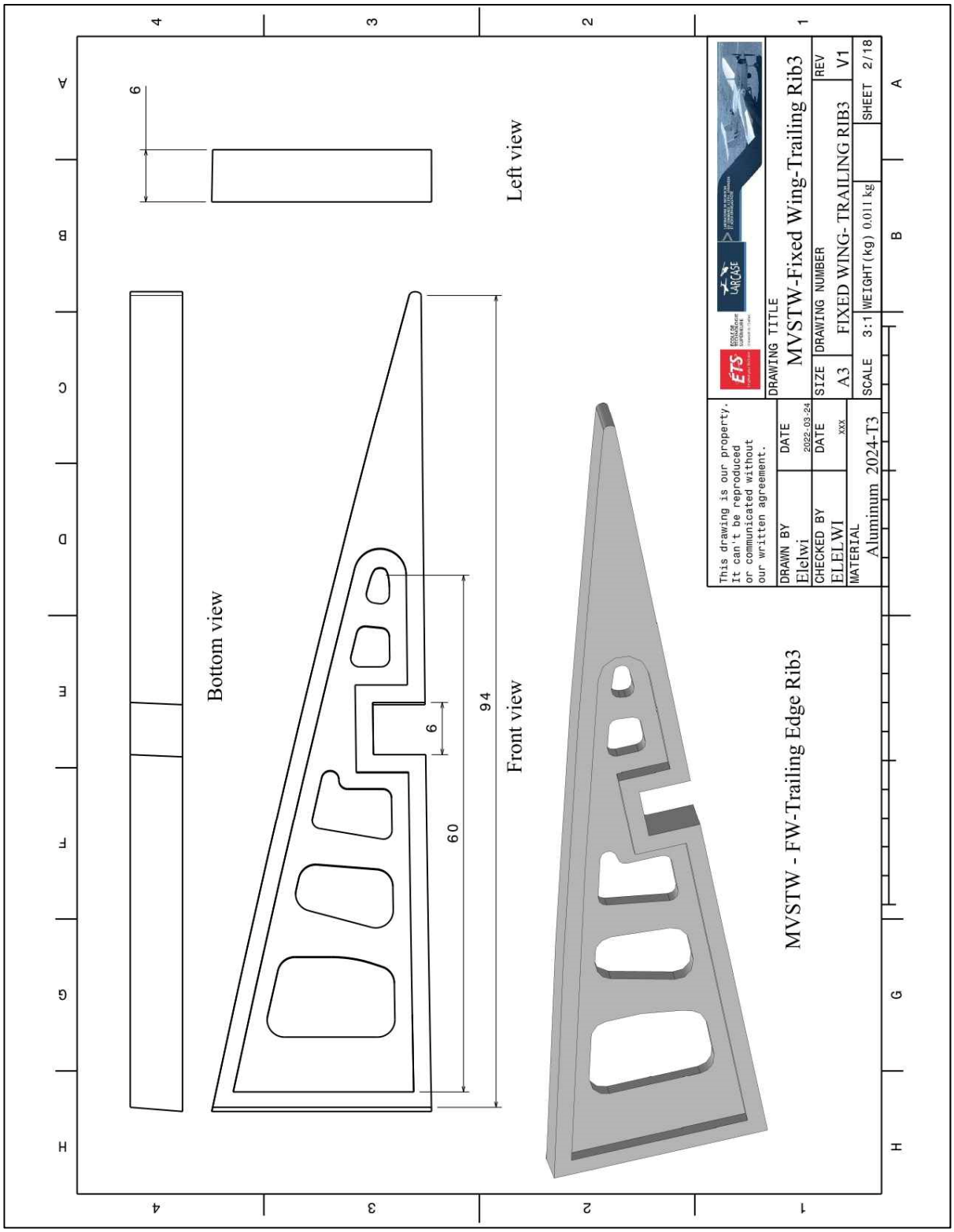

Figure-B II-26 MVSTW Fixed Wing Trailing Edge Rib3 Using Al 2024-T3

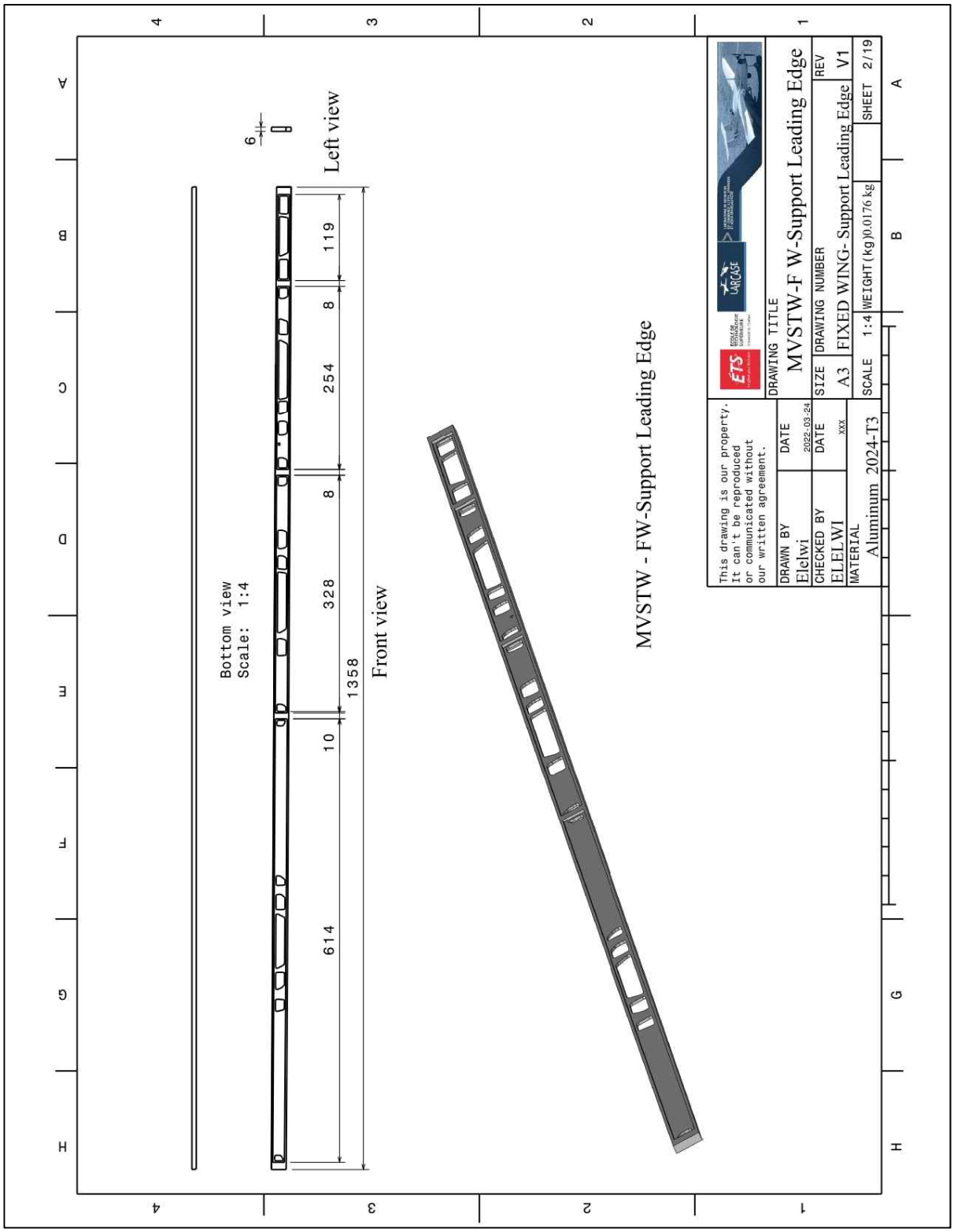

Figure-B II-27 MVSTW Fixed Wing Support Leading Edge Using Al 2024-T3

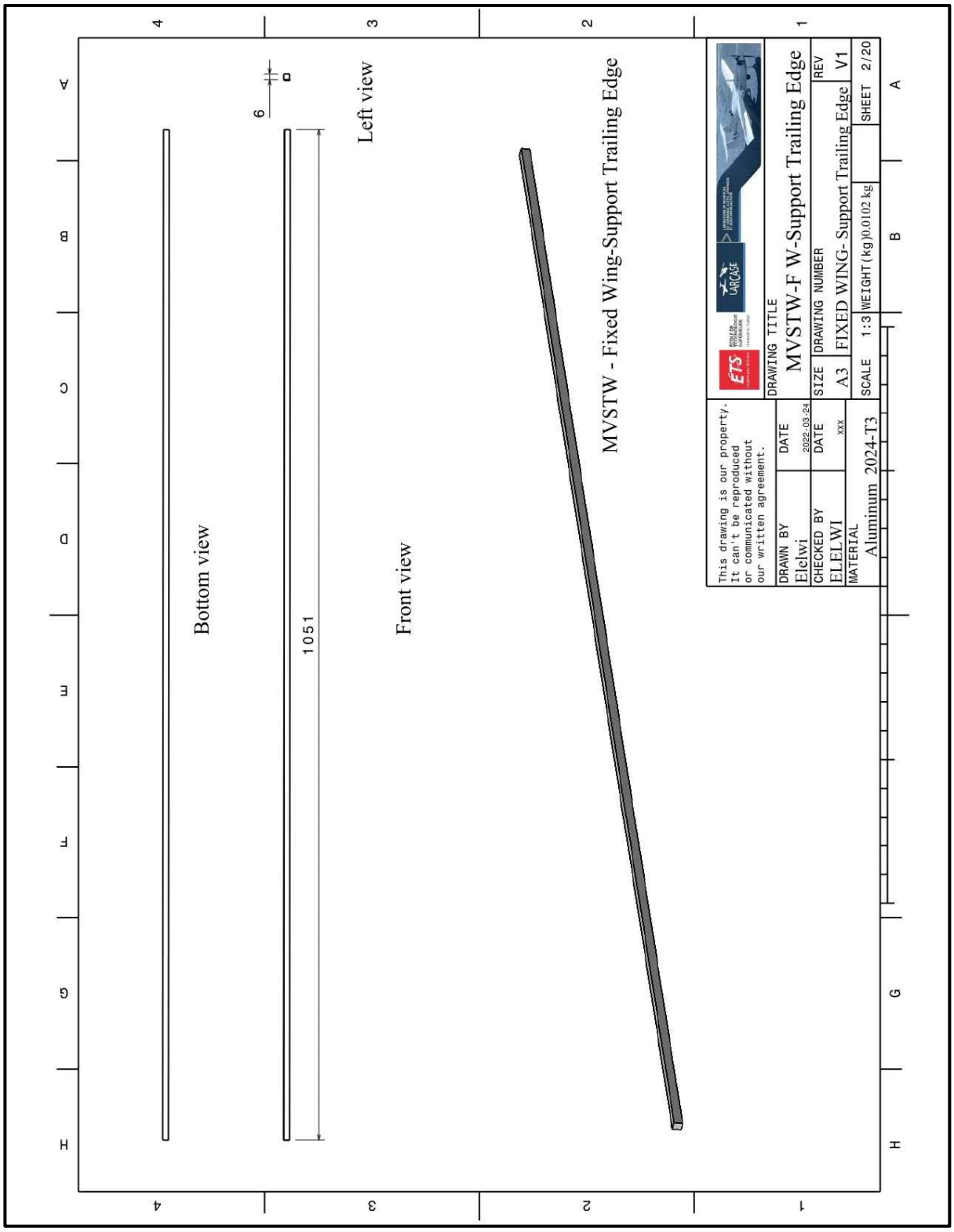

Figure-B II-28 MVSTW Fixed Wing Support Trailing Edge Using Al 2024-T3

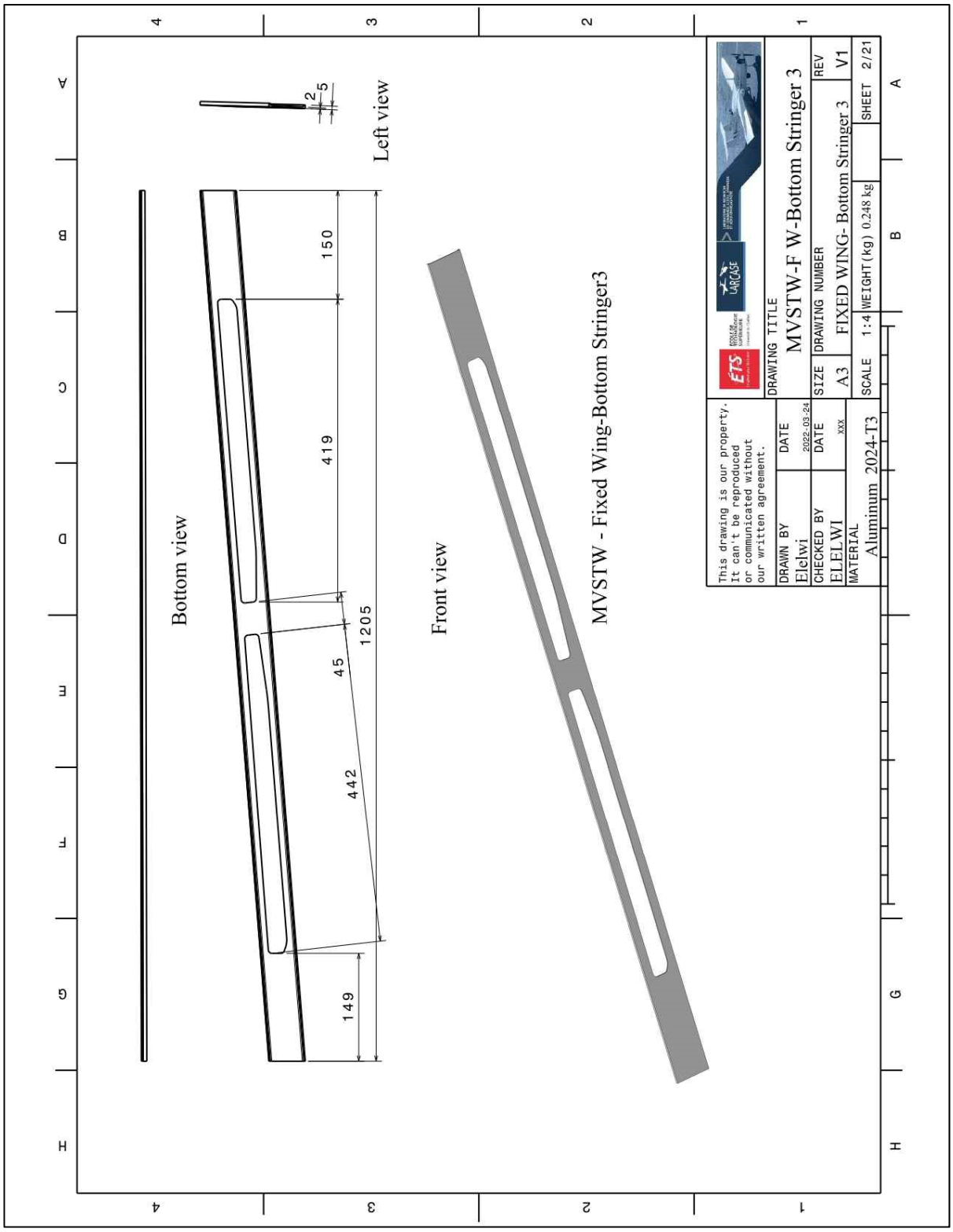

Figure-B II-29 MVSTW Fixed Wing Bottom Stringer3 Using Al 2024-T3

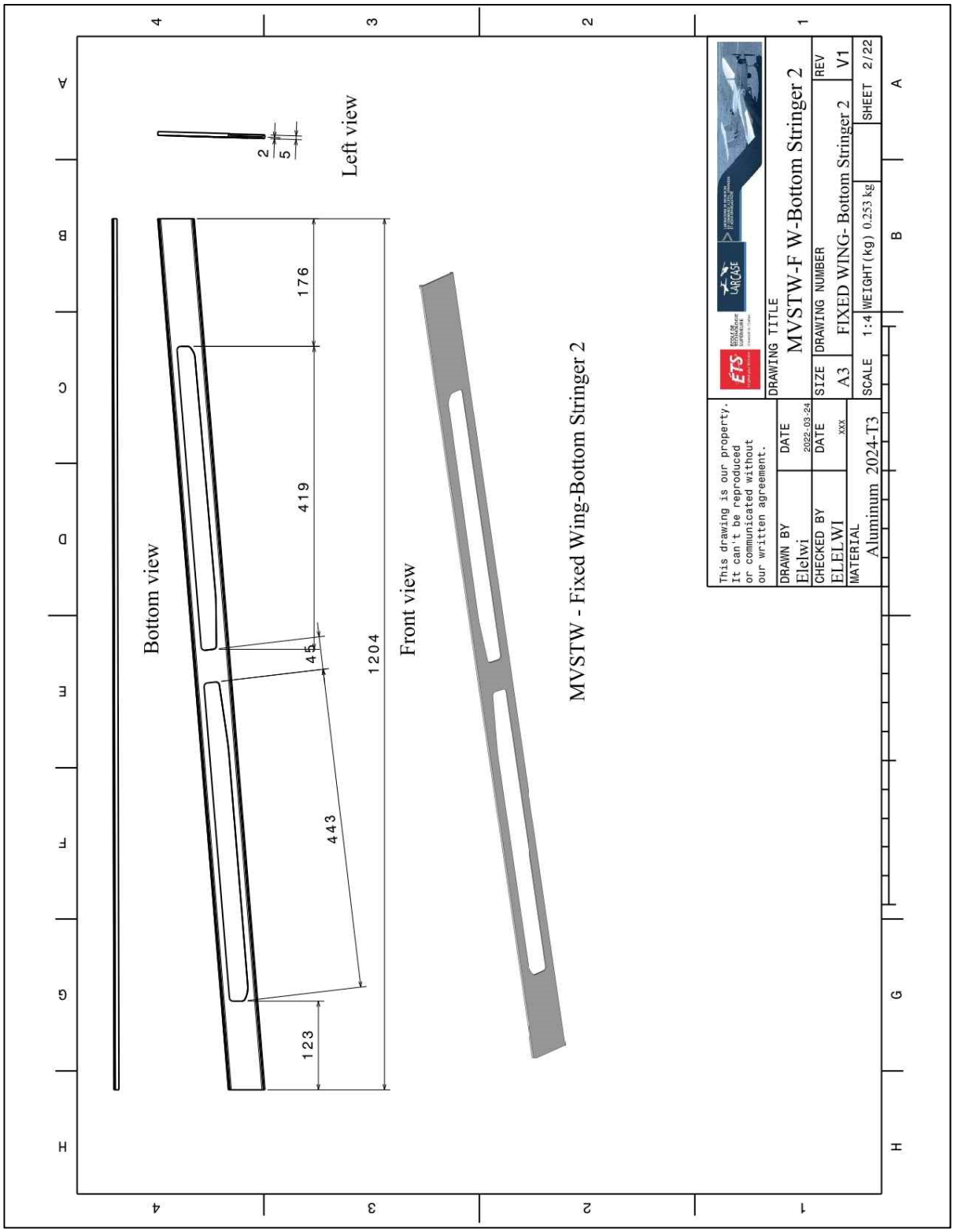

Figure-B II-30 MVSTW Fixed Wing Bottom Stringer2 Using Al 2024-T3

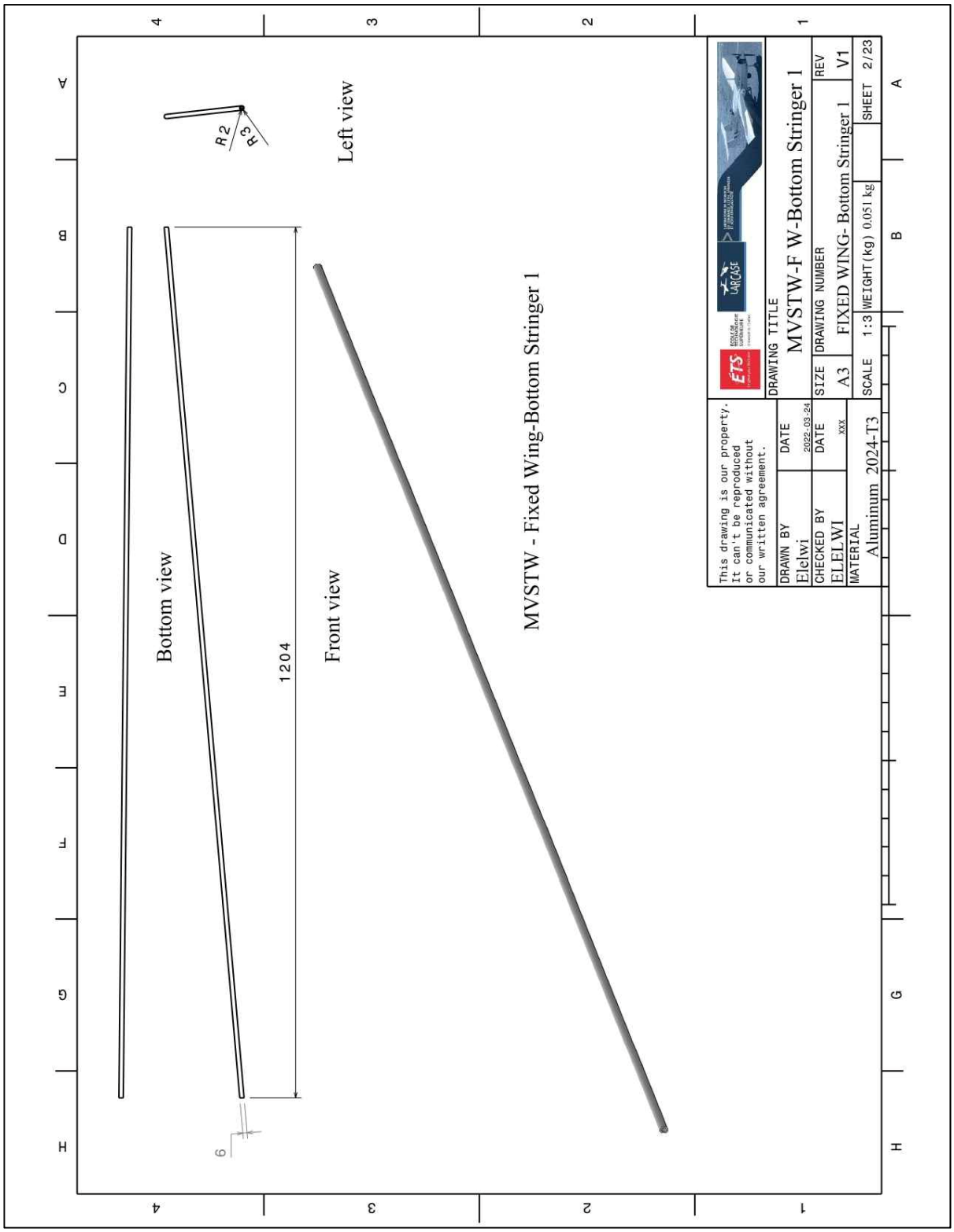

Figure-B II-31 MVSTW Fixed Wing Bottom Stringer1 Using Al 2024-T3

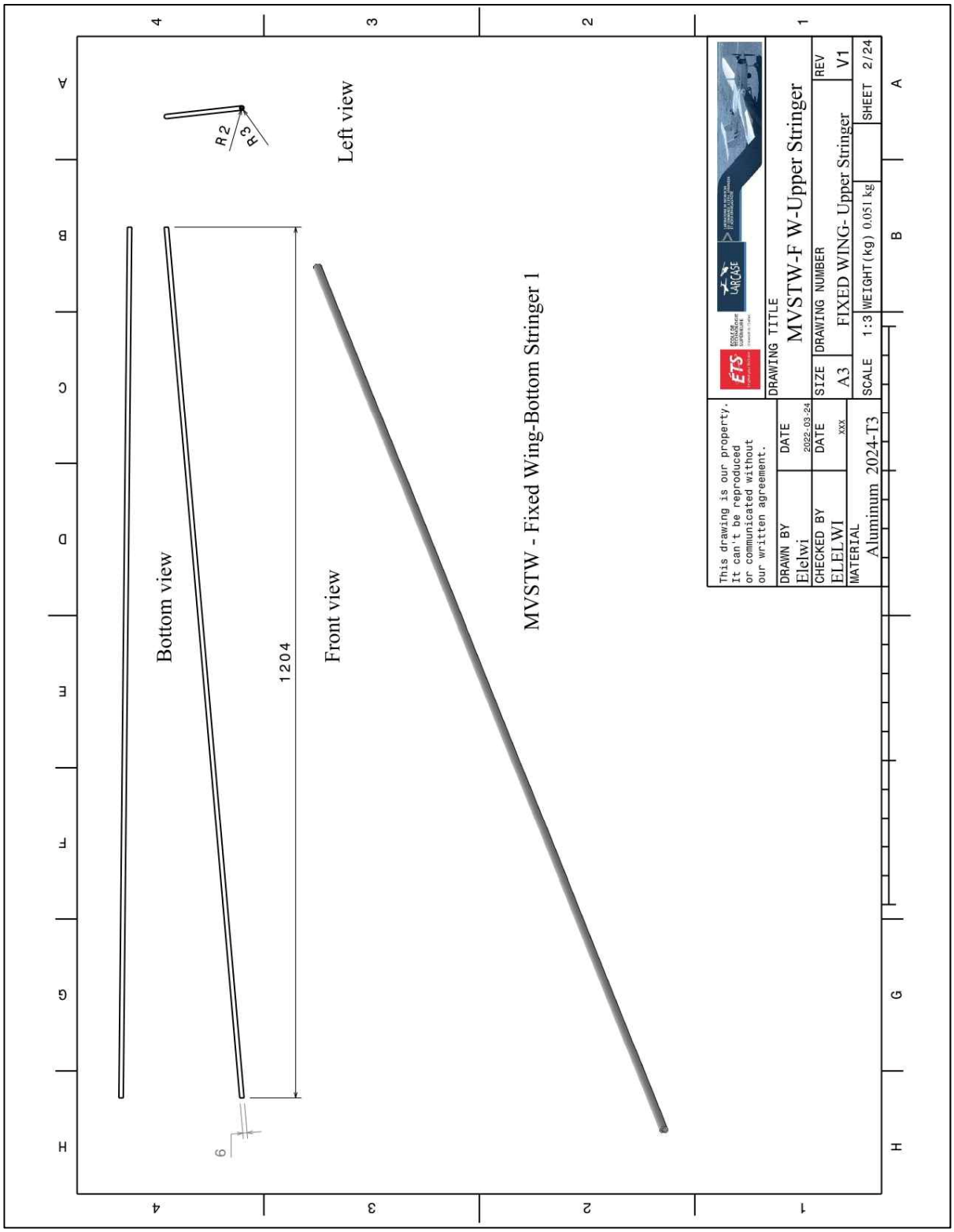

Figure-B II-32 MVSTW Fixed Wing Upper Stringer Using Al 2024-T3

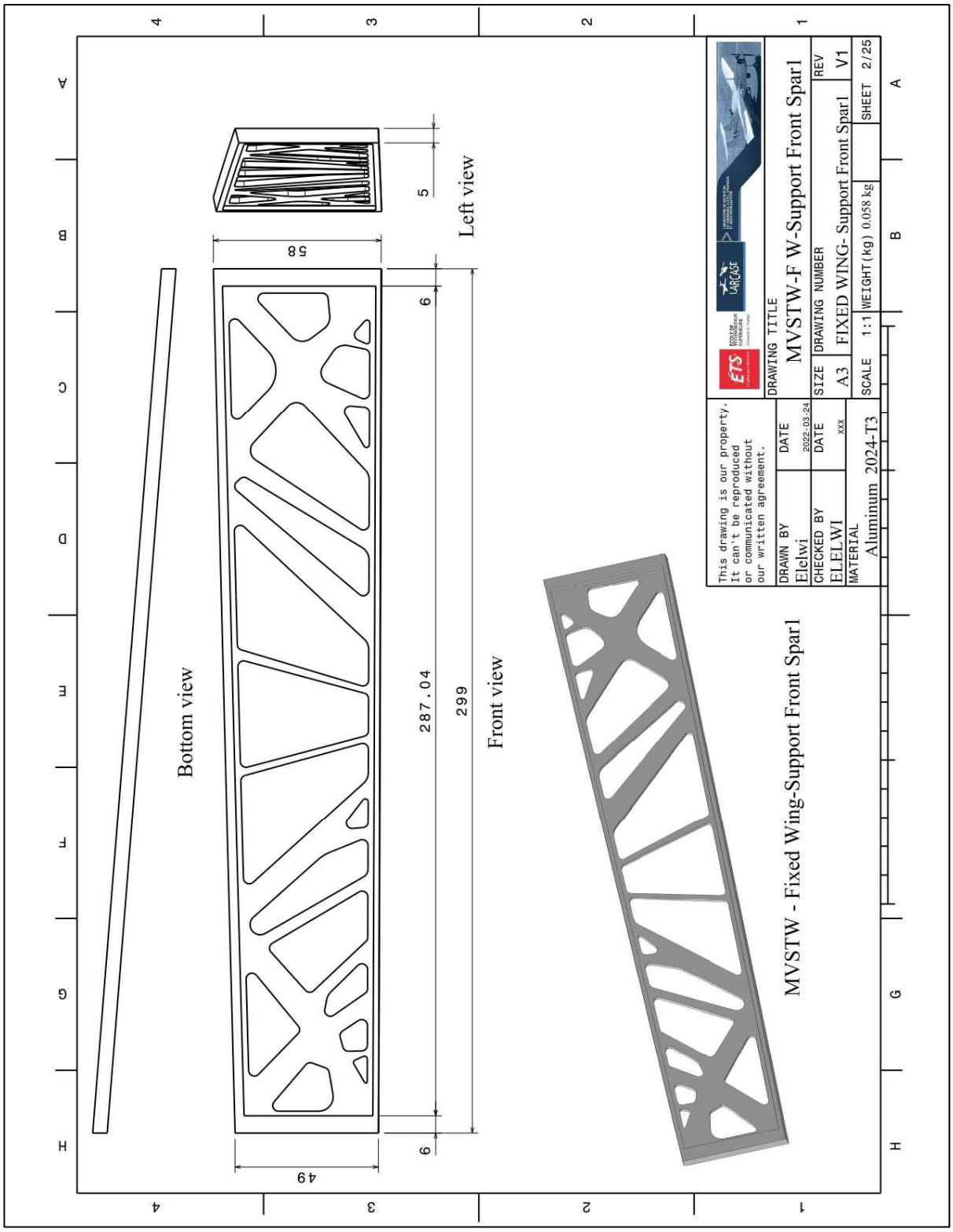

Figure-B II-33 MVSTW Fixed Wing Support front Spar1 Using Al 2024-T3

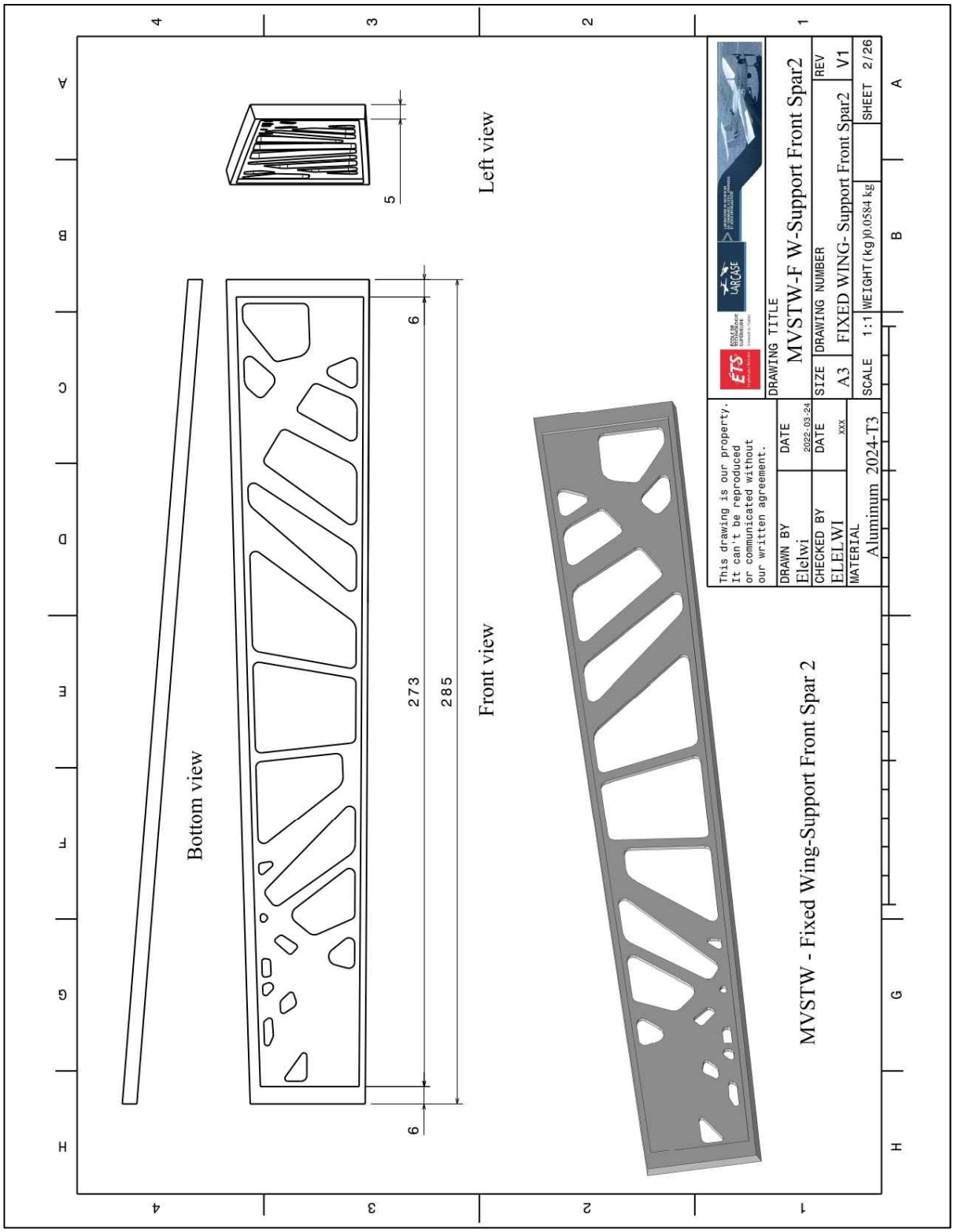

Figure-B II-34 MVSTW Fixed Wing Support Front Spar2 Using Al 2024-T3

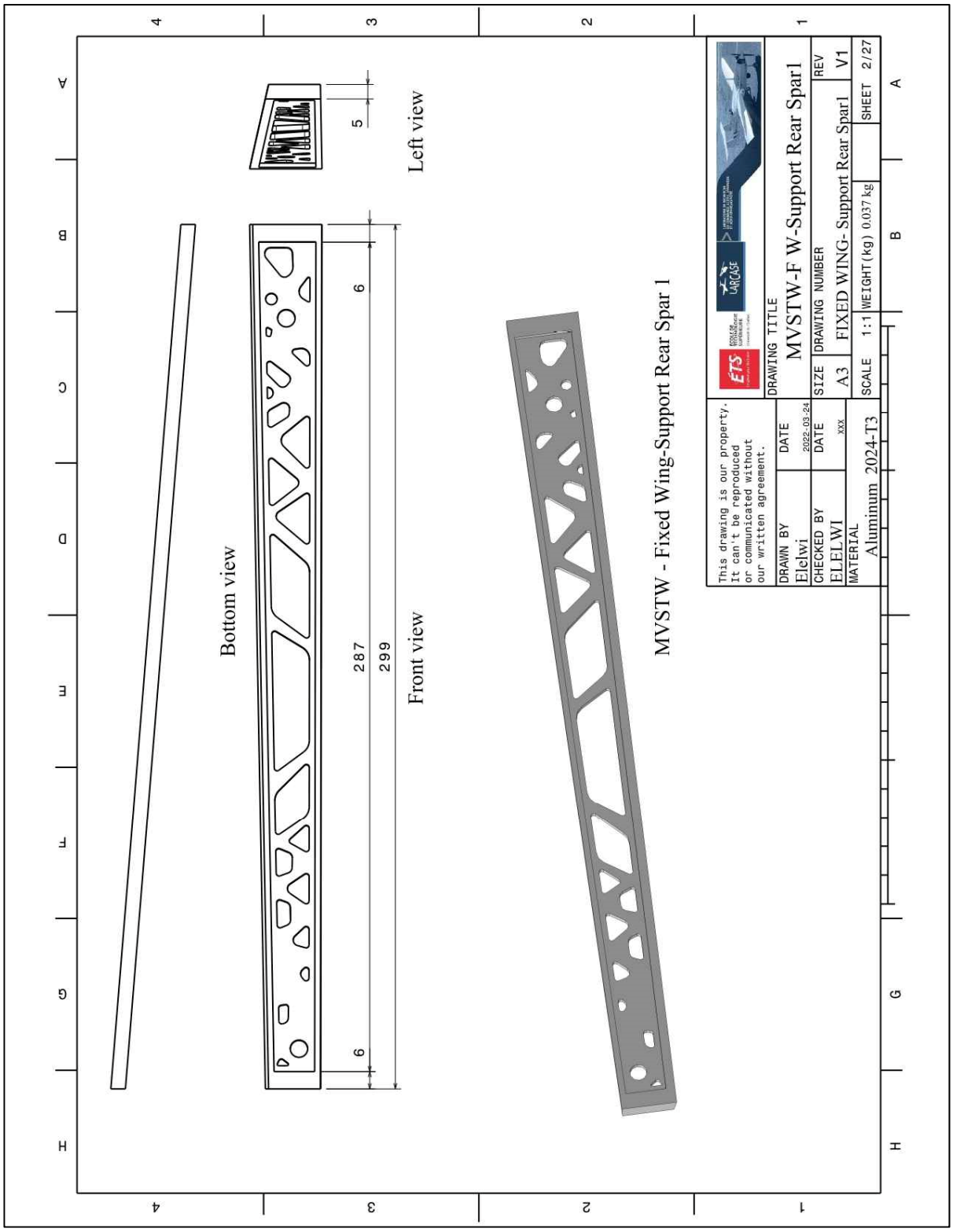

Figure-B II-35 MVSTW Fixed Wing Support Rear Spar1 Using Al 2024-T3

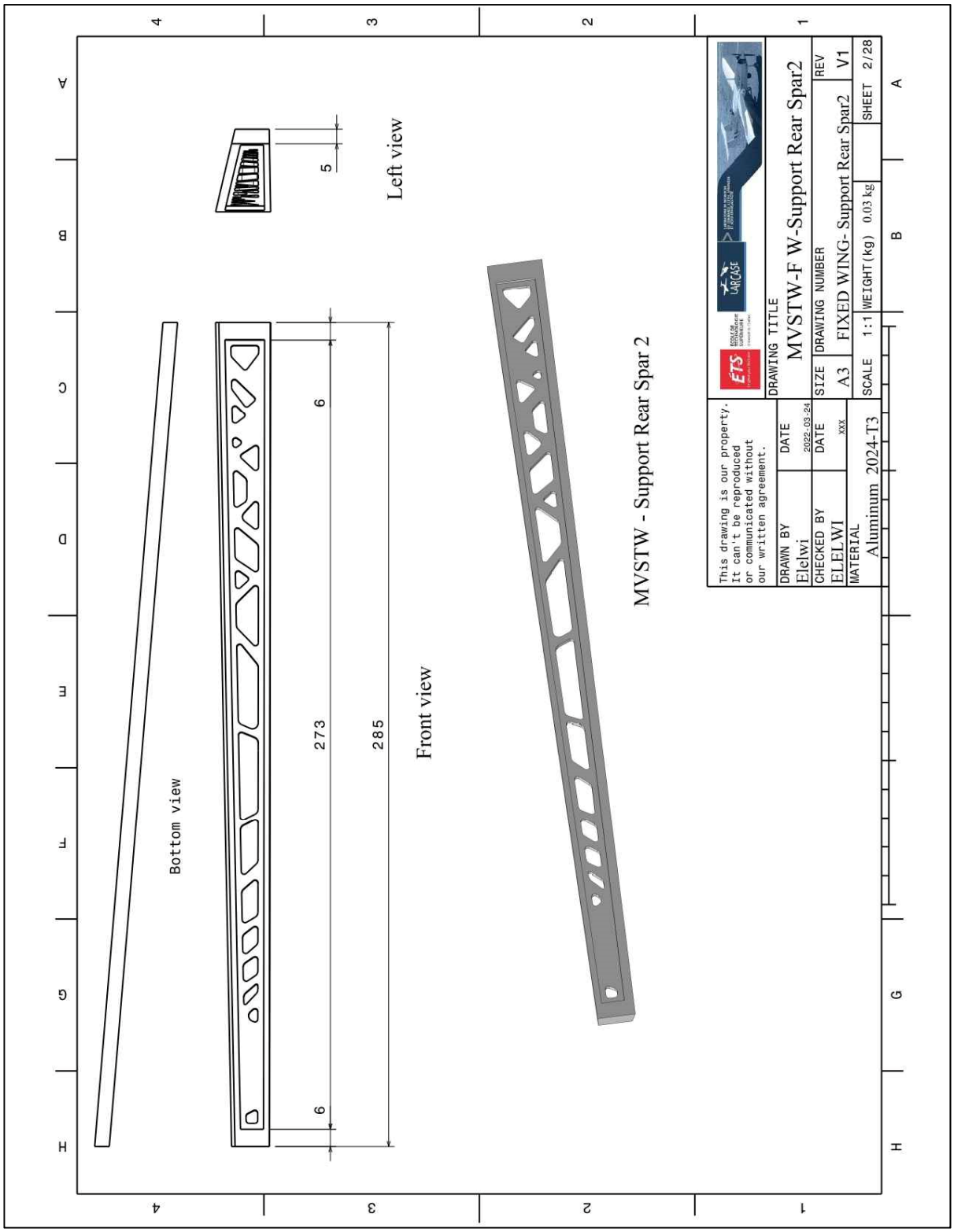

Figure-B II-36 MVSTW Fixed Wing Support Rear Spar2 Using Al 2024-T3

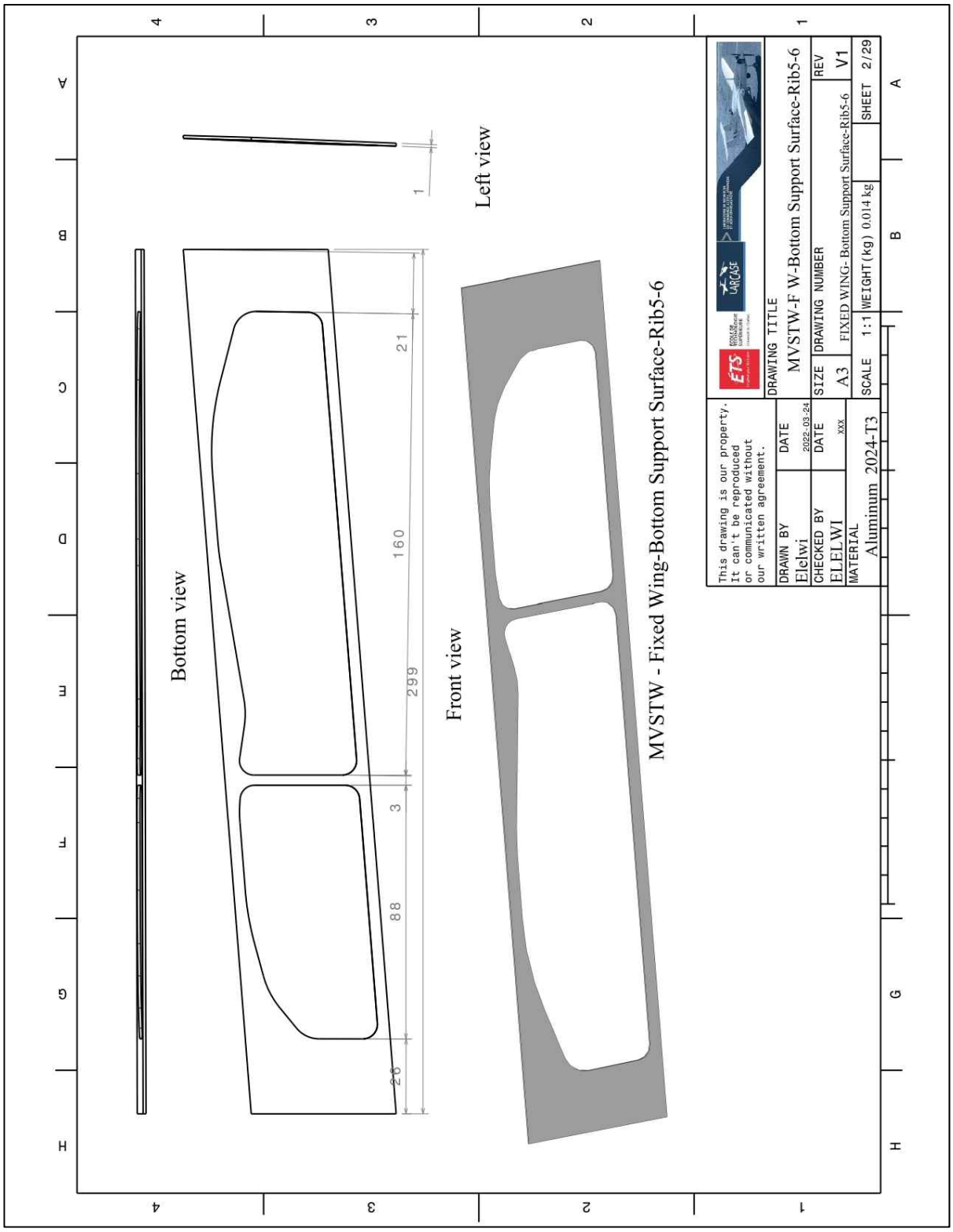

Figure-B II-37 MVSTW Fixed Wing Support Surface Rib 5-6 Using Al 2024-T3

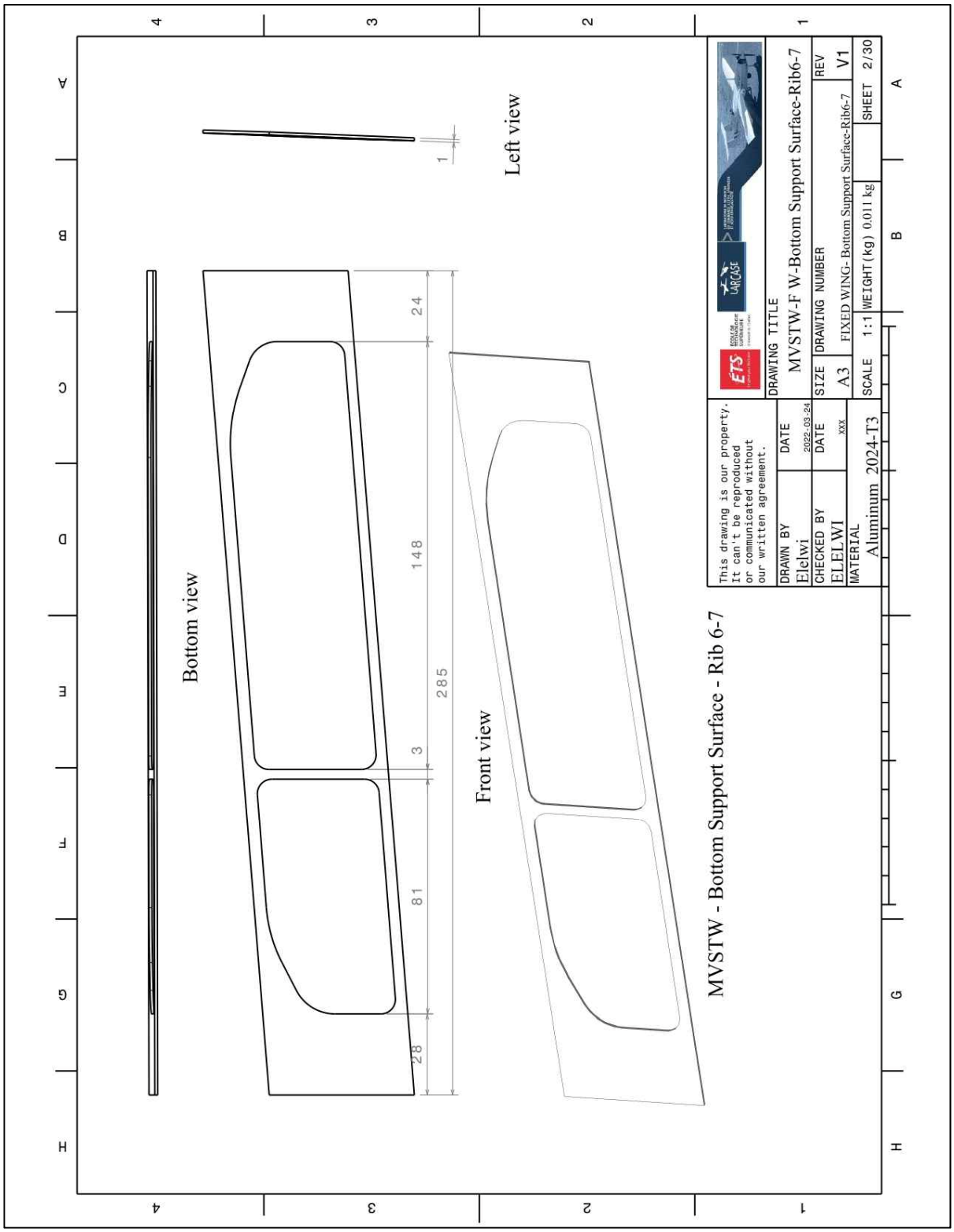

Figure-B II-38 MVSTW Fixed Wing Support Surface Rib 6-7 Using Al 2024-T3

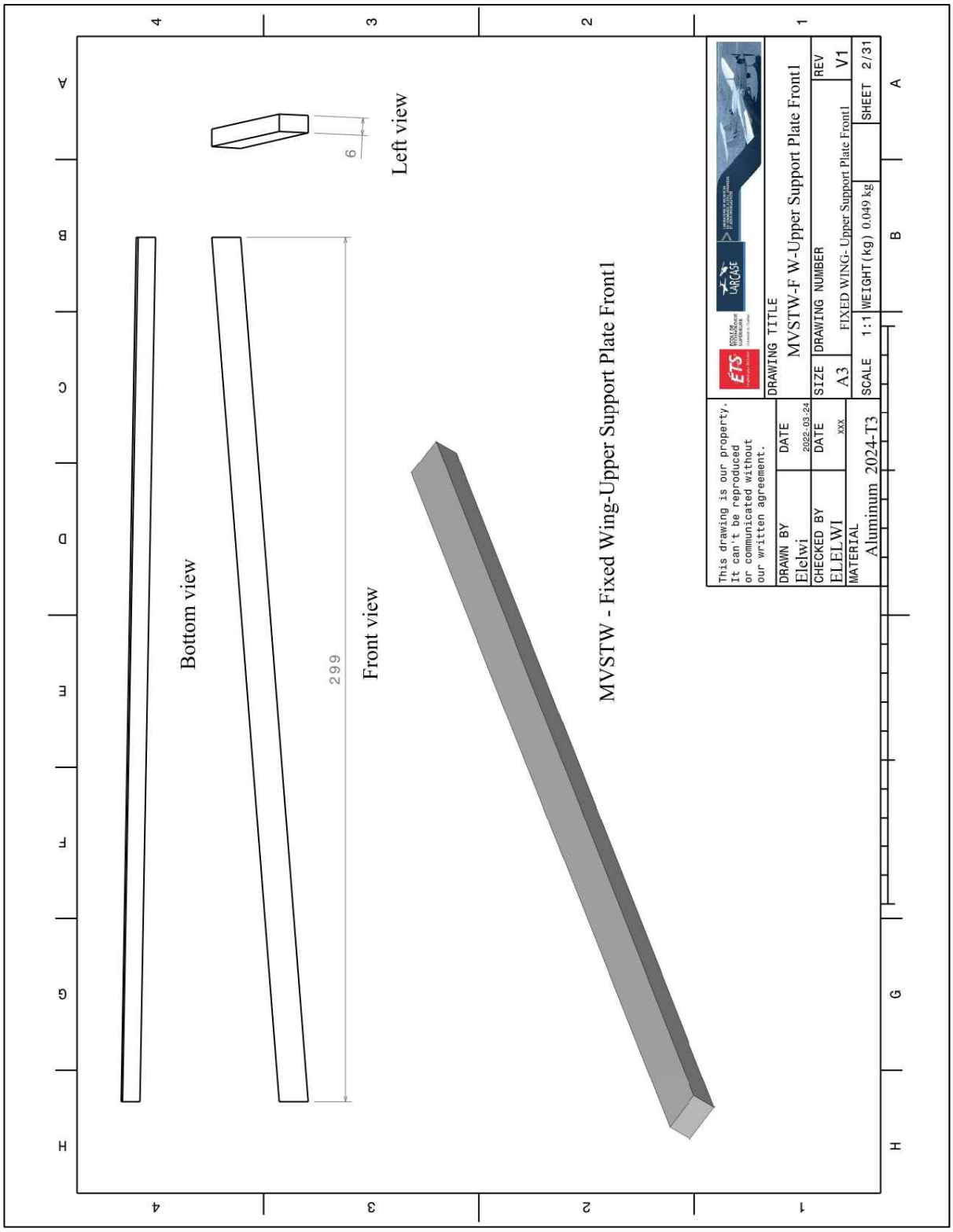

Figure-B II-39 MVSTW Fixed Wing Upper Support Plate Front Using Al 2024-T3

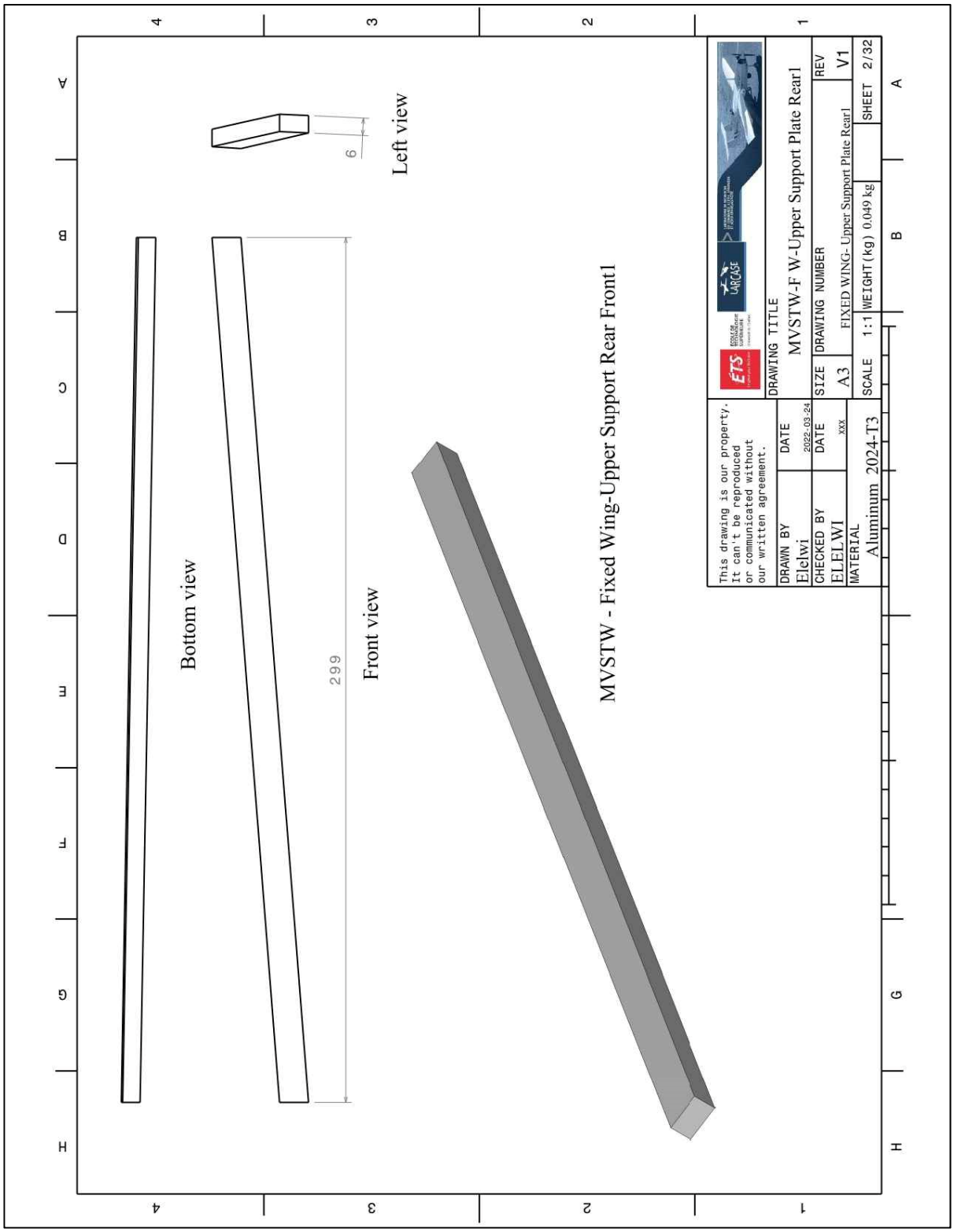

Figure-B II-40 MVSTW Fixed Wing Upper Support Plate Rear1 Using Al 2024-T3

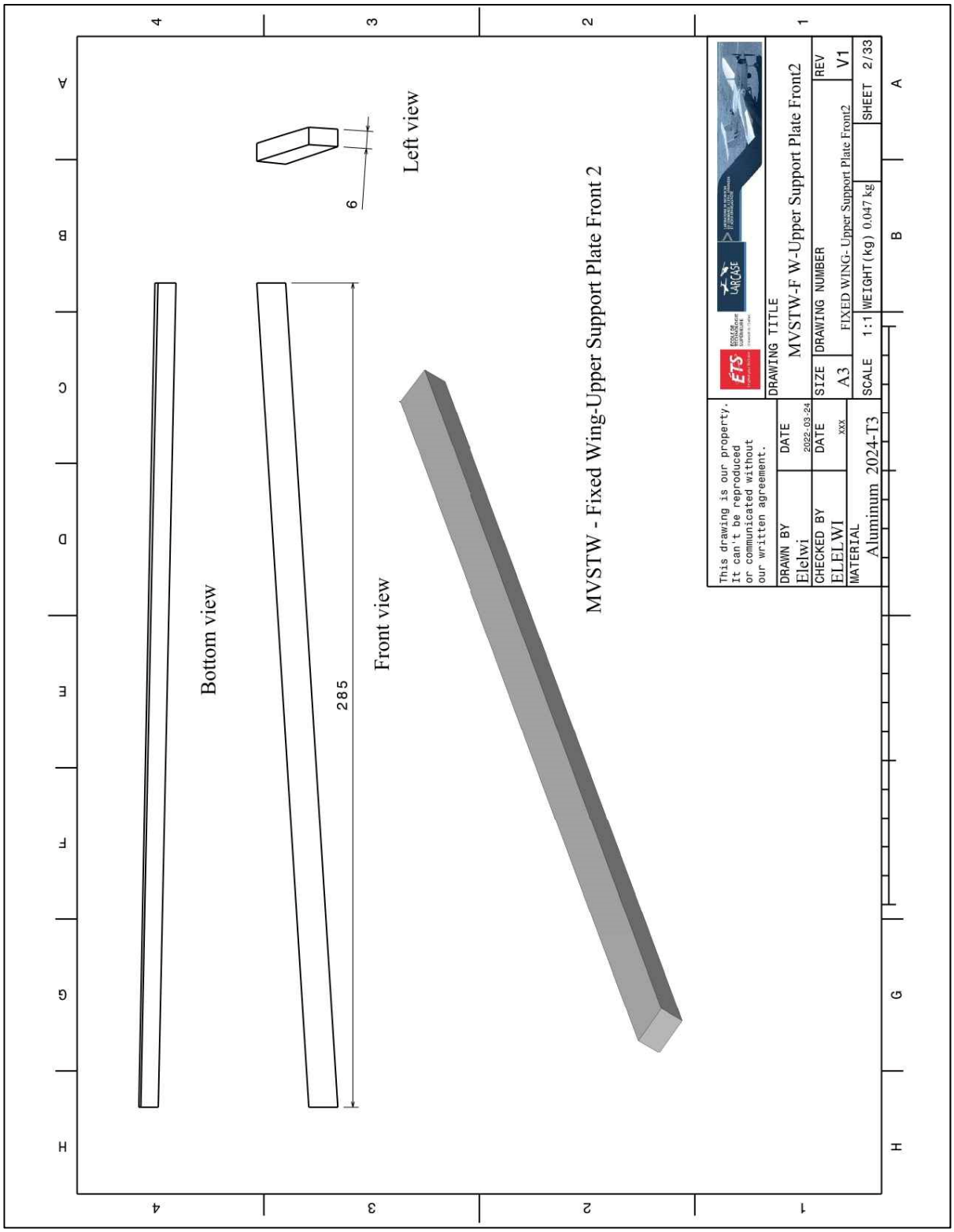

Figure-B II-41 MVSTW Fixed Wing Upper Support Plate Front2 Using Al 2024-T3

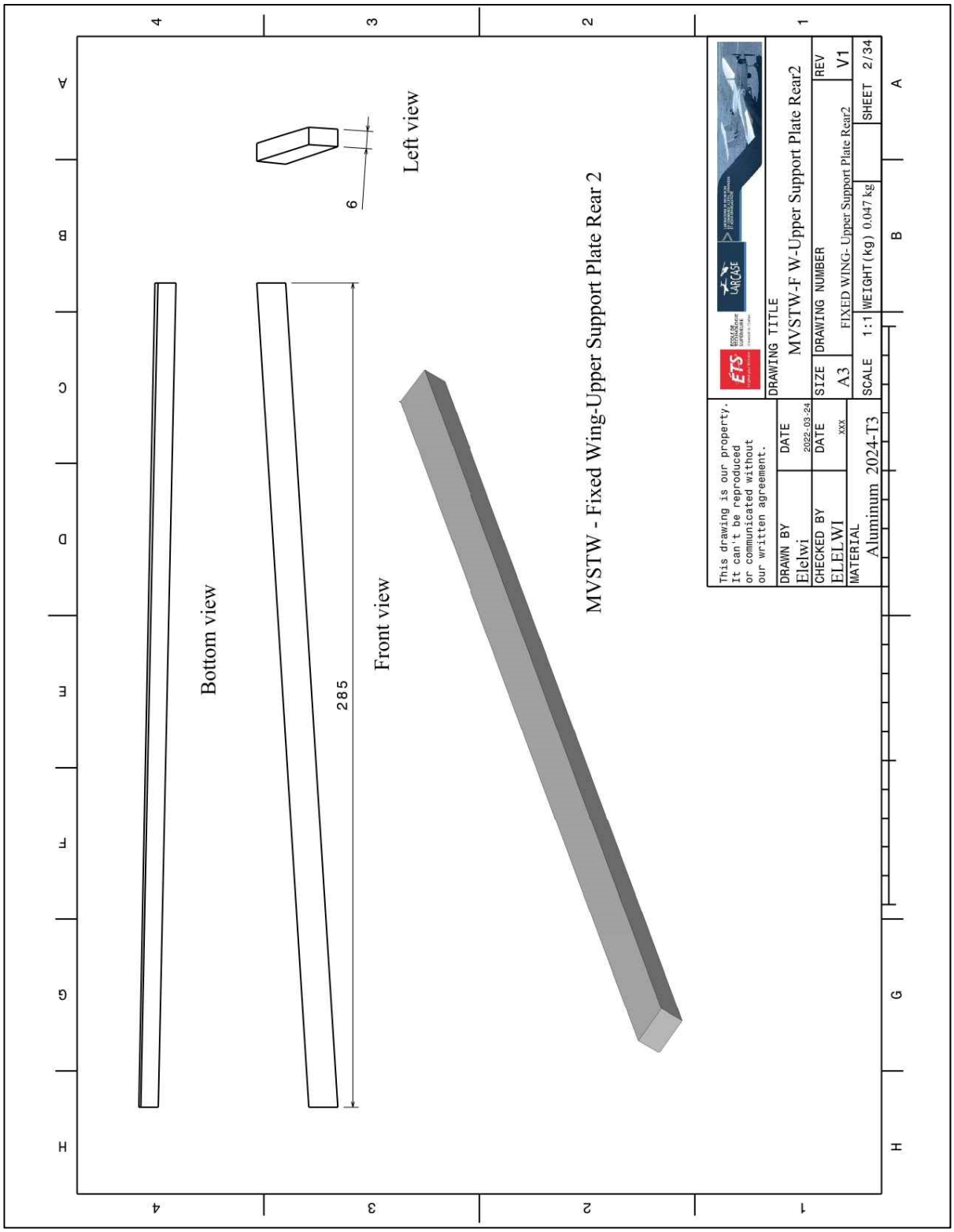

Figure-B II-42 MVSTW Fixed Wing Upper Support Plate Rear2 Using Al 2024-T3

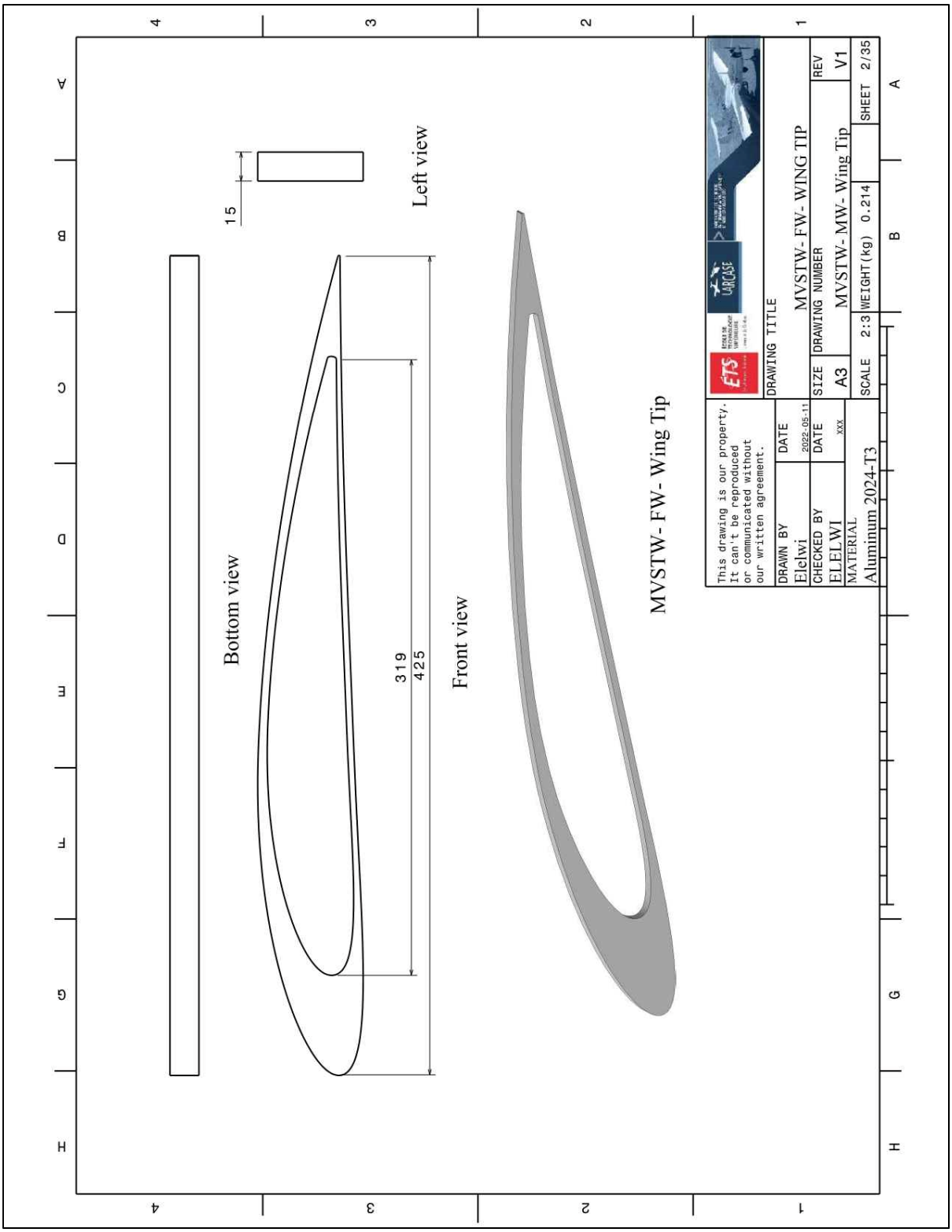

Figure-B II-43 MVSTW Fixed Wing - Wing Tip Using Al 2024-T3

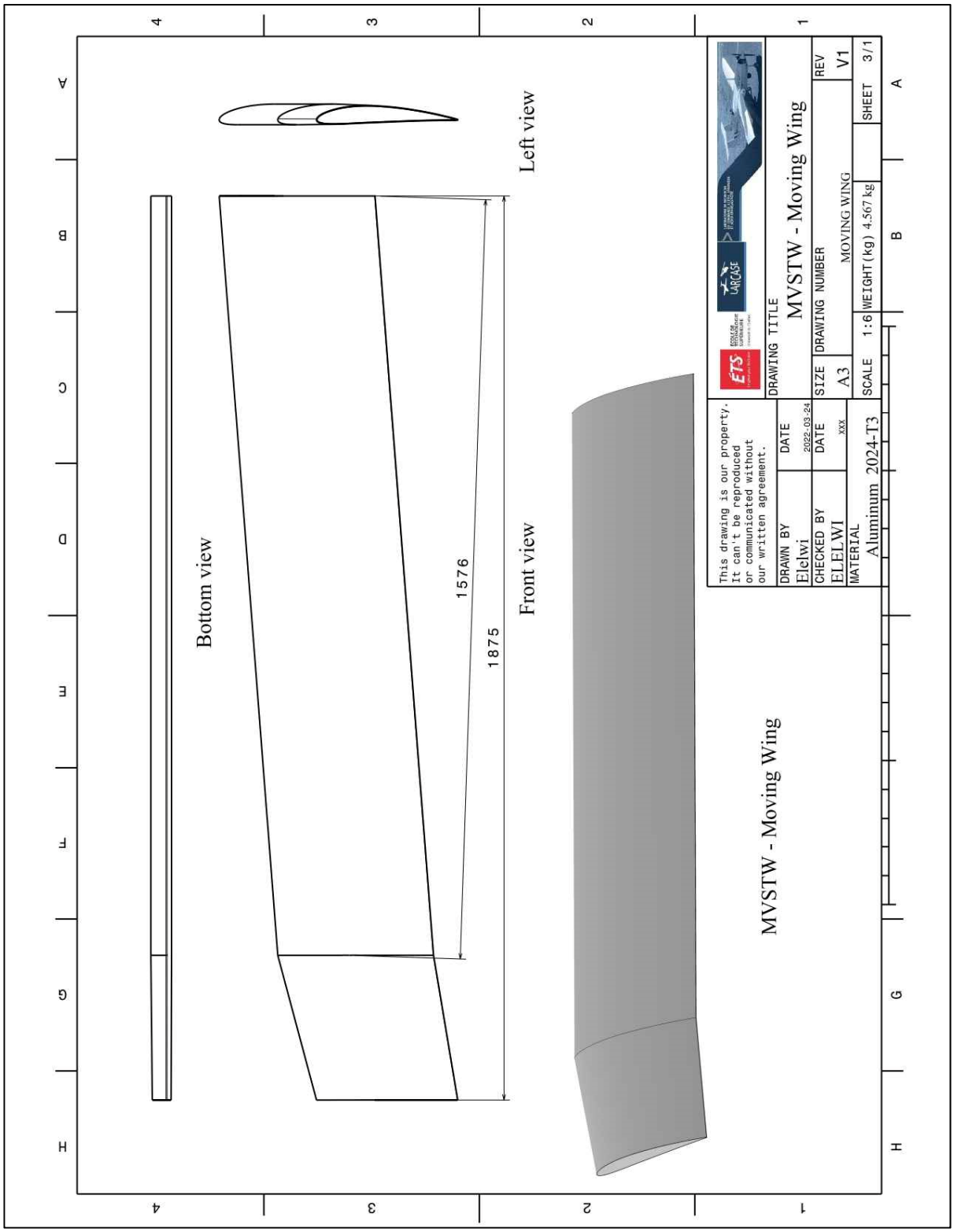

Figure-B II-44 MVSTW Moving Wing Using Al 2024-T3

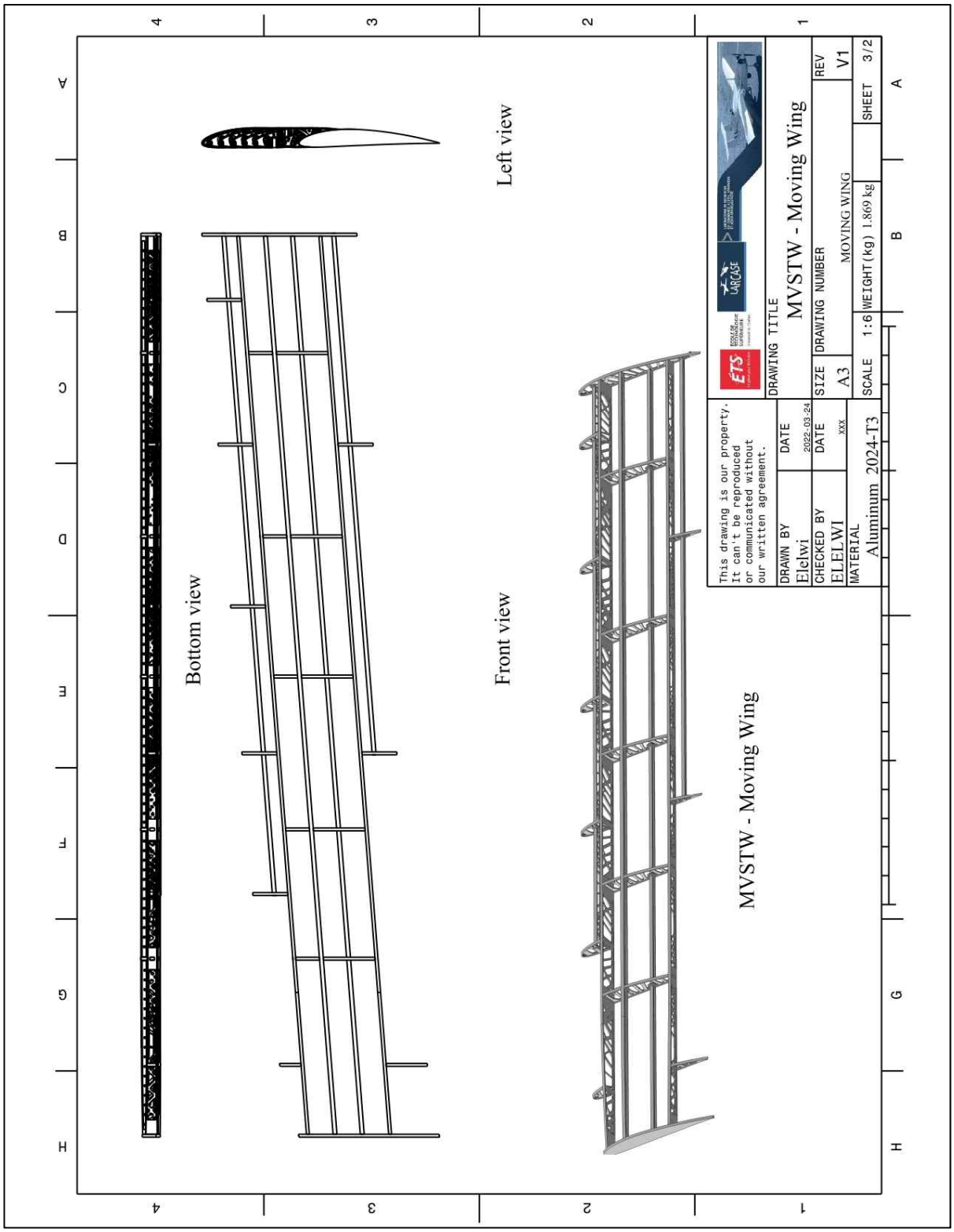

Figure-B II-45 MVSTW Moving Wing Skeleton Using Al 2024-T3

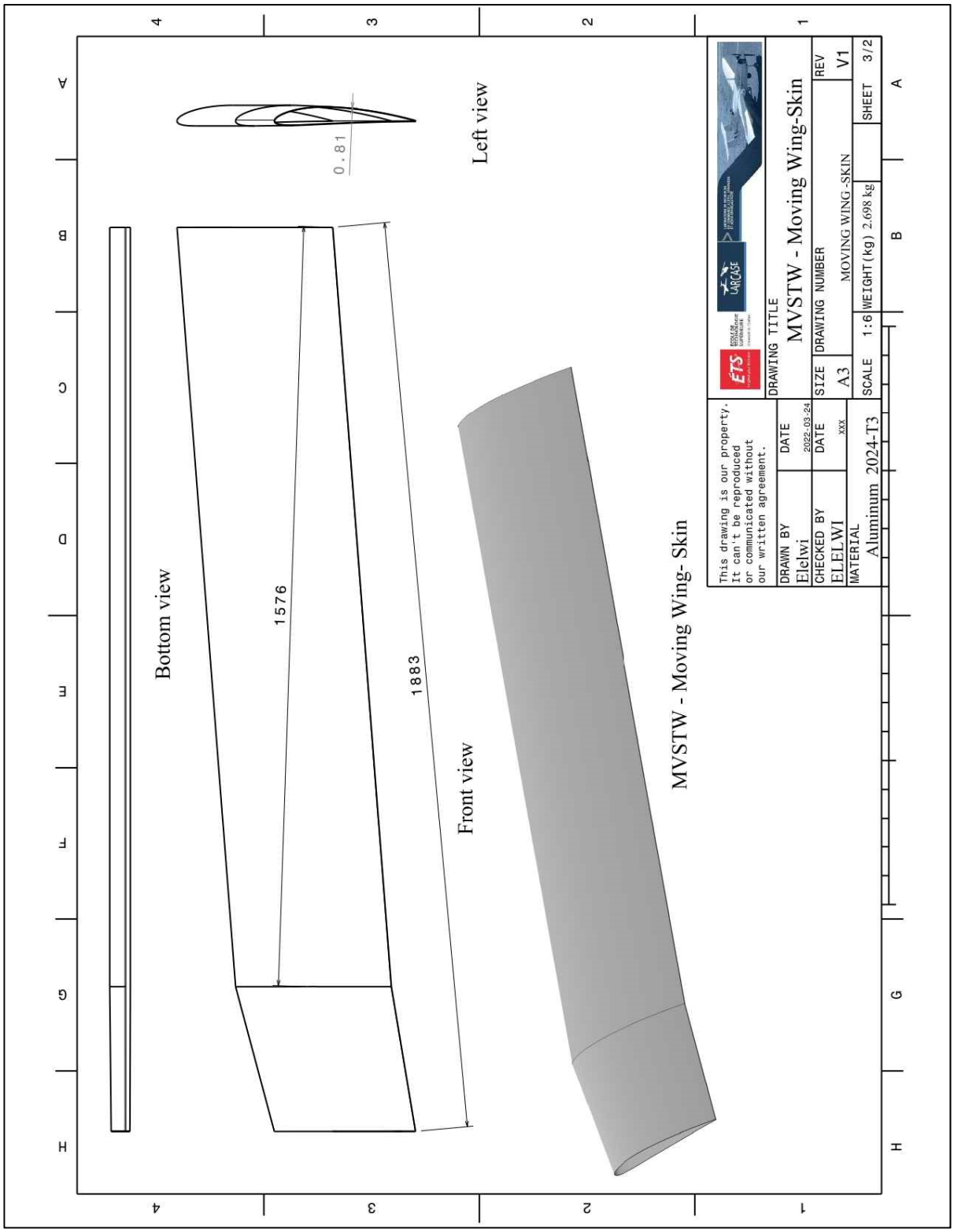

Figure-B II-46 MVSTW Moving Wing Skin Using Al 2024-T3

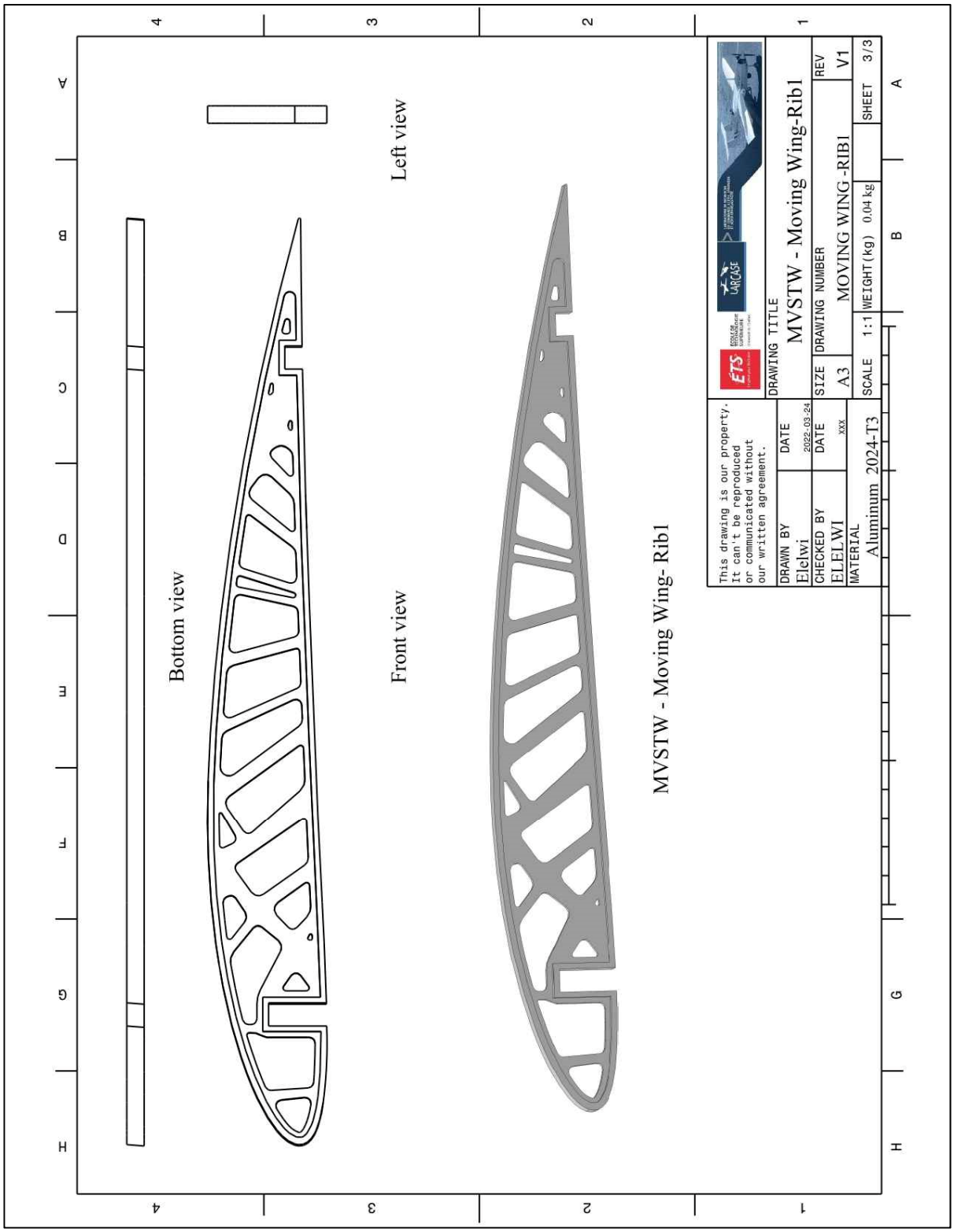

Figure-B II-47 MVSTW Moving Wing Rib1 Using Al 2024-T3

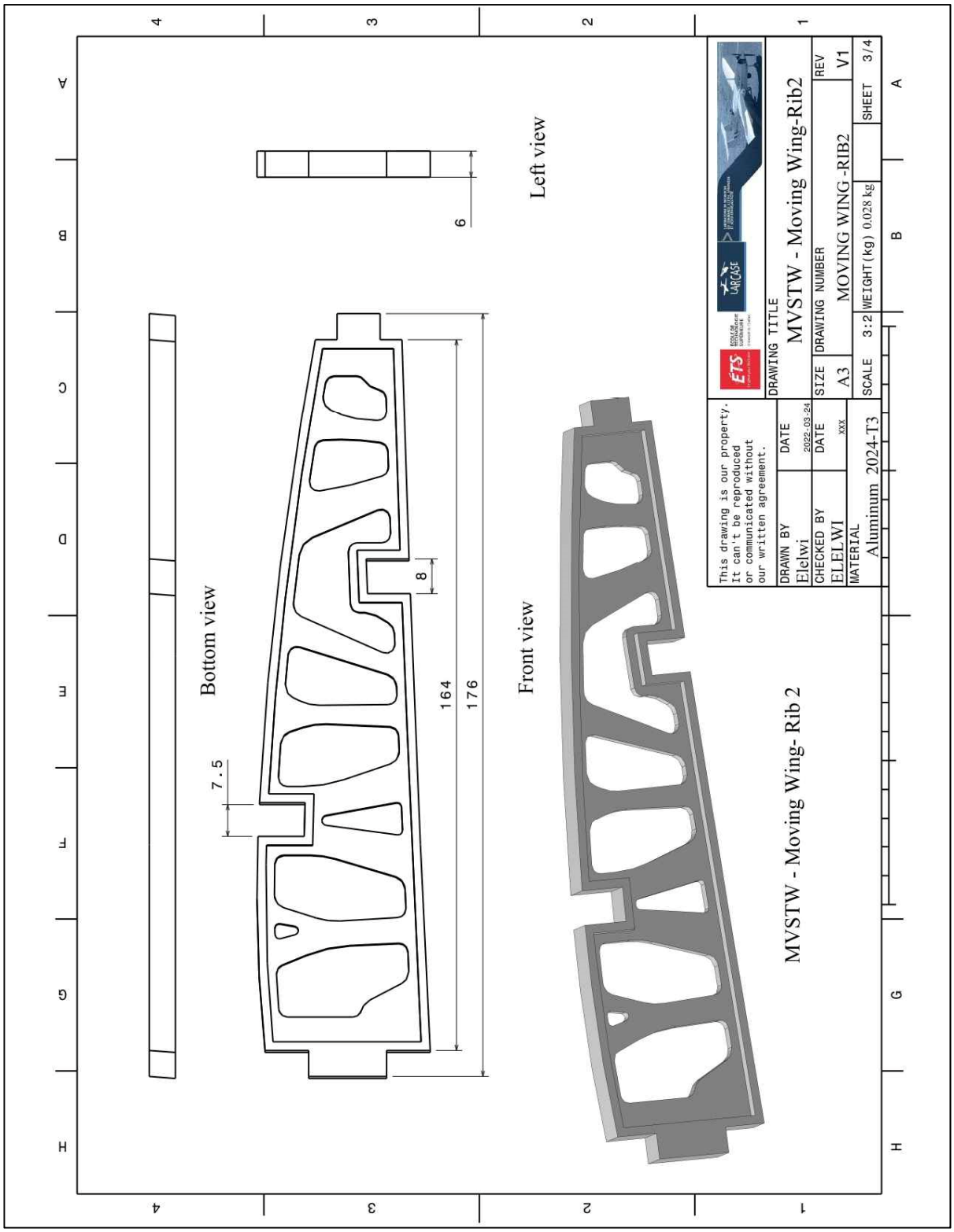

Figure-B II-48 MVSTW Moving Wing Rib2 Using Al 2024-T3

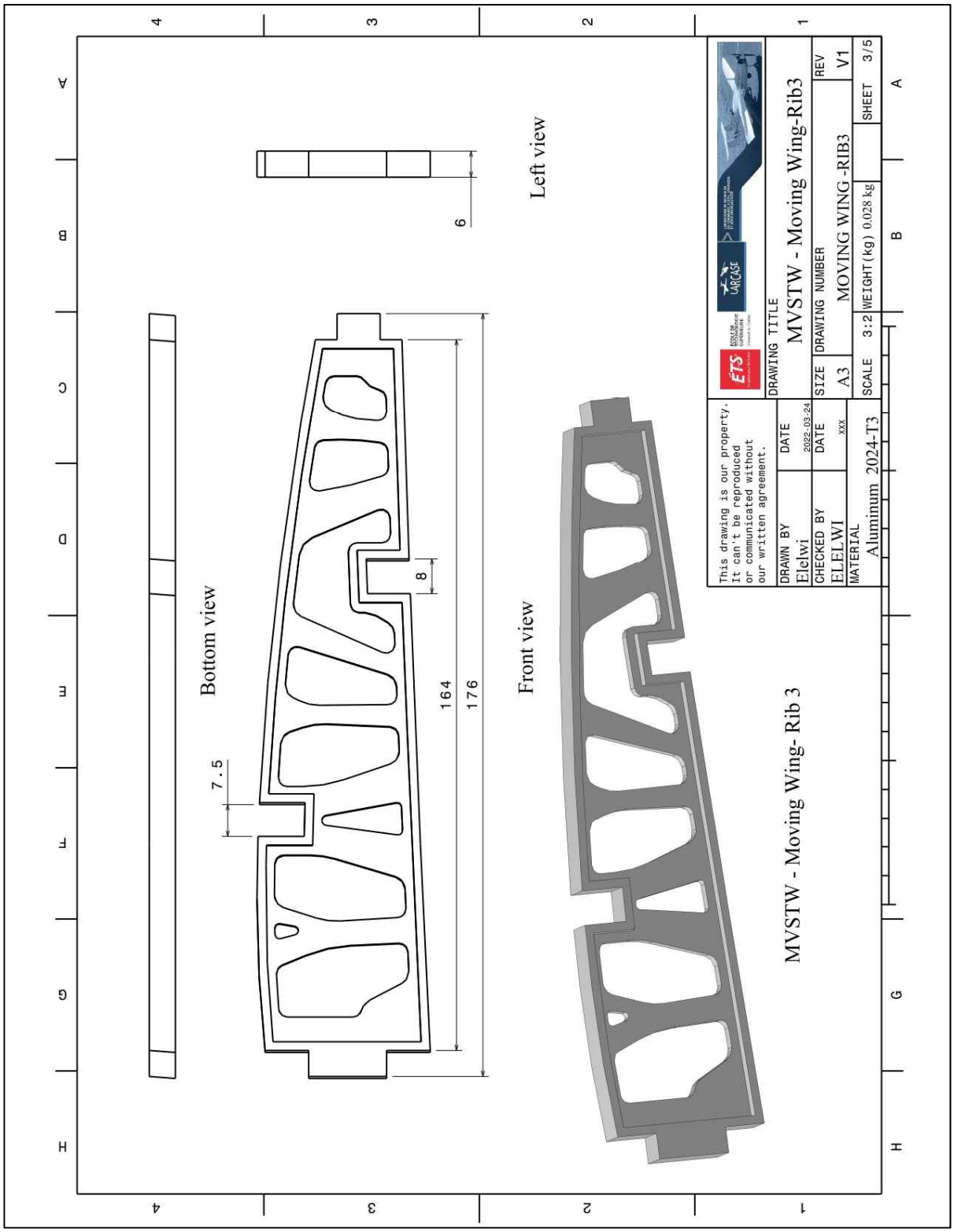

Figure-B II-49 MVSTW Moving Wing Rib3 Using Al 2024-T3

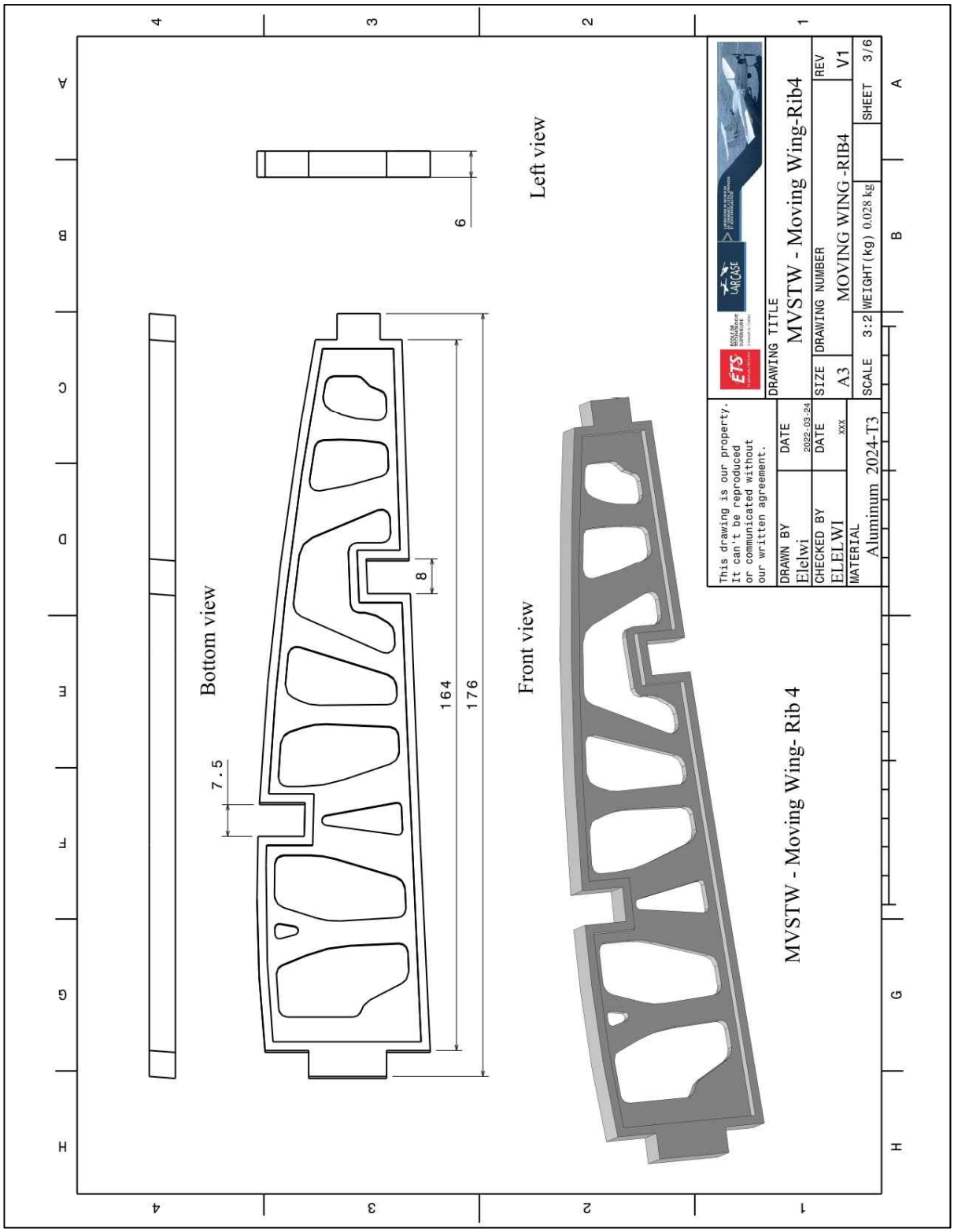

Figure-B II-50 MVSTW Moving Wing Rib4 Using Al 2024-T3

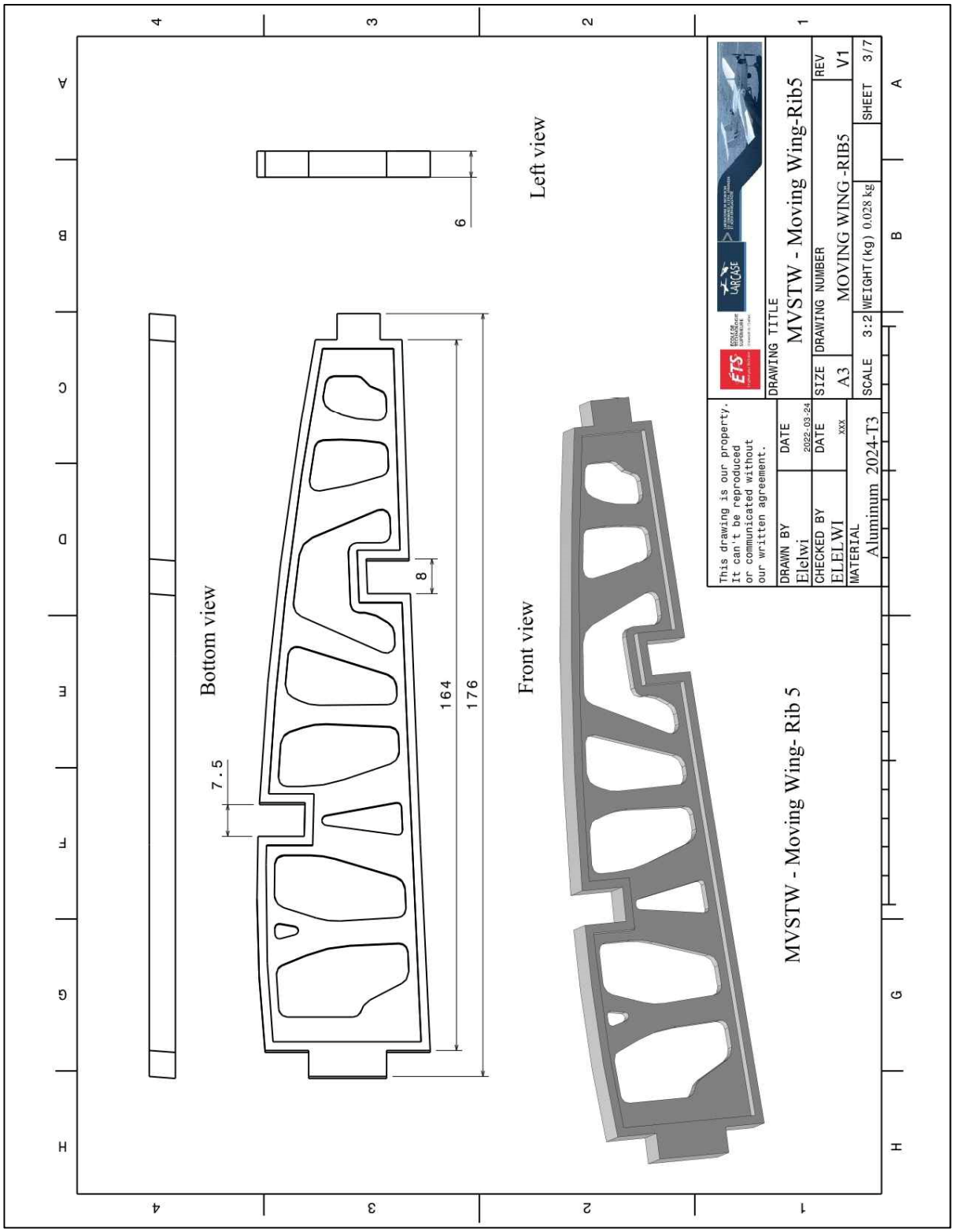

Figure-B II-51 MVSTW Moving Wing Rib5 Using Al 2024-T3

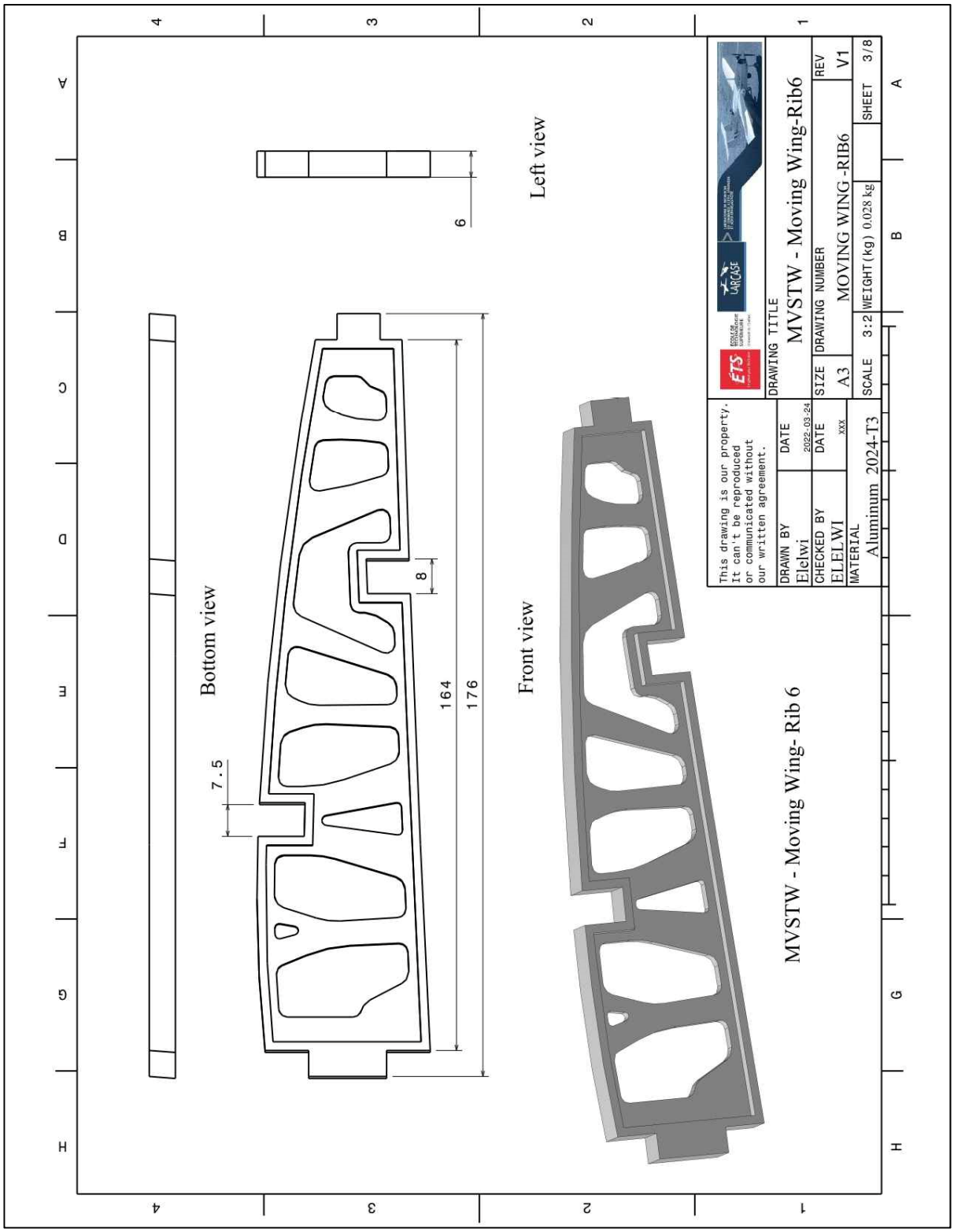

Figure-B II-52 MVSTW Moving Wing Rib6 Using Al 2024-T3

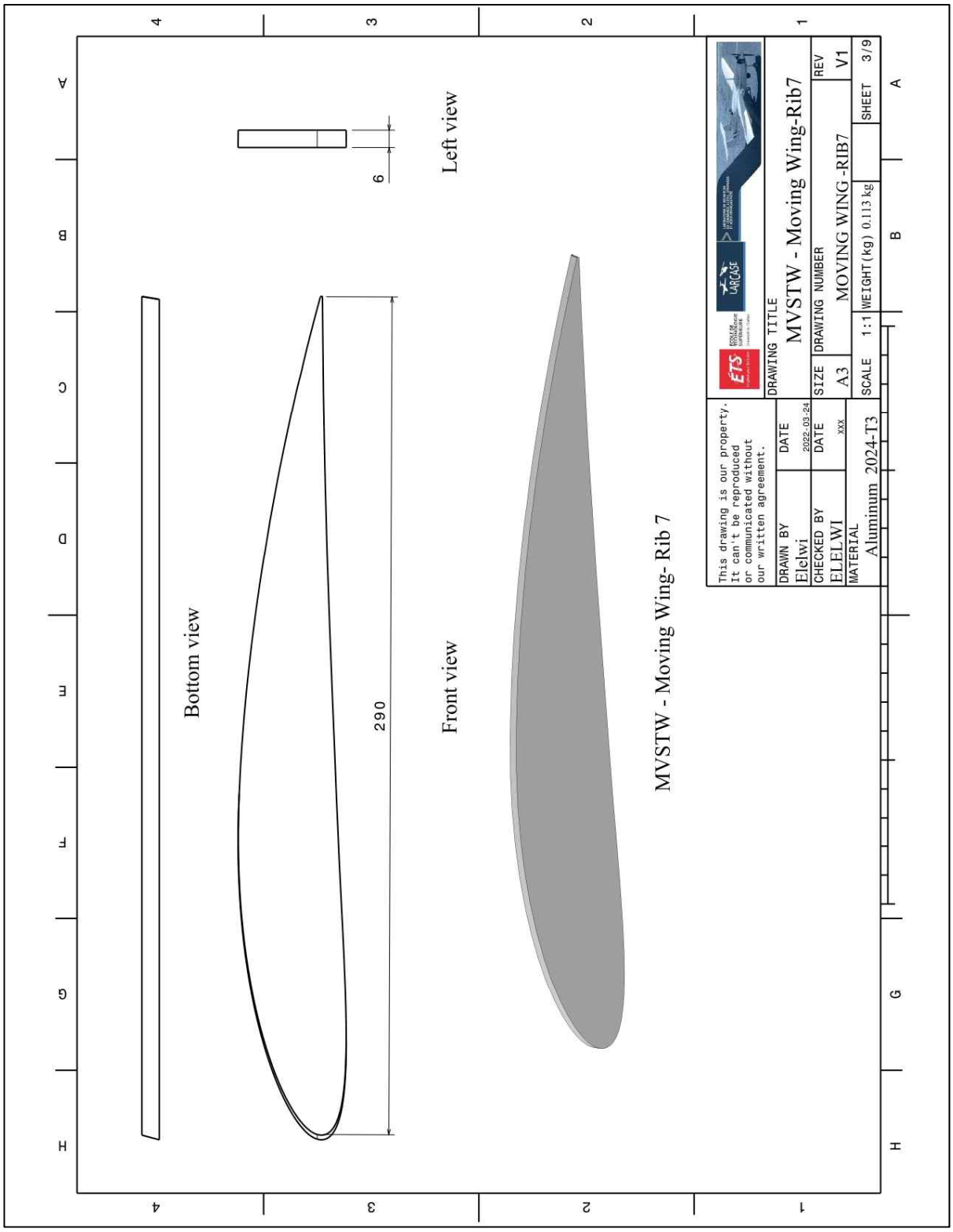

Figure-B II-53 MVSTW Moving Wing Rib7 Using Al 2024-T3

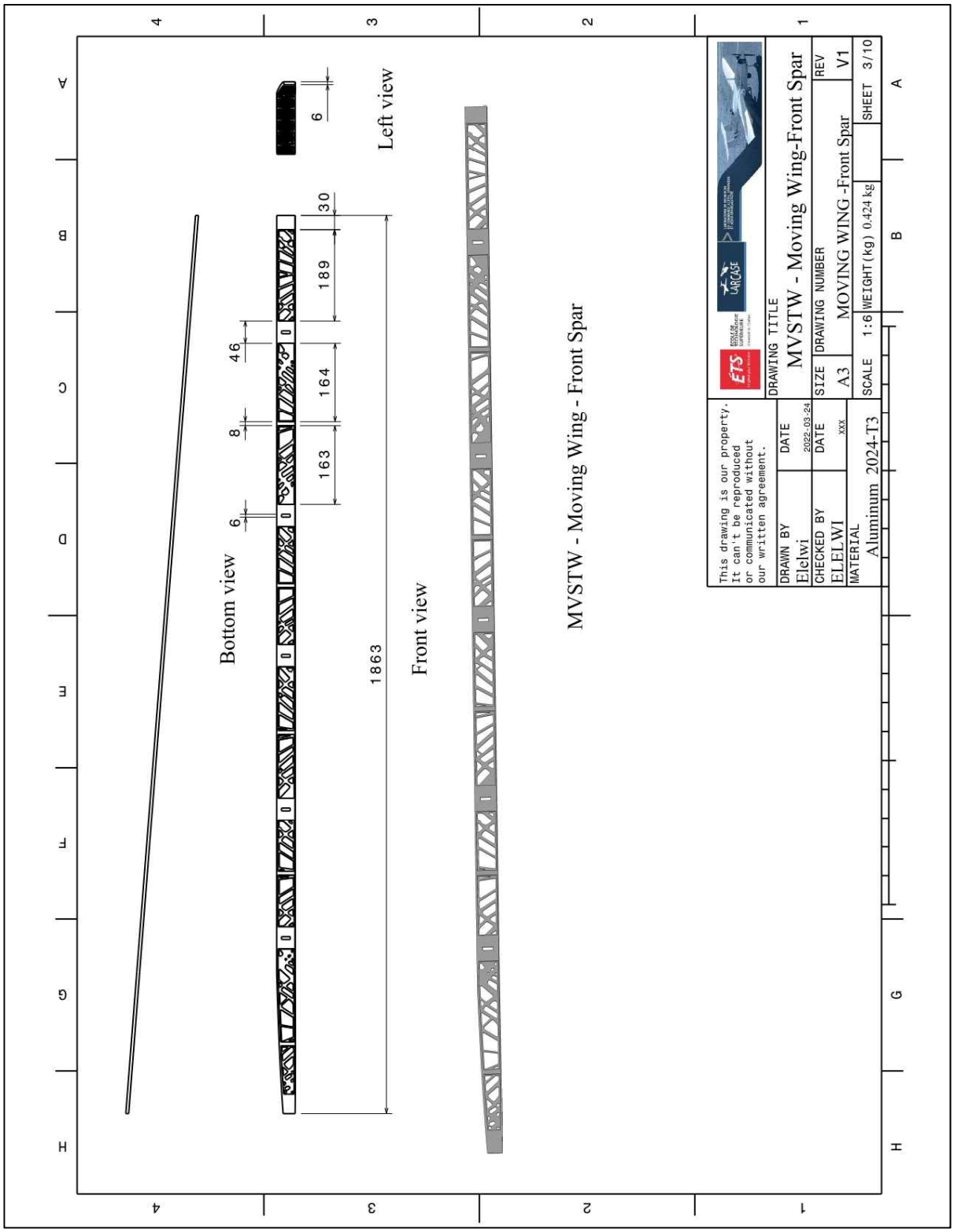

Figure-B II-54 MVSTW Moving Wing Front Spar Using Al 2024-T3

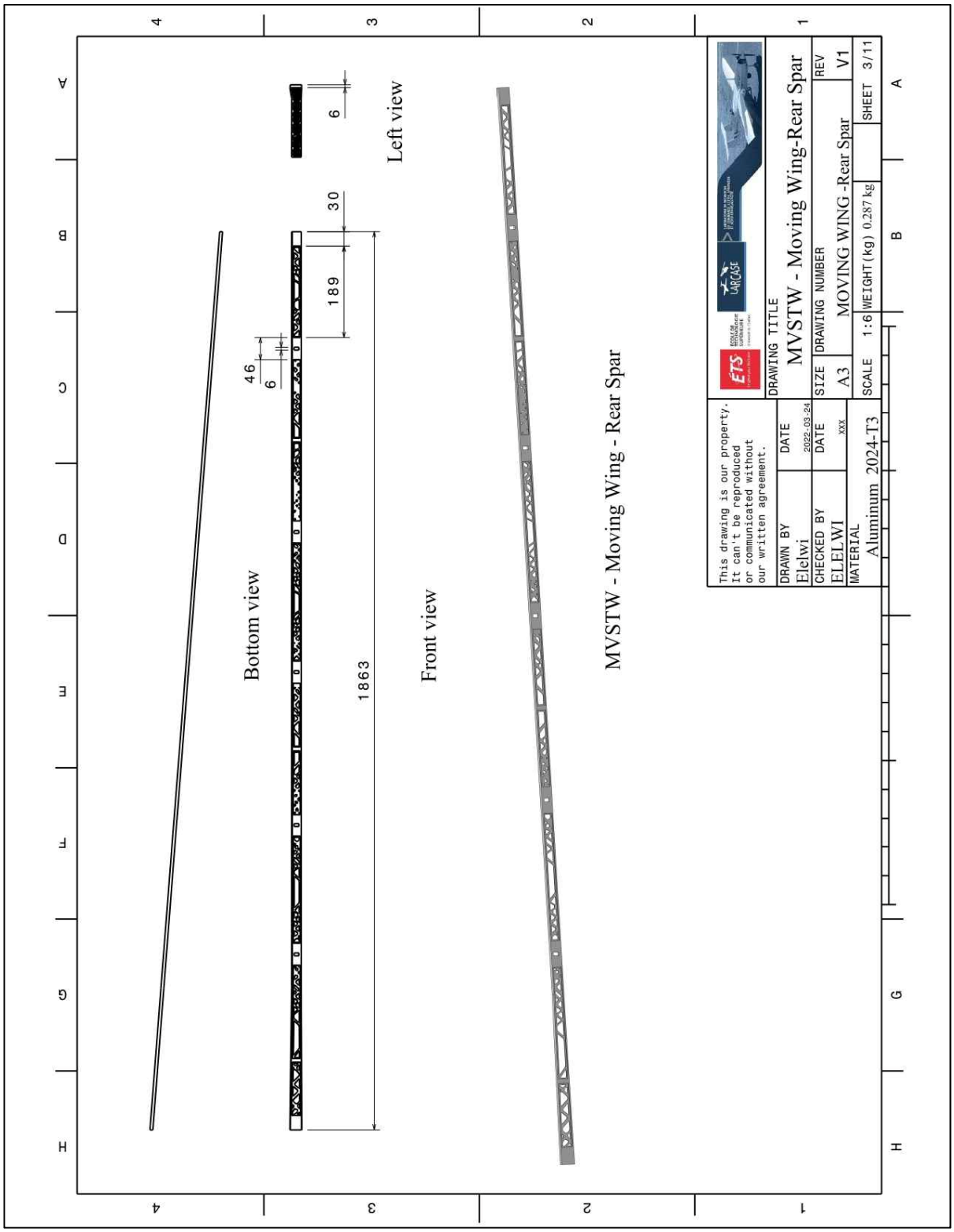

Figure-B II-55 MVSTW Moving Wing Rear Spar Using Al 2024-T3

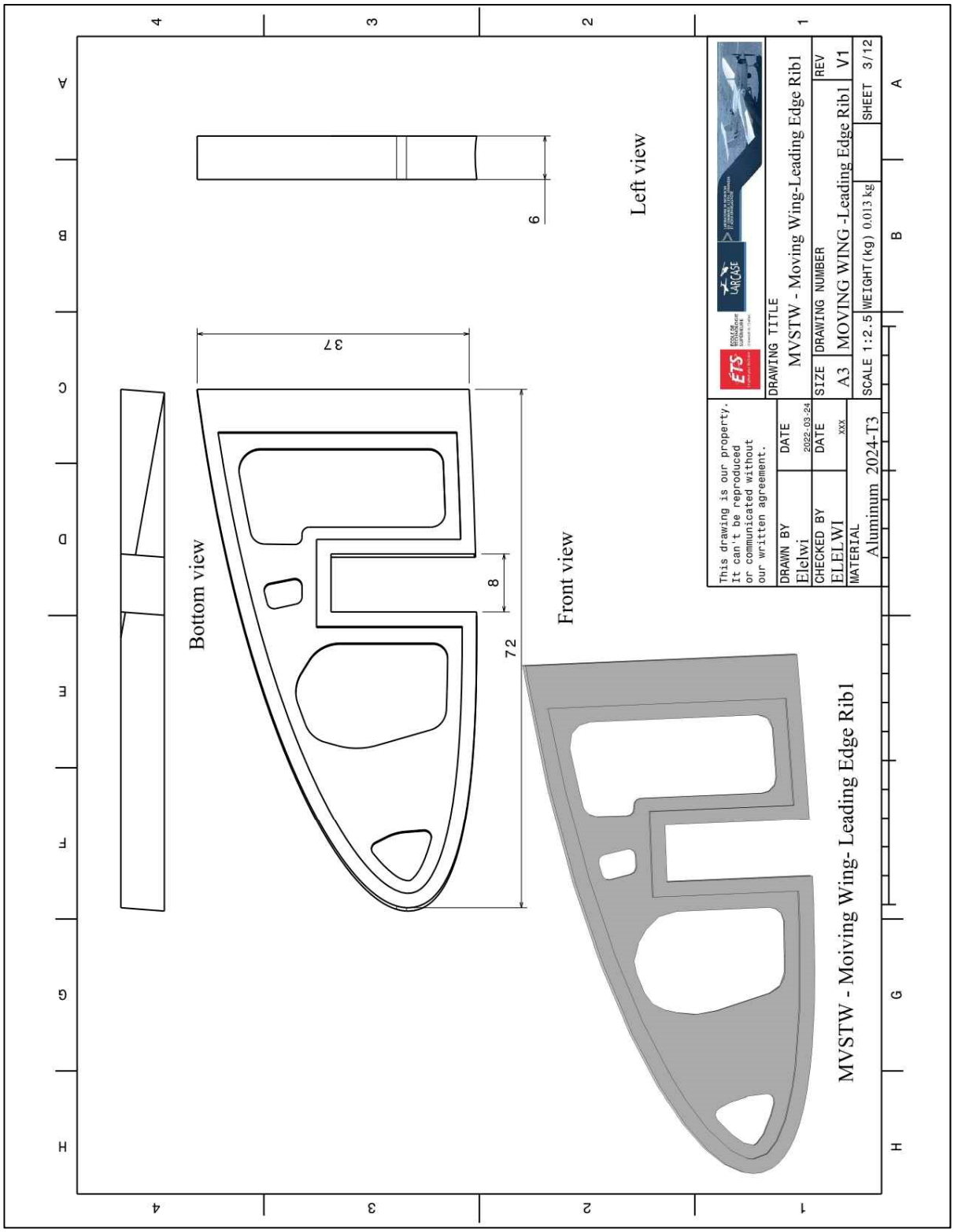

Figure-B II-56 MVSTW Moving Wing Leading Edge Rib1 Using Al 2024-T3

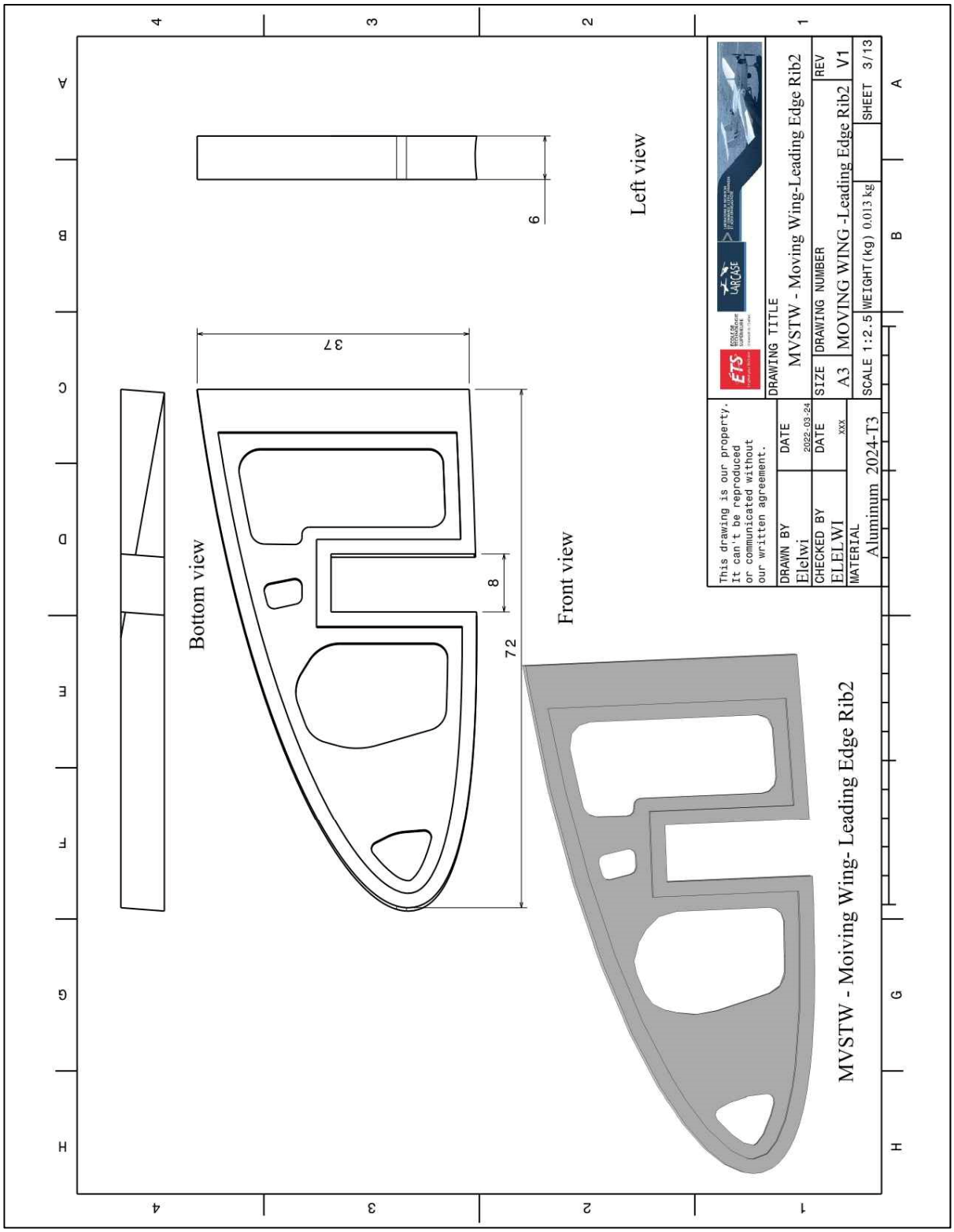

Figure-B II-57 MVSTW Moving Wing Leading Edge Rib2 Using Al 2024-T3

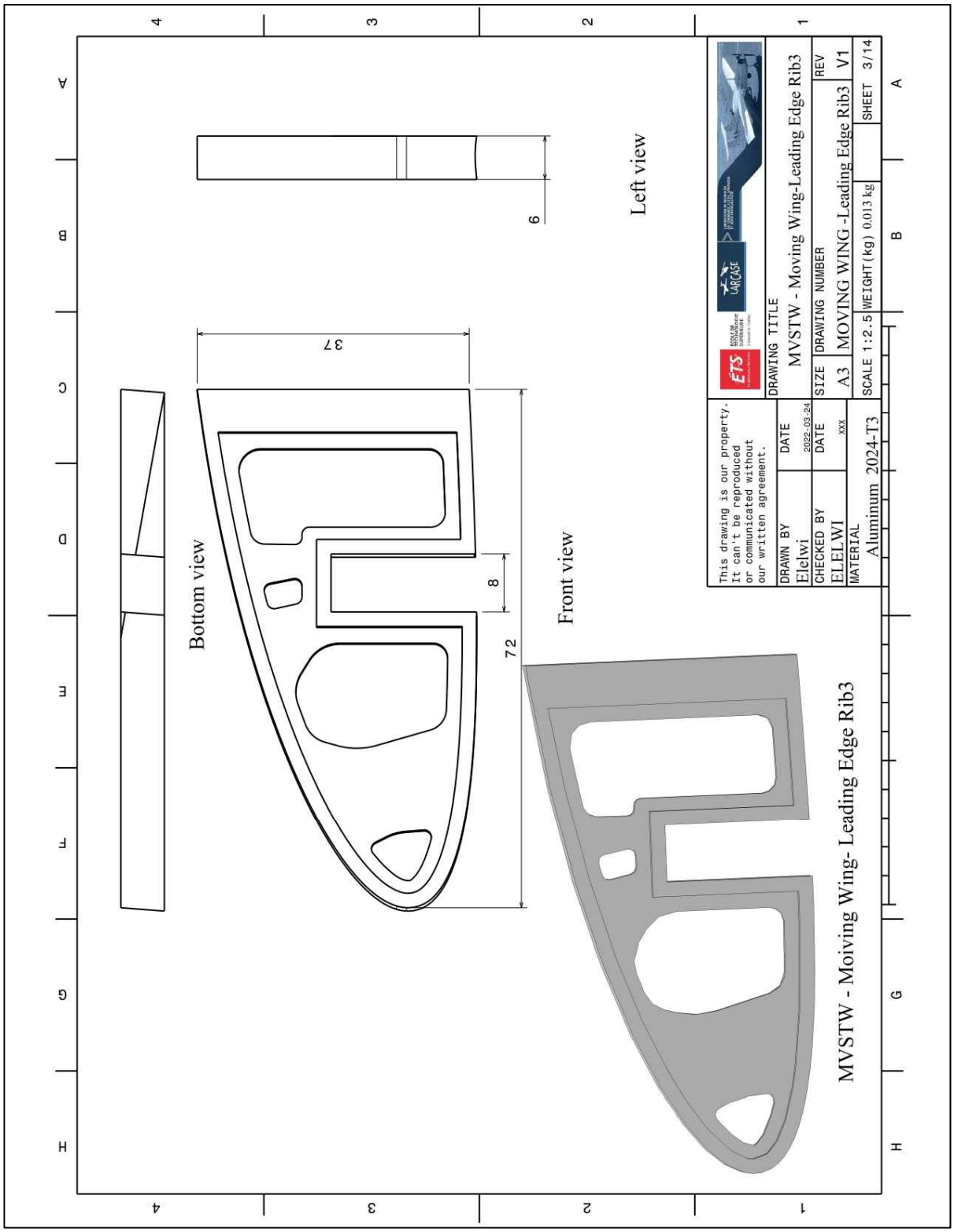

Figure-B II-58 MVSTW Moving Wing Leading Edge rib3 Using Al 2024-T3

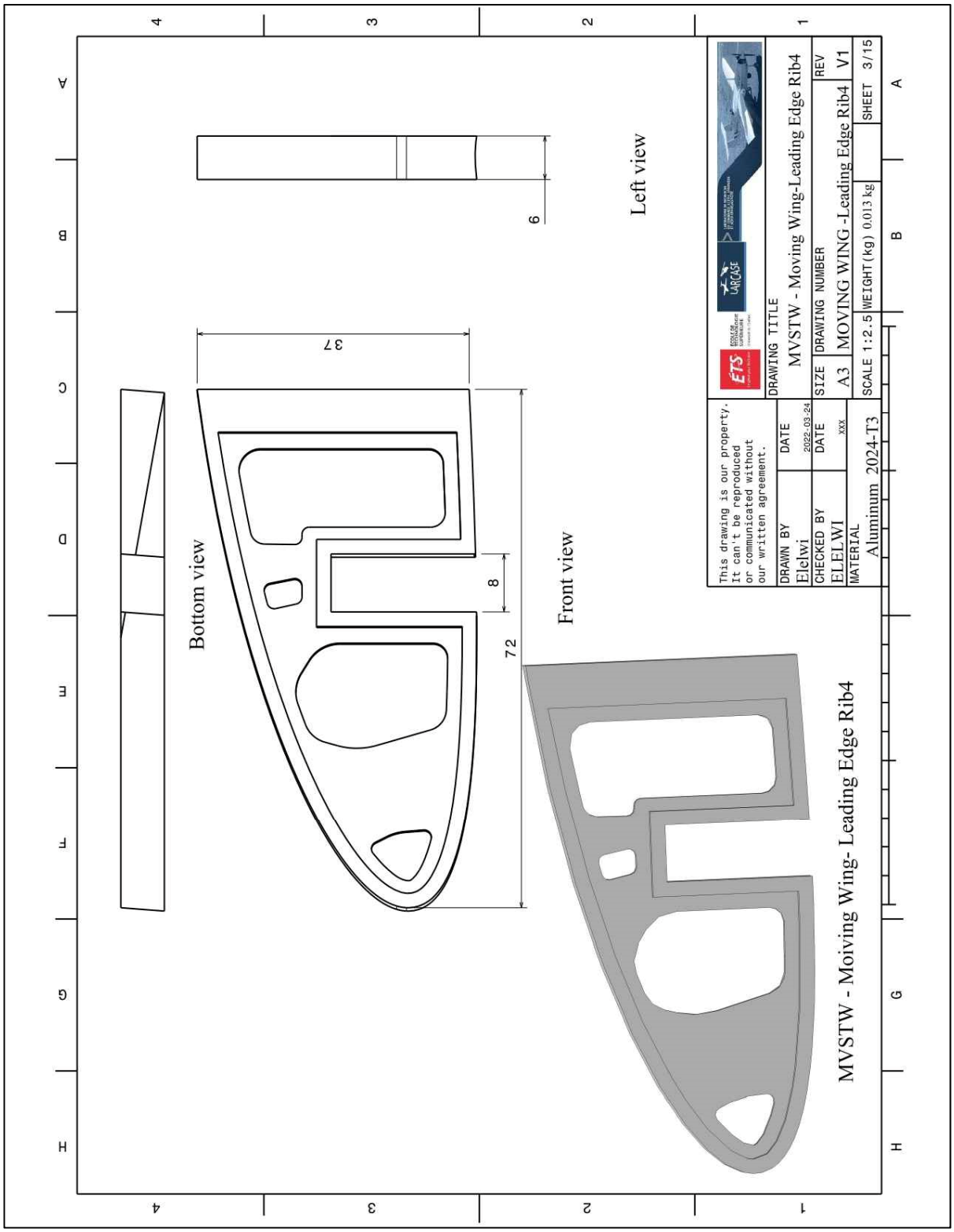

Figure-B II-59 MVSTW Moving Wing leading Edge Rib4 Using Al 2024-T3

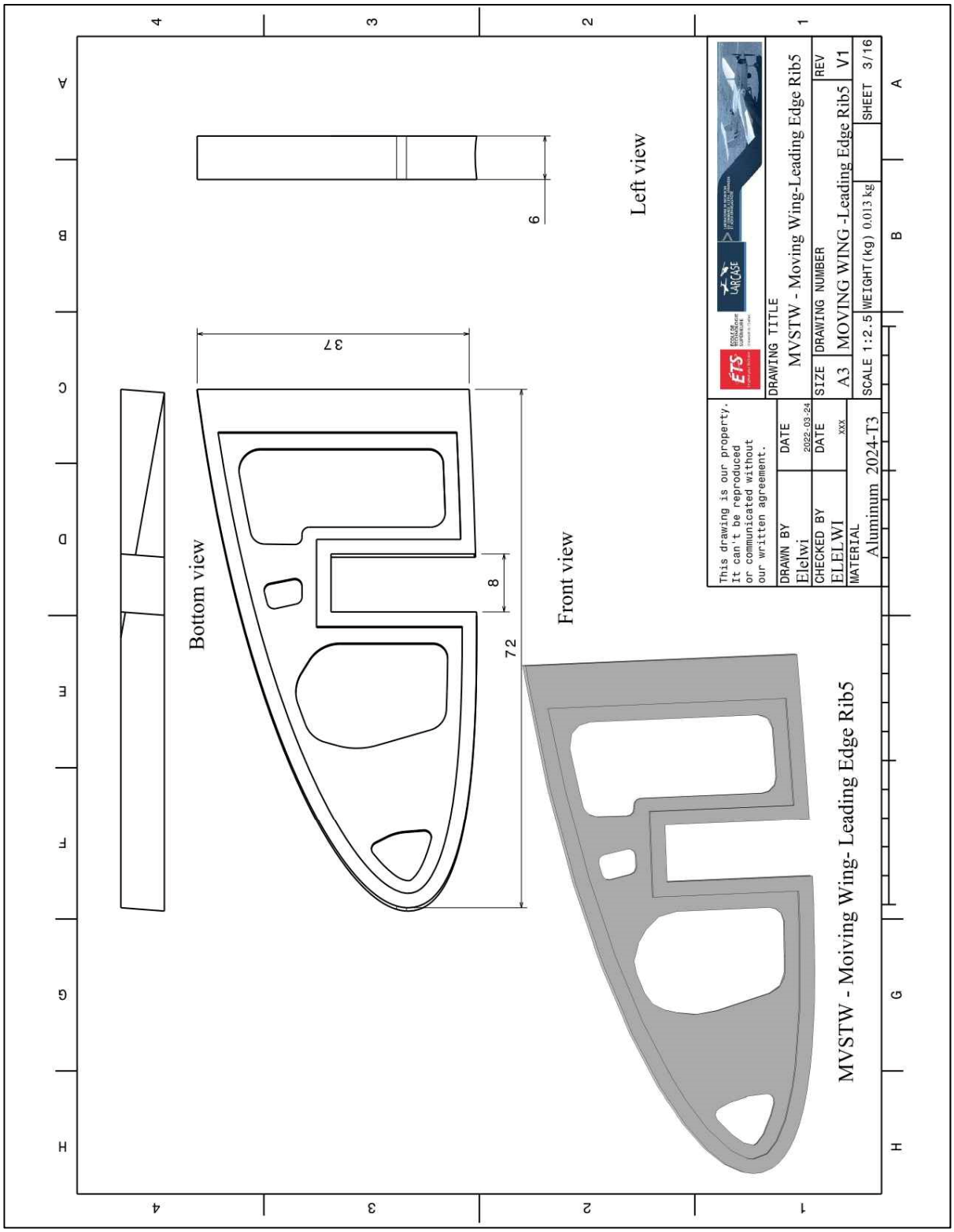

Figure-B II-60 MVSTW Moving Wing Leading Edge Rib5 Using Al 2024-T3

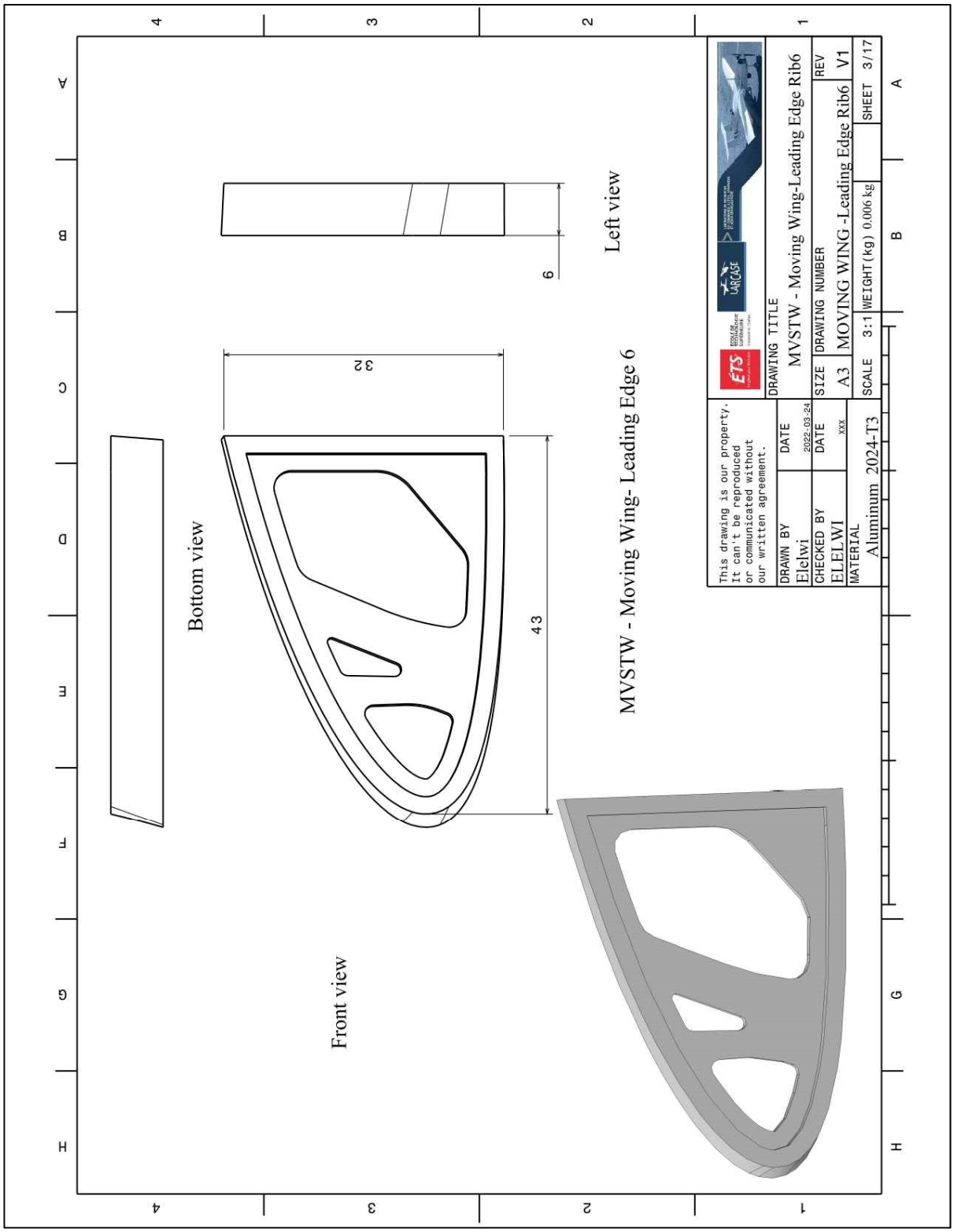

Figure-B II-61 MVSTW Moving Wing Leading Edge Rib6 Using Al 2024-T3

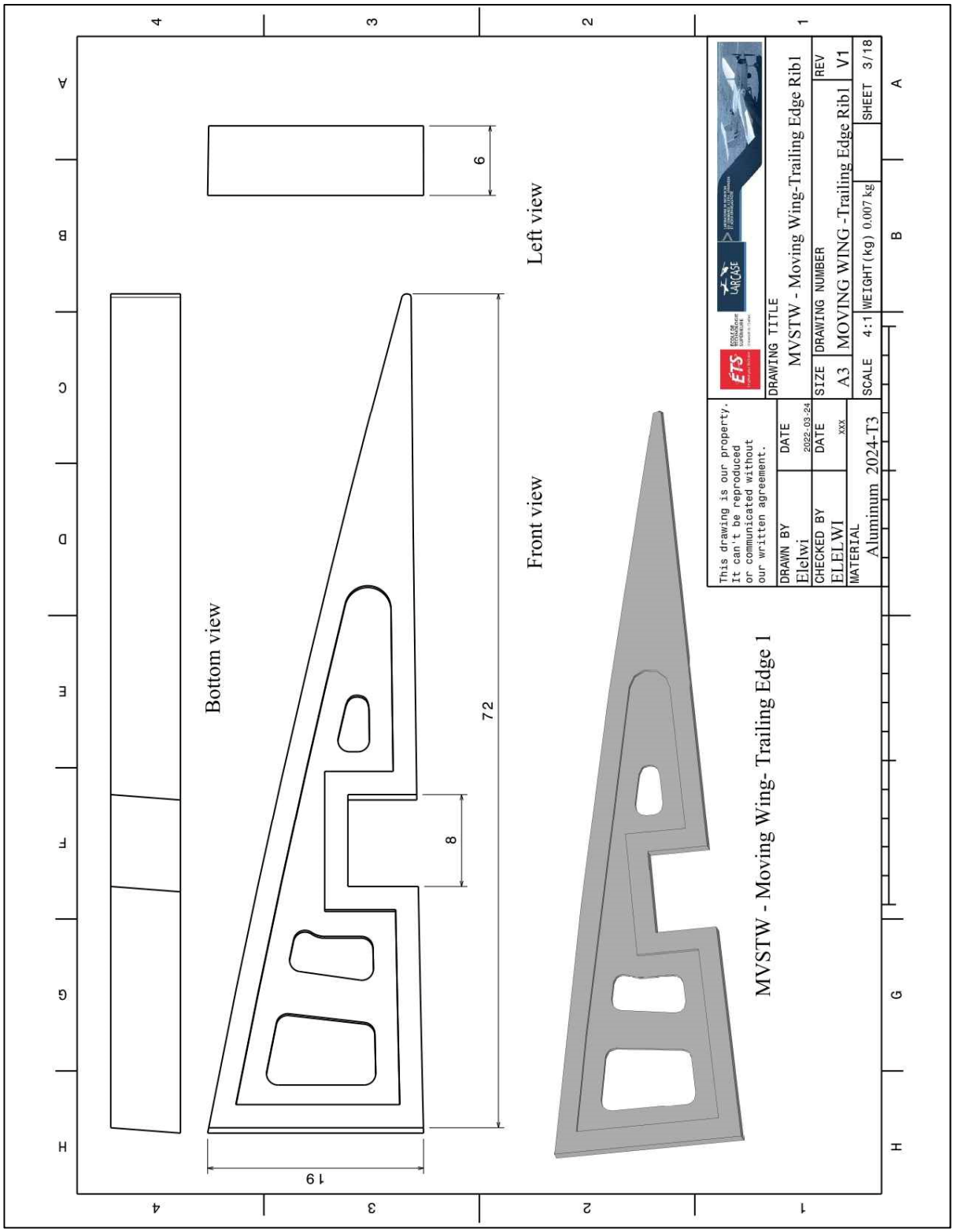

Figure-B II-62 MVSTW Moving Wing Trailing Edge Rib1 Using Al 2024-T3

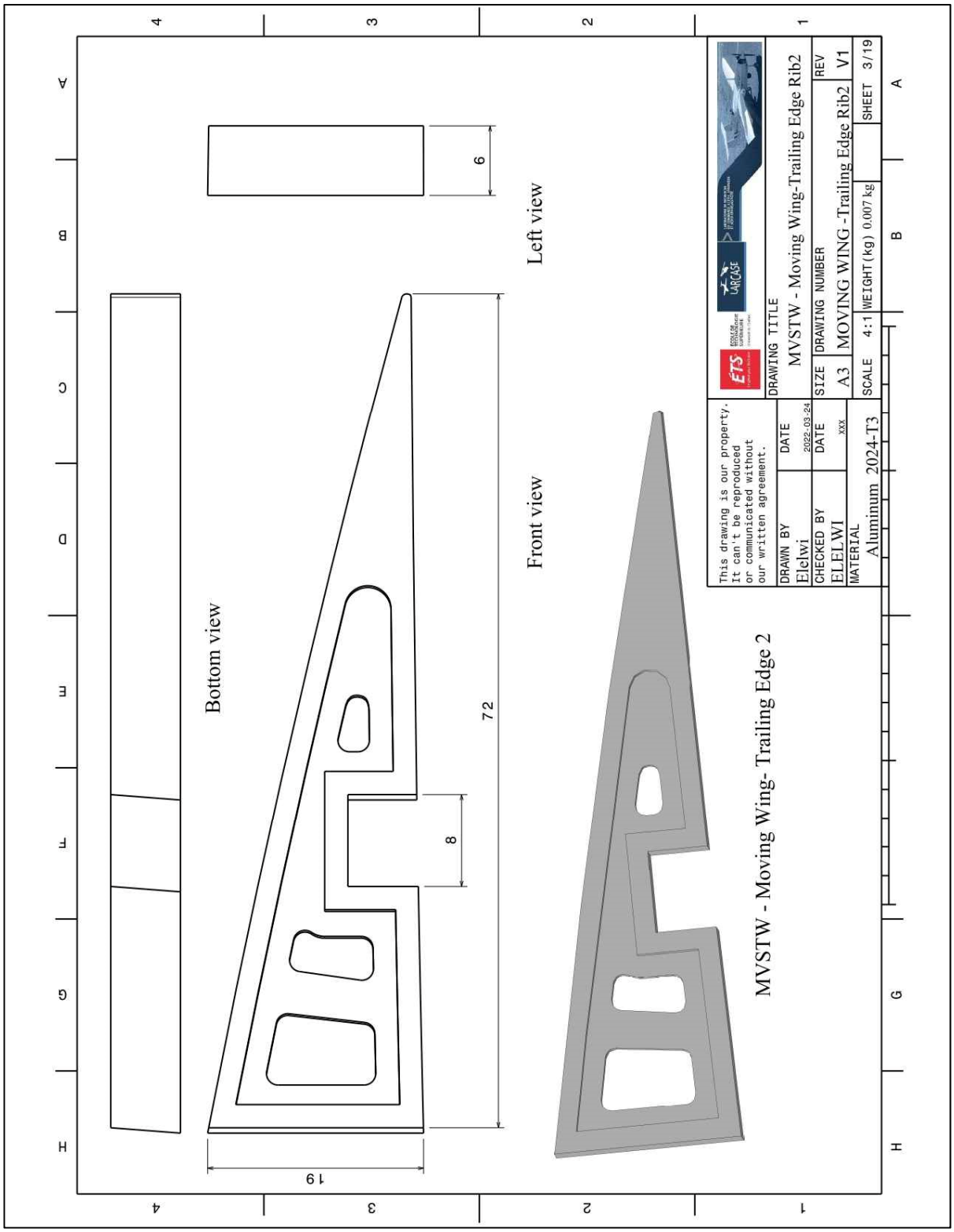

Figure-B II-63 MVSTW Moving Wing trailing Edge Rib2 Using Al 2024-T3

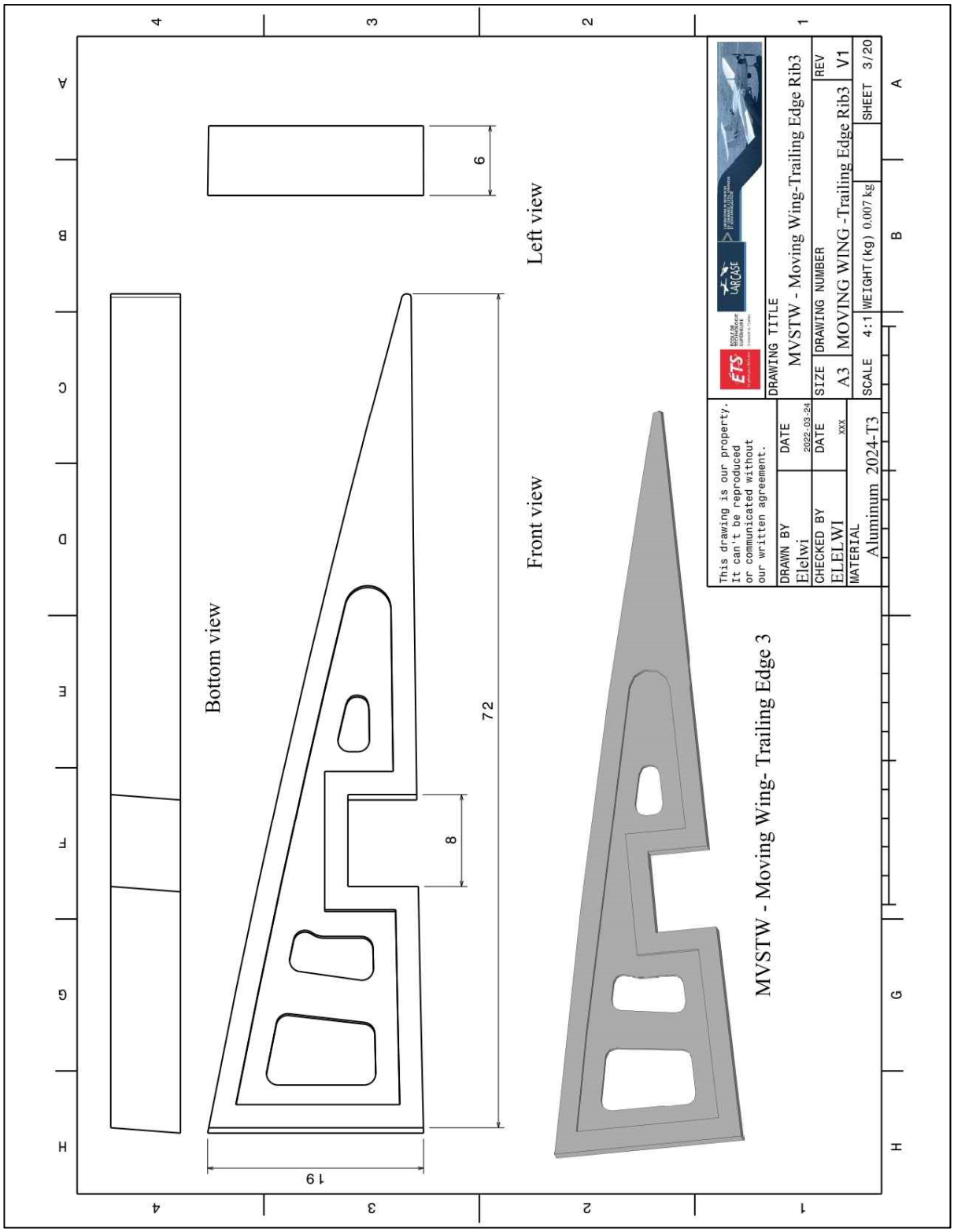

Figure-B II-64 MVSTW Moving Wing Trailing Edge Rib3 Using Al 2024-T3

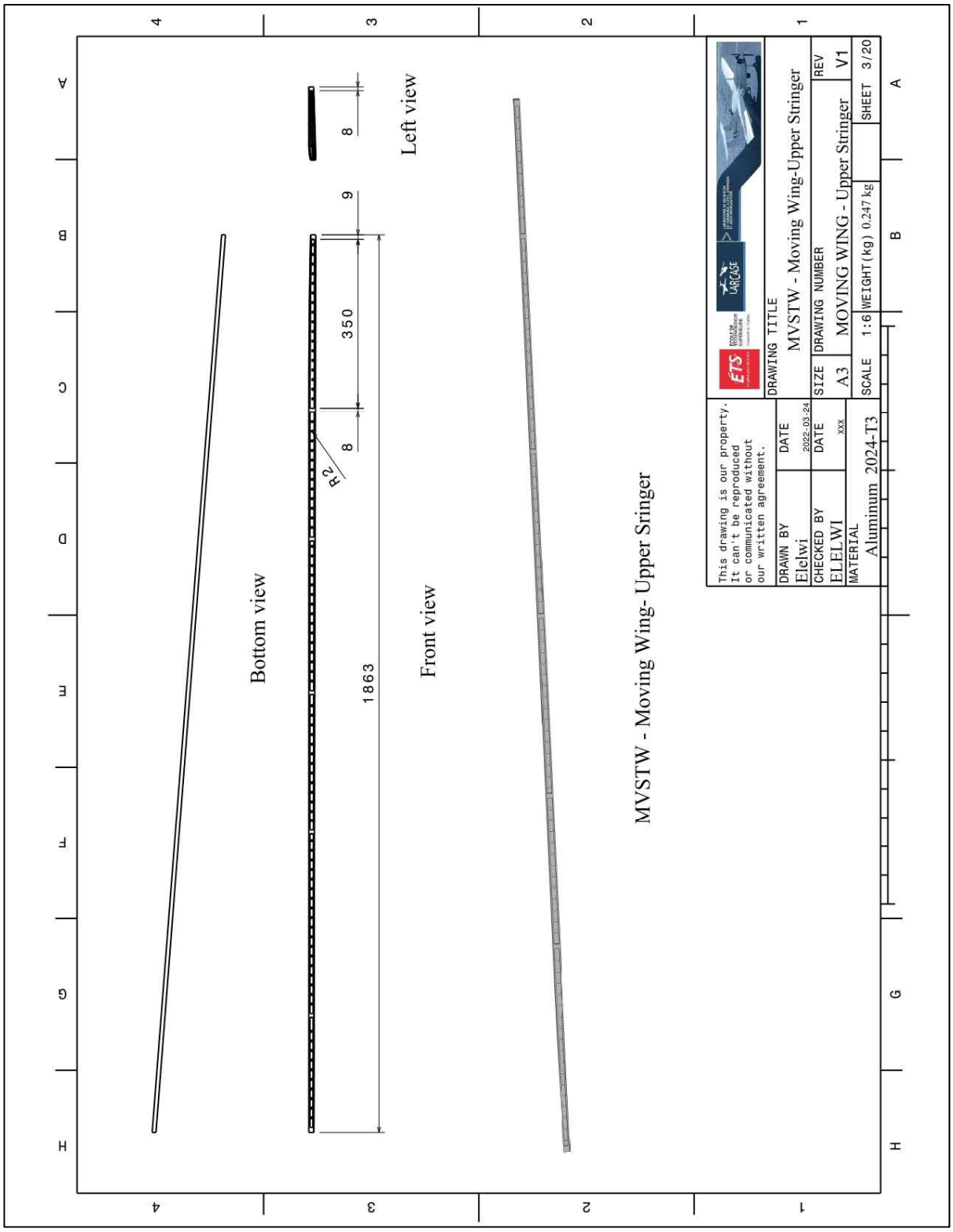

Figure-B II-65 MVSTW Moving Wing Upper Stringer Using Al 2024-T3

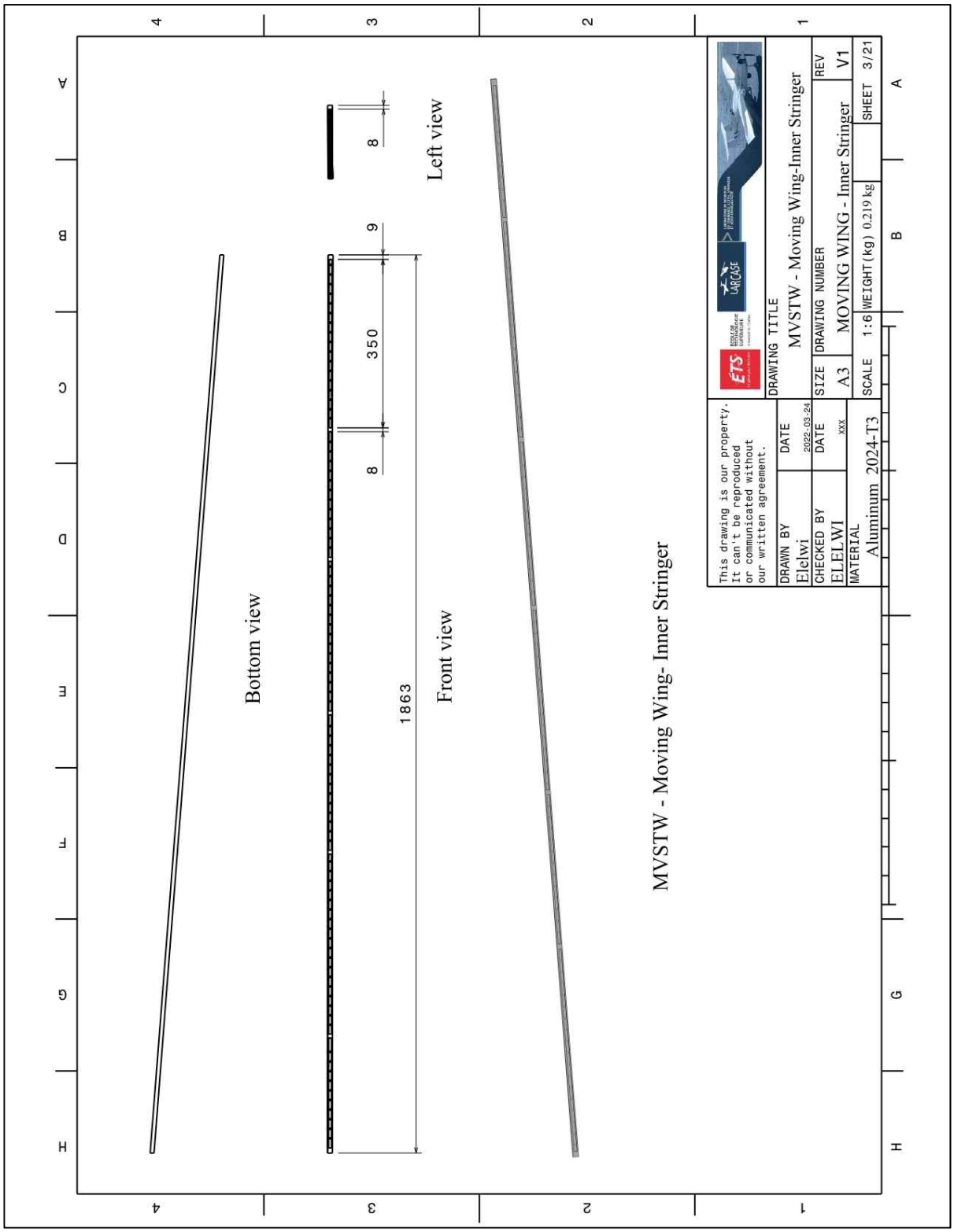

Figure-B II-66 MVSTW Moving Wing Inner Stringer Using Al 2024-T3

APPENDIX III

MVSTW USING ALUMINUM COMPOSITE MATERIALS

This appendix is for the detailed design of MVSTW and its components using composite materials. It depicts the MVSTW with various wingspan extensions based on the location of the moving segment with the fixed wing. The detailed design also includes information such as the weight of each component, composite material type for each component, and the design scale.

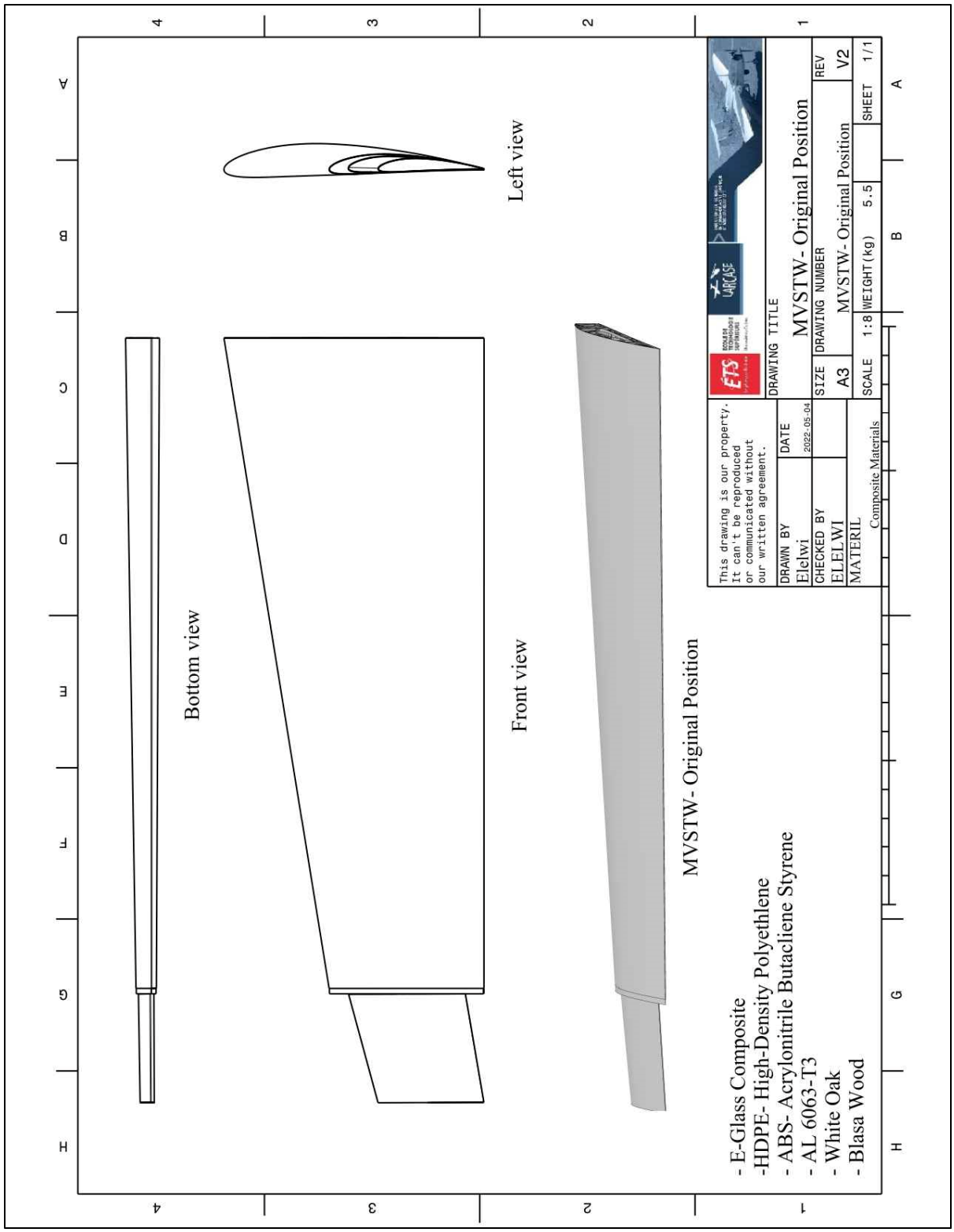

Figure-C III-1 MVSTW at Original Position Using Composite Materials

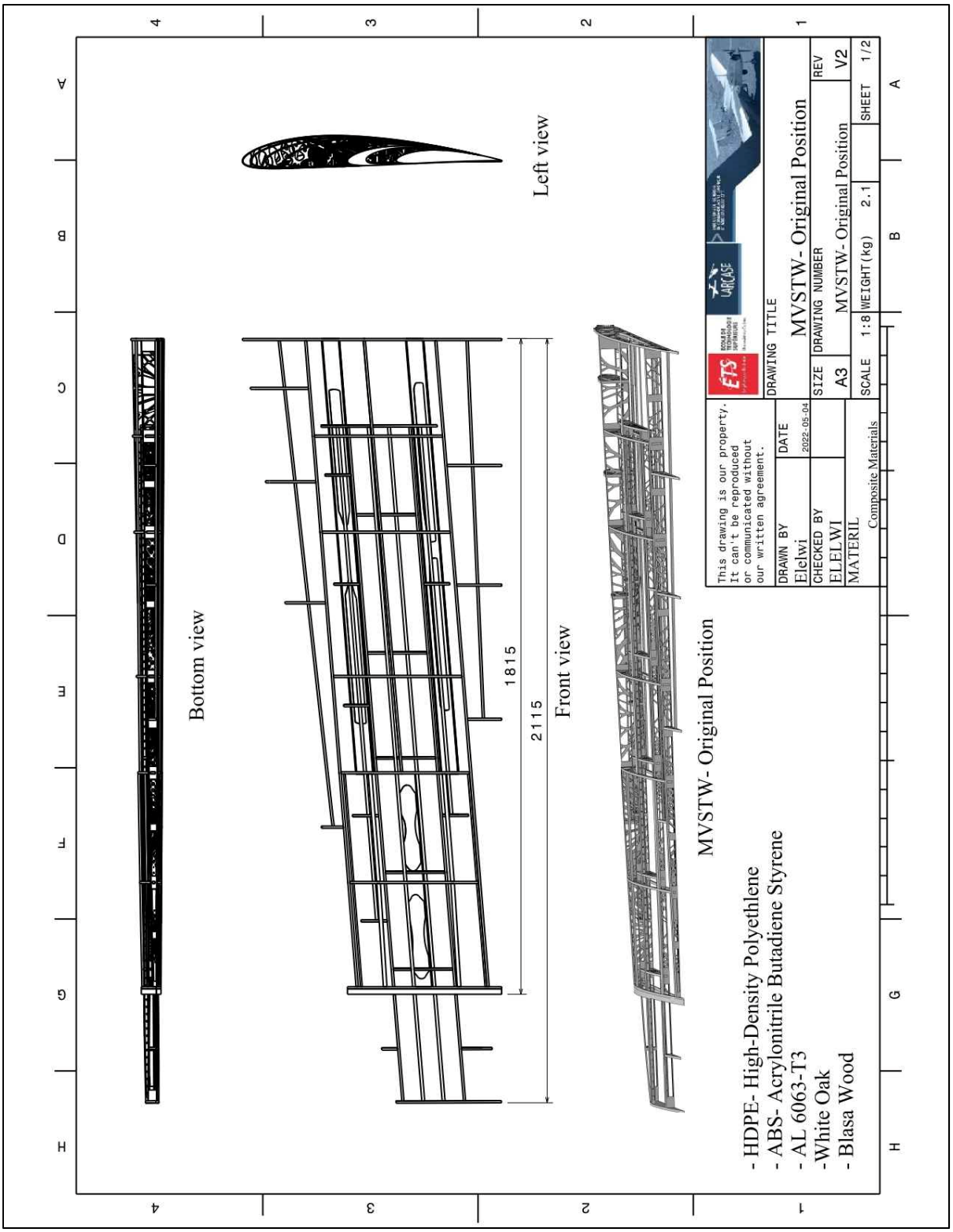

Figure-C III-2 MVSTW Skeleton at Original Position Using Composite Materials

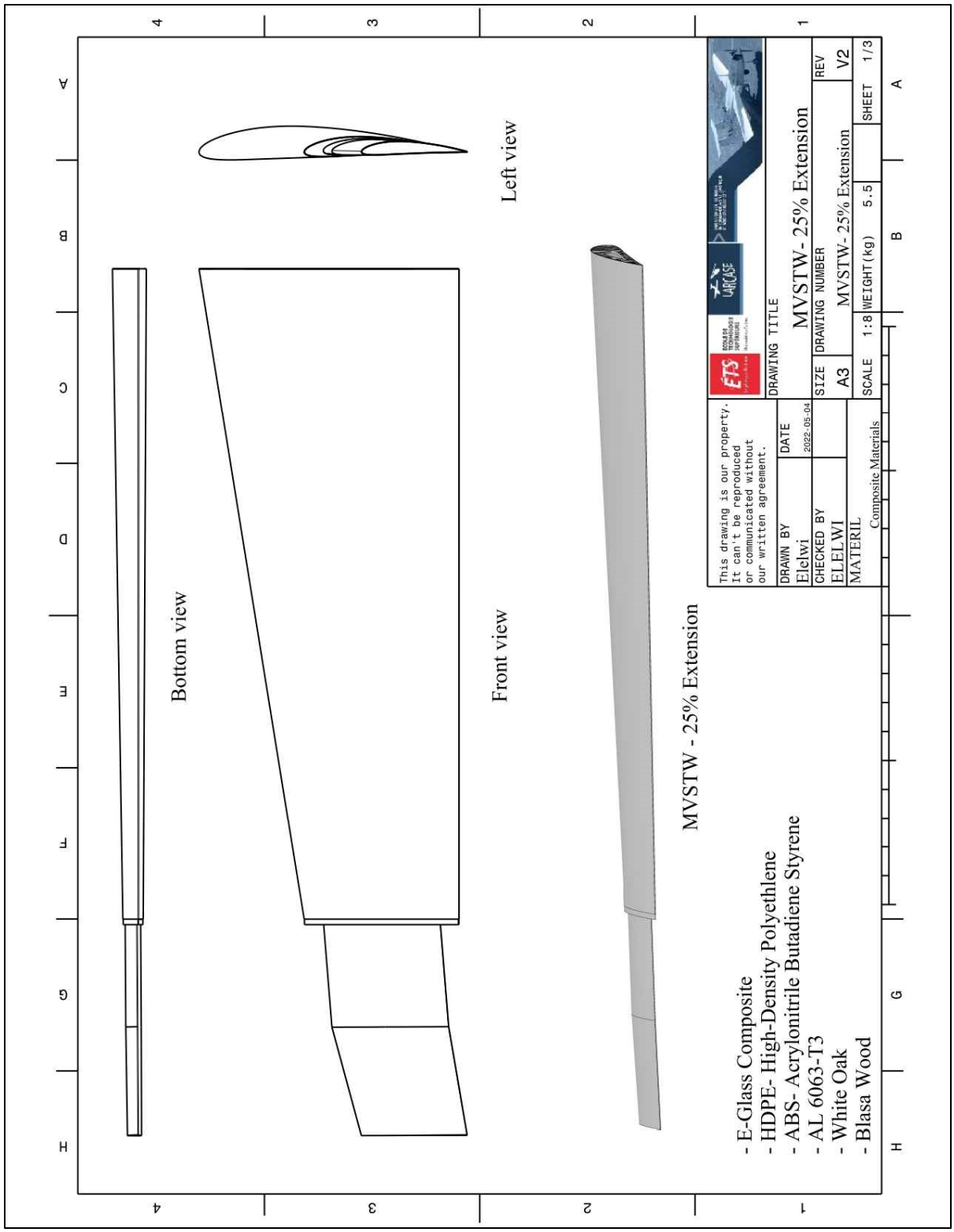

Figure-C III-3 MVSTW at 25% from its Original Position Using Composite Materials

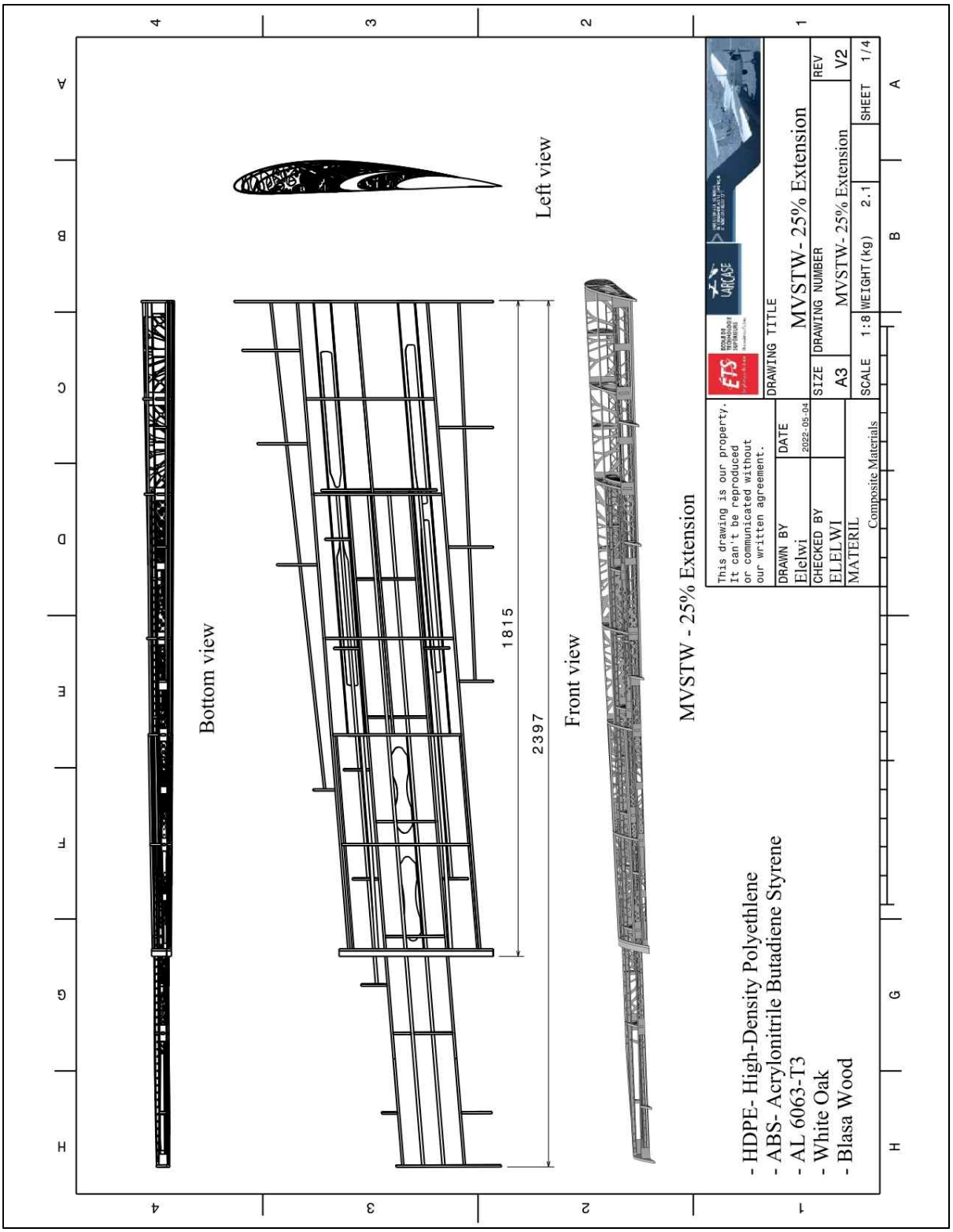

Figure-C III-4 MVSTW Skeleton at 25% from its Original Position Using Composite Materials

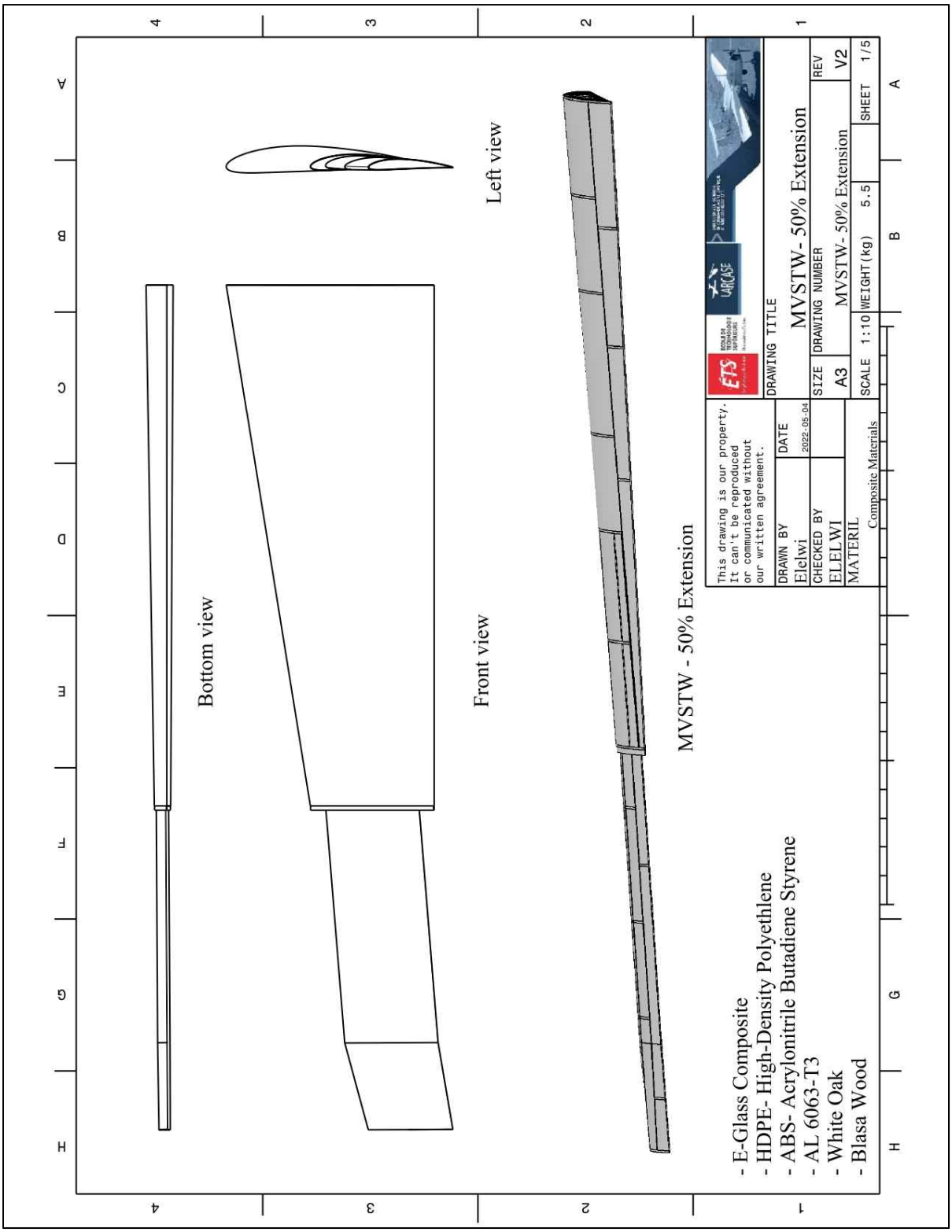

Figure-C III-5 MVSTW at 50% from its Original Position Using Composite Materials

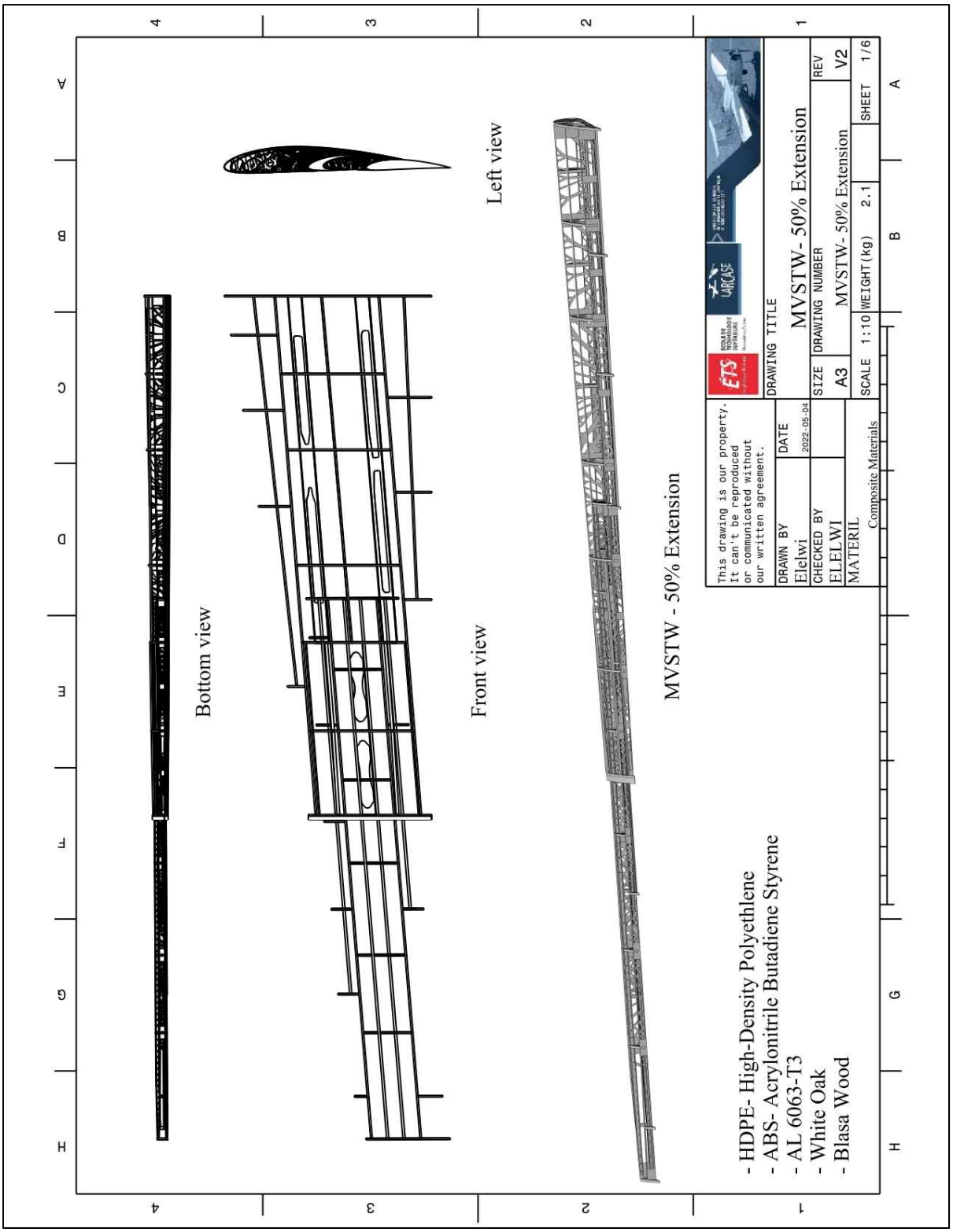

Figure-C III-6 MVSTW Skelton at 50% from its Original Position Using Composite Materials

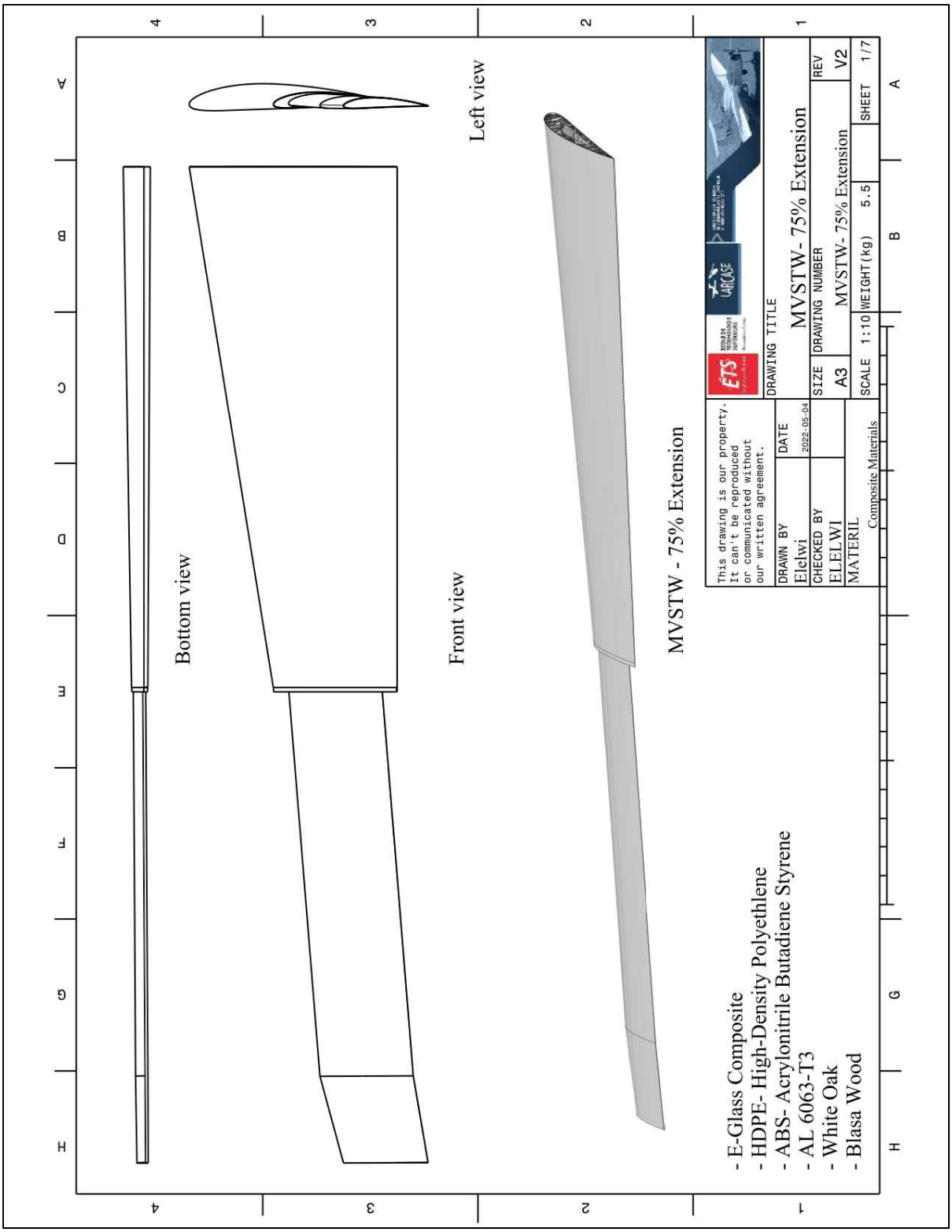

Figure-C III-7 MVSTW at 75% from its Original Position Using Composite Materials

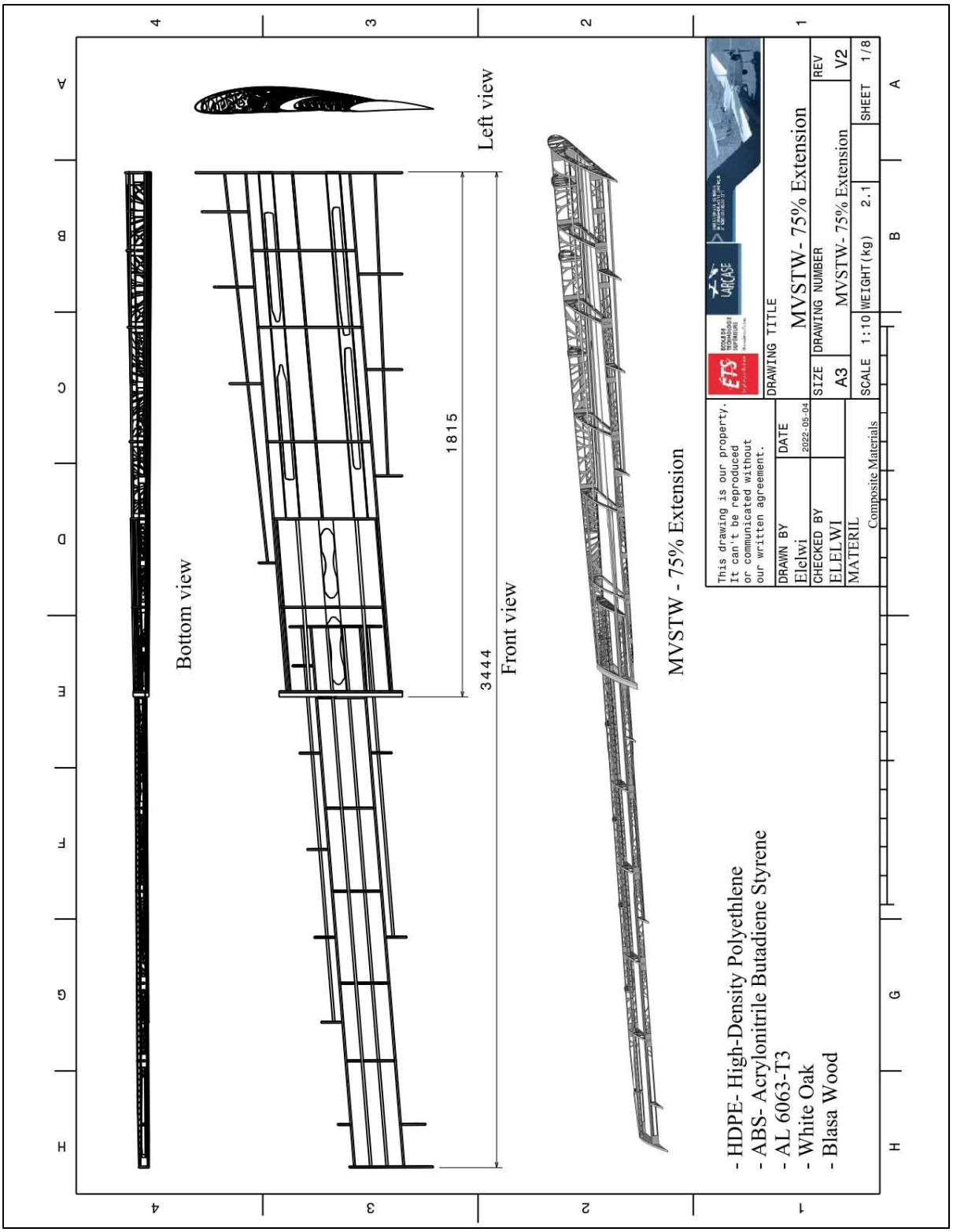

Figure-C III-8 MVSTW Skeleton at 75% from its Original Position Using Composite Materials

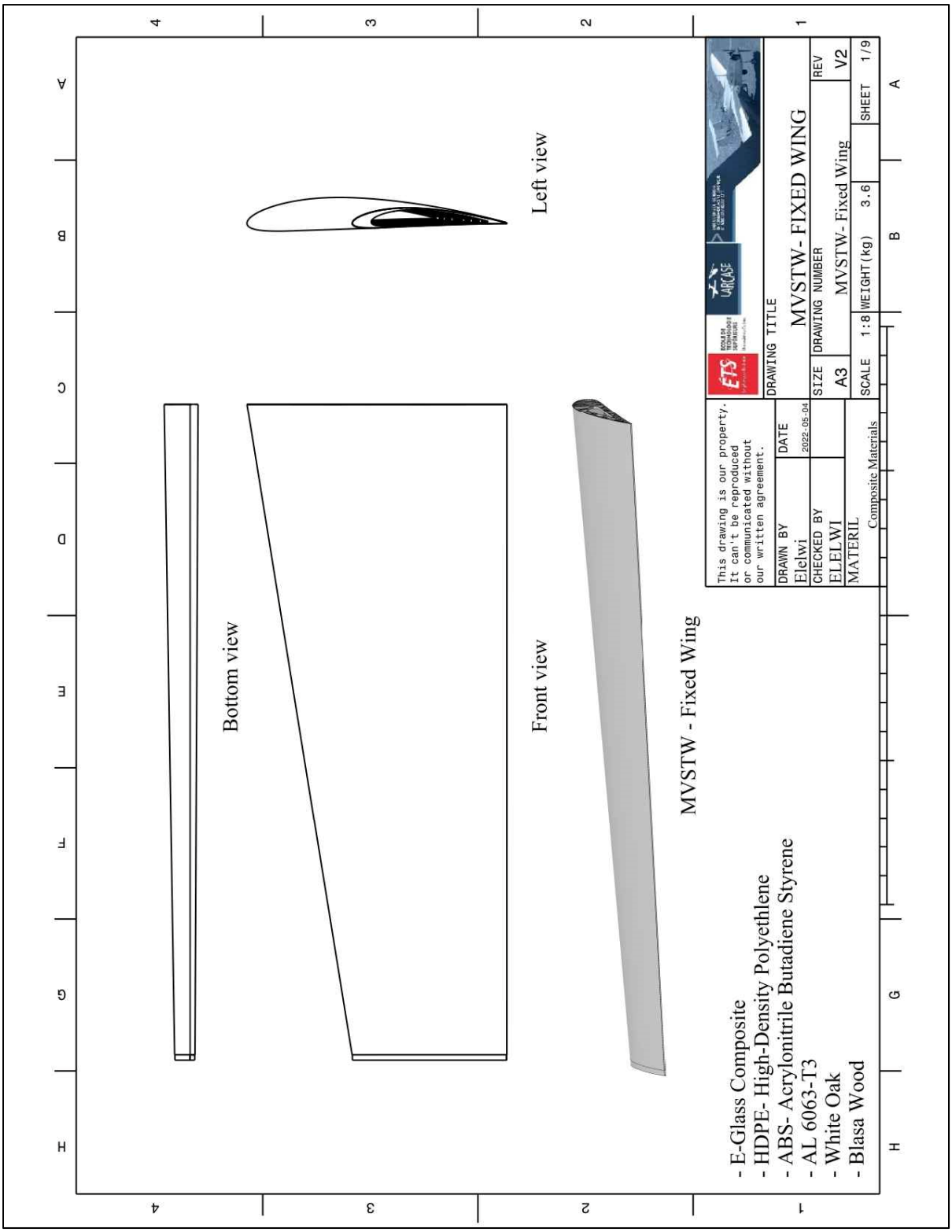

Figure-C III-9 MVSTW Fixed Wing Using Composite Materials

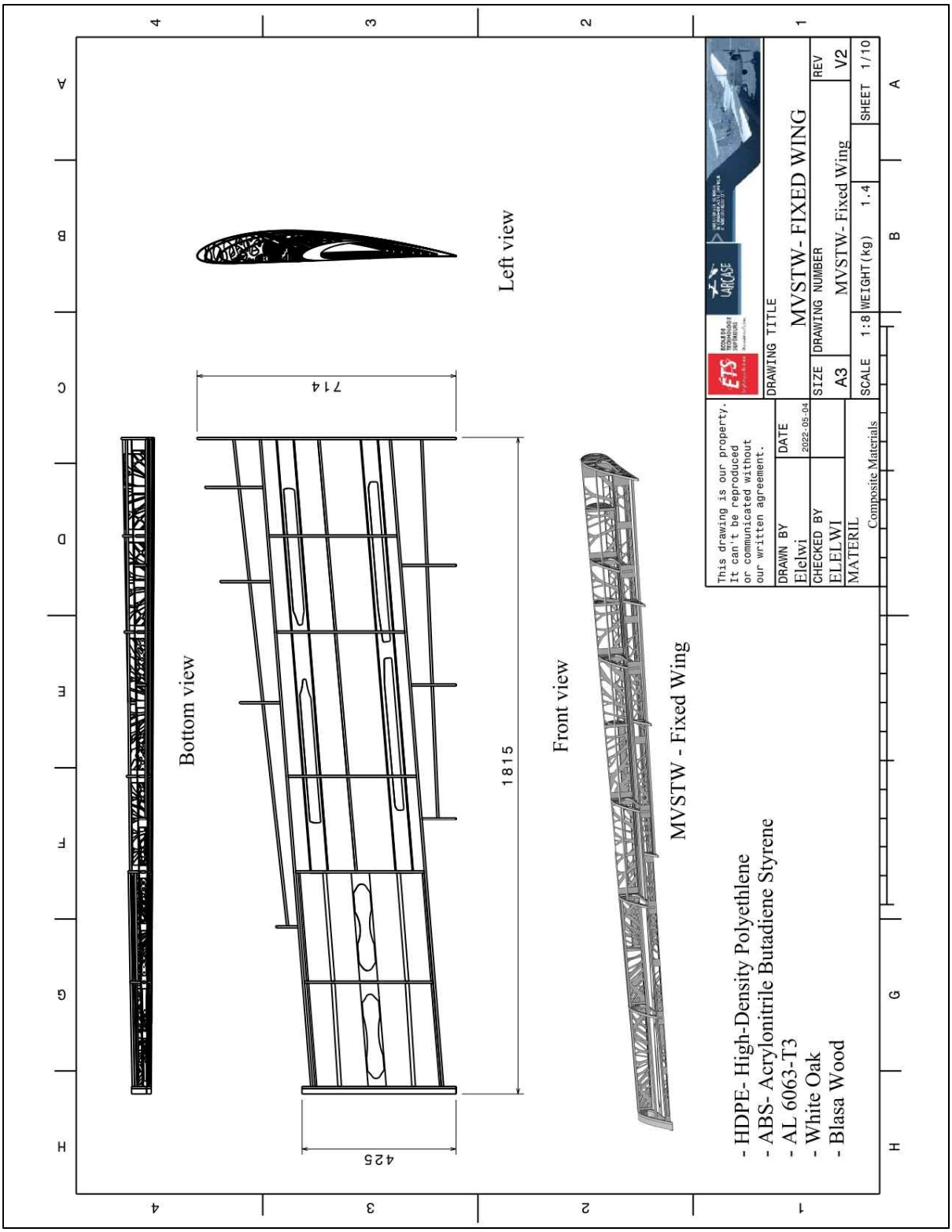

Figure-C III-10 MVSTW Fixed Wing Skelton Using Composite Materials

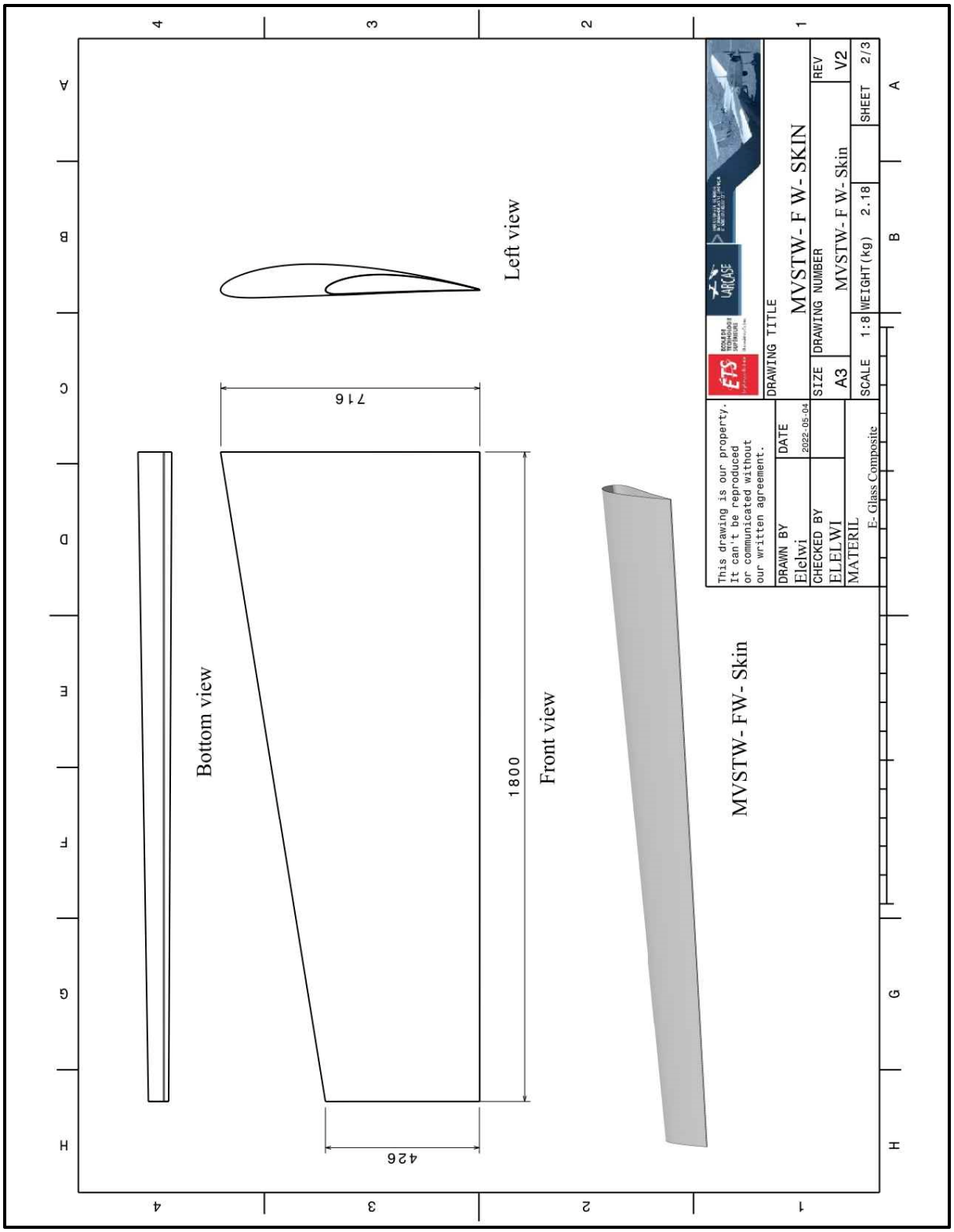

Figure-C III-11 MVSTW Fixed Wing Skin Using E-glass Composite

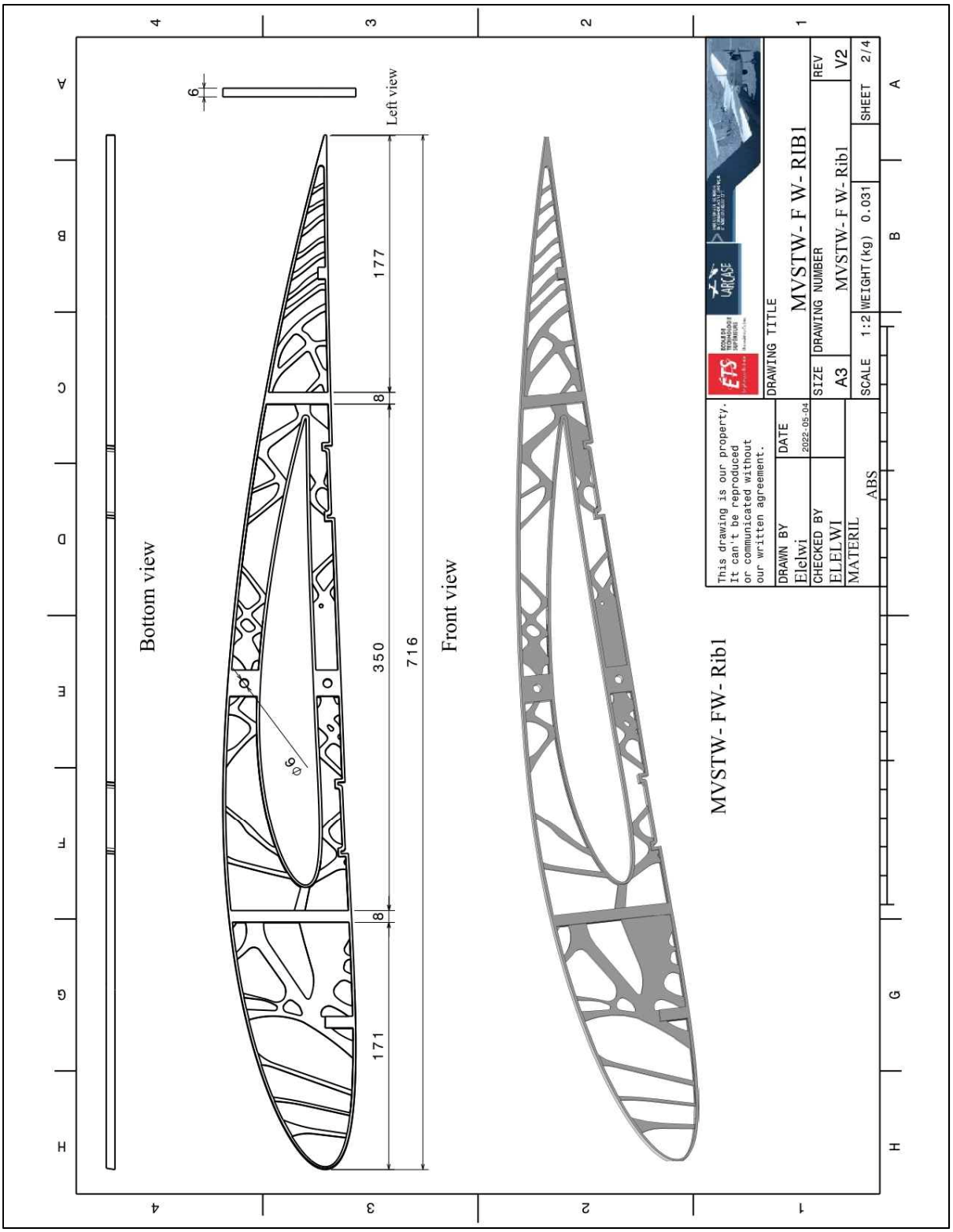

Figure-C III-12 MVSTW Fixed Wing Rib1 Using ABS

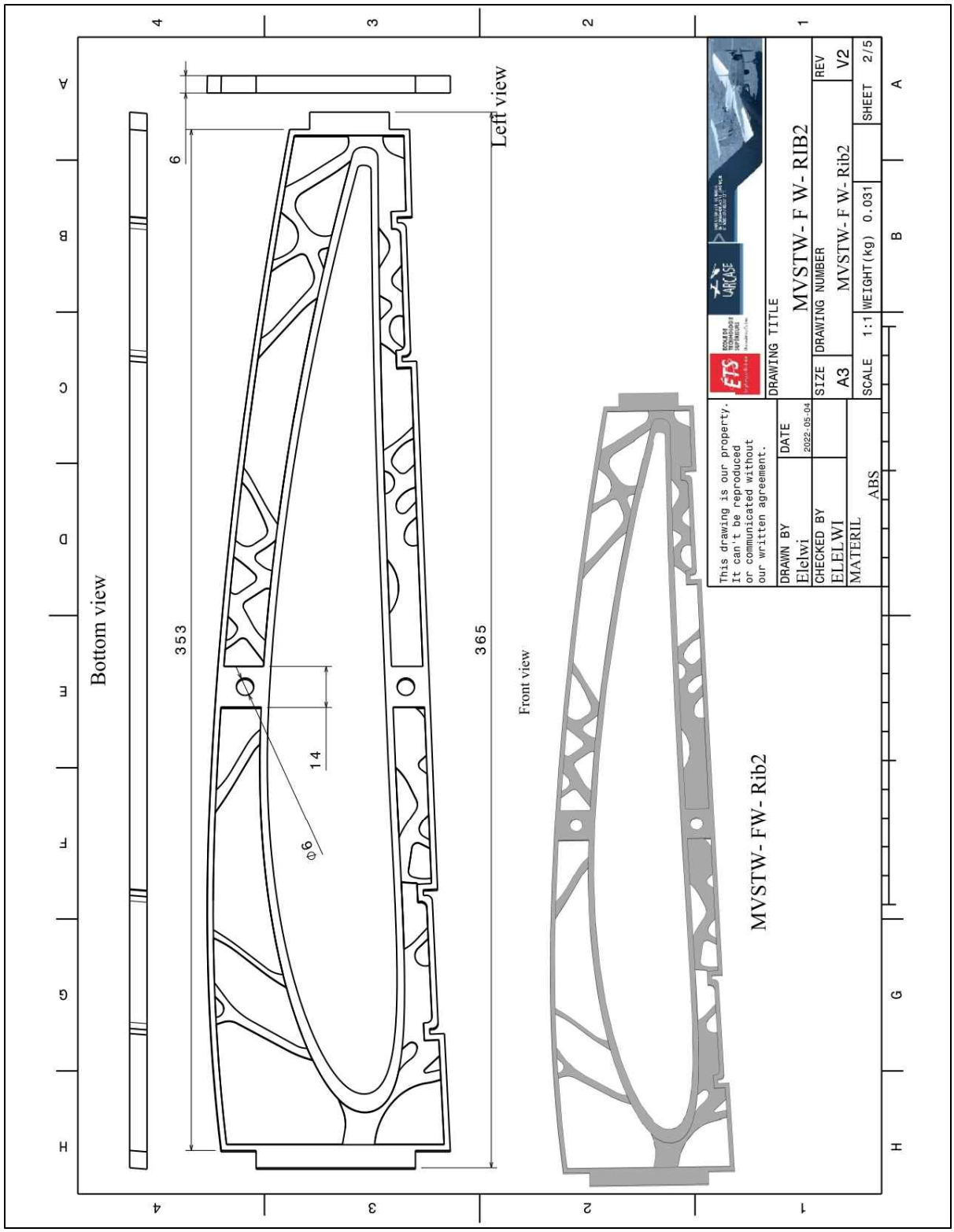

Figure-C III-13 MVSTW Fixed Wing Rib2 Using ABS

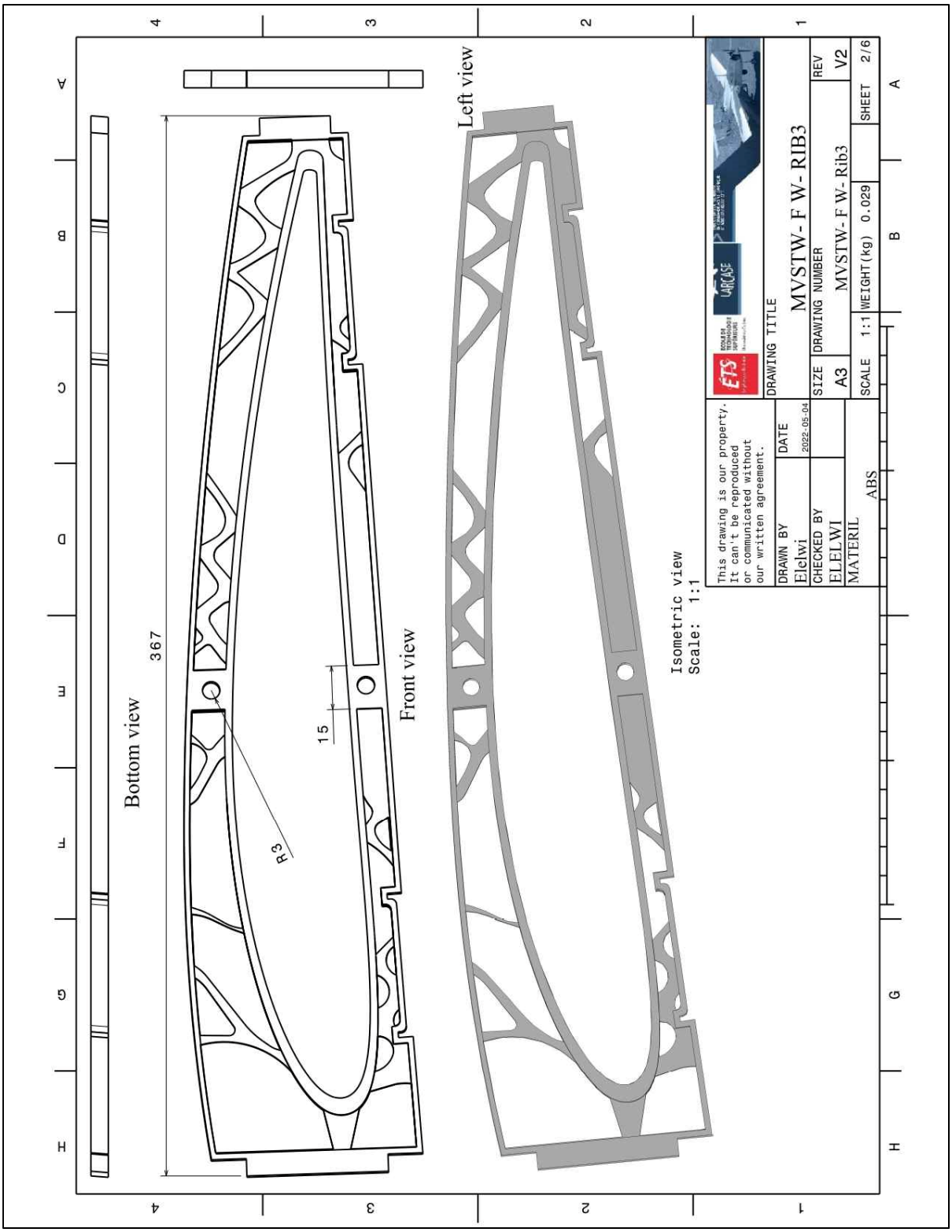

Figure-C III-14 MVSTW Fixed Wing Rib3 Using ABS

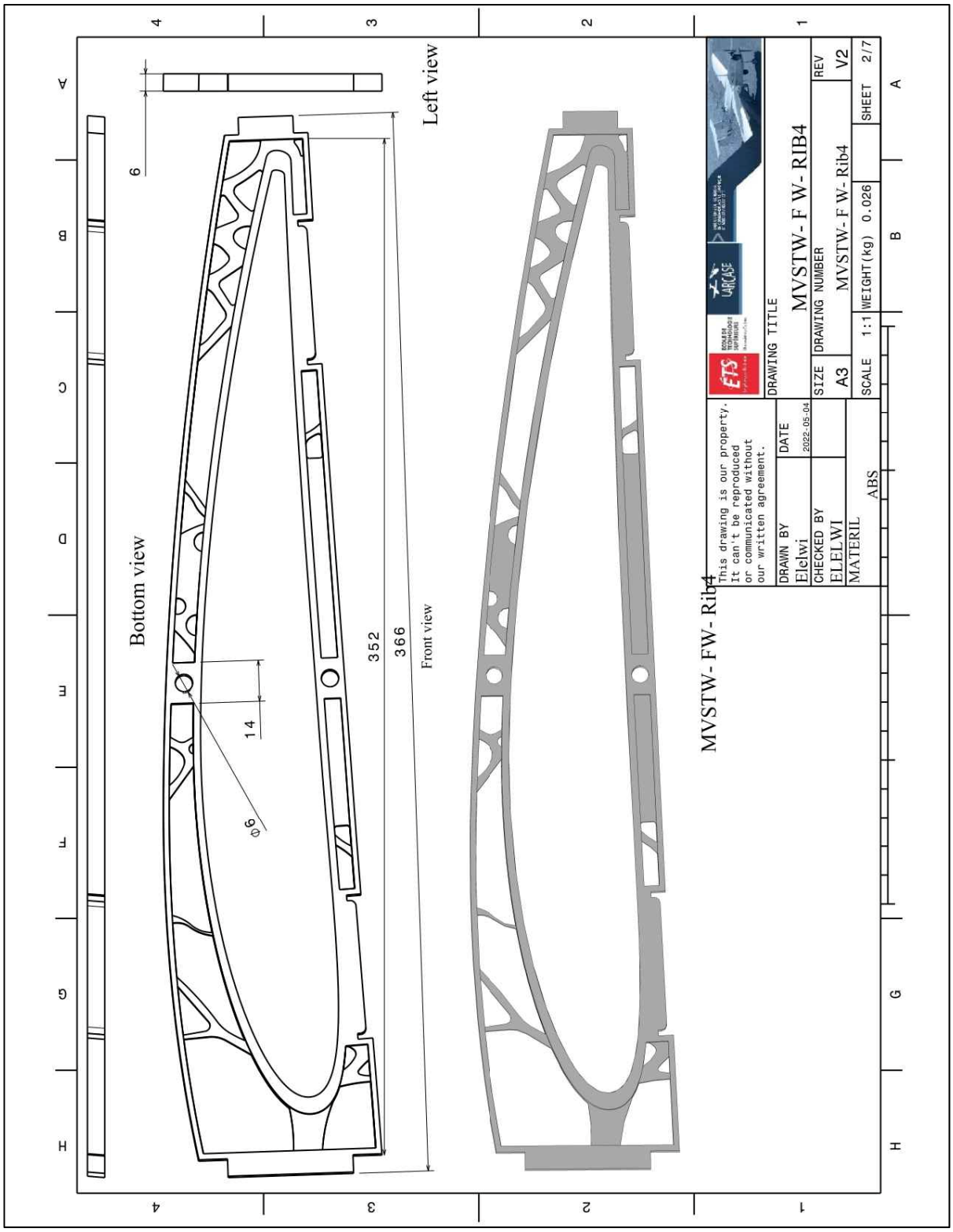

Figure-C III-15 MVSTW Fixed Wing Rib4 Using ABS

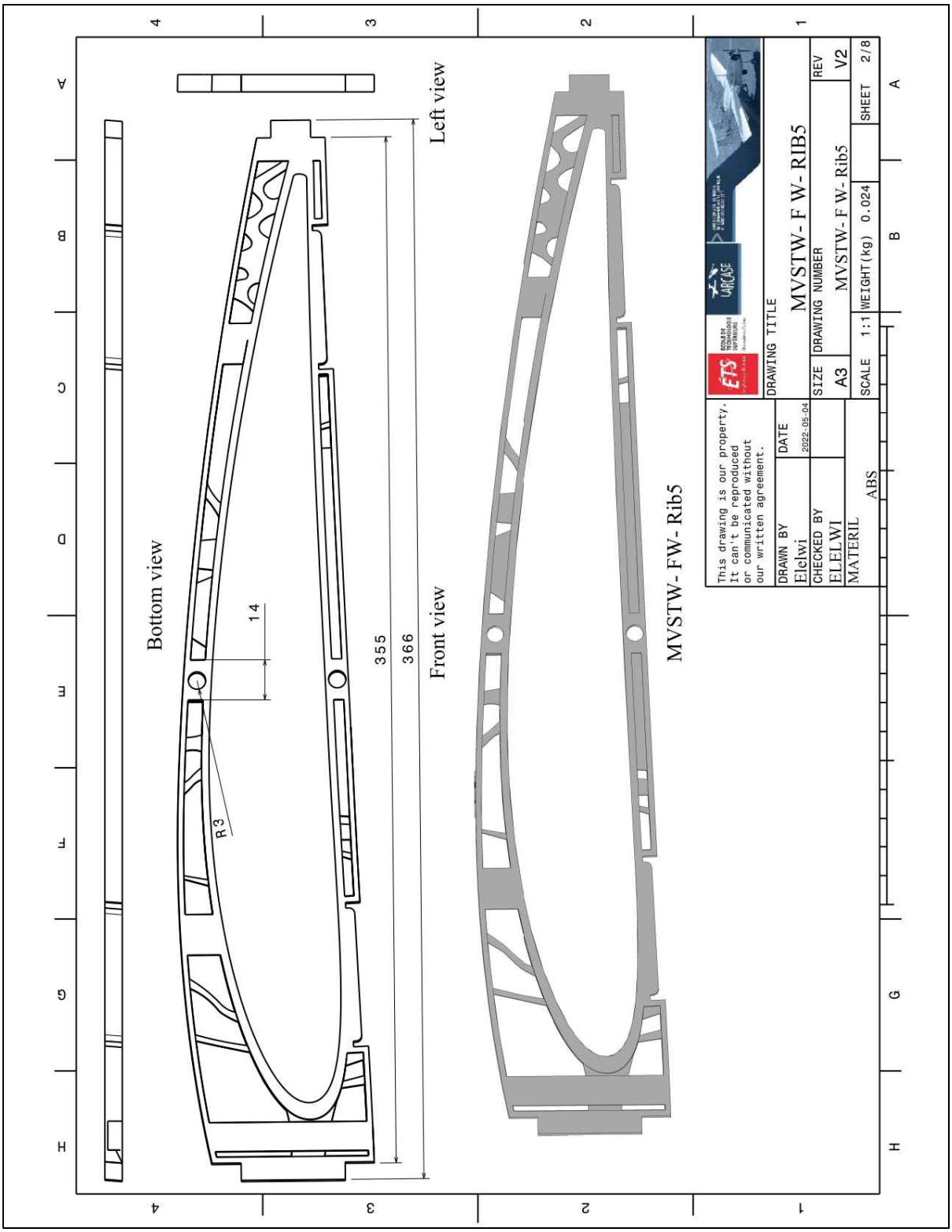

Figure-C III-16 MVSTW Fixed Wing Rib5 Using ABS

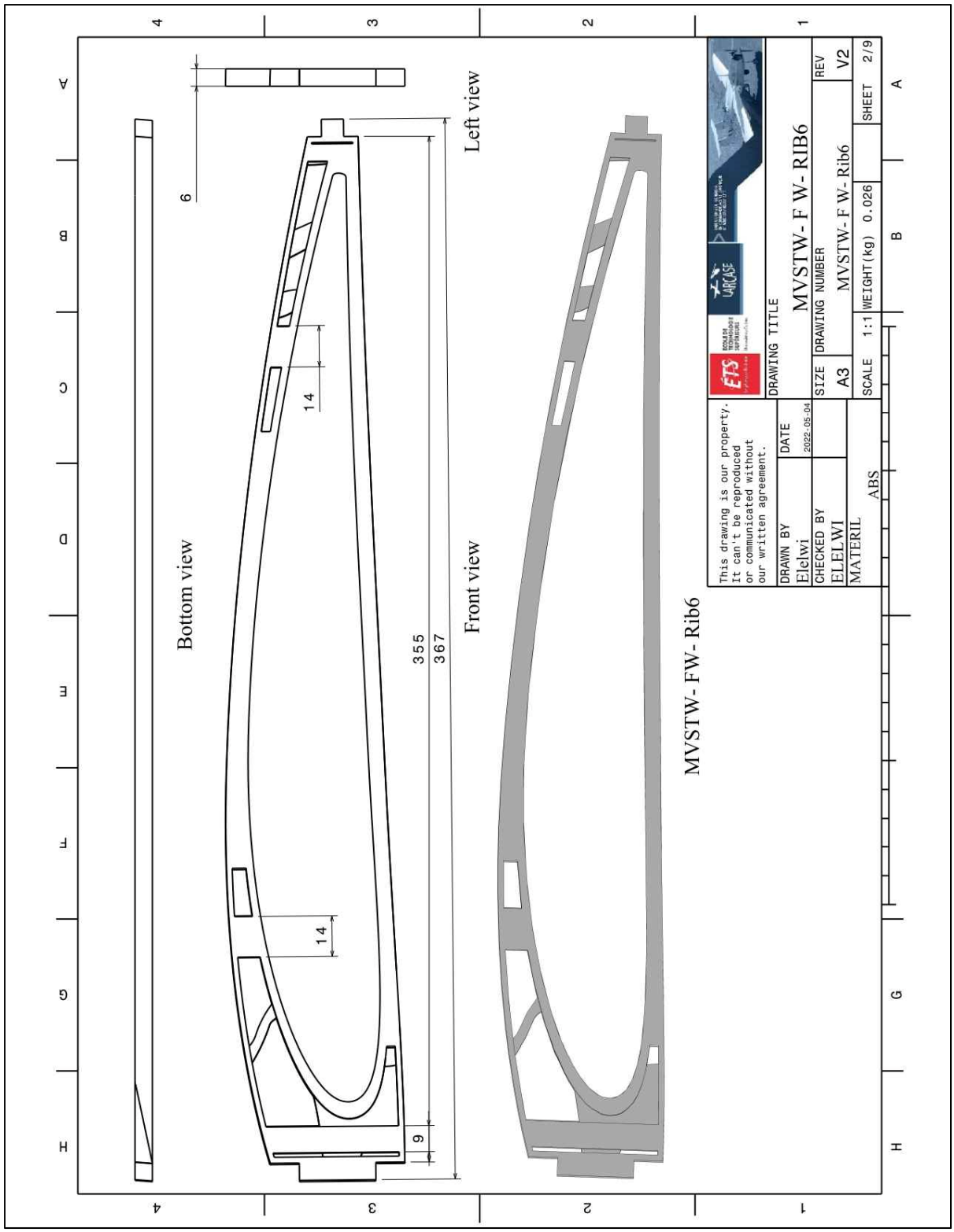

Figure-C III-17 MVSTW Fixed Wing Rib6 Using ABS

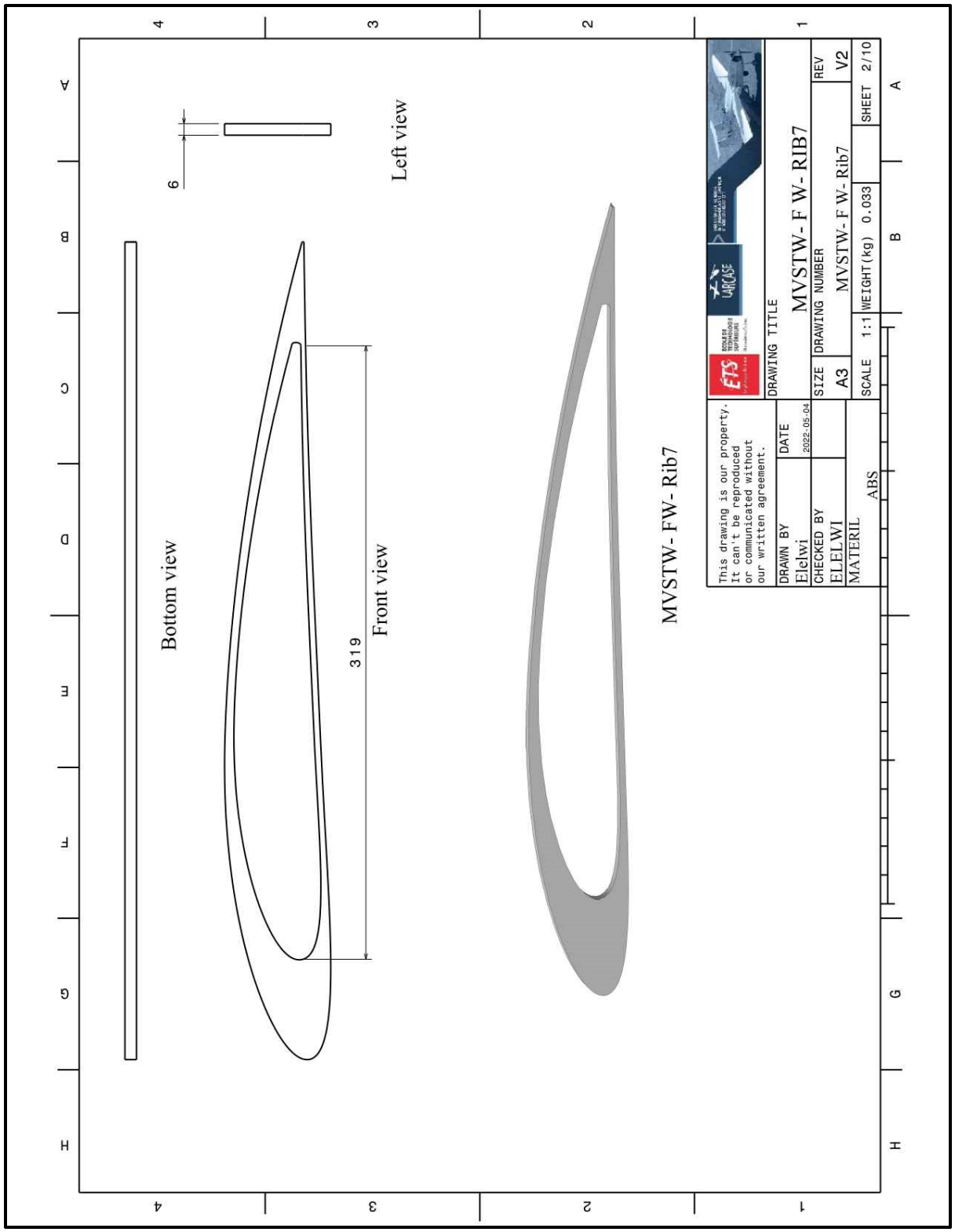

Figure-C III-18 MVSTW Fixed Wing Rib7 Using ABS

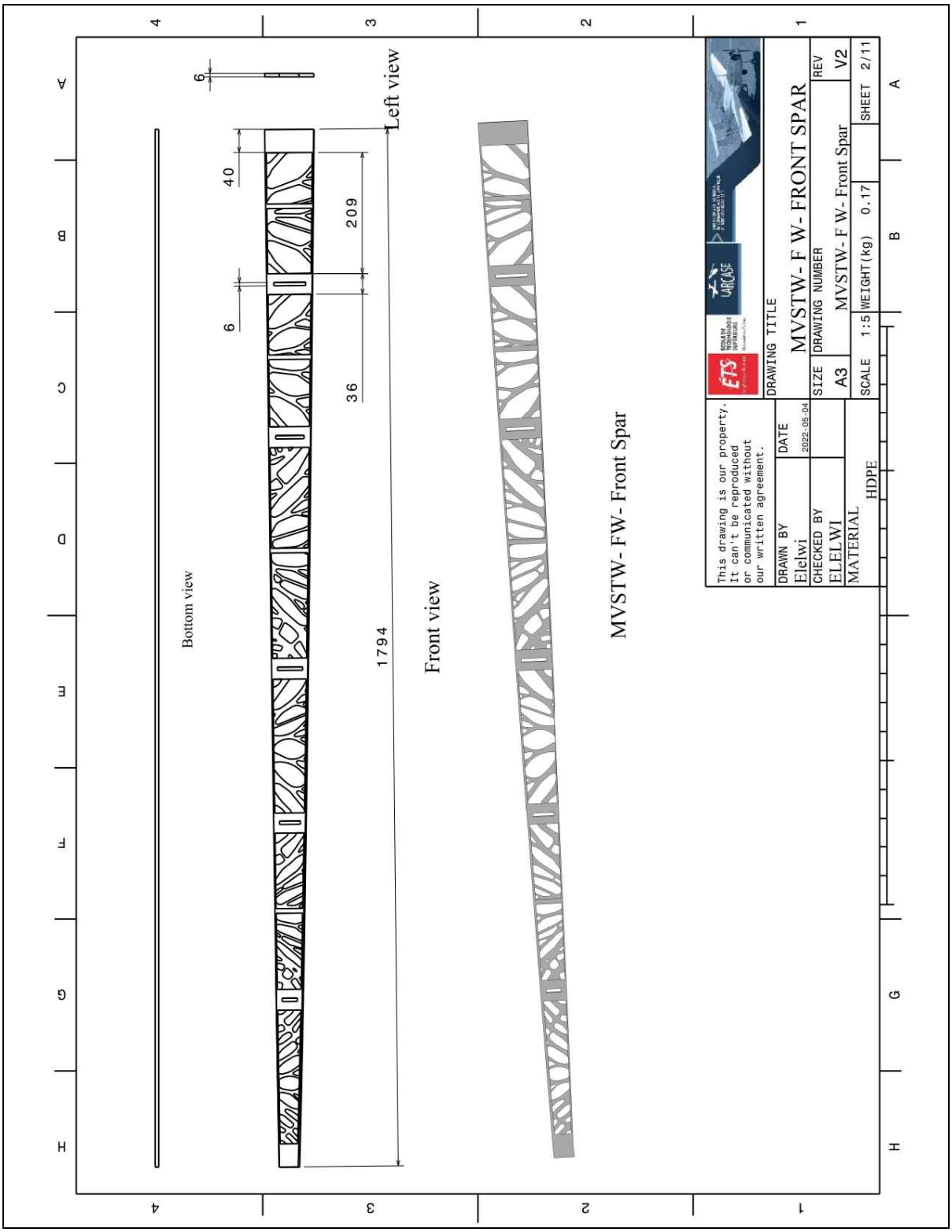

Figure-C III-19 MVSTW Fixed Wing Front Spar Using HDPE

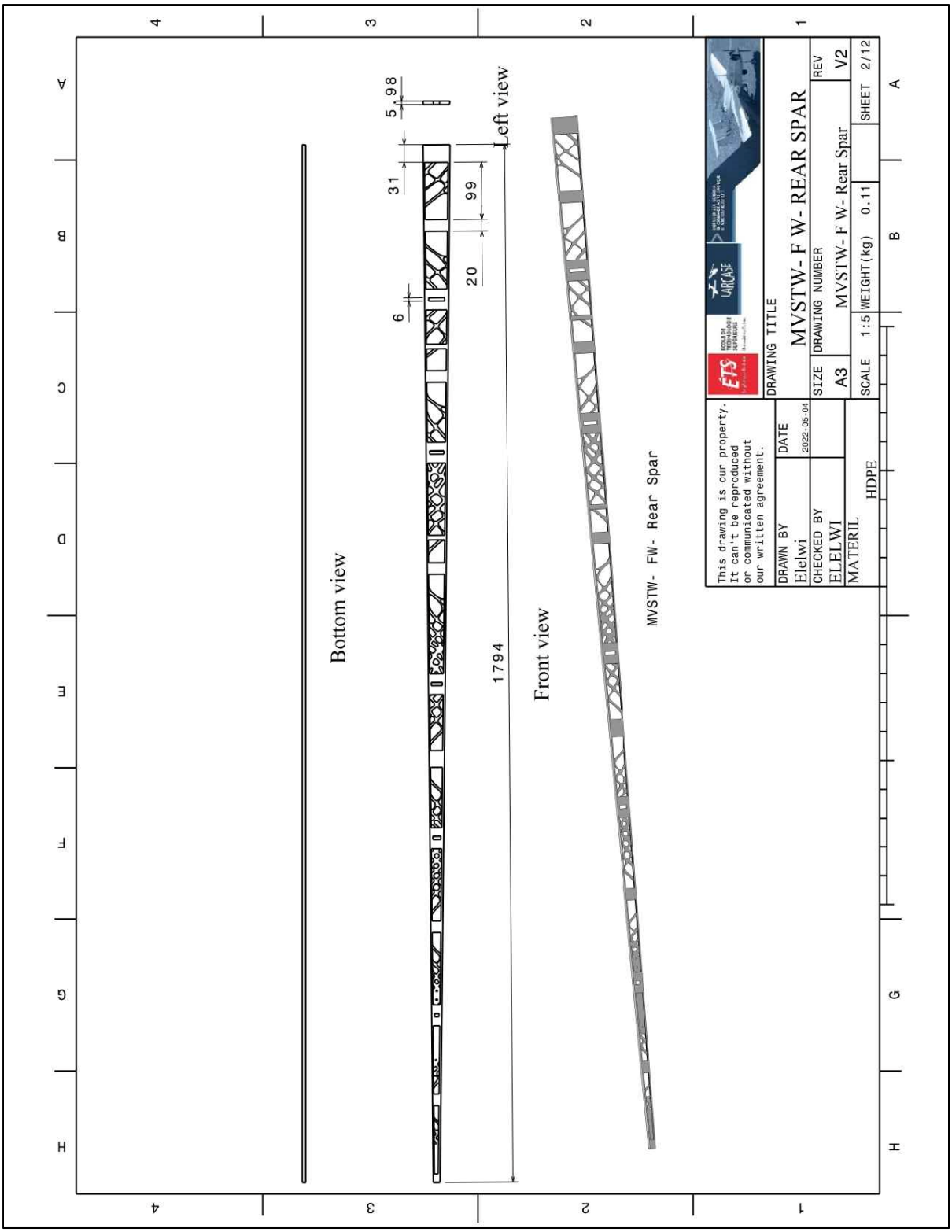

Figure-C III-20 MVSTW Fixed Wing Rear Spar Using HDPE

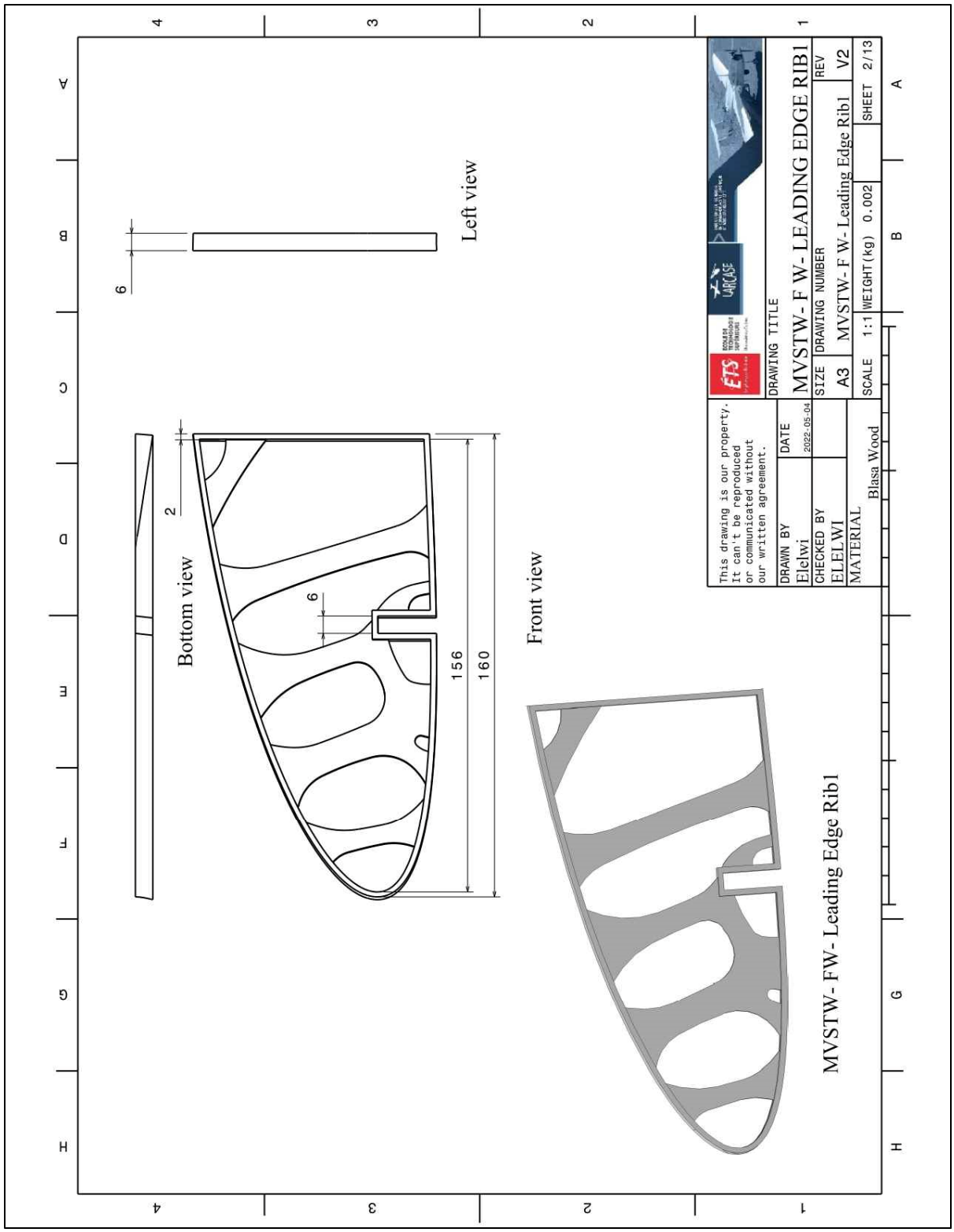

Figure-C III-21 MVSTW Fixed Wing Leading Edge Rib1 Using Balsa Wood

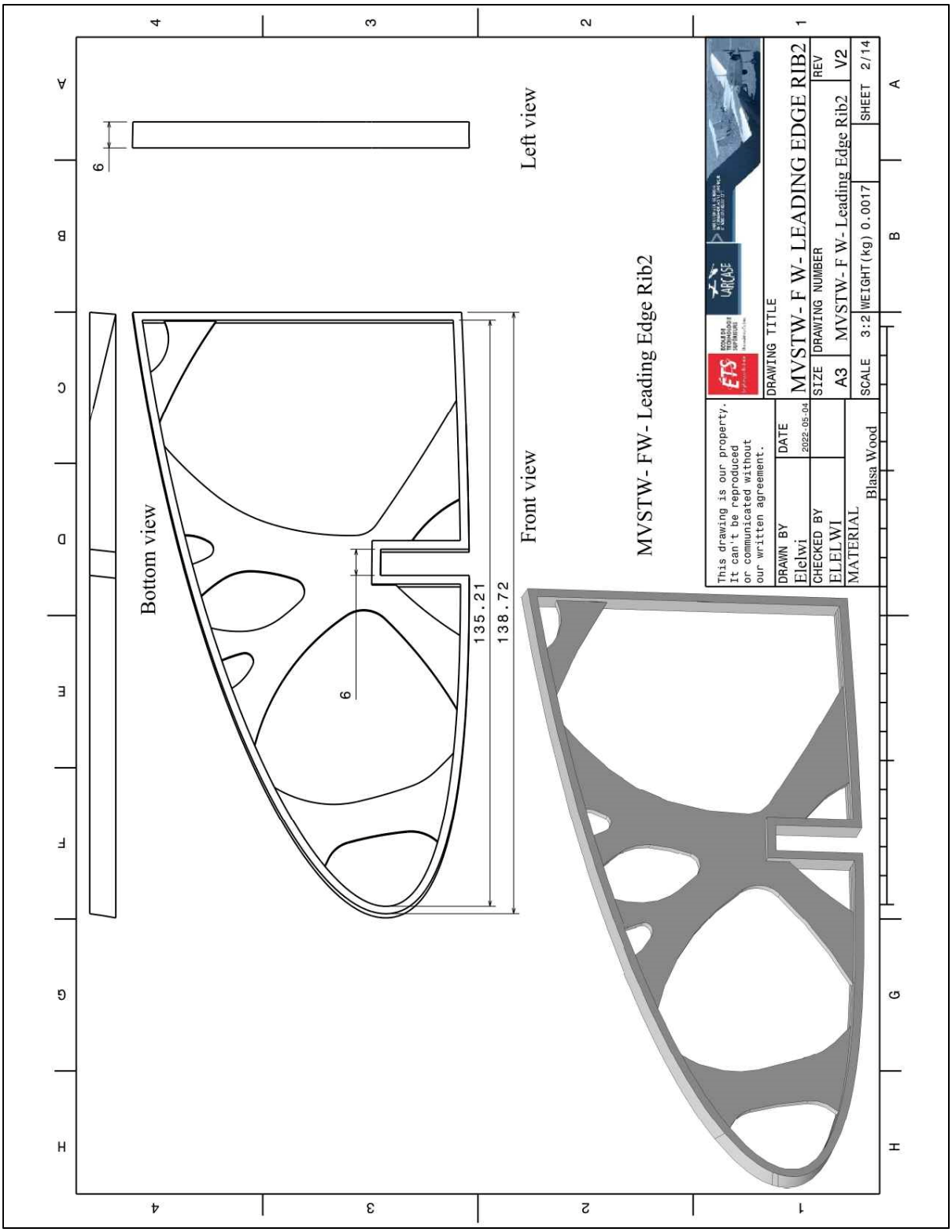

Figure-C III-22 MVSTW Fixed Wing Leading Edge Rib2 Using Balsa Wood

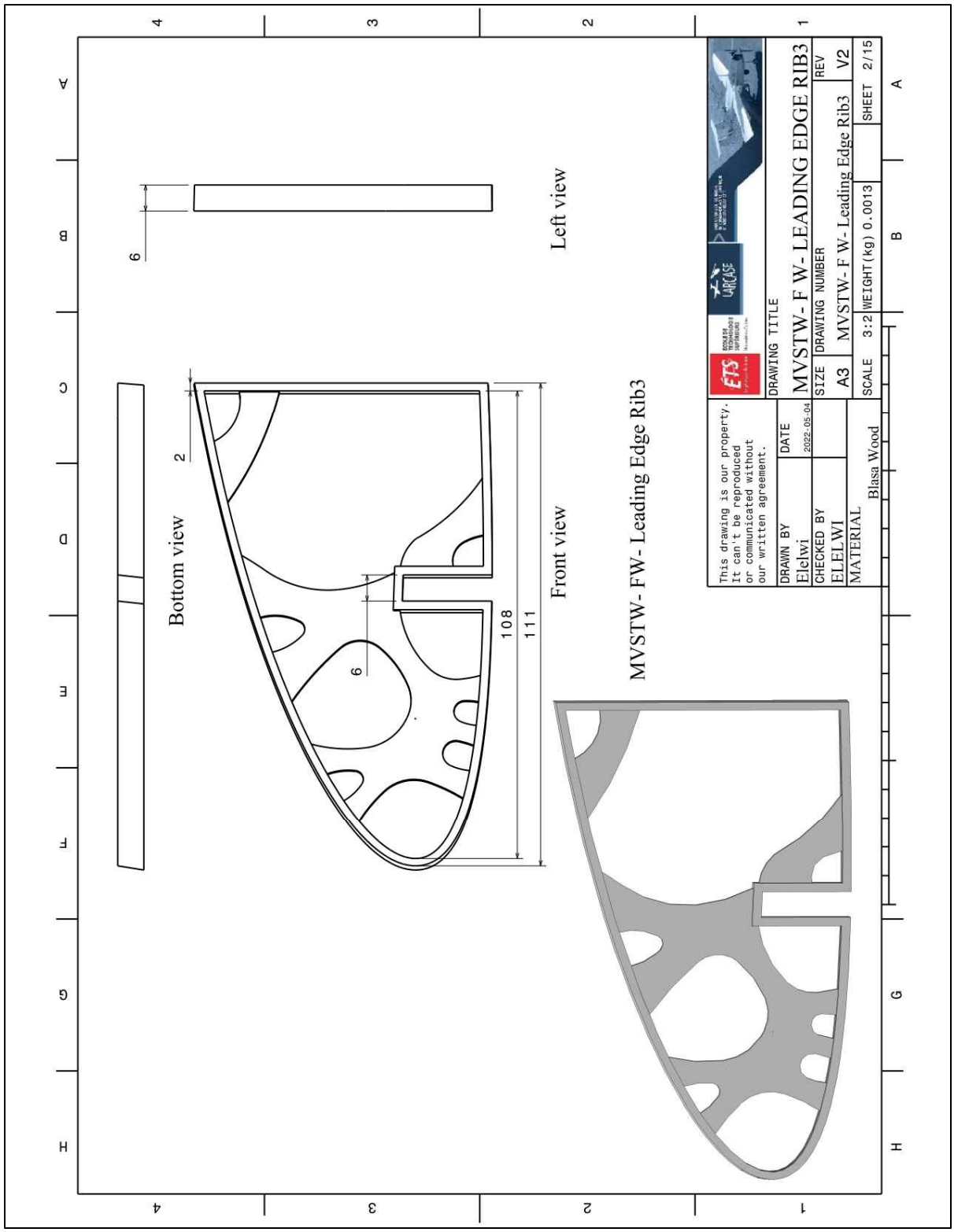

Figure-C III-23 MVSTW Fixed Wing Leading Edge Rib3 Using Balsa Wood

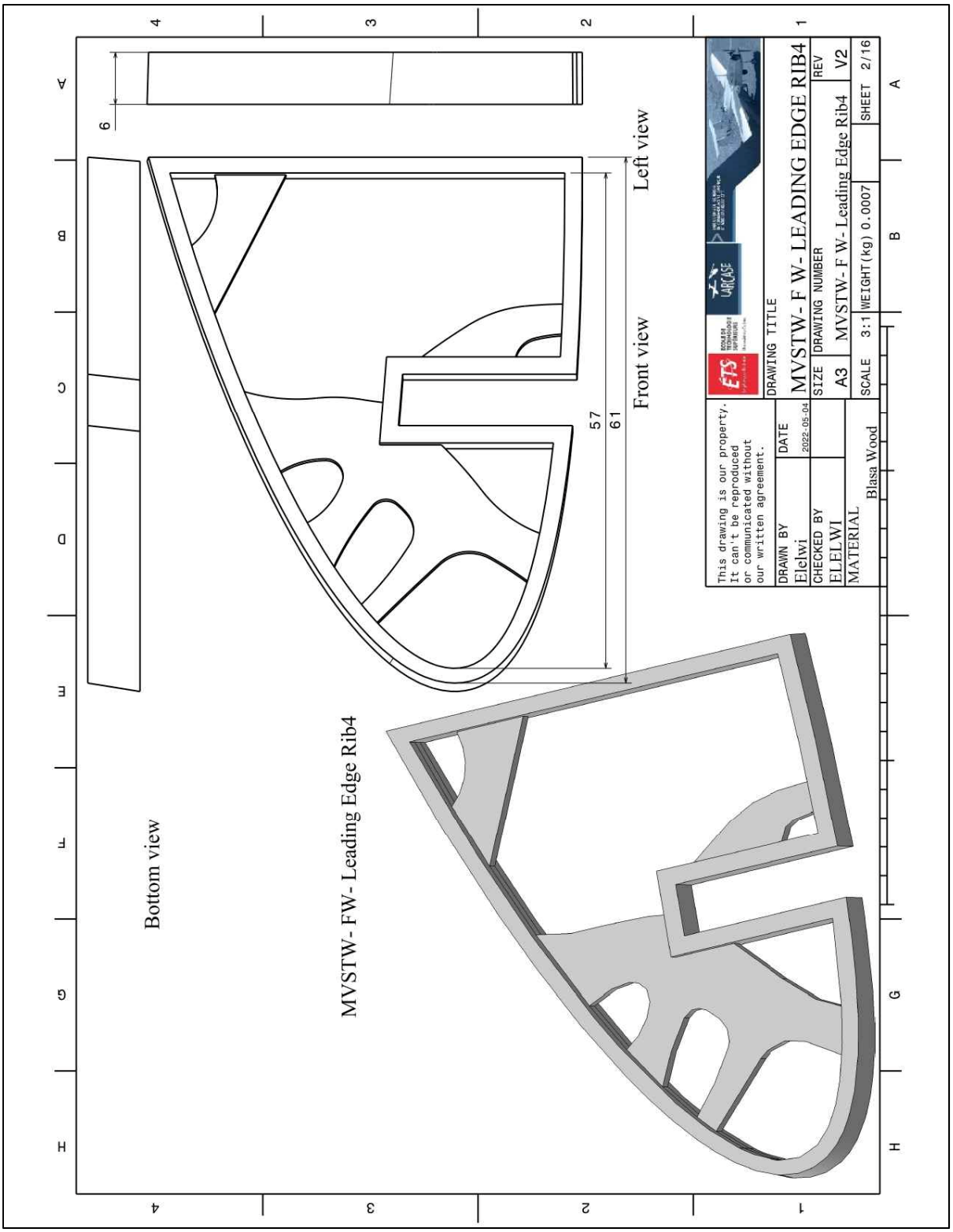

Figure-C III-24 MVSTW Fixed Wing Leading Edge Rib4 Using Balsa Wood

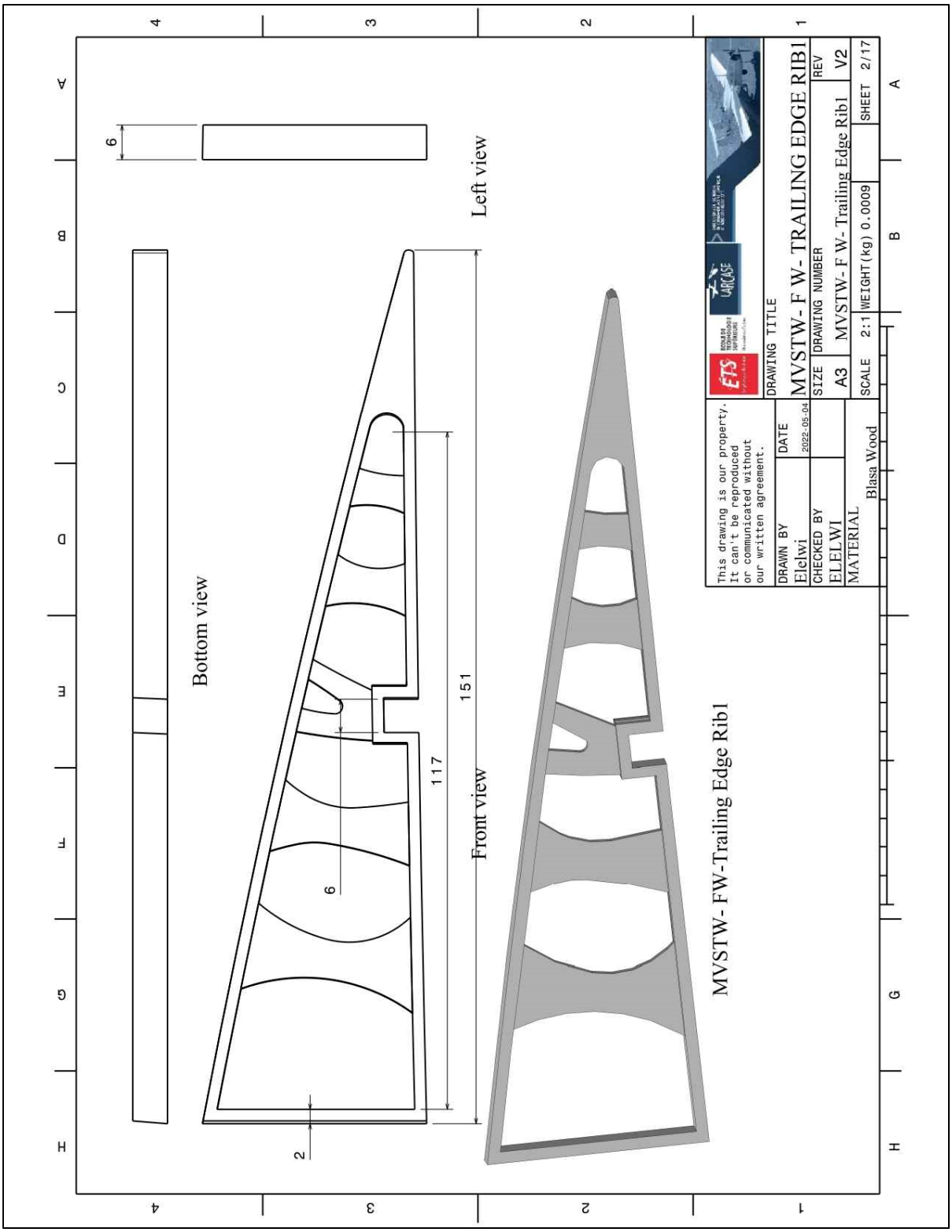

Figure-C III-25 MVSTW Fixed Wing Trailing Edge Rib1 Using Balsa Wood

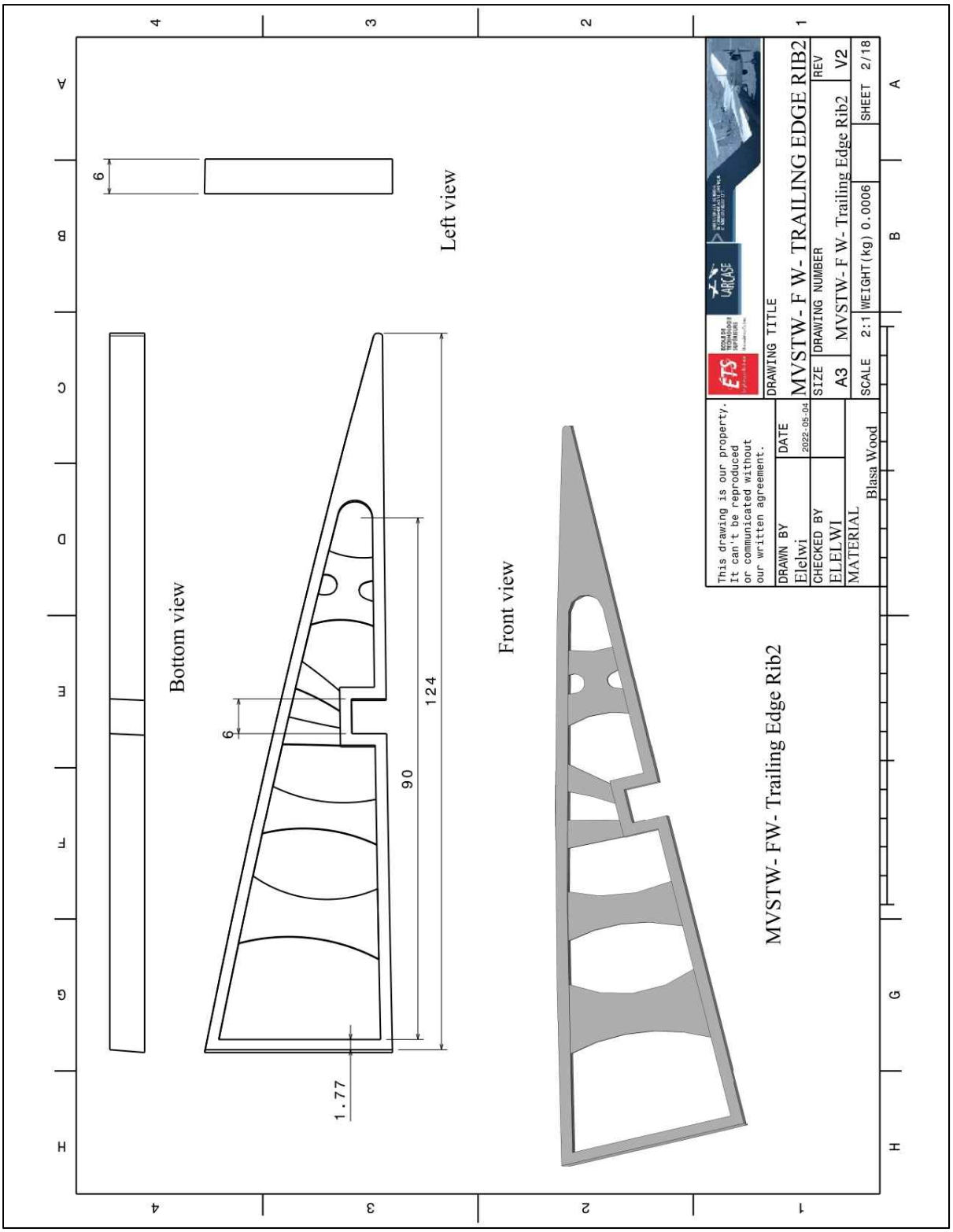

Figure-C III-26 MVSTW Fixed Wing Trailing Edge Rib2 Using balsa Wood

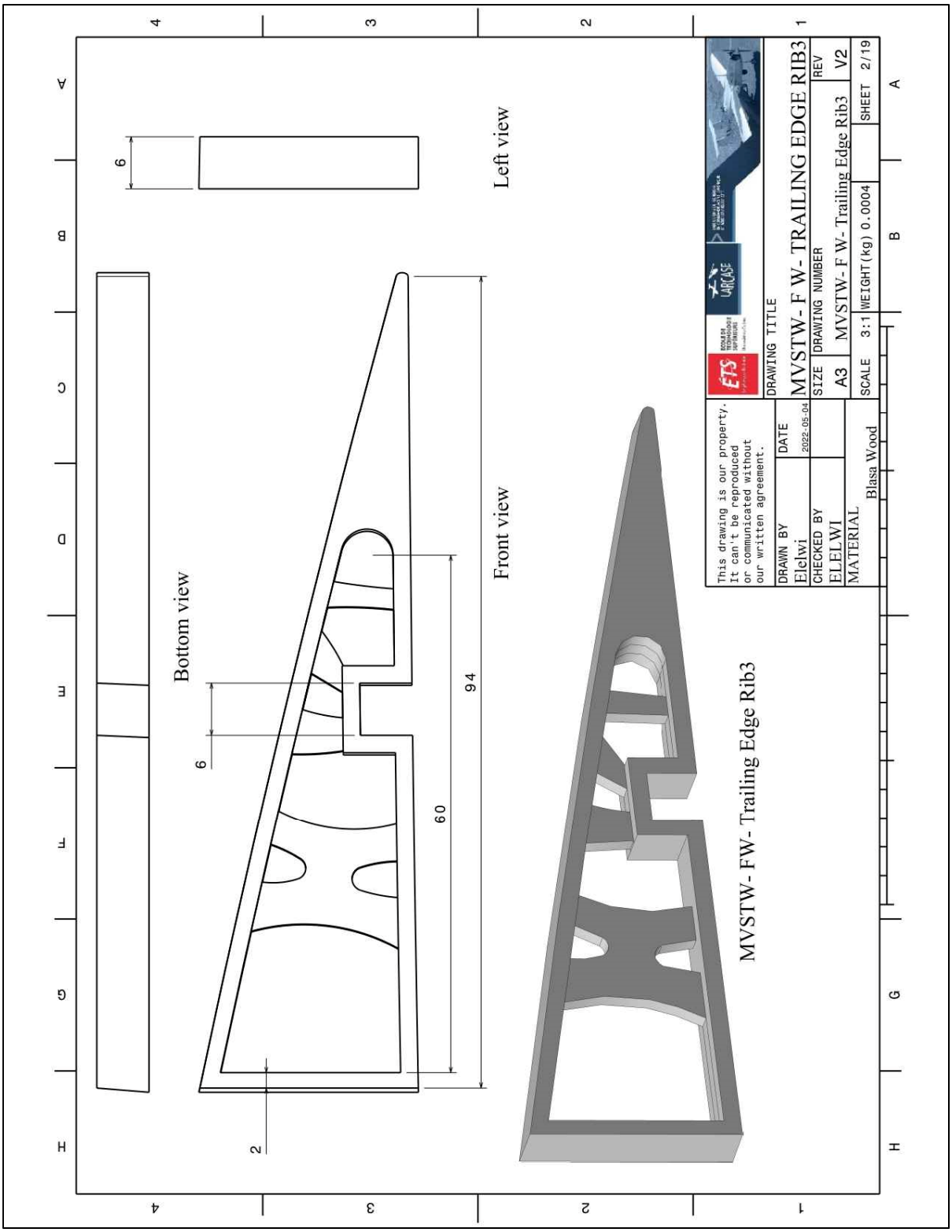

Figure-C III-27 MVSTW Fixed Wing Trailing Edge Rib3 Using Baalsa Wood

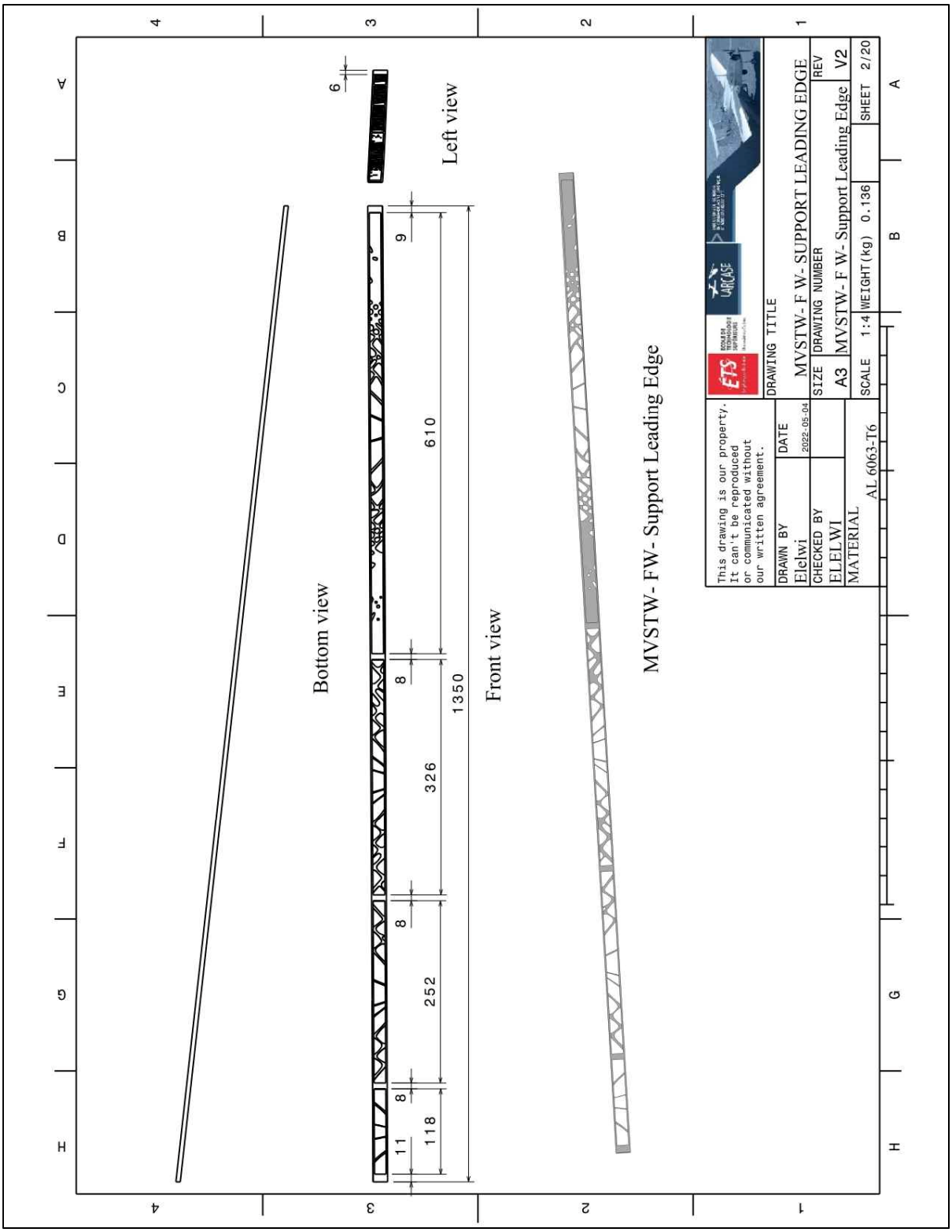

Figure-C III-28 MVSTW Fixed Wing Support Leading Edge Using Al 6063-T6

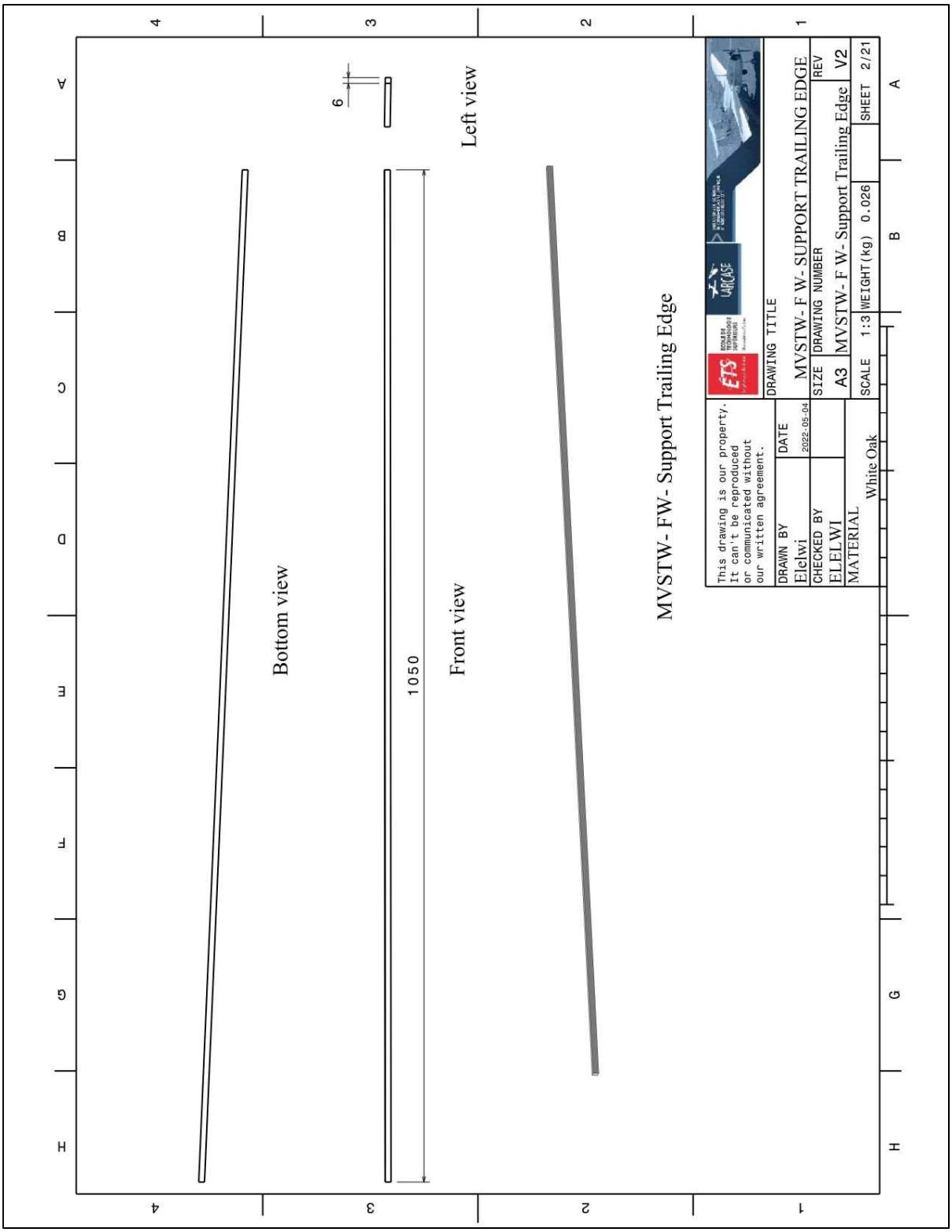

Figure-C III-29 MVSTW Fixed Wing Support Trailing Edge Using White Oak

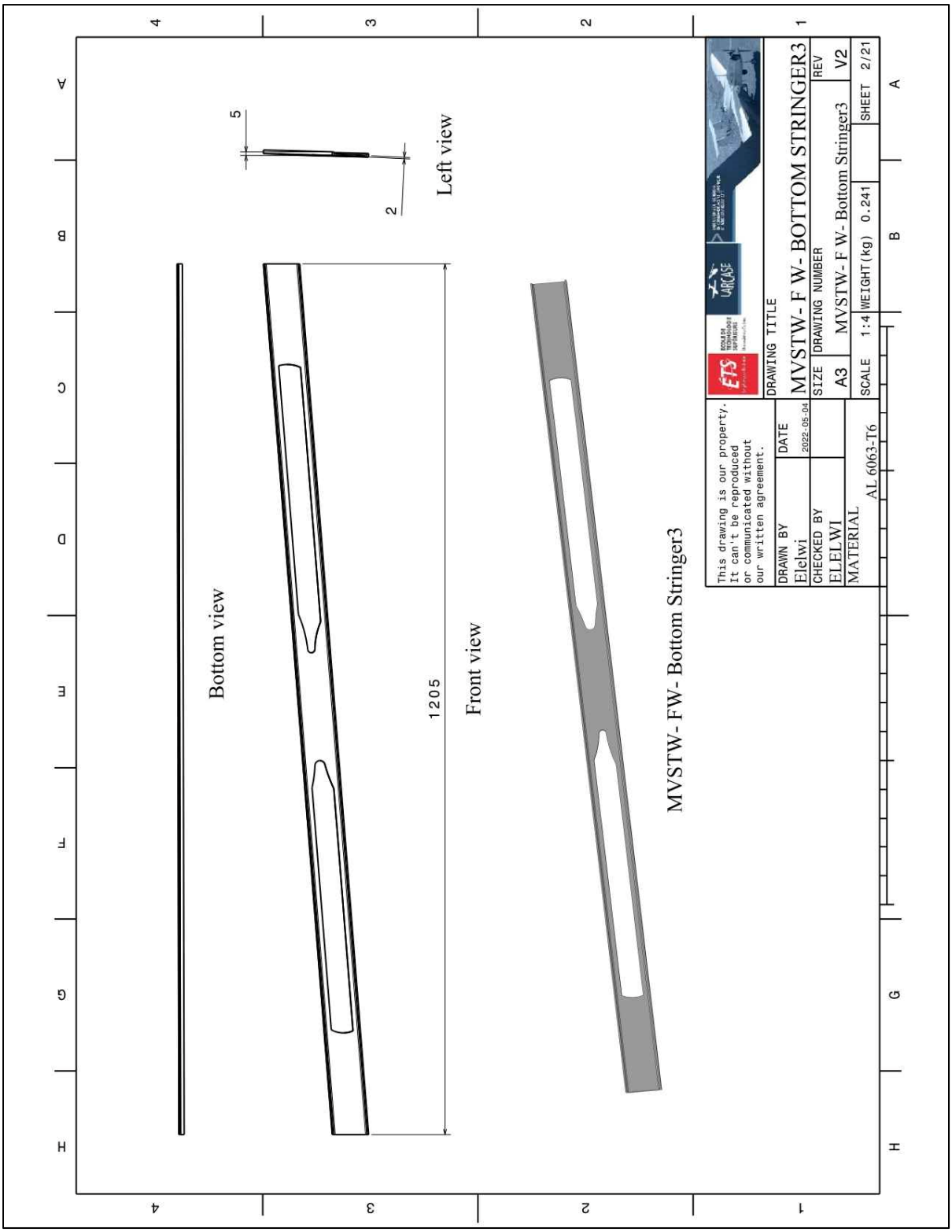

Figure-C III-30 MVSTW Fixed Wing Bottom Stringer3 Using Al 6063-T6

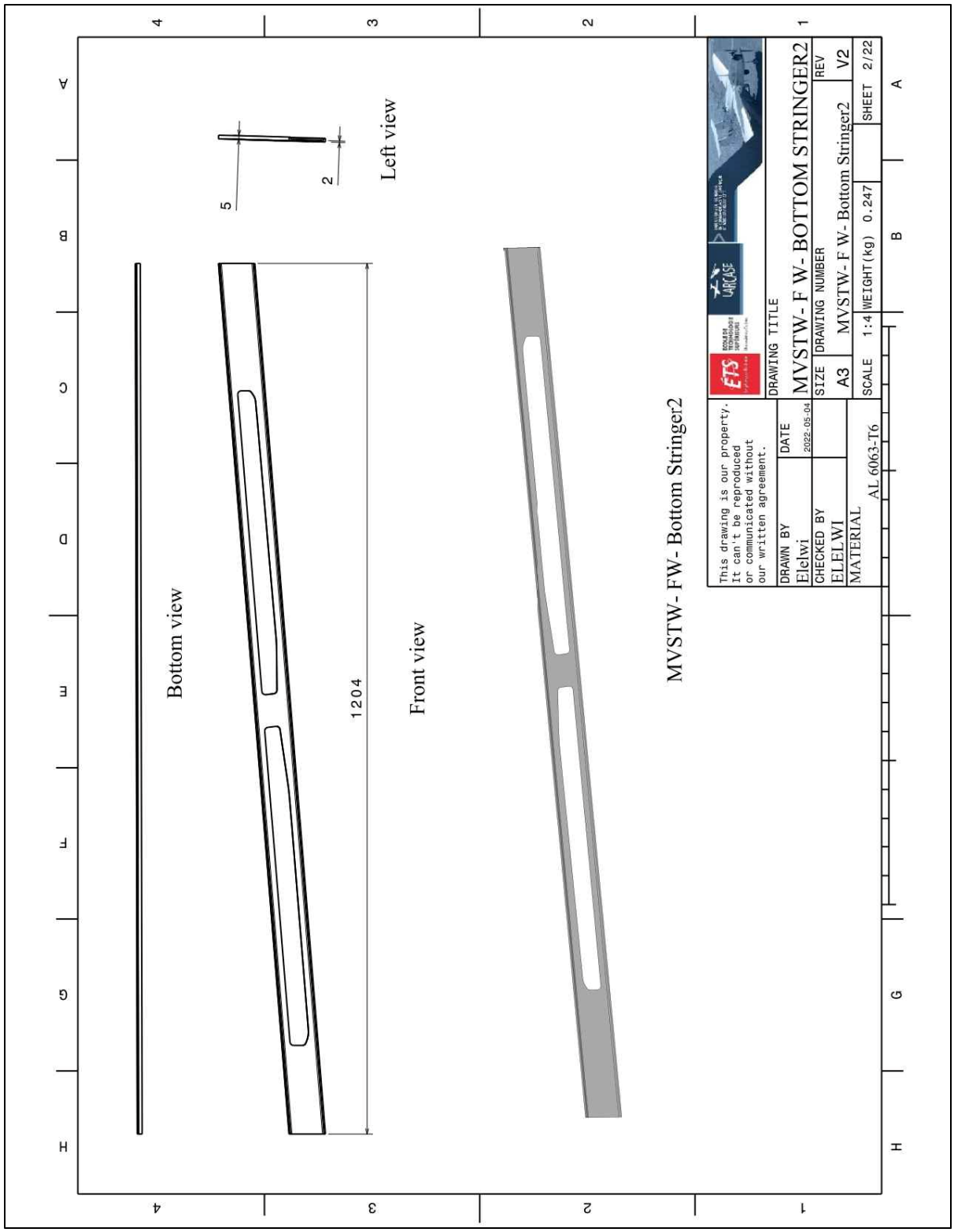

Figure-C III-31 MVSTW Fixed Wing Bottom Stringer2 Using Al 6063-T6

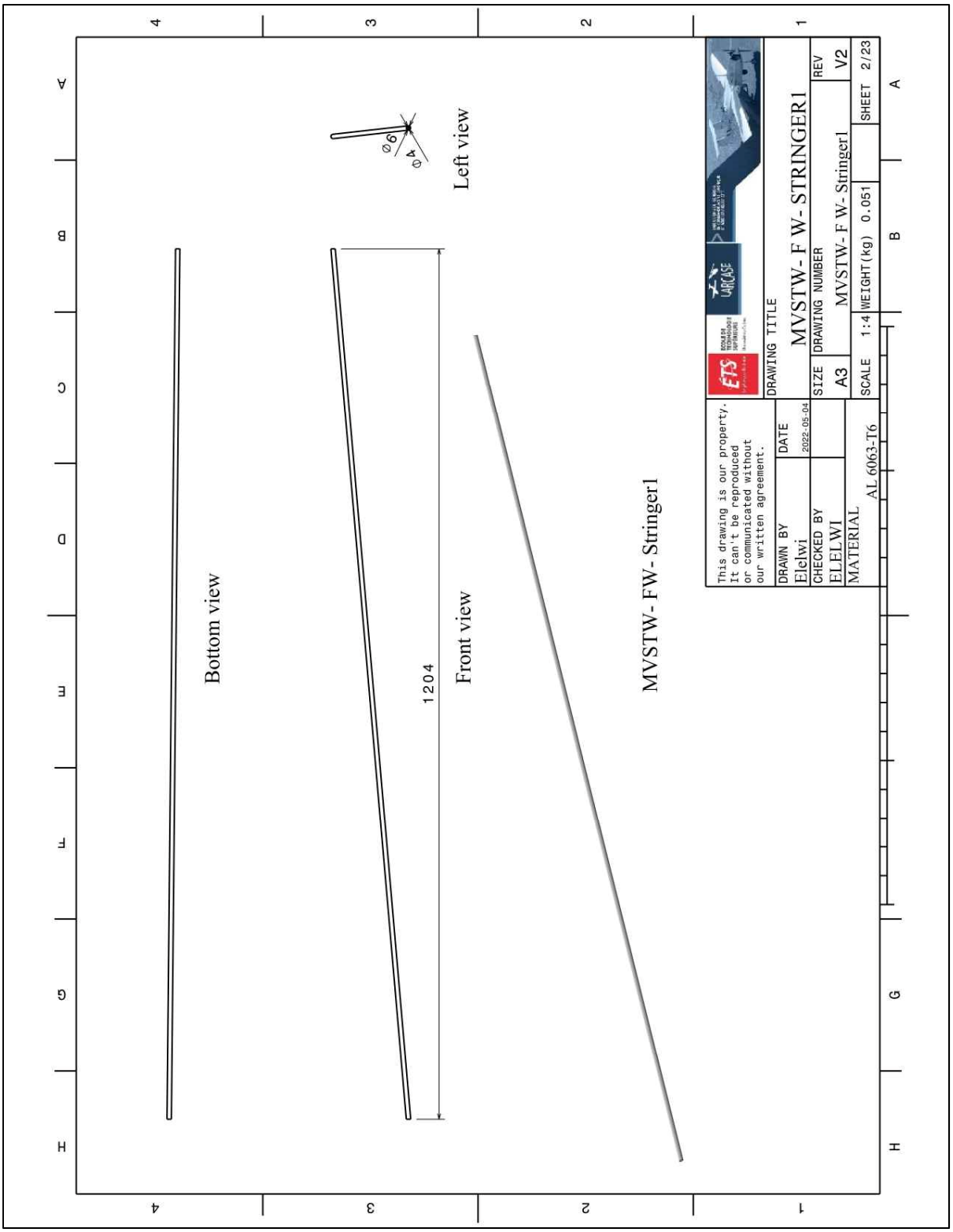

Figure-C III-32 MVSTW Fixed Wing Stringer1 Using Al 6063-T6

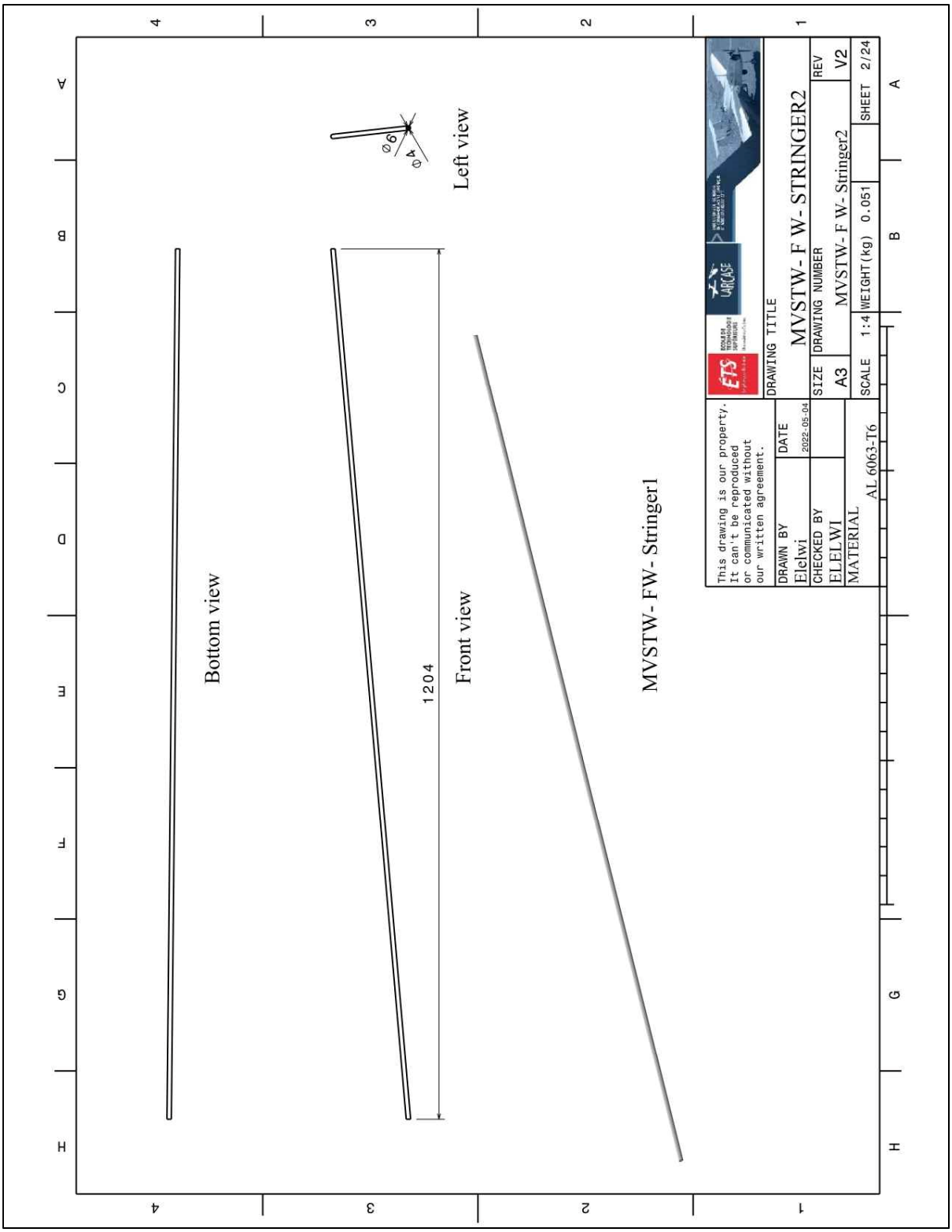

Figure-C III-33 MVSTW Fixed Wing Stringer2 Using Al 6063-T6

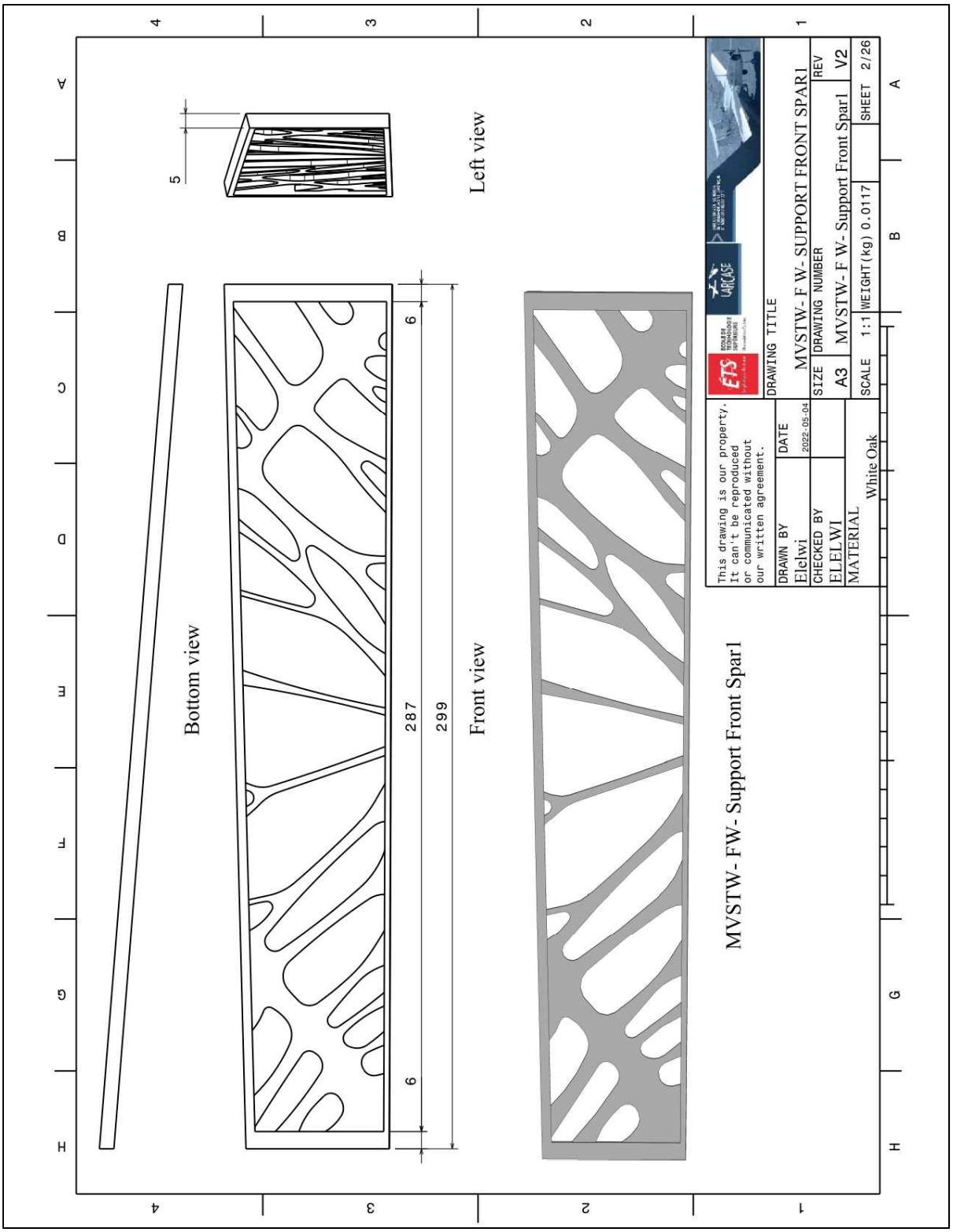

Figure-C III-34 MVSTW Fixed Wing Support front Spar1 Using White Oak

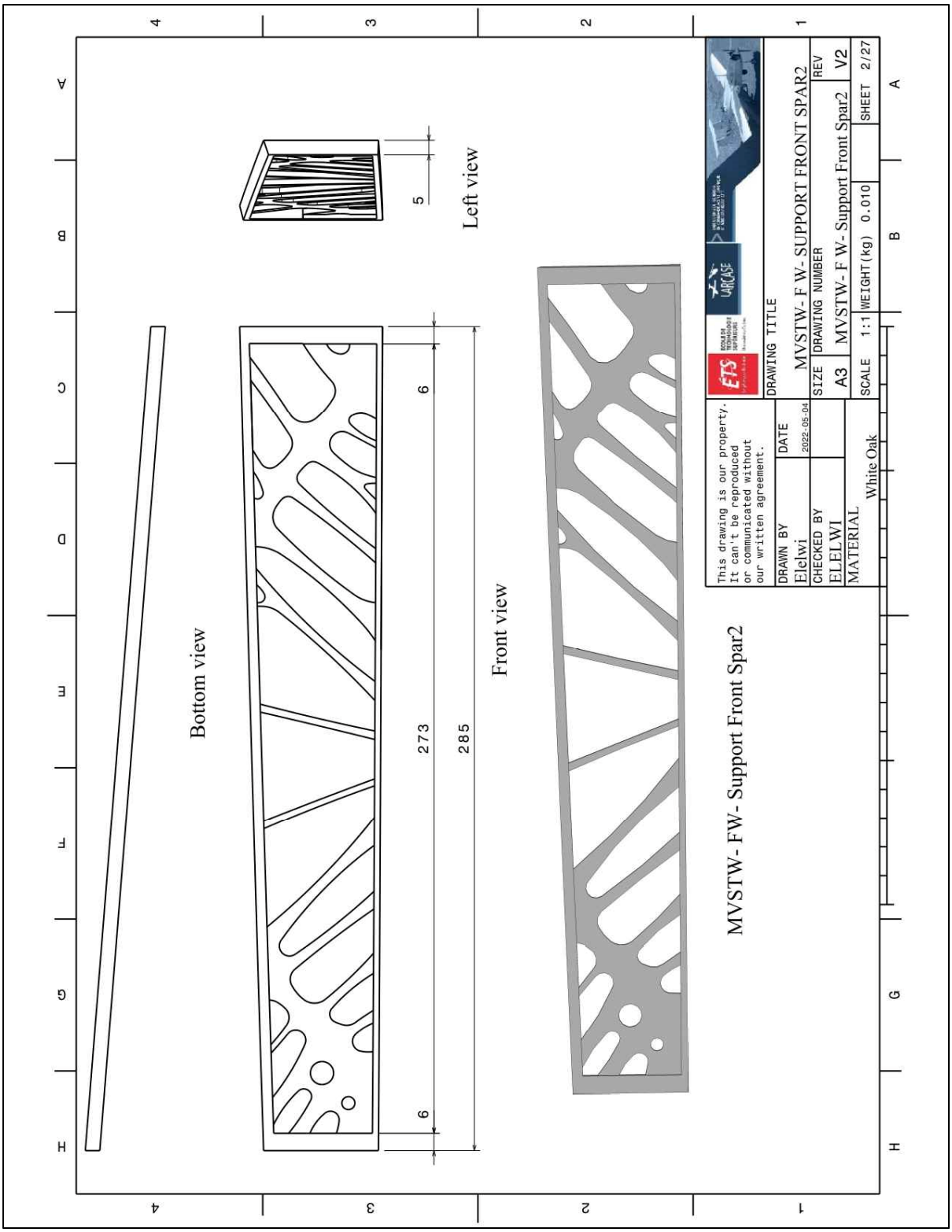

Figure-C III-35 MVSTW Fixed Wing Support Front Spar2 Using White Oak

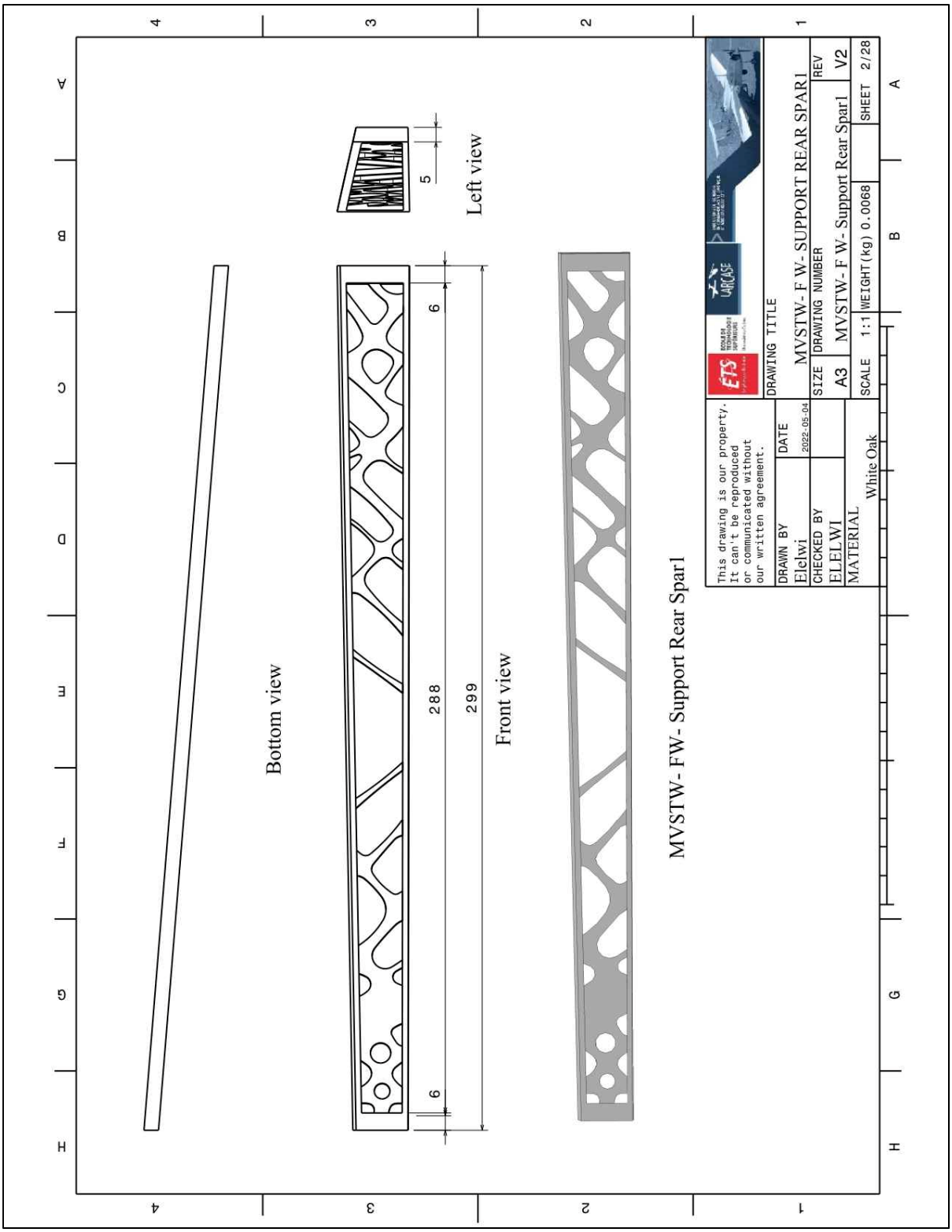

Figure-C III-36 MVSTW Fixed Wing Support Rear Spar1 Using White Oak

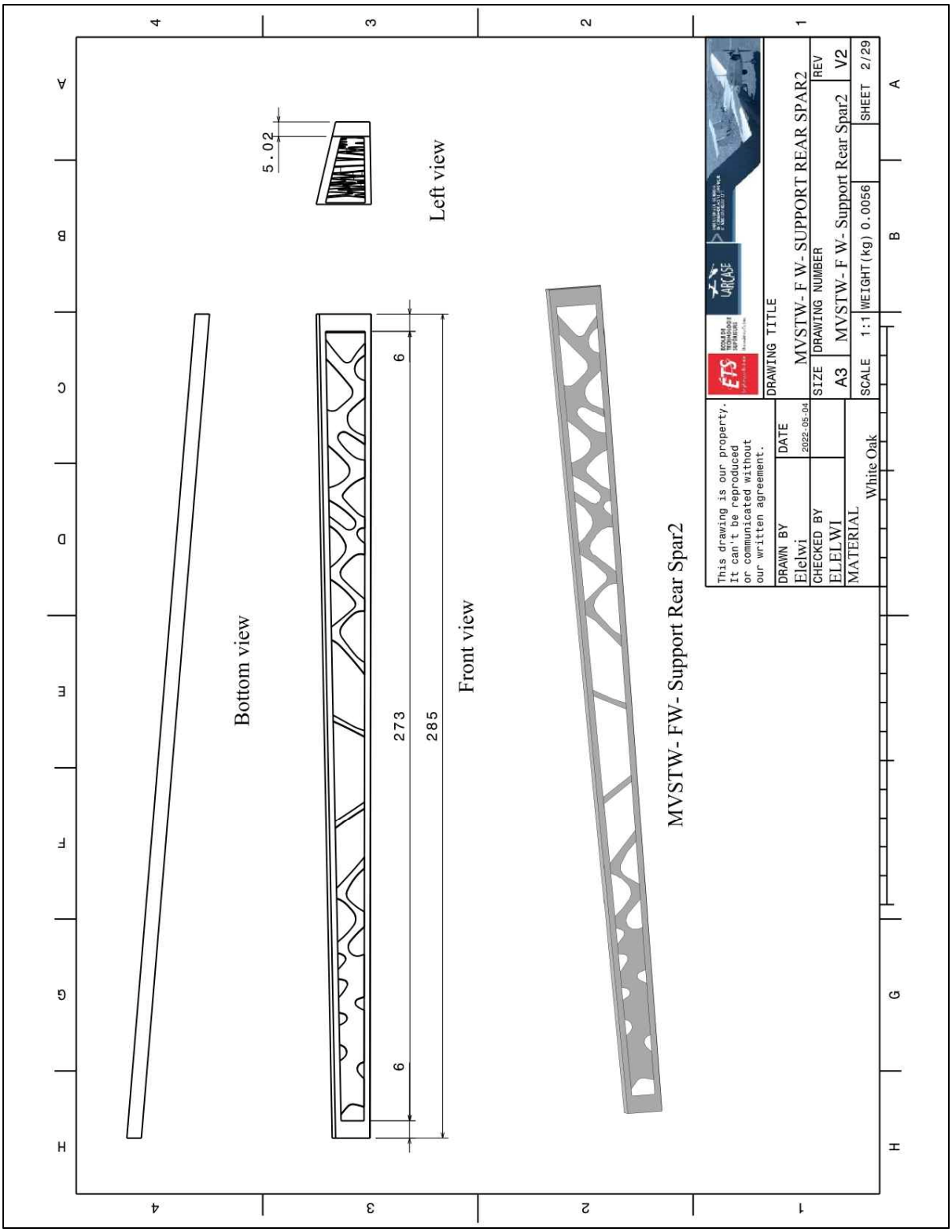

Figure-C III-37 MVSTW Fixed Wing Support Rear Spar2 Using White Oak

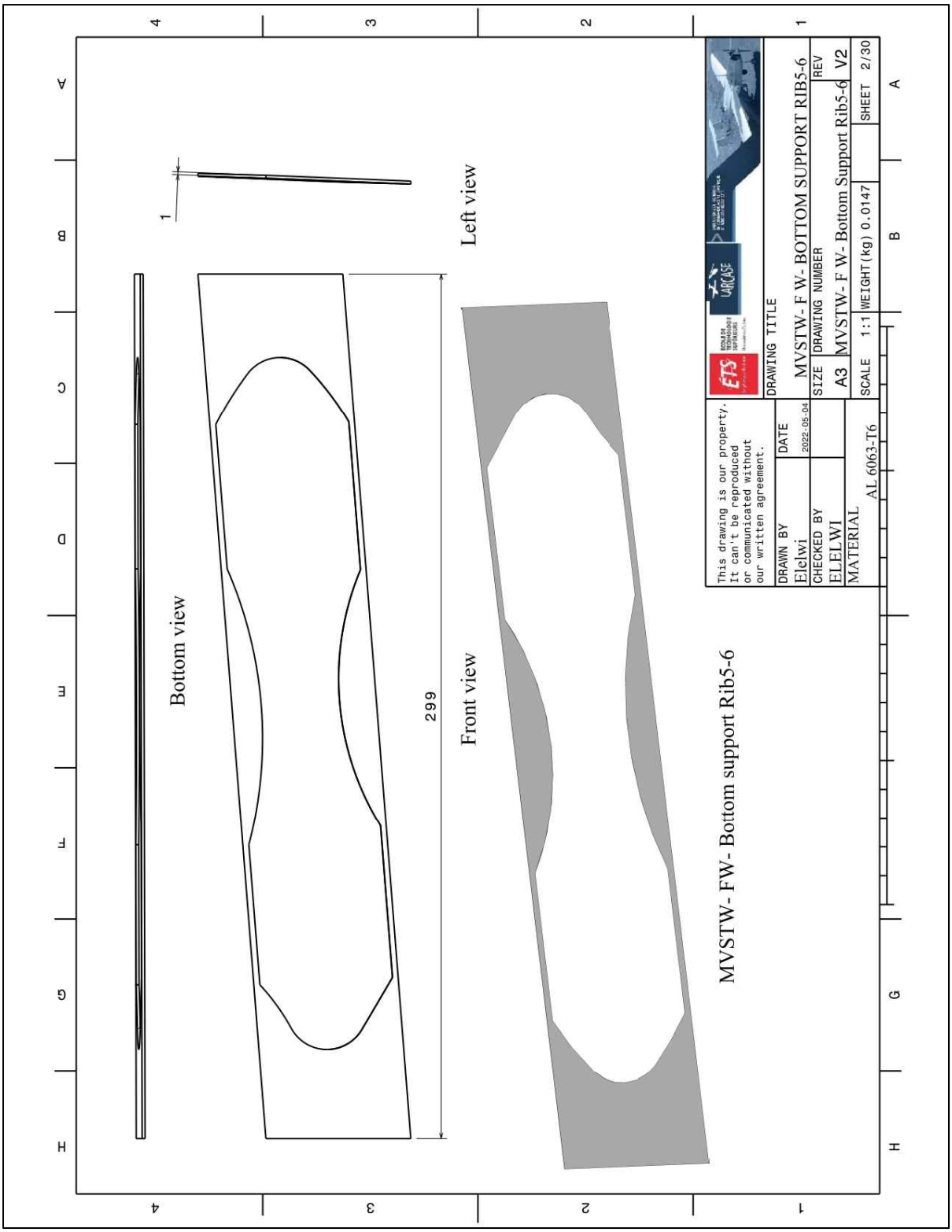

Figure-C III-38 MVSTW Fixed Wing Bottom Support Rib 5-6 Using Al 6063-T6

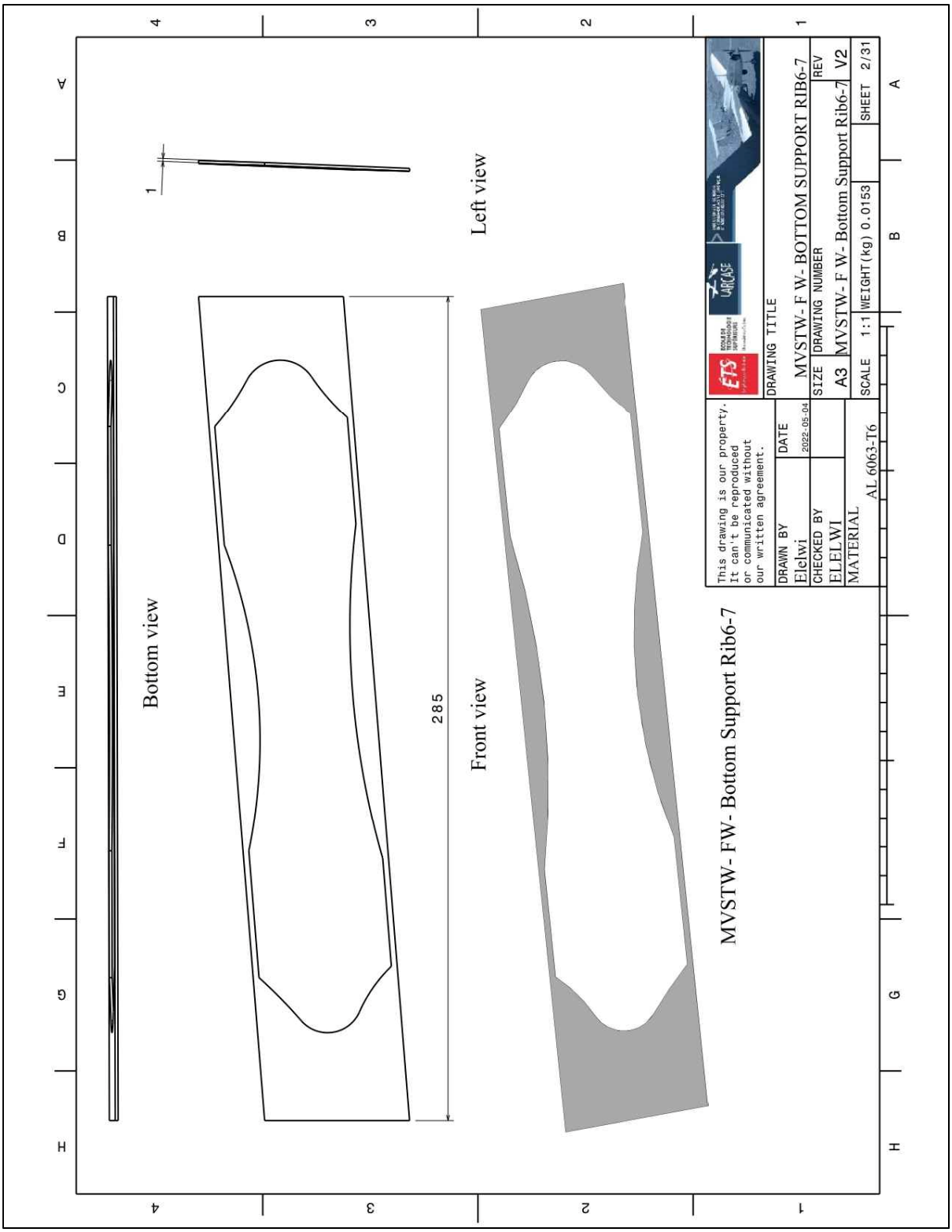

Figure-C III-39 MVSTW Fixed Wing Bottom Support Rib 6-7 Using Al 6063-T6

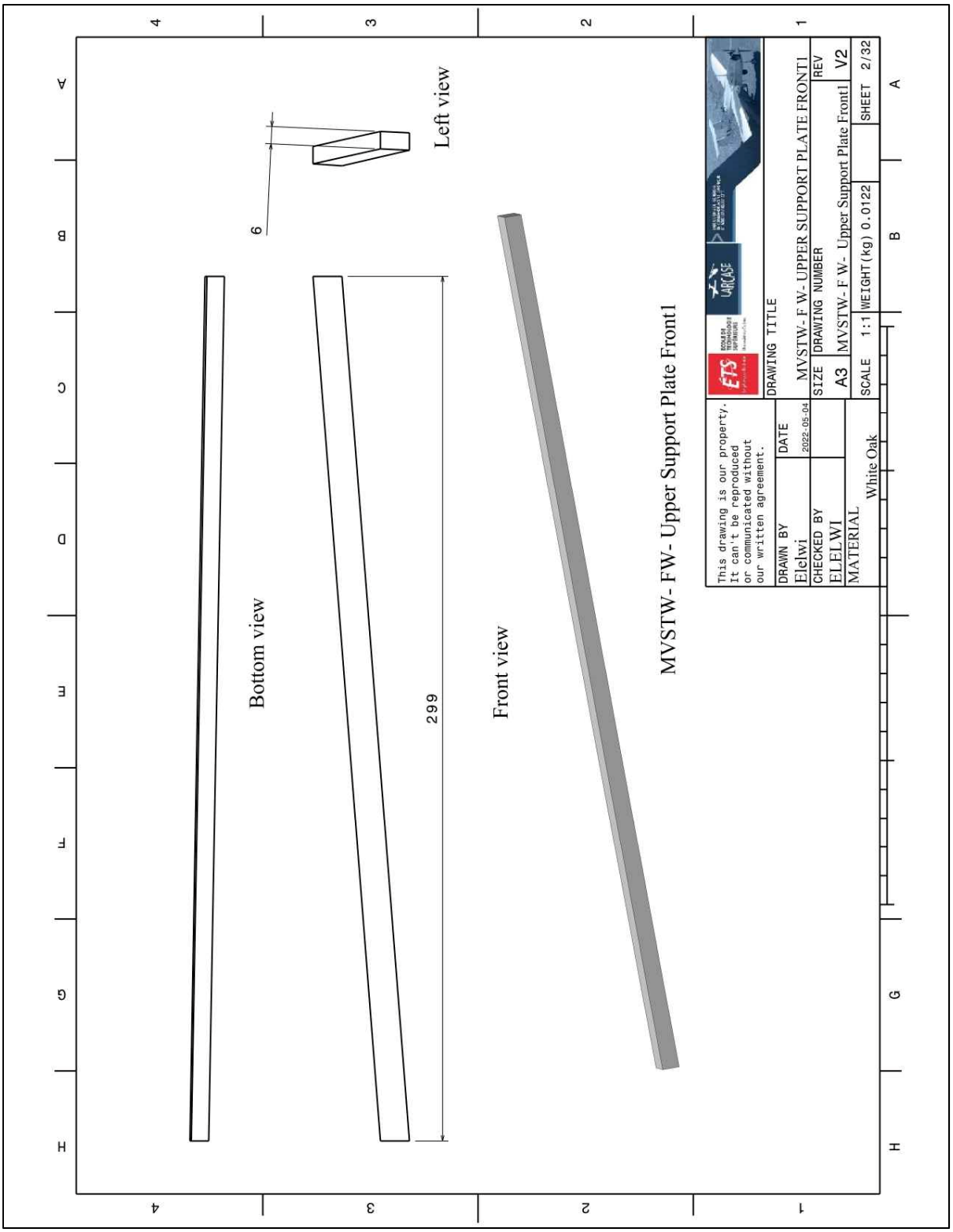

Figure-C III-40 MVSTW Fixed Wing Upper Support Plate Front1 Using White Oak

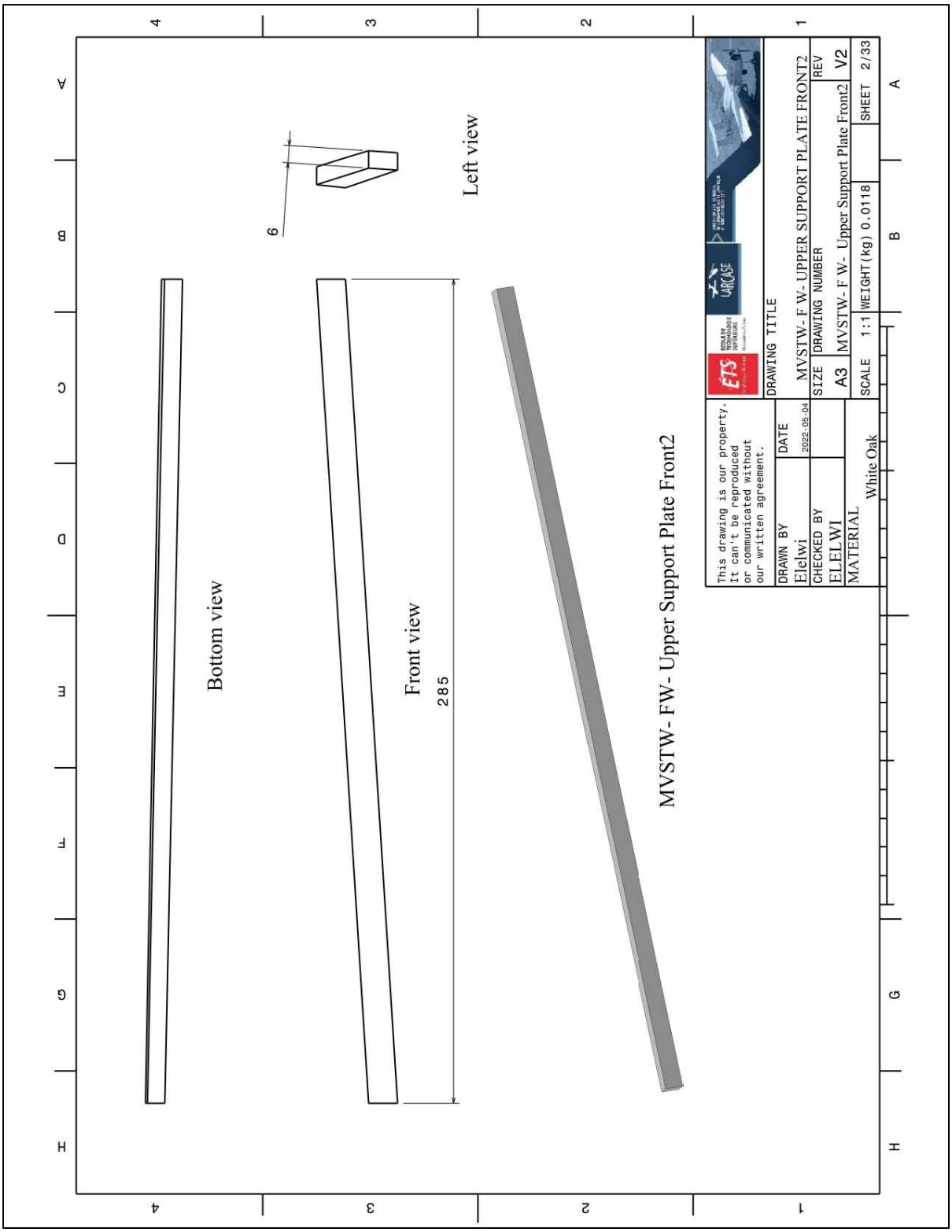

Figure-C III-41 MVSTW Fixed Wing Upper Support plate Front2 Using White Oak

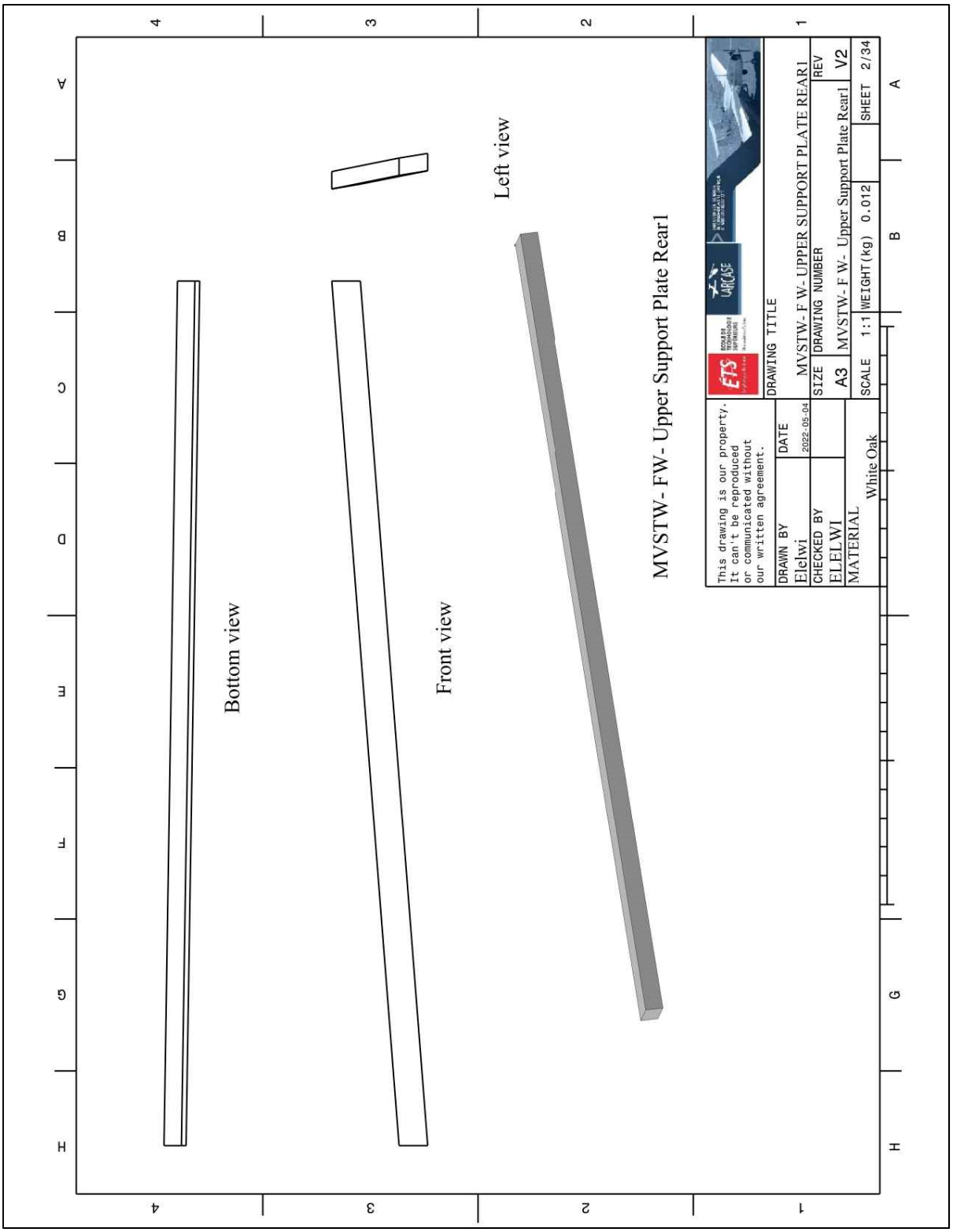

Figure-C III-42 MVSTW Fixed Wing Upper Support Plate Rear1 Using White Oak

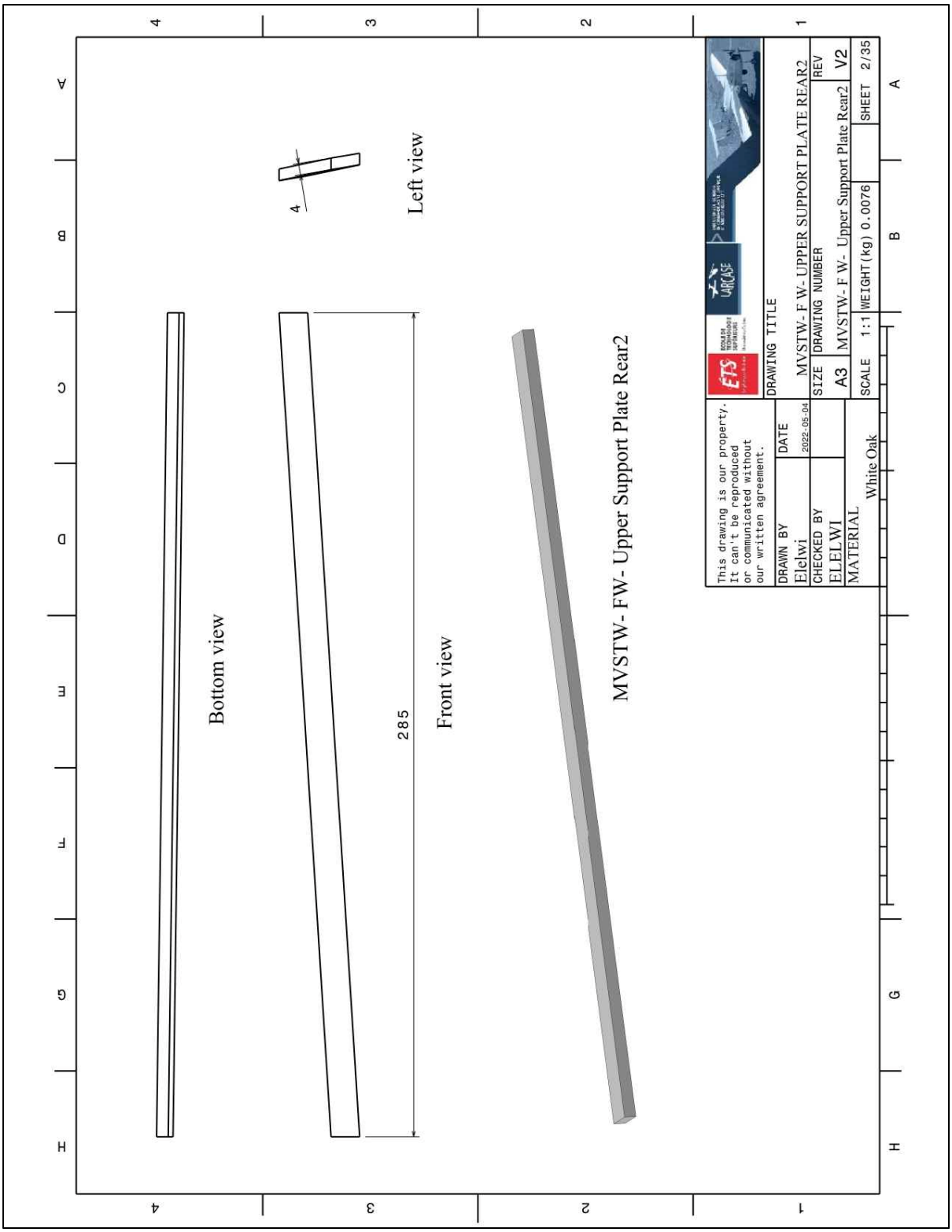

Figure-C III-43 MVSTW Fixed Wing Upper Support Plate Rear2 Using White Oak

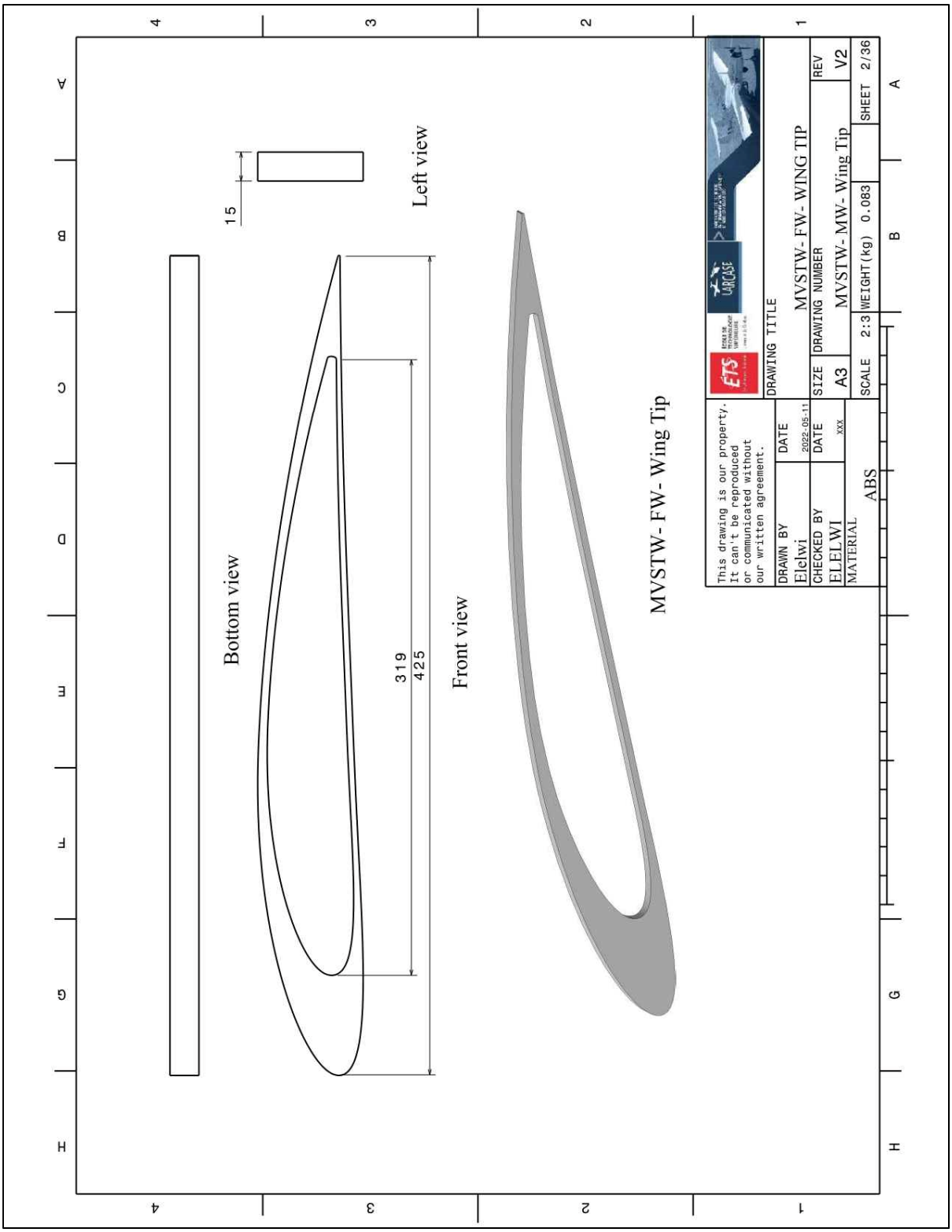

Figure-C III-44 MVSTW Fixed Wing- Wing Tip Using ABS

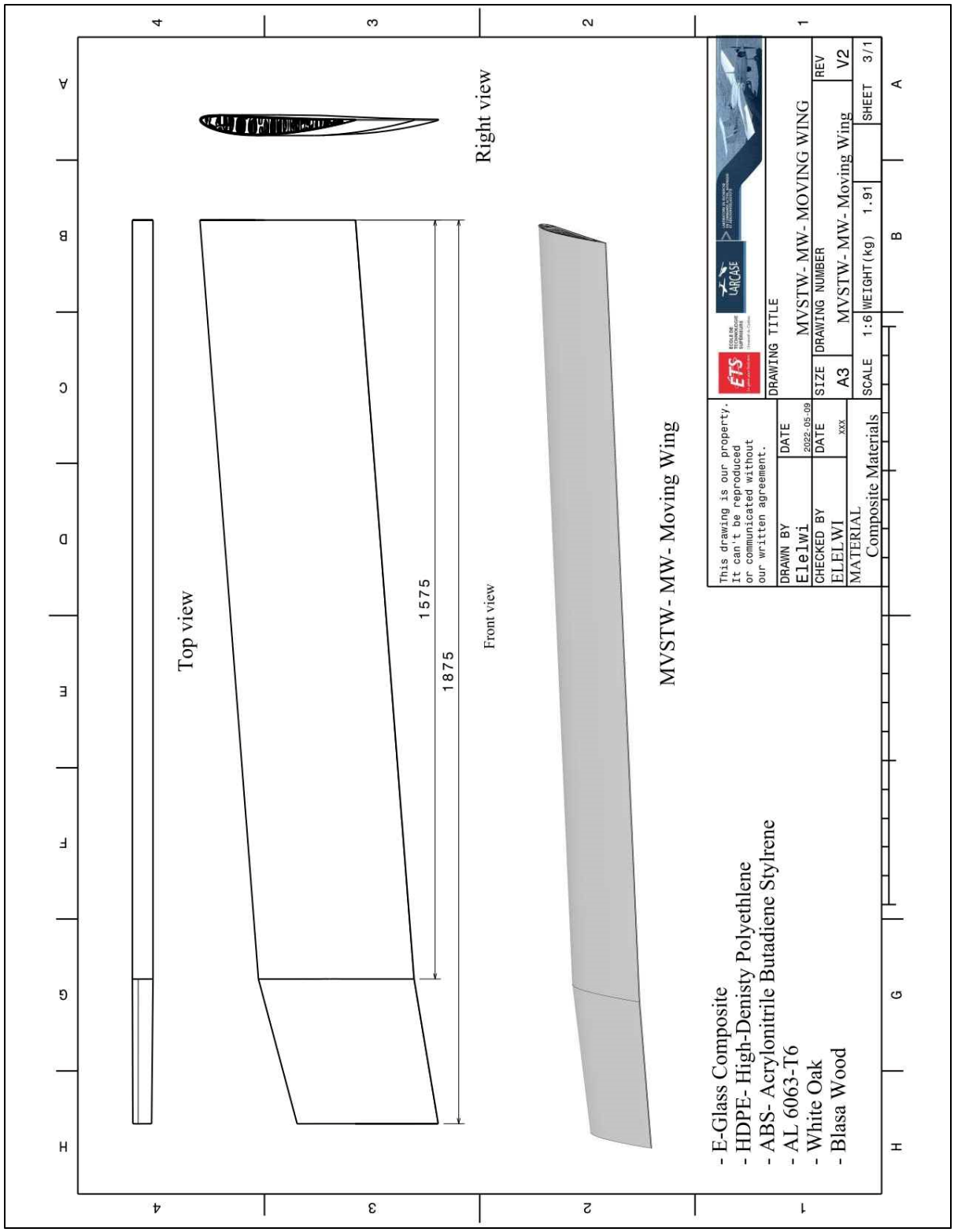

Figure-C III-45 MVSTW Moving Wing Using Composite Materials

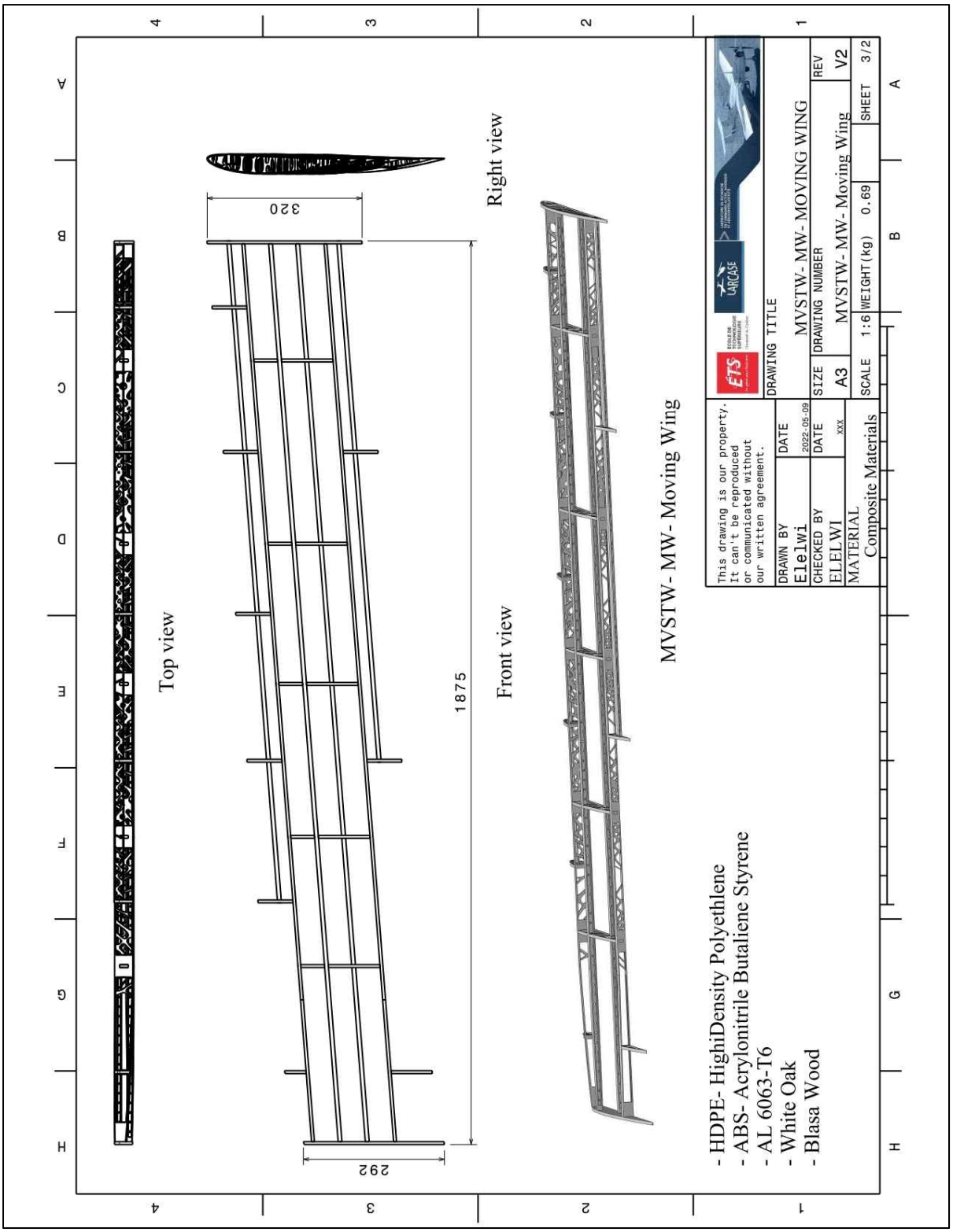

Figure-C III-46 MVSTW Moving Wing Skeleton Using Composite Materials

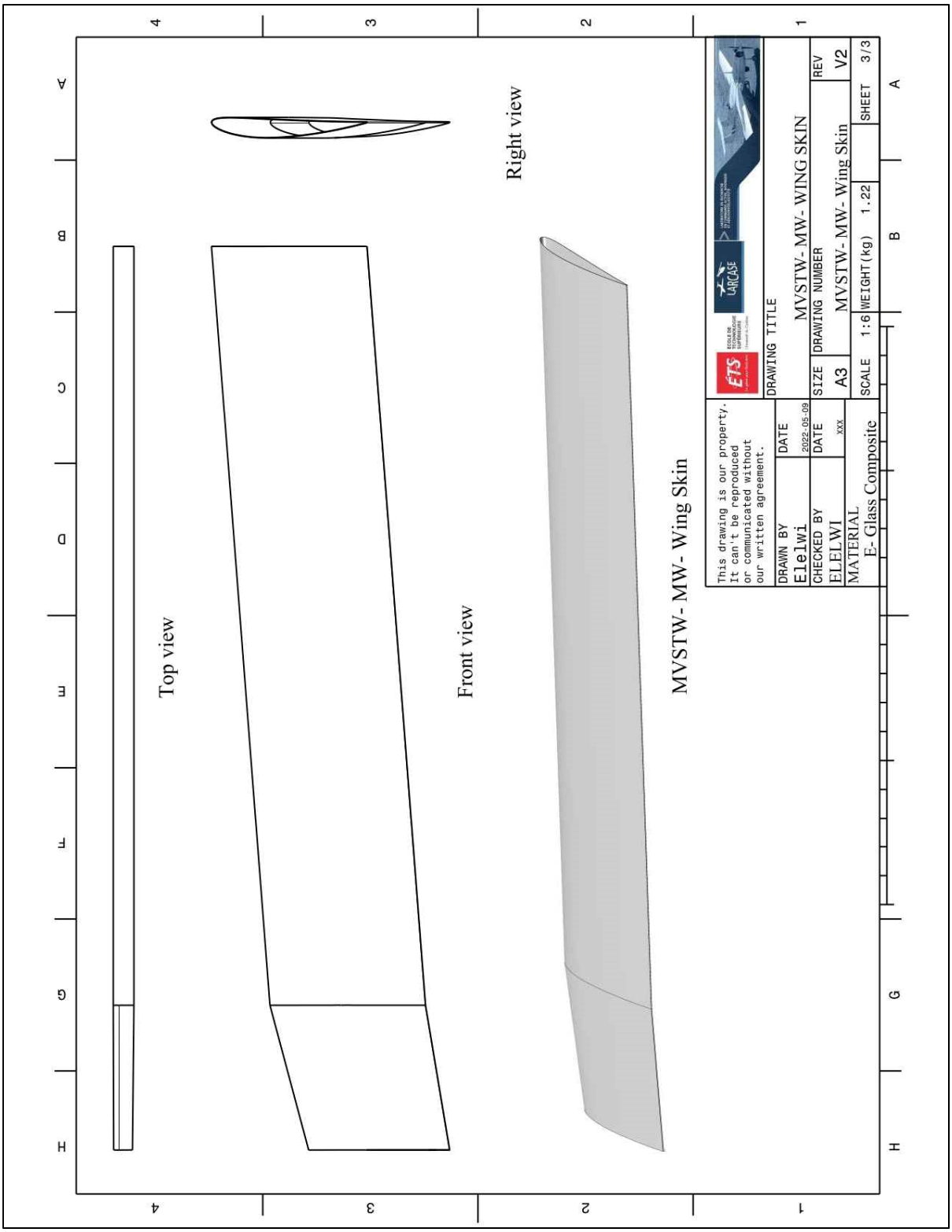

Figure-C III-47 MVSTW Moving Wing Skin Using E-Glass Composite

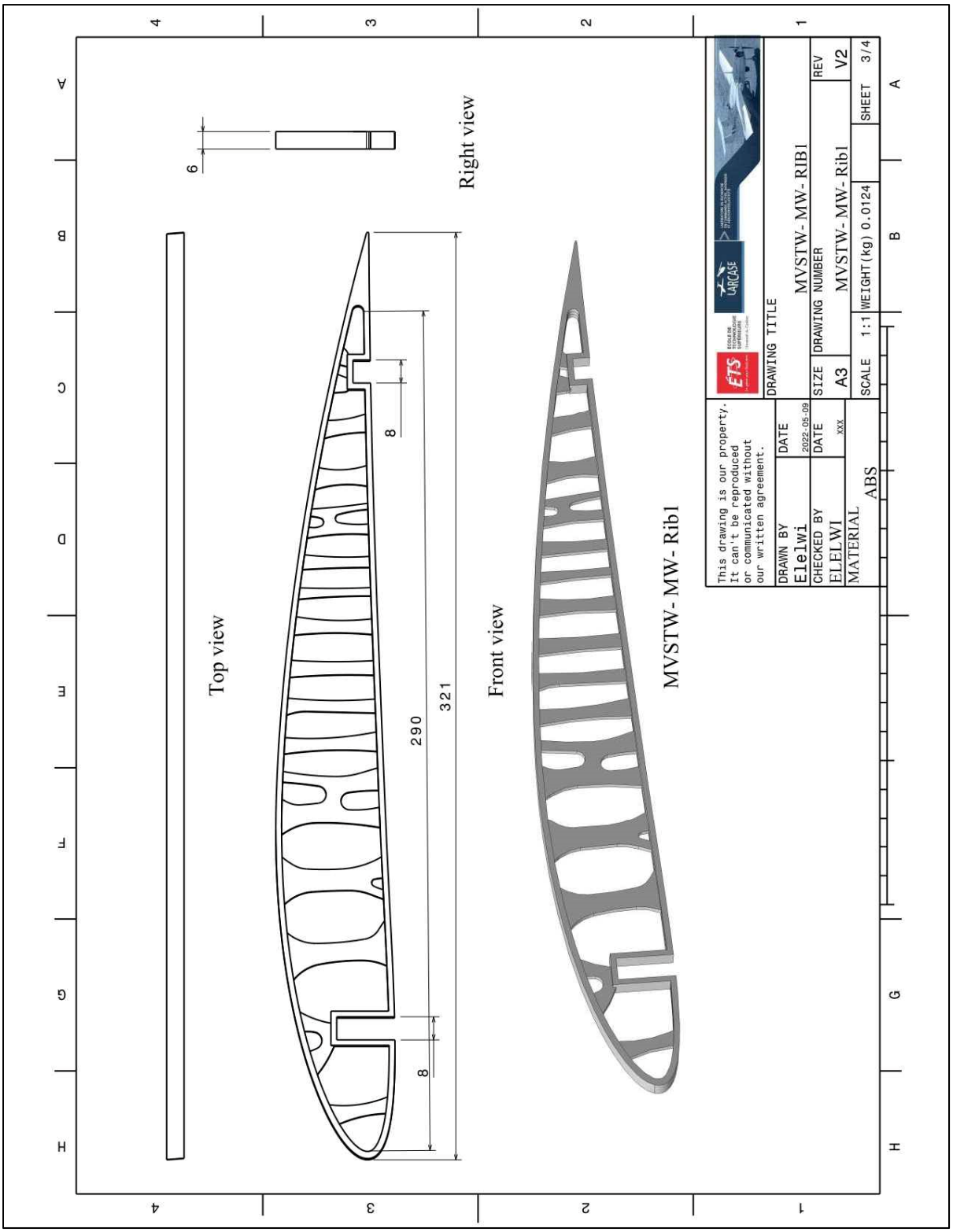

Figure-C III-48 MVSTW Moving Rib1 Wing Using ABS

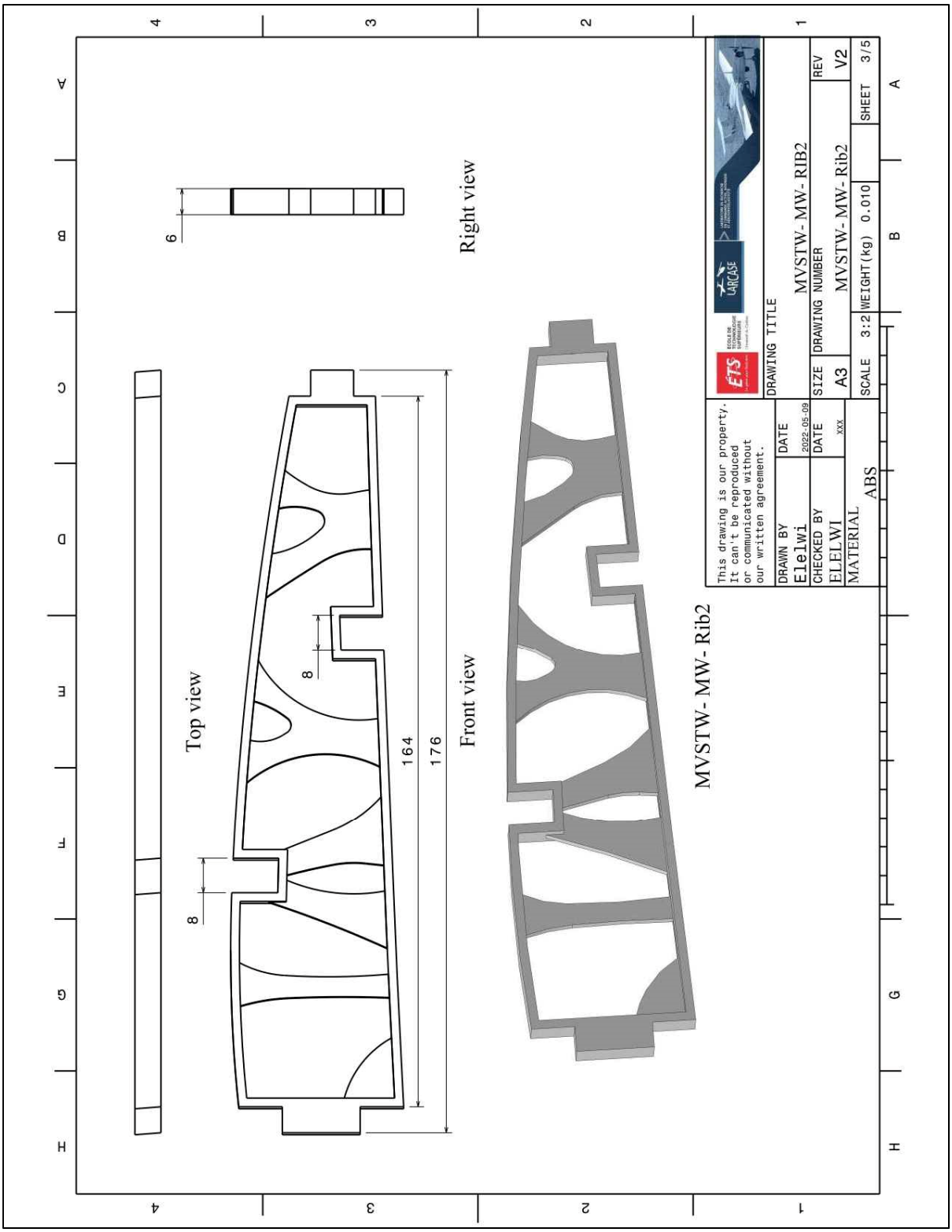

Figure-C III-49 MVSTW Moving Rib2 Wing Using ABS

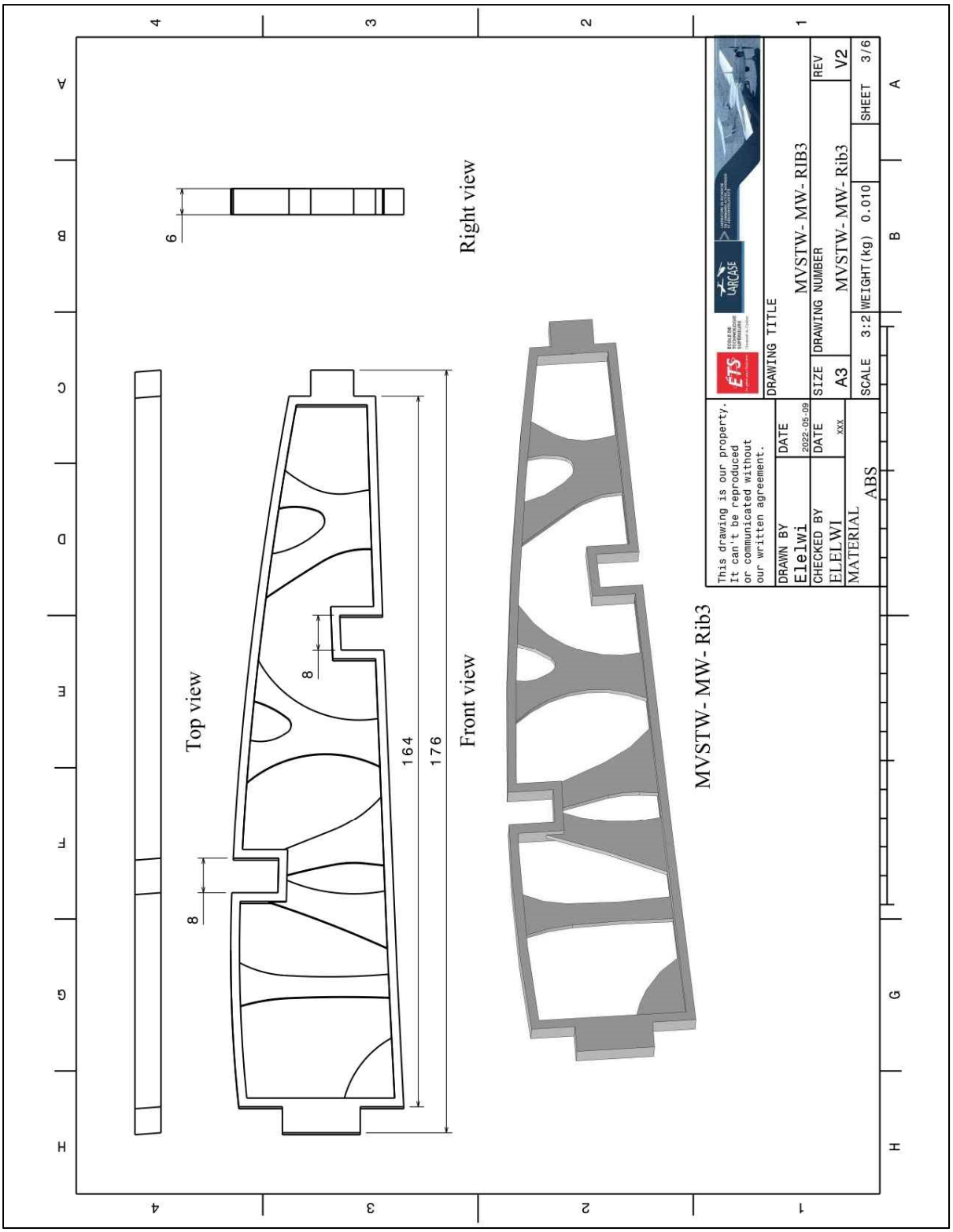

Figure-C III-50 MVSTW Moving Rib3 Wing Using ABS

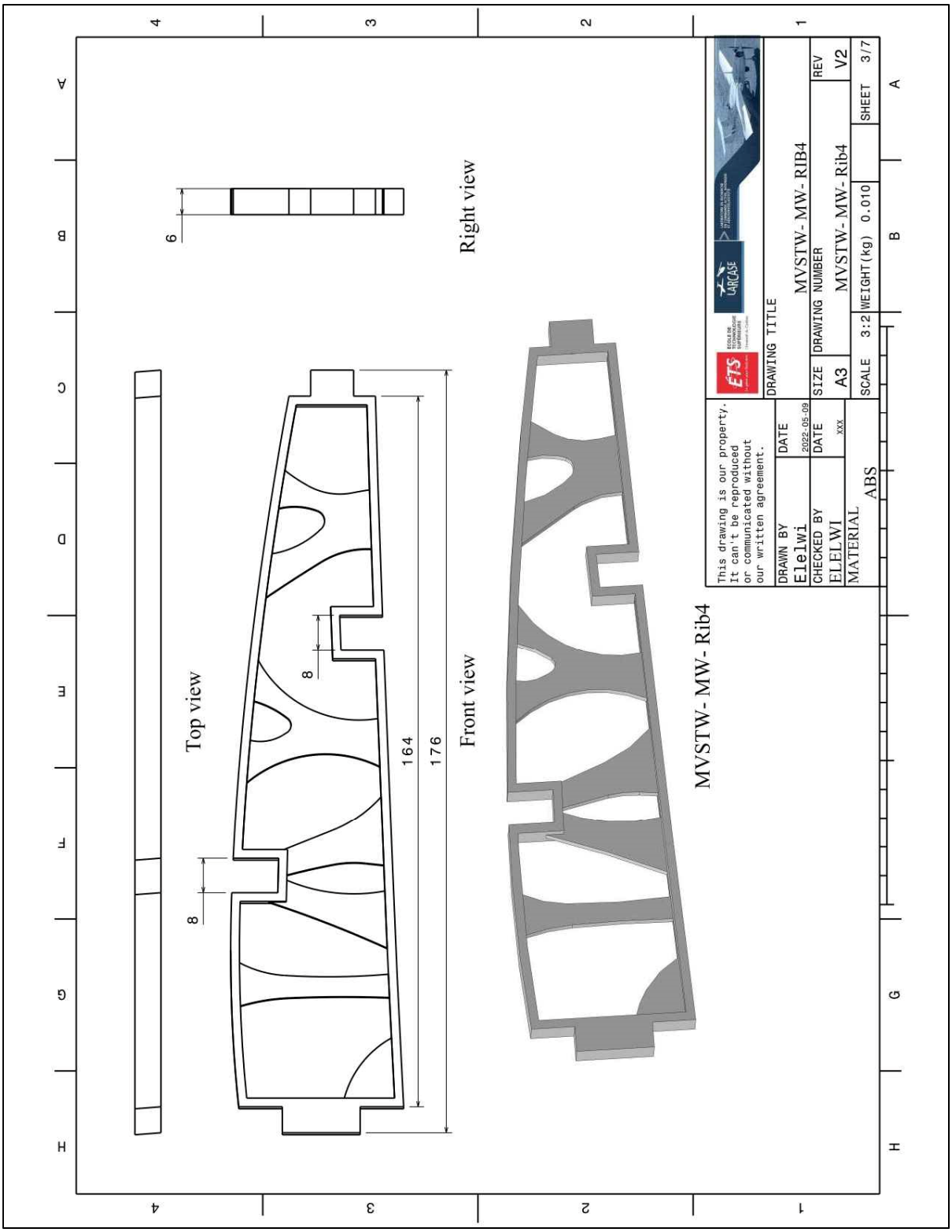

Figure-C III-51 MVSTW Moving Rib4 Wing Using ABS

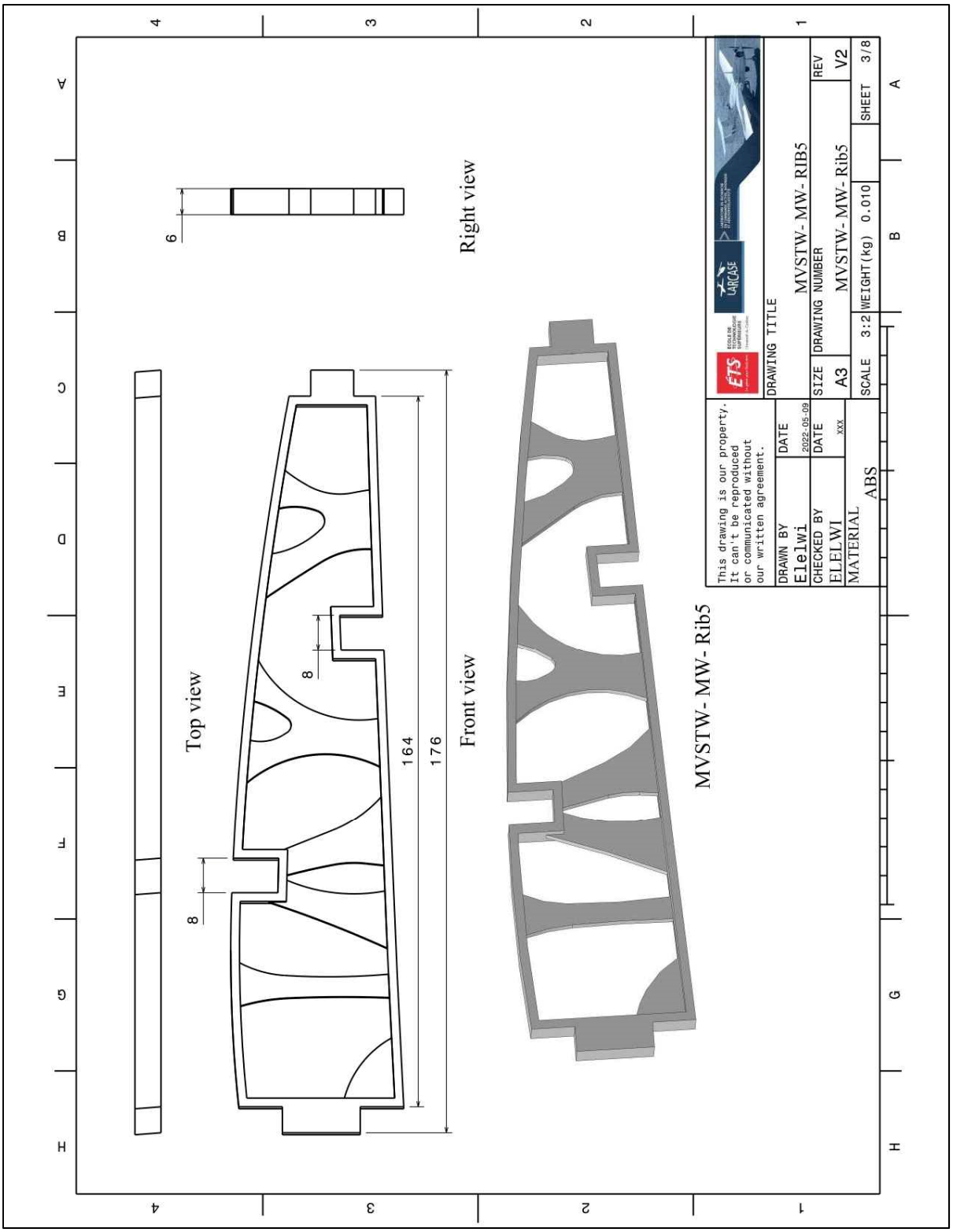

Figure-C III-52 MVSTW Moving Rib5 Wing Using ABS

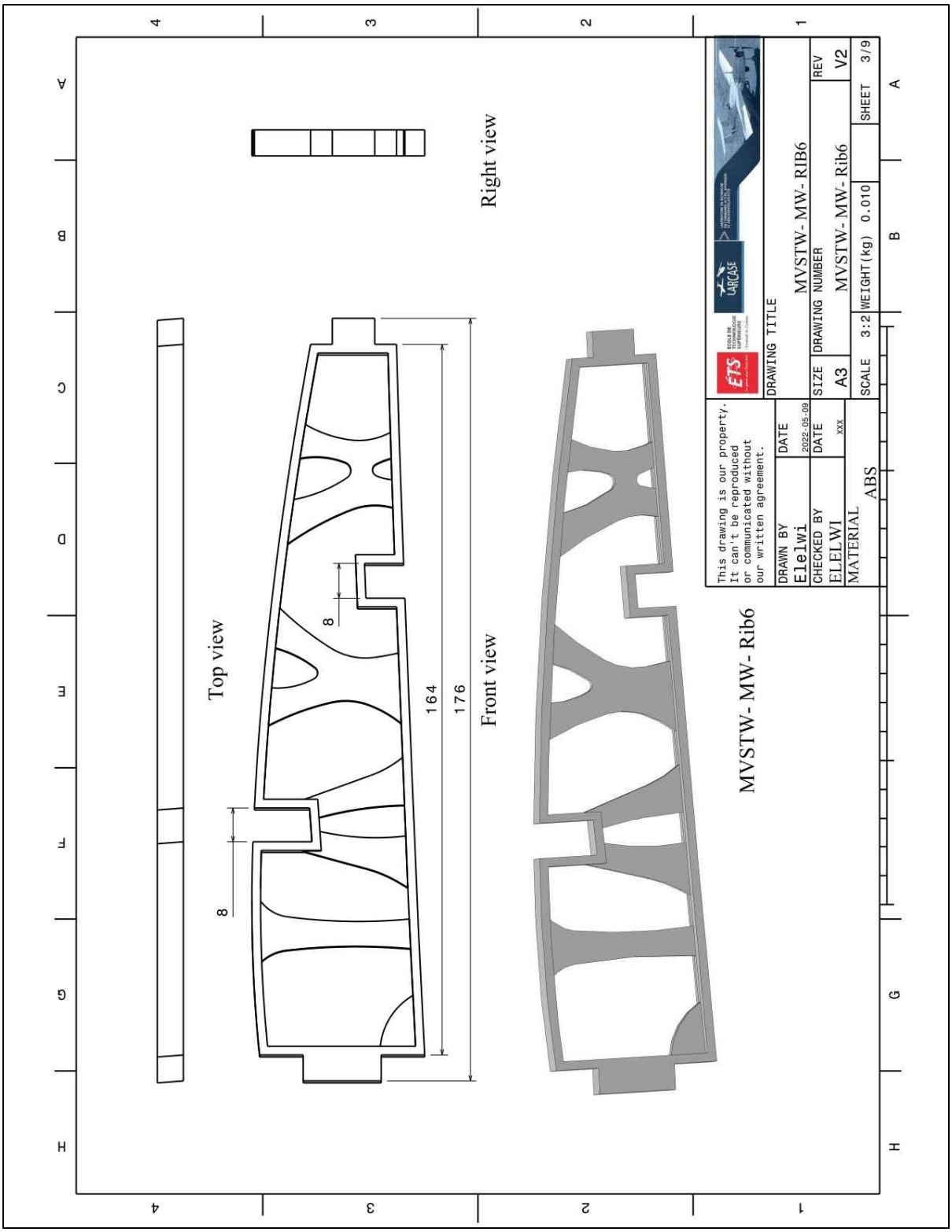

Figure-C III-53 MVSTW Moving Rib6 Wing Using ABS

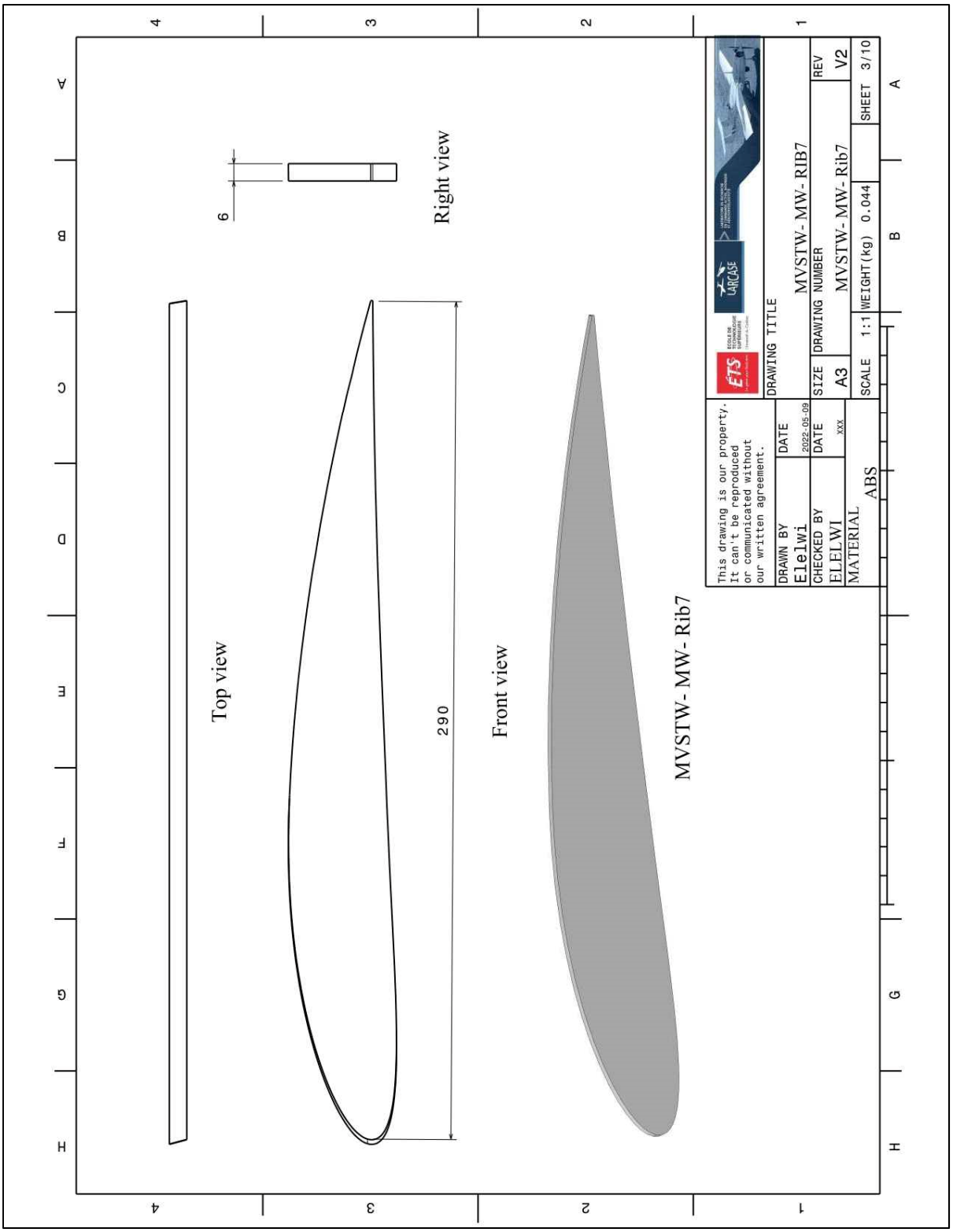

Figure-C III-54 MVSTW Moving Rib7 Wing Using ABS

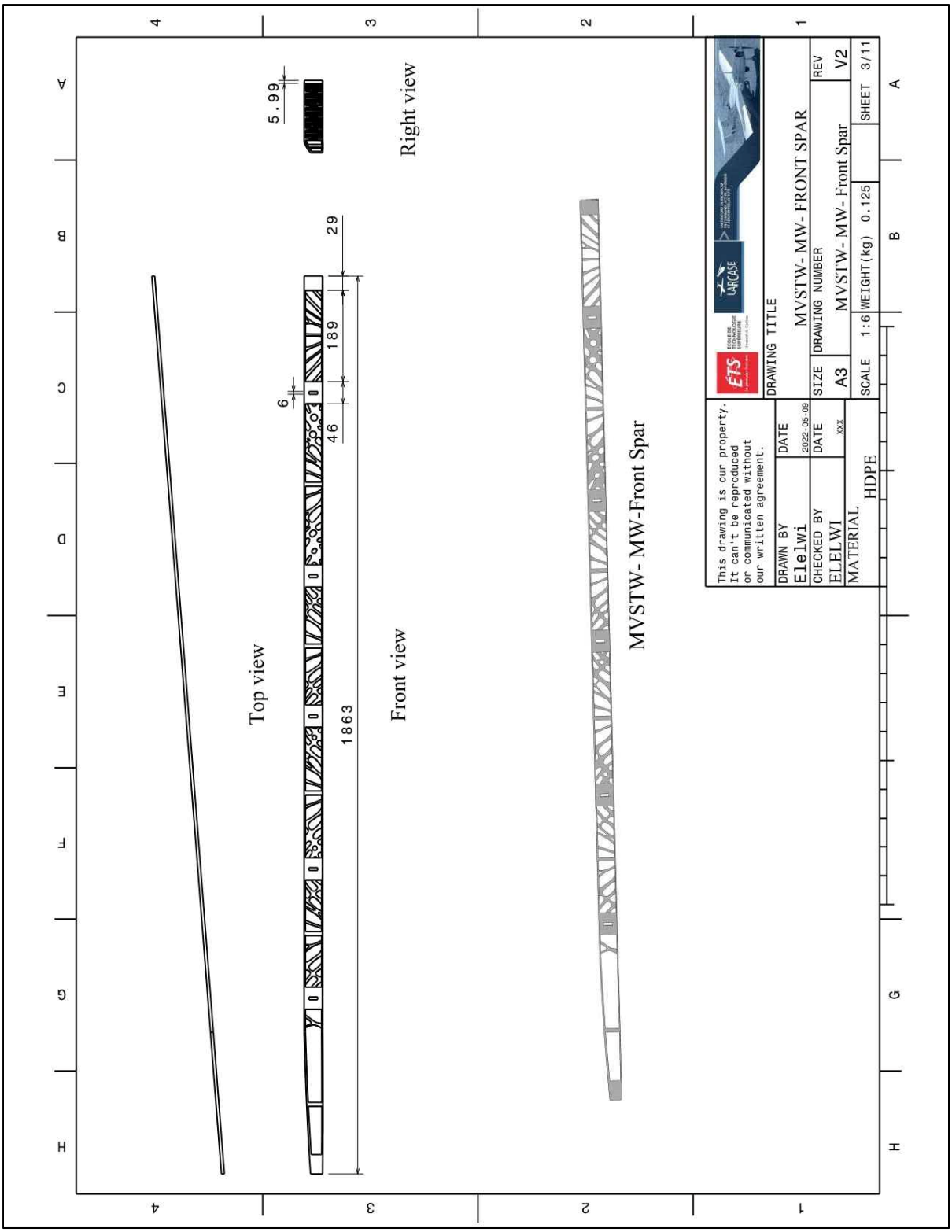

Figure-C III-55 MVSTW Moving Front Spar Wing Using HDPE

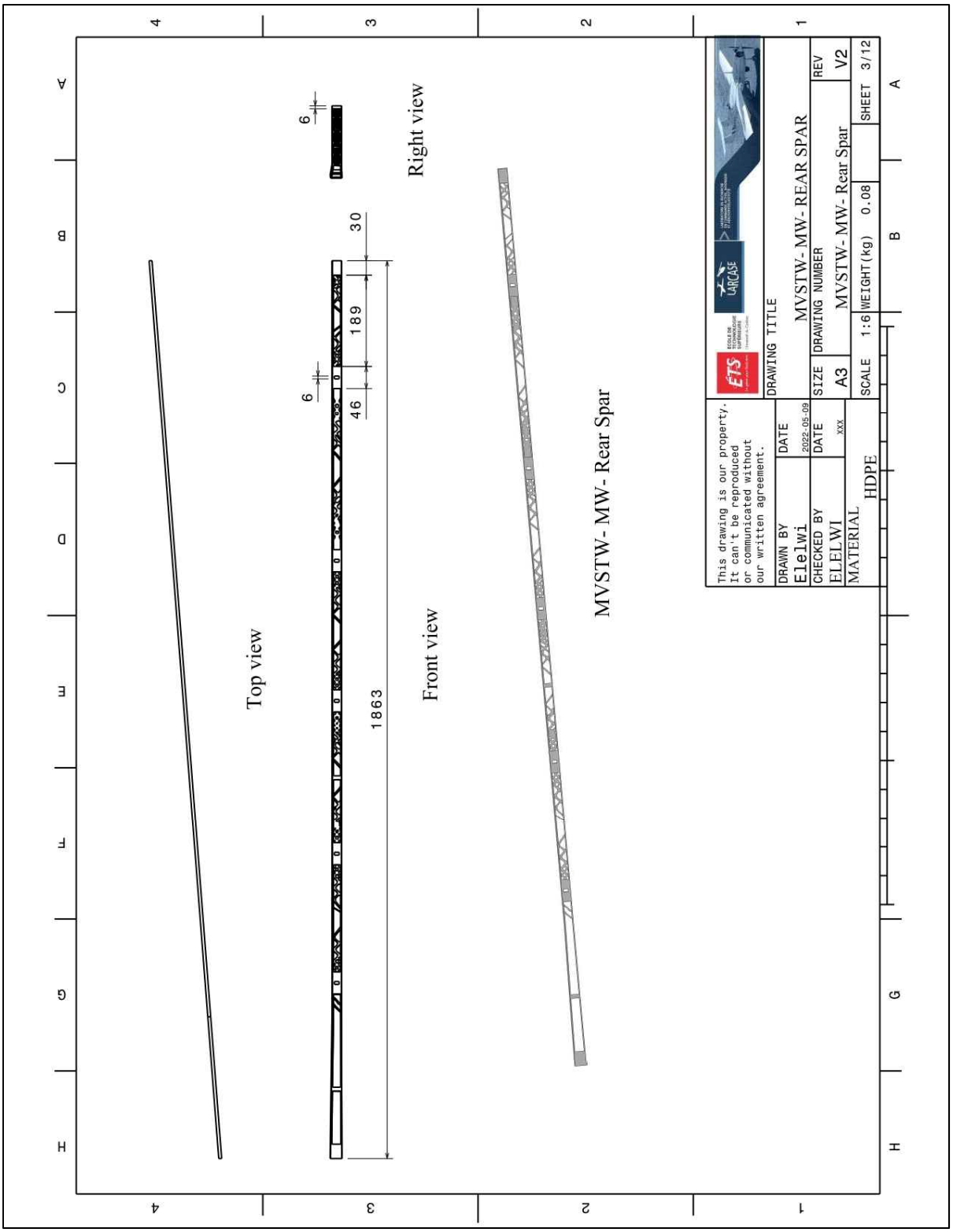

Figure-C III-56 MVSTW Moving Rear Spar Wing Using HDPE

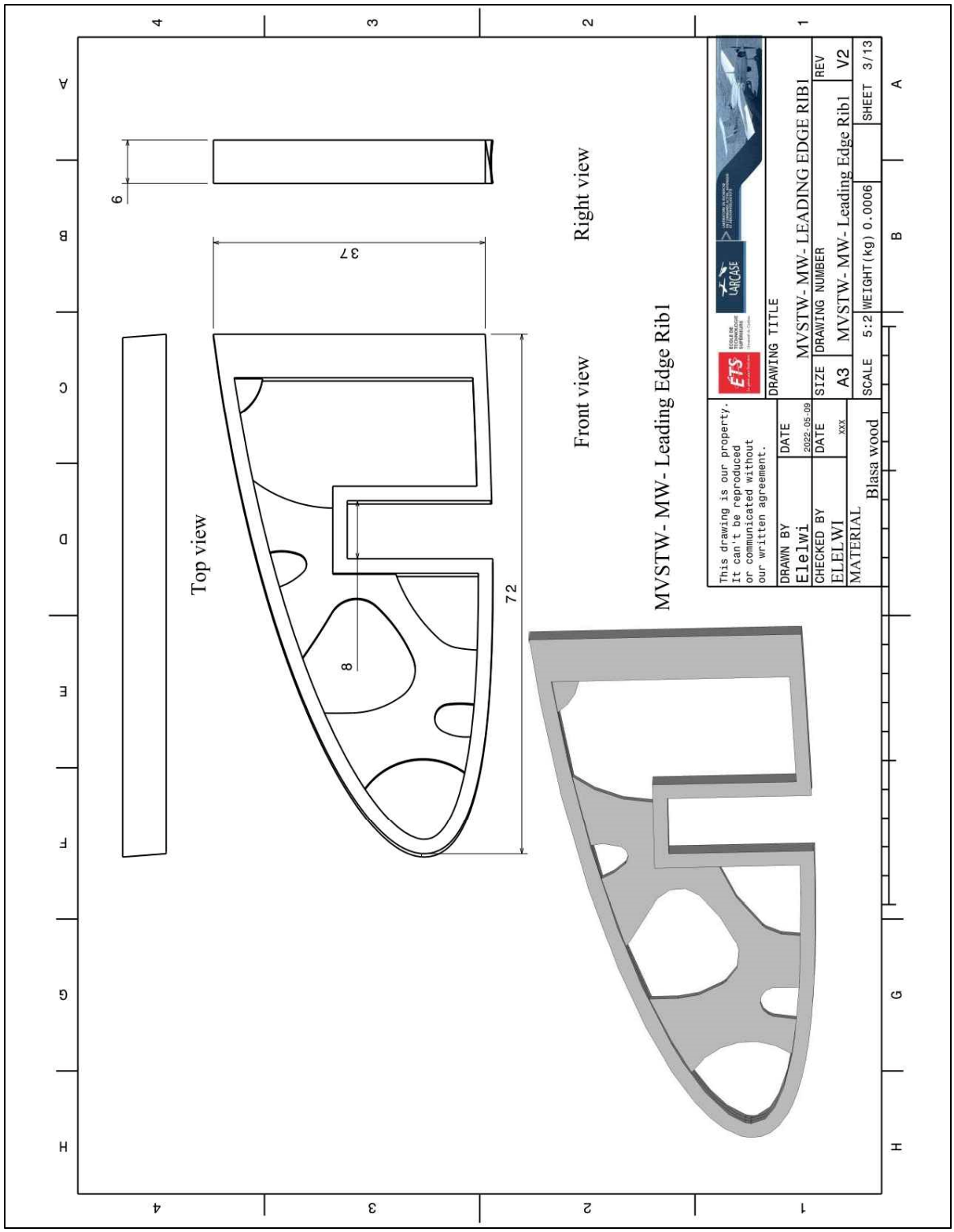

Figure-C III-57 MVSTW Moving Leading Edge Rib1 Wing Using Balsa Wood

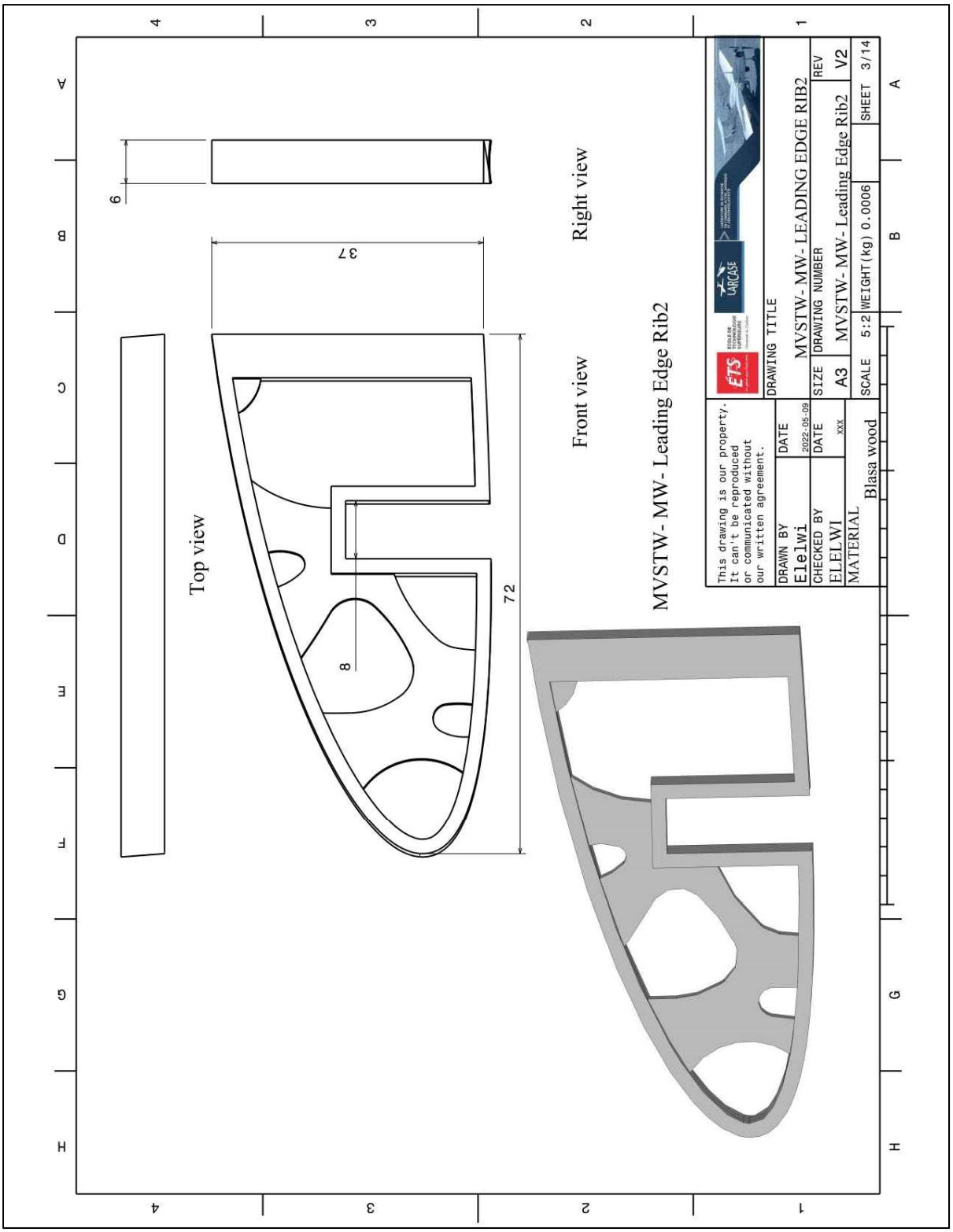

Figure-C III-58 Moving Leading Edge Rib2 Wing Using Balsa Wood

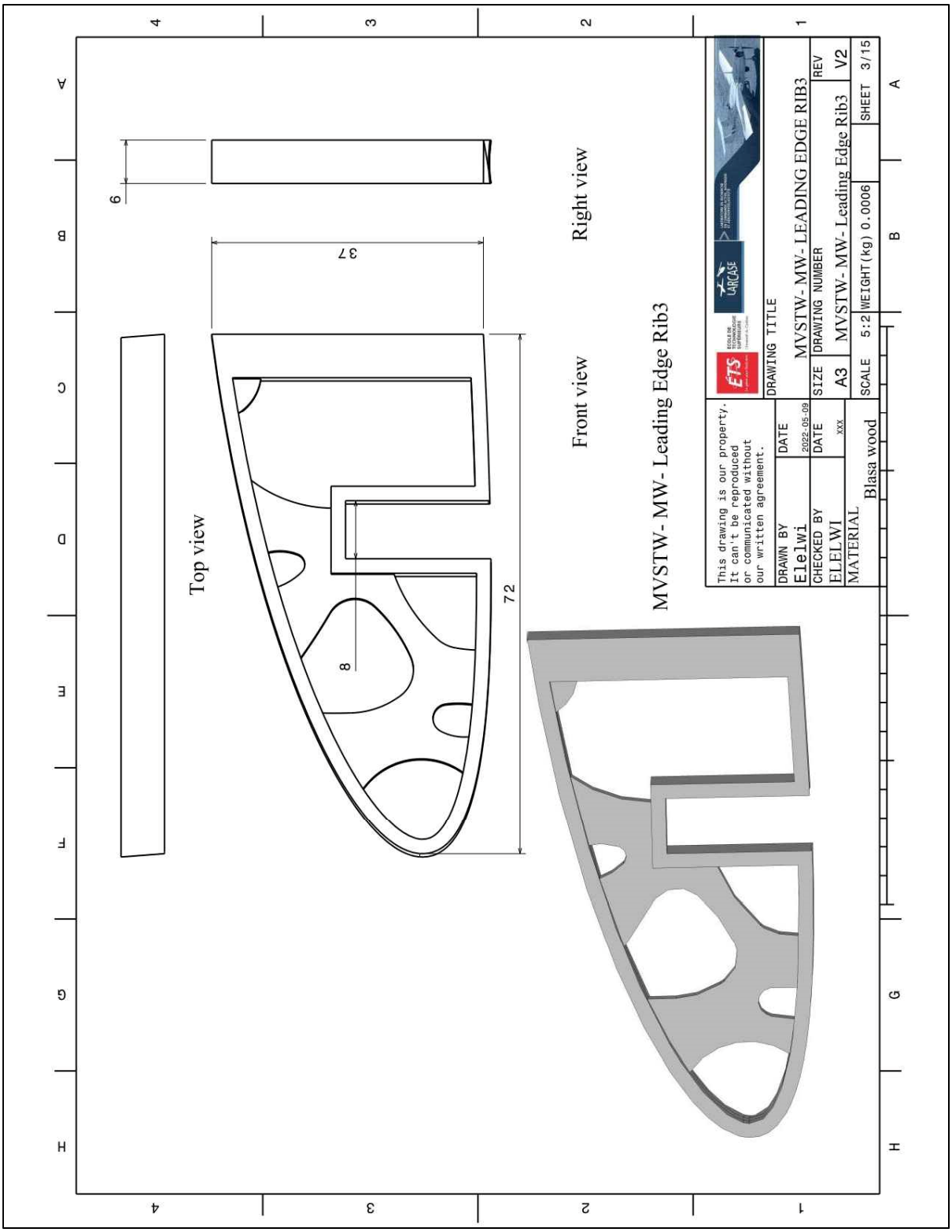

Figure-C III-59 Moving Leading Edge Rib3 Wing Using Balsa Wood

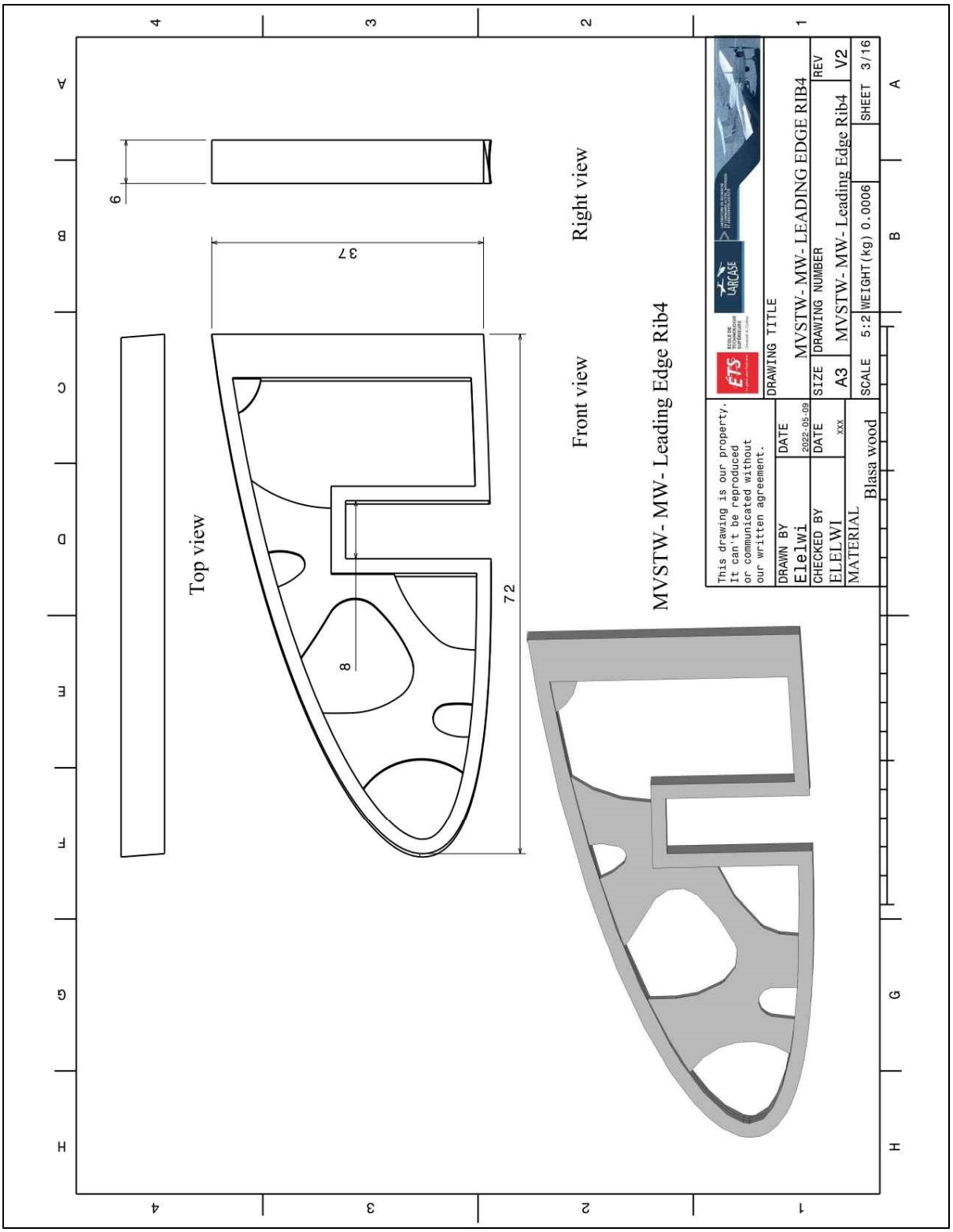

Figure-C III-60 Moving Leading Edge Rib4 Wing Using Balsa Wood

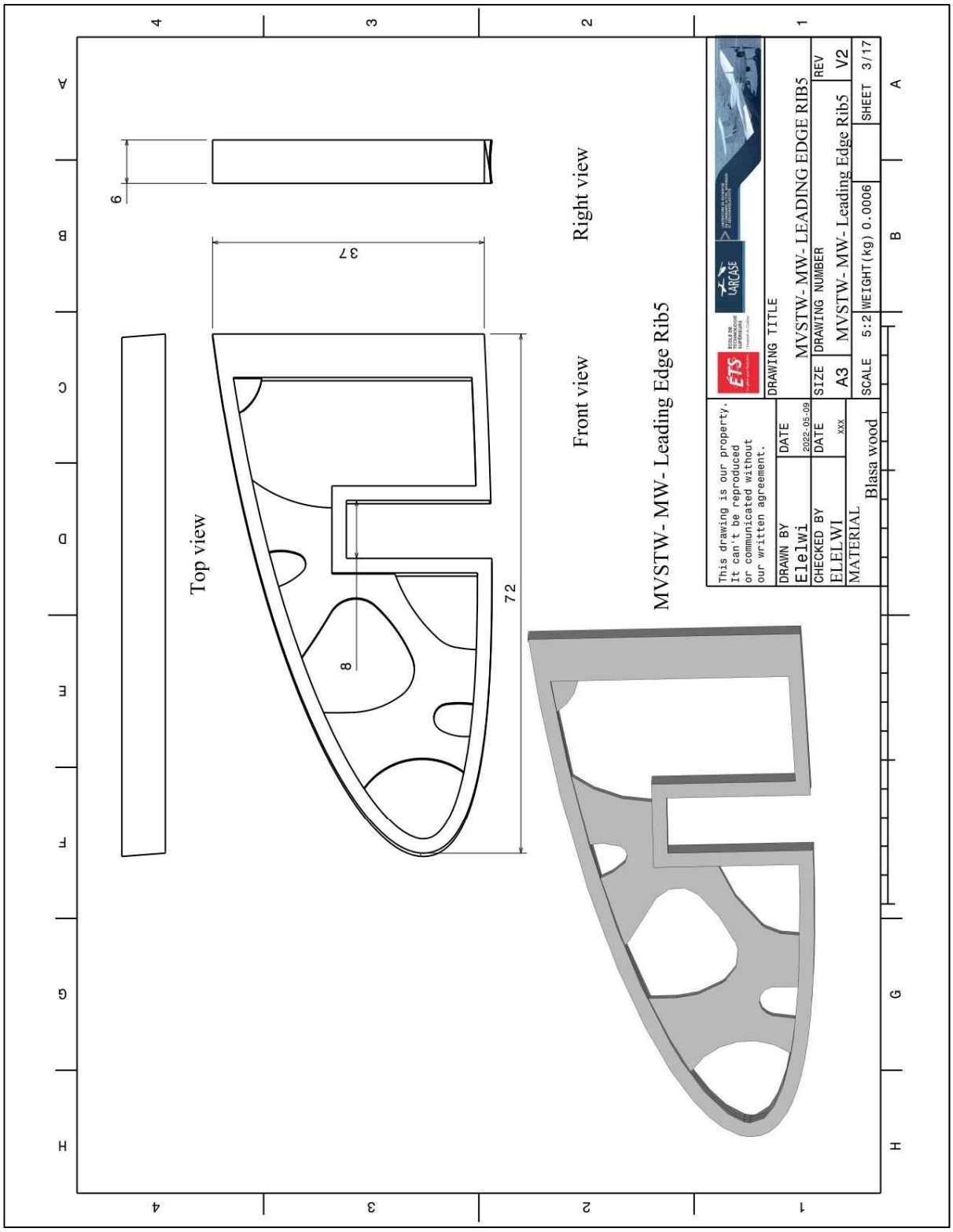

Figure-C III-61 Moving Leading Edge Rib5 Wing Using Balsa Wood

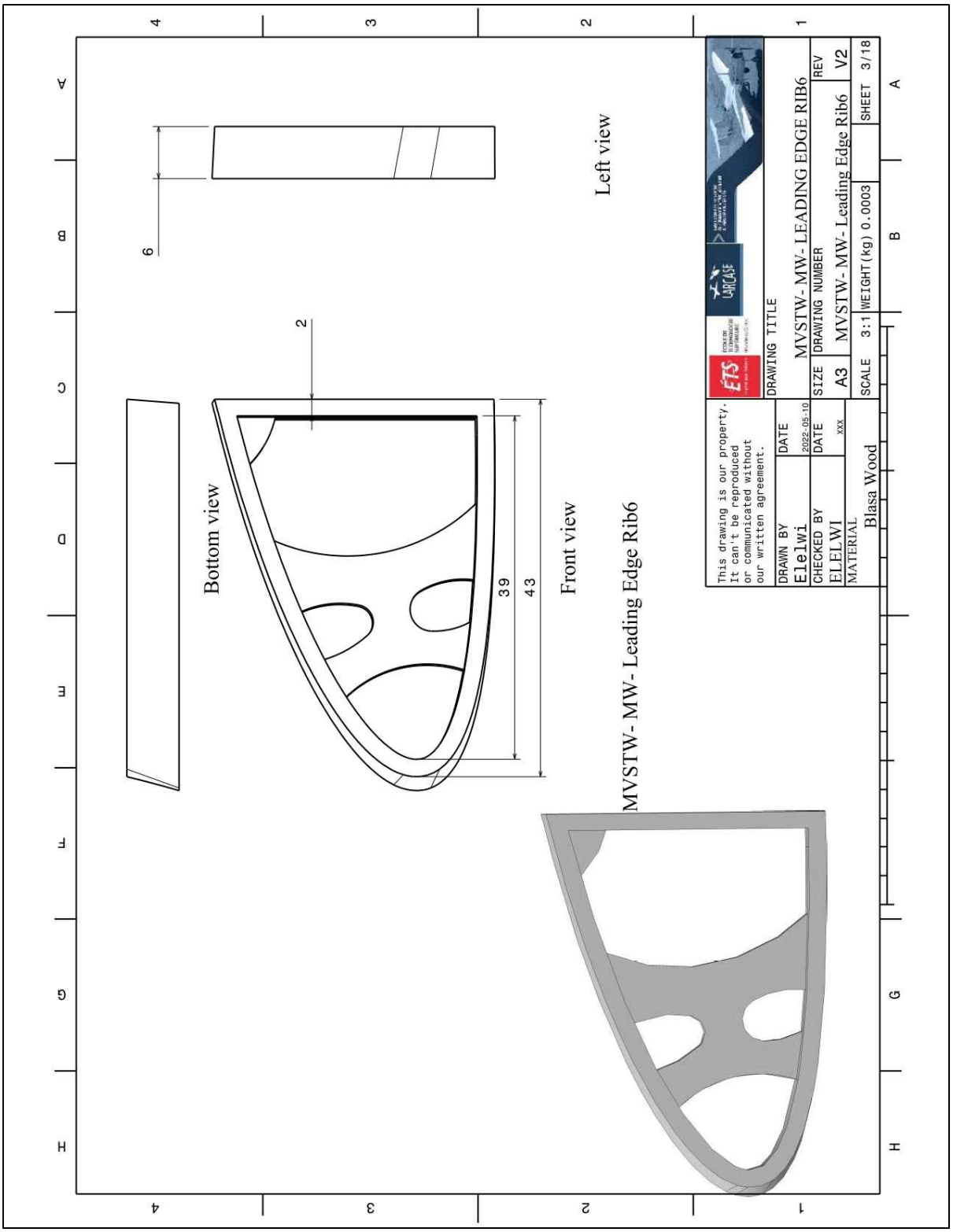

Figure-C III-62 Moving Leading Edge Rib6 Wing Using Balsa Wood

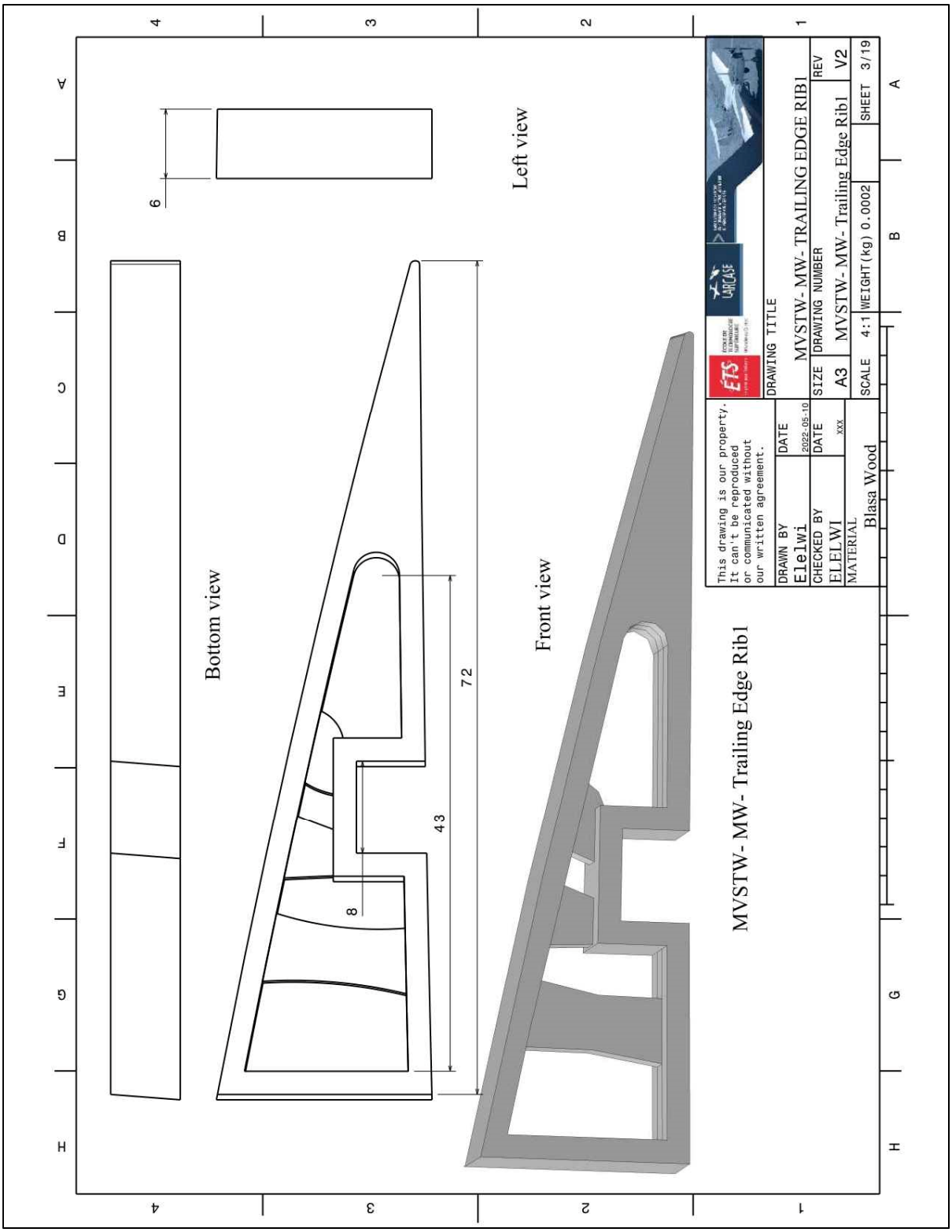

Figure-C III-63 Moving Trailing Edge Rib1 Wing Using Balsa Wood

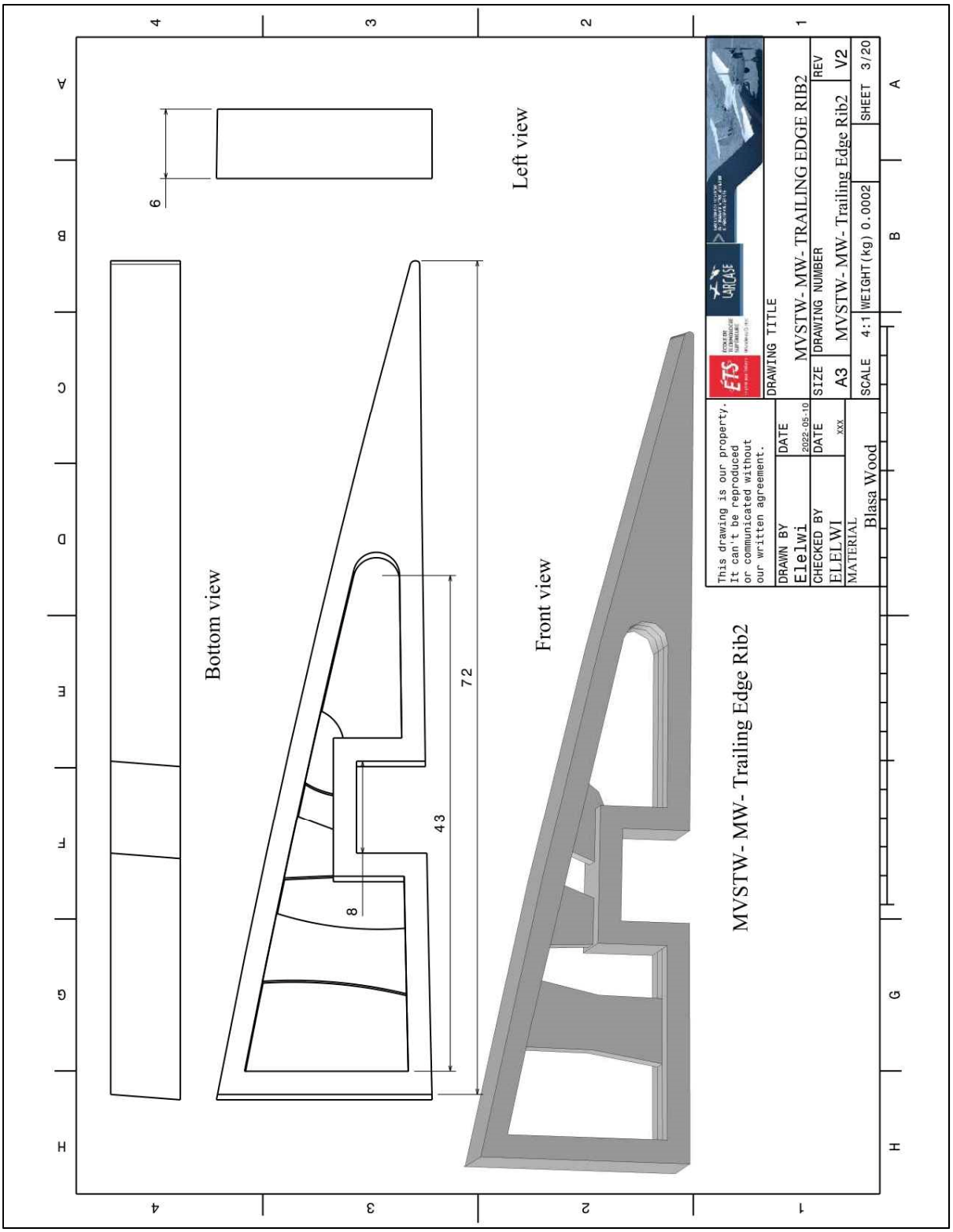

Figure-C III-64 Moving Trailing Edge Rib2 Wing Using Balsa Wood

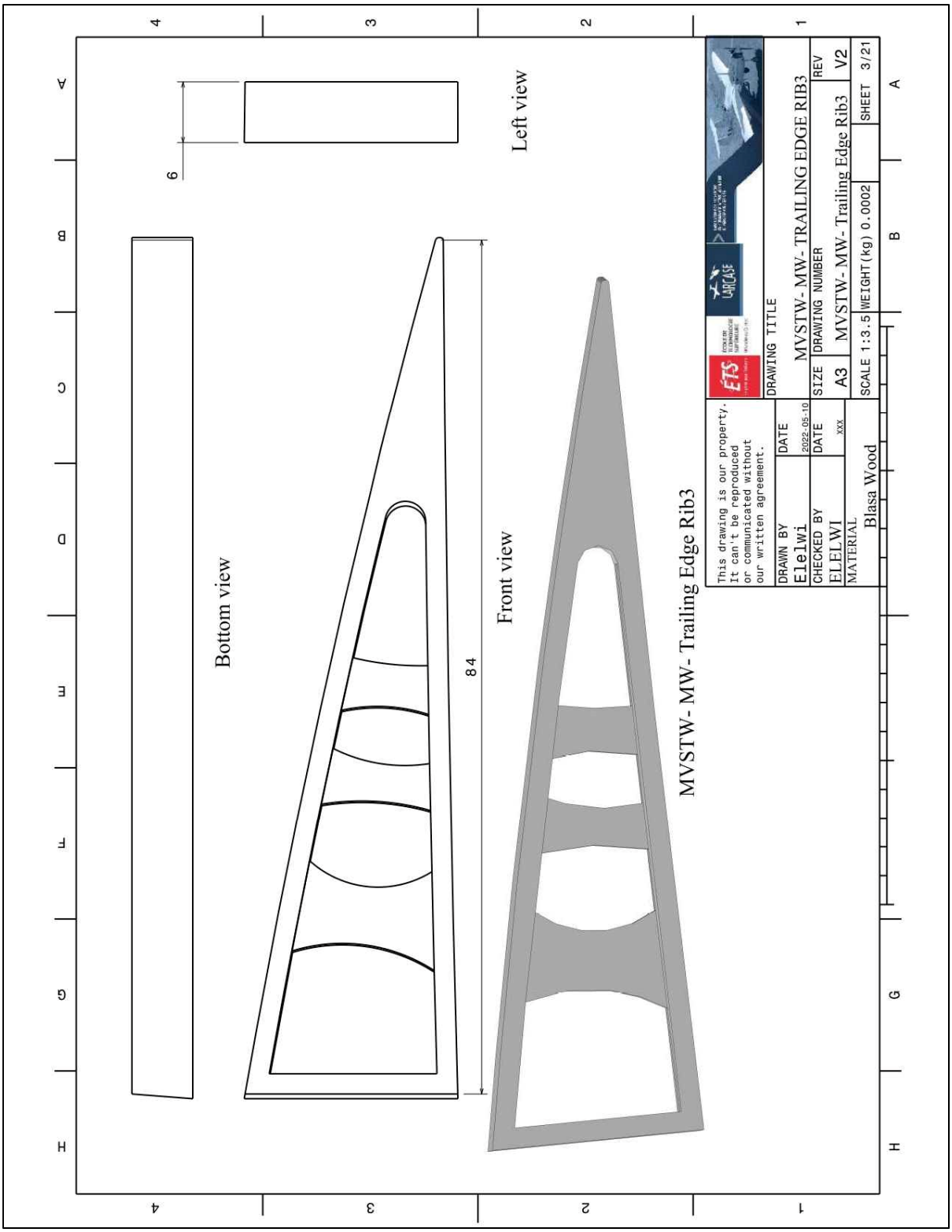

Figure-C III-65 Moving Trailing Edge Rib3 Wing Using Balsa Wood

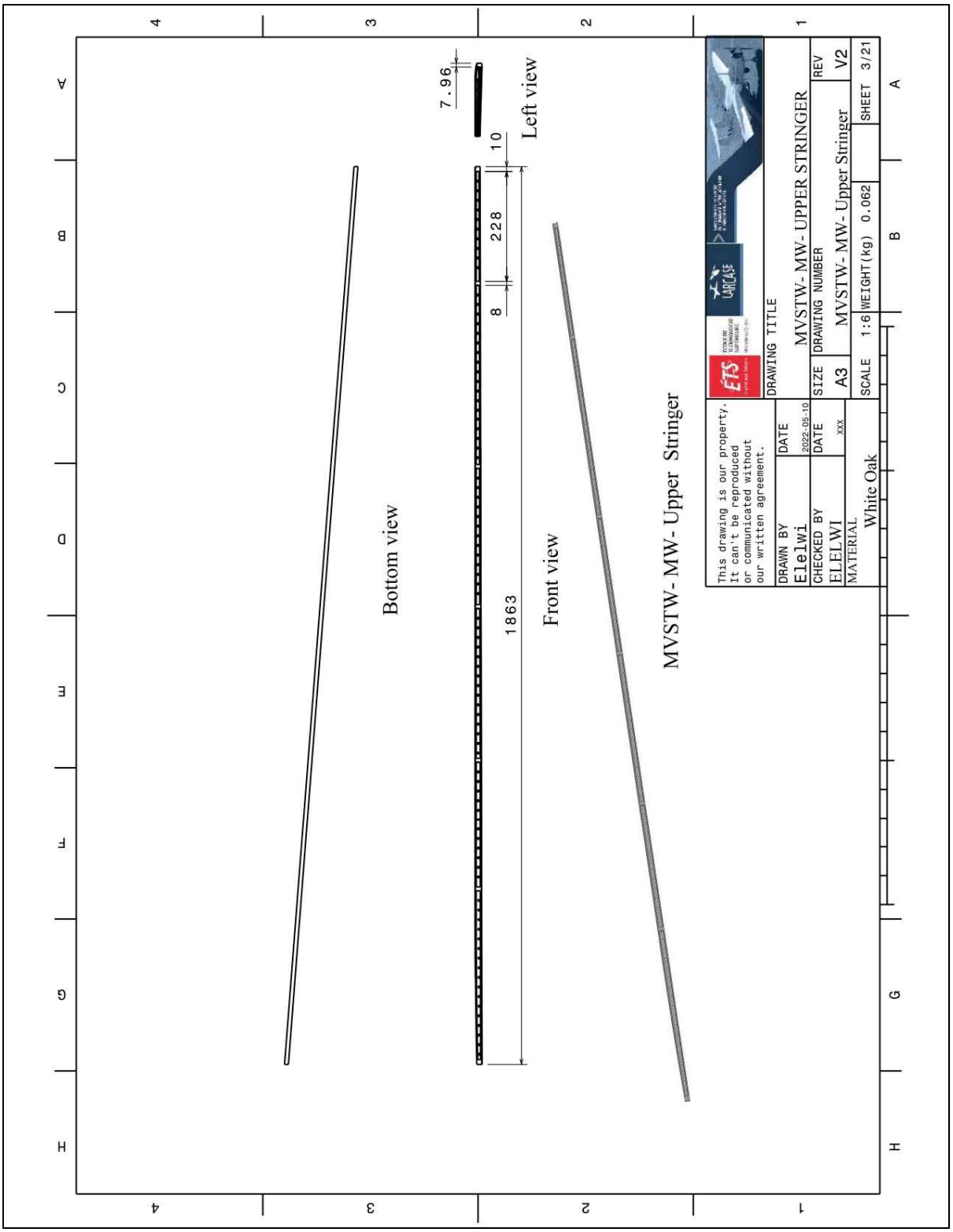

Figure-C 66 Moving Upper Stringer Wing Using White Oak

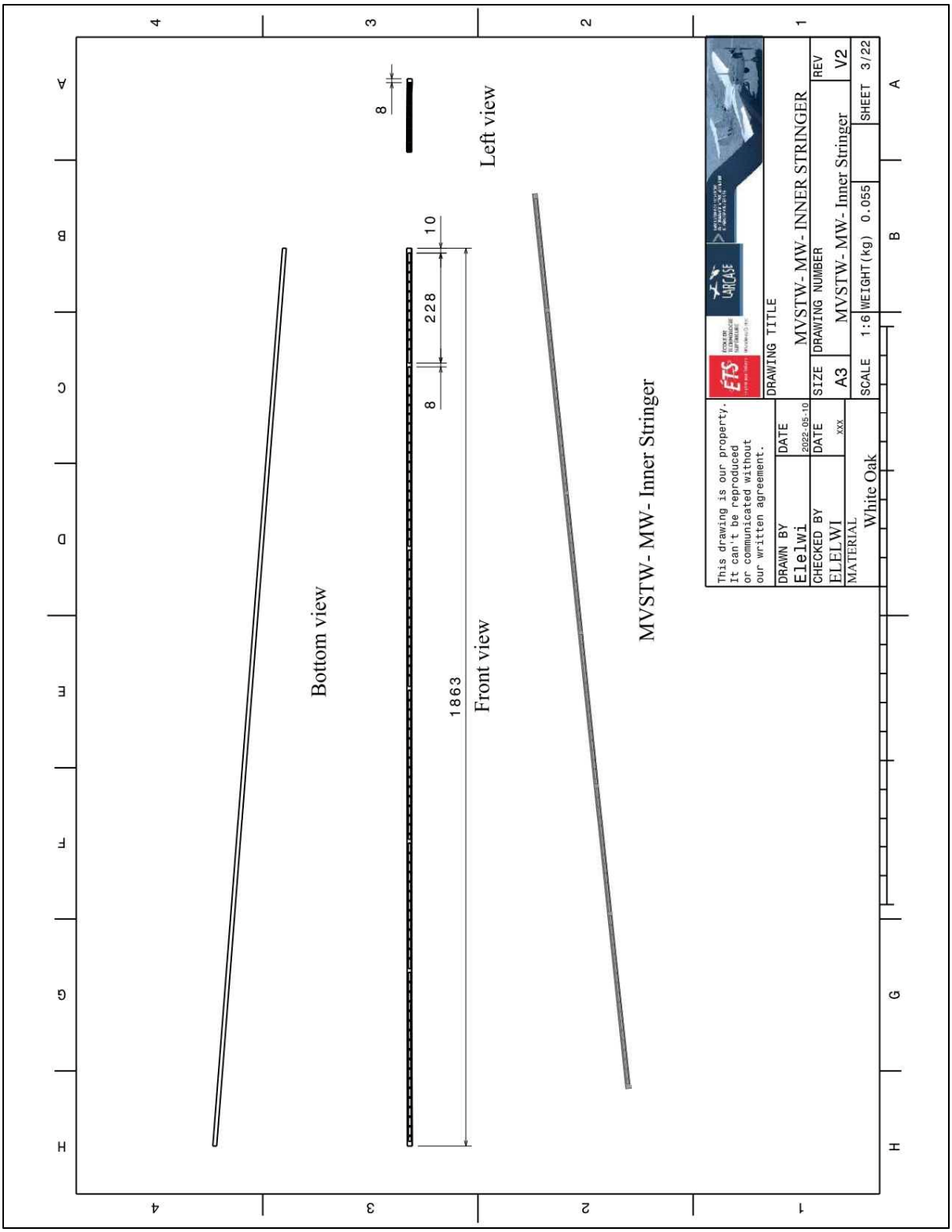

Figure-C III-67 Moving Inner Stringer Wing Using White Oak

LIST OF BIBLIOGRAPHICAL REFERENCES

Aage, N., Andreassen, E., Lazarov, B. S., & Sigmund, O. (2017). Giga-voxel computational morphogenesis for structural design. *Nature, 550*(7674), 84-86. doi:10.1038/nature23911

Aamir, M., Tolouei-Rad, M., Giasin, K., & Nosrati, A. (2019). Recent advances in drilling of carbon fiber–reinforced polymers for aerospace applications: A review. *The International Journal of Advanced Manufacturing Technology, 105*(5), 2289-2308.

Abdelkefi, A., & Ghommem, M. (2013). Piezoelectric energy harvesting from morphing wing motions for micro air vehicles. *Theoretical and Applied Mechanics Letters, 3*(5), 052004.

Acar, E., Haftka, R. T., & Kim, N. H. (2010). Effects of structural tests on aircraft safety. *AIAA Journal, 48*(10), 2235-2248.

Ajaj, R., Bourchak, M., & Friswell, M. (2014). Span morphing using the GNAT spar for a mini-UAV: designing and testing.

Ajaj, R., Flores, E. S., Friswell, M., Allegri, G., Woods, B., Isikveren, A., & Dettmer, W. (2013). The Zigzag wingbox for a span morphing wing. *Aerospace Science and technology, 28*(1), 364-375.

Ajaj, R., Friswell, M., Saavedra Flores, E., Little, O., & Isikveren, A. (2012). *Span morphing: a conceptual design study.* Paper presented at the 53rd AIAA/ASME/ASCE/AHS/ASC structures, structural dynamics and materials conference 20th AIAA/ASME/AHS adaptive structures conference 14th AIAA.

Ajaj, R. M., Friswell, M. I., I Saavedra Flores, E., Keane, A., Isikveren, A. T., Allegri, G., & Adhikari, S. (2014). An integrated conceptual design study using span morphing technology. *Journal of Intelligent material systems and structures, 25*(8), 989-1008.

Allen, M. J. (2003). *Modeling aircraft wing loads from flight data using neural networks*: National Aeronautics and Space Administration, Dryden Flight Research Center.

Ameduri, S., & Concilio, A. (2020). Morphing wings review: aims, challenges, and current open issues of a technology. *Proceedings of the Institution of Mechanical Engineers, Part C: Journal of Mechanical Engineering Science*, 0954406220944423. doi:10.1177/0954406220944423

Amendola, G., Dimino, I., Amoroso, F., & Pecora, R. (2016). *Experimental characterization of an adaptive aileron: Lab tests and FE correlation.* Paper presented at the Sensors

and Smart Structures Technologies for Civil, Mechanical, and Aerospace Systems 2016.

Anderson, J. D., & Bowden, M. L. (2005). Introduction to flight.

Arena, M., Concilio, A., & Pecora, R. (2019). Aero-servo-elastic design of a morphing wing trailing edge system for enhanced cruise performance. *Aerospace Science and technology, 86*, 215-235.

Armendáriz, I., Millán, J. S., Encinas, J. M., & Olarrea, J. (2016). Strategies for dynamic failure analysis on aerospace structures. In *Handbook of Materials Failure Analysis with Case Studies from the Aerospace and Automotive Industries* (pp. 29-55): Elsevier.

Assimi, H., Jamali, A., & Nariman-zadeh, N. (2017). Sizing and topology optimization of truss structures using genetic programming. *Swarm and Evolutionary Computation, 37*, 90-103. doi:https://doi.org/10.1016/j.swevo.2017.05.009

Awad, A. H., El Gamasy, R., Abd El Wahab, A., & Abdellatif, M. H. (2019). Mechanical and Physical Properties of PP and HDPE. *Engineering Science, 4*(2), 34-42.

Baier, H., & Datashvili, L. (2011). Active and morphing aerospace structures-a synthesis between advanced materials, structures and mechanisms. *International Journal of Aeronautical and Space Sciences, 12*(3), 225-240.

Bakhtiarinejad, M. (2015). *Topology optimization based on morphing mesh for simultaneous component relocation and frame structure design*: University of Maryland, Baltimore County.

Barbarino, S., Bilgen, O., Ajaj, R. M., Friswell, M. I., & Inman, D. J. (2011). A review of morphing aircraft. *Journal of Intelligent material systems and structures, 22*(9), 823-877.

Bashir, M., Longtin-Martel, S., Botez, R. M., & Wong, T. (2021). Aerodynamic Design Optimization of a Morphing Leading Edge and Trailing Edge Airfoil–Application on the UAS-S45. *Applied Sciences, 11*(4), 1664. Retrieved from https://www.mdpi.com/2076-3417/11/4/1664

Batista, N. L., Helal, E., Kurusu, R. S., Moghimian, N., David, E., Demarquette, N. R., & Hubert, P. (2019). Mass-produced graphene—HDPE nanocomposites: thermal, rheological, electrical, and mechanical properties. *Polymer Engineering & Science, 59*(4), 675-682.

Beaverstock, C. S., Fincham, J., Friswell, M. I., Ajaj, R. M., De Breuker, R., & Werter, N. (2014). *Effect of symmetric & asymmetric span morphing on flight dynamics.* Paper presented at the AIAA Atmospheric flight mechanics conference.

Beaverstock, C. S., Woods, B. K. S., Fincham, J. H. S.-M., & Friswell, M. I. (2015). Performance comparison between optimised camber and span for a morphing wing. *Aerospace, 2*(3), 524-554.

Bendsøe, M. P. (1989). Optimal shape design as a material distribution problem. *Structural optimization, 1*(4), 193-202.

Bendsøe, M. P., & Sigmund, O. (1999). Material interpolation schemes in topology optimization. *Archive of Applied Mechanics, 69*(9), 635-654. doi:10.1007/s004190050248

Beutel, A. (2014). NASA tests revolutionary shape changing aircraft flap for the first time. *Washington (DC): NASA*.

Bilgen, O., Friswell, M., Kochersberger, K., & Inman, D. (2011). *Surface actuated variable-camber and variable-twist morphing wings using piezocomposites.* Paper presented at the 52nd AIAA/ASME/ASCE/AHS/ASC Structures, Structural Dynamics and Materials Conference 19th AIAA/ASME/AHS Adaptive Structures Conference 13t.

Blondeau, J., & Pines, D. (2004). *Pneumatic morphing aspect ratio wing.* Paper presented at the 45th AIAA/ASME/ASCE/AHS/ASC Structures, Structural Dynamics & Materials Conference.

Borrega, M., & Gibson, L. J. (2015). Mechanics of balsa (Ochroma pyramidale) wood. *Mechanics of Materials, 84*, 75-90. doi:https://doi.org/10.1016/j.mechmat.2015.01.014

Botez, R. (2018). Morphing wing, UAV and aircraft multidisciplinary studies at the Laboratory of Applied Research in Active Controls, Avionics and AeroServoElasticity LARCASE. *Aerospace Lab*(14), 1-11.

Botez, R., Koreanschi, A., Gabor, O., Tondji, Y., Guezguez, M., Kammegne, J., . . . Mamou, M. (2018). Numerical and experimental transition results evaluation for a morphing wing and aileron system. *The Aeronautical Journal, 122*(1251), 747-784.

Botez, R. M. (2018). Morphing Wing, UAV and Aircraft Multidisciplinary Studies at the Laboratory of Applied Research in Active Controls, Avionics and AeroServoElasticity LARCASE. *Aerospace Lab*(14), 1-11. doi:10.12762/2018.Al14-02

Botez, R. M. (2022). *Overview of Morphing Aircraft and Unmanned Aerial Systems Methodologies and Results–Application on the Cessna Citation X, CRJ-700, UAS-S4 and UAS-S45.* Paper presented at the AIAA SCITECH 2022 Forum.

Botez, R. M., Grigorie, T. L., Khan, S., Mamou, M., & Mebarki, Y. (2021). *A smart controlled morphing wing experimental model with the structure based on a full-scaled portion of a real wing.* Paper presented at the AIAA Scitech 2021 Forum.

Botez, R. M., Koreanschi, A., Oliviu, S. G., Mebarki, Y., Mamou, M., Tondji, Y., . . . Amendola, G. (2017). *Numerical and experimental testing of a morphing upper surface wing equipped with conventional and morphing ailerons.* Paper presented at the 55th AIAA Aerospace Sciences Meeting.

Botez, R. M., Molaret, P., & Laurendeau, E. (2007). *Laminar flow control on a research wing project presentation covering a three year period.* Paper presented at the Canadian aeronautics and space institute annual general meeting.

Buchanan, S. (2007). *Development of a wingbox rib for a passenger jet aircraft using design optimization and constrained to traditional design and manufacture requirements.* Paper presented at the Altair Engineering CAE Technology Conference, Michigan.

Burdette, D. A., Kenway, G. K., Lyu, Z., & Martins, J. R. (2015). *Aerostructural design optimization of an adaptive morphing trailing edge wing.* Paper presented at the 56th AIAA/ASCE/AHS/ASC Structures, Structural Dynamics, and Materials Conference.

Cantrell, J., Rohde, S., Damiani, D., Gurnani, R., DiSandro, L., Anton, J., . . . Ifju, P. (2017). *Experimental Characterization of the Mechanical Properties of 3D Printed ABS and Polycarbonate Parts*, Cham.

Carossa, G. M., Ricci, S., De Gaspari, A., Liauzun, C., Dumont, A., & Steinbuch, M. (2016). Adaptive trailing edge: specifications, aerodynamics, and exploitation. In *Smart intelligent aircraft structures (SARISTU)* (pp. 143-158): Springer.

Cascio, M. L., Milazzo, A., Amendola, G., Arena, M., & Dimino, I. (2018). *Optimisation design process of a morphing winglet.* Paper presented at the Bioinspiration, Biomimetics, and Bioreplication VIII.

Cauzard, V., Antoine, S., & Botez, R. M. (2013). *Aerodynamics simulation of the hydra technologies unmanned aerial systems UAS S4 wing using the fluent code* (0148-7191). Retrieved from

Chen, L., Guo, Z., & Wang, W. (2016). *Dynamic model and analysis of asymmetric telescopic wing for morphing aircraft.* Paper presented at the MATEC Web of Conferences.

Chethan, K., Zuber, M., Shenoy, S., & Kini, C. R. (2019). Static structural analysis of different stem designs used in total hip arthroplasty using finite element method. *Heliyon, 5*(6), e01767.

Communier, D., Botez, R. M., & Wong, T. (2020). Design and validation of a new morphing camber system by testing in the price—Païdoussis subsonic wind tunnel. *Aerospace, 7*(3), 23.

Communier, D., Salinas, M. F., Carranza Moyao, O., & Botez, R. M. (2015). *Aero structural modeling of a wing using CATIA V5 and XFLR5 software and experimental validation using the Price-Païdoussis wing tunnel.* Paper presented at the AIAA atmospheric flight mechanics conference, Dallas, TX, USA.

Concilio, A., Dimino, I., Ciminello, M., Pecora, R., Amoroso, F., & Magnifico, M. (2018). An adaptive trailing edge. In *Morphing Wing Technologies* (pp. 517-545): Elsevier.

Concilio, A., Dimino, I., Lecce, L., Pecora, R., Ricci, S., Aliabadi, F. M. H., . . . Semperlotti, F. (2017). *"Morphing Wing Technologies: Large Commercial Aircraft and Civil Helicopters"*: Elsevier Science.

Concilio, A., Dimino, I., & Pecora, R. (2021). SARISTU: Adaptive Trailing Edge Device (ATED) design process review. *Chinese Journal of Aeronautics, 34*(7), 187-210. doi:https://doi.org/10.1016/j.cja.2020.08.036

Concilio, A., Dimino, I., Pecora, R., & Ciminello, M. (2016). *Structural design of an adaptive wing trailing edge for enhanced cruise performance.* Paper presented at the 24th AIAA/AHS adaptive structures conference.

Contino, M., Andena, L., La Valle, V., Rink, M., Marra, G., & Resta, S. (2020). A comparison between K $ K $ and G $ G $ approaches for a viscoelastic material: the case of environmental stress cracking of HDPE. *Mechanics of Time-Dependent Materials, 24*(3), 381-394.

Coroian, A., & Lupea, I. (2013). Improving the sound pressure level for a simplified passenger cabin by using modal participation and size optimization. *Romanian Journal of Acoustics and Vibration, 10*(1), 47.

Costa, I. L. M., Zanini, N. C., & Mulinari, D. R. (2021). Thermal and Mechanical Properties of HDPE Reinforced with Al2O3 Nanoparticles Processed by Thermokinectic Mixer. *Journal of Inorganic and Organometallic Polymers and Materials, 31*(1), 220-228. doi:10.1007/s10904-020-01709-0

Coughtrie, A., Borman, D., & Sleigh, P. (2013). Effects of turbulence modelling on prediction of flow characteristics in a bench-scale anaerobic gas-lift digester. *Bioresource technology, 138*, 297-306.

Daynes, S., Feih, S., Lu, W. F., & Wei, J. (2017). Optimisation of functionally graded lattice structures using isostatic lines. *Materials & Design, 127*, 215-223. doi:https://doi.org/10.1016/j.matdes.2017.04.082

Degertekin, S. O., Lamberti, L., & Ugur, I. B. (2019). Discrete sizing/layout/topology optimization of truss structures with an advanced Jaya algorithm. *Applied Soft Computing, 79*, 363-390. doi:https://doi.org/10.1016/j.asoc.2019.03.058

Della Vecchia, P., Corcione, S., Pecora, R., Nicolosi, F., Dimino, I., & Concilio, A. (2017). Design and integration sensitivity of a morphing trailing edge on a reference airfoil: The effect on high-altitude long-endurance aircraft performance. *Journal of Intelligent material systems and structures, 28*(20), 2933-2946.

Deperrois, A. (2009). XFLR5 Analysis of foils and wings operating at low Reynolds numbers. *Guidelines for XFLR5, 142*.

Dillinger, J., Klimmek, T., Abdalla, M. M., & Gürdal, Z. (2013). Stiffness optimization of composite wings with aeroelastic constraints. *Journal of Aircraft, 50*(4), 1159-1168.

Dimino, I., Andreutti, G., Moens, F., Fonte, F., & Pecora, R. (2021). Integrated Design of a Morphing Winglet for Active Load Control and Alleviation of Turboprop Regional Aircraft. *Applied Sciences, 11*(5), 2439.

Dimino, I., Flauto, D., Diodati, G., & Pecora, R. (2014). Actuation system design for a morphing wing trailing edge. *Recent Patents on Mechanical Engineering, 7*(2), 138-148.

Dimino, I., Lecce, L., & Pecora, R. (2017). *Morphing wing technologies: Large commercial aircraft and civil helicopters*: Butterworth-Heinemann.

Diodati, G., Ricci, S., De Gaspari, A., Huvelin, F., Dumont, A., & Godard, J.-L. (2013). *Estimated performance of an adaptive trailing-edge device aimed at reducing fuel consumption on a medium-size aircraft.* Paper presented at the Industrial and Commercial Applications of Smart Structures Technologies 2013.

Easter, S., Turman, J., Sheffler, D., Balazs, M., & Rotner, J. (2013). *Using advanced manufacturing to produce unmanned aerial vehicles: a feasibility study.* Paper presented at the Ground/Air Multisensor Interoperability, Integration, and Networking for Persistent ISR IV.

Elelwi, M., Botez, R. M., & Dao, T.-M. (2021). Structural Sizing and Topology Optimization Based on Weight Minimization of a Variable Tapered Span-Morphing Wing for Aerodynamic Performance Improvements. *Biomimetics, 6*(4), 55. Retrieved from https://www.mdpi.com/2313-7673/6/4/55

Elelwi, M., Calvet, T., Botez, R. M., & Dao, T. M. (2021). Wing component allocation for a morphing variable span of tapered wing using finite element method and topology

optimisation – application to the UAS-S4. *The Aeronautical Journal*, 1-24. doi:10.1017/aer.2021.29

Elelwi, M., Kuitche, M. A., Botez, R. M., & Dao, T. M. (2020). Comparison and analyses of a variable span-morphing of the tapered wing with a varying sweep angle. *The Aeronautical Journal, 124*(1278), 1146-1169. doi:10.1017/aer.2020.19

Erchiqui, F., Annasabi, Z., & Diagne, M. (2021). Investigation of the radiofrequency heating of anisotropic dielectric materials with a phase change: application to frozen Douglas-fir and white oak woods. *Wood Science and Technology*. doi:10.1007/s00226-021-01345-y

Eves, J., Toropov, V., Thompson, H., Gaskell, P., Doherty, J., & Harris, J. (2009). Topology optimization of aircraft with non-conventional configurations.

Fincham, J., Beaverstock, C. S., Coles, A. B., Parsons, L. L., Friswell, M. I., & Ajaj, R. M. (2014). Aerodynamic forces on morphing wings during span extension. *Advanced aero concepts, design, and operations*.

Fincham, J., & Friswell, M. (2015). Aerodynamic optimisation of a camber morphing aerofoil. *Aerospace Science and technology, 43*, 245-255.

Gabor, O. Ş., Koreanschi, A., & Botez, R. M. (2016). A new non-linear vortex lattice method: Applications to wing aerodynamic optimizations. *Chinese Journal of Aeronautics, 29*(5), 1178-1195.

Gabor, O. Ş., Koreanschi, A., Botez, R. M., Mamou, M., & Mebarki, Y. (2016). Numerical simulation and wind tunnel tests investigation and validation of a morphing wing-tip demonstrator aerodynamic performance. *Aerospace Science and technology, 53*, 136-153.

Gabor, O. S., Simon, A., Koreanschi, A., & Botez, R. (2014). *Numerical optimization of the S4 Éhecatl UAS airfoil using a morphing wing approach.* Paper presented at the American Institute of Aeronautics and Astronautics AIAA 32nd Applied Aerodynamics Conference, Atlanta, GA, USA.

Gamboa, P., Aleixo, P., Vale, J., Lau, F., & Suleman, A. (2007). *Design and Testing of a Morphing Wing for an Experimental UAV*. Retrieved from

Gao, B., Kang, R., & Chen, Y. (2016). Deployable mechanism design for span morphing wing aircraft. In *Mechanism and Machine Science* (pp. 801-813): Springer.

Gao, L., Jin, H., Zhao, J., Cai, H., & Zhu, Y. (2018). Flight dynamics modeling and control of a novel catapult launched tandem-wing micro aerial vehicle with variable sweep. *IEEE Access, 6*, 42294-42308.

Gawel, D., Nowak, M., Hausa, H., & Roszak, R. (2017). New biomimetic approach to the aircraft wing structural design based on aeroelastic analysis. *Bulletin of the Polish Academy of Sciences: Technical Sciences DOI - 10.1515/bpasts-2017-0080, 65*(No 5 (Special Section on Multilevel Converters)), 741-750-741-750. Retrieved from http://journals.pan.pl/dlibra/publication/edition/105785

Ghosh, R., Ghosh, S., Ghimire, S., & Barman, D. R. (2016). Static analysis of multi-leaf spring using ansys workbench 16.0. *International Journal of Mechanical Engineering and Technology (IJMET), 7*(5), 241-249.

Gibson, R. F. (2016). *Principles of composite material mechanics*: CRC press.

Gibson, R. F., & Plunkett, R. (1976). Dynamic mechanical behavior of fiber-reinforced composites: measurement and analysis. *Journal of Composite Materials, 10*(4), 325-341.

Girennavar, M., Soumya, H., Subodh, H., Heraje, T. J., & PY, D. R. (2017). Design, Analysis and Testing of Wing Spar for Optimum Weight. *International Journal of Research and Scientific Innovation (IJRSI), 4*(VII), 104-112.

Grbović, A., Kastratović, G., Sedmak, A., Balać, I., & Popović, M. D. (2019). Fatigue crack paths in light aircraft wing spars. *International Journal of Fatigue, 123*, 96-104. doi:https://doi.org/10.1016/j.ijfatigue.2019.02.013

Grihon, S., Krog, L., & Hertel, K. (2004). A380 weight savings using numerical structural optimization. *Inproceedings of 20th AAAF Colloqium" Material for Aerospace Application", Paris, France*.

Grisval, J.-P., & Liauzun, C. (1999). Application of the finite element method to aeroelasticity. *Revue Européenne des Éléments Finis, 8*(5-6), 553-579. doi:10.1080/12506559.1999.10511397

Gross, A., Fasel, H. F., & Gaster, M. (2015). Criterion for Spanwise Spacing of Stall Cells. *AIAA Journal, 53*(1), 272-274. doi:10.2514/1.J053347

Gunwant, D., & Misra, A. (2012). Topology Optimization of sheet metal brackets using ANSYS. *MIT International Journal of Mechanical Engineering, 2*(2), 120-126.

Guo, S. (2007). Aeroelastic optimization of an aerobatic aircraft wing structure. *Aerospace Science and technology, 11*(5), 396-404.

Höke, Ö., & Bozca, M. (2020). Topology Optimisation of Engine Cross Members for Lightweight Structure in Light Commercial Vehicles. *International Journal of*

Precision Engineering and Manufacturing, 21(3), 465-482. doi:10.1007/s12541-019-00228-4

Ivanco, T., Scott, R., Love, M., Zink, S., & Weisshaar, T. (2007). *Validation of the Lockheed Martin morphing concept with wind tunnel testing.* Paper presented at the 48th AIAA/ASME/ASCE/AHS/ASC structures, structural dynamics, and materials conference.

James, K. A., Kennedy, G. J., & Martins, J. R. R. A. (2014). Concurrent aerostructural topology optimization of a wing box. *Computers & Structures, 134*, 1-17. doi:https://doi.org/10.1016/j.compstruc.2013.12.007

Jankovics, D., Gohari, H., Tayefeh, M., & Barari, A. (2018). Developing topology optimization with additive manufacturing constraints in ANSYS®. *IFAC-PapersOnLine, 51*(11), 1359-1364.

Jensen, F. (2018). Topology Optimization of Turbine Manifold in the Rocket Engine Demonstrator Prometheus. In.

Jerome, P. (2001). *Composite materials in the airbus A380-from history to future.* Paper presented at the Beijing: Proceedings 13th International Conference on Composite Materials (ICCM-13).

Joshi, S., Tidwell, Z., Crossley, W., & Ramakrishnan, S. (2004). *Comparison of morphing wing stategies based upon aircraft performance impacts.* Paper presented at the 45th AIAA/ASME/ASCE/AHS/ASC Structures, Structural Dynamics & Materials Conference.

Judge, J. F. (1969). Composite materials- The coming revolution(Filamentary composite materials for commercial aircraft and engine construction noting boron, graphite and glass reinforcement). *Airline Management and Marketing Including American Aviation, 1*, 85.

Kammegne, M. J. T., Botez, R. M., Grigorie, T. L., Manou, M., & Mebarki, Y. (2016). A fuel saving way in aerospace engineering based on morphing wing technology: a new multidisciplinary experimental model. *International Journal of Contemporary ENERGY, 2*(2). doi:10.14621/ce.20160202

Kennedy, G., & Martins, J. R. (2012). *A comparison of metallic and composite aircraft wings using aerostructural design optimization.* Paper presented at the 12th AIAA Aviation Technology, Integration, and Operations (ATIO) Conference and 14th AIAA/ISSMO Multidisciplinary Analysis and Optimization Conference.

Kennedy, G. J., Kenway, G. K., & Martins, J. R. (2014). *A comparison of metallic, composite and nanocomposite optimal transonic transport wings*: National Aeronautics and Space Administration, Langley Research Center.

Kenway, G. K., Kennedy, G. J., & Martins, J. R. (2014). Scalable parallel approach for high-fidelity steady-state aeroelastic analysis and adjoint derivative computations. *AIAA Journal, 52*(5), 935-951.

Kevadiya, M., & Vaidya, H. A. (2013). 2D analysis of NACA 4412 airfoil. *International Journal of Innovative Research in Science, Engineering and Technology, 2*(5), 1686-1691.

Komarov, V., Kishov, E., Kurkin, E., & Charkviani, R. (2015). Aircraft composite spoiler fitting design using the variable density model. *Procedia Computer Science, 65*, 99-106.

Koreanschi, A., Sugar-Gabor, O., & Botez, R. M. (2016a). Drag optimisation of a wing equipped with a morphing upper surface. *The Aeronautical Journal, 120*(1225), 473-493.

Koreanschi, A., Sugar-Gabor, O., & Botez, R. M. (2016b). Numerical and experimental validation of a morphed wing geometry using Price-Païdoussis wind-tunnel testing. *The Aeronautical Journal, 120*(1227), 757-795.

Körpe, D. S., Çetin, K., Altınok, A. S., Morasata, R., Eren, B., Demircan, O. M., . . . Kunnathur, N. S. (2016). Design of a UAV with Variable-Span Morphing Wing.

Krog, L., Tucker, A., Kemp, M., & Boyd, R. (2004). *Topology optimisation of aircraft wing box ribs.* Paper presented at the 10th AIAA/ISSMO multidisciplinary analysis and optimization conference.

Kuitche, M. A. J., & Botez, R. M. (2019). Modeling novel methodologies for unmanned aerial systems – Applications to the UAS-S4 Ehecatl and the UAS-S45 Bálaam. *Chinese Journal of Aeronautics, 32*(1), 58-77. doi:https://doi.org/10.1016/j.cja.2018.10.012

Kuitche, M. A. J., Botez, R. M., Guillemin, A., & Communier, D. (2020). Aerodynamic modelling of unmanned aerial system through nonlinear vortex lattice method, computational fluid dynamics and experimental validation-application to the uas-s45 bàlaam: Part 1. *INCAS Bulletin, 12*(1), 91-103. doi:DOI: 10.13111/2066-8201.2020.12.1.9

Kuitche, M. A. J., Botez, R. M., Viso, R., Maunand, J. C., & Moyao, O. C. (2020). Blade element momentum new methodology and wind tunnel test performance evaluation for the UAS-S45 Bàlaam propeller. *CEAS Aeronautical Journal, 11*(4), 937-953. doi:10.1007/s13272-020-00462-x

Langtry, R. B., & Menter, F. R. (2009). Correlation-based transition modeling for unstructured parallelized computational fluid dynamics codes. *AIAA Journal, 47*(12), 2894-2906.

Lee, H.-A., & Park, G.-J. (2015). Nonlinear dynamic response topology optimization using the equivalent static loads method. *Computer Methods in Applied Mechanics and Engineering, 283*, 956-970.

Leng, J., Lan, X., Liu, Y., & Du, S. (2011). Shape-memory polymers and their composites: stimulus methods and applications. *Progress in Materials Science, 56*(7), 1077-1135.

Li, C., Kim, I. Y., & Jeswiet, J. (2015). Conceptual and detailed design of an automotive engine cradle by using topology, shape, and size optimization. *Structural and Multidisciplinary Optimization, 51*(2), 547-564. doi:10.1007/s00158-014-1151-6

Li, W., & Jin, D. (2018). Flutter suppression and stability analysis for a variable-span wing via morphing technology. *Journal of Sound and Vibration, 412*, 410-423.

Li, X.-p., Zhao, L.-y., & Liu, Z.-z. (2017). *Topological optimization of continuum structure based on ANSYS.* Paper presented at the MATEC Web of Conferences.

Liauzun, C., Daniel Mortchéléwicz, G., & Lepage, A. (2019, 2019-06-10). *Assessment of CFD methods taking into account laminar-turbulent transition for aeroelasticity of laminar wings. Evaluation de méthodes CFD avec prise en compte de la transition laminaire-turbulent pour l'aéroélasticité des voilures laminaires.* Paper presented at the IFASD 2019, SAVANNAH, United States.

Liauzun, C., Le Bihan, D., David, J.-M., Joly, D., & Paluch, B. (2018). Study of morphing winglet concepts aimed at improving load control and the aeroelastic behavior of civil transport aircraft. *Aerospace Lab*(14), 1-15.

Liauzun, C. d. (2006). *Assessment of CFD techniques for wind turbine aeroelasticity.* Paper presented at the ASME Pressure Vessels and Piping Conference.

Liauzun, C. d. (2010). *Aeroelastic response to gust using CFD techniques.* Paper presented at the Fluids Engineering Division Summer Meeting.

Liu, Q., Mulani, S. B., & Kapania, R. K. (2014). *Global/local multidisciplinary design optimization of subsonic wing.* Paper presented at the 10th AIAA Multidisciplinary Design Optimization Conference.

Locatelli, D., Mulani, S. B., & Kapania, R. K. (2014). Parameterization of curvilinear spars and ribs for optimum wing structural design. *Journal of Aircraft, 51*(2), 532-546.

Lubin, G. (2013). *Handbook of composites*: Springer Science & Business Media.

Lyu, Z., Xu, Z., & Martins, J. (2014). *Benchmarking optimization algorithms for wing aerodynamic design optimization.* Paper presented at the Proceedings of the 8th International Conference on Computational Fluid Dynamics, Chengdu, Sichuan, China.

McCormick, B. W. (1995). The lifting-line model, aerodynamics, aeronautics and flight mechanics. In: New York: Wiley.

Mestrinho, J., Gamboa, P., & Santos, P. (2011). *Design optimization of a variable-span morphing wing for a small UAV.* Paper presented at the 52nd AIAA/ASME/ASCE/AHS/ASC Structures, Structural Dynamics and Materials Conference 19th AIAA/ASME/AHS Adaptive Structures Conference 13t.

Michaud, F., Joncas, S., & Botez, R. (2013). Design, manufacturing and testing of a small-scale composite morphing wing. *In Proceedings of the 19th International Conference on Composite Materials-ICCM19 (Montreal, QC, Canada, July 28-Aug. 2, 2013)*. doi:https://espace2.etsmtl.ca/id/eprint/8930/

Mieloszyk, J., Tarnowski, A., Kowalik, M., Perz, R., & Rzadkowski, W. (2019). Preliminary design of 3D printed fittings for UAV. *Aircraft Engineering and Aerospace Technology*.

Mitropoulou, C. C., Fourkiotis, Y., Lagaros, N. D., & Karlaftis, M. G. (2013). Evolution strategies-based metaheuristics in structural design optimization. *Metaheuristic Applications in Structures and Infrastructures*, 79-102.

Morlier, J., & Charlotte, M. (2012, 2012-09-04). *Structural wingbox optimization in a coupled FSI problem of a flexible wing: FEA sol200 versus surrogate models.* Paper presented at the 8th International Conference on Engineering Computational Technology (CST 2012), Dubrovnik, Croatia.

Mou, B., He, B.-J., Zhao, D.-X., & Chau, K.-w. (2017). Numerical simulation of the effects of building dimensional variation on wind pressure distribution. *Engineering Applications of Computational Fluid Mechanics, 11*(1), 293-309. doi:10.1080/19942060.2017.1281845

Muneiah, T., Bhaskar, E., & Rajesh, C. V. (2014). Design and Developemnt of Aircraft Droop Nose Ribs by Using Optistruct. *International Journal of Advanced Engineering Research and Studies, 3*(4), 18-21.

Murugan, S., Woods, B., & Friswell, M. (2015). Hierarchical modeling and optimization of camber morphing airfoil. *Aerospace Science and technology, 42*, 31-38.

Nelson, R. C. (1998). *Flight stability and automatic control* (Vol. 2): WCB/McGraw Hill New York.

Nomani, J., Wilson, D., Paulino, M., & Mohammed, M. I. (2020). Effect of layer thickness and cross-section geometry on the tensile and compression properties of 3D printed ABS. *Materials Today Communications, 22*, 100626. doi:https://doi.org/10.1016/j.mtcomm.2019.100626

Noviello, M. C., Dimino, I., Amoroso, F., & Pecora, R. (2019). Aeroelastic assessments and functional hazard analysis of a regional aircraft equipped with morphing winglets. *Aerospace, 6*(10), 104.

Oktay, E., Akay, H. U., & Merttopcuoglu, O. (2011). Parallelized structural topology optimization and CFD coupling for design of aircraft wing structures. *Computers & Fluids, 49*(1), 141-145. doi:https://doi.org/10.1016/j.compfluid.2011.05.005

Oktay, E., Akay, H. U., & Sehitoglu, O. T. (2014). Three-dimensional structural topology optimization of aerial vehicles under aerodynamic loads. *Computers & Fluids, 92*, 225-232. doi:https://doi.org/10.1016/j.compfluid.2013.11.018

Oliviu, S. G., Koreanschi, A., & Botez, R. M. (2015). *Numerical study of UAS-S4 Éhecatl aerodynamic performance improvement obtained with the use of a morphing wing approach.* Paper presented at the 33rd AIAA Applied Aerodynamics Conference.

Pecora, R. (2021). Morphing wing flaps for large civil aircraft: Evolution of a smart technology across the Clean Sky program. *Chinese Journal of Aeronautics, 34*(7), 13-28.

Pecora, R., Amoroso, F., & Lecce, L. (2012). Effectiveness of wing twist morphing in roll control. *Journal of Aircraft, 49*(6), 1666-1674.

Pecora, R., Barbarino, S., Concilio, A., Lecce, L., & Russo, S. (2011). Design and functional test of a morphing high-lift device for a regional aircraft. *Journal of Intelligent material systems and structures, 22*(10), 1005-1023.

Plocher, J., & Panesar, A. (2019). Review on design and structural optimisation in additive manufacturing: Towards next-generation lightweight structures. *Materials & Design, 183*, 108164.

Popov, A. V., Grigorie, T. L., Botez, R. M., Mébarki, Y., & Mamou, M. (2010). Modeling and testing of a morphing wing in open-loop architecture. *Journal of Aircraft, 47*(3), 917-923.

Prakash, T., & Pant, R. S. (2017). *Studies in telescopic span morphing of HALE UAV.* Paper presented at the 2017 8th International Conference on Mechanical and Aerospace Engineering (ICMAE).

Raheel, M., & Toropov, V. (2018). *Topology Optimization of an Aircraft Wing with an Outboard X-Stabilizer.* Paper presented at the 2018 Multidisciplinary Analysis and Optimization Conference.

Rajak, D. K., Pagar, D. D., Kumar, R., & Pruncu, C. I. (2019). Recent progress of reinforcement materials: a comprehensive overview of composite materials. *Journal of Materials Research and Technology, 8*(6), 6354-6374.

Rajak, D. K., Pagar, D. D., Menezes, P. L., & Linul, E. (2019). Fiber-reinforced polymer composites: Manufacturing, properties, and applications. *Polymers, 11*(10), 1667.

Ramesh, S., Handal, R., Jensen, M. J., & Rusovici, R. (2020). Topology optimization and finite element analysis of a jet dragster engine mount. *Cogent Engineering, 7*(1), 1723821.

Rao, J., Kiran, S., Kamesh, J., Padmanabhan, M. A., & Chandra, S. (2009). Topology optimization of aircraft wing. *Journal of Aerospace Science and Technologies, 61*(3), 402.

Rathod, V. T., Kumar, J. S., & Jain, A. (2017). Polymer and ceramic nanocomposites for aerospace applications. *Applied Nanoscience, 7*(8), 519-548.

Rinku, A., & Ananthasuresh, G. (2015). *Topology and Size Optimization of Modular Ribs in Aircraft Wings.* Paper presented at the 11th World Congress on Structural and Multidisciplinary Optimisation.

Sadler, R. L., Sharpe, M., Panduranga, R., & Shivakumar, K. (2009). Water immersion effect on swelling and compression properties of Eco-Core, PVC foam and balsa wood. *Composite Structures, 90*(3), 330-336. doi:https://doi.org/10.1016/j.compstruct.2009.03.016

Segui, M., Kuitche, M., & Botez, R. M. (2017). *Longitudinal aerodynamic coefficients of hydra technologies UAS-S4 from geometrical data.* Paper presented at the AIAA Modeling and Simulation Technologies Conference.

Seigler, T. M. (2005). *Dynamics and control of morphing aircraft.* Virginia Tech,

Setlak, L., & Kowalik, R. (2019). Examination of multi-pulse rectifiers of PES systems used on airplanes compliant with the concept of electrified aircraft. *Applied Sciences, 9*(8), 1520.

Setlak, L., Kowalik, R., & Lusiak, T. (2021). Practical Use of Composite Materials Used in Military Aircraft. *Materials, 14*(17), 4812.

Shokrieh, M. M., & Moshrefzadeh-Sani, H. (2016). On the constant parameters of Halpin-Tsai equation. *Polymer, 106*, 14-20.

Sigmund, O., & Petersson, J. (1998). Numerical instabilities in topology optimization: a survey on procedures dealing with checkerboards, mesh-dependencies and local minima. *Structural optimization, 16*(1), 68-75.

Singh, A., & Agrawal, A. (2015). Investigation of surface residual stress distribution in deformation machining process for aluminum alloy. *Journal of Materials Processing Technology, 225*, 195-202. doi:https://doi.org/10.1016/j.jmatprotec.2015.05.025

Sofla, A., Meguid, S., Tan, K., & Yeo, W. (2010). Shape morphing of aircraft wing: Status and challenges. *Materials & Design, 31*(3), 1284-1292.

Stanford, B. K., Jutte, C. V., & Coker, C. A. (2019). Aeroelastic Sizing and Layout Design of a Wingbox Through Nested Optimization. *AIAA Journal, 57*(2), 848-857.

Sugar-Gabor, O. (2019). Nonlinear lifting-line model using a vector formulation of the unsteady Kutta-Joukowski theorem. *INCAS Bulletin, 11*(1), 189-203.

Sullivan, J. M. (2006). Evolution or revolution? The rise of UAVs. *IEEE Technology and Society Magazine, 25*(3), 43-49.

Sun, J., Guan, Q., Liu, Y., & Leng, J. (2016). Morphing aircraft based on smart materials and structures: A state-of-the-art review. *Journal of Intelligent material systems and structures, 27*(17), 2289-2312.

Tamta, S., & Saxena, R. (2016). Topological optimization of continuum structures using optimality criterion in ANSYS. *Int Res J Eng Technol, 3*(7), 1483-1488.

Tang, J., Xi, P., Zhang, B., & Hu, B. (2013). A finite element parametric modeling technique of aircraft wing structures. *Chinese Journal of Aeronautics, 26*(5), 1202-1210. doi:https://doi.org/10.1016/j.cja.2013.07.019

Tarabi, A., Ghasemloo, S., & Mani, M. (2016). Experimental investigation of a variable-span morphing wing model for an unmanned aerial vehicle. *Journal of the Brazilian Society of Mechanical Sciences and Engineering, 38*(7), 1833-1841.

Tchatchueng Kammegne, M. J., Grigorie, T. L., & Botez, R. (2016). Morphing wing design to reduce airplane fuel consumption. *Substance ÉTS*.

Tchatchueng Kammegne, M. J., Tondji, Y., Botez, R. M., Grigorie, L. T., Mamou, M., & Mébarki, Y. (2018). New control methodology for a morphing wing demonstrator. *Proceedings of the Institution of Mechanical Engineers, Part G: Journal of Aerospace Engineering, 232*(8), 1479-1494.

Tondji, Y., & Botez, R. (2016). *Semi-empirical estimation and experimental validation of the mass and the center of gravity location of the unmanned aerial system—UAS-S4 of hydra technologies.* Paper presented at the 2016 international conference on unmanned aircraft systems (ICUAS).

Tondji, Y., & Botez, R. M. (2017). Semi-empirical estimation and experimental method for determining inertial properties of the Unmanned Aerial System – UAS-S4 of Hydra Technologies. *The Aeronautical Journal, 121*(1245), 1648-1682. doi:10.1017/aer.2017.105

Torenbeek, E. (2013). *Advanced aircraft design: conceptual design, analysis and optimization of subsonic civil airplanes*: John Wiley & Sons.

Traub, L. W., Botero, E., Waghela, R., Callahan, R., & Watson, A. (2015). Effect of taper ratio at low reynolds number. *Journal of Aircraft, 52*(3), 734-747.

Usher, T. D., Ulibarri, K. R., & Camargo, G. S. (2013). Piezoelectric microfiber composite actuators for morphing wings. *International Scholarly Research Notices, 2013*.

Vale, J., Leite, A., Lau, F., & Suleman, A. (2011). Aero-structural optimization and performance evaluation of a morphing wing with variable span and camber. *Journal of Intelligent material systems and structures, 22*(10), 1057-1073.

Vasconcelos, G. d. C., Basso, B. B., & Valera, T. S. (2019). Effect of impurity content on long term performance of recycled HDPE for structural application. *AIP Conference Proceedings, 2065*(1), 040005. doi:10.1063/1.5088325

Vasista, S., De Gaspari, A., Ricci, S., Riemenschneider, J., Monner, H. P., & van de Kamp, B. (2016). Compliant structures-based wing and wingtip morphing devices. *Aircraft Engineering and Aerospace Technology: An International Journal, 88*(2), 311-330. doi:10.1108/AEAT-02-2015-0067

Wang, Q., Lu, Z., & Zhou, C. (2011). New Topology Optimization Method for Wing Leading-Edge Ribs. *Journal of Aircraft, 48*(5), 1741-1748. doi:10.2514/1.C031362

Wang, W., Guo, S., & Yang, W. (2011). Simultaneous partial topology and size optimization of a wing structure using ant colony and gradient based methods. *Engineering Optimization, 43*(4), 433-446.

Weisshaar, T. A. (2006). Morphing aircraft technology-new shapes for aircraft design.

Williams, R. B., Park, G., Inman, D. J., & Wilkie, W. K. (2002). An overview of composite actuators with piezoceramic fibers. *Proceeding of IMAC XX, 47*, 130.

Zhang, Q., & Liu, H. H. T. (2017). Aerodynamics Modeling and Analysis of Close Formation Flight. *Journal of Aircraft, 54*(6), 2192-2204. doi:10.2514/1.C034271

Zhang, X., Zhao, Y., & Si, F. (2018). *Analysis of wing flexure deformation based on ANSYS.* Paper presented at the 2018 IEEE/ION Position, Location and Navigation Symposium (PLANS).

Zhao, L., Li, K., Chang, Y., & Li, J. (2019). Topology Optimization Design of Compliant Mechanism of Composite Wing Leading Edge. *Journal of Physics: Conference Series, 1215*, 012002. doi:10.1088/1742-6596/1215/1/012002

Zhao, Y.-b., Guo, W.-j., Duan, S.-h., & Xing, L.-g. (2017). A novel substructure-based topology optimization method for the design of wing structure. *Int. J. Simul. Multisci. Des. Optim., 8*, A5. doi:https://doi.org/10.1051/smdo/2016013

Zhu, J.-H., Zhang, W.-H., & Xia, L. (2016). Topology Optimization in Aircraft and Aerospace Structures Design. *Archives of Computational Methods in Engineering, 23*(4), 595-622. doi:10.1007/s11831-015-9151-2

Zingg, D., Diosady, L., & Billing, L. (2006). *Adaptive airfoils for drag reduction at transonic speeds.* Paper presented at the 24th AIAA applied aerodynamics conference.